Spin Systems and Long-Range Interactions for Quantum Memories and Quantum Computing

creative commons

Namensnennung-Keine kommerzielle Nutzung-Keine Bearbeitung 2.5 Schweiz

Sie dürfen:

das Werk vervielfältigen, verbreiten und öffentlich zugänglich machen

Zu den folgenden Bedingungen:

Namensnennung. Sie müssen den Namen des Autors/Rechteinhabers in der von ihm festgelegten Weise nennen (wodurch aber nicht der Eindruck entstehen darf, Sie oder die Nutzung des Werkes durch Sie würden entlohnt).

Keine kommerzielle Nutzung. Dieses Werk darf nicht für kommerzielle Zwecke verwendet werden.

Keine Bearbeitung. Dieses Werk darf nicht bearbeitet oder in anderer Weise verändert werden.

- Im Falle einer Verbreitung müssen Sie anderen die Lizenzbedingungen, unter welche dieses Werk fällt, mitteilen. Am Einfachsten ist es, einen Link auf diese Seite einzubinden.

- Jede der vorgenannten Bedingungen kann aufgehoben werden, sofern Sie die Einwilligung des Rechteinhabers dazu erhalten.

- Diese Lizenz lässt die Urheberpersönlichkeitsrechte unberührt.

Quelle: http://creativecommons.org/licenses/by-nc-nd/2.5/ch/   Datum: 3.4.2009

Genehmigt von der Philosophisch-Naturwissenschaftlichen Fakultät auf Antrag von

Prof. Dr. Daniel Loss

Prof. Dr. David DiVincenzo

Basel, den 17. September 2013

Prof. Dr. Jörg Schibler
Dekan

Acknowledgments

I would like to start by thanking my advisor Prof. Daniel Loss who accepted me as a PhD student in his group and who gave me the opportunity to work on many different and exciting research projects. His enthusiasm for Physics was contagious and I am very grateful for his guidance, help, and support during the four years of my PhD. His door was always open for me to discuss with him and he shared his ideas with the greatest generosity. His constant encouragements and his positive attitude towards my work have been of inestimable value.

I would also like to thank Prof. Arthur Jaffe whom I had the chance to meet during his sabbatical at the University of Basel. I had the opportunity to collaborate with him on exciting problems in Mathematical Physics where Prof. Jaffe's expertise is unique. This was a very productive and stimulating period, during which I developed a nice and friendly relationship with him.

Further, I am grateful to Prof. David DiVincenzo who kindly accepted to co-referee my thesis and to Prof. Christoph Bruder who chaired my PhD defense exam.

During my PhD studies, I shared the office with three successive colleagues and friends that made the working time very enjoyable. I thank Dr. Jan Fischer for his help and support at the beginning of my PhD. I am very grateful to Dr. Stefano Chesi with whom I collaborated on various projects. He was very patient and always happy to share his broad knowledge with me. I thank Dr. Diego Rainis who made the life in the office and in the whole institute very lively. The many physics discussions I had with him were not only pleasant but also useful for my research.

The work presented in this thesis would not have been possible without the help of very talented researchers. My deepest gratitude goes to Dr. Stefano Chesi, Dr. Suhas Gangadharaiah, Adrian Hutter, Luka Trifunovic, and Dr. James Wootton, who all were open to share their expertise with me.

vi

Summary

Since the seminal work by Shor who proposed a quantum algorithm factorizing integers into prime factors, it has become manifest that the laws of quantum mechanics provide resources for computation that overpower classical physics. The computational advantages that quantum physics offers have stimulated a tremendous amount of theoretical and experimental research. In this context, spin systems have played a major role, given that the spin degree of freedom – with the paradigmatic case of the spin-$1/2$ of electrons – represents an obvious candidate for the encoding of an elementary bit of quantum information (qubit).

On the other hand, however, quantum objects are very fragile entities, being very susceptible to the environment they reside in. This fragility of qubits is one of the main obstacles in the realization of a quantum computer.

In this thesis, we mainly address the two following questions relevant to quantum computation.

i) How is it possible to realize quantum gates in a reliable and scalable way?

ii) How can we store quantum information in a way that is resilient to the errors caused by the thermal environment? We focus on spin systems and demonstrate that long-range spin-spin interactions in the models considered can have beneficial effects.

In their pioneering work, Loss and DiVincenzo proposed a way to perform quantum computation in a semiconductor-based architecture where the spin state of an electron trapped in a quantum dot is chosen to encode the elementary qubit. In this proposal, the spins are required to lie spatially close to each other, and this might complicate the realization of a scalable architecture.

In the first part of the thesis we thus propose a scheme that allows the constraint on the positioning of the qubits to be relaxed. This is achieved by introducing a ferromagnetic coupler between the distant qubits, to which it is coupled via a dipolar interaction. Most importantly, our pro-

posal is applicable to *any type of spin qubits* and in particular to the technologically very relevant silicon-based qubits and NV-centers in diamond to which previous coupling schemes do not apply.

As additional key element, a quantum computer needs a memory capable of reliably storing quantum information in the presence of thermal fluctuations. In this context, systems with topological order are very promising in that they are immune to local static perturbations.

This brings us to the second part of this thesis, where we consider self-correcting memories, for which the protection against thermal noise is built-in at the hardware level. We propose physical models that exhibit these self-correcting properties, using as a starting point the well known topologically ordered toric code. In particular, we investigate how to induce long-range interactions between the spins of the toric code, since such interactions help increase the memory lifetime.

As a first step, we study a honeycomb quantum spin model coupled to delocalized cavity modes. We investigate the properties of the low-energy toric code Hamiltonian and show that the coupling to cavity modes prolongs the lifetime of the memory and offers a method to detect the presence of excitations. While the introduction of extended bosonic modes makes the model non-local, we also propose a purely local model consisting of a toric code embedded in a three-dimensional cubic lattice of hopping bosons; the low-energy sector of a toric code coupled to a three-dimensional Heisenberg ferromagnet in a broken-symmetry state realizes this model. Our analysis leads to an energy penalty for the creation of defects that grows linearly with the size L of the memory and thus to a lifetime increasing exponentially with L.

In the third part of this thesis, we study spin systems that support anyons, i.e., particles with fractional statistics. As anyons are assumed to be well separated from each other, local perturbations cannot fuse them and thus cannot introduce any transitions between different states of the anyonic Hilbert space. Similar to the toric code, such systems are topologically ordered: they are immune to local perturbations and quantum gates are implemented by non-local operations, namely the exchange of anyons, whose outcomes depend only on the topology of the exchange. Here again the fault-tolerance is achieved at the level of the hardware and physical systems supporting non-abelian anyons are thus promising platforms for quantum computation.

We focus on spin systems that exhibit some of these properties and specifically on variations of the honeycomb quantum spin model. We first investigate the exact solution of the honeycomb model in detail and derive an explicit formula for the projector onto the physical subspace.

We use this result to study inhomogeneous open spin ladders, related to the honeycomb model, which can be tuned between topological and non-topological phases. We test the robustness of Majorana end states (MES) which emerge at the boundary between sections in different topological phases. Furthermore, we present a trijunction setup where MES can be braided. This is of interest since MES in these spin ladders potentially follow non-abelian braiding statistics. Finally, we study the ground states of the aforementioned ladders and show that they are free of vortices when the signs of the spin couplings are all positive or negative. To prove this, we use exact reflection-positivity-based methods as well as approximate methods. We discuss why the absence of vortices in the ground states of the spin ladders is relevant for quantum computation.

In the last part of the thesis, we provide an extension of the Mermin-Wagner theorem to a system of lattice spins that are spin-coupled to itinerant and interacting charge carriers. We prove that neither (anti-) ferromagnetic nor helical long-range order is possible in one and two dimensions at any finite temperature (in the absence of spin-orbit). The fundamental question whether spontaneous ordering of the lattice spins occurs in these systems is of interest in the context of quantum computation; the polarization of nuclear spins coupled to a two-dimensional electron gas is a possible route towards the reduction of decoherence induced by the fluctuating Overhauser field in gate-defined quantum dots.

Contents

II Self-Correcting Quantum Memories and Long-Range Interactions

Introduction

Spin systems lie at the heart of many important research areas of modern solid-state physics, among which solid-state-based quantum computation has generated a lot a research over the last decades. The realization of a quantum computer, capable of performing calculations much more efficiently than classical computers, is one of the major challenges of contemporary physics. In fact, quantum mechanics provides resources for computation that overpower classical physics; for instance a quantum algorithm factorizing integers into prime factors (undoable with a classical computer in a reasonable amount of time) was proposed in a seminal work by Shor. [1] However, quantum objects are very fragile and very susceptible to the environment they are residing in. It is thus a very subtle and perplexed task to reliably store and to process quantum information in a way that allows to perform powerful quantum algorithms.

Pioneering ideas to implement a scalable quantum computer are due to Loss and DiVincenzo. [2] They proposed a semiconductor-based quantum computer where the elementary quantum bit (qubit) of information is chosen to be encoded in the spin state of the electron. The proposed setup was such that it could satisfy stringent criteria essential for the realization of quantum computing architectures. These are known as the DiVincenzo criteria, which can be synthesized as follows: [3]

- Definition of the logical qubits,

- initialization in a chosen state with high fidelity,
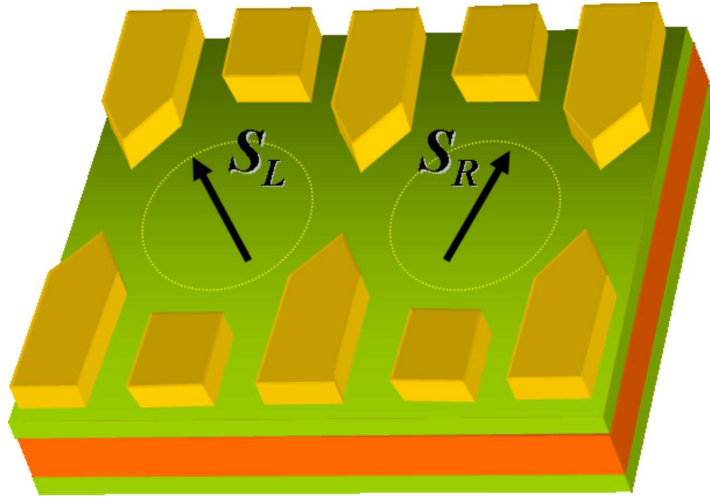
Figure 1.1: Double quantum dot. The electrons are trapped in the quantum dots by means of electric gates (yellow). The spin S_L (S_R) of the left (right) electron is depicted by an arrow. The spin states define the states of the logical qubits. The coupling between the qubits is tuned by electrically controlling (through the two gates in the middle) the overlap of the associated electronic wavefunctions.

- long coherence times; any coherent superposition of the qubit states must survive for a sufficiently long time compared to the gate operation time,

- ability to coherently control a single qubit and to induce coherent interactions between different qubits,

- method to read-out the final state of the qubit,

- scalabilty; if one wants to apply the proposal in forthcoming technologies, the possibility to scale up the number of qubits is crucial.

The basic building elements of the of the Loss-DiVincenzo quantum computer are depicted in Fig. 1.1. Each qubit is encoded in the spin (arrow) of an electron that is trapped in a gate-defined quantum dot. Most of the experimental implementations of such qubits are done in GaAs two-dimensional electron gases (2DEGs). Impressive experimental progress has been achieved in the realization and control of such systems (for a review see for example [4, 5, 6]) making GaAs spin qubits a very appealing platform. The qubit basis states are defined through

$$|0\rangle = |\uparrow\rangle \qquad \text{and} \qquad |1\rangle = |\downarrow\rangle, \qquad (1.1)$$

with $|\uparrow\rangle$ and $|\downarrow\rangle$ the basis states of the electron spin. A general qubit state is then an arbitrary superposition of the basis states, namely

$$|\psi\rangle = \alpha|0\rangle + \beta|1\rangle \,, \tag{1.2}$$

with $|\alpha|^2 + |\beta|^2 = 1$.

Let us now sketch the main ideas of the proposal. Initialization of the qubit state is performed by applying an external magnetic field. The single qubit operations are performed by applying *locally* time-dependent magnetic fields. Producing time-dependent localized magnetic fields is technologically challenging, however it is possible to effectively create such fields with a spatially varying g-tensor or spin-orbit coupling for example. In these cases the control is fully electrical. Two-qubit gates are performed by exploiting the direct exchange interaction of adjacent spins. The exchange interaction is controlled electrically by tuning the tunnel barrier between the quantum dots. In this case the interaction between nearby spin qubits $\boldsymbol{S}_1$ and $\boldsymbol{S}_2$ can be mapped to a time-dependent Heisenberg model

$$H_{12} = J(t)\boldsymbol{S}_1 \cdot \boldsymbol{S}_2 \,, \tag{1.3}$$

where $J(t)$ is the time-dependent exchange coupling. Another DiVincenzo criterion that needs to be satisfied is the possibility to read-out the state of the qubit after quantum computation. In the above setup, this can be achieved by converting the spin states into charge states, which can then be detected electrostatically.

In the original Loss-DiVincenzo proposal, direct exchange interaction between the quantum dots is exploited and requires the qubits to lie very close to each other. This is not optimal as it reduces the space left for the auxiliary gates needed to define the quantum dots and also because it requires strong localization of the fields for the single-qubit operations. These stringent conditions on the position of the quantum dots as well as on the localization of the fields can represent a hinder to the last DiVincenzo criterion, namely scalability. In this context it is thus of relevance to propose methods to couple qubits that allow for more freedom in the relative positioning of the quantum dots.

Over the last years another type of spin qubits has emerged as a very promising alternative to GaAs quantum dots, namely *atomistic* qubits such as silicon-based qubits and NV-centers. [7, 8, 9] The former are defined by the electron or nuclear spin of a phosphorus atom implanted in a silicon wafer. In the latter case, the qubit is encoded in a level doublet of a nitrogen-vacancy center in diamond. As both types of spin qubits can be isotopically purified and the noise due to surrounding nuclear spins can

be avoided, these systems are very stable with impressively long coherence times. They thus also represent good candidates for the encoding of elementary qubits.

The possibility to purify the material from its nuclear spins is very favorable but unfortunately not always possible. In GaAs quantum dots for example, a main source of decoherence is due to the fluctuating nuclear Overhauser field. However, polarization of the the nuclear spins would increase the decoherence times of the qubit. In this context, the question whether ordering might occur spontaneously in systems of lattice spins coupled to a 2DEG is relevant. We address this problem in Part IV of this thesis and extend the Mermin-Wagner theorem to a system of lattice spins which are spin-coupled to itinerant and interacting charge carriers. We use the Bogoliubov inequality to rigorously prove that neither (anti-) ferromagnetic nor helical long-range order is possible in one and two dimensions at any finite temperature. When Rashba and/or Dresselhaus spin-orbit interaction is present, our proof becomes generally inconclusive.

After this small digression, let us come back to our main subject of interest here, namely the coupling of distant spin qubits. While proposals to couple spin qubits over large distances already exist (see Chapters 3 and 4 for references), none of them apply to atomisitc qubits and the question about their coupling remains open. The main reason for that is that these qubits are very confined and have very weak spin-orbit interaction. The first property hinders easily tunnel coupling to these systems and the second one precludes the possibility to use electrostatic couplings.

In this thesis we tackle this problem and propose a mechanism of coherent coupling between distant spin qubits interacting dipolarly with a ferromagnet. We derive an effective two-spin interaction Hamiltonian and estimate the coupling strength to be about $10^{-8}\,eV$ for qubits separated by distances of about one micron. We present a sequence for the implementation of the entangling CNOT gate and estimate the corresponding operation time to be a few tens of nanoseconds. Our proposal applies to *any type of spin qubits*. Finally, we discuss the mechanisms of decoherence induced solely by the coupling to the ferromagnet and show that there is a regime where it is negligible. A particularly promising application of our proposal is to atomistic spin-qubits such as silicon-based qubits and NV-centers in diamond. We also investigate its applicability to singlet-triplet qubits. The details of the proposal as well as important references to the subject matter can be found in Chapters 3 and 4.

As the above example shows, long-range spin-spin interactions medi-

ated by a coupler represent a powerful resource for the field of quantum computation. Below we argue that long-range interactions play also a central role in stabilizing quantum memories.

In this thesis we generally define as "long-ranged" an interaction with a $1/r^\alpha$ spatial decay where $0 \leqslant \alpha \leqslant 2$. Archetypical examples are the gravitational interaction between masses and the Coulomb interaction between charged particles.

1.1 Self-correcting quantum memories

Every quantum computer needs a memory that allows to reliably store the quantum information in the presence of a thermal environment. Although the decoherence times of single-qubit quantum dots have been considerably improved over the years, such qubits remain very susceptible to the coupling to the environment and they quickly decohere. An interesting idea to overcome these negative effects induced by a thermal environment is to encode a single *logical qubit* into a large number of *physical qubits*. [10, 11] This allows one to use the additional degrees of freedom of the enlarged Hilbert space in order to perform non-destructive measurements on the system: the state of the qubit is not affected by the measurement and the presence of errors can be detected. This is done by measuring certain *check operators* and the outcome is called *error syndrome*. These so-called *quantum error-correcting codes* require the ability to measure the error syndrome repeatedly and to actively correct the errors produced by the environment. While this method works in principle, it leads to a high degree of technological challenge since a large number of measurements and entangling operations need to be performed very accurately.

In this context, it is of relevance to find systems that are *self-correcting*, i.e., resilient to errors on the level of the hardware. It is well known that this is possible in the classical case. The prototypical example of a classical memory (classical hard-drive in modern computers) is the 2D Ising model or the 3D Heisenberg ferromagnet in a broken-symmetry state below the Curie temperature. The bit states are then defined by the direction of the magnetization

$$\text{up} \leftrightarrow |0\rangle \qquad \text{and} \qquad \text{down} \leftrightarrow |1\rangle. \tag{1.4}$$

These systems are self-correcting in the sense that they do not require to actively cure the errors induced by the environment, but the magnet itself does it for you. Indeed, assume the classical ferromagnet to have

all spins pointing along a certain direction with total magnetization S. At time t^* introduce a certain number of bit flips and reduce the magnetization to $S - s$. Due to the exchange interaction between the spins, recovering of bit-flip errors is promoted and the magnetization S is recovered after a certain time $t > t^*$, i.e., the memory corrects itself the errors introduced by the environment. This recovery is due to the energy barrier imposed by the exchange interaction that favors a spin to flip back rather than creating large domains of spins with opposite direction. As a direct consequence, the lifetime of the magnetization (and thus of the encoded classical bit) increases with the number of spins. In other words, the lifetime of the memory increases with the size of the system; this is the characteristic property of what we define as a self-correcting memory.

Such considerations lead to the following natural question: is it possible to build a quantum analog? In other words, can we find a quantum mechanical system that allows to store quantum information in a reliable way without the need to perform active operations such as measurements or entangling operations? So-called *topological phases of matter* have attracted a lot of attention and have been argued to represent a good place to store quantum information. Such phases of matter can arise as the ground state degenerate subspace of certain many-body Hamiltonians. For a rigorous definition of topological order we recommend the reader to have a look at Ref. [12], however it can partially be understood as the property that local operations cannot distinguish between the different ground states. Therefore only highly non-local operations cause transitions between the ground states and the system is immune to local perturbations. One of the most important and well-studied examples of topological phases of matter is the toric code introduced by Kitaev in Refs. [13, 14] and later investigated in the framework of quantum memories in Ref. [15].

The toric code corresponds to the subspace of a frustration free Hamiltonian defined on a lattice in two dimensions with toric boundary conditions. For a surface with genus g, one can show that the degeneracy of the ground-state subspace (the so-called code space) is 4^g. We can thus encode $2g$ logical qubits in the toric code space. The toric code is topologically ordered and robust against local pertubations at zero temperature: [12] the effect of such perturbations on the energy splitting of the ground-state manifold is exponentially suppressed with the linear size L of the lattice. In other words, the toric code represents a stable quantum memory at zero temperature. This is not the case in the presence of coupling to a thermal environment; contrary to a classical memory the lifetime of the

toric code does not increase with L. References to improved versions of the toric code as well as a more detailed discussion of its thermal fragility can be found in Chapter 5. As the toric code is of central importance in a big part of this work, we present the most important aspects of it in Chapter 5 .

The above considerations allow us to attempt a good definition for a *self-correcting* quantum memory: a quantum-mechanical system that stores logical qubits in a topologically ordered ground-state subspace and whose lifetime increases with the linear size L of the system in the presence of a thermal environment (similar to a classical hard-drive). In order to make this definition closer to reality, we generally require additional properties in the definition. Here we synthesize all the important characteristics that we think a model for a self-correcting quantum memory should satisfy:

- The quantum information is stored in a *topologically ordered ground-state subspace* of a gapped Hamiltonian H,

- the linear size L required to obtain a lifetime t should obey $L = \text{poly}(t)$ when the memory is in contact with a thermal environment. In other words, the lifetime of the memory should grow at least ploynomially with L,

- the memory is realizable in our three-dimensional space,

- the Hamiltonian H involves only few-body *local* interactions of *bounded* strength.

The first condition ensures that the memory is protected against weak, static, and local perturbations of the Hamiltonian. The presence of a gap allows to unambiguously define the ground-state subspace and the memory is stable if a perturbation is sufficiently smaller than the gap. The second condition defines thermal stability of the quantum memory. Finally, the third and fourth conditions make the model closer to what is expected to be practically realizable.

In Part II, we study variations of the toric code. In particular we propose in Chapter 6 a way to realize long-range interactions between defects (called anyons in this context) by coupling the honeycomb quantum spin model to extended cavity modes. We study the properties of the low-energy toric code model perturbatively by making use of the Schrieffer-Wolff transformation and show that, depending on the specific setup, the cavity modes can be useful in several ways. They allow to detect the presence of anyons through frequency shifts and to prolong the

lifetime of the memory by enhancing the anyon excitation energy or me-
diating long-range anyon-anyon interactions with tunable sign. Indeed,
it has been shown in Ref. [16] that repulsive long-range interactions be-
tween the defects of the toric code lead to a memory lifetime growing
polynomially with L.

   As the coupling to cavity modes requires the introduction of non-local
terms in the Hamiltonian and thus break one of the above criteria, we
propose in Chapter 7 a second model that is purely local and that leads
to an energy barrier for the anyons that grows linearly with L and thus to
a lifetime that grows exponentially with L. The model is composed of a
toric code embedded in a three-dimensional system of hopping bosons.
Furthermore we propose and study another model that allows to realize
the coupling to hopping bosons in its low-energy sector. This model is
realized by locally coupling toric code operators to individual spins of a
three-dimensional Heisenberg ferromagnet in a broken-symmetry state
at finite temperature. This setup presents similarties to the one studied
in Part I for the long-distance coupling of spin qubits. In this case the
spins are replaced by toric code operators and the long-range interaction
between these operators (mediated by the bosonic field) is at the origin
of the energy barrier for the creation of defects.

1.2   Topological quantum computation by anyons

In physical implementations of quantum computers, the realization of
quantum gates is subject to errors and imperfections due to the cou-
pling to noise sources that are unavoidable in these setups. However,
if the quantum gates are sufficiently precise it is possible to perform
quantum computation in a fault-tolerant (i.e. resilent to imperfections)
way. Unfortunately the fidelity of the gates needs to be very high and
this represents a considerable technological challenge. It is thus of inter-
est to determine whether it is possible to achieve fault-tolerant quantum
computation at the level of the hardware similar to classical (and quan-
tum) self-correcting memories which are intrinsically resilient to errors.
Kitaev demonstrated a deep connection between quasiparticle-like ex-
citations with fractional statistics (there is a long history of excitations
with fractional statistics, called *anyons* by Wilczeck [17], see for example
Refs. [18, 19]) and quantum computation; [14] nowdays this field is re-
ferred to as *topological quantum computation*, see for example [20, 21] for a

good introduction to this exciting subject and for more details about the material presented here.

It is well established that particles in three dimensions follow either fermionic or bosonic statistics. Consider two indistinguishable particles in three dimensions and take one of the particles around the second particle along a closed path $\mathcal{C}_1$. As statistical behavior depends only on the topology of the path, we can continuously deform the closed path $\mathcal{C}_1$ to a point and thus conclude that the wavefunction $|\psi\rangle$ of the two particles remains unchanged. As the motion of one particle around the closed path $\mathcal{C}_1$ corresponds to two consecutive exchanges of the particles, we infer that a single exchange leads to the following transformation of the wavefunction $|\psi\rangle$:

$$|\psi\rangle \rightarrow e^{i\phi}|\psi\rangle\,, \qquad \begin{aligned} \phi &= 0\,, \text{ for bosons }, \\ \phi &= \pi\,, \text{ for fermions}. \end{aligned} \tag{1.5}$$

In two dimensions the above arguments do not apply because a closed loop is not always topologically equivalent to a point. It is thus clear that the two-dimensional world offers a wider range of possible statistical evolutions than our three-dimensional space does. In two dimensions, the two-particle wavefunction can pick any possible phase $e^{i\phi}$ under exchange, with $\phi \in [0, 2\pi]$. When the statistical evolution is described by a phase factor, we denote the corresponding particles *abelian anyons*. However, more complicated statistical evolution can arise for so-called *non-abelian anyons* that we now describe in more detail.

Models for non-abelian anyons contain a set of particles

$$1 \text{ vaccuum}\,, \quad a\,, \quad b\,, \quad c\,, \quad d \ldots\,, \tag{1.6}$$

and a set of non-trivial fusion rules

$$a \times b = N^c_{ab}\, c + N^d_{ab}\, d + \cdots\,. \tag{1.7}$$

The anyonic Hilbert space where the quantum information is stored and processed is then the degenerate fusion space of the set of anyons. As anyons are assumed to be well-separated from each other, local perturbations cannot fuse the quasiparticles and thus cannot introduce transitions between the different states. Similar to the toric code, such systems are topologically ordered: they are immune to local perturbations and quantum gates are implemented by non-local operations, namely exchange of anyons, that only depend on the topology of the exchange. The statistical evolution is then described by a unitary matrix acting on the anyonic

Hilbert space. Consider for example four anyons labeled 1, 2, 3, and 4. The exchange $1 \leftrightarrow 2$ implements a unitary that we denote U_{12} and the exchange $2 \leftrightarrow 3$ implements the unitary U_{23}. As matrices generally do not mutually commute, i.e. $[U_{12}, U_{23}] \neq 0$, the adjective non-abelian is justified to qualify these anyons. The built-in fault-tolerance of anyonic quantum computation renders this theory very appealing for the realization of quantum computing architectures.

Non-abelian anyons do not only represent a nice theoretical concept but Ising anyons for example are expected to be realized in certain physical systems: in fractional quantum Hall systems, [22] in vortices of p-wave superconductors, [23] in proximity-induced superconducting wires, [24, 25, 26] as well as in lattice spin models. [27] The quasiparticles of the Ising anyon model are labeled: 1 (vacuum), ϵ, and σ. Their fusion rules are

$$\epsilon \times \epsilon = 1\,, \quad \epsilon \times \sigma = \sigma\,, \quad \sigma \times \sigma = 1 + \epsilon\,. \tag{1.8}$$

While Ising anyons are not universal for quantum computation, their potential physical realization makes them very interesting and has motivated a lot of work. Furthermore, schemes to make Ising anyons universal have been investigated. [28]

In part III we study quantum spin systems that support Ising anyons. We focus on the compass model originally introduced by Kugel and Khomskii [29] to study the Jahn-Teller effect. A two-dimensional honeycomb version of the compass model has been extensively studied by Kitaev in Ref. [27]. Kitaev showed that this spin model has a rich structure and supports two phases (that we denote by A and B here) in the spin-spin interaction parameter space. In phase A the model is gapped and is equivalent to the toric code Hamiltonian in lowest-order. In this case the vortex excitations are similar to the toric code anyons and are abelian. [14] On the contrary phase B is gapless but Kitaev showed that the introduction of an external magnetic field (or of any perturbation that breaks time-reversal invariance) opens a gap. In this case the vortex excitations carry a Majorana in their center and are non-abelian Ising anyons. The simplicity of the honeycomb model makes it promising for the physical realization of an anyon model; the honeycomb model has become closer to reality thanks to several recent proposals. [30, 31, 32, 33]

Quasi one-dimensional versions of the honeycomb model in form of a ladder have been studied. [34, 35, 36] It has been shown in Ref. [36] that such ladders support localized Majorana states at the junction between topological and non-topological phases. Similar to Majorana end states in p-wave wires, they might follow non-abelian braiding statistics.

In Chapter 9 we study many aspects of the exact solution of the honeycomb model. In particular, in the context of the spin-to-Majoranas mapping used by Kitaev to solve the model, the Hilbert space gets enlarged and unphysical states needs to be discriminated from the physical ones. We derive an explicit formula for the projector onto the physical subspace and show that physical states are simply characterized by the parity of the total occupation of the fermionic eigenmodes.

In Chapter 10 we propose an inhomogeneous open spin ladder, related to the Kitaev honeycomb model, which can be tuned between topological and nontopological phases. We investigate the robustness of the Majorana bound states that arise at the junction between topological and non-topological regions and propose a way to exchange them in a trijunction setup. This is of interest as Majorana end states in these ladders are susceptible to follow non-abelian braiding statistics.

In Chapter 11 we establish reflection positivity for Gibbs trace states defined by a certain class of Hamiltonians that describe the interaction of Majoranas. This turns out to be pertinent to the study of the honeycomb model and its variations.

In Chapter 12 we use exact reflection-positivity-based methods to investigate the role that vortex loops play in characterizing eigenstates of certain Majorana Hamiltonians realized by the honeycomb quantum spin model and the associated ladder. Among other results, we show that for reflection symmetric open ladders the ground states of the spin Hamiltonians are vortex-free when the signs of the spin couplings are all positive or negative. Furthermore, for non-symmetric open (and closed) ladders we use approximate methods and find evidence that the same is true. These results find application in the context of topological quantum computation: as we discuss in detail in Chapter 10, the presence of freely moving vortices in the ground states of spin ladders would alter in a dramatic way the outcome of exchanging the Majorana end states; the parity of the encoded qubit depends on the position of the vortices.

Part I

Long-Range Indirect Interaction of Spins Mediated by a Ferromagnet

CHAPTER 2

Introduction

Quantum coherence and entanglement lie at the heart of quantum information processing. One of the basic requirements for implementing quantum computing is to generate, control, and measure entanglement in a given quantum system. This is a rather challenging task, as it requires to overcome several obstacles, the most important one being decoherence processes. These negative effects have their origin in the unavoidable coupling of the quantum systems to the environment they are residing in.

A guiding principle in the search for a good system to encode qubits is the smaller the system the more coherence, or, more precisely, the fewer degrees of freedom the weaker the coupling to the environment. Simultaneously, one needs to be able to coherently manipulate the individual quantum objects, which is more efficient for larger systems. This immediately forces us to compromise between manipulation and decoherence requirements.

Following this principle, among the most promising candidates for encoding a qubit we find *atomistic* two-level systems, such as NV-centers and silicon-based spin qubits. [37, 38, 39, 40, 41, 42, 43, 44, 45, 46, 48, 49] The latter are composed of nuclear (electron) spins of phosphorus atoms in a silicon nanostructure. They have very long T_2 times of $60\,ms$ [8] for nuclei and of $200\mu s$ for electrons. [7] Recently, high fidelity single qubit gates and readout have been demonstrated experimentally. [7] Nitrogen-vacancy centers [9] in diamond have also been demonstrated experimentally to be very stable with long decoherence times of $T_2^* \approx 20\,\mu s$ and $T_2 \approx 1.8\,ms$. [50] Both types of spin qubits have the additional advantage

that noise due to surrounding nuclear spins can be avoided by isotopi-
cally purifying the material.

Unfortunately, it is hardly possible to make these spin qubits inter-
act with each other in a controlled and scalable fashion. They are very
localized and their position in the host material is given and cannot be
adjusted easily. Therefore, if during their production two qubits turn out
to lie close to each other they will always be coupled, while if they are
well-isolated from each other they will never interact. It is thus of high
interest to propose a scheme to couple such atomistic qubits in a way that
allows a high degree of control. While there have been various propos-
als over the last years in order to couple spin qubits over large distances,
[56, 57, 58, 59, 60, 61, 62, 63, 64, 65, 66, 67] none of these methods apply
straightforwardly to atomisitc qubits such as silicon-based qubits and N-
V centers.

Alternative successful candidates for encoding a qubit are an elec-
tron spin localized in a semiconductor quantum dot, gate-defined or self-
assembled, or a singlet-triplet qubit with two electrons in a double quan-
tum well. [6, 84] These natural two-level systems are very long-lived (re-
laxation time $T_1 \sim 1s$, see Ref. [51], and decoherence time $T_2 > 200\mu s$, see
Ref. [52]), they can be controlled efficiently by both electric and magnetic
fields, [53, 54, 55] and, eventually, may be scaled into a large network. It
has been experimentally demonstrated that qubit-qubit couplings can be
generated and controlled efficiently for these systems. [66] However the
separation between the quantum dots needs to be small ($\sim 100nm$) and
this renders their scaling to a very large number of qubits a perplexed
task. Indeed, the physical implementation of quantum dot networks re-
quires some space between the qubits for the different physical auxiliary
components (metallic gates, etc.). In this context, it is therefore also im-
portant to find a way to couple such qubits over sufficiently large dis-
tances (micrometer scale) to satisfy the space constraint.

In this work we propose a mechanism of long-range coherent inter-
action between *any kind of spin qubits*. The idea is to use the dipolar cou-
pling of spin qubits to the spins of a dogbone-shaped ferromagnet. We
show that coupling strengths of about $10^{-8}eV$ are achievable between
spin qubits separated by a distance of about $1\,\mu m$. Our scheme is demon-
strated to be applicable to singlet-triplet qubits as well. Furthermore, we
explicitly construct the required sequences to implement a CNOT gate
and estimate the corresponding operation times. The additional deco-
herence induced by the coupling to the ferromagnet is studied and we
find a regime where fluctuations are under control and no significant ad-
ditional decoherence is introduced. A particularly promising application

of our proposal is to atomistic spin-qubits such as silicon-based qubits and NV-centers in diamond to which previous coupling schemes do not apply.

Long-Distance Entanglement of Spin-Qubits via Ferromagnet

We propose a mechanism of coherent coupling between distant spin qubits interacting dipolarly with a ferromagnet. We derive an effective two-spin interaction Hamiltonian and estimate the coupling strength. We discuss the mechanisms of decoherence induced solely by the coupling to the ferromagnet and show that there is a regime where it is negligible. Finally, we present a sequence for the implementation of the entangling CNOT gate and estimate the corresponding operation time to be a few tens of nanoseconds. A particularly promising application of our proposal is to atomistic spin-qubits such as silicon-based qubits and NV-centers in diamond to which previous coupling schemes do not apply.

3.1   Introduction

Addressing the issue of coupling atomisitc qubits in this work, we fill the gap and propose a setup to couple two spin qubits separated by a relatively large distance on the order of micrometers, see Fig. 3.1. The

coupling is mediated via a ferromagnet with gapped excitations to which the spin qubits are coupled by magnetic dipole-dipole interaction. Since the ferromagnet is gapped only virtual magnons are excited but in order to obtain the sizable coupling one needs to tune the splitting of the qubit close to resonance with the gap of the ferromagnet. The *on* and *off* switching of the qubit-qubit interaction is therefore achieved by tuning qubits off resonance (see below). The resulting system is thus realizable with state-of-the-art semiconductor technologies. We point out that our analysis is not restricted to a precise type of spin qubit but is in principle applicable to any system that dipolarly interact with the spins of a ferromagnet. In particular, our proposal is also applicable to an electron spin localized in a semiconductor quantum dot, gate-defined or self-assembled. [2, 6] While other schemes exist to couple such qubits over large distances, [65, 66, 58, 60, 63] none of them is applicable to atomistic qubits. The main novelty of our proposal is thus the possibility to *also* couple atomistic qubits that are of high technological relevance.

Before we proceed with the quantitative analysis, let us first give an intuitive picture of the qubit-qubit coupling. The coupling between two distant qubits is mediated via a *coupler* system. The relevant quantity of this coupler is its spin-spin susceptibility—in order to have a long-range coupling, a slowly spatially decaying susceptibility is required. The dimensionality of the coupler plays an important role since, in general, it strongly influences the spatial decay of the susceptibility, which can be anticipated from purely geometric considerations. Furthermore, since the coupler interacts with the qubits via magnetic dipolar forces, we require that a large part of the coupler lies close to the qubits. To this end we immediately see that a dog-bone shape depicted in Fig. 3.1 satisfies these two requirements—strong dipolar coupling to the qubits and slow spatial, practically 1D, susceptibility decay between the qubits.

3.2   Model

The system we consider consists of two spin-$\frac{1}{2}$ qubits coupled dipolarly to the ferromagnet

$$H = H_\sigma + H_\text{F} + H_\text{I}, \tag{3.1}$$

where H_F is for the moment unspecified Hamiltonian of the dog-bone shaped ferromagnet that is assumed to be polarized along the x-axis. We first assume that the qubits are also polarized along the x-axis, $H_\sigma = \sum_{i=1,2} \frac{\Delta_i}{2} \sigma_i^x$, while the ferromagnet disc axes are along z, see Fig. 3.1. The magnetic dipole coupling between the ferromagnet and the spin-qubits
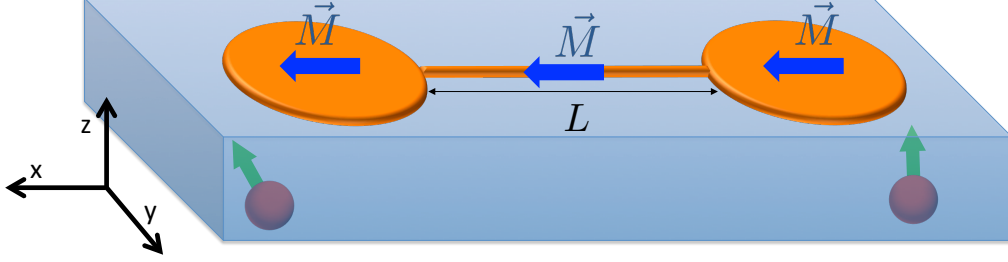
Figure 3.1: The schematics of the ferromagnetic coupler setup. The orange dog-bone shape denotes the ferromagnet that is coupled via magnetic dipole interaction to spins of nearby quantum dots (red sphere with green arrow). The ferromagnet is assumed to be a monodomain and its magnetization is denoted by blue arrows (M) that can take arbitrary orientation. The length of the quasi-1D ferromagnetic channel that is approximately equal to the distance between the qubits is denoted by L. The shape of the ferromagnetic coupler is chosen such that it enables strong coupling to the spin-qubits while maintaining the spatially slowly decaying 1D susceptibility between the two discs.

can be written as

$$
\begin{aligned}
H_{\mathrm{I}} =\ & \frac{\mu_0 \mu_b \mu}{4\pi a^3} \sum_{i=1,2} \int d\boldsymbol{r}\, S_{\boldsymbol{r}}^x \left[\left(\frac{3i A_{i,\boldsymbol{r}}'}{2} + \frac{3 C_{i,\boldsymbol{r}}''}{4} \right) \sigma_i^+ + \mathrm{h.c.} \right. \\
& \left. + \frac{1}{2} \left(B_{i,\boldsymbol{r}} - 3 C_{i,\boldsymbol{r}}' \right) \sigma_i^z \right] \\
& + S_{\boldsymbol{r}}^+ \left[\left(\frac{3}{8} C_{i,\boldsymbol{r}}' - \frac{3i}{2} A_{i,\boldsymbol{r}}'' + \frac{3}{8} B_{i,\boldsymbol{r}} \right) \sigma_i^+ \right. \\
& \left. - \frac{1}{8} \left(B_{i,\boldsymbol{r}} - 3 C_{i,\boldsymbol{r}}' \right) \sigma_i^- + \left(\frac{3 C_{i,\boldsymbol{r}}''}{4} + \frac{3i A_{i,\boldsymbol{r}}'}{2} \right) \sigma_i^z \right] \\
& + \mathrm{h.c},
\end{aligned}
\tag{3.2}
$$

where $A_{\boldsymbol{r}}$, $B_{\boldsymbol{r}}$, $C_{\boldsymbol{r}}$ are given by

$$
A_{\boldsymbol{r}} = \frac{1}{a^3} \frac{r^z r^+}{r^5} ,
\tag{3.3}
$$

$$
C_{\boldsymbol{r}} = \frac{1}{a^3} \frac{(r^+)^2}{r^5} ,
\tag{3.4}
$$

$$
B_{\boldsymbol{r}} = \frac{1}{a^3} \frac{1}{r^3} \left(2 - \frac{3 r^+ r^-}{r^2} \right) ,
\tag{3.5}
$$

with $S_{\boldsymbol{r}}^{\pm} = S_{\boldsymbol{r}}^y \pm i S_{\boldsymbol{r}}^z$ and lattice constant a. Here we denote the real part of a complex number with prime and the imaginary part with double prime. The operator $\boldsymbol{S_r}$ describes the spin of the ferromagnet at the position $\boldsymbol{r}$.

Next, we release the assumptions about the mutual orientation of the disc axes, the axes of polarization of the ferromagnet, and the direction of the qubits splitting and assume that these can take arbitrary directions. Now the interaction Hamiltonian reads

$$
\begin{aligned}
H_{\mathrm{I}} =& \frac{\mu_0 \mu_b \mu}{4\pi a^3} \sum_{i=1,2} \int d\boldsymbol{r}\, S_{\boldsymbol{r}}^{\tilde{z}} \left[a_{i,\boldsymbol{r}} \sigma_i^z + b_{i,\boldsymbol{r}} \sigma_i^+ + \text{h.c.} \right] + \\
& S_{\boldsymbol{r}}^{\tilde{+}} \left[c_{i,\boldsymbol{r}} \sigma_i^z + d_{i,\boldsymbol{r}} \sigma_i^+ + e_{i,\boldsymbol{r}} \sigma_i^- \right] + \text{h.c},
\end{aligned}
\tag{3.6}
$$

where $\boldsymbol{S_r}$ and $\boldsymbol{\sigma_r}$ have, in general, different quantization axes. The expressions of the coefficients in Eq. (3.6) are now more complicated, nevertheless it is important to note that the integrals of these coefficients are *experimentally accessible*. The qubits can be used to measure the stray field of the ferromagnet which is given by $B_s = (b_i', b_i'', a_i)$, where $\{a_i, \ldots, e_i\} = \frac{\mu_0 \mu}{4\pi a^3} \int d\boldsymbol{r} \{a_i, \ldots, e_i\}_{\boldsymbol{r}}$. In order to measure the remaining coefficients, one needs to apply the magnetic field externally in order to polarize sequentially the ferromagnet along the two perpendicular directions to the ferromagnet easy axis. The coefficients are obtained then by measuring again the stray fields (with the aid of the qubits) which now are given by $(d' + e', d'' - e'', c')$ and $(d'' + e'', d' - e', c'')$. Furthermore, all the results that we are going to obtain for the qubit-qubit coupling as well as the estimates of the decoherence will depend only on the integrals of the coefficients, i.e., on $\{a_i, \ldots, e_i\}$ rather than $\{a_i, \ldots, e_i\}_{\boldsymbol{r}}$.

Coherent coupling

We proceed to derive the effective qubit-qubit coupling by performing a Schrieffer-Wolff (SW) transformation. [75] We assume that the excitations in the ferromagnet are gapped due to some magnetic anisotropy (e.g. shape-anisotropy), with the gap being denoted by Δ_F. This is important because when the qubit splitting Δ is smaller than Δ_F, flipping the qubit spin cannot excite magnons in the ferromagnet, thus there are only virtual magnons excited via coupling to the qubits—otherwise such a coupling would lead to strong decoherence in the qubits. Due to the presence of the gap in the ferromagnet, its transversal susceptibility $\chi_\perp(\omega, \boldsymbol{r})$ decays exponentially for $\omega < \Delta_F$ with the characteristic length $l_F \propto$

$1/\sqrt{\Delta_F - \omega}$, thus we take into account only terms with $\omega \sim \Delta_F$, see Appendix 3.B. Straightforward application of lowest order SW transformation accompanied by tracing out the degrees of freedom of the ferromagnet yields the effective qubit-qubit coupling Hamiltonian

$$H_{eff} = H_\sigma + \chi_\perp^{1D}(\Delta_1, L) e_1 \sigma_1^- (c_2 \sigma_2^z + d_2 \sigma_2^+ + e_2 \sigma_2^-)^\dagger +$$
$$1 \leftrightarrow 2 + \text{h.c.}, \tag{3.7}$$

where $\chi_\perp^{1D}$ is the transverse susceptibility (i.e. transverse to the $\widetilde{z}$ direction) of a quasi-1D ferromagnet, since we assumed a dog-bone shaped ferromagnet. We have neglected the longitudinal susceptibility $\chi_\parallel$ since it is smaller by factor of $1/S$ compared to the transverse one and it is suppressed by temperature, see Appendix 3.C. It is readily seen from the above expression that in order to obtain a sizable coupling between the qubits we have to tune at least one of the qubits close to resonance, $\Delta_i \sim \Delta_F$. This can be achieved by conveniently positioning the qubit such that the Zeeman splitting produced by the stray field of the ferromagnet is close to the excitation gap of the ferromagnet. The fine tuning can be then achieved by applying locally a small external magnetic field from a coil. The on resonance requirement offers an elegant way to switch on/off the coupling between the qubits. The idea is to tune the qubit splitting close to resonance to switch on the mediated interaction and to tune it off resonance to switch off the mediated interaction. [1]

For the sake of completeness, in the Appendix 3.D we present a detailed discussion of the effective coupling mediated by the dog-bone when the qubits are exchange coupled to the ferromagnet which requires a tunnel coupling between spin qubit and ferromagnet.

Implementation of two-qubit gates

Two qubits interacting via the ferromagnet evolve according to the Hamiltonian H_{eff}, see Eq. (3.7). The Hamiltonian is therefore the sum of Zeeman terms and qubit-qubit interaction. These terms, by and large, do not commute, making it difficult to use the evolution to implement standard entangling gates. Nevertheless, if we assume that $\Delta_1 = \Delta_2$, H_σ acts only in the subspace spanned by $\{|\uparrow,\uparrow\rangle, |\downarrow,\downarrow\rangle\}$ and the Zeeman splitting of the qubits is much larger than the effective qubit-qubit coupling, we can neglect the effect of H_{eff} in this part of the subspace and approximate it

---

[1]Another possibility is to keep one of the qubits off resonance and then tuning the other one on and off.

by its projection in the space spanned by the vectors $\{|\uparrow,\downarrow\rangle, |\downarrow,\uparrow\rangle\}$

$$H'_{\text{eff}} = H_\sigma + \alpha(\sigma_1^x\sigma_2^x - \sigma_1^y\sigma_2^y) + \beta(\sigma_1^x\sigma_2^y + \sigma_1^y\sigma_2^x), \tag{3.8}$$

where $\alpha = -8\text{Re}(e_1 e_2^*)$ and $\beta = -4\text{Re}(d_1 e_2^* + d_2 e_1^*)$. Within this approximation, the coupling in H'_{eff} and the Zeeman terms now commute. From here we readily see that the stray field components, a_i, b_i, as well as the coefficient c_i do not determine the operation time of the two qubit gates—the operation time depends only on d_i and e_i. To proceed we perform a rotation on the first qubit around the z-axis by an angle $\tan\theta = \beta/\alpha$ and arrive at the Hamiltonian

$$H'_{\text{eff}} = H_\sigma + \sqrt{\alpha^2 + \beta^2}(\sigma_1^x\tilde{\sigma}_2^x - \sigma_1^y\tilde{\sigma}_2^y). \tag{3.9}$$

We consider the implementation of the iSWAP gate $U_{\text{iSWAP}} = e^{i(\sigma_1^x\tilde{\sigma}_2^x + \sigma_1^y\tilde{\sigma}_2^y)\pi/4}$, which can be used to implement the CNOT gate. [11] The Hamiltonian H' can be transformed to the desired form by changing the sign of $\sigma_1^x\tilde{\sigma}_2^x$ term. This is achieved with the following sequence [68]

$$U_{\text{iSWAP}} = \sigma_1^y e^{iH_\sigma t} e^{-iH'_{\text{eff}}t}\sigma_1^y, \tag{3.10}$$

where $t = \pi/(4\sqrt{\alpha^2 + \beta^2})$. When iSWAP is available, the CNOT gate can be constructed in the standard way [69]

$$U_{\text{C}NOT} = e^{-i\frac{\pi}{4}\sigma_1^z}e^{i\frac{\pi}{4}\sigma_2^x}e^{i\frac{\pi}{4}\sigma_2^z}U_{\text{i}SWAP}e^{-i\frac{\pi}{4}\sigma_1^x}U_{\text{i}SWAP}e^{i\frac{\pi}{4}\sigma_2^z}. \tag{3.11}$$

Since H'_{eff} is an approximation of H_{eff}, the above sequence will yield approximate CNOT, $U'_{\text{C}NOT}$, when used with the full the Hamiltonian. The success of the sequences therefore depends on the fidelity of the gates, $F(U'_{\text{C}NOT})$. Ideally this would be defined using a minimization over all possible states of two qubits. However, to characterize the fidelity of an imperfect CNOT it is sufficient to consider the following four logical states of two qubits: [65] $|+,\uparrow\rangle, |+,\downarrow\rangle, |-,\uparrow\rangle$, and $|-,\downarrow\rangle$. These are product states which, when acted upon by a perfect CNOT, become the four maximally entangled Bell states $|\Phi^+\rangle, |\Psi^+\rangle, |\Phi^-\rangle$, and $|\Psi^-\rangle$, respectively. As such, the fidelity of an imperfect CNOT may be defined,

$$F(U'_{\text{C}NOT}) = \min_{i\in\{+,-\}, j\in\{0,1\}} |\langle i,j|U_{\text{C}NOT}^\dagger U'_{\text{C}NOT}|i,j\rangle|^2. \tag{3.12}$$

The choice of basis used here ensures that $F(U'_{\text{C}NOT})$ gives a good characterization of the properties of $U'_{\text{C}NOT}$ in comparison to a perfect CNOT, especially for the required task of generating entanglement. For realistic parameters, with the Zeeman terms two order of magnitude stronger

than the qubit-qubit coupling, the above sequence yields fidelity for the CNOT gate of 99.976%.

To compare these values to the thresholds found in schemes for quantum computation, we must first note that imperfect CNOTs in these cases are usually modeled by the perfect implementation of the gate followed by depolarizing noise at a certain probability. It is known that such noisy CNOTs can be used for quantum computation in the surface code if the depolarizing probability is less than 1.1%. [70] This corresponds to a fidelity, according to the definition above, of 99.17%. The fidelities that may be achieved in the schemes proposed here are well above this value and hence, though they do not correspond to the same noise model, we can expect these gates to be equally suitable for fault-tolerant quantum computation.

3.3 Decoherence

In this section we study the dynamics of a single qubit coupled to the ferromagnet. In particular we want to answer the question whether the effective coupling derived in the previous section is *coherent*, i.e., whether the decoherence time due solely to the dipolar coupling to the ferromagnet is larger than the qubit operation time.

A ferromagnet has two types of fluctuations—longitudinal and transverse ones. The longitudinal noise stems from fluctuations of the $S^{\tilde{z}}$ component (we recall that the ferromagnet is polarized along $\tilde{z}$), while the transverse one is related to fluctuations of $S^{\tilde{\pm}}$. In what follows we study these two noise sources separately. The general noise model that describes both types of noise is then given by

$$H = H_{\mathrm{F}} + \frac{\Delta}{2}\sigma^z + \sigma^z \otimes X + \sigma^+ \otimes Y + \mathrm{h.c.}, \tag{3.13}$$

where the ferromagnet operators X (Y) couple longitudinally (transversally) to the qubit. The noise model given in Eq. (3.13) leads to the following relaxation and decoherence times within Born-Markov approximation [74]

$$T_1^{-1} = S_Y(\omega = \Delta), \tag{3.14}$$

$$T_2^{-1} = \frac{1}{2}T_1^{-1} + S_X(\omega = 0), \tag{3.15}$$

where we defined the fluctuation power spectrum of an operator A in the following way, $S_A(\omega) = \int dt e^{-i\omega t}\{A^\dagger(t), A(0)\}$. In order to obtain

estimates for the decoherence times we need a specific model for the ferromagnet Hamiltonian, herein taken to be a gapped Heisenberg model $H_F = -J \sum_{\langle r,r' \rangle} \boldsymbol{S_r} \cdot \boldsymbol{S_{r'}} + \Delta_F \sum_r S_r^z$, J being the exchange coupling and Δ_F the excitation gap induced by some magnetic anisotropy.

Longitudinal noise

The power spectrum of longitudinal fluctuations is given by the following expression (see Appendix 3.C)

$$S_\parallel^{3D}(\omega) = \frac{\alpha\sqrt{\beta\omega}}{2\beta^2 D^3} e^{-\beta\Delta_F} \coth(\beta\omega/2), \tag{3.16}$$

where $D = 2JS$. We readily observe that the power spectrum is subohmic, i.e., it diverges at low frequencies $S_\parallel^{3D}(\omega) \propto 1/\sqrt{\omega}$—this is a direct consequence of the fact that longitudinal fluctuations are gapless. Due to this divergence, the perturbation theory (Born approximation) cannot be used when there is longitudinal coupling to the longitudinal noise. In order to deal with this singularity, we study transverse (Y) and longitudinal (X) coupling separately. The transverse coupling can be treated perturbatively, while for the longitudinal coupling we solve the problem exactly.

Transverse coupling to longitudinal noise

The part of the Hamiltonian that describes transverse coupling to the longitudinal noise reads

$$H = H_F + \sigma^+ \otimes \int d\boldsymbol{r} b_{\boldsymbol{r}} S_{\boldsymbol{r}}^{\tilde{z}} + \text{h.c.} \tag{3.17}$$

Using Eq. (3.15) and the inequality

$$S_\parallel^{3D}(\omega, \boldsymbol{r}) \leq S_\parallel^{3D}(\omega, \boldsymbol{r} = 0),$$

we obtain the relaxation time

$$\begin{aligned} T_1^{-1} &= \int d\boldsymbol{r} d\boldsymbol{r}' b_{\boldsymbol{r}} b_{\boldsymbol{r}'} S_\parallel^{3D}(\Delta, \boldsymbol{r} - r') \\ &\leq \int d\boldsymbol{r} d\boldsymbol{r}' b_{\boldsymbol{r}} b_{\boldsymbol{r}'} S_\parallel^{3D}(\Delta, \boldsymbol{r} = 0) \\ &= b^2 S_\parallel^{3D}(\Delta). \end{aligned} \tag{3.18}$$

The above expression readily shows that relaxation time can be tailored arbitrarily by choosing the ratio T/Δ_F sufficiently small.

Longitudinal coupling to longitudinal noise

Here we consider only longitudinal coupling to longitudinal noise thus the Hamiltonian reads

$$H = H_F + \epsilon \, \sigma_z + \sigma^z \otimes V \,, \tag{3.19}$$

with $V = \int d\boldsymbol{r} a_{\boldsymbol{r}} S_{\boldsymbol{r}}^{\tilde{z}}$. To simplify the problem further, [71] we substitute $S_{\boldsymbol{r}}^{\tilde{z}} \to S_{\boldsymbol{r}}^{\tilde{x}}$ since the latter is linear in magnon operators while the former is quadratic. When the final formula for the decoherence time is obtained we substitute back the power spectrum of $S_{\boldsymbol{r}}^{\tilde{z}}$ instead of $S_{\boldsymbol{r}}^{\tilde{x}}$.

In order to study decoherence we have to calculate the following quantity [71]

$$\langle \sigma^-(t) \rangle = e^{i\varepsilon t/\hbar} \langle \sigma^-(0) \rangle \times \tag{3.20}$$

$$\times \left\langle \tilde{T} \exp\left(i \int_0^t V \, dt' \right) T \exp\left(i \int_0^t V \, dt' \right) \right\rangle \,,$$

with $(\tilde{T})$ T the (anti-) time ordering operator. The average in the above expression can be evaluated using a cluster expansion [72] and since the perturbation V is linear in the bosonic operators, only the second order cluster contributes. Therefore, the final exact result for the time-evolution of $\sigma^-(t)$ reads

$$\langle \sigma^-(t) \rangle = e^{i\varepsilon t/\hbar} \langle \sigma^-(0) \rangle e^{-\frac{1}{2} \int_0^t \int_0^t S(t_2 - t_1) dt_1 dt_2} \,, \tag{3.21}$$

where $S(t) = \langle [V(t), V(0)]_+ \rangle$. After performing the Fourier transformation we obtain

$$\langle \sigma_-(t) \rangle = e^{i\varepsilon t/\hbar} \langle \sigma_-(0) \rangle \times \tag{3.22}$$

$$\times \exp\left(-\frac{1}{2} \int \frac{d\omega}{2\pi} S(\omega) \frac{\sin^2(\omega t/2)}{(\omega/2)^2} \right) \,.$$

Note that this expression is of exactly the same form as the one for a *classical* Gaussian noise. [73] Now we substitute back $S_{\boldsymbol{r}}^{\tilde{x}} \to S_{\boldsymbol{r}}^{\tilde{z}}$

$$\langle \sigma^-(t) \rangle = e^{i\varepsilon t/\hbar} \langle \sigma^-(0) \rangle \times$$

$$\times \exp\left(-\frac{1}{2} \int \frac{d\omega}{2\pi} \int d\boldsymbol{r} d\boldsymbol{r}' a_{\boldsymbol{r}} a_{\boldsymbol{r}'} S_{\parallel}^{3D}(\omega, \boldsymbol{r} - r') \frac{\sin^2(\omega t/2)}{(\omega/2)^2} \right) \,.$$

$$\tag{3.23}$$

For long times $t \gg \hbar/T$ the dynamics is of the form

$$\langle \sigma^-(t) \rangle \sim e^{-2\sqrt{2\pi}a^2 T^{5/2} e^{-\beta \Delta_F} t^{3/2}/(3D^3) + i\Delta t}, \tag{3.24}$$

where we have used the inequality $S_\parallel^{3D}(\omega, \boldsymbol{r}) \leq S_\parallel^{3D}(\omega, \boldsymbol{r} = 0)$. Thus, this type of decoherence can be suppressed by choosing the ratio T/Δ_F sufficiently small.

Transverse noise

The power spectrum of transverse fluctuations of the ferromagnet is gapped and thus vanishes for $\omega < \Delta_F$ (see Appendix 3.B),

$$S_\perp^{3D}(\omega) = 0, \qquad\qquad \omega < \Delta_F, \tag{3.25}$$

$$S_\perp^{3D}(\omega) = \frac{S\sqrt{\omega - \Delta_F}}{D^{3/2}} \coth(\beta\omega/2), \quad \omega > \Delta_F. \tag{3.26}$$

Since the transverse fluctuations are gapped and the precession frequency of the qubits is below the gap, this noise source does not contribute in the second order (Born approximation) because only virtual magnons can be excited. In this section we choose the quantization axes such that qubit splitting is along the z-axis, while the ferromagnet is polarized along the x-axis (see Fig. 3.1), this is done solely for simplicity and all the conclusions are also valid for the most general case. The Hamiltonian of the coupled system is of the form Eq. (3.13) with operators X (Y)

$$X = \frac{i}{2} \int d\boldsymbol{r} c_{\boldsymbol{r}} (S_{\boldsymbol{r}}^+ - S_{\boldsymbol{r}}^-), \tag{3.27}$$

$$Y^+ = -\frac{i}{8} \int d\boldsymbol{r} (a_{\boldsymbol{r}} S_{\boldsymbol{r}}^+ + b_{\boldsymbol{r}} S_{\boldsymbol{r}}^-), \tag{3.28}$$

with $S_{\boldsymbol{r}}^\pm = S_{\boldsymbol{r}}^y \pm i S_{\boldsymbol{r}}^z$ and the definitions

$$a_{\boldsymbol{r}} = B_{\boldsymbol{r}} + 3C_{\boldsymbol{r}} - 6A_{\boldsymbol{r}}, \tag{3.29}$$

$$b_{\boldsymbol{r}} = B_{\boldsymbol{r}} + 3C_{\boldsymbol{r}} + 6A_{\boldsymbol{r}}, \tag{3.30}$$

$$c_{\boldsymbol{r}} = B_{\boldsymbol{r}} - 3A_{\boldsymbol{r}}'', \tag{3.31}$$

where $A_{\boldsymbol{r}}$, $B_{\boldsymbol{r}}$, $C_{\boldsymbol{r}}$ are given by Eqs. (4.24)-(6.65). To proceed further we perform the SW transformation on the Hamiltonian given by Eq. (3.13). We ignore the Lamb and Stark shifts and obtain the effective Hamiltonian

$$H = H_{\mathrm{F}} + \frac{\Delta}{2}\sigma^z + \sigma^z \otimes \tilde{X}_2 + \sigma^+ \otimes \tilde{Y}_2^- + \sigma^- \otimes \tilde{Y}_2^+, \tag{3.32}$$

where

$$\tilde{X}_2 = X_2 - \langle X_2 \rangle, \tag{3.33}$$

$$\tilde{Y}_2^{\pm} = Y_2^{\pm} - \langle Y_2^{\pm} \rangle, \tag{3.34}$$

with the following notation

$$X_2 = 4(Y_\Delta^+ Y^- + Y^+ Y_\Delta^-), \tag{3.35}$$

$$Y_2^+ = 2(Y_\Delta^+ X - X_0 Y^+), \tag{3.36}$$

$$X_\omega = \frac{i}{2} \int d\boldsymbol{r}\boldsymbol{r}' \chi_\perp(\omega, \boldsymbol{r} - \boldsymbol{r}') c_{\boldsymbol{r}}(S_{\boldsymbol{r}'}^+ - S_{\boldsymbol{r}'}^-), \tag{3.37}$$

$$Y_\omega^+ = -\frac{i}{8} \int d\boldsymbol{r}\boldsymbol{r}' \chi_\perp(\omega, \boldsymbol{r} - \boldsymbol{r}')(a_{\boldsymbol{r}} S_{\boldsymbol{r}'}^+ + b_{\boldsymbol{r}} S_{\boldsymbol{r}'}^-). \tag{3.38}$$

The model given by Eq. (3.13) yields the following expressions for the relaxation and decoherence times

$$T_1^{-1} = S_{\tilde{Y}_2^-}(\omega = \Delta), \tag{3.39}$$

$$T_2^{-1} = \frac{1}{2}T_1^{-1} + S_{\tilde{X}_2}(\omega = 0). \tag{3.40}$$

After a lengthy calculation we obtain the following expressions for T_1 and T_2 (see Appendix 3.E for a detailed derivation)

$$T_1^{-1} \leq \frac{B^4 S^2 \Delta_F^2}{2D^3} \left(\frac{1}{\Delta_F} + \frac{1}{\Delta_F - \Delta} \right)^2 f\left(\frac{\Delta}{\Delta_F}, \beta\Delta_F \right), \tag{3.41}$$

$$T_2^{-1} \leq \frac{B^4 S^2 \Delta_F^2}{4D^3} \left(\frac{1}{\Delta_F} + \frac{1}{\Delta_F - \Delta} \right)^2 f\left(\frac{\Delta}{\Delta_F}, \beta\Delta_F \right) +$$

$$\frac{B^4 S^2 \Delta_F^2}{2D^3(\Delta_F - \Delta)^2} f(0, \beta\Delta_F), \tag{3.42}$$

with the function $f(x, y)$ defined as follows

$$f(x, y) = \int_{1+x}^{\infty} dz \frac{\sqrt{z-1}}{e^{yz} - 1} \frac{\sqrt{z - x - 1}}{e^{y(z-x)} - 1}. \tag{3.43}$$

It is important to note that $f(x, y) \propto e^{-y}$, i.e., we obtain, as before for the longitudinal noise, that the effect of transverse fluctuations can be suppressed by choosing the temperature much smaller than the excitation gap of the ferromagnet. As anticipated, Eq. (3.42) shows that the transverse noise becomes more important as the resonance is approached ($\Delta \sim \Delta_F$).

3.4 Estimates

In this section we give numerical estimates for the coherent coupling mediated by the ferromagnet and the associated decoherence times. These estimates are valid for both silicon-based and NV-center qubits.

Assume that the qubits lie close to the disc axis at a distance $h = 25\,nm$ below the disc and that the ferromagnet has in-plane polarization (along x-axis). Assume the thickness of the disk to be $20\,nm$, its radius to be $50\,nm$, and a lattice constant of 4Å. In this case the stray field at the position $x = 0$ is along x and has a magnitude that can reach values close to $1\,T$ depending on the precise position of the qubit. Similarly, when the ferromagnet is polarized out-of-plane (along the z-axis), then the stray field at position $x = y = 0$ is along z and can take values up to $1\,T$. For these cases and when the qubit splitting is brought close to resonance, $\Delta_F - \Delta \approx 10^{-2}\mu eV$, we obtain operation times on the order of tens of nanoseconds when the qubits are separated by a distance of about $1\,\mu m$. The decoherence times T_2 depend strongly on the ratio $k_B T/\Delta_F$ and the additional decoherence source can be made negligible if this ratio is sufficiently small. For a magnon gap $\Delta_F = 100\,\mu eV$ (corresponding to a magnetic field of about $1\,T$) and a temperature $T = 0.1\,K$, we obtain decoherence times solely due to the coupling to the ferromagnet that are much bigger than the operation times and the typical decoherence times of the qubits.

3.5 Conclusions

We propose a scheme to coherently couple two *atomistic* qubits separated over distances on the order of a micron. We present a sequence for the implementation of the entangling CNOT gate and obtain operation times on the order of a few tens of nanoseconds. We show that there is a regime where all fluctuations of the ferromagnet are under control and the induced decoherence is non-detrimental: this is achieved when the temperature is smaller than the excitation gap of the ferromagnet. The main novel aspect of our proposal is its applicability to the technologically very important silicon qubits and NV-centers to which previous coupling methods do not apply.

3.6 Acknowledgements

3.A Holstein-Primakoff transformation

For the sake of completeness we derive in this Appendix explicit expressions for the different spin-spin correlators used in this work

$$C^{\alpha\beta}(\omega, \boldsymbol{q}) = \langle S_{\boldsymbol{q}}^{\alpha}(\omega) S_{-\boldsymbol{q}}^{\beta}(0) \rangle. \tag{3.44}$$

For this purpose, we make use of a Holstein-Primakoff transformation

$$S_i^z = -S + n_i, \ \ S_i^- = \sqrt{2S}\sqrt{1 - \frac{n_i}{2S}} a_i, \ \text{and}$$

$$S_i^+ = \left(S_i^-\right)^\dagger, \tag{3.45}$$

in the limit $n_i \ll 2S$, with a_i satisfying bosonic commutation relations and $n_i = a_i^\dagger a_i$. [47] The creation operators $a_i^\dagger$ and annihilation operators a_i satisfy bosonic commutation relations and the associated particles are called magnons. The corresponding Fourier transforms are straightforwardly defined as $a_{\boldsymbol{q}}^\dagger = \frac{1}{\sqrt{N}} \sum_i e^{-i\boldsymbol{q}\cdot\boldsymbol{R}_i} a_i$. In harmonic approximation, the Heisenberg Hamiltonian H_F reads

$$H_F \approx \sum_{\boldsymbol{q}} \epsilon_{\boldsymbol{q}} a_{\boldsymbol{q}}^\dagger a_{\boldsymbol{q}}, \tag{3.46}$$

where $\epsilon_{\boldsymbol{q}} = \omega_{\boldsymbol{q}} + \Delta_F = 4JS[3 - (\cos(q_x) + \cos(q_y) + \cos(q_z))] + \Delta_F$ is the spectrum for a cubic lattice with lattice constant $a = 1$ and the gap Δ_F is induced by the external magnetic field or anisotropy of the ferromagnet.

3.B Transverse correlators $\langle S_{\boldsymbol{q}}^+(t) S_{-\boldsymbol{q}}^-(0) \rangle$

Let us now define the Fourier transforms in the harmonic approximation

$$S_{\boldsymbol{q}}^+ = \frac{1}{\sqrt{N}} \sum_i e^{-i\boldsymbol{q}\boldsymbol{r}_i} S_i^+ = \frac{\sqrt{2S}}{\sqrt{N}} \sum_i e^{-i\boldsymbol{q}\boldsymbol{r}_i} a_i^\dagger = \sqrt{2S} a_{-\boldsymbol{q}}^\dagger,$$

$$S_{-\boldsymbol{q}}^- = \frac{1}{\sqrt{N}} \sum_i e^{i\boldsymbol{q}\boldsymbol{r}_i} S_i^- = \frac{\sqrt{2S}}{\sqrt{N}} \sum_i e^{i\boldsymbol{q}\boldsymbol{r}_i} a_i = \sqrt{2S} a_{-\boldsymbol{q}}. \tag{3.47}$$

From this it directly follows that

$$
\begin{aligned}
C^{+-}(t, \boldsymbol{q}) &= \langle S_{\boldsymbol{q}}^+(t) S_{-\boldsymbol{q}}^-(0) \rangle \\
&= 2S \langle a_{-\boldsymbol{q}}^\dagger(t) a_{-\boldsymbol{q}} \rangle = 2S e^{i\epsilon_q t} n_{\boldsymbol{q}} ,
\end{aligned}
\tag{3.48}
$$

with $\epsilon_q \approx D q^2 + \Delta_F$ in the harmonic approximation.

The Fourier transform is then simply given by

$$
\begin{aligned}
C^{+-}(\omega, \boldsymbol{q}) &= \frac{1}{\sqrt{2\pi}} \int_{-\infty}^{\infty} dt \, e^{-i\omega t} C^{+-}(t, \boldsymbol{q}) \\
&= \underbrace{\frac{1}{\sqrt{2\pi}} \int_{-\infty}^{\infty} dt \, e^{i(\epsilon_q - \omega) t} 2S n_{\boldsymbol{q}}}_{\sqrt{2\pi} \delta(\epsilon_q - \omega)} \\
&= \sqrt{2\pi} 2S \delta(\epsilon_{\boldsymbol{q}} - \omega) \frac{1}{e^{\beta\omega} - 1} .
\end{aligned}
\tag{3.49}
$$

The corresponding correlator in real space is then simply given by ($q := |\boldsymbol{q}|$)

$$
\begin{aligned}
C^{+-}(\omega, \boldsymbol{r}) &= \frac{1}{(2\pi)^{3/2}} \int d\boldsymbol{q} \, e^{i\boldsymbol{q}\boldsymbol{r}} C^{+-}(\omega, \boldsymbol{q}) \tag{3.50} \\
&= \frac{\sqrt{2\pi}}{(2\pi)^{3/2}} 2S \frac{1}{e^{\beta\omega} - 1} \int d\boldsymbol{q} \, \delta(D q^2 + \Delta_F - \omega) e^{i\boldsymbol{q}\boldsymbol{r}} \\
&= \frac{2S}{e^{\beta\omega} - 1} \int_{-1}^{1} \int_{0}^{\infty} dq \, dx \, q^2 \delta(D q^2 + \Delta_F - \omega) e^{iqrx} \\
&= \frac{4S}{r} \frac{1}{e^{\beta\omega} - 1} \int_{0}^{\infty} dq \, q \, \delta(D q^2 + \Delta_F - \omega) \sin(qr) .
\end{aligned}
$$

Let us now perform the following substitution

$$
y = D q^2,
\tag{3.51}
$$

which gives for $\omega > \Delta_F$

$$
\begin{aligned}
C^{+-}(\omega, \boldsymbol{r}) &= \frac{4S/r}{2D(e^{\beta\omega} - 1)} \int_{0}^{\infty} dy \, \delta(y + \Delta_F - \omega) \sin\left(\sqrt{\frac{y}{D}} r \right) \\
&= \frac{2S}{D} \frac{1}{e^{\beta\omega} - 1} \frac{\sin(\sqrt{(\omega - \Delta_F)/D} r)}{r} .
\end{aligned}
\tag{3.52}
$$

We remark that

$$
C^{+-}(\omega, \boldsymbol{r}) = 0, \quad \omega < \Delta_F.
\tag{3.53}
$$

We note the diverging behavior of the above correlation function for $\Delta_F = 0$ and $\omega \to 0$, namely

$$\frac{1}{e^{\beta\omega} - 1} \frac{\sin\left(\sqrt{\frac{\omega}{D}} r\right)}{r} \to \frac{1}{\sqrt{D}\beta} \frac{1}{\sqrt{\omega}}. \tag{3.54}$$

Similarly, it is now easy to calculate the corresponding commutators and anticommutators. Let us define

$$S_\perp(t, \boldsymbol{q}) := \frac{1}{2}\{S_q^+(t), S_{-q}^-(0)\}. \tag{3.55}$$

It is then straightforward to show that

$$S_\perp(t, \boldsymbol{q}) \;=\; S e^{i\epsilon_q t}(1 + 2n_q), \tag{3.56}$$

and therefore

$$S_\perp(\omega, \boldsymbol{q}) \;=\; \frac{S}{\sqrt{2\pi}} \int_{-\infty}^{\infty} e^{i(\epsilon_q - \omega)t}(1 + 2n_q)$$

$$=\; S\sqrt{2\pi}\delta(\epsilon_q - \omega)\left(1 + 2\frac{1}{e^{\beta\omega} - 1}\right). \tag{3.57}$$

Following essentially the same steps as the one performed above, we obtain the 3D real space anticommutator for $\omega > \Delta_F$

$$S_\perp^{3D}(\omega, \boldsymbol{q}) \;=\; S \coth(\beta\omega/2) \times \tag{3.58}$$

$$\times \int_{-1}^{1} \int_{0}^{\infty} dx\,dq\,q^2 e^{iqrx}\delta(\epsilon_q - \omega)$$

$$=\; \frac{S}{D} \coth(\beta\omega/2) \frac{\sin(\sqrt{(\omega - \Delta_F)/D}\,r)}{r}. \tag{3.59}$$

Let us now finally calculate the transverse susceptibility defined as

$$\chi_\perp(t, \boldsymbol{q}) \;=\; -i\theta(t)[S_q^+(t), S_{-q}^-(0)]. \tag{3.60}$$

As before, in the harmonic approximation, one finds

$$\chi_\perp(t, \boldsymbol{q}) \;=\; i\theta(t)2S e^{i\epsilon_q t}. \tag{3.61}$$

In the frequency domain, we then have

$$\chi_\perp(\omega, \boldsymbol{q}) = \frac{2iS}{\sqrt{2\pi}} \int_0^\infty dt\, e^{i(\epsilon_q - \omega)t - \eta t} \tag{3.62}$$

$$=\; -\frac{2S}{\sqrt{2\pi}} \frac{1}{\epsilon_q - \omega + i\eta},$$

and thus in the small q expansion

$$\chi_\perp(\omega, \boldsymbol{q}) = -\frac{2S}{\sqrt{2\pi}} \frac{1}{D\boldsymbol{q}^2 + \Delta_F - \omega + i\eta}. \tag{3.63}$$

In real space, for the three-dimensional case, we obtain

$$\begin{aligned}
\chi_\perp^{3D}(\omega, \boldsymbol{r}) &= -\frac{2S}{\sqrt{2\pi}} \frac{2\pi}{(2\pi)^{3/2}} \int_0^\infty \int_{-1}^1 dx dq q^2 \frac{1}{D\boldsymbol{q}^2 + \Delta_F - \omega + i\eta} e^{iqrx} \\
&= -\frac{4S}{\sqrt{2\pi}} \frac{2\pi}{(2\pi)^{3/2}} \frac{1}{r} \int_0^\infty dq q \frac{1}{D\boldsymbol{q}^2 + \Delta_F - \omega + i\eta} \sin(qr).
\end{aligned} \tag{3.64}$$

Making use of the Plemelj formula we obtain for $\omega > \Delta_F$

$$\begin{aligned}
\chi_\perp^{3D}(\omega, \boldsymbol{r}) &= -\frac{2S}{\sqrt{2\pi}} \frac{2\pi}{(2\pi)^{3/2}} \frac{1}{r} \int_{-\infty}^\infty dq q \frac{1}{D\boldsymbol{q}^2 + \Delta_F - \omega + i\eta} \sin(qr) \\
&= -\frac{2S}{\sqrt{2\pi}} \frac{2\pi}{(2\pi)^{3/2}} \frac{1}{r} P \int_{-\infty}^\infty dq \frac{q}{Dq^2 + \Delta_F - \omega} \sin(qr) \\
&\quad + i\frac{2S}{\sqrt{2\pi}} \frac{2\pi^2}{(2\pi)^{3/2}} \frac{1}{r} \int_{-\infty}^\infty dq q \delta(Dq^2 + \Delta_F - \omega) \sin(qr) \\
&= -\frac{S}{D} \frac{\cos(r\sqrt{(\omega - \Delta_F)/D})}{r} + i\frac{S}{2D} \frac{\sin(\sqrt{(\omega - \Delta_F)/D}r)}{r}.
\end{aligned} \tag{3.65}$$

It is worth pointing out that the imaginary part of the susceptibility vanishes,

$$\chi_\perp^{3D}(\omega, \boldsymbol{r})'' = 0, \quad \omega < \Delta_F, \tag{3.66}$$

and therefore the susceptibility is purely real and takes the form of a Yukawa potential

$$\chi_\perp^{3D}(\omega, \boldsymbol{r}) = -\frac{S}{D} \frac{e^{-r/l_F}}{r}, \quad \omega < \Delta_F, \tag{3.67}$$

where $l_F = \sqrt{\frac{D}{\Delta_F - \omega}}$.

Note also that the imaginary part of the transverse susceptibility satisfies the well-know fluctuation-dissipation theorem

$$S_\perp^{3D}(\omega, \boldsymbol{r}) = \coth(\beta\omega/2)\chi_\perp^{3D}(\omega, \boldsymbol{r})''. \tag{3.68}$$

In three dimensions the susceptibility decay as $1/r$, where r is measured in lattice constants. For distances of order of $1\mu m$ this leads to four orders of magnitude reduction.

For quasi one-dimensional ferromagnets such a reduction is absent and the transverse susceptibility reads

$$\chi_{\perp}^{\text{1D}}(\omega, r) = -\frac{S}{D} l_F e^{-r/l_F}, \quad \omega < \Delta_F, \tag{3.69}$$

where l_F is defined as above and the imaginary part vanishes as above, i.e.,

$$\chi_{\perp}^{\text{1D}}(\omega, r)'' = 0, \quad \omega < \Delta_F. \tag{3.70}$$

Similarly for $\omega > \Delta_F$ we have

$$\chi_{\perp}^{\text{1D}}(\omega, r) = S \frac{\sin\left(\sqrt{(\omega - \Delta_F)/D}r\right)}{\sqrt{D(\omega - \Delta_F)}}, \tag{3.71}$$

and

$$\chi_{\perp}^{\text{1D}}(\omega, r)'' = \frac{S}{2D} \sqrt{\frac{D}{\omega - \Delta_F}} \cos\left(\sqrt{(\omega - \Delta_F)/D}r\right). \tag{3.72}$$

3.C Longitudinal correlators $\langle S_{\boldsymbol{q}}^z(t) S_{-\boldsymbol{q}}^z(0) \rangle$

The longitudinal susceptibility reads

$$
\begin{aligned}
\chi_{\parallel}(t, \boldsymbol{q}) &= -i\theta(t)[S_{\boldsymbol{q}}^z(t), S_{-\boldsymbol{q}}^z(0)] \\
&= -\theta(t)\frac{1}{N} \sum_{\boldsymbol{q}', \boldsymbol{q}''} e^{it(\epsilon_{\boldsymbol{q}'} - \epsilon_{\boldsymbol{q}'+\boldsymbol{q}})} \langle [a_{\boldsymbol{q}'}^{\dagger} a_{\boldsymbol{q}'+\boldsymbol{q}}, a_{\boldsymbol{q}''}^{\dagger} a_{\boldsymbol{q}''-\boldsymbol{q}}] \rangle.
\end{aligned}
\tag{3.73}
$$

Applying Wick's theorem and performing a Fourier transform, we obtain the susceptibility in frequency domain

$$\chi_{\parallel}(\omega, \boldsymbol{q}) = -\frac{1}{N} \sum_{\boldsymbol{k}} \frac{n_{\boldsymbol{k}} - n_{\boldsymbol{k}+\boldsymbol{q}}}{\omega - \epsilon_{\boldsymbol{k}+\boldsymbol{q}} + \epsilon_{\boldsymbol{k}} + i\eta}, \tag{3.74}$$

where $n_{\boldsymbol{k}}$ is the magnon occupation number given by the Bose-Einstein distribution

$$n_k = \frac{1}{e^{\beta \epsilon_k} - 1}, \tag{3.75}$$

where $\epsilon_{\boldsymbol{k}}$ is again the magnon spectrum ($\epsilon_{\boldsymbol{k}} = \omega_{\boldsymbol{k}} + \Delta_F \approx D\boldsymbol{k}^2 + \Delta_F$ for small k). Note that the longitudinal susceptibility is proportional to $1/S$, due to the fact that $\epsilon_{\boldsymbol{k}} - \epsilon_{\boldsymbol{k}+\boldsymbol{q}} = \omega_{\boldsymbol{k}} - \omega_{\boldsymbol{k}+\boldsymbol{q}} \propto S$.

Since we are interested in the decoherence processes caused by the longitudinal fluctuations, we calculate the imaginary part of $\chi_{\parallel}(\omega, \boldsymbol{q})$ which

is related to the fluctuations via the fluctuation-dissipation theorem. Performing a small q expansion and assuming without loss of generality $\omega > 0$, we obtain for the imaginary part

$$
\begin{aligned}
\chi_{\parallel}^{3D}(\omega, \boldsymbol{q})'' &= \frac{\pi}{(2\pi)^3} \int d\boldsymbol{k}(n_{\boldsymbol{k}} - n_{\boldsymbol{k}+\boldsymbol{q}})\delta(\omega_{\boldsymbol{k}} - \omega_{\boldsymbol{k}+\boldsymbol{q}} + \omega) \\
&= \frac{1}{4\pi}\int_0^\infty dk k^2 \int_{-1}^1 dx \left(\frac{1}{e^{\beta(\Delta_F + Dk^2)} - 1} - \frac{1}{e^{\beta(\omega + \Delta_F + Dk^2)} - 1} \right) \times \\
&\qquad\qquad\qquad\qquad\qquad\qquad\qquad \times \delta(\omega - Dq^2 - 2Dkqx) \\
&= \frac{1}{4\pi}\int_0^\infty dk k^2 \int_{-1}^1 dx \left(\frac{1}{e^{\beta(\Delta_F + Dk^2)} - 1} - \frac{1}{e^{\beta(\omega + \Delta_F + Dk^2)} - 1} \right) \times \\
&\qquad\qquad\qquad\qquad\qquad\qquad \times \delta\left(k - \frac{\omega - Dq^2}{2Dqx} \right) \left| \frac{1}{2Dqx} \right| \\
&= \frac{1}{4\pi}\int_{-1}^1 dx \left| \frac{1}{2Dqx} \right| \left(\frac{\omega - Dq^2}{2Dqx} \right)^2 \theta\left(\frac{\omega - Dq^2}{2Dqx} \right) \times \\
&\qquad \times \left(\frac{1}{e^{\beta\left(\Delta_F + D\left(\frac{\omega - Dq^2}{2Dqx}\right)^2\right)} - 1} - \frac{1}{e^{\beta\left(\omega + \Delta_F + D\left(\frac{\omega - Dq^2}{2Dqx}\right)^2\right)} - 1} \right) \\
&= \frac{1}{4\pi}\int_0^1 dx \frac{1}{2Dqx} \left(\frac{\omega - Dq^2}{2Dqx} \right)^2 \times \\
&\qquad \left(\frac{1}{e^{\beta\left(\Delta_F + D\left(\frac{\omega - Dq^2}{2Dqx}\right)^2\right)} - 1} - \frac{1}{e^{\beta\left(\omega + \Delta_F + D\left(\frac{\omega - Dq^2}{2Dqx}\right)^2\right)} - 1} \right). \text{ (3.76)}
\end{aligned}
$$

Next, since we are interested in the regime where $\omega \gg T$ (and thus $\beta\omega \gg 1$), we have $n_{\boldsymbol{k}} \gg n_{\boldsymbol{k}+\boldsymbol{q}}$. Furthermore, we approximate the distribution function $n_{\boldsymbol{k}} = \frac{e^{-\beta(\Delta_F + \omega_{\boldsymbol{k}})}}{1 - e^{-\beta\Delta_F + \beta\omega_{\boldsymbol{k}}}}$ (this is valid when $\beta\omega_{\boldsymbol{k}} \ll 1$) and arrive at the following expression

$$
\begin{aligned}
\chi_{\parallel}^{3D}(\omega, \boldsymbol{q})'' &= \frac{1}{4\pi}\int_0^1 dx \frac{1}{2Dqx} \left(\frac{\omega - Dq^2}{2Dqx} \right)^2 \frac{e^{-\beta\left(\Delta_F + D\left(\frac{\omega - Dq^2}{2Dqx}\right)^2\right)}}{1 - e^{-\beta\Delta_F} + \beta D\left(\frac{\omega - Dq^2}{2Dqx}\right)^2} \\
&= -\frac{e^{1 - e^{-\beta\Delta_F} - \beta\Delta_F}}{4\beta D^2 q}\text{Ei}\left(e^{-\beta\Delta_F} + \frac{1}{4}\left(-4 - \beta Dq^2 + 2\beta\omega - \frac{\beta\omega^2}{Dq^2} \right) \right),
\end{aligned}
$$
(3.77)

where $\text{Ei}(z)$ is the exponential integral function. We also need the the real

space representation obtained after inverse Fourier transformation,

$$\chi_\parallel^{\text{3D}}(\omega, \boldsymbol{r})'' = \sqrt{\frac{2}{\pi}} \frac{1}{r} \int_0^\infty dq\, q \chi_\parallel^{\text{3D}}(\omega, q)'' \sin(qr)\,. \tag{3.78}$$

In order to perform the above integral we note that the imaginary part of the longitudinal susceptibility, given by Eq. (3.77), is peaked around $q = \sqrt{\omega/D}$ with the width of the peak $(1/\sqrt{\beta D})$ much smaller than its position in the regime we are working in ($\omega \gg T$). For $\boldsymbol{r} = 0$, the integration over q can be then performed approximately and yields the following expression

$$
\begin{aligned}
\chi_\parallel^{\text{3D}}(\omega, \boldsymbol{r} = 0)'' = {} & \frac{\sqrt{\pi} e^{-e^{-\beta \Delta_F} - 3\beta \Delta_F/2}}{2\beta^2 D^3} \left(e^{e^{-\beta \Delta_F} + \beta \Delta_F/2} \right. \\
& - e\sqrt{\pi}\sqrt{e^{\beta \Delta_F} - 1} \\
& \left. \times \operatorname{Erfc}(e^{-\beta \Delta_F/2}\sqrt{e^{\beta \Delta_F} - 1}) \right) \sqrt{\beta \omega}\,,
\end{aligned}
\tag{3.79}
$$

where $\operatorname{Erfc}(z)$ denotes the complementary error function. It is readily observed from the above expression that the longitudinal fluctuations are exponentially suppressed by the gap. Assuming that $\Delta_F \gg T$, we obtain the following simplified expression

$$\chi_\parallel^{\text{3D}}(\omega, \boldsymbol{r} = 0)'' = \frac{\sqrt{\pi} - e\pi \operatorname{Erfc}(1)}{2\beta^2 D^3} e^{-\beta \Delta_F} \sqrt{\beta \omega}\,. \tag{3.80}$$

We observe that, since $J(\omega) = \chi_\parallel(\omega, \boldsymbol{r})''$, the longitudinal noise of the ferromagnet is—as the transverse one—sub-ohmic. [74]

It is interesting to obtain the behavior of the longitudinal susceptibility in the opposite limit, when $\beta\omega \ll 1$. In this limit, the difference of the two Boltzmann factors in Eq. (3.76) can be expanded to the lowest order in the small quantity $\beta\omega$,

$$
\begin{aligned}
\chi_\parallel^{3D}(\omega, \boldsymbol{q})'' &= \int_0^1 dx \frac{1}{8\pi Dqx} \left(\frac{\omega - Dq^2}{2Dqx} \right)^2 \times \\
&\qquad \frac{\beta\omega}{\operatorname{ch}\left(\beta \Delta_F + \beta D \left(\frac{\omega - Dq^2}{2Dqx} \right)^2 \right) - 1} \\
&= \frac{\omega}{16\pi D^2 q \left(e^{\beta \Delta_F + \frac{\beta(\omega - Dq^2)^2}{4Dq^2}} - 1 \right)}\,.
\end{aligned}
\tag{3.81}
$$

In order to calculate the Fourier transform to real space, we note that for $\beta\omega \ll 1$ the denominator of the above expression depends only weakly on ω, thus we ignore this dependence and obtain the Fourier transform for $\boldsymbol{r} = 0$

$$\chi_{\parallel}^{3D}(\omega)'' = \frac{\ln(1 + n_{\boldsymbol{k}=0})}{16\pi\beta D^3}\omega. \tag{3.82}$$

The above formula shows that the longitudinal noise of a ferromagnet at high temperatures ($\beta\omega \ll 1$) behaves as ohmic rather than sub-ohmic bath.

Next we calculate the longitudinal fluctuations for the case of a quasi-one-dimensional ferromagnet ($\Delta_F \gg T$) and obtain

$$
\begin{aligned}
\chi_{\parallel}^{1D}(\omega, r = 0)'' &= \frac{1}{4\pi}\int_{-\infty}^{\infty} dk \int_{-\infty}^{\infty} dq \left(\frac{1}{e^{\beta(\Delta_F + Dk^2)} - 1} \right. \\
&\quad \left. - \frac{1}{e^{\beta(\omega + \Delta_F + Dk^2)} - 1} \right) \delta(\omega - Dq^2 - 2Dkq) \\
&= \int_{-\infty}^{\infty} dk \frac{e^{-\beta Dk^2}}{1 - e^{-\beta\Delta_F} + \beta Dk^2} \frac{1}{D\sqrt{k^2 + \omega/D}} \\
&= \frac{\gamma}{D\sqrt{\beta\omega}} e^{-\beta\Delta_F},
\end{aligned}
\tag{3.83}
$$

where γ is a numerical factor of order unity. Note that $S_{\parallel}(\omega, \boldsymbol{r})$ is defined through the fluctuation dissipation theorem as

$$S_{\parallel}(\omega, \boldsymbol{r}) = \coth(\beta\omega/2)\chi_{\perp}(\omega, \boldsymbol{r})''. \tag{3.84}$$

3.D   Exchange coupling to the ferromagnet

Exchange coupling

The Hamiltonian we consider is of the following form

$$H = H_F + H_\sigma + A \sum_i \boldsymbol{\sigma}_i \cdot \boldsymbol{S}_{\boldsymbol{r}_i}, \tag{3.85}$$

where A is the exchange coupling constant between the qubit spins and the ferromagnet. The ferromagnet is assumed to be below the Curie temperature with the magnetization pointing along the out-of-plane z-direction. The qubit Hamiltonian is assumed to be without splitting initially, that is $H_\sigma^{(0)} = 0$. Nevertheless, since the ferromagnet is in the ordered phase, there exists a first order effect due to coupling to the ferromagnet which gives rise to the term of the form $A \sum_i \sigma_i^z \langle S_{\boldsymbol{r}_i}^z \rangle$. Such

a splitting is undesirable if one is interested in *coherent* interaction—we remedy this by coupling the spins to another ferromagnet, albeit with anti-parallel magnetization [2]. Since we allow for some misalignment between orientation of the magnetization of the two ferromagnets, the final Hamiltonian for the qubits in the spin space after taking into account the first order corrections due to coupling to the ferromagnet reads

$$H_\sigma = \frac{1}{2}\Delta \sum_i \sigma_i^x . \tag{3.86}$$

The splitting in the x-direction of the qubit (or equivalently along the y-direction) is beneficial since it reduces decoherence due to longitudinal noise of the ferromagnet: the effect of such noise spectrum can significantly influence decoherence times for the case of no splitting of the qubit because the longitudinal noise is gapless.

Coherent coupling

We proceed with the derivation of an effective two-spin interaction Hamiltonian for $A \ll J$ by employing a perturbative Schrieffer-Wolff transformation [75] up to the second order

$$H_{\text{eff}} = H_\sigma + \frac{A^2}{8}\chi_\perp(\Delta)(2\sigma_1^y\sigma_2^y + \sigma_1^z\sigma_2^x + \sigma_1^x\sigma_2^z) , \tag{3.87}$$

where we introduced the notation $\chi_\perp(\omega) = \chi_\perp(\omega, L)$ ($L = |\boldsymbol{r}_2 - \boldsymbol{r}_1|$) and $\chi_\perp(\omega, \boldsymbol{r})$ is the transverse real space spin susceptibility of the ferromagnet. Note that we have neglected $\chi_\perp^{\text{3D}}(-\Delta)$ and $\chi_\perp^{\text{3D}}(0)$ in comparison to $\chi_\perp^{\text{1D}}(\Delta)$, as well as the longitudinal susceptibility $\chi_\parallel$ since it is smaller by factor of $1/S$ compared to the transverse one and it is suppressed by temperature. The real space transverse susceptibility of the 3D ferromagnet is given by

$$\chi_\perp^{\text{3D}}(\omega, \boldsymbol{r}) = -\frac{S}{D}\frac{e^{-r/l_F}}{r}, \quad \omega < \Delta_F, \tag{3.88}$$

where Δ_F is the gap induced via applied external magnetic field or due to internal anisotropy of the ferromagnet, $l_F = \sqrt{\frac{D}{\Delta_F - \omega}}$ and $D = 2JS$. In what follows, we assume that the external gap is always larger than the qubit splitting, $\Delta < \Delta_F$, as this ensures that the transverse noise is not contributing to decoherence in second order since transverse noise is

---

[2]Note that the z-component of the magnetization of both the ferromagnets does not need to cancel exactly. We only require the splitting along z to be smaller that Δ_F.

related to the vanishing imaginary part of the transverse susceptibility, $\chi_\perp(\omega)'' = 0$ ($\omega < \Delta_F$). The spatial dependence of the effective two spin coupling given by Eq. (3.88) is of Yukawa type due to presence of the external gap. If we assume a realistic tunnel coupling to the ferromagnet of $100\mu eV$, [76, 77] the Curie temperature of $550K$ [as for example for yttrium iron garnet (YIG)] and a gap of $\Delta_F = 100\mu eV$, and the qubit splitting close to the resonance $\Delta_F - \Delta = 3 \times 10^{-3}\mu eV$ (corresponding to a magnetic field of about $B = 60\mu T$) we obtain for the qubit-qubit coupling strength a value on the order of 4×10^{-11} eV for a lattice constant of about 4Å. This coupling strength gives rise to the operation times of $5\mu s$—significantly below the relaxation and decoherence times of the spin qubit, $T_1 = 1s$ [51] and $T_2 > 200\mu s$ [52] respectively. Furthermore, the error threshold—defined as the ratio between the two-qubit gate operation time to the decoherence time—we obtain with such an operation time is about 10^{-2}, which is good enough for implementing the surface code error correction. [78] Here we used T_2 instead of T_2^* since spin-echo can be performed together with two-qubit gates. [79] Alternatively, the decoherence time of GaAs qubits can be increased without spin-echo by narrowing the state of the nuclear spins. [80, 81]

The dimensionality of the ferromagnet plays an important role—if we assume $10nm$ width of the trench where the ferromagnet is placed, then, for energies below $0.1meV$, the ferromagnet behaves as quasi one-dimensional (1D). In this case we obtain

$$\chi_\perp^{1D}(\omega, r) = -\frac{S}{D}l_F e^{-r/l_F}, \quad \omega < \Delta_F, \tag{3.89}$$

wherefrom it is evident that at distances $r \lesssim l_F$ the susceptibility of a quasi-1D ferromagnet is practically constant in contrast to the 3D case, where a $1/r$ decay is obtained, see Eq. (3.88). Additionally, we require $l_F \lesssim D/(AS) = 2J/A$ for the perturbation theory to be valid. Thus, for the same parameters as above, but without the need to tune very close to the resonance (we set herein $\Delta_F - \Delta = 0.5\mu eV$, corresponding to about $B = 10mT$) a coupling strength of $10^{-8}eV$ is obtained.

For 1D case there is yet another rather promising possibility—to use magnetic semiconductors. [82] These materials are characterized by a particularly low Curie temperature of $30K$ or below, [82] and the distance between the ions that are magnetically ordered via RKKY interaction is about $10 - 100nm$. Such a large lattice constant is very beneficial for the long range coupling—if we take the lattice constant to be $10nm$, the coupling to the ferromagnet $A = 15\mu eV$ and the qubit splitting close to resonance ($\Delta_F - \Delta = 0.5\mu eV$, corresponding to about $B = 10mT$),

the qubit-qubit coupling becomes of the order of 1μeV. Such a coupling strength in turn leads to an error threshold on the order of 10^{-8}. Therefore, even the standard error correction protocol can be used in this case.

Derivation of the effective Hamiltonian (exchange coupling)

Here we give a detailed derivation of the qubit-qubit effective Hamiltonian. As stated above, the total Hamiltonian of the system reads

$$H = H_F + H_\sigma + A \sum_i \left(\frac{1}{2} (\sigma_i^+ S_{\boldsymbol{r}_i}^- + \sigma_i^- S_{\boldsymbol{r}_i}^+) + \sigma_i^z S_{\boldsymbol{r}_i}^z \right), \tag{3.90}$$

where we identify the main part as $H_0 = H_F + H_\sigma$ and the small perturbation as the exchange coupling $V = A \sum_i \boldsymbol{\sigma}_i \cdot \boldsymbol{S}_{\boldsymbol{r}_i}$. The Hamiltonian of the ferromagnet reads $H_F = -J \sum_{\langle \boldsymbol{r}, \boldsymbol{r}' \rangle} \boldsymbol{S}_{\boldsymbol{r}} \cdot \boldsymbol{S}_{\boldsymbol{r}'}$, while the Hamiltonian for the two distant qubits is $H_\sigma = \frac{\Delta}{2} \sum_{i=1,2} \sigma_i^x$.

The second order effective Hamiltonian [75] is given by $H_{\text{eff}}^{(2)} = H_0 + U$, where

$$U = -\frac{i}{2} \lim_{\eta \to 0^+} \int_0^\infty dt e^{-\eta t} [V(t), V], \tag{3.91}$$

where $V(t) = e^{iH_0 t} V e^{-iH_0 t}$.

We have

$$\sigma_i^+(t) = \frac{1 + \cos(\Delta t)}{2} \sigma_i^+ + \frac{1 - \cos(\Delta t)}{2} \sigma_i^- - i \sin(\Delta t) \sigma_i^z, \tag{3.92}$$

and $\sigma_i^-(t) = \sigma_i^+(t)^\dagger$.

Recalling that the zz susceptibility can be neglected and that only the transverse susceptibility contributes, we obtain the following result from Eq. (3.91), $U = \lim_{\eta \to 0^+} \int_0^\infty dt e^{-\eta t} \sum_{ij} U_{ij}$

$$U_{ij} = -\frac{iA^2}{8} \left([\sigma_i^-(t) S_{\boldsymbol{r}_i}^+(t), \sigma_j^+ S_{\boldsymbol{r}_j}^-] + \text{h.c.} \right)$$

$$= -\frac{iA^2}{8} \left(\sigma_i^-(t) \sigma_j^+ [S_{\boldsymbol{r}_i}^+(t), S_{\boldsymbol{r}_j}^-] + \text{h.c.} \right) \tag{3.93}$$

Finally, by rewriting $\cos(\Delta t) = \frac{e^{i\Delta t} + e^{-i\Delta t}}{2}$, $\sin(\Delta t) = \frac{e^{i\Delta t} - e^{-i\Delta t}}{2i}$, and using the definition of the real space transverse spin susceptibility

$$\chi_\perp(\omega, \boldsymbol{r}_i - \boldsymbol{r}_j) = -i \lim_{\eta \to 0^+} \int_0^\infty dt e^{-(i\omega + \eta)t} [S_{\boldsymbol{r}_i}^+(t), S_{\boldsymbol{r}_j}^-], \tag{3.94}$$

we obtain by inserting Eq. (3.92) into Eq. (3.93)

$$
\begin{aligned}
U =& \frac{A^2}{8} \sum_{ij} \left(\frac{\chi_\perp(0)}{2} + \frac{\chi_\perp(\Delta) + \chi_\perp(-\Delta)}{4} \right) \sigma_i^- \sigma_j^+ \\
&+ \frac{A^2}{8} \sum_{ij} \left(\frac{\chi_\perp(0)}{2} - \frac{\chi_\perp(\Delta) + \chi_\perp(-\Delta)}{4} \right) \sigma_i^+ \sigma_j^+ \\
&- \frac{A^2}{8} \sum_{ij} \frac{\chi_\perp(\Delta) - \chi_\perp(-\Delta)}{2} \sigma_i^z \sigma_j^+ + \text{h.c.}
\end{aligned}
\tag{3.95}
$$

Since the decay length of the susceptibility $\chi(\omega, \boldsymbol{r})$ is large only close to the resonance, $\Delta_F \sim \Delta$, we can simplify the above equation by neglecting $\chi(-\Delta, \boldsymbol{r})$ and $\chi(0, \boldsymbol{r})$ in comparison to $\chi(\Delta, \boldsymbol{r})$ which is assumed to be close to the resonance. Within this approximation we arrive at Eq. (3.87) of the main text.

3.E Fourth order contributions to decoherence

In this section we determine the effect of the transverse noise in the lowest non-vanishing order due to coupling dipolarly to the ferromagnet. Here we choose quantizations axes such that the qubit splitting is along the z-axis, while the ferromagnet is polarized along x-axis. The Hamiltonian of the coupled system reads

$$
H = H_{\text{F}} + \frac{\Delta}{2}\sigma^z + \sigma^z \otimes X + \sigma^+ \otimes Y^- + \sigma^- \otimes Y^+,
\tag{3.96}
$$

where the operator X (Y) that couples longitudinally (transversally) to the qubit is linear in the transverse operators of the ferromagnet

$$
X = \frac{i}{2} \int d\boldsymbol{r} c_{\boldsymbol{r}} (S_{\boldsymbol{r}}^+ - S_{\boldsymbol{r}}^-),
\tag{3.97}
$$

$$
Y^+ = -\frac{i}{8} \int d\boldsymbol{r} (a_{\boldsymbol{r}} S_{\boldsymbol{r}}^+ + b_{\boldsymbol{r}} S_{\boldsymbol{r}}^-),
\tag{3.98}
$$

with $S_{\boldsymbol{r}}^{\pm} = S_{\boldsymbol{r}}^y \pm iS_{\boldsymbol{r}}^z$ and the definitions of the coefficients

$$a_{\boldsymbol{r}} = B_{\boldsymbol{r}} + 3C_{\boldsymbol{r}} - 6A_{\boldsymbol{r}}, \tag{3.99}$$

$$b_{\boldsymbol{r}} = B_{\boldsymbol{r}} + 3C_{\boldsymbol{r}} + 6A_{\boldsymbol{r}}, \tag{3.100}$$

$$c_{\boldsymbol{r}} = B_{\boldsymbol{r}} - 3A_{\boldsymbol{r}}'', \tag{3.101}$$

$$A_{\boldsymbol{r}} = \frac{1}{a^3}\frac{r^z r^+}{r^5}, \tag{3.102}$$

$$C_{\boldsymbol{r}} = \frac{1}{a^3}\frac{(r^+)^2}{r^5}, \tag{3.103}$$

$$B_{\boldsymbol{r}} = \frac{1}{a^3}\frac{1}{r^3}\left(2 - \frac{3r^+ r^-}{r^2}\right). \tag{3.104}$$

To proceed further we perform the SW transformation on the Hamiltonian given by Eq. (3.96). We ignore the Lamb and Stark shifts and obtain the effective Hamiltonian

$$H = H_{\mathrm{F}} + \frac{\Delta}{2}\sigma^z + \sigma^z \otimes \tilde{X}_2 + \sigma^+ \otimes \tilde{Y}_2^- + \sigma^- \otimes \tilde{Y}_2^+, \tag{3.105}$$

where

$$\tilde{X}_2 = X_2 - \langle X_2 \rangle, \tag{3.106}$$

$$\tilde{Y}_2^{\pm} = Y_2^{\pm} - \langle Y_2^{\pm} \rangle, \tag{3.107}$$

with the following notation

$$X_2 = 4(Y_\Delta^+ Y^- + Y^+ Y_\Delta^-), \tag{3.108}$$

$$Y_2^+ = 2(Y_\Delta^+ X - X_0 Y^+), \tag{3.109}$$

$$X_\omega = \frac{i}{2}\int d\boldsymbol{r}\boldsymbol{r}'\chi_\perp(\omega, \boldsymbol{r} - \boldsymbol{r}')c_{\boldsymbol{r}}(S_{\boldsymbol{r}'}^+ - S_{\boldsymbol{r}'}^-), \tag{3.110}$$

$$Y_\omega^+ = -\frac{i}{8}\int d\boldsymbol{r}\boldsymbol{r}'\chi_\perp(\omega, \boldsymbol{r} - \boldsymbol{r}')(a_{\boldsymbol{r}}S_{\boldsymbol{r}'}^+ + b_{\boldsymbol{r}}S_{\boldsymbol{r}'}^-), \tag{3.111}$$

The model given by Eq. (3.105) yields the following expressions for the relaxation and decoherence times

$$T_1^{-1} = S_{\tilde{Y}_2^-}(\omega = \Delta), \tag{3.112}$$

$$T_2^{-1} = \frac{1}{2}T_1^{-1} + S_{\tilde{X}_2}(\omega = 0), \tag{3.113}$$

where, again, $S_A(\omega) = \int dt e^{-i\omega t}\{A^\dagger(t), A(0)\}$.

After a lengthy calculation we obtain the expressions for $S_{\tilde{X}_2}(\omega = 0)$ and $S_{\tilde{Y}_2^-}(\omega = \Delta)$,

$$S_{\tilde{X}_2}(0) = \frac{1}{128} \int d\nu dr_1 r_2 r_3 r_4 r_5 r_6 C^{-+}(\nu, \boldsymbol{r}_3 - \boldsymbol{r}_4) C^{+-}(-\nu, \boldsymbol{r}_1 - \boldsymbol{r}_2) \times \tag{3.114}$$

$$\begin{aligned}
&((a_{\boldsymbol{r}_5} a^*_{\boldsymbol{r}_3} + b_{\boldsymbol{r}_3} b^*_{\boldsymbol{r}_1})(a_{\boldsymbol{r}_4} a^*_{\boldsymbol{r}_2} + b_{\boldsymbol{r}_6} b^*_{\boldsymbol{r}_4}) \chi_\perp(\Delta, \boldsymbol{r}_1 - \boldsymbol{r}_5) \chi_\perp(\Delta, \boldsymbol{r}_2 - \boldsymbol{r}_6) + \\
&(a_{\boldsymbol{r}_4} a^*_{\boldsymbol{r}_2} + b_{\boldsymbol{r}_5} b^*_{\boldsymbol{r}_4})(a_{\boldsymbol{r}_1} a^*_{\boldsymbol{r}_3} + b_{\boldsymbol{r}_6} b^*_{\boldsymbol{r}_1}) \chi_\perp(\Delta, \boldsymbol{r}_2 - \boldsymbol{r}_5) \chi_\perp(\Delta, \boldsymbol{r}_3 - \boldsymbol{r}_6) + \\
&(a_{\boldsymbol{r}_6} a^*_{\boldsymbol{r}_2} + b_{\boldsymbol{r}_2} b^*_{\boldsymbol{r}_4})(a_{\boldsymbol{r}_5} a^*_{\boldsymbol{r}_3} + b_{\boldsymbol{r}_3} b^*_{\boldsymbol{r}_1}) \chi_\perp(\Delta, \boldsymbol{r}_1 - \boldsymbol{r}_5) \chi_\perp(\Delta, \boldsymbol{r}_4 - \boldsymbol{r}_6) + \\
&(a_{\boldsymbol{r}_6} a^*_{\boldsymbol{r}_2} + b_{\boldsymbol{r}_2} b^*_{\boldsymbol{r}_4})(a_{\boldsymbol{r}_1} a^*_{\boldsymbol{r}_3} + b_{\boldsymbol{r}_5} b^*_{\boldsymbol{r}_1}) \chi_\perp(\Delta, \boldsymbol{r}_3 - \boldsymbol{r}_5) \chi_\perp(\Delta, \boldsymbol{r}_4 - \boldsymbol{r}_6)),
\end{aligned}$$

$$S_{\tilde{Y}_2^-}(\Delta) = \frac{1}{64} \int d\nu dr_1 r_2 r_3 r_4 r_5 r_6 C^{-+}(\nu, \boldsymbol{r}_3 - \boldsymbol{r}_4) C^{+-}(\Delta - \nu, \boldsymbol{r}_1 - \boldsymbol{r}_2) \times \tag{3.115}$$

$$\begin{aligned}
&(c_{\boldsymbol{r}_3} c_{\boldsymbol{r}_6}(a_{\boldsymbol{r}_4} b^*_{\boldsymbol{r}_1} + a_{\boldsymbol{r}_5} b^*_{\boldsymbol{r}_4}) \chi_\perp(0, \boldsymbol{r}_2 - \boldsymbol{r}_6) \chi_\perp(\Delta, \boldsymbol{r}_1 - \boldsymbol{r}_5) \\
&- c_{\boldsymbol{r}_3} c_{\boldsymbol{r}_6}(a_{\boldsymbol{r}_5} a^*_{\boldsymbol{r}_2} + b_{\boldsymbol{r}_2} b^*_{\boldsymbol{r}_1}) \chi_\perp(0, \boldsymbol{r}_4 - \boldsymbol{r}_6) \chi_\perp(\Delta, \boldsymbol{r}_1 - \boldsymbol{r}_5) - \\
&c_{\boldsymbol{r}_4} c_{\boldsymbol{r}_6}(a_{\boldsymbol{r}_1} a^*_{\boldsymbol{r}_2} + b_{\boldsymbol{r}_5} b^*_{\boldsymbol{r}_1}) \chi_\perp(0, \boldsymbol{r}_3 - \boldsymbol{r}_6) \chi_\perp(\Delta, \boldsymbol{r}_2 - \boldsymbol{r}_5) \\
&+ c_{\boldsymbol{r}_1} c_{\boldsymbol{r}_6}(b_{\boldsymbol{r}_5} a^*_{\boldsymbol{r}_2} + b_{\boldsymbol{r}_2} a^*_{\boldsymbol{r}_3}) \chi_\perp(0, \boldsymbol{r}_4 - \boldsymbol{r}_6) \chi_\perp(\Delta, \boldsymbol{r}_3 - \boldsymbol{r}_5) + \\
&c_{\boldsymbol{r}_4} c_{\boldsymbol{r}_5}(b_{\boldsymbol{r}_3} a^*_{\boldsymbol{r}_2} + b_{\boldsymbol{r}_6} a^*_{\boldsymbol{r}_3}) \chi_\perp(0, \boldsymbol{r}_1 - \boldsymbol{r}_5) \chi_\perp(\Delta, \boldsymbol{r}_2 - \boldsymbol{r}_6) \\
&+ c_{\boldsymbol{r}_3} c_{\boldsymbol{r}_4}(a_{\boldsymbol{r}_5} a^*_{\boldsymbol{r}_2} + b_{\boldsymbol{r}_6} b^*_{\boldsymbol{r}_1}) \chi_\perp(\Delta, \boldsymbol{r}_1 - \boldsymbol{r}_5) \chi_\perp(\Delta, \boldsymbol{r}_2 - \boldsymbol{r}_6) - \\
&c_{\boldsymbol{r}_1} c_{\boldsymbol{r}_5}(a_{\boldsymbol{r}_4} a^*_{\boldsymbol{r}_3} + b_{\boldsymbol{r}_6} b^*_{\boldsymbol{r}_4}) \chi_\perp(0, \boldsymbol{r}_2 - \boldsymbol{r}_5) \chi_\perp(\Delta, \boldsymbol{r}_3 - \boldsymbol{r}_6) \\
&- c_{\boldsymbol{r}_1} c_{\boldsymbol{r}_4}(b_{\boldsymbol{r}_6} a^*_{\boldsymbol{r}_2} + b_{\boldsymbol{r}_5} a^*_{\boldsymbol{r}_3}) \chi_\perp(\Delta, \boldsymbol{r}_2 - \boldsymbol{r}_5) \chi_\perp(\Delta, \boldsymbol{r}_3 - \boldsymbol{r}_6) - \\
&c_{\boldsymbol{r}_2} c_{\boldsymbol{r}_5}(a_{\boldsymbol{r}_6} a^*_{\boldsymbol{r}_3} + b_{\boldsymbol{r}_3} b^*_{\boldsymbol{r}_4}) \chi_\perp(0, \boldsymbol{r}_1 - \boldsymbol{r}_5) \chi_\perp(\Delta, \boldsymbol{r}_4 - \boldsymbol{r}_6) \\
&+ c_{\boldsymbol{r}_2} c_{\boldsymbol{r}_5}(a_{\boldsymbol{r}_6} b^*_{\boldsymbol{r}_1} + a_{\boldsymbol{r}_1} b^*_{\boldsymbol{r}_4}) \chi_\perp(0, \boldsymbol{r}_3 - \boldsymbol{r}_5) \chi_\perp(\Delta, \boldsymbol{r}_4 - \boldsymbol{r}_6) - \\
&c_{\boldsymbol{r}_2} c_{\boldsymbol{r}_3}(a_{\boldsymbol{r}_6} b^*_{\boldsymbol{r}_1} + a_{\boldsymbol{r}_5} b^*_{\boldsymbol{r}_4}) \chi_\perp(\Delta, \boldsymbol{r}_1 - \boldsymbol{r}_5) \chi_\perp(\Delta, \boldsymbol{r}_4 - \boldsymbol{r}_6) \\
&+ c_{\boldsymbol{r}_1} c_{\boldsymbol{r}_2}(a_{\boldsymbol{r}_6} a^*_{\boldsymbol{r}_3} + b_{\boldsymbol{r}_5} b^*_{\boldsymbol{r}_4}) \chi_\perp(\Delta, \boldsymbol{r}_3 - \boldsymbol{r}_5) \chi_\perp(\Delta, \boldsymbol{r}_4 - \boldsymbol{r}_6) + \\
&c_{\boldsymbol{r}_5} c_{\boldsymbol{r}_6}(a_{\boldsymbol{r}_4} a^*_{\boldsymbol{r}_3} + b_{\boldsymbol{r}_3} b^*_{\boldsymbol{r}_4}) \chi_\perp(0, \boldsymbol{r}_1 - \boldsymbol{r}_5) \chi_\perp(0, \boldsymbol{r}_2 - \boldsymbol{r}_6) \\
&- c_{\boldsymbol{r}_5} c_{\boldsymbol{r}_6}(a_{\boldsymbol{r}_4} b^*_{\boldsymbol{r}_1} + a_{\boldsymbol{r}_1} b^*_{\boldsymbol{r}_4}) \chi_\perp(0, \boldsymbol{r}_2 - \boldsymbol{r}_5) \chi_\perp(0, \boldsymbol{r}_3 - \boldsymbol{r}_6) - \\
&c_{\boldsymbol{r}_5} c_{\boldsymbol{r}_6}(b_{\boldsymbol{r}_3} a^*_{\boldsymbol{r}_2} + b_{\boldsymbol{r}_2} a^*_{\boldsymbol{r}_3}) \chi_\perp(0, \boldsymbol{r}_1 - \boldsymbol{r}_5) \chi_\perp(0, \boldsymbol{r}_4 - \boldsymbol{r}_6) \\
&+ c_{\boldsymbol{r}_5} c_{\boldsymbol{r}_6}(a_{\boldsymbol{r}_1} a^*_{\boldsymbol{r}_2} + b_{\boldsymbol{r}_2} b^*_{\boldsymbol{r}_1}) \chi_\perp(0, \boldsymbol{r}_3 - \boldsymbol{r}_5) \chi_\perp(0, \boldsymbol{r}_4 - \boldsymbol{r}_6)).
\end{aligned}$$

In order to obtain the estimates for relaxation and decoherence time, we consider the ferromagnet to be in shape of infinite plane. Furthermore, we are not aiming at performing an exact evaluation of the integrals in Eqs. (3.115)-(3.116), but rather at finding the lower bound for the relaxation and decoherence times. To this end we note that $|C^{+-}(\omega, \boldsymbol{r} - \boldsymbol{r}')| \leq |C^{+-}(\omega, \boldsymbol{r} = 0)|$ and arrive at the following inequalities

$$S_{\tilde{X}_2}(0) \leq \frac{B^4}{8(\Delta_F - \Delta)^2} \int_{\Delta_F}^{\infty} d\nu\, C^{+-}(\nu)^2, \tag{3.116}$$

$$S_{\tilde{Y}_2^-}(\Delta) \leq \frac{B^4}{8} \left(\frac{1}{\Delta_F} + \frac{1}{\Delta_F - \Delta} \right)^2 \times$$

$$\int_{\Delta_F + \Delta}^{\infty} d\nu\, C^{+-}(\nu) C^{+-}(\nu - \Delta), \tag{3.117}$$

where we used notation $B = \int d\mathbf{r}\, B_{\mathbf{r}}$. Finally we arrive at the estimates for the relaxation and decoherence times

$$T_1^{-1} \leq \frac{B^4 S^2 \Delta_F^2}{2D^3} \left(\frac{1}{\Delta_F} + \frac{1}{\Delta_F - \Delta} \right)^2 f\left(\frac{\Delta}{\Delta_F}, \beta\Delta_F \right), \tag{3.118}$$

$$T_2^{-1} \leq \frac{B^4 S^2 \Delta_F^2}{4D^3} \left(\frac{1}{\Delta_F} + \frac{1}{\Delta_F - \Delta} \right)^2 f\left(\frac{\Delta}{\Delta_F}, \beta\Delta_F \right) +$$

$$\frac{B^4 S^2 \Delta_F^2}{2D^3(\Delta_F - \Delta)^2} f\left(0, \beta\Delta_F \right). \tag{3.119}$$

with the function $f(x, y)$ defined as follows

$$f(x, y) = \int_{1+x}^{\infty} dz \frac{\sqrt{z-1}}{e^{yz} - 1} \frac{\sqrt{z - x - 1}}{e^{y(z-x)} - 1}. \tag{3.120}$$

Assuming the same parameters as in the main text, we obtain decoherence times of about 0.5 hours, while the relaxation time is on the order of 1000 hours. It is worth noting that this result depends sensitively on the ratio Δ_F/T, thus if we assume a temperature of 4K, we obtain $T_1 \geq 200\mu s$ and $T_2 \geq 30\mu s$.

Long-Range Interaction of Spin-Qubits via Ferromagnets

We propose a mechanism of a long-range coherent interaction between two singlet-triplet qubits dipolarly coupled to a dogbone-shaped ferromagnet. An effective qubit-qubit interaction Hamiltonian is derived and the coupling strength is estimated. Furthermore we derive the effective coupling between two spin-$1/2$ qubits that are coupled via dipolar interaction to the ferromagnet and that lie at arbitrary positions and deduce the optimal positioning. We consider hybrid systems consisting of spin-$1/2$ and ST qubits and derive the effective Hamiltonian for this case. We then show that operation times vary between 1MHz and 100MHz and give explicit estimates for GaAs, Silicon, and NV-center based spin qubits. Finally, we explicitly construct the required sequences to implement a CNOT gate. The resulting quantum computing architecture retains all the single qubit gates and measurement aspects of earlier approaches, but allows qubit spacing at distances of order $1\,\mu$m for two-qubit gates, achievable with current semiconductor technology.

4.1 Introduction

In this work, we propose and study a system that allows for coherent coupling between ST-qubits as well as between spin-$1/2$ qubits over distances of about one micrometer. The coupler is a ferromagnet composed of two disks separated by a thin quasi-1D region, see Fig. 4.1. The qubits are coupled to the ferromagnet via dipolar interaction and they are positioned in the vicinity of each disk. The relevant quantity of the coupler, describing the effective coupling between the distant qubits, is its spin-spin susceptibility—a slowly spatially decaying real part of the susceptibility is required in order to mediate interactions over long distances. Additionally, in order to have *coherent* coupling, the imaginary part of the susceptibility should be sufficiently small. The spatial decay of the spin susceptibility depends strongly on the dimensionality of the ferromagnet— it is longer ranged in lower dimensions. The dogbone shape of the coupler considered here is thus optimal: it allows for strong coupling to the ferromagnet because many spins of each disk lie close to the qubits, while the coherent interaction between them is mediated by the quasi-1D channel. Actually the statement on the optimal shape of the *coupler* is quite general if we consider a realistic interaction between the qubit and the coupler, i.e., a Coulomb [65] or a dipolar one as herein.

Likewise, we derive a Hamiltonian for the effective interaction between the distant qubits positioned arbitrarily with respect to each disk of the dogbone and determine what is the optimal position for the coupling to be strongest. For ST-qubit the optimal coupling is obtain if one quantum well is positioned directly below the disk center and the other one below the edge of the disk, while for the spin-$1/2$ qubits it is optimal to place them at the edge of the disk. Similar conclusions about the optimal positioning of the qubits with respect to the coupler were previously obtained for the case of electrostatic interaction. [65]

In the most favorable scenarios described above the coupling strength of $10^{-2}\mu eV$ are achieved for ST-qubits as well as for spin-$1/2$ qubits. The clock speed for such coupling schemes thus varies between 1MHz and 100MHz. We summarize in Tables 4.1 and 4.2 of Section 4.8 the coupling strengths and corresponding operation times achievable with our scheme.

In order to be useful for quantum computation, one needs to be able to turn on and off the coupling between the qubits. This is efficiently achieved by putting the qubit splitting off-resonance with the internal splitting of the ferromagnet. As we argue below, a modification in the qubit splitting of about one percent of Δ_F is enough to interrupt the in-
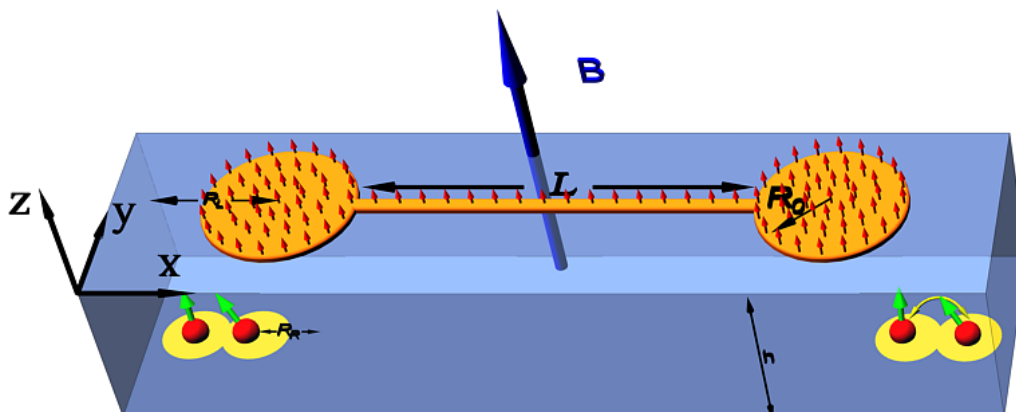
Figure 4.1: Model system consisting of two identical double-QDs in the xy-plane and the dogbone-shaped coupler. The dogbone coupler consists of two ferromagnetic disks of radius R_0 connected by a thin ferromagnetic wire of length L. Each double-QD can accommodate one (two) electrons, defining the spin-$1/2$ (ST-) qubit. Absence of tunneling between the separate double-QD is assumed. Here R_{L} (R_{R}) is the in-plane distance between the left (right) well and the corresponding disk center, while h is vertical distance between the QD and the gate. The red arrow on top of the ferromagnet denote the orientation of its magnetization which is assumed to be monodomain.

teraction between the qubits. Finally we derive for both qubit systems the sequence to implement the entangling gates CNOT (and iSWAP) that can be achieved with a gate fidelity exceeding 99.9%. The additional decoherence effects induced solely by the coupling to the ferromagnet are negligible for sufficiently low temperatures ($T \lesssim 0.1K$). [83] We then obtain error thresholds—defined as the ratio between the two-qubit gate operation time to the decoherence time—of about 10^{-4} for ST-qubits as well as for spin-$1/2$ qubits and this is good enough to implement the surface code error correction in such setups. This quantum computing architecture thus retains all the single qubit gates and measurement aspects of earlier approaches, but allows qubit spacing at distances of order $1\,\mu$m for two-qubit gates, achievable with current semiconductor technology.

The paper is organized as follows. In Sections 4.2 and 4.3 we introduce the ferromagnet and ST-qubit Hamiltonian, respectively. In Sec. 4.3 we derive the effective dipolar coupling between the ST-qubit and the ferromagnet. In Sec. 4.3 we make use of a perturbative Scrhieffer-Wolff transformation to derive the effective coupling between the two ST-qubits that is mediated by the ferromagnet. We determine the optimal position

of the qubits relative to the disks of the dogbone. In Sec. 4.3 we construct the sequence to implement the CNOT (and iSWAP) gate and calculate the corresponding fidelity of the sequence. In Sec. 4.4 we study the coupling between two spin-$1/2$ qubits positioned at arbitrary location with respect to the adjacent disk of the dogbone-shaped ferromagnet. We derive an effective Hamiltonian for the interaction of the two spin-$1/2$ qubits mediated by the ferromagnet and determine the optimal position of the qubits. In Sec. 4.4 we derive the sequence to implement the CNOT (and iSWAP) gate. In Sec. 4.5, we show that spin-$1/2$ and ST qubits can be cross-coupled leading to hybrid qubits and we derive the effective Hamiltonian for this case. In Sec. 7.5, we discuss the range of validity of our effective theory. The *on/off* switching mechanisms of the qubit-qubit coupling are discussed in Sec. 4.7. In Sec. 4.8, we present a table with the effective coupling strengths and operation times achievable in our setup for four experimentally relevant systems, namely GaAs spin-$1/2$ quantum dots, GaAs singlet-triplet quantum dots, silicon-based qubits, and N-V centers. Finally, Sec. 4.9 contains our final remarks and the Appendices additional details on the models and derivations.

4.2   Ferromagnet

We denote by $\boldsymbol{S_r}$ the spins (of size S) of the ferromagnet at site $\boldsymbol{r}$ on a cubic lattice and $\boldsymbol{\sigma}_i$ stands for the spin-$1/2$ qubit spins. The ferromagnet Hamiltonian we consider is of the following form

$$H_F = -J \sum_{\langle \boldsymbol{r},\boldsymbol{r'} \rangle} \boldsymbol{S_r} \cdot \boldsymbol{S_{r'}} + \Delta_F \sum_{\boldsymbol{r}} S_{\boldsymbol{r}}^z, \tag{4.1}$$

with $J > 0$ and $\Delta_F = \mu B$, where B is externally applied magnetic field (see Fig. 4.1) and μ is the magnetic moment of the ferromagnet spin. The above Hamiltonian is the three-dimensional (3D) Heisenberg model with the sum restricted to nearest-neighbor sites $\langle \boldsymbol{r}, \boldsymbol{r'} \rangle$. The ferromagnet is assumed to be monodomain and below the Curie temperature with the magnetization pointing along the z-direction.

We would like to stress at this point that even though herein we analyze a specific model for the ferromagnet (Heisenberg model), all our conclusions rely only on the generic features of the ferromagnet susceptibility, i.e., its long-range nature. Furthermore, the gap in the magnon spectrum can originate also from anisotropy. The presence of the gap is an important feature since it suppresses the fluctuations, albeit the sus-

ceptibility is cut-off after some characteristic length given by the gap and the frequency at which the ferromagnet is probed.

4.3 Coupling between ST-qubits

The Hamiltonian we consider is of the following form

$$H = H_F + H_\tau + H_I, \tag{4.2}$$

where H_τ is Hamiltonian of the two ST-qubits [84, 85] and H_I is the dipolar coupling between the ferromagnet and the ST-qubits (see below).

Singlet-triplet qubit Hamiltonian

A Singlet-Triplet (ST) qubit is a system that consists of two electrons confined in a double quantum well. Herein we assume that the wells are steep enough so that we can consider only one lowest orbital level of each well. Following Ref. [86], we consider also the spin space of the two electrons and write down the total of six basis states

$$
\begin{aligned}
|(2,0)S\rangle &= c_{\text{L}\uparrow}^{\dagger} c_{\text{L}\downarrow}^{\dagger} |0\rangle, \\
|(0,2)S\rangle &= c_{\text{R}\uparrow}^{\dagger} c_{\text{R}\downarrow}^{\dagger} |0\rangle, \\
|(1,1)S\rangle &= \frac{1}{\sqrt{2}} \left(c_{\text{L}\uparrow}^{\dagger} c_{\text{R}\downarrow}^{\dagger} - c_{\text{L}\downarrow}^{\dagger} c_{\text{R}\uparrow}^{\dagger} \right) |0\rangle, \\
|T_+\rangle &= c_{\text{L}\uparrow}^{\dagger} c_{\text{R}\uparrow}^{\dagger} |0\rangle, \\
|T_0\rangle &= \frac{1}{\sqrt{2}} \left(c_{\text{L}\uparrow}^{\dagger} c_{\text{R}\downarrow}^{\dagger} + c_{\text{L}\downarrow}^{\dagger} c_{\text{R}\uparrow}^{\dagger} \right) |0\rangle, \\
|T_-\rangle &= c_{\text{L}\downarrow}^{\dagger} c_{\text{R}\downarrow}^{\dagger} |0\rangle,
\end{aligned}
\tag{4.3}
$$

where $c_{\text{L}}^{\dagger}$ ($c_{\text{R}}^{\dagger}$) creates an electron in the Wannier state Φ_{L} (Φ_{R}). The Wannier states are $\Phi_{L,R} = \frac{1}{\sqrt{1-2sg+g^2}} (\varphi_{1,2} - g\varphi_{2,1})$, where

$$s = \langle \varphi_1 | \varphi_2 \rangle = \exp[-\left(a/a_{\text{B}}\right)^2]$$

is the overlap of the harmonic oscillator ground state wave functions of the two wells, $a_{\text{B}} = \sqrt{\hbar/m\omega_0}$ is the Bohr radius of a single quantum dot, $\hbar\omega_0$ is the single-particle level spacing, and $2a = l$ is the interdot distance. The mixing factor of the Wannier states is $g = (1 - \sqrt{1 - s^2})/s$. Using these six basis states we can represent the Hamiltonian of the ST-qubits

$$H_0 = \begin{pmatrix} H_{\text{S}S} & 0 \\ 0 & H_{\text{T}T,0} \end{pmatrix}. \tag{4.4}$$

In writing the above equation we have neglected the spin-orbit interaction (SOI), thus there are no matrix elements coupling the singlet and triplet blocks. The effect of SOI in ST-qubit was studied in Ref. [86] and no major influence on the qubit spectra was found.

The two qubit states are $|T_0\rangle$ and, in the absence of SOI, the linear combination of the singlet states $|S\rangle = \alpha|(2,0)S\rangle + \beta|(1,1)S\rangle + \gamma|(0,2)S\rangle$, where the coefficients α, β, γ depend on the detuning ε between the two quantum wells. In particular, when $\varepsilon = 0$ we have $|S\rangle = |(1,1)S\rangle$. In what follows, we always consider Hamiltonians only in the qubit subspace, thus the Hamiltonian of two ST-qubits reads

$$H_\tau = -\frac{\Delta}{2} \sum_{i=1,2} \tau_i^z, \tag{4.5}$$

where $\tau^{x,y,z}$ are the Pauli matrices acting in the space spanned by vectors $\{|S\rangle, |T_0\rangle\}$ and Δ is the ST-qubit splitting.

Dipolar coupling to ST-qubit

In this section we derive the dipolar coupling between the ferromagnet and the ST-qubit. To this end we first project the Zeeman coupling to the ST-qubit system on the two-dimensional qubit subspace

$$H_Z = g^* \mu_B \left(\boldsymbol{B}_L \cdot \boldsymbol{S}_L + \boldsymbol{B}_R \cdot \boldsymbol{S}_R \right), \tag{4.6}$$

where $\boldsymbol{B}_L$ ($\boldsymbol{B}_R$) is the magnetic field in the left (right) quantum well, $S_{L,R}^i = (\sigma^i)_{ss'} c_{L,R,s}^\dagger c_{L,R,s'}$ and g^* is the effective Landé factor. After projecting on the qubit space we obtain

$$H_Z = g^* \mu_B (B_L^z - B_R^z) \tau^x. \tag{4.7}$$

With this result we are ready to write down the ferromagnet/ST-qubit interaction Hamiltonian

$$H_I = \sum_{i=1,2} g^* \mu_0 \mu_B \left(\hat{B}_L^z(i) - \hat{B}_R^z(i) \right) \tau_i^x, \tag{4.8}$$

where index i enumerates ST-qubits, and the magnetic field from the ferromagnet can be express through the integral over the ferromagnet

$$\hat{B}_{L,R}^z(i) = \frac{\mu_0 \mu}{4\pi a^3} \int d\boldsymbol{r}(i)_{L,R} \frac{1}{r(i)_{L,R}^3} \times \tag{4.9}$$
$$\left(S_{\boldsymbol{r}(i)_{L,R}}^z - \frac{3(\boldsymbol{S}_{\boldsymbol{r}(i)_{L,R}} \cdot \boldsymbol{r}(i)_{L,R}) r(i)_{L,R}^z}{r(i)_{L,R}^2} \right),$$

where the coordinate system for $\boldsymbol{r}(i)_{\mathrm{L}}$ ($\boldsymbol{r}(i)_{\mathrm{R}}$) is positioned in left (right) quantum well of the i-th qubit.

Effective coupling between two ST-qubits

Given the total Hamitonian, Eq. (14.16), we can easily derive the effective qubit-qubit coupling with help of Schrieffer-Wolff transformation

$$H_{eff} = H_\tau - \lim_{\nu \to 0^+} \frac{i}{2} \int_0^\infty dt e^{-\nu t} \left[H_I(t), H_I \right], \tag{4.10}$$

with $H_I(t) = e^{iH_\tau t} H_I e^{-iH_\tau t}$.

We assume that the radius of the two disks is much smaller than the distance between their centers ($R_0 \ll L$). Within this assumption we can take for the susceptibility between two points at opposite disks the same as the 1D susceptibility. Next we take only on-resonance susceptibility and make use of the expression $\tau^x(\Delta) = \frac{1}{2}(\tau^x + i\tau^y)$, where $\tau^x(\omega)$ is the Fourier transform of $\tau^x(t) = e^{iH_\tau t}\tau^x e^{-iH_\tau t}$. We define the transverse susceptibility in the standard way

$$\chi_\perp(\omega, \boldsymbol{r}_i - \boldsymbol{r}_j) = -i \lim_{\eta \to 0^+} \int_0^\infty dt e^{(-i\omega - \eta)t} [S_{\boldsymbol{r}_i}^+(t), S_{\boldsymbol{r}_j}^-]. \tag{4.11}$$

The longitudinal susceptibility, defined via

$$\chi_\parallel(\omega, \boldsymbol{r}_i - \boldsymbol{r}_j) = -i \lim_{\eta \to 0^+} \int_0^\infty dt e^{(-i\omega - \eta)t} [S_{\boldsymbol{r}_i}^z(t), S_{\boldsymbol{r}_j}^z], \tag{4.12}$$

can be neglected compared to the transverse one because the former is smaller by a factor $1/S$ and is proportional to the magnon occupation number, see Eq. (3.74) in Appendix 3.C . Therefore the longitudinal susceptibility vanishes at zero temperature, while the is not the case for the transverse susceptibility. We arrive finally at the following expression

$$H_{eff} = H_\tau + \frac{9}{4} \mathcal{B} \chi_\perp^{1D}(\Delta, L) \tau_1^x \tau_2^x, \tag{4.13}$$

where $\mathcal{B} = (\mu_0 \mu)^2 (g^* \mu_B)^2 (A_L^1 - A_R^1)(A_L^2 - A_R^2)/16\pi^2 a^6$, $\chi_\perp^{1D}$ is given in Eq. (3.69) and

$$A_{\mathrm{L},R}^i = \int d\boldsymbol{r}(i)_{\mathrm{L},R} \frac{r(i)_{\mathrm{L},R}^- r(i)_{\mathrm{L},R}^z}{r(i)_{\mathrm{L},R}^5}. \tag{4.14}$$

Assuming the dogbone shape of the ferromagnet in the above integral
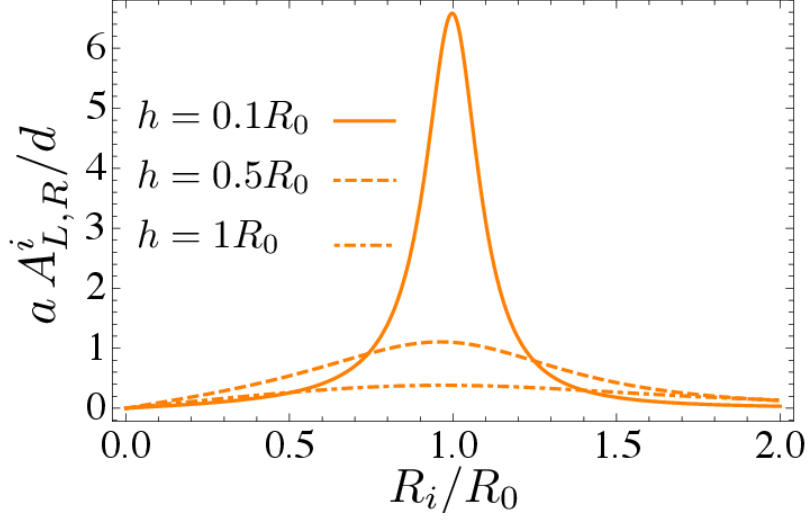
Figure 4.2: Plot of $aA_{L,R}^i/d$ defined through Eq. (4.14) as function of R_i/R_0 for different values of h. We see that the value of $aA_{L,R}^i/d$ is bigger when the ST-qubit is closer to the disk of the dogbone as expected. Furthermore, by placing the right dot at distance R_0 of the disk axis and the left dot on the disk axis, we obtain the strongest value for the effective coupling between the two ST-qubits, see Eq. (4.13).

and integration only over the adjacent disk, we obtain

$$
A_{L,R}^i = \frac{2ihd}{a} \left(\frac{2R_{L,R}^i R_0 \left(F(\mathrm{acsc}(w_{L,R}^i), {w_{L,R}^i}^2) - K({w_{L,R}^i}^2) \right)}{3R_{L,R}^i \left((R_{L,R}^i - R_0)^2 + h^2 \right) \sqrt{(R_{L,R}^i + R_0)^2 + h^2}} \right.
$$
$$
\left. + \frac{u_{L,R}^i E({w_{L,R}^i}^2) - u_{L,R}^i E(\mathrm{acsc}(w_{L,R}^i), {w_{L,R}^i}^2)}{3R_{L,R}^i \left((R_{L,R}^i - R_0)^2 + h^2 \right) \sqrt{(R_{L,R}^i + R_0)^2 + h^2}} \right), \quad (4.15)
$$

where R_0 is the disk radius, $R_{L,R}^i$ is the distance from the adjacent disk axis to the left or right quantum well of the i-th qubit, $\mathrm{acsc}(x)$ is the inverse cosecant; $F(x,y)$, $K(x)$ and $E(x,y)$ are the corresponding elliptic integrals. Furthermore, we introduced the notation $u_{L,R}^i = {R_{L,R}^i}^2 + R_0^2 + h^2$ and $w_{L,R}^i = \sqrt{1 - \frac{4R_{L,R}^i R_0}{(R_{L,R}^i + R_0)^2 + h^2}}$, where h is the distance in the z-direction between the ST-qubit plane and the adjacent disk bottom and d is the disk thickness, see Fig. 4.1.

Figure 4.2 illustrates the dependence of the $A_{L,R}^i$ integrals on the position of the quantum wells. Since the coupling constant is given by the

difference of this integrals for left and right quantum well, we conclude that the strongest coupling is obtained if one quantum well of the ST-qubit is positioned below the disk center and the other exactly below the edge. Furthermore, when $h \ll R_0$ the value of the integral is strongly peaked around $R \sim R_0$ and this can be exploited as yet another switching mechanism—moving one quantum well away from the edge of the disk.

Sequence for CNOT gate

Two qubits interacting via the ferromagnet evolve according to the Hamiltonian H_{eff}, see Eq. (4.13). The Hamiltonian is therefore the sum of Zeeman terms and qubit-qubit interaction. These terms do not commute, making it difficult to use the evolution to implement standard entangling gates. Nevertheless, since H_τ acts only in the subspace spanned by $\{| \uparrow\uparrow \rangle, | \downarrow\downarrow \rangle\}$ and $\Delta \gg J_{12} = 9\mathcal{B}\chi_\perp(\Delta)/4$, we can neglect the effect of H_{eff} in this part of the space and approximate it by its projection in the space spanned by vectors $\{| \uparrow\downarrow \rangle, | \downarrow\uparrow \rangle\}$

$$H'_{\text{eff}} = H_\tau + J_{12}(\tau_1^x \tau_2^x + \tau_1^y \tau_2^y). \tag{4.16}$$

Within this approximation, the coupling in H'_{eff} and Zeeman terms now commute.

We consider the implementation of the iSWAP gate [68]

$$U_{\text{iSWAP}} = e^{-i(\tau_1^x \tau_2^x + \tau_1^y \tau_2^y)3\pi/4},$$

which can be used to implement the CNOT gate:

$$U_{\text{iSWAP}} = e^{iH_\tau t} e^{-iH'_{\text{eff}} t}, \tag{4.17}$$

where $t = 3\pi/(4J_{12})$. When iSWAP is available, the CNOT gate can be constructed in the standard way [69]

$$U_{\text{CNOT}} = e^{-i\frac{\pi}{4}\tau_1^z} e^{i\frac{\pi}{4}\tau_2^x} e^{i\frac{\pi}{4}\tau_2^z} U_{\text{iSWAP}} e^{-i\frac{\pi}{4}\tau_1^x} U_{\text{iSWAP}} e^{i\frac{\pi}{4}\tau_2^z}. \tag{4.18}$$

Since H'_{eff} is an approximation of H_{eff}, the above sequence will yield approximate CNOT, U'_{CNOT}, when used with the full Hamiltonian. The success of the sequences therefore depends on the fidelity of the gates, $F(U'_{\text{CNOT}})$. Ideally this would be defined using a minimization over all possible states of two qubits. However, to characterize the fidelity of an imperfect CNOT it is sufficient to consider the following four logical states of two qubits: [65, 83] $|+, 0\rangle, |+, 1\rangle, |-, 0\rangle$, and $|-, 1\rangle$. These are

product states which, when acted upon by a perfect CNOT, become the four maximally entangled Bell states $|\Phi^+\rangle, |\Psi^+\rangle, |\Phi^-\rangle$, and $|\Psi^-\rangle$, respectively. As such, the fidelity of an imperfect CNOT may be defined,

$$F(U'_{\mathrm{CNOT}}) = \min_{i\in\{+,-\},j\in\{0,1\}} |\langle i,j|U^\dagger_{CNOT}U'_{CNOT}|i,j\rangle|^2. \qquad (4.19)$$

The choice of basis used here ensures that $F(U'_{\mathrm{CNOT}})$ gives a good characterization of the properties of U'_{CNOT} in comparison to a perfect CNOT, especially for the required task of generating entanglement. For realistic parameters, with the Zeeman terms two order of magnitude stronger than the qubit-qubit coupling, the above sequence yields fidelity for the CNOT gate of 99.976%.

To compare these values to the thresholds found in schemes for quantum computation, we must first note that imperfect CNOT's in these cases are usually modelled by the perfect implementation of the gate followed by depolarizing noise at a certain probability. It is known that such noisy CNOT's can be used for quantum computation in the surface code if the depolarizing probability is less than 1.1%. [70] This corresponds to a fidelity, according to the definition above, of 99.17%. The fidelities that may be achieved in the schemes proposed here are well above this value and hence, though they do not correspond to the same noise model, we can expect these gates to be equally suitable for fault-tolerant quantum computation.

4.4 Coupling between spin-$1/2$ qubits

In this section we study the coupling of two spin-1/2 quantum dots via interaction with a dog-bone shaped ferromagnet. The Hamiltonian has again the form as in Eq. (14.16) and we allow for splittings of the spin-1/2 qubits both along x and z direction,

$$H_\sigma = \frac{\Delta_x}{2}\sum_{i=1,2}\sigma_i^x + \frac{\Delta_z}{2}\sum_{i=1,2}\sigma_i^z, \qquad (4.20)$$

where $\boldsymbol{\sigma}_i$ are the Pauli operators of the ith spin-1/2 quantum dot. Hamiltonian (4.20) is a generalized version of the Hamiltonian studied in Ref. [83] where we considered splitting along x only. We present here a detailed derivation of the effective coupling between two quantum dots located at an arbitrary position with respect to the dogbone shaped ferromagnet, i.e., contrary to Ref. [83] we do not assume that the quantum dots are positioned at a highly symmetric point but consider the most general case.

This allows us to determine the optimal positioning of the qubit in order to achieve the strongest coupling between the qubits.

The dipolar coupling between the ferromagnet and the spin-1/2 qubits is given by

$$H_I = \sum_{i,\boldsymbol{r}} \frac{g^* \mu_0 \mu_B \mu}{4\pi r^3} \left(\boldsymbol{\sigma}_i \cdot \boldsymbol{S_r} - \frac{3(\boldsymbol{\sigma}_i \cdot \boldsymbol{r})(\boldsymbol{S_r} \cdot \boldsymbol{r})}{r^2} \right), \tag{4.21}$$

where μ_D is the magnetic moment of the spin-1/2 qubit. The explicit expressions for the time evolution of the Pauli operators in Heisenberg picture is

$$
\begin{aligned}
\sigma_i^+(t) &= -\frac{1}{\Delta^2}(i\Delta\cos(\Delta t/2) - \Delta_z\sin(\Delta t/2))^2 \sigma_i^+ \\
&\quad -\frac{\Delta_x^2}{2\Delta^2}(\cos(t\Delta) - 1)\sigma_i^- \\
&\quad +\frac{\Delta_x}{\Delta^2}(\Delta_z - \Delta_z\cos(t\Delta) - i\Delta\sin(t\Delta))\sigma_i^z, \\
\sigma_i^z(t) &= \frac{\Delta_x}{2\Delta^2}(\Delta_z - \Delta_z\cos(t\Delta) - i\Delta\sin(t\Delta))\sigma_i^+ \\
&\quad +\frac{\Delta_x}{2\Delta^2}(\Delta_z - \Delta_z\cos(t\Delta) + i\Delta\sin(t\Delta))\sigma_i^- \\
&\quad +\frac{\Delta_z^2 + \Delta_x^2\cos(t\Delta)}{\Delta^2}\sigma_i^z,
\end{aligned}
\tag{4.22}
$$

where we introduced the notation $\Delta = \sqrt{\Delta_x^2 + \Delta_z^2}$. We also assume that $\Delta < \Delta_F$ such that the susceptibility $\chi_\perp(\Delta, \boldsymbol{r})$ is purely real—thus the transverse noise is gapped. By replacing the above expressions in Eq. (4.10), we obtain the effective qubit-qubit coupling

$$
\begin{aligned}
H_{\text{eff}} = H_\sigma &+ \frac{(g^*\mu_0\mu_B\mu)^2}{16\pi^2 a^6}\Big(\frac{9}{8}A_1^* A_2 \chi_\perp^{1D}(\Delta)\sigma_1^z(\Delta)\sigma_2^z \\
&+ \frac{3}{16}(3A_2 C_1^* \chi_\perp^{1D}(\Delta) - B_1 A_2^* \chi_\perp^{1D}(\Delta))\sigma_1^+(\Delta)\sigma_2^z \\
&+ \frac{3}{16}(3A_1 C_2^* \chi_\perp^{1D}(\Delta) - B_2 A_1^* \chi_\perp^{1D}(\Delta))\sigma_1^z(\Delta)\sigma_2^+ \\
&+ \frac{1}{32}(B_1 B_2 \chi_\perp^{1D}(\Delta) + 9 C_1 C_2^* \chi_\perp^{1D}(\Delta))\sigma_1^-(\Delta)\sigma_2^+ \\
&- \frac{3}{32}(B_1 C_2 \chi_\perp^{1D}(\Delta) + B_2 C_1 \chi_\perp^{1D}(\Delta))\sigma_1^-(\Delta)\sigma_2^- \\
&+ \text{h.c.}\Big) + 1 \leftrightarrow 2,
\end{aligned}
\tag{4.23}
$$

where we have denoted $\chi_\perp^{1D}(\Delta) = \chi_\perp^{1D}(\Delta, L)$ and introduced the follow-
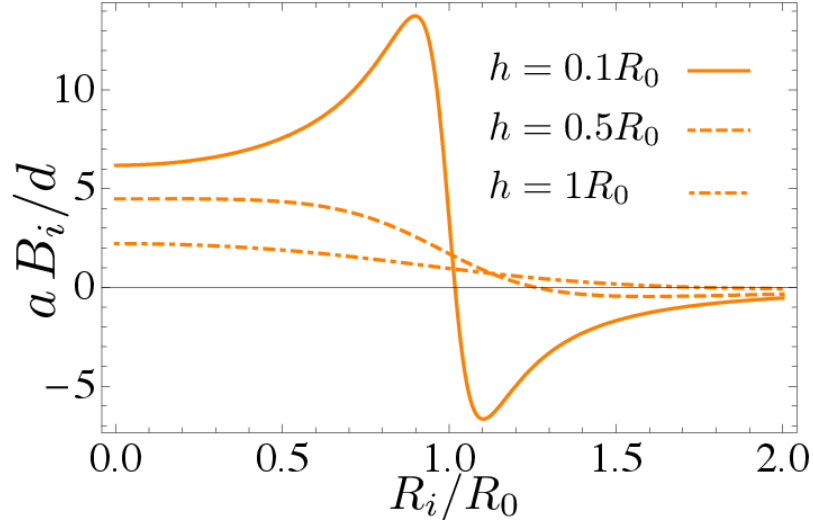
Figure 4.3: Plot of aB_i/d defined in Eq. (6.65) as function of R_i/R_0 for different values of h. The value of the integral increases in general by decreasing the value of h.

ing notation for the integrals

$$A_i = \int d\boldsymbol{r}_i \frac{r_i^z r_i^+}{r_i^5} , \tag{4.24}$$

$$C_i = \int d\boldsymbol{r}_i \frac{(r_i^+)^2}{r_i^5} , \tag{4.25}$$

$$B_i = \int d\boldsymbol{r}_i \frac{1}{r_i^3} \left(2 - \frac{3r_i^+ r_i^-}{r_i^2} \right) , \tag{4.26}$$

with the coordinate origin for $\boldsymbol{r}_i$ at the i-th qubit and the integration goes over the adjacent disk. We also defined the Fourier transforms of the time evolution of Pauli matrices $\boldsymbol{\sigma}(t) = e^{iH_\sigma t} \boldsymbol{\sigma} e^{-iH_\sigma t}$ as

$$\begin{aligned}
\sigma_i^+(\Delta) &= -\frac{1}{\Delta^2} \left(-\frac{\Delta^2}{4} + \frac{\Delta_z \Delta}{2} - \frac{\Delta_z^2}{4} \right) \sigma_i^+ \\
&\quad + \frac{\Delta_x}{\Delta^2} \left(-\frac{\Delta_z}{2} + \frac{\Delta}{2} \right) \sigma_i^z - \frac{\Delta_x^2}{4\Delta^2} \sigma_i^- ,
\end{aligned}$$

and

$$\begin{aligned}
\sigma_i^z(\Delta) &= \frac{\Delta_x}{2\Delta^2} \left(-\frac{\Delta_z}{2} + \frac{\Delta}{2} \right) \sigma_i^+ + \frac{\Delta_x}{2\Delta^2} \left(-\frac{\Delta_z}{2} - \frac{\Delta}{2} \right) \sigma_i^- \\
&\quad + \frac{\Delta_x^2}{2\Delta^2} \sigma_i^z . \tag{4.27}
\end{aligned}$$
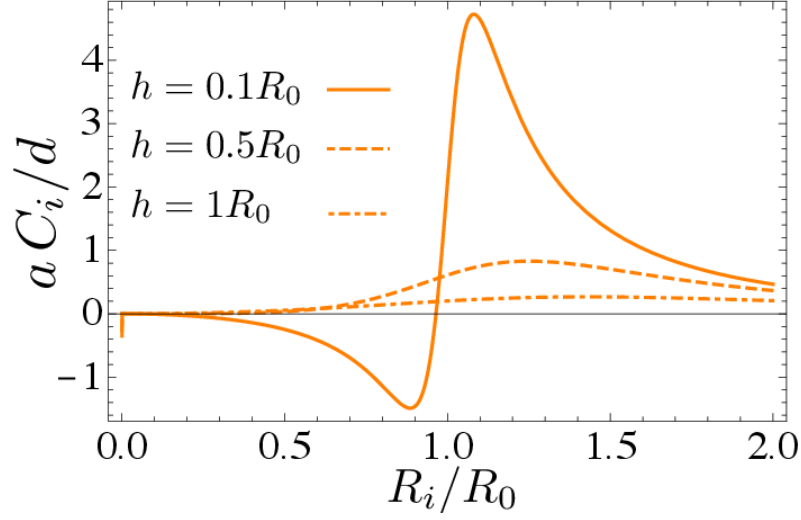
Figure 4.4: Plot of aC_i/d defined in Eq. (11.24) as function of R_i/R_0 for different values of h. The value of the integral is peaked around $R_i \sim R_0$ and it increases in general by decreasing the value of h.

By assuming a dogbone-shaped ferromagnet and integrating only over the adjacent disk as above, we obtain A_i given in Eq. (4.15) with $R^i_{L,R}$ replaced by R_i since there is now only one spin-$1/2$ qubit below each disk of the dogbone. The remaining integrals yield the following results

$$
\begin{aligned}
B_i &= -\frac{2d}{3a} \left(\frac{\left(R_i^4 + 3R_i^2\left(h^2 - R_0^2\right) + \left(R_0^2 + h^2\right)^2 \right) E\left(1 - w_i^2\right)}{R_i^2 \left((R_i - R_0)^2 + h^2\right)\sqrt{(R_i + R_0)^2 + h^2}} \right. \\
&\qquad \left. - \frac{\left((R_i - R_0)^2 + h^2\right)\left(R_i^2 + 2\left(R_0^2 + h^2\right)\right) K\left(1 - w_i^2\right)}{R_i^2 \left((R_i - R_0)^2 + h^2\right)\sqrt{(R_i + R_0)^2 + h^2}} \right) \\
C_i &= \frac{2d}{a} \frac{\left((R_i - R_0)^2 + h^2\right) K\left(1 - w_i^2\right) - 2\left(R_i^2 - R_0^2 + h^2\right) E\left(1 - w_i^2\right)}{\left((R_i - R_0)^2 + h^2\right)\sqrt{(R_i + R_0)^2 + h^2}},
\end{aligned}
$$
$$\tag{4.28}$$

where $w_i = \sqrt{1 - \frac{4R_iR_0}{(R_i + R_0)^2 + h^2}}$, R_0 is the radius of each disk, R_i is the distance of the i-th qubit to the adjacent dog bone axis, and R_0 and h are defined as in Sec. 4.3. In deriving Eq. (4.23) we took again only 'on-resonance' terms into account (i.e. we neglected $\chi_\perp^{1D}(0)$ and $\chi_\perp^{1D}(-\Delta)$). Furthermore we assumed, as above, that the susceptibility between two points on different disks of the dogbone is well approximated by the 1D transverse susceptibility. In the limit where each quantum dot lies on the

vertical axis going through the center of each cylinder of the dogbone, the axial symmetry leads to $A_1 = A_2 = C_1 = C_2 = 0$, $B_1 = B_2 = B$, and with $\Delta_z = 0$ we recover the result

$$H_{\text{eff}} = H_\sigma + \frac{(g^*\mu_0\mu_B\mu)^2}{16\pi^2 a^6}\frac{B^2}{32}\chi_\perp^{1D}(\Delta)(2\sigma_1^y\sigma_2^y + \sigma_1^z\sigma_2^x + \sigma_1^x\sigma_2^z) \qquad (4.29)$$

derived in Ref. [83]. The analysis carried out herein assumes arbitrary positioning of the qubit and allow us to determine the optimal positioning for the strongest coupling. To this end, we analyze integrals A_i, B_i, C_i, see Figs. 4.2-4.4. It is readily observed that the coupling strength increases as the vertical distance between the qubit and coupler plane, h, decreases. Additionally, we observe that the strongest coupling strength is obtained when the qubit is positioned below the edge of the adjacent disk.

The derived coupling is valid for any dogbone-like shape of the ferromagnet, i.e., it is not crucial to assume disk shape.

Sequence for CNOT gate

The effective Hamiltonian derived in previous section, Eq. (4.23), can be re-expressed in the following form

$$H_{\text{eff}} = \frac{(g^*\mu_0\mu_B\mu)^2}{16\pi^2 a^6}\chi_\perp^{1D}(\Delta, L)\boldsymbol{\sigma}_1^T \cdot \hat{\mathcal{H}} \cdot \boldsymbol{\sigma}_2 + \frac{1}{2}\boldsymbol{\Delta} \cdot (\boldsymbol{\sigma}_1 + \boldsymbol{\sigma}_2), \qquad (4.30)$$

with $\boldsymbol{\Delta} = (\Delta_x, 0, \Delta_z)^T$ and $\hat{\mathcal{H}}$ being the symmetric matrix with all entries being non-zero. The question now arises how to construct the CNOT gate sequence for such a general Hamiltonian. We tackle this problem by taking first the quantization axis to be along the total magnetic field acting on the two qubits and denote by $\tilde{\boldsymbol{\sigma}}_i$ Pauli matrix vector with respect to this new quantization axis. The Hamiltonian now reads

$$H_{\text{eff}} = \frac{(g^*\mu_0\mu_B\mu)^2}{16\pi^2 a^6}\chi_\perp^{1D}(\Delta, L)\,\tilde{\boldsymbol{\sigma}}_1^T \cdot \hat{\tilde{\mathcal{H}}} \cdot \tilde{\boldsymbol{\sigma}}_2 + \frac{1}{2}\Delta(\tilde{\sigma}_1^z + \tilde{\sigma}_2^z), \qquad (4.31)$$

where the components of the matrix $\hat{\tilde{\mathcal{H}}}$ are given in Appendix 4.A.

We proceed further along the lines presented in Sec. 4.3, i.e., we project the rotated Hamiltonian, Eq. (4.31), on the subspace spanned by vectors $\{|\tilde{\uparrow}\tilde{\downarrow}\rangle, |\tilde{\downarrow}\tilde{\uparrow}\rangle\}$. This procedure yields the following result

$$H'_{\text{eff}} = \tilde{J}_{12}(\tilde{\sigma}_1^x\tilde{\sigma}_2^x + \tilde{\sigma}_1^y\tilde{\sigma}_2^y) + \Delta(\tilde{\sigma}_1^z + \tilde{\sigma}_2^z), \qquad (4.32)$$

$\tilde{J}_{12} = \frac{(\mu_0 g^* \mu_B \mu)^2}{(4\pi)^2 a^6} \frac{\chi_\perp^{1D}(\Delta, L)}{32} \tilde{A}_{12}$. The dimensionless constant $\tilde{A}_{12}$ is defined through the following expression

$$
\begin{aligned}
\tilde{A}_{12} = \;& \frac{\Delta_x{}^2 \left(36 A_1 A_2 + (B_1 + 3C_1)(B_2 + 3C_2)\right)}{16\Delta^2} \\
& + \frac{6\Delta_x \Delta_z \left(A_2 (B_1 - 3C_1) + A_1 (B_2 - 3C_2)\right)}{16\Delta^2} \\
& + \frac{2\Delta_z (B_1 B_2 + 9 C_1 C_2)(\Delta + \Delta_z)}{16\Delta^2}.
\end{aligned}
\tag{4.33}
$$

The projected Hamiltonian in Eq. (4.32) is identical to the one already considered in Sec. 4.3, Eq. (4.16). Thus the CNOT gate sequence can be obtained in exactly same way, namely via Eqs. (4.17) and (4.18).

Similar to the previously studied case of ST-qubits, the CNOT gate sequence described in this section is only approximate one. For realistic parameters, with the Zeeman terms two order of magnitude stronger than the qubit-qubit coupling, this approximate sequence yields fidelity for the CNOT gate similar to the one previously found in Sec. 4.3.
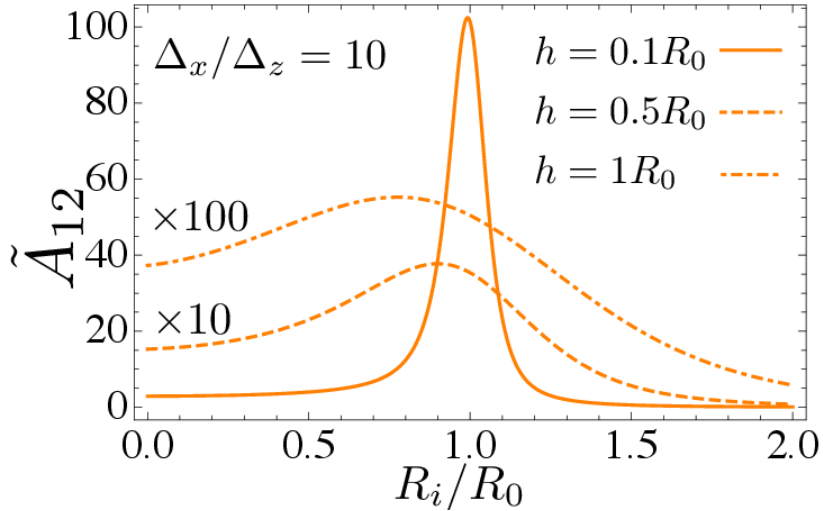
Figure 4.5: Plot of $\tilde{A}_{12}$ defined in Eq. (4.33) as function of R_i/R_0 for different values of h, assuming $R_1 = R_2$ and $\Delta_x = 10\Delta_z$. The value of the integral is peaked around $R_i \sim R_0$ and it increases in general by decreasing the value of h.

We now use Eq. (4.33) to determine the optimal positioning of the qubits in order to obtain shortest possible gate operation times. If we assume that the qubit splitting is predominantly along the x-axis ($\Delta_x \gg$

Δ_z), we obtain the behavior illustrated in Fig. 4.5. We conclude that for all values of h the optimal positioning is below the edge of the adjacent disk. It is interesting to note that when $h \ll R_0$ one can obtain more than two orders of magnitude enhancement compared to the positioning previously studied in Ref. [83]. In the opposite limit, $\Delta_x \ll \Delta_z$, we observe behavior illustrated in Fig. 4.6. When also $h \ll R_0$ we recover the same optimal positioning as before—below the edge of the disk, while when $h \sim R_0$, positioning the qubit anywhere below the disk yields approximately same coupling strength.
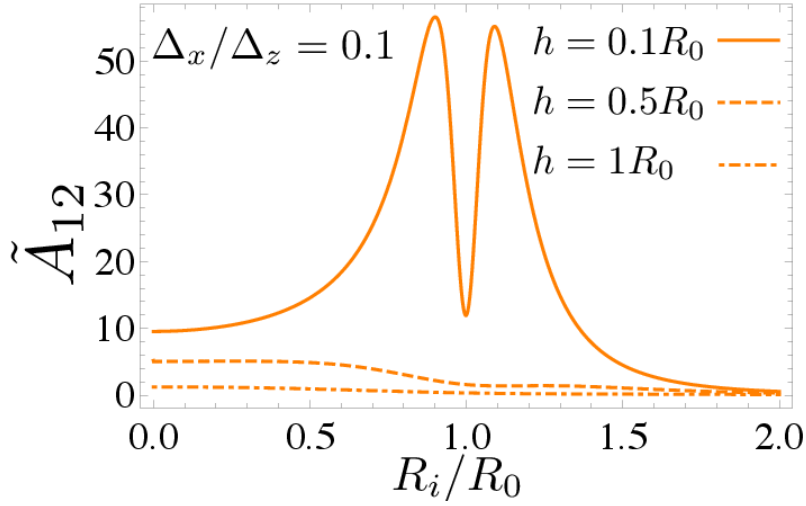
Figure 4.6: Plot of $\tilde{A}_{12}$ defined in Eq. (4.33) as function of R_i/R_0 for different values of h, assuming $R_1 = R_2$ and $\Delta_x = 0.1\Delta_z$. The value of the integral is peaked around $R_i \sim R_0$ only for $h \ll R_0$ and it increases in general by decreasing the value of h.

4.5   Coupling between spin-$1/2$ and ST-qubits

In the previous sections we have considered the coupling of both spin-$1/2$ and ST qubits individually. Since each setup has its own advantages and challenges, it is interesting to show these qubits can be cross-coupled to each other and thus that hybrid spin-qubits can be formed. This opens up the possibility to take advantage of the 'best of both worlds.

The Hamiltonian of such a hybrid system reads

$$H = H_F + H_\sigma + H_\tau + H_I, \qquad (4.34)$$

where the first three term on left-hand side are given by omitting the summation over i in Eqns. (4.1), (4.20) and (4.5), respectively. The interaction term H_I has the following form

$$H_I = \sum_{\boldsymbol{r}} \frac{g^* \mu_0 \mu_B \mu}{4\pi r^3} \left(\boldsymbol{\sigma} \cdot \boldsymbol{S_r} - \frac{3(\boldsymbol{\sigma} \cdot \boldsymbol{r})(\boldsymbol{S_r} \cdot \boldsymbol{r})}{r^2} \right)$$
$$+ g^* \mu_B \left(\hat{B}_{\mathrm{L}}^z - \hat{B}_{\mathrm{R}}^z \right) \tau_i^x, \tag{4.35}$$

with $\hat{B}_{\mathrm{L,R}}$ being given in Eq. (4.9) when index i is omitted. Continuing along the lines of the previous sections, we perform the second order SW transformation and obtain the effective coupling between the qubits

$$H_{eff} = \frac{3(\mu_0 g^* \mu_B \mu)^2}{256\pi^2 a^6} \chi_{\perp}^{\mathrm{1D}}(\Delta) \left(\mathrm{Re}[3A(A_L - A_R)^*] \tau^x \sigma^z(\Delta) \right.$$
$$+ (C^*(A_L - A_R) - 3B(A_L - A_R)^*) \tau^x \sigma^+(\Delta) + \mathrm{h.c})$$
$$+ \{ \sigma^i(\Delta) \to \sigma^i, \tau^x \to \tau^x(\Delta) \}, \tag{4.36}$$

where $A_{\mathrm{L,R}}$ and A are calculated in Eq. (4.15), while B and C are given in Eq. (4.28).

Similarly as in the previous sections, we find that the optimal coupling for the hybrid case is obtained when the spin-$1/2$ qubit is positioned below the edge of one of the two discs while one quantum well of the ST-qubit is positioned below the other disc center with the other well being below the disc edge.

4.6 Validity of the effective Hamiltonian

We discuss herein the validity of the effective Hamiltonian derived in Sec. 4.3 and Sec. 4.4.

Special care has to be taken for the validity of the perturbation theory employed herein, since we are working close to resonance, i.e., $\Delta - \Delta_F$ has to be small but still much larger than the coupling of a qubit to an individual spin of the ferromagnet. For the perturbation theory to be valid we also require the tilt of each ferromagnet spin to be sufficiently small (i.e. $\langle S_{\boldsymbol{r}}^{\pm} \rangle \ll 1$). The tilt of the central spin of the ferromagnetic disk can be estimated by the integral over the dogbone disk D

$$\langle S_{\boldsymbol{r}}^{\pm} \rangle = \int_D \chi_{\perp}(\boldsymbol{r}) B_{\perp}(\boldsymbol{r}). \tag{4.37}$$

Using cylindrical coordinates we then obtain

$$\langle S_{\boldsymbol{r}}^{\pm} \rangle \sim \frac{\mu_0 \mu_B^2}{2a} \int_0^R \rho d\rho \frac{1}{(\rho^2 + h^2)^{3/2}} \frac{S}{D\rho}, \qquad (4.38)$$

where $\frac{S}{D\rho}$ is the spatial decay of the transversal susceptibility and $\frac{1}{(\rho^2+h^2)^{3/2}}$ is the decay of the dipolar field causing the perturbation of the ferromagnet. Even though each spin is just slightly tilted, we obtain a sizable coupling due to big number of spins involved in mediating the coupling.

4.7   Switching mechanisms

In this section we briefly discuss possible switching *on/off* mechanisms. These include changing the splitting of the qubits and moving them spatially. The former mechanism is based on the dependence of the susceptibility decay length on frequency, [83] see Eq. (3.69). It is enough to detune the qubit splitting by less then a percent to switch the qubit-qubit coupling effectively off. This is particularly feasible for the ST-qubits where qubit splitting can be controlled by all electrical means. Furthermore, the ST-qubits coupling can be switched off also by rotating them such that $A_\mathrm{L} = A_\mathrm{R}$, see Eq. (4.14).

The spin-$1/2$ qubits can be switched either by detuning its splitting off-resonance with the magnon gap Δ_F or by moving them away from the dogbone disk, see Figs. 4.5-4.6.

4.8   Coupling strengths and operation times

In Tables 4.1 and 4.2 we present a summary of the effective coupling strengths and operation times that can be obtained in the proposed setup. We assume that the qubits are separated by a distance of $1\mu m$ and we give the remaining parameters in the table captions.

The column captions correspond to four experimentally relevant setups considered in this work (GaAs ST and spin-$1/2$ quantum dots, silicon-based quantum dots, and NV-centers). The row captions denote respectively the vertical distance h between the qubit and the disk of the ferromagnet, the difference between the qubit splitting Δ and the internal splitting Δ_F of the ferromagnet (given in units of energy and in units of magnetic field), the obtained effective qubit-qubit interaction, and the corresponding operation time.

Table 4.1: The parameters used to obtain the numbers below are: Landé factor of the ferromagnet $g_F = 2$; disk radius $R_0 = 50nm$; disk thickness $d = 20nm$; Curie temperature $T = 550K$ and thus exchange coupling $J/k_B \approx 824K$; lattice constant of the ferromagent $a = 4\text{Å}$. We consider the case $\Delta_x \ll \Delta_z$.

$\Delta_x \ll \Delta_z$	GaAs ST QD $\|g^*\| = 0.4$	GaAs ST QD $\|g^*\| = 0.4$	GaAs spin-1/2 QD $\|g^*\| = 0.4$
Distance h	$50\,nm$	$50\,nm$	$50\,nm$
Splitting $\Delta_F - \Delta$	$1\,\mu eV\ (43.2\,mT)$	$0.5\mu eV\ (21.6mT)$	$10^{-2}\,\mu eV\ (0.4\,mT)$
Coupling strength (CS)	$1.4 \times 10^{-9}\,eV$	1.4×10^{-8}	$2 \times 10^{-10}\,eV$
Operation time (OS)	$470\,ns$	$47ns$	$3.3\,\mu s$

$\Delta_x \ll \Delta_z$	Silicon-based QD	NV-center
Distance h	$25\,nm$	$5\,nm$
Splitting $\Delta_F - \Delta$	$10^{-2}\,\mu eV\ (0.1\,mT)$	$10^{-1}\,\mu eV\ (0.9\,mT)$
Coupling Strength (CS)	$2.4 \times 10^{-8}\,eV$	$1.8 \times 10^{-8}\,eV$
Operation Time (OT)	$27.4\,ns$	$36.6\,ns$

The operation times obtained in Tables 4.1 and 4.2 are significantly below the relaxation and decoherence times of the corresponding qubits. Indeed, for GaAs quantum dots $T_1 = 1s$ (see Ref. [51]), and $T_2 > 200\mu s$ (see Ref. [52]), respectively. Here we compare to T_2 instead of T_2^* since spin-echo can be performed together with two-qubit gates. [79] Alternatively, the T_2^* of GaAs qubits can be increased without spin-echo by narrowing the state of the nuclear spins. [80, 81]

For silicon-based qubits decoherence time up to $T_2 \approx 200\mu s$ is achievable. [8] Finally decoherence times of $T_2^* \approx 20\mu s$ and $T_2 \approx 1.8ms$ have been obtained for N-V centers in diamond. [50]

In Table 4.3, we summarize the obtained coupling strengths and operation times obtained when a ST-qubit is cross coupled with a spin-1/2 qubit.

We have verified that the tilting of the ferromagnet spins given in Eq. (4.38) remains small. The biggest tilt we obtain (for $h = 5\,nm$) is $\langle S_{\boldsymbol{r}}^{\pm} \rangle \approx 10^{-7} \ll 1$. Thus all the result are within the range of validity of the perturbation theory.

Table 4.2: We use the same parameters as in Table 4.1 but consider the case $\Delta_x \gg \Delta_z$.

$\Delta_x \gg \Delta_z$	GaAs spin-$1/2$ QD $|g^*| = 0.4$	Silicon-based QD $|g^*| = 2$	NV-center $|g^*| = 2$
Distance h	$50\,nm$	$25\,nm$	$5\,nm$
Splitting $\Delta_F - \Delta$	$10^{-2}\,\mu eV\ (0.4\,mT)$	$10^{-2}\,\mu eV\ (0.1\,mT)$	$10^{-1}\,\mu eV\ (0.9\,mT)$
Coupling strength	$1.2 \times 10^{-10}\,eV$	$1.8 \times 10^{-8}\,eV$	$3.6 \times 10^{-8}\,eV$
Operation time	$5.5\,\mu s$	$36.6\,ns$	$18.3\,ns$

Table 4.3: We use the same parameters as in Table 4.1 and choose the splitting $\Delta_F - \Delta = 10^{-2}\,\mu eV$ for the ST-qubit (the splitting of the other qubit is taken from Table 4.1) to determine the coupling strengths and operation times achieved in the hybrid case. The column caption of the table labels GaAs ST-QD, while the row captions label the three other qubit systems, considered in this work, to which it can be hybridized. The left panel corresponds to the case $\Delta_x \ll \Delta_z$ while the right panel corresponds to $\Delta_x \gg \Delta_z$.

$\Delta_x \ll \Delta_z$	GaAs ST QD	
	Coupling strength	Operation time
GaAs spin-$1/2$ QD	$1.7 \times 10^{-9}\,eV$	$387\,ns$
Silicon-based QD	$1.8 \times 10^{-8}\,eV$	$36.6\,ns$
NV-center	$1.6 \times 10^{-8}\,eV$	$41.1\,ns$

$\Delta_x \gg \Delta_z$	GaAs ST QD	
	Coupling strength	Operation time
GaAs spin-$1/2$ QD	$1.3 \times 10^{-9}\,eV$	$506\,ns$
Silicon-based QD	$1.6 \times 10^{-8}\,eV$	$41.1\,ns$
NV-center	$2.2 \times 10^{-8}\,eV$	$29.9\,ns\,ns$

4.9 Conclusions

We have proposed and studied a model that allows coherent coupling of distant spin qubits. The idea is to introduce a piece of ferromagnetic material between qubits to which they couple dipolarly. A dogbone shape of the ferromagnet is the best compromise since it allows both strong coupling of the qubits to the ferromagnet and long-distance coupling because of its slowly decaying 1D spin-spin susceptibility. We have derived an effective Hamiltonian for the qubits in the most general case where the qubits are positioned arbitrarily with respect to the dogbone. We have calculated the optimal position for the effective qubit-qubit coupling to be strongest and estimated it. For both the singlet-triplet (ST) and spin-$1/2$ qubits, interaction strengths of $10^{-2}\mu eV$ can be achieved. Since decoherence effects induced by the coupling to the ferromagnet are negligible, [83] we obtain error thresholds of about 10^{-4} for ST-qubits and for spin-$1/2$ qubits. In both cases this is good enough to implement the surface code error correction. [78] Finally, for both types of qubits we have explicitly constructed the sequence to implement a CNOT gate achievable with a fidelity of more than 99.9%

Our analysis is general and is not restricted to any special types of qubits as long as they couple dipolarly to the ferromagnet. Furthermore, the only relevant quantity of the coupler is its spin-spin susceptibility. Hence, our analysis is valid for any kind of coupler (and not just a ferromagnet) that has a sufficiently slowly decaying susceptibility.

This quantum computing architecture retains all the single qubit gates and measurement aspects of earlier approaches, but allows qubit spacing at distances of order 1 μm for two- qubit gates, achievable with the state-of-the-art semiconductor technology.

4.10 Acknowledgment

4.A   Rotated Hamiltonian for CNOT gate

Here we give the general form of the matrix $\tilde{\tilde{H}}$ entering Eq. (4.31).

$$
\begin{aligned}
\tilde{\mathcal{H}}_{12} =\ & \frac{3\Delta_z\Delta_z^-(C_2'''(-6\Delta_xA_1'+B_1\Delta_z^-+3C_1'\Delta_z^+)+2\Delta_xA_1''(B_2+3C_2'))}{32\Delta^3} \\
& \frac{6\Delta_z\Delta_z^-C_1''(B_2\Delta_z^--3C_2'\Delta_z^+)+3\Delta_xi\left(12A_2\Delta\Delta_xA_1^*-12A_1\Delta\Delta_xA_2^*\right)}{64\Delta^3} \\
& +\frac{\Delta_x\left(-4\Delta_xA_1'(B_2+3C_2)+4A_1B_2\Delta_x+\Delta_z^-\left(3C_1C_2^*+2i(B_1C_2''+B_2C_1'')\right)\right)}{64\Delta^3} \\
& +\frac{3\Delta_xi\left(12A_1\Delta_x^2C_2'+3C_1^*\Delta_z^-\left(2A_2\Delta-C_2\Delta_x\right)+(2B_1\Delta A_2''\Delta_z^-+3iC_1\Delta A_2^*\Delta_z^-)\right)}{64\Delta^3}\ ,
\end{aligned}
$$

$$\tag{4.39}$$

$$
\begin{aligned}
\tilde{\mathcal{H}}_{13} =\ & \frac{2\left(\Delta_z^z(B_2\Delta_x(B_1-3C_1')-3B_1(2\Delta_zA_2'+\Delta_xC_2'))-6B_2\Delta_x^2A_1'\right)}{64\Delta^2} \\
& +\frac{9\Delta_xC_2^*(2A_1\Delta_x+C_1\Delta-C_1\Delta_z)+9C_1^*\Delta_z^-(2A_2\Delta_z+C_2\Delta_x)}{64\Delta^2} \\
& +\frac{18\Delta_xA_1^*(2A_2\Delta_z+C_2\Delta_x)+18\Delta_zA_2^*(2A_1\Delta_x+C_1\Delta-C_1\Delta_z)}{64\Delta^2}\ ,
\end{aligned}
$$

$$\tag{4.40}$$

$$
\begin{aligned}
\tilde{\mathcal{H}}_{23} =\ & \frac{3i\left(2i(\Delta_x(\Delta_z^-(B_1C_2''+B_2C_1''')+2iB_2\Delta_xA_1')+2iB_1\Delta_zA_2'\Delta_z^-)\right)}{64\Delta^2} \\
& +\frac{12i\left(A_1B_2\Delta_x^2+A_2B_1\Delta_z\Delta_z^-\right)+9i\Delta_xC_2^*(2A_1\Delta_x-C_1\Delta+C_1\Delta_z)}{64\Delta^2} \\
& +\frac{3i\left(6\Delta_zA_2^*(-2A_1\Delta_x-C_1\Delta+C_1\Delta_z)-6\Delta_xA_1^*(C_2\Delta_x-2A_2\Delta_z)\right)}{64\Delta^2} \\
& +\frac{3i\left(3C_1^*\Delta_z^-(2A_2\Delta_z+C_2\Delta_x)\right)}{64\Delta^2}\ ,
\end{aligned}
$$

$$\tag{4.41}$$

$$\tilde{\mathcal{H}}_{11} = \frac{2(6B_2\Delta_x\Delta_z A_1' - \Delta_z^-(6B_1\Delta_x A_2' + B_2\Delta_z(B_1 - 3C_1') - 3B_1\Delta_z C_2'))}{32\Delta^2}$$
$$+\frac{18\Delta_x A_2^*(2A_1\Delta_x + C_1\Delta - C_1\Delta_z) - 9C_1^*\Delta_z^-(C_2\Delta_z - 2A_2\Delta_x)}{32\Delta^2}$$
$$+\frac{18\Delta_x A_1^*(2A_2\Delta_x - C_2\Delta_z) + 9\Delta_z C_2^*(-2A_1\Delta_x - C_1\Delta + C_1\Delta_z)}{32\Delta^2},$$

$$(4.42)$$

$$\tilde{\mathcal{H}}_{22} = -\frac{9C_2^*(2A_1\Delta_x - C_1\Delta + C_1\Delta_z) + 18C_2\Delta_x A_1^* + 9C_2 C_1^*\Delta_z^-}{32\Delta^2}$$
$$+\frac{2(6B_2\Delta_x A_1' + \Delta_z^-(B_1(B_2 + 3C_2') + 3B_2 C_1'))}{32\Delta^2},$$

$$(4.43)$$

$$\tilde{\mathcal{H}}_{33} = 0, \tag{4.44}$$

and the rest of the components $\tilde{\mathcal{H}}_{ij}$ are obtain from $\tilde{\mathcal{H}}_{ji}$ by exchanging $i \leftrightarrow j$.

Part II

Self-Correcting Quantum Memories and Long-Range Interactions

CHAPTER 5

Introduction

Realizing qubits with long coherence time is a basic requirement for quantum information processing. [88] A promising strategy to achieve this goal is to make use of quantum error correcting codes, where a single logical qubit is represented by suitable entangled states of a collection of many spins. This allows to detect and correct a finite number of errors acting on the individual physical spins of the code. [11] Furthermore, if the quantum code is the ground space of a gapped Hamiltonian, errors in the memory lead to excitations in the spin system and they can be suppressed at low temperature. In this respect, stabilizer Hamiltonians (given by a sum of mutually commuting Pauli operators) are of special importance [11, 89] and a particularly interesting class are stabilizer Hamiltonians with topological order, where the distance of the code grows as a power of the system size L (see Refs. [12, 90] for a rigorous definition of topological quantum order and the consequences on the stability of the ground subspace under local Hamiltonian perturbations). Models with topological order were already known in the context of lattice gauge theory [91, 92] and a pioneering example applied to quantum information is the toric code proposed by Kitaev. [14]

However, several limitations of this type of models appear when put in contact with an external environment. [15, 16, 93, 94, 95, 96, 97, 98, 99, 100, 101, 102, 103] Most importantly, it was shown that at any finite temperature the lifetime of the toric code does not grow with system size. [15, 16, 94, 95] This is a generic feature of stabilizer Hamiltonians with short-range interactions in one and two dimensions since, while the distance of the code increases with L, the energy barrier to perform a logical error is bounded by a constant. Indeed, it was shown that not only the

toric code but a large class of 1-, 2-, and 3-dimensional Hamiltonians suffer from the aforementioned thermal instability of quantum information. [98, 104, 105] This is in contrast to the classical case, where magnetic devices allow the construction of self-correcting hard drives that are stable against both local perturbations and thermal excitations. In the case of the toric code, the excitations of the system can be represented as pairs of classical diffusing anyons and the aforementioned energy barrier is simply the energy cost to create a single anyon pair. Therefore, it is of crucial importance to devise new architectures where such gap is enhanced and the anyon population is exponentially suppressed. A four-dimensional generalization of the toric code has been proposed and studied [15, 106]. In this model, the logical operators are membranes and not strings, and therefore the energy barrier to perform a logical operation increases with the size of the memory. This is the only model that is truly self-correcting and that has a lifetime growing exponentially with L. Unfortunately, this models is not directly realizable in our three-dimensional space. Proposals for three-diemnsional spin Hamiltonians with local few-spin interactions that do not fall victim to the aforementioned no-go results exist [107, 108, 109, 110] but none of them is expected to allow for a storage time increasing arbitrarily with system size

On the positive side, it has been shown that repulsive long-range interactions between anyons lead to storage times that grow polynomially in L. [16, 111, 112, 113] The toric code can be realized as a low-energy effective Hamiltonian of the Kitaev honeycomb model, [27, 114] and long-range interactions between anyons appear in the presence of a non-local coupling with cavity modes extending over the whole memory. [16] Such memories are called *self-correcting*, as their stability against errors caused by the thermal environment is "built in" in the sense that no active (measurement-based) error correction is required. In similar approaches, long-range attractive interaction between anyons as a way to suppress their motion across the memory has been proposed in Ref. [15] and later studied in Ref. [97] by coupling the toric code to a bosonic bath. In this case the diffusion of anyons is reduced by the attractive interaction and the memory lifetime increases polynomially with L, but the model requires unbounded-strength interactions between anyon operators and the bosonic bath [97]. References [115, 116] studied disorder as a means to hinder quantum propagation of anyons.

In Chapter 6, we propose a way to engineer the replulsive long-range interactions between anyons of the toric code. Anyon-anyon interactions correspond to eight-body interactions and as such cannot directly be realized in nature. We thus start from the honeycomb model (involving only

two-body interactions) and introduce a linear modification of the Ising interactions due to the presence of quantized cavity fields. This allows to control the properties of the low-energy toric code Hamiltonian, which can serve as a quantum memory, by tuning the physical parameters of the cavity modes, like frequencies, photon occupations, and coupling strengths. We study the properties of the model perturbatively by making use of the Schrieffer-Wolff transformation and show that, depending on the specific setup, the cavity modes can be useful in several ways. They allow to detect the presence of anyons through frequency shifts and to prolong the lifetime of the memory by enhancing the anyon excitation energy or mediating long-range anyon-anyon interactions with tunable sign.

In Chapter 7, we propose the first model for a self-correcting quantum memory that satisfies all the criteria listed in Section 1. This is achieved by locally coupling a 2D toric code to a 3D system. We propose to embed the toric code into a 3D cubic lattice of hopping bosons. The stabilizer operators of the toric code are then locally coupled to the bosonic annihilation and creation operators. This system is closely related to another model that we study, namely a toric code coupled to a 3D bulk ferromagnet in a broken-symmetry state at finite temperature. In both cases an effective Hamiltonian is derived for the toric code in which the energy penalty required to create anyons grows linearly with L, and thus the lifetime of the quantum memory grows exponentially with L (for the ferromagnet this is true only in the presence of sufficiently slow thermal noise). While we make use of perturbation theory to study the toric code coupled to the FM, the coupling to the hopping boson system is exactly solvable via a polaron transformation.

Before going into more details, we would like to present the main aspects of the two-dimensional toric code as it is an essential building block of the following models. Our discussion is mainly based on Refs. [14, 15].

5.1 The toric code

The toric code [13, 14] of linear size L consists of $2L^2$ spin-$1/2$ qubits located at each edge of a square lattice with toric boundary conditions, see Fig. 5.1. Associated to each square unit cell of the lattice, define a plaquette p as the union of the four sites around the corresponding unit cell. Similary, a star s is defined as the union of the four sites surrounding

vertex s. Associated to each plaquette and star we define the operators

$$Z_p = \prod_{i\in\text{plaquette}(p)} \sigma_i^z \quad \text{and} \quad X_s = \prod_{i\in\text{star}(s)} \sigma_i^x\,. \tag{5.1}$$

Here $\boldsymbol{\sigma}_i = (\sigma_i^x, \sigma_i^y, \sigma_i^z)$ are the usual Pauli operators. The plaquette and star operators mutually commute, commute with each other, and have eigenvalues ± 1. We can thus define the following frustration free Hamiltonian

$$H = -J\sum_p Z_p - J\sum_s X_s\,, \tag{5.2}$$

where $J > 0$. The ground state manifold of H is the space $\mathcal{L}$ of states that are invariant under the action of Z_p and X_s,

$$\mathcal{L} = \{|\Omega_0\rangle \ : \ Z_p|\Omega_0\rangle = X_s|\Omega_0\rangle = |\Omega_0\rangle,\ \forall\, p, s\}\,. \tag{5.3}$$

We refer to Z_p and X_s as *stabilizer operators*. We identity $\mathcal{L}$ as the *code subspace* where the quantum information is encoded. As a side remark, note that the toric code is a specific example of the more general *stabilizer codes* [11] and the corresponding *stabilizer Hamiltonians* are defined by a sum of commuting Pauli operators.

A straightforward counting argument allows one to conclude that $\dim(\mathcal{L}) = 4$ and therefore that two logical qubits can be stored in $\mathcal{L}$. Indeed, the number of spins being $2L^2$ the dimension of the Hilbert space is 2^{2L^2}. However, only $2L^2 - 2$ stabilizers are independent since

$$\prod_s X_s = \prod_p Z_p = 1\,. \tag{5.4}$$

Therefore, the dimension of $\mathcal{L}$ is given by $2^{2L^2}/2^{2L^2-2} = 4$. More generally, when the lattice resides on a surface with genus g, the ground-state degeneracy is 4^g.

Define *logical operators* as the operators that cause transitions between the states of the logical qubits. From Eq. (5.3), we infer that the logical operators must commute with all stabilizers but cannot be written as products of Z_p' s and X_s's.

Define the path operators

$$S^x(\ell) = \prod_{i\in\ell} \sigma_i^x \qquad \text{and} \qquad S^z(\ell) = \prod_{i\in\ell} \sigma_i^z\,, \tag{5.5}$$

where the path $\ell = \{i_1, i_2, \ldots, i_n\}$ is a (ordered) sequence of nearest-neighbor sites. By definition, when $\ell = \ell_c$ is a loop, then $S^{x,z}(\ell_c)$ commute

with all stabilizer operators. However, one needs to distinguish between two kinds of loops: topologically trivial (i.e. contractible) loops ℓ_c^t and topologically nontrivial (i.e. non-contractible) loops ℓ_c^{nt}. It is easy to show that the operators $S^x(\ell_c^t)$ and $S^z(\ell_c^t)$ can always be written as a product of stabilizers and thus that they act trivially on the code subspace. On the contrary, operators of the form $S^x(\ell_c^{nt})$ and $S^z(\ell_c^{nt})$ commute with all stabilizer operators but are not generated by products of X_s's and Z_p's. We thus define

$$X_{1,2} = \prod_{i \in \ell_{1,2}} \sigma_i^x \qquad \text{and} \qquad Z_{1,2} = \prod_{i \in \ell'_{1,2}} \sigma_i^z, \qquad (5.6)$$

as the four logical operators, with $\ell_{1,2}$ and $\ell'_{1,2}$ topologically nontrivial, see Fig. 5.1. We thus conclude that local operations do not allow to distinguish between the states of the logical qubits and highly non-local operations are required. In connection to this, it has been demonstrated in Ref. [12] that Hamiltonian (5.2) is protected against sufficiently weak, local, and static perturbations of the Hamiltonian; the effect of such perturbations on the energy splitting of the ground-state manifold is exponentially suppressed with the linear size L of the lattice. The toric code thus represents a stable quantum memory at zero temperature.

Quasiparticle-like Excitations and Error Correction

A state $|\Psi\rangle$ carries a quasiparticle-like excitation whenever it exsists a plaquette p_1 or a star s_1 such that $Z_{p_1}|\Psi\rangle = -|\Psi\rangle$ or $X_{s_1}|\Psi\rangle = -|\Psi\rangle$. On the torus, due to condition (5.4), excitations can only be created in pairs. Since σ_i^x anticommutes with two Z_p's and σ_j^z anticommutes with two X_s's, a two-particle state takes the form

$$|\Psi(\ell)_x\rangle = S^x(\ell)|\Omega_0\rangle \qquad \text{or} \qquad |\Psi(\ell)_z\rangle = S^z(\ell)|\Omega_0\rangle, \qquad (5.7)$$

where ℓ is an open path on the lattice. The operators $S^x(\ell)$ and $S^z(\ell)$ correspond to strings of bit-flip errors σ_i^x and phase errors σ_i^z respectively. The operator $S^x(\ell)$ creates two excited plaquettes at the ends of the path ℓ, these are x-type excitations. Similarly, the operator $S^z(\ell)$ creates two excited stars at the ends of ℓ, these are z-type excitations. From Eq. (5.2) we infer that the energy to create a pair of excitations is $4J$ and that it does not require any further energy to separate the quasiparticles. Both z- and x-type excitations are (abelian) *anyons* as their statistics is neither bosonic, nor fermionic. Consider the initial state $|\psi_i\rangle = S^x(\ell)S^z(\ell')|\Omega_0\rangle$
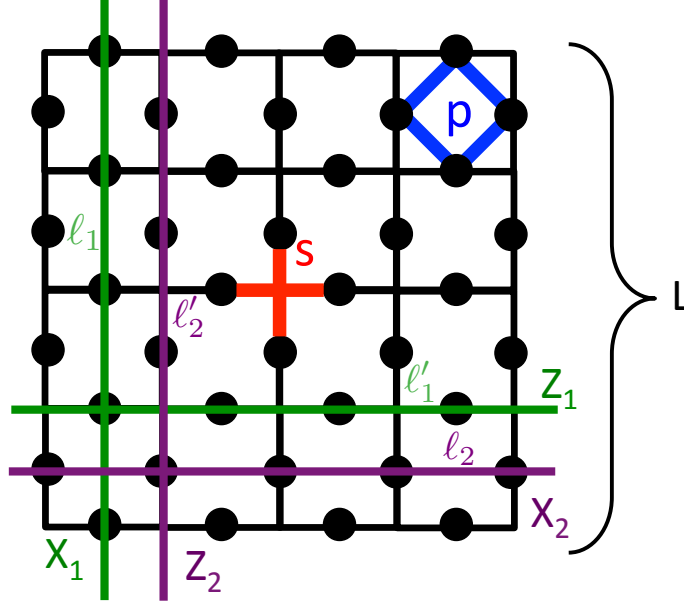
Figure 5.1: Toric code lattice. The black dots represent spin-$1/2$ particles residing on each edge of the quadratic lattice with toric boundary conditions. Associated to each plaquette p and star s we define plaquette operators Z_p and star operators X_s as in Eq. (5.1). The four logical operators $X_{1,2}$ ands $Z_{1,2}$ are defined in (5.6) and are associated to the topologically nontrivial loops $\ell_{1,2}$ and $\ell'_{1,2}$.

containing two x-type particles at the end of path ℓ and two z-type particles at the end of path ℓ'. Apply an operator $S^z(c)$ that moves one of the z-type particles around a x-type particle along a topologically trivial loop c. Since ℓ and c have an odd number of sites in common, it is clear that $\{S^z(c), S^x(\ell)\} = 0$. The final state reads

$$\begin{aligned}
|\psi_f\rangle &= S^z(c)S^x(\ell)S^z(\ell')|\Omega_0\rangle = -S^x(\ell)S^z(c)S^z(\ell')|\Omega_0\rangle \\
&= -S^x(\ell)S^z(\ell')|\Omega_0\rangle = -|\psi_i\rangle,
\end{aligned} \tag{5.8}$$

where we have used the facts that $[S^z(c), S^z(\ell)] = 0$ and $S^z(c)$ can be written as a product of Z_p's.

Let us now consider a general loop ℓ_c. The operators $S^{x,z}(\ell_c)$ do not produce any anyons and $S^{x,z}(\ell_c)|\Omega_0\rangle$ is a groundstate of H. We are thus interested in the effect of such loops of bit-flip or phase errors (that we now generically call physical errors) on the code subspace. Again we have to disitnguish between trivial loops ℓ_c^{t} and nontrivial loops ℓ_c^{nt} of

physical errors. Trivial loops cross $\ell_{1,2}$ and $\ell'_{1,2}$ an even number of times and $S^{x,z}(\ell_c^{\mathrm{t}})$ commutes with all logical operators. Nontrivial loops do not cross all the paths $\ell_{1,2}$ and $\ell'_{1,2}$ an even number of times; $S^{x,z}(\ell_c^{\mathrm{nt}})$ anticommutes with one logical operator and implements a logical error in the code subspace $\mathcal{L}$. Since the weight of the minimal-weight Pauli operator that induces transitions between states in $\mathcal{L}$ is L, we say that the toric code has *distance* L.

Error Correction and Thermal Stability

Assume that the the toric code is subject to random bit-flip errors (X) and phase errors (Z) with probability p, namely

$$\rho \to (1-p)^2 I\rho I + p(1-p)X\rho X + p(1-p)Z\rho Z + p^2 Y\rho Y . \tag{5.9}$$

Such an error scheme leads to creation of anyons, to annihilation of existing anyons, or to hopping of an anyon to a nearby plaquette or star.

Here we summarize how error correction is envisioned. After a certain time, the external observer measures the position of the excitations outputs an error syndrome. It is assumed that the position of anyons can be measured but no additional information about the actual position of the strings of physical errors can be extracted. In order to return into the groundsubspace, the external observer performs an error correcting scheme which consists in annihilating pairs of ayons. In doing so, the observer involves either only topologically trivial loops or some topologically nontrivial loops of physical errors. In the first scenario the original stored quantum information is retrieved, while in the second scenario a logical operator is applied onto the code subspace and the stored quantum information is lost.

For the error channel (5.9), the toric code can be mapped to a random-bond Ising model. [15] This procedure allows one to derive a critical fraction of physical errors $f_c = 0.11$. Below f_c, error correction succeeds with probability one in the thermodynamic limit. Above f_c retrieval of the stored quantum information is not possible.

In the presence of thermal environment, it it has been shown that the toric code does not represent a stable quantum memory (see discussion above for a list of references). Here we follow the same line of reasoning as in Ref. [16] and explain intuitively the reason for such a thermal fragility. The coupling of the toric code to a thermal bath leads to creation of anyon pairs with rate $\gamma(-4J)$, to annihilation of existing anyon pairs with a rate $\gamma(4J) = \gamma(-4J)e^{4J\beta}$ (detailed balance condition), and to

hopping of an anyon to a nearest-neighbor site with rate $\gamma(0)$ (that we assume to be different than zero). The precise form of the rates γ depends on the precise nature of the thermal environment. Assume that N anyons are present in the system. After a time t, the fraction f of physical errors can be estimated to be

$$f \approx N\gamma(0)t/2L^2\,.\tag{5.10}$$

As we argued above, error correction fails for $f \geq f_c$, or in other words after a time

$$\tau \approx 2f_c\frac{e^{\beta J} + 1}{\gamma(0)}\,,\tag{5.11}$$

where the density of anyons $N/L^2 = 1/(e^{\beta J} + 1)$ is given by the Fermi-Dirac distribution at temperature $T = 1/\beta$. From Eq. (5.11) we infer that the lifetime τ does not depend on the size of the memory and thus cannot be improved by increasing L. This negative result has its origin in the fact that as soon as a pair of anyons is created at constant energy cost $4J$, the anyons can move through the whole memory without additional energy penalty. In other words the energy barrier to perform a logical operation is constant.

The scope of Part II is to modify Hamiltonian (5.2) in order to make the quantum memory stable against thermal noise. In particular, in Chapter 7 we propose a model that satisfies all the four criteria for a self-correcting quantum memory presented in Chapter 1.

Quantum Memory Coupled to Cavity Modes

Inspired by spin-electric couplings in molecular magnets, we introduce in the Kitaev honeycomb model a linear modification of the Ising interactions due to the presence of quantized cavity fields. This allows to control the properties of the low-energy toric code Hamiltonian, which can serve as a quantum memory, by tuning the physical parameters of the cavity modes, like frequencies, photon occupations, and coupling strengths. We study the properties of the model perturbatively by making use of the Schrieffer-Wolff transformation and show that, depending on the specific setup, the cavity modes can be useful in several ways. They allow to detect the presence of anyons through frequency shifts and to prolong the lifetime of the memory by enhancing the anyon excitation energy or mediating long-range anyon-anyon interactions with tunable sign. We consider both resonant and largely detuned cavity modes.

6.1 Introduction

In analogy to the spin-electric coupling in molecular magnets, [117, 118, 119] we consider a modification of the Ising couplings of the type $J_{x,y} \to J_{x,y} + \delta_{x,y}(a + a^\dagger)$. In this paper we study in detail the effect of such a coupling in the honeycomb model by making use of perturbation theory and show that cavity modes can be useful in several ways, not only to mediate long-range interactions between anyons.

For example, they allow to realize a basic operation such as the read-out of the error syndrome or, in other words, to detect the presence of anyons across the memory. To achieve this, it is sufficient to couple locally a single cavity mode to the desired read-out site and to detect its frequency shift, similar to a scheme demonstrated for superconducting qubits. [120, 121] As we will see in the next sections, a single cavity mode can also be used to resonantly enhance the anyon gap while, to generate an anyon-anyon interaction of the desired sign, two cavity modes are required. Such a variety of situations corresponds to different specific configurations for the interaction between the cavity modes and the spin model, which we analyze by making use of perturbation theory. Our work is based on the Schrieffer-Wolff transformation, [122, 75] which can be easily applied to the Kitaev honeycomb model, even in the presence of cavity modes, to obtain explicit expressions for the parameters of the quantum memory.

The detailed outline of the paper is as follows: we start with Sec. 6.2 by introducing the model Hamiltonian and discuss the physical motivation of the coupling. We then describe in Sec. 6.3 the perturbative framework in general terms. In Sec. 6.4 we consider different read-out schemes. In Sec. 6.5 we study the enhancement of the gap produced by a single resonant cavity mode. In Sec. 6.6 we obtain long-range anyon-anyon interactions from a specific coupling scheme with two resonant cavity modes. We conclude with Sec. 6.7 by studying the effect of off-resonant cavity modes and present in Appendices 6.A-6.D an extended discussion of several technical aspects and derivations.

6.2 Model

The Kitaev honeycomb model [27] is a two dimensional version of the quantum compass model defined on a Honeycomb lattice. [29, 31] It consists of $2N$ spin-$1/2$ particles located at the sites of a honeycomb lattice with nearest-neighbor Ising interactions and is illustrated in Fig. 6.1b).
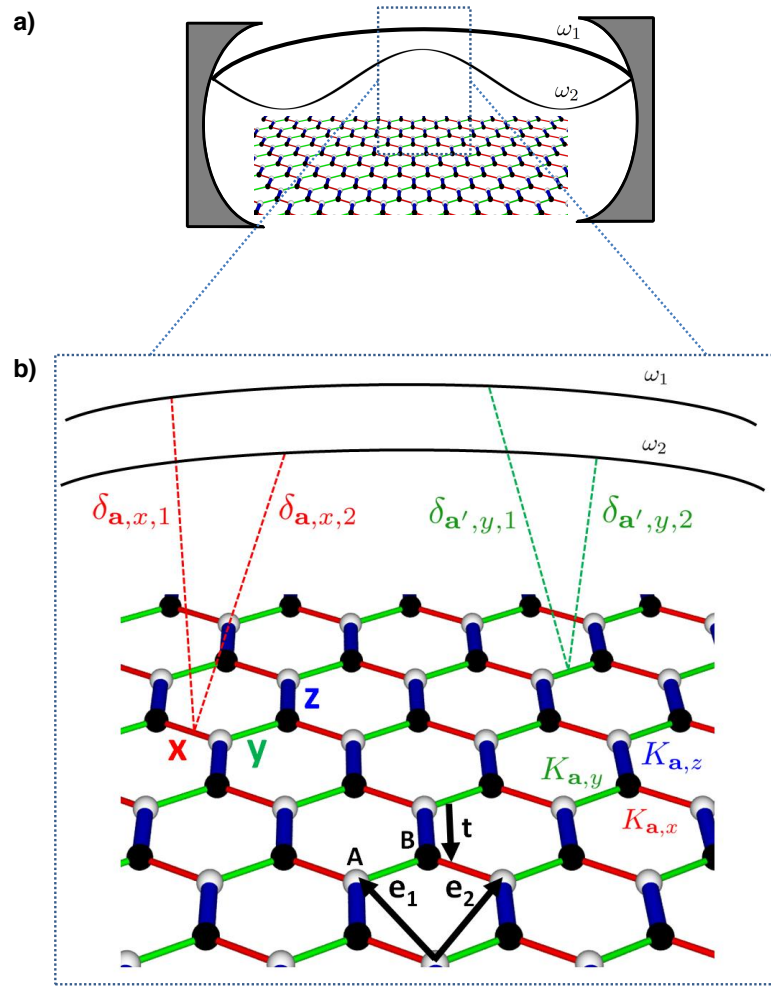
Figure 6.1: Illustration of the Kitaev honeycomb model with cavity modes. a) Schematic view of the honeycomb model at the center of an optical or microwave cavity. The two shaded areas represent mirrors and the curves in the middle two quantized cavity modes with frequencies $\omega_{1,2}$ to which the spin model couples according to Eq. (6.2). b) Kitaev honeycomb lattice. The spins are represented by white or black dots respectively belonging to the A or B sublattice. Ising interactions of type $\sigma^x\sigma^x$ along x-links (red), $\sigma^y\sigma^y$ along y-links (green), or $\sigma^z\sigma^z$ along z-links (blue) are represented by colored links with different directions (see the upmost schematic diagram). Strongly interacting z-dimers are depicted by thick blue links and form a lattice with basis vectors $\boldsymbol{e}_{1,2}$ while $\boldsymbol{t}$ is a vector which connects A- and B- sublattice sites. Cavity modes (here, two of them, with frequencies $\omega_{1,2}$) modify the Ising interactions of certain links (as indicated by dashed lines), according to Eq. (6.2).

The interaction between two neighboring spins is either $\sigma^x \sigma^x$, $\sigma^y \sigma^y$, or $\sigma^z \sigma^z$, depending on the direction of the link connecting the two spins. In this work we are interested in the limit when the $\sigma^z \sigma^z$-couplings are much stronger than the other ones. Therefore, the model can be seen as consisting of N weakly coupled dimers, forming a triangular lattice with unit vectors $e_{1,2}$, as shown in Fig. 6.1b).

In this work, we consider the following generalization of the Kitaev honeycomb Hamiltonian

$$
\begin{aligned}
H \;=\; & \sum_\alpha \omega_\alpha a_\alpha^\dagger a_\alpha - \sum_{\boldsymbol{a}} K_{\boldsymbol{a},z} \sigma_{\boldsymbol{a}}^z \sigma_{\boldsymbol{a}+\boldsymbol{t}}^z \\
& - \sum_{\boldsymbol{a}} K_{\boldsymbol{a},x} \sigma_{\boldsymbol{a}}^x \sigma_{\boldsymbol{a}+e_1+\boldsymbol{t}}^x - \sum_{\boldsymbol{a}} K_{\boldsymbol{a},y} \sigma_{\boldsymbol{a}}^y \sigma_{\boldsymbol{a}+e_2+\boldsymbol{t}}^y,
\end{aligned}
\tag{6.1}
$$

where the three last sums run over all vectors $\boldsymbol{a} = n_1 e_1 + n_2 e_2$ ($n_{1,2} \in \mathbb{Z}$) pointing to a A-sublattice site (white dots), $\boldsymbol{t}$ is a vector which connects A- (white dots) and B- (black dots) sublattice sites and $\sigma^{x,y,z}$ are the usual spin Pauli operators. In Eq. (6.1), we have assumed that the Ising couplings $K_{\boldsymbol{a},k}$ (with $k = x, y, z$) are site dependent. Furthermore, we introduced a collection of cavity modes labeled by α, with frequency ω_α, and annihilation operators a_α. We propose that they are coupled to the spin model as follows:

$$
K_{\boldsymbol{a},k} = J_{\boldsymbol{a},k} + \sum_\alpha \delta_{\boldsymbol{a},k,\alpha}(a_\alpha + a_\alpha^\dagger),
\tag{6.2}
$$

where $J_{\boldsymbol{a},k}$ are the unperturbed Ising couplings, and $\delta_{\boldsymbol{a},k,\alpha}$ describe the linear change due to the cavity modes (see Fig. 6.1). The original Kitaev model is recovered for $\delta_{\boldsymbol{a},k,\alpha} = 0$ and $J_{\boldsymbol{a},k} = J_k$, independent of the lattice site. For simplicity, we also assume in the rest of this work $K_z = J_z$, but we keep the more general form of coupling [Eq. (6.2)] for $K_{\boldsymbol{a},x}$ and $K_{\boldsymbol{a},y}$.

To physically justify Eq. (6.2), we note that Ising couplings can be engineered in a variety of systems, for example between quantum dots, [123] Josephson Junction qubits, [124, 125, 32], atoms in optical lattices, [30, 126] and doped coupled cavities.[127] Anisotropic spin interactions are also present in molecular magnets [117, 118, 119] and between pseudo-spin orbital states. [29] Recently, theoretical proposals to engineer the honeycomb model in Mott insulators with strong spin-orbit coupling were discussed in Refs. [31, 128]. Metal-oxide compounds (layered iridates of type $A_2\text{IrO}_3$, with $A = \text{Li}, \text{Na}$) were considered there as promising materials. In these systems, the strength of the magnetic interaction
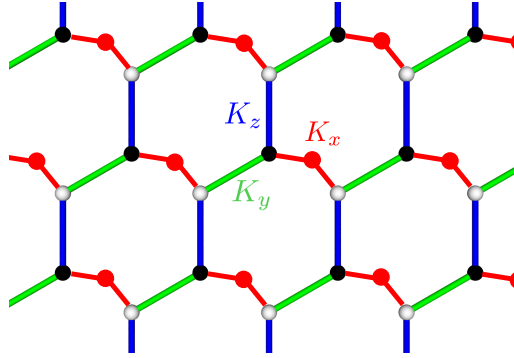
Figure 6.2: Pictorial representation of superexchange interactions. The bridge sites (dots in the middle of each x-link) mediate the magnetic $\sigma^x \sigma^x$ interactions between the spins (dots at each site of the honeycomb lattice). Here, the x-links have a nonvanishing dipole moment and can thus be linearly coupled to external electric fields. By controlling the equilibrium position of the bridge sites, the coupling to the cavity modes can in principle be tuned locally.

can be modified by external perturbations, in particular electric and magnetic fields. [125, 123, 117, 118, 119] Such perturbations can be generated by charged nanomechanical systems (e.g., cantilevers) or quantized electromagnetic fields (e.g., in cavities and transmission line resonators [120, 121, 129]), thus realizing a coupling of the type of Eq. (6.2). As a more specific example, we would like to mention molecular magnets. In this case, electric fields can be used to modify the overlap of the orbital wavefunctions and thus the resulting magnetic interactions, which are determined by exchange or super-exchange mechanisms. Strongly anisotropic (Ising-like) magnetic interactions can arise here in the presence of spin-orbit coupling. [117, 118, 119]

A linear effect in the electric field, as in Eq. (6.2), can only exist if the electric-dipole of the underlying bond is not zero or, in other terms, if the inversion symmetry of that bond is broken. This is illustrated in Fig. 6.2 for the x-links, assuming the presence of superexchange interactions mediated via an auxiliary site (the so-called bridge site). Figure 6.2 also illustrates that only selected links can be coupled to the cavity modes since y- and z-bonds have no dipole moment and thus $\delta_{\boldsymbol{a},k,\alpha} = 0$. Finally, Fig. 6.2 suggests that $\delta_{\boldsymbol{a},k,\alpha}$ can be controlled locally. By realizing Fig. 6.2 in a quantum dot setup, $\delta_{\boldsymbol{a},k,\alpha}$ could be made zero or not by changing the equilibrium position of the bridge sites with static electric gates.
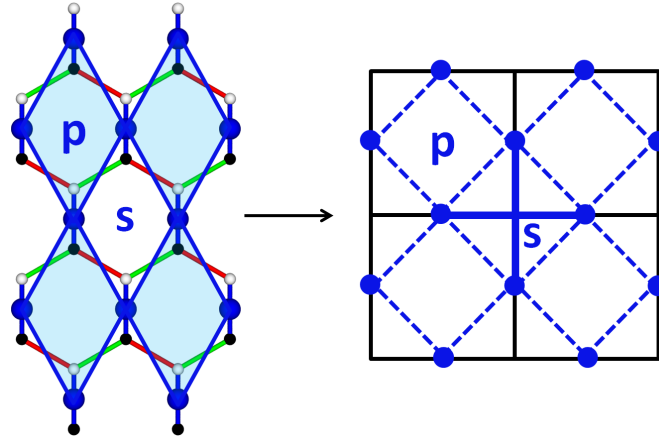
Figure 6.3: Mapping of the Kitaev honeycomb model to the toric code. Left-hand side: each z-dimer, formed by a black and a white spin [see also Fig. 6.1b)], corresponds to a new lattice site (large blue dots). To these new sites, hard-core bosons and effective spins are associated. A low-energy (zero hard-core bosons) toric code Hamiltonian for the effective spins is obtained by perturbation theory. The resulting toric code model is schematically illustrated on the right-hand side. The dark and white unit cells on the left-hand-side correspond now to plaquette (p) and star (s) operators, respectively.

6.3   Perturbative approach

Exact results for the Kitaev honeycomb model exist for arbitrary values of $J_{x,y,z}$ [27] but they do not include couplings to the cavity modes. Therefore, we study Eq. (6.1) with perturbation theory. This is indeed appropriate if the model is intended to be a quantum memory, since for $J_{x,y} \ll J_z$ the honeycomb model can be mapped to the toric code. [27, 114] Without cavity modes, perturbative treatments of the honeycomb model can be found in Ref. [27] where the author makes use of Green's functions, and more recently in Ref. [114] with the perturbative continuous unitary transformation method. [130, 131] This work is based on a different approach, namely on the Schrieffer-Wolff (SW) transformation, [122, 75] which can be applied in a straightforward way to Eq. (6.1), as we will see in the next sections.

Hard-core boson transformation

The first step of our analysis consists in the hard-core boson transformation presented in Ref. [114], which maps each z-dimer to a particle and an effective spin, see Fig. 6.3. The two spins of each z-dimer can be either parallel or anti-parallel and, if we assume that $J_z > 0$, the parallel configuration has lower energy than the anti-parallel one. The excited dimers can thus be in terpreted as particles (hard-core bosons) with energy $2J_z$, and the remaining degree of freedom as an effective spin-1/2. More explicitly:

$$| \uparrow \rangle_a \otimes | \uparrow \rangle_{a+t}, = | \Uparrow 0 \rangle_a, \qquad | \downarrow \rangle_a \otimes | \downarrow \rangle_{a+t} = | \Downarrow 0 \rangle_a,$$
$$| \downarrow \rangle_a \otimes | \uparrow \rangle_{a+t} = | \Uparrow 1 \rangle_a, \qquad | \uparrow \rangle_a \otimes | \downarrow \rangle_{a+t}, = | \Downarrow 1 \rangle_a,$$

where the four possible spin configurations of a given dimer (left-hand sides) are mapped to states with $0, 1$ hard-core boson and $\Downarrow, \Uparrow$ effective spin. If we rewrite the above transformation in operator language we obtain

$$\begin{aligned}
\sigma^x_{a+t} &= \tau^x_a(b^\dagger_a + b_a), & \sigma^x_a &= b^\dagger_a + b_a, \\
\sigma^y_{a+t} &= \tau^y_a(b^\dagger_a + b_a), & \sigma^y_a &= i\tau^z_a(b^\dagger_a - b_a), \\
\sigma^z_{a+t} &= \tau^z_a, & \sigma^z_a &= \tau^z_a(1 - 2b^\dagger_a b_a),
\end{aligned} \qquad (6.3)$$

where $b^\dagger_a$ (b_a) creates (destroys) a hard-core boson and $\tau^{x,y,z}_a$ are the Pauli operators of the effective spin-1/2 at site a. At distinct sites a and a', bosonic commutation relations are satisfied:

$$[b_a, b^\dagger_{a'}] = 0, \qquad \mathrm{i}f\ a \neq a'. \qquad (6.4)$$

Furthermore, $\{b_a, b^\dagger_a\} = 1$.

By making use of these bosonic operators, we can rewrite the first line of Eq. (6.1) simply as

$$H_0 = \sum_\alpha \omega_\alpha a^\dagger_\alpha a_\alpha + 2J_z \sum_a b^\dagger_a b_a, \qquad (6.5)$$

which represents the unperturbed Hamiltonian. Here and in the rest of the paper we drop an inessential constant $-J_z N$.

Perturbation operators

We now consider the second line of Eq. (6.1), which constitutes our perturbation. By rewriting the spin operators by making use of Eq. (6.3), we obtain that Eq. (6.1) takes the following form

$$H = H_0 + T_0 + T_{-2} + T_{+2}, \qquad (6.6)$$

where

$$T_0 = -\sum_{\boldsymbol{a},k}(K_{\boldsymbol{a},k}t_{\boldsymbol{a},k} + \text{h.c.}) := f_0(K_{\boldsymbol{a},k}), \tag{6.7}$$

$$T_{+2} = -\sum_{\boldsymbol{a},k} K_{\boldsymbol{a},k}v_{\boldsymbol{a},k} := f_{+2}(K_{\boldsymbol{a},k}), \tag{6.8}$$

$$T_{-2} = (T_{+2})^\dagger := f_{-2}(K_{\boldsymbol{a},k}), \tag{6.9}$$

with $k = x, y$. As in Ref. [114], we defined the hopping operators

$$t_{\boldsymbol{a},x} = b^\dagger_{\boldsymbol{a}+\boldsymbol{e}_1}b_{\boldsymbol{a}}\tau^x_{\boldsymbol{a}+\boldsymbol{e}_1}, \tag{6.10}$$

$$t_{\boldsymbol{a},y} = -ib^\dagger_{\boldsymbol{a}+\boldsymbol{e}_2}b_{\boldsymbol{a}}\tau^y_{\boldsymbol{a}+\boldsymbol{e}_2}\tau^z_{\boldsymbol{a}}, \tag{6.11}$$

and the hard-core boson creation operators

$$v_{\boldsymbol{a},x} = b^\dagger_{\boldsymbol{a}+\boldsymbol{e}_1}b^\dagger_{\boldsymbol{a}}\tau^x_{\boldsymbol{a}+\boldsymbol{e}_1}, \tag{6.12}$$

$$v_{\boldsymbol{a},y} = ib^\dagger_{\boldsymbol{a}+\boldsymbol{e}_2}b^\dagger_{\boldsymbol{a}}\tau^y_{\boldsymbol{a}+\boldsymbol{e}_2}\tau^z_{\boldsymbol{a}}. \tag{6.13}$$

In other words, $T_{+2(-2)}$ creates (destroys) two nearest-neighbor hard-core bosons and T_0 makes a hard-core boson hop to a nearest-neighbor unoccupied dimer.

It is also useful to keep track of the change in the number of photons: whenever a hard-core boson is created, destroyed, or hops from one site to another, a photon might be simultaneously created or destroyed. Therefore, we introduce $T^{m\alpha}_n$ operators, where the lower label ($n = 0, \pm2$, as before) refers to the change in the number of hard-core bosons, while the upper label ($m = 0, \pm1$) indicates that the number of photons in mode α changes by m. Such operators are simply defined by substituting in Eqs. (6.7-6.9) the full couplings $K_{\boldsymbol{a},k}$ by the appropriate quantity, $J_{\boldsymbol{a},k}$, $\delta_{\boldsymbol{a},k,\alpha}a_\alpha$, or $\delta_{\boldsymbol{a},k,\alpha}a^\dagger_\alpha$. By using the notation introduced in Eqs. (6.7-6.9), which define the f_n functions, we can write

$$T^0_n = f_n(J_{\boldsymbol{a},k}), \tag{6.14}$$

$$T^{+\alpha}_n = f_n(\delta_{\boldsymbol{a},k,\alpha})a^\dagger_\alpha, \tag{6.15}$$

$$T^{-\alpha}_n = f_n(\delta_{\boldsymbol{a},k,\alpha})a_\alpha. \tag{6.16}$$

Clearly, the T_n is also given by a sum of the $T^{m\alpha}_n$:

$$T_n = T^0_n + \sum_{\alpha,\pm} T^{\pm\alpha}_n. \tag{6.17}$$

Furthermore, the energy change corresponding to $T^{m\alpha}_n$ is immediately obtained from the energies $2J_z$ and ω_α of the hard-core bosons and the

photons respectively, and can be expressed through the following commutation relations

$$[H_0, T_n^{m\alpha}] = (2nJ_z + m\omega_\alpha)T_n^{m\alpha}. \tag{6.18}$$

Note that we use here the convention $0\alpha \equiv 0$ such that T_0^0 and $T_{\pm 2}^0$, which do not change the state of the cavity, are defined independently of the value of α.

SW transformation and correspondence to the toric code

In the perturbative limit we are interested in, the SW transformation allows to obtain an effective Hamiltonian in a desired subspace up to an arbitrary order in perturbation theory. For the convenience of the reader, we summarize the general procedure in Appendix 6.A, and provide there the general formulas appropriate for the type of Hamiltonian of interest in this work, up to the fourth perturbative order. Since the quantum information is encoded in the spin degrees of freedom, we always consider the low-energy subspace where no hard-core boson is present. On the other hand, we will generally allow the modes of the cavity to be excited, to study how the presence of a finite photon population affects the properties of the memory. While the treatment of Appendix 6.A is completely general, the resulting fourth-order expressions involve too many terms to be presented here. It is instead interesting to consider specific coupling schemes and physically relevant regimes, in which only a few dominant contributions are important. Several examples will be examined in detail in the following sections.

In the remaining of this section we restrict ourselves to the case without cavity modes, and derive the toric code from the formulas of Appendix 6.A. By setting all the $\delta_{a,k,\alpha}$ to zero, the T_n operators coincide with T_n^0 and all the summations on the photon indexes i, j, k, r in Eqs. (6.90-6.92) can be dropped. By applying such formulas in the subspace with zero hard-core bosons we obtain

$$
\begin{aligned}
H_{\text{eff}} = \quad &-\frac{1}{4J_z}T_{-2}T_{+2} + \frac{1}{16J_z^2}T_{-2}T_0T_{+2} \\
&-\frac{1}{128J_z^3}T_{-2}T_{-2}T_{+2}T_{+2} - \frac{1}{64J_z^3}T_{-2}T_0T_0T_{+2} \\
&+\frac{1}{64J_z^3}T_{-2}T_{+2}T_{-2}T_{+2},
\end{aligned} \tag{6.19}
$$

were we wrote explicitly the third-order term in the second line, even if it gives no contribution: a hardcore-boson pair created by T_{+2} from the
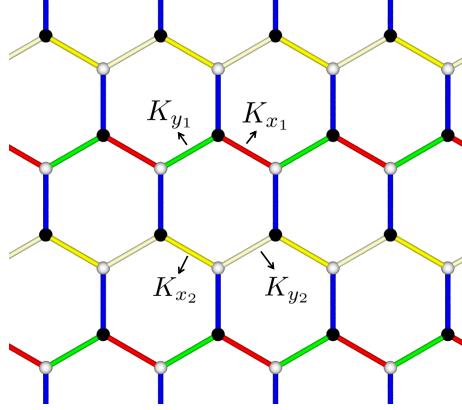
Figure 6.4: Honeycomb lattice with two distinct x-couplings $K_{x_{1,2}}$ and two distinct y-couplings $K_{y_{1,2}}$.

vacuum, followed by a T_0 hopping process, cannot be annihilated by the T_{-2} operator. In general, only even orders appear in the perturbation theory and Eq. (6.91) always evaluates to zero. It is also worth pointing out that Eq. (6.19) is the same as the one derived in Ref. [114] with the perturbative continuous unitary transformation approach.

If we now explicitly write Eq. (6.19) in terms of spin operators, by using Eqs. (6.7-6.9) with $K_{a,k} = J_k$, the toric code Hamiltonain is obtained. [14] As a slight generalization, we consider here the case when four distinct couplings enter, namely $J_{x_{1,2}}$ and $J_{y_{1,2}}$. This specific scheme is illustrated in Fig. 6.4 and leads to

$$
\begin{aligned}
H_{\text{eff}} = & -\frac{J_{x_1}^2 + J_{x_2}^2}{4J_z}\frac{N}{2} - \frac{J_{y_1}^2 + J_{y_2}^2}{4J_z}\frac{N}{2} \\
& -\frac{J_{x_1}^2 J_{y_1}^2 + J_{x_2}^2 J_{y_2}^2}{16J_z^3}\frac{N}{2} + \frac{J_{x_1}^2 J_{y_2}^2 + J_{x_2}^2 J_{y_1}^2}{16J_z^3}\frac{N}{2} \\
& -\frac{2(J_{x_1}^2 J_{x_2}^2 + J_{y_1}^2 J_{y_2}^2)}{64J_z^3}N + \frac{J_{x_1}^4 + J_{x_2}^4}{64J_z^3}\frac{N}{2} + \frac{J_{y_1}^4 + J_{y_2}^4}{64J_z^3}\frac{N}{2} \\
& -\frac{J_{x_1} J_{y_1} J_{x_2} J_{y_2}}{16J_z^3}\sum_{\boldsymbol{a}} W_{\boldsymbol{a}}.
\end{aligned}
\tag{6.20}
$$

This result will be useful later, when in Sec. 6.7 we will discuss the non-resonant coupling of the cavity modes to the spin Hamiltonian. The first three lines are a constant and can thus be dropped for the moment. We have kept them here since they will become important in Sec. 6.7, when the $J_{x_{1,2}}$, $J_{y_{1,2}}$ will be generalized to full couplings $K_{x_{1,2}}$, $K_{y_{1,2}}$, including the cavity modes.

The last line of Eq. (6.20) is expressed in terms of the spin operators W_a, defined as

$$W_a = \tau_a^z \tau_{a+e_2}^y \tau_{a+e_1}^y \tau_{a+e_1+e_2}^z. \tag{6.21}$$

Note that the W_a operator involves four dimers, connected by two x-links and two y-links. We will use sometimes the expression that such links 'belong to' the corresponding operator W_a. The W_a operators are mutually commuting and can be rewritten in terms of stars and plaquettes of the toric code, as introduced in Ref. [14]. In order to see this correspondence, we perform a spin rotation. [114] If the spin lies at a site which is the bottom corner of a dark unit cell (see the left-hand side of Fig. 6.3)

$$\tau^x = -s^y, \quad \tau^y = s^x, \quad \tau^z = s^z, \tag{6.22}$$

otherwise

$$\tau^x = s^y, \quad \tau^y = s^z, \quad \tau^z = s^x. \tag{6.23}$$

We have now that half of the unit cells of the lattice of dimers (the dark unit cells in the left-hand side of Fig. 6.3) corresponds to plaquette operators B_p of the form $s^z s^z s^z s^z$. The other half of the cells (the empty ones in the left-hand side of Fig. 6.3) corresponds to star operators A_s of the form $s^x s^x s^x s^x$. By setting $J_{x_1} = J_{x_2} = J_x$ and $J_{y_1} = J_{y_2} = J_y$, Eq. (6.20) gives back the result of Refs. [14, 114]

$$\begin{aligned} H_{\text{eff}} = \quad & -\frac{J_x^2 + J_y^2}{4J_z}N - \frac{J_x^4 + J_y^4}{64J_z^3}N \\ & -\frac{J_x^2 J_y^2}{16J_z^3}\left(\sum_s A_s + \sum_p B_p\right). \end{aligned} \tag{6.24}$$

In the following we will use the simpler notation in terms of the W_a operators, by keeping in mind that

$$\sum_a W_a = \sum_s A_s + \sum_p B_p. \tag{6.25}$$

6.4   Read-out schemes

As a first application of the coupling of the honeycomb spin model to cavity modes, we show that it allows the read-out of the eigenvalues of the star and plaquette operators. This is a basic requirement if the toric code model is aimed to be a quantum memory, since the knowledge of

such eigenvalues (the error syndrome) is needed to perform the error-correction algorithm and to retrieve the encoded information.

We start by discussing an example when a single cavity mode, with unperturbed frequency ω and annihilation operator a, allows to read the eigenvalue of a single operator $W_{\boldsymbol{a}_r}$, for a given site $\boldsymbol{a}_r$. The specific coupling scheme we consider for Eq. (6.2) is as follows, for the x-links:

$$K_{\boldsymbol{a}_r,x} = K_{\boldsymbol{a}_r+\boldsymbol{e}_2,x} = J_x + \delta_x(a + a^\dagger), \tag{6.26}$$

and $K_{\boldsymbol{a},x} = J_x$ otherwise. Furthermore, $K_{\boldsymbol{a},y} = J_y$ for all the y-links. In other terms, only the two x-links which belong to the $W_{\boldsymbol{a}_r}$ operator are coupled to the cavity mode. This allows to read-out the eigenvalue of $W_{\boldsymbol{a}_r}$ from an indirect measurement since we obtain the following effective Hamiltonian

$$H_{eff} = \left[\omega - \frac{2\delta_x^2}{4J_z - \omega} - \frac{4\delta_x^2 J_y^2}{(4J_z - \omega)^3}W_{\boldsymbol{a}_r}\right] a^\dagger a, \tag{6.27}$$

which is derived from Eq. (6.1) by applying the general formalism of Appendix 6.A. In particular, as described in more detail in Appendix 6.B, we have evaluated Eqs. (6.90) and (6.92) for the specific coupling scheme under consideration, keeping only the terms diagonal in the number of photons and assuming the resonant condition

$$(4J_z - \omega) \ll 4J_z, \omega. \tag{6.28}$$

This implies that, at each order, only resonant terms contribute to Eq. (6.27), i.e., the ones where only powers of $(4J_z - \omega)$ appear in the energy denominators. Here, and in the rest of this work, we also assume $(4J_z - \omega) > 0$, such that the state with zero hard-core bosons is the unperturbed ground state of the resonant subspace.

Equation (6.27) shows that the frequency of the cavity is now

$$\omega - \frac{2\delta_x^2}{4J_z - \omega} \mp \frac{4\delta_x^2 J_y^2}{(4J_z - \omega)^3}. \tag{6.29}$$

Therefore, it is sufficient to detect the change in the frequency of the cavity mode, which is conditioned by the eigenvalue of $W_{\boldsymbol{a}_r}(\pm 1)$. Let's also recall from Sec. 6.3 that the lattice site $\boldsymbol{a}_r$ determines if the operator $W_{\boldsymbol{a}_r}$, defined in Eq. (6.21), corresponds to a star (empty unit cells in the left hand side of Fig. 6.3) or a plaquette (dark unit cells in the left hand side of Fig. 6.3) of the toric code model.

It is worth mentioning that a similar read-out scheme was demonstrated in superconducting circuits for a single qubit: in that case the role of $W_{\boldsymbol{a}_r}$ is played by σ_z of the qubit being read, dispersively coupled to a transmission line resonator. [120, 121] The frequency shift of the cavity mode can be determined in transmission measurements. Indeed, proposals for the realization of the honeycomb spin Hamiltonian with superconducting circuits already exist, [32] and it is conceivable that our readout scheme could also be realized in this type of systems. Note that the read-out must take place in a time interval which is much smaller than the typical time for a spin to flip. This condition can be satisfied for a single superconducting qubit, since the relaxation time can reach about 10 μs, while the response time of the measurement is a few hundred nanoseconds. [121] However, the signal to noise ratio is presently too low to allow single shot read-out. Besides superconducting systems, also spin qubits in semiconductor nanostructures can be coupled to transmission line resonators via spin-orbit interactions. In particular, InAs nanowire quantum dots were discussed in Ref. [132].

We now address the problem of measuring all the stars and plaquettes of the memory. As discussed already at the end of Sec. 9.2, we can imagine that all the couplings $\delta_{\boldsymbol{a},x,\alpha}$ can be switched on/off. For our read-out scheme, this implies that the site $\boldsymbol{a}_r$ can be freely chosen and all plaquettes and stars can be successively measured, one after the other. This method is not efficient in terms of the total read-out time for the whole memory, but has the advantage of using a single cavity mode. Having at disposal many cavity modes (ideally, one for each site of the memory), much more efficient schemes can be realized.

Consider in particular a set of sites $\Omega = \{\boldsymbol{a}_\alpha\}$, each of them corresponding to an operator $W_{\boldsymbol{a}_\alpha}$ which we would like to measure with a cavity mode α. For simplicity, we assume that all frequencies and couplings are equal, which can be realized with an array of identical resonators. Each mode α (in particular, the read-out of its frequency) can be addressed individually and is coupled to the two x-links of the corresponding $W_{\boldsymbol{a}_\alpha}$ operator in the following way

$$K_{\boldsymbol{a}_\alpha,x} = K_{\boldsymbol{a}_\alpha+\boldsymbol{e}_2,x} = J_x + \delta_x(a_\alpha + a_\alpha^\dagger), \tag{6.30}$$

while $K_{\boldsymbol{a},x} = J_x$ and $K_{\boldsymbol{a},y} = J_y$ for all the remaining links. We further require that

$$\text{if } \boldsymbol{a}_\alpha \in \Omega, \text{ then } \boldsymbol{a}_\alpha \pm \boldsymbol{e}_2 \notin \Omega, \tag{6.31}$$

such that two operators $W_{\boldsymbol{a}_{\alpha_1}}$, $W_{\boldsymbol{a}_{\alpha_2}}$ never share a x-link and thus no virtual process couples the $W_{\boldsymbol{a}_\alpha}$ operators to more than one cavity mode

in lowest-order. Then, the read-out of a single site can be generalized to
obtain the following effective Hamiltonian:

$$H_{eff} = \sum_{\boldsymbol{a}_\alpha \in \Omega} \left[\omega - \frac{2\delta_x^2}{4J_z - \omega} - \frac{4\delta_x^2 J_y^2}{(4J_z - \omega)^3} W_{\boldsymbol{a}_\alpha} \right] a_\alpha^\dagger a_\alpha, \qquad (6.32)$$

Therefore, we can read-out simultaneously the eigenvalues of all $W_{\boldsymbol{a}_\alpha}$
through the shifts of the corresponding cavity mode frequencies. This
procedure can be used to measure the state of the full memory in two
steps only. This requires to have a cavity mode for each $W_{\boldsymbol{a}}$ operator and
being able to turn on/off all the spin-electric couplings. Then, we can
apply the above procedure twice in a checkerboard configuration where,
in the first step, we turn on the couplings of only the plaquette operators
and, in the second step, the couplings of only the star operators.

6.5 Resonant enhancement of the gap from a single cavity mode

We discuss in this and the following sections how the cavity modes can
be used to prolong the lifetime of the encoded information. As shown in
Sec. 6.3, the honeycomb model (6.1) in the absence of cavity modes and
with uniform couplings ($K_{\boldsymbol{a},x} = J_x$ and $K_{\boldsymbol{a},y} = J_y$) is equivalent to the
toric code model of Eq. (6.24), up to fourth order in perturbation theory.
This effective model can be used as a quantum memory encoding two
qubits in the ground space, and the lifetime is essentially determined
by the energy gap. [14] As it can be seen in Eq. (6.24), the excitations
correspond to sites where $W_{\boldsymbol{a}} = -1$. They can also be interpreted as
anyons, [14] with anyon numbers $n_{\boldsymbol{a}}$ defined as

$$W_{\boldsymbol{a}} = 1 - 2n_{\boldsymbol{a}}, \qquad (6.33)$$

at each site $\boldsymbol{a}$ of the lattice. If $W_{\boldsymbol{a}} = +1$, then no anyon is present, i.e.
$n_{\boldsymbol{a}} = 0$. Instead, if $W_{\boldsymbol{a}} = -1$ one anyon is present, i.e. $n_{\boldsymbol{a}} = +1$. In
Eq. (6.24), the anyons are noninteracting particles with energy

$$\mu_0 = \frac{J_x^2 J_y^2}{8J_z^3}. \qquad (6.34)$$

In the present section, we consider how to obtain a noninteracting toric
model in the presence of a single cavity mode, and how the gap of the

model is affected by the cavity. We refer to the next section for a discussion of anyon interactions induced by two cavity modes, as proposed in Ref. [16].

As for the single-site read-out discussed in Sec. 6.4, the cavity mode has unperturbed frequency ω and annihilation operator a, but the coupling scheme is as follows, for all the x-links:

$$K_{\boldsymbol{a},x} = J_x + \delta_x(a + a^\dagger), \tag{6.35}$$

while $K_{\boldsymbol{a},y} = J_y$ for all the y-links. Our analysis can also be simply extended to non-homogeneous couplings, when δ_x becomes site-dependent. The read-out scheme of Eq. (6.26), where only two x-links are affected by the cavity, provides an explicit example.

To obtain an effective Hamiltonian, we assume again here the resonant condition of Eq. (6.28), which allows us to keep only the leading term (with resonant energy denominators) in the perturbative contributions of Eqs. (6.90) and (6.92). The interested reader can find more details of the derivation in Appendix 6.B. The final result reads

$$H_{\text{eff}} = \omega a^\dagger a - \frac{\delta_x^2 N}{4J_z - \omega}a^\dagger a - \frac{4\delta_x^2 J_y^2}{(4J_z - \omega)^3}a^\dagger a \sum_{\boldsymbol{a}} W_{\boldsymbol{a}}, \tag{6.36}$$

where the modified gap of the model is immediately seen to be

$$\mu = \frac{8\delta_x^2 J_y^2}{(4J_z - \omega)^3}\langle a^\dagger a\rangle, \tag{6.37}$$

which is proportional to the number of photons populating the cavity mode. In fact, comparing μ to the bare gap μ_0 of Eq. (6.34), the quantity $\delta_x^2\langle a^\dagger a\rangle$ appears instead of J_x^2. Furthermore, the denominator is in terms of $(4J_z - \omega)$, which can be made smaller by simply changing the frequency of the cavity, in contrast to the bare value J_z. Indeed, we assumed $(4J_z - \omega) \ll J_z$, see Eq. (6.28). These facts make the effect of that cavity very interesting, because the resonant gap μ can be made larger than μ_0. Here and in the rest of this work, we assume that the cavity is driven out of equilibrium. The average $\langle a^\dagger a\rangle$ appearing in Eq. (6.37) corresponds to the non-equilibrium photon population of the cavity and can be large.

Note however that the gap cannot be made arbitrarily large. In particular, the perturbative expansion requires $\delta_x\sqrt{\langle a^\dagger a\rangle}, J_{x,y} < (4J_z - \omega)$, which implies $\mu < J_y$. Still, for given values $J_{x,y} \ll J_z$, an enhancement

factor of the bare gap μ_0 of order $J_z^3/J_x^2 J_y$ can be achieved, by an appropriate design of the cavity and excitation of the resonant mode. Such increase in the gap has a dramatic effect on the life-time of the quantum memory, if μ can become larger than the temperature T. In this case, the population of anyons is exponentially suppressed and the life-time τ increases accordingly. The following approximate formula was proposed [95, 97, 16]

$$\tau \simeq 2 f_c \frac{e^{\mu/k_B T} + 1}{D}, \qquad (6.38)$$

where D is the diffusion constant of the anyons and the prefactor f_c can be interpreted as a critical fraction of errors. [16] The value of D depends on the details of the thermal bath, especially whether it is Ohmic or super-Ohmic, and can also contain a dependence on μ (see Ref. [16] for an extended discussion).

Finally, we recall that the exact solution in the absence of cavity modes [27] also displays a gapless phase, away from the perturbative regime (i.e., when $J_{x,y,z}$ have comparable values). The influence of the cavity mode on this gapless phase is an interesting question: since in the resonant case the role of $4J_z$ is played by $4J_z - \omega$, it can be expected that not only the gap of the system can be modified by tuning ω around $4J_z$, but also a transition from the gapped to the gapless phase could be induced by changing the parameters of the cavity. These nonperturbative aspects will be the subject of future investigations.

6.6   Long-Range interactions

It was shown in Ref. [16] that repulsive long-range interactions between anyons have a beneficial effect on the memory. Since cavity modes spatially uniform across the memory realize interactions with constant strength, we consider the following effective model

$$H_{eff} = \mu \sum_{\boldsymbol{a}} n_{\boldsymbol{a}} + \frac{A}{2} \sum_{\boldsymbol{a},\boldsymbol{a}'} n_{\boldsymbol{a}} n_{\boldsymbol{a}'}, \qquad (6.39)$$

where $\boldsymbol{a}, \boldsymbol{a}'$ run over all the N sites of the lattice [1] and the anyon numbers $n_{\boldsymbol{a}} = 0, 1$ are defined as in Eq. (6.33). Note that, differently from Ref. [16], we do not distinguish here between star and plaquette anyons, but all of them interact among each other. The effect of the interactions on the memory lifetime can be understood in terms of a mean-field gap μ_{mf},

---

[1]We also include in the interaction term of Eq. (6.39) a self-energy correction $A/2$.

which includes the repulsion energy (if $A > 0$) from the average anyon density $n_{\mathrm{m}f}$:

$$\mu_{\mathrm{mf}} = \mu + n_{\mathrm{mf}} A N, \tag{6.40}$$

where n_{mf} is determined self-consistently as $n_{\mathrm{mf}} = 1/(e^{\mu_{\mathrm{mf}}/k_B T} + 1)$ assuming an equilibrium density of anyons at temperature T.

It is the purpose of this section to study how the model (6.39) is realized perturbatively and when the effect of the interactions becomes relevant. A noticeable feature of Eq. (6.40) is that, assuming constant μ, A, the mean-field gap increases with N. This is because the contribution from the interaction (second term) grows and becomes eventually the dominant term for sufficiently large N. The effect is to reduce the anyon density $n_{\mathrm{m}f}$ and prolong the memory lifetime. [16] However, two main differences appear in the explicit perturbative derivation:

(i) The parameters μ and A acquire in general a nontrivial dependence on N. Therefore, it is possible that the anyon gap μ dominates the size-dependence of the gap, instead of the interaction contribution.

(ii) The requirement to strictly remain in the perturbative regime imposes restrictions to the size of the system, below which in many cases the interaction contribution is small with respect to μ.

However, we also find specific coupling schemes and appropriate range of parameters for which the interactions become the dominant effect.

Coupling scheme and resonant effective Hamiltonian

As suggested in Ref. [16], we consider two cavity modes with frequencies $\omega_{x,y}$ and annihilation operators $a_{x,y}$. To have two modes is useful because it allows to change the sign of the interaction, by choosing the frequencies and photon occupations of the two cavity modes. The first (second) mode couples to one half of the $x(y)$-couplings. In particular, by referring to the color code of Fig. 6.4, we assume

$$K_{\boldsymbol{a},x} = J_x + \delta_x(a_x^\dagger + a_x), \text{ for the red } x\text{-links}, \tag{6.41}$$

while $K_{\boldsymbol{a},x} = J_x$ for the yellow x-links and

$$K_{\boldsymbol{a},y} = J_y + \delta_y(a_y^\dagger + a_y), \text{ for the green } y\text{-links}, \tag{6.42}$$

while $K_{\boldsymbol{a},y} = J_y$ for the white y-links.

We obtain the effective Hamiltonian for the toric code model from a
SW transformation by assuming, as in the previous sections, that the two
modes are resonant

$$(4J_z - \omega_{x,y}) \ll J_z, \omega_{x,y}. \tag{6.43}$$

Although this considerably simplifies the treatment, still several contri-
butions are present when evaluating the second and fourth order expres-
sions, as discussed in more detail in Appendix 6.C. The following much
simpler expression is obtained

$$H_{\text{eff}} = \omega'_x a^\dagger_x a_x + \omega'_y a^\dagger_y a_y$$
$$-\frac{1}{2} \left[\sum_{\alpha=x,y} \frac{J_x J_y \delta_x \delta_y}{(4J_z - \omega_\alpha)^3} \right] \left(a^\dagger_x a_y + a_x a^\dagger_y \right) \sum_{\boldsymbol{a}} W_{\boldsymbol{a}}, \tag{6.44}$$

by imposing the more restrictive condition

$$|\omega'_x - \omega'_y| \ll (4J_z - \omega_{x,y}) \ll J_z, \omega_{x,y}. \tag{6.45}$$

In Eqs. (6.44) and (6.45) we defined

$$\omega'_\alpha = \omega_\alpha - \frac{N}{2} \frac{\delta^2_\alpha}{4J_z - \omega_\alpha}, \tag{6.46}$$

where the second term is generally a small correction to the frequencies,
due to perturbative restrictions to the size of the system [see Eq. (6.100)].
A feature of the scheme considered here is that no term diagonal in the
photon modes which couples to $\sum_{\boldsymbol{a}} W_{\boldsymbol{a}}$ appears at fourth order. This is
because each cavity mode only interacts with a single link of each $W_{\boldsymbol{a}}$
operator, and thus at most one photon operator per mode can appear in
combination with $\sum_{\boldsymbol{a}} W_{\boldsymbol{a}}$. Therefore, all the couplings to $W_{\boldsymbol{a}}$ in the effec-
tive fourth-order Hamiltonian are off-diagonal in the photon operators.
As a first approximation, due to Eq. (6.45), we only kept one of these
terms, namely the one appearing in the second line of Eq. (6.44) which is
resonant in the difference of the two cavity mode frequencies.

By performing a second SW transformation of Eq. (6.44) in the photon
modes (in the same way described in Ref. [16]) and keeping only terms
involving spin operators, we obtain

$$H_{eff} = \frac{A}{8} \left(\sum_{\boldsymbol{a}} W_{\boldsymbol{a}} \right)^2, \tag{6.47}$$

where A is is given by

$$A = 2 \left[\sum_{\alpha=x,y} \frac{J_x J_y \delta_x \delta_y}{(4J_z - \omega_\alpha)^3} \right]^2 \frac{\langle a_x^\dagger a_x \rangle - \langle a_y^\dagger a_y \rangle}{\omega_x' - \omega_y'}. \tag{6.48}$$

By rewriting Eq. (6.47) in terms of anyons we obtain:

$$H_{eff} = -\frac{AN}{2} \sum_{\boldsymbol{a}} n_{\boldsymbol{a}} + \frac{A}{2} \sum_{\boldsymbol{a},\boldsymbol{a}'} n_{\boldsymbol{a}} n_{\boldsymbol{a}'}. \tag{6.49}$$

As announced, the effective parameters μ and A have a dependence on N which in the case of the interaction strength A can be quite weak [it appears through the denominator $\omega_x' - \omega_y'$, see Eqs. (6.48) and (6.46)]. Instead, the chemical potential is approximately linear in N

$$\mu = -\frac{AN}{2}, \tag{6.50}$$

which makes it the dominant effect. Therefore, it is required for the stability of the $n_{\boldsymbol{a}} = 0$ ground state that $A < 0$, which leads to $\mu > 0$ and can be realized by an appropriate choice of the frequencies ω_α' and photon occupations $\langle a_\alpha^\dagger a_\alpha \rangle$. The anyon interaction is in this case negative, which has the unfavorable effect of reducing the non-interacting gap, but it becomes quickly negligible with N. Note that, for a gap which grows linearly with system size, the lifetime is prolonged exponentially with N at low temperature, as shown in Eq. (6.38).

Interpretation in terms of anyon-holes

An interesting aspect of Eq. (6.47) is that it is symmetric with respect to the change of sign of all the $W_{\boldsymbol{a}}$. Therefore, it is useful to define the anyon-hole number

$$\bar{n}_{\boldsymbol{a}} = 1 - n_{\boldsymbol{a}}, \tag{6.51}$$

which describe excitations of the ground state with $W_{\boldsymbol{a}} = -1$ for every $\boldsymbol{a}$. Clearly, transforming Eq. (6.47) in terms of the $\bar{n}_{\boldsymbol{a}}$ leads to an Hamiltonian with the same form of Eq. (6.49). Another interesting way to rewrite Eq. (6.47) in a symmetric way is by considering both types of particles present in the memory (i.e., at each site either an anyon or an anyon-hole is present). This gives:

$$H_{eff} = -\frac{A}{2} \sum_{\boldsymbol{a},\boldsymbol{a}'} \bar{n}_{\boldsymbol{a}} n_{\boldsymbol{a}'}, \tag{6.52}$$

describing a long-range interaction between anyons and anyon-holes. For for $A < 0$ such interaction is repulsive and the ground state is completely occupied with one type of particles, say anyon-holes. The appearance of anyons in the memory then results in a repulsive contribution from the $\sim N$ anyon-holes already present in the ground-state. This picture provides a natural interpretation of the system size dependence of the gap, in terms of long-range interactions.

As a side remark, we consider again the model Hamiltonian Eq. (6.39), but with with constant coefficients μ, A. By rewriting Eq. (6.39) in terms of anyon-holes we obtain:

$$H_{eff} = -(\mu + AN) \sum_{\boldsymbol{a}} \bar{n}_{\boldsymbol{a}} + \frac{A}{2} \sum_{\boldsymbol{a},\boldsymbol{a}'} \bar{n}_{\boldsymbol{a}} \bar{n}_{\boldsymbol{a}'}. \tag{6.53}$$

Differently from Ref. [16], we now assume $A < 0$. Then, the first term of Hamiltonian (6.53) is a size-dependent chemical potential which for large system size becomes positive, while the second term describes a long-range attractive interaction. Therefore, if we want to use this system as a quantum memory, we can encode a state in the memory full of anyons ($W_{\boldsymbol{a}} = -1$ for every $\boldsymbol{a}$, instead of $+1$). In this situation, the role of the anyons and the anyon-holes is interchanged. For example, a spin-flip will now produce a pair of anyon-holes which diffuse in the memory and destroy the information. However, since the chemical potential of the anyon-holes increases linearly with the system size, one can prolong the lifetime of the memory by making the system size bigger.

Off-resonant contributions to the anyon gap

We have assumed so far the resonant condition (6.45), such that we could keep only a single term which couples to the star and plaquette operators [the second line of Eq. (6.44)]. However, many contributions to the gap and interactions exist in general and we show here that for some regime of parameters it is possible that μ in Eq. (6.39) becomes zero. In this case, the interactions between anyons have a dominant effect.

We consider again the effective photon Hamiltonian up to fourth order, obtained from Eqs. (6.89) and (6.92), but keep two additional terms

with respect to Eq. (6.44)

$$
\begin{aligned}
H_{\text{eff}} \quad &= \omega'_x a^\dagger_x a_x + \omega'_y a^\dagger_y a_y - \frac{N}{4} \sum_{\alpha=x,y} \frac{J_\alpha \delta_\alpha}{4J_z - \omega_\alpha} \left(a_\alpha + a^\dagger_\alpha\right) \\
&\quad - \left[\sum_{\alpha=x,y} \frac{J^2_{\bar\alpha} J_\alpha \delta_\alpha}{(4J_z - \omega_\alpha)^3}(a_\alpha + a^\dagger_\alpha)\right] \sum_{\boldsymbol{a}} W_{\boldsymbol{a}} \\
&\quad - \left[\sum_{\alpha=x,y} \frac{J_x J_y \delta_x \delta_y}{2(4J_z - \omega_\alpha)^3}\right] \left(a^\dagger_x a_y + a_x a^\dagger_y\right) \sum_{\boldsymbol{a}} W_{\boldsymbol{a}}, \qquad (6.54)
\end{aligned}
$$

where in the second line $\bar\alpha = y$ if $\alpha = x$ and vice-versa. For some details on the derivation of this expression, we refer to Appendix 6.C. In Eq. (6.54), the second line generates now a chemical potential for the anyons in combination with the second-order term in the first line. Therefore, Eq. (6.50) gets modified as follows

$$
\mu = -\frac{AN}{2} + \sum_{\alpha=x,y} \frac{J^2_x J^2_y \delta^2_\alpha}{(4J_z - \omega_\alpha)^4 \omega'_\alpha} N. \qquad (6.55)
$$

Equation (6.55) shows that the effect of the off-resonant terms becomes negligible if ω'_α is sufficiently large. However, this new contribution to the chemical potential appears to lower order in the perturbation expansion than the first term (sixth order in the parameters $J_{x,y}, \delta_{x,y}$ instead of eighth order). Therefore, it is possible to make the off-resonant contribution of the same size of the resonant one by slightly relaxing the condition (6.45). Note that the second term in Eq. (6.55) is always positive and can only be canceled if $A > 0$, which is possible by choosing suitable frequencies and photon occupations of the two modes [see Eq. (6.48)]. The anyon interaction is therefore repulsive and the final Hamiltonian is similar to the case studied in Ref. [16].

As a specific example, we plot μ in Fig. 6.5 as function of N, by using in Eq. (6.55) suitable numerical values of the couplings, such that μ is approximately zero. Since the dependence on N of Eq. (6.55) is not exactly linear for both terms (due to A and ω'_α), μ cannot be made zero identically for arbitrary N. Nevertheless, in a range of parameters, it is sufficiently small that the repulsive anyon interaction becomes the dominant effect. This we show by plotting in Fig. 6.5 the mean-field gap μ_{mf}, obtained from Eq. (6.40), which can be much larger than the non-interacting gap μ.

The effect of the interactions is very beneficial since it allows to obtain μ_{mf} in the mK range, while the original gap without cavities is $J^2_x J^2_y / 8J^3_z \simeq$
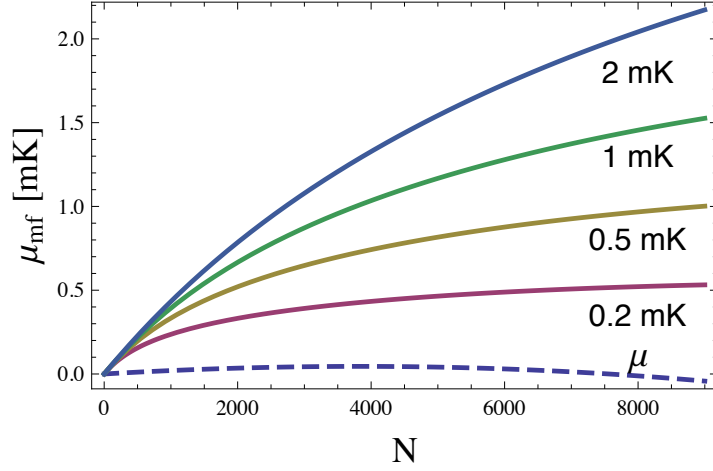
Figure 6.5: Mean-field gap μ_{mf}, given by Eq. (6.40) with A as in Eq. (6.48), plotted for different temperatures (solid curves). The dashed curve is the bare gap μ of Eq. (6.55). We used $J_z = 1011$ K, $J_{x_{1,2}} = J_{y_{1,2}} = 22$ K, $\langle a_x^\dagger a_x \rangle = 100$, $\langle a_y^\dagger a_y \rangle = 0$, $\delta_x = \delta_y = 0.21$ K, $\omega_x = 3991$ K, and $\omega_y = 3980$ K.

30 μK. However, although the interacting regime presents interesting aspects, it seems more useful in practice to take advantage of the resonant enhancement of the gap discussed in Sec. 6.5. This is realized if each mode couples to all the corresponding (x- or y-) links, instead of half of them. The final result is the same of Eq. (6.37), including two resonant modes

$$\mu \simeq \sum_\alpha \frac{8\delta_\alpha^2 J_{\bar\alpha}^2}{(4J_z - \omega_\alpha)^3} \langle a_\alpha^\dagger a_\alpha \rangle. \tag{6.56}$$

With the same parameters of Fig. 6.5, Eq. (6.56) gives $\mu \simeq 0.1$ K, much larger than the maximum value $\mu_{mf} \simeq 1$ mK of Fig. 6.5. As discussed, the effect of the interaction becomes larger with system size, but unfortunately the perturbative treatment is only strictly applicable within a limited range of values of N. Conditions for N are discussed in Appendixes 6.B and 6.C, and lead to an upper bound for N similar to the largest value in Fig. 6.5.

6.7   Cavity modes out of resonance

In the previous sections, we generally assumed that the different cavity modes are resonantly coupled to the memory, i.e., $\omega_\alpha \simeq 4J_z$. We now consider the case of largely detuned modes. Since cavity modes with large

frequency $\omega_\alpha \gg J_z$ have a small effect on the spin model, we consider the opposite limit:

$$\omega_\alpha \ll 4J_z, \tag{6.57}$$

and show that many results of the previous sections have an analog in this regime. As before, we can still compute the SW effective Hamiltonian given by Eqs. (6.90) and (6.92), but it is not possible now to pick a few resonant terms at each order of perturbation theory. However, as shown in Appendix 6.D, the final result can be obtained from the calculation without cavity modes, by substituting $J_{a,x}$, $J_{a,y}$ with the corresponding full couplings (6.2):

$$J_{a,x} \to K_{a,x}, \qquad J_{a,y} \to K_{a,y}. \tag{6.58}$$

Given this simple prescription, the expression Eq. (6.20) for the Kitaev model with four distinct couplings $J_{x_{1,2}}$, $J_{y_{1,2}}$ proves to be useful for several configurations.

We consider first a single cavity mode coupled homogeneously to the x-links as in Eq. (6.35), which amounts to set

$$J_{x_{1,2}} \to J_x + \delta_x(a + a^\dagger), \quad J_{y_{1,2}} \to J_y, \tag{6.59}$$

in Eq. (6.20). As in Sec. 6.5, we can neglect the off-diagonal terms in the photon Hamiltonian and obtain

$$H_{\text{eff}} = \left(\omega - \frac{\delta_x^2 N}{2J_z}\right) a^\dagger a - \frac{J_y^2[J_x^2 + \delta_x^2(2a^\dagger a + 1)]}{16J_z^3} \sum_a W_a, \tag{6.60}$$

which shows an enhancement of the gap from the cavity mode. Even if the gap from Eq. (6.60) does not have a resonant denominator, it is still possible to increase it by driving the cavity to a large photon population. From the point of view of the perturbative treatment, the only condition to be satisfied in Eq. (6.60) for the number of photons is $\delta_x \sqrt{\langle a^\dagger a \rangle} \ll J_z$.

We now consider the anyon interactions and choose the same coupling scheme of Sec. 6.6 with two cavity modes $a_{x,y}$ respectively coupled to half of the x- or y-links. More explicitly, we set in Eq. (6.20)

$$J_{\alpha_1} \to J_\alpha + \delta_\alpha(a_\alpha + a_\alpha^\dagger), \quad J_{\alpha_2} \to J_\alpha, \tag{6.61}$$

where $\alpha = x, y$. By keeping only terms which are relevant for the star and plaquette operators (see Appendix 6.D), we obtain

$$
\begin{aligned}
H_{\text{eff}} = {} & \omega_x'' a_x^\dagger a_x + \omega_y'' a_y^\dagger a_y - \frac{N}{4J_z} \sum_{\alpha=x,y} J_\alpha \delta_\alpha (a_\alpha + a_\alpha^\dagger) \\
& - \frac{J_x^2 J_y^2}{16 J_z^3} \sum_{\boldsymbol{a}} W_{\boldsymbol{a}} - \left[\sum_{\alpha=x,y} \frac{J_{\bar\alpha}^2 J_\alpha \delta_\alpha}{16 J_z^3} (a_\alpha + a_\alpha^\dagger) \right] \sum_{\boldsymbol{a}} W_{\boldsymbol{a}} \\
& - \frac{J_x J_y \delta_x \delta_y}{16 J_z^3} \left(a_x a_y^\dagger + a_y^\dagger a_x \right) \sum_{\boldsymbol{a}} W_{\boldsymbol{a}}
\end{aligned}
\tag{6.62}
$$

which is in complete analogy with Eq. (6.54), except that the first $\sum_{\boldsymbol{a}} W_{\boldsymbol{a}}$ term in the second line (present even without cavity modes) is not neglected here, since all the energy denominators are non-resonant. In Eq. (6.62) we defined

$$
\omega_\alpha'' = \omega_\alpha - \frac{N}{4J_z} \delta_\alpha^2,
\tag{6.63}
$$

where the second term is generally a small correction in the perturbative regime. As in the previous section, we perform a second SW transformation in the photon field and obtain the following effective Hamiltonian by making use of the resonant condition $\omega_x'' \simeq \omega_y''$

$$
H = \frac{A}{8} \left(\sum_{\boldsymbol{a}} W_{\boldsymbol{a}} \right)^2,
\tag{6.64}
$$

where

$$
A = 2 \left(\frac{J_x J_y \delta_x \delta_y}{8 J_z^3} \right)^2 \frac{\langle a_x^\dagger a_x \rangle - \langle a_y^\dagger a_y \rangle}{\omega_x'' - \omega_y''}.
\tag{6.65}
$$

Similar to Sec. 6.6, we can rewrite Eq. (6.64) in terms of the anyon numbers $n_{\boldsymbol{a}}$, in the form of Eq. (6.39), with A given by Eq. (6.65) above and a chemical potential $\mu = -AN/2$, approximately proportional to the system size. We recall again that A can be made either positive or negative, depending on the sign of $\langle a_x^\dagger a_x \rangle - \langle a_y^\dagger a_y \rangle$ and $(\omega_x'' - \omega_y'')$, with $A < 0$ leading to a stable memory. As in Sec. 6.6, if we stay a little bit away from the $\omega_x'' \simeq \omega_y''$ resonance, the lower-order terms become relevant and we can write the following expression for the chemical potential of the anyons

$$
\mu = -\frac{AN}{2} + \frac{J_x^2 J_y^2}{8 J_z^3} + \sum_{\alpha=x,y} \frac{J_x^2 J_y^2 \delta_\alpha^2 N}{16 J_z^4 \omega_\alpha''},
\tag{6.66}
$$

which can be put to zero by choosing $A > 0$ and for some specific choice of parameters. This allows to recover the same situation of Sec. 6.6, when the dynamics of the system is solely determined by the long-range positive interaction between the anyons.

6.8 Conclusion

In this paper we have analyzed a generalization of the Kitaev honeycomb model, which includes the influence of quantized cavity modes. The coupling is realized by a linear modification of the Ising interactions which should be relevant for a variety of systems. [29, 30, 31, 32, 117, 118, 119, 120, 121, 123, 124, 125, 126, 127] We have studied this model in the perturbative regime, when the low-energy Hamiltonian is a generalization of the toric code and the setup can thus be seen as a quantum memory. We have considered different coupling schemes and shown that the presence of cavity modes can be useful in several ways.

More specifically, cavity modes allow to read-out the state of the star and plaquette operators. An efficient read-out scheme of the error syndrome is an essential prerequisite to perform any error-correction algorithm. [15, 133] The simplest way to achieve this goal is to couple one cavity mode to the desired star or plaquette and to detect the corresponding frequency shift, similarly to a read-out scheme for single superconducting qubit in circuit quantum electrodynamics. [120, 121] An array of multiple resonators allows to measure all the star or plaquette operators simultaneously.

Secondly, we studied cavity modes coupled homogeneously across the whole memory. We have considered both setups with one and two cavity modes, resonantly coupled or with very small frequencies. For the case of a single cavity we have obtained the dependence of the anyon gap from the photon number and frequency of the mode, and shown that a large enhancement is possible with an excited cavity at resonance. Having two cavity modes allows to realize long-range interactions with tunable sign among anyons and a size-dependent chemical potential. In this case, the relevant excitation energy is a mean-field gap [16] which, in some parameter regimes, is essentially due to the anyon interactions and is generally much larger than the original gap without cavities. Since the lifetime of the memory depends exponentially on the value of the gap at low temperature, these results might lead to a dramatic prolongation of the memory lifetime. From a more general perspective, the extension of the honeycomb Hamiltonian considered in this work allows to have

additional control on the properties of the model, through the specific features of the coupling scheme and the possibility of tuning the parameters characterizing the cavity modes.

6.9 Acknowledgments

6.A SW transformation

For the convenience of the reader, we summarize here the formalism of the Schrieffer-Wolff (SW) transformation [122, 75] and show how it can be applied to the general class of Hamiltonians of interest in this work.

General formalism

Consider a Hamiltonian H with a projector P_H on an invariant subspace (i.e., a direct sum of eigenspaces) and two known projectors P and $Q = 1 - P$, such that the subspace of P has the same dimension of the one of P_H. A SW transformation is defined as a unitary transformation $U = e^S$ with block off-diagonal S which maps the subspace of P_H into P. Therefore, $P = e^S P_H$ and the transformed Hamiltonian $H_\mathrm{d} = UHU^\dagger$ is block diagonal:

$$PSP = QSQ = 0, \tag{6.67}$$

and

$$PH_\mathrm{d}Q = QH_\mathrm{d}P = 0. \tag{6.68}$$

It is useful to define the superoperator L as

$$LA = [S, A], \tag{6.69}$$

such that, in the superoperator language, the transformed Hamiltonian H_d takes the following compact form:

$$H_\mathrm{d} = e^L H. \tag{6.70}$$

Let's now consider an Hamiltonian that can be decomposed in a dominant part H_0 and a small perturbation $V = V_\mathrm{d} + V_\mathrm{od}$, where the spectrum

of H_0 is divided in a low-energy space (P projects onto the low-energy space) and a high-energy space ($Q = 1 - P$ projects onto the high-energy space). By definition, the diagonal perturbation V_d and the off-diagonal perturbation V_od satisfy the following equations

$$
\begin{aligned}
P V_\mathrm{d} Q &= Q V_\mathrm{d} P = 0, \\
P V_\mathrm{od} P &= Q V_\mathrm{od} Q = 0.
\end{aligned}
\tag{6.71}
$$

Since V is assumed to be small, we can expand S and L in a series, namely

$$
S = \sum_{n=1} S_n, \quad \text{and} \quad L = \sum_{n=1} L_n,
\tag{6.72}
$$

where $L_n A := [S_n, A]$. If we require that the off-diagonal part vanishes at each order, we find the following recursive relations for the S_n operators[75] ($n = 1, 2, 3, ...$)

$$
S_1 = L_0^{-1} V_\mathrm{od},
\tag{6.73}
$$

$$
S_2 = L_0^{-1} L_1 V_\mathrm{d},
\tag{6.74}
$$

$$
S_3 = -\frac{1}{3} L_0^{-1} L_1^3 (H_0) + L_0^{-1} L_2 V_\mathrm{d},
\tag{6.75}
$$

$$
\cdots
$$

where $L_0 A := [H_0, A]$. It is now possible to find general expressions for the low-energy effective Hamiltonian at each order, namely

$$
H_\mathrm{eff}^{(1)} = P V_\mathrm{d} P,
\tag{6.76}
$$

$$
H_\mathrm{eff}^{(2)} = \frac{1}{2} P L_1 V_\mathrm{od} P,
\tag{6.77}
$$

$$
H_\mathrm{eff}^{(3)} = \frac{1}{2} P L_2 V_\mathrm{od} P,
\tag{6.78}
$$

$$
H_\mathrm{eff}^{(4)} = \frac{1}{2} P L_3 V_\mathrm{od} P - \frac{1}{24} P L_1^3 V_\mathrm{od} P,
\tag{6.79}
$$

$$
\cdots
$$

Application to a general class of Hamiltonians

In this section, we want to apply the formalism presented above to a general class of Hamiltonians relevant to this work:

$$
H = H_0 + \sum_{j,n} T_n^j,
\tag{6.80}
$$

defined on a product Hilbert space $\mathcal{H}_1 \otimes \mathcal{H}_2$. From Eq. (6.17), it is clear that H of Eq. (6.1) has the above form. The unperturbed spectrum (given by H_0) can be described in terms of a single type of excitations in $\mathcal{H}_1$ (in our case, hard-core bosons) and a set of excitations in $\mathcal{H}_2$, labeled by an index α (in our case, photons belonging to different cavity modes). The operators T_n^j acts on $\mathcal{H}_1$ by changing the number of hard-core bosons by n (in our case, $n = 0, \pm 2$) and on $\mathcal{H}_2$ according to the index j. This can assume the values $j = m\alpha$, indicating that the number of photons of type α changes by m (in our case, $m = 0, \pm 1$). As discussed in the main text, we also use the convention $0\alpha \equiv 0$, such that there is a unique set of T_n^0 operators (which do not change the photon number of any mode).

At this point, we define the low-energy space of this system as the lowest energy eigenspace in $\mathcal{H}_1$. Therefore, P is the projector onto the subspace with no hard-core bosons, and $Q = 1 - P$ in the subspace where some hard-core boson is present. The diagonal and off-diagonal perturbations are given by

$$V_\mathrm{d} = \sum_j T_0^j + Q \underbrace{\sum_j \sum_{n \neq 0} T_n^j}_{=:B} Q, \tag{6.81}$$

$$V_\mathrm{od} = PBQ + QBP. \tag{6.82}$$

We assume in the following, as appropriate for our case,

$$PT_0^j = T_0^j P = 0, \tag{6.83}$$

and that the energy change due to the T_n^j operators is given by $\delta\epsilon_n^j$. Therefore, the following commutation relations hold:

$$\left[H_0, T_n^j\right] = \delta\epsilon_n^j \, T_n^j. \tag{6.84}$$

In the simplest case, the excitations also correspond to energy quanta, as in Eq. (6.18).

It is now possible to calculate $S_{1,2,3}$ according to Eqs. (6.73-6.75), which

give

$$S_1 = \sum_i \sum_n \left[\frac{PT_n^i Q}{\delta\epsilon_n^i} - \text{h.c.} \right], \tag{6.85}$$

$$S_2 = \sum_{i,j} \sum_{n,m} \left[\frac{PT_n^i Q T_m^j Q}{\delta\epsilon_n^i (\delta\epsilon_n^i + \delta\epsilon_m^j)} - \text{h.c.} \right], \tag{6.86}$$

$$S_3 = \sum_{i,j,k} \sum_{n,m,l} \left[\frac{PT_n^i Q T_m^j Q T_l^k Q}{\delta\epsilon_n^i (\delta\epsilon_n^i + \delta\epsilon_m^j)(\delta\epsilon_n^i + \delta\epsilon_m^j + \delta\epsilon_l^k)} \right.$$
$$+ \frac{1}{3} \frac{PT_n^i Q T_l^k PT_m^j Q + PT_m^j Q T_n^i PT_l^k Q}{\delta\epsilon_n^i \delta\epsilon_l^k (\delta\epsilon_n^i + \delta\epsilon_m^j + \delta\epsilon_l^k)}$$
$$\left. - \frac{2}{3} \frac{PT_n^i Q T_m^j PT_l^k Q}{\delta\epsilon_n^i \delta\epsilon_l^k (\delta\epsilon_n^i + \delta\epsilon_m^j + \delta\epsilon_l^k)} - \text{h.c.} \right], \tag{6.87}$$

where every term with $n = 0$ vanishes because of Eq. (6.83) and h.c. denotes hermitian conjugates (note that all the S_p are anti-hermitian). These hermitian conjugate terms can be written in a form similar to the ones explicitly appearing in the square parenthesis, by making use of

$$\left(T_n^i \right)^\dagger = T_{-n}^{-i}, \quad \text{a}nd \quad \delta\epsilon_{-n}^{-i} = -\delta\epsilon_n^i. \tag{6.88}$$

With the help of Eqs. (6.76-6.79), we finally obtain the low-energy effective Hamiltonian up to fourth order:

$$H_{\text{eff}}^{(1)} = 0, \tag{6.89}$$

$$H_{\text{eff}}^{(2)} = \frac{1}{2} \sum_{i,j} \sum_{n,m} \left[\frac{PT_n^i Q T_m^j P}{\delta\epsilon_n^i} + \text{h.c.} \right], \tag{6.90}$$

$$H_{\text{eff}}^{(3)} = \frac{1}{2} \sum_{i,j,k} \sum_{n,m,l} \left[\frac{PT_n^i Q T_m^j Q T_l^k P}{\delta\epsilon_n^i (\delta\epsilon_n^i + \delta\epsilon_m^j)} + \text{h.c.} \right], \tag{6.91}$$

$$H_{\text{eff}}^{(4)} = \frac{1}{2} \sum_{i,j,k,r} \sum_{n,m,l,q} \left[\frac{2}{3} \frac{-PT_n^i Q T_m^j PT_l^k Q T_q^r P}{\delta\epsilon_n^i \delta\epsilon_l^k (\delta\epsilon_n^i + \delta\epsilon_m^j + \delta\epsilon_l^k)} \right.$$
$$+ \frac{1}{3} \frac{PT_n^i Q T_l^k PT_m^j Q T_q^r P + PT_m^j Q T_n^i PT_l^k Q T_q^r P}{\delta\epsilon_n^i \delta\epsilon_l^k (\delta\epsilon_n^i + \delta\epsilon_m^j + \delta\epsilon_l^k)}$$
$$- \frac{1}{12} \frac{PT_n^i Q T_m^j PT_l^k Q T_q^r P + 3PT_n^i Q T_q^r PT_m^j Q T_l^k P}{\delta\epsilon_n^i \delta\epsilon_m^j \delta\epsilon_l^k}$$
$$\left. + \frac{PT_n^i Q T_m^j Q T_l^k Q T_q^r P}{\delta\epsilon_n^i (\delta\epsilon_n^i + \delta\epsilon_m^j)(\delta\epsilon_n^i + \delta\epsilon_m^j + \delta\epsilon_l^k)} + \text{h.c.} \right], \tag{6.92}$$

where again h.c. are hermitian conjugate terms.

6.B   SW transformation with a single cavity mode

We consider in this Appendix the application of the SW formalism to the case when a single cavity mode is present, coupled only to x-links. This is useful for both Secs. 6.4 and 6.5, where a read-out scheme and the effect of the cavity mode on the gap were studied.

Derivation of the effective Hamiltonian

In this case, the perturbation is given by T_n^0 and $T_n^\pm$ operators, where we drop the index α since only one mode is present. The treatment of the previous Appendix 6.A can be easily applied to this case, where $\delta\epsilon_n^j$ of Eq. (6.84) is as in Eq. (6.18), with $\omega_\alpha = \omega$. Since we are interested in the resonant case $(4J_z - \omega) \ll 4J_z, \omega$, the relevant energy differences are

$$\delta\epsilon_{+2}^- = -\delta\epsilon_{-2}^+ = 4J_z - \omega, \tag{6.93}$$

$$\delta\epsilon_0^0 = 0. \tag{6.94}$$

It is then possible to directly apply Eqs. (6.90) and (6.92), keeping only the terms where the energy denominators are obtained from $\delta\epsilon_{+2}^-$, $\delta\epsilon_{-2}^+$, and $\delta\epsilon_0^0$, which leads to

$$H_{\text{eff}} = \omega a^\dagger a - \frac{1}{4J_z - \omega}\left(\frac{1}{2}T_{-2}^+ T_{+2} + \text{h.c.}\right)$$

$$+ \frac{1}{(4J_z - \omega)^3}\left(\frac{5}{8}T_{-2}^+ T_{+2}^- T_{-2}^+ T_{+2} - \frac{1}{4}T_{-2}^+ T_{-2}^+ T_{+2}^- T_{+2}\right.$$

$$\left. - \frac{1}{8}T_{-2}^+ T_{+2} T_{-2}^+ T_{+2}^- - \frac{1}{2}T_{-2}^+ T_0^0 T_0^0 T_{+2} + \text{h.c.}\right). \tag{6.95}$$

where $T_{+2} = T_{+2}^0 + T_{+2}^+ + T_{+2}^-$, as defined in Eq. (6.17).

The effective Hamiltonian (6.95) is valid in the subspace with zero hard-core bosons, but is not diagonal in the number of photons. Therefore, it represents an effective Hamiltonian for the cavity and it requires to be further diagonalized to obtain the energy eigenstates. The explicit form of the photon Hamiltonian depends on the specific coupling scheme of the cavity to the links of the model, which is reflected in the T_n^j operators. As an example, we assume the homogeneous coupling scheme

(6.35), to all the x-links of the model, and consider first the terms up to second-order. Evaluating the first line of Eq. (6.95) in terms of effective spins and photon operators gives

$$
\begin{aligned}
H_{\text{eff}} = \quad & \omega a^\dagger a - \frac{\delta_x^2 N}{4 J_z - \omega} a^\dagger a - \frac{J_x \delta_x}{4 J_z - \omega} \left(a + a^\dagger \right) \frac{N}{2} \\
& - \frac{\delta_x^2}{4 J_z - \omega} \left(a^2 + a^{\dagger 2} \right) \frac{N}{2} + \dots .
\end{aligned}
\tag{6.96}
$$

The first two terms appear in Eq. (6.36) while the off-diagonal terms can be eliminated with a second SW transformation, in the photon operators only. Such off-diagonal terms involve excitations with energy ω or 2ω and therefore give small corrections in the resonant limit we are interested. Therefore, we have neglected them in Eq. (6.36).

Evaluating all the fourth-order terms appearing in Eq. (6.95) is cumbersome, but this is not necessary for our purposes. As explained above, we keep only the terms already diagonal in the photon number, while the other ones give only small non-resonant corrections. Therefore, we can simply substitute all the T_n operators in Eq. (6.95) by T_n^-. Furthermore, we are interested to the coupling of the photon mode to the W_a operators, which are the product of spin operators involving four *distinct* links of the model (of which two are x-links and two y-links). To understand the relevant terms at fourth order we note that, for the specific coupling scheme (6.35), only the x-links are coupled to the cavity mode. Therefore: (i) the T_n^0 operators involve a sum of terms with all the links of the model, while (ii) the $T_n^\pm$ operators are sums of terms with only x-links. Since only the T_0^0 operators contain terms relative to the y-links, it becomes clear that only the $T_{-2}^+ T_0^0 T_0^0 T_{+2}^-$ combination can couple to the W_a operators. Finally, (6.95) can be simplified to the following form

$$
H_{\text{eff}} = \omega a^\dagger a - \frac{T_{-2}^+ T_{+2}^-}{4 J_z - \omega} - \frac{T_{-2}^+ T_0^0 T_0^0 T_{+2}^-}{\left(4 J_z - \omega \right)^3},
\tag{6.97}
$$

which evaluates to Eq. (6.36), by expressing it in terms of photon and effective spin operators. As it turns out, the same reasonings apply to the read-out methods we discussed in Sec. 6.4, where as well only couplings to the x-links appear. Therefore, Eq. (6.97) is also the relevant effective Hamiltonian for the coupling schemes (6.26) and (6.30), which evaluate to Eqs. (6.27) and (6.32) respectively. Note that we have always neglected in the final results a sub-leading constant correction of the cavity frequency, i.e., the $a^\dagger a$ term appearing in fourth order and independent of the W_a operators.
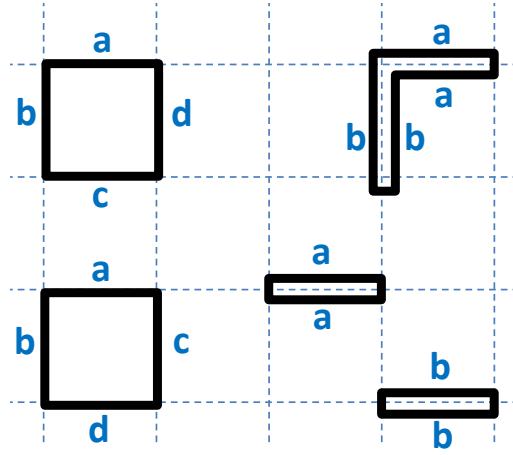
Figure 6.6: Pictorial representation of the connected and disconnected terms entering the perturbation expansion (6.95). Both loops $abcd$ and $abba$ represent the different contributions arising from the connected term $T_{-2}^{+} T_0^0 T_0^0 T_{+2}^{-}$. We see that only $abcd$ loops lead to terms proportional to W_a, since all four links are different. This is not the case for the $abba$ loop and the corresponding terms are constants. The remaining fourth-order terms entering Eq. (6.95) can be represented by two disconnected loops aa and bb. Since the number of different positions of each aa and bb loop is proportional to N, the contribution of the disconnected terms is $\sim N^2$.

Disconnected terms

We would like to comment here on a special aspect which arises in the presence of cavity modes, i.e., the appearance in the perturbative expansion of non-extensive terms in the size of the system N. These originate from disconnected terms in the perturbation expansion which, if the Hamiltonian is local, give a vanishing contribution. [75] This result, known as linked-cluster theorem, is not valid here because of the long-range nature of the coupling of the photon modes, which are delocalized and can interact simultaneously with links at any distance across the lattice.

For the case of interest here, the only connected fourth-order term appearing in Eq. (6.95) is the last one, with its hermitian conjugate. Consider in fact the action of $T_{-2}^{+} T_0^0 T_0^0 T_{+2}^{-}$: the first operator from right to left, T_{+2}, creates two hard-core bosons on a certain link. The second and third operators make such hard-core bosons hop, and therefore they have to act on links where only one hard-core boson is present. Finally, the last

operator T^+_{-2} annihilates the two hard-core bosons. Therefore the links involved form a single closed loop, of the form $abcd$ (if all four links are different, which contributes with a term proportional to W_a) or $abba$ (if the links are repeated, which contributes with a term without W_a), see Fig. 6.6.

On the other hand, the remaining three fourth-order terms appearing in Eq. (6.95), with their hermitian conjugates, are disconnected. To see this, we note that at most one of the four operators, the $T_{\pm 2}$, can act on a y-link, while the other three, of the form $T^\pm_n$, only contain x-link terms. Therefore, the only possibility is that two pairs of hard-core bosons are created on distinct x-links and annihilated on the same two links, a processes that can be represented with two small disconnected loops aa and bb, see Fig. 6.6. These processes can contribute with terms which are of order N^2 instead of N. Clearly, this does not occur for the read-out schemes discussed in Sec. 6.4, where each cavity mode is coupled locally to a single plaquette or star, but is relevant for Sec. 6.5. By assuming the homogeneous coupling scheme (6.35), the disconnected terms of Eq. (6.95) evaluate to

$$
\begin{aligned}
&- \frac{1}{2} \frac{\delta_x^3 (N^2 - 3N)}{(4J_z - \omega_1)^3} (J_x a^{\dagger 2} a + \delta_x a^{\dagger 2} a^2 + \delta_x a^{\dagger 2} a a^\dagger + \text{h.c.}) \\
&+ \frac{5}{8} \frac{\delta_x^3 N^2}{(4J_z - \omega_1)^3} (J_x a^\dagger a a^\dagger + \delta_x a^\dagger a a^\dagger a + \delta_x a^\dagger a a^{\dagger 2} + \text{h.c.}) \\
&- \frac{1}{8} \frac{\delta_x^3 N^2}{(4Jz - \omega_1)^3} (J_x a^{\dagger 2} a + \delta_x a^\dagger a a^\dagger a + \delta_x a^{\dagger 3} a + \text{h.c.}).
\end{aligned}
$$

(6.98)

It is immediate to check that, if the photon operators are replaced by complex numbers, i.e., $a^{(\dagger)} \to \alpha^{(*)}$, Eq. (6.98) gives an extensive contribution since all the N^2 terms cancel, in agreement with the linked-cluster theorem. If we use the bosonic commutation relation $[a, a^\dagger] = 1$, then we can simplify Eq. (6.98) to the following form

$$
\begin{aligned}
&- \frac{3N}{2} \delta_x^3 [\delta_x (a^{\dagger 2} a^2 + a^{\dagger 2} a a^\dagger + \text{h.c.}) + J_x (a^{\dagger 2} a + a^\dagger a^2)] \\
&+ \frac{N^2}{8} \delta_x^3 [8 \delta_x a^\dagger a + 5 J_x (a + a^\dagger) + 6 \delta_x (a^2 + a^{\dagger 2})],
\end{aligned}
$$

(6.99)

where the N^2 contribution (second line) does not vanish.

This result does not represent a fundamental problem since, for a finite system, terms proportional to N^2 or higher powers of N can certainly exist. However, the final perturbative expressions are not extensive quantities in the thermodynamic limit $N \to \infty$. This behavior can

be attributed to the failure of the perturbative treatment since, besides the conditions $J_{x,y}$, $\delta_x\sqrt{\langle a^\dagger a\rangle} \ll (4J_z - \omega)$, the requirement to have a power series in terms of small expansion parameters also leads to an upper bound on the size of N, namely

$$\delta_x\sqrt{N} \ll (4J_z - \omega_x). \tag{6.100}$$

This condition is not very restrictive, since the coupling δ_x is expected to be small. Furthermore, an interesting limit is obtained for a vanishing coupling δ_x and a large number of photons $\langle a^\dagger a\rangle$. In this case, for system size $N \ll \langle a^\dagger a\rangle$, the non-extensive terms can be generally neglected in comparison to the extensive ones. For example, in Eq. (6.99) this condition would give $\delta_x^3 N\langle a^\dagger a\rangle^2 \gg \delta_x^3 N^2\langle a^\dagger a\rangle$, by comparing the first and second line.

6.C   SW transformation in the presence of four different links and two resonant cavity modes

In this section we present how the SW transformation is applied to the scheme of Sec. 6.6 for which the four links belonging to each W_a operator have all distinct couplings, see Eqs. (6.41), (6.42), and Fig. 6.4. By using Eqs. (6.90) and (6.92) one can obtain the zero hard-core boson effective Hamiltonian up to fourth order. Since we are interested in a regime where $(4J_z - \omega_{x,y}) \ll \omega_{x,y}$, we keep the resonant terms only. Furthermore, it is sufficient to keep at fourth order only the terms that couple to the star and plaquette operators. This leads to:

$$H_{\text{eff}} = \sum_{\alpha=x,y}\left[\omega_\alpha a_\alpha^\dagger a_\alpha - \frac{T_{-2}^\alpha(T_{+2}^0 + T_{+2}^\alpha + T_{+2}^{-\alpha}) + \text{h.c.}}{2(4J_z - \omega_\alpha)}\right.$$
$$\left. - \frac{T_{-2}^{+\alpha}T_0^0 T_0^0(T_{+2}^0 + T_{+2}^{-\bar\alpha}) + \text{h.c.}}{2(4J_z - \omega_\alpha)^3}\right]. \tag{6.101}$$

where $\bar\alpha = y$ if $\alpha = x$ and vice-versa. In the above expression, terms like $T_{-2}^\alpha T_{+2}^\beta T_{-2}^\gamma T_{+2}^\zeta$ or $T_{-2}^\alpha T_{-2}^\beta T_{+2}^\gamma T_{+2}^\zeta$ do not appear, because they do not contribute to the resonant coupling to the W_a operators. It is worth mentioning that the conditions in order to treat the Hamiltonian within perturbation theory are the same as in Appendix 6.B, namely

$$J_\alpha,\ \delta_\alpha\sqrt{\langle a_\alpha^\dagger a_\alpha\rangle},\ \delta_\alpha\sqrt{N} \ll \min(4J_z - \omega_{x,y}). \tag{6.102}$$

By writing Hamiltonian (6.101) explicitly in terms of effective spin operators and photon operators, we obtain the following zero hard-core boson effective Hamiltonian

$$
\begin{aligned}
H_{\text{eff}} \quad = \sum_{\alpha=x,y} \Bigg[&\omega'_\alpha a^\dagger_\alpha a_\alpha - \frac{J_\alpha \delta_\alpha}{4J_z - \omega_\alpha} \left(a_\alpha + a^\dagger_\alpha\right) \frac{N}{4} \\
&- \frac{\delta_\alpha^2}{4J_z - \omega_\alpha} \left(a_\alpha^2 + a_\alpha^{\dagger 2}\right) \frac{N}{4} \\
&- \frac{J_{\bar\alpha}^2 J_\alpha \delta_\alpha}{(4J_z - \omega_\alpha)^3} \left(a_\alpha + a^\dagger_\alpha\right) \sum_{\boldsymbol{a}} W_{\boldsymbol{a}} \\
&- \frac{J_x J_y \delta_x \delta_y}{2(4J_z - \omega_\alpha)^3} \left(a^\dagger_x a_y + a_x a^\dagger_y\right) \sum_{\boldsymbol{a}} W_{\boldsymbol{a}} \Bigg].
\end{aligned}
$$
(6.103)

In the strictly resonant case [see Eq. (6.45)] we can drop all the non-diagonal terms except the last line, which leads to Eq. (6.44). If we want to calculate the leading non-resonant correction to the chemical potential, we have to keep also the $(a_\alpha + a^\dagger_\alpha)$ terms in the first and third line, which leads to Eq. (6.54). This is because, as explained in Sec. 6.6, these two non-diagonal terms combine to a higher-order $\sum_{\boldsymbol{a}} W_{\boldsymbol{a}}$ contribution, diagonal in the photon modes, after a second SW transformation. On the other hand, $(a_\alpha^2 + a_\alpha^{\dagger 2})$ does not appear together with $\sum_{\boldsymbol{a}} W_{\boldsymbol{a}}$ and therefore can be dropped, for the purpose of obtaining corrections to the star and plaquette couplings. Finally we note that the third line, after the second SW transformation in the photon operators, also leads to a interaction term $(\sum_{\boldsymbol{a}} W_{\boldsymbol{a}})^2$, but this is generally negligible compared to the one from the last line of Eq. (6.103) and is not considered in Sec. 6.6.

As a last note, a conservative requirement to perform the SW on Eq. (6.103) is that that the off-diagonal operators are much smaller than the corresponding gaps. From the first line of Eq. (6.103) we obtain

$$
\frac{J_\alpha \delta_\alpha \sqrt{\langle a_\alpha a^\dagger_\alpha \rangle}}{4J_z - \omega_\alpha} \frac{N}{4} \ll \omega'_\alpha,
$$
(6.104)

and from the fourth line

$$
\frac{J_x J_y \delta_x \delta_y \sqrt{\langle a_x a^\dagger_x \rangle \langle a_y a^\dagger_y \rangle}}{2(4J_z - \omega_\alpha)^3} N \ll |\omega'_x - \omega'_y|.
$$
(6.105)

Finally, the condition from the third line of Eq. (6.103) is less restrictive than Eq. (6.104), because of an additional small factor $J_{\bar\alpha}^2/(4J_z - \omega_\alpha)^2$. These conditions, together with Eq. (6.102), pose a restriction onto the size N at which the perturbative treatment is justified.

6.D SW transformation in the presence of small frequency modes

The main purpose of this section is to prove the prescription (6.58) of Sec. 6.7 to obtain the effective Hamiltonian in the presence of off-resonant cavity modes.

First we note that, if no cavity is present, only the T_n^0 operators are non-vanishing and $T_n = T_n^0$. Therefore, we can drop in Eqs. (6.89-6.92) the summations in the photon indexes i, j, k, r and set all the T_n^i operators equal to T_n. On the other hand, by making use of Eq. (6.57) for the case with small frequency modes, we can approximate $\delta\epsilon_n^i \simeq 2nJ_z$, i.e., neglect the photon frequency shifts in the denominators of Eqs. (6.89-6.92). This allows to perform the summations in the photon indexes and express Eqs. (6.89-6.92) in terms of the T_n operators, as for the case without photon modes discussed above. The difference is that the T_n are now photon operators, simply obtained from the ones without cavities by substituting $J_{a,k} \to K_{a,k}$ (where $k = x, y$). Furthermore, it is also clear from Eq. (6.2) that the $K_{a,k}$ are all commuting operators, and therefore they can be treated in the same way of the $J_{a,k}$ in the derivation of the effective Hamiltonian. This shows that it is sufficient to apply Eq. (6.58), if the effective Hamiltonian without cavity modes is known.

By applying this prescription to the second coupling scheme of Sec. 6.7 [see Eq. (6.61)], we obtain the following effective Hamiltonian

$$
\begin{aligned}
H_{\text{eff}} = \sum_{\alpha=x,y} &\left[\omega''_\alpha a_\alpha^\dagger a_\alpha - \frac{J_\alpha \delta_\alpha}{4J_z}(a_\alpha + a_\alpha^\dagger)N \right.\\
&\left. - \frac{\delta_\alpha^2}{4J_z}(a_\alpha^2 + a_\alpha^{\dagger 2})\frac{N}{2} - \frac{J_\alpha^2 J_\alpha \delta_\alpha}{16J_z^3}(a_\alpha + a_\alpha^\dagger)\sum_a W_a \right]\\
&- \frac{J_x^2 J_y^2}{16J_z^3}\sum_a W_a - \frac{J_x J_y \delta_x \delta_y}{16J_z^3}\left(a_x a_y^\dagger + a_y^\dagger a_x\right)\sum_a W_a\\
&- \frac{J_x J_y \delta_x \delta_y}{16J_z^3}\left(a_x a_y + a_x^\dagger a_y^\dagger\right)\sum_a W_a
\end{aligned}
\tag{6.106}
$$

where ω''_α are defined in Eq. (6.63). In Eq. (6.106), we only kept terms from the first and last lines of Eq. (6.20) while dropping all the fourth order terms which do not couple to the W_a operators and some inessential constants.

We note now that the $(a_\alpha^2 + a_\alpha^{\dagger 2})$ term, in the second line of Eq. (6.106), does not have a corresponding $\sum_a W_a$ term, and that the off-resonant

coupling to the W_a operators in the last line does not have a corresponding $\left(a_x a_y + a_x^\dagger a_y^\dagger\right)$ term at lower order. Therefore, after a second SW transformation of Eq. (6.106), these two terms give negligible corrections to the effective Hamiltonian for the star and plaquette operators and we have dropped them in Eq. (6.62).

Towards a Local 3D Hamiltonian as a Thermally Stable Surface Code

119

We propose and study two examples of quantum memories that present self-correcting properties. This is achieved by locally coupling a 2D $L \times L$ toric code to a 3D system. The first is to embed the toric code into a 3D Heisenberg ferromagnet (FM) in a broken-symmetry state at finite temperature. The stabilizer operators of the toric code are then locally coupled to individual spins of the FM. The second is to similarly couple the toric code to a system of bosons hopping on a cubic lattice. In both cases an effective Hamiltonian is derived for the toric code in which the energy penalty required to create anyons grows linearly with L, and thus the lifetime of the quantum memory grows exponentially with L. While we make use of perturbation theory to study the toric code coupled to the FM, the coupling to the hopping boson system is exactly solvable via a polaron transformation. Furthermore, we show how to choose an appropriate coupling scheme in order to hinder the hopping of anyons (and not only their creation) with energy barriers that also grow proportionally to L. We study the backaction of the toric code onto the FM both analytically and with a Monte-Carlo simulation and show a tilting of the spins close to the code after a time t_r independent of L. When $t > t_r$ two scenarios are conceivable. Either magnetic pulses are applied to the FM at constant time intervals t_r in order to refresh the FM and thus maintain a $O(L)$ energy penalty for the anyons, or the spins of the FM reach the new equilibrium position and the energy penalty scales only with $\ln(L)$ (and so the lifetime as poly L). Our analysis provides evidence that the first model is stable against *adiabatic* errors. However, since the effective Hamiltonian is derived within the framework of perturbation theory, our study does not represent a full proof of self-correction which remains an open problem for the ferromagnet model. This is in contrast with the second model that we have solved exactly. In this case we show that our model with strictly local bounded-strength interactions in three dimensions has an energy barrier that grows linearly with the system size and thus a lifetime of the memory that grows exponentially with L.

7.1 Introduction

In this work, we propose two three-dimensional (3D) models with purely local interactions of bounded strength that present self-correcting properties. First, we consider a surface code embedded in a bulk ferromagnet (FM) and find an anyon chemical potential increasing linearly with L and thus a memory lifetime increasing exponentially with L. This scaling of the lifetime coincides with the four-dimensional toric code, [15, 106]

which constitutes so far the only known example of a truly self-correcting quantum memory.

The origin of this favorable behavior resides in the long-range character of the ferromagnetic transverse susceptibility in the ordered phase since it describes the effective attractive interactions between stabilizer operators. This long-range behavior is based on the low-energy modes of the FM in the broken-symmetry phase. This result is general and does not depend on damping effects and temperature T as long as the FM stays in the ordered phase. The effect of the FM can then be understood in terms of virtual emission and absorption of magnons which mediate long-range interactions between the stabilizer operators. Our analysis is based on the derivation of an effective Hamiltonian within the framework of perturbation theory. As such, the effective theory is expected to describe accurately the low-energy physics of our model. The necessary assumptions for the validity of the effective theory are given in Section 7.5: the effective Hamiltonian is valid in the low-energy and long-wavelength approximation and the quantum memory is expected to be protected against *adiabatic errors* only. Being based on perturbation theory, our analysis does not represent a full proof of self-correction: this remains an interesting open problem. In the harmonic approximation, the Hamiltonian can be solved exactly and allows to give an exact expression for the chemical potential of the anyons which is in complete agreement with the one-magnon result.

We study a second model consisting of a toric code coupled to a reservoir of hopping bosons on a cubic lattice. This model retains all the positive aspects of the previous model, namely it only involves local interactions of bounded-strength in three dimensions and it has the additional advantage to be exactly solvable via a polaron transformation. The coupling to the bosons again lead to an energy penalty for the anyons that grows linearly with L and thus to a lifetime that increases exponentially with L. Contrary to the analysis of the FM model, our study of the hopping bosons system is exact. Nevertheless, as bosonic operators are unbounded, the self-correcting nature of this model is less surprising than would be a similar behavior for the FM model. We note that both models are related to each other since the FM Hamiltonian in the harmonic approximation coincides with the hopping boson Hamiltonian as we show below.

We study backaction effects of the surface code onto the FM both analytically and with a Metropolis simulation. We show that the surface code leads to a tilting of the spins close to the code after a time t_r which depends only on the parameters of the FM and the coupling between the

surface code plaquettes and the spins of the FM (but not on the size L). Applying a magnetic pulse at fixed time intervals allows one to keep the spins of the FM along z and thus renders backaction effects negligible. Although this procedure is sufficient to stabilize the quantum memory, it is not necessary. When the ferromagnetic spins reach their new equilibrium position, the coupling between stabilizers is then given by the longitudinal susceptibility which is shorter-ranged. However, this still leads to a chemical potential scaling with $\ln(L)$ and a memory lifetime increasing polynomially with L.

Finally we present a coupling scheme, that applies to the FM as well as to the hopping bosons, in order to hinder hopping of anyons, and not only their creation, by an $O(L)$ energy barrier. This is useful since imperfections in the initialization process might lead to a finite density of anyons.

7.2 Coupling to the ferromagnet

We introduce two sets of spins, namely $\boldsymbol{S}_j$ for the spins of the 3D FM located at site j of a cubic lattice and $\boldsymbol{I}_j$ for the physical spins-$1/2$ of the 2D surface code. Both spins satisfy the usual commutation relations. The Hamiltonian we consider is purely local and given by

$$H = H_{\mathrm{F}} + A \sum_{\boldsymbol{p}} W_{\boldsymbol{p}} S_{\boldsymbol{p}}^x \,, \tag{7.1}$$

where A is the coupling constant between the spins of the surface code and the FM. Here, the plaquette (stabilizer) operator $W_{\boldsymbol{p}} = I_{\boldsymbol{p},1}^z I_{\boldsymbol{p},2}^y I_{\boldsymbol{p},3}^z I_{\boldsymbol{p},4}^y$ is the poduct of spins around the square plaquette centered at $\boldsymbol{p}$, which are defined on a square lattice of linear size L with periodic boundary conditions (we set the lattice constant to unity). The 3D vector $\boldsymbol{p}$ points towards the spin $\boldsymbol{S}_{\boldsymbol{p}}$ of the FM located in the center of a plaquette, see Fig. 7.1. Note that this definition of $W_{\boldsymbol{p}}$ ensures that the blue and white plaquettes are equivalent to the usual toric code star and plaquette operators. [14]

Here, $H_{\mathrm{F}} = -J \sum_{\langle i,j \rangle} \boldsymbol{S}_i \cdot \boldsymbol{S}_j + h_z \sum_i S_i^z$ is the Hamiltonian of the 3D Heisenberg FM of linear size $\Lambda \gg L$, where $J > 0$ is the exchange constant and the sum is restricted to nearest-neighbor lattice sites. The FM is assumed to be below the Curie temperature and the spins ordered along the z-direction. To break the symmetry of the FM, a small magnetic field h_z in z-direction is applied. This field also stabilizes the FM against the effective magnetic field produced by the surface code (see below). The
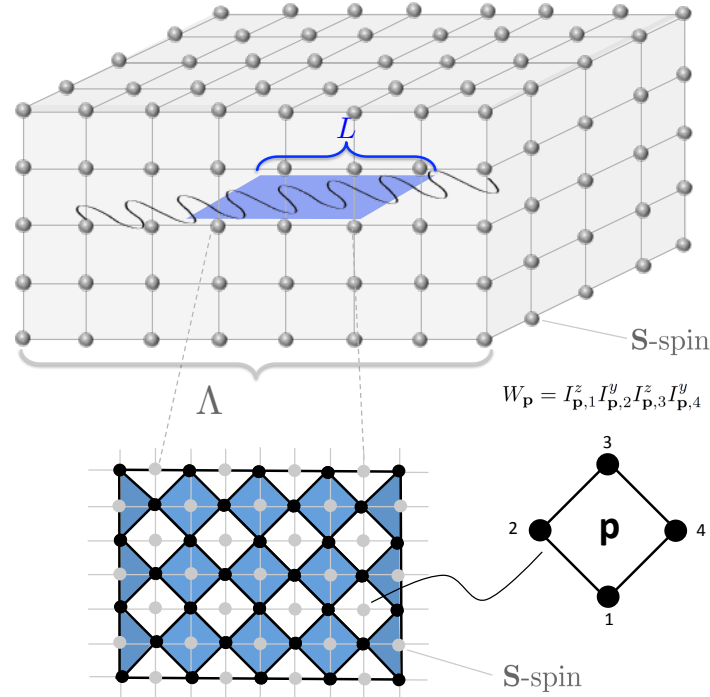
Figure 7.1: A 2D surface code (blue area in xy-plane) of size L^2 is centered inside a cubic 3D Heisenberg ferromagnet of lattice size Λ^3 which is in a broken-symmetry state (magnetization along the z-axis). The stabilizers $W_{\boldsymbol{p}}$ of the surface code locally couple to the S-spins (grey dots) of the FM. The low-energy magnons (wiggly line) in the FM mediate attractive interactions between the stabilizers. Alternatively the toric code can be coupled to a system of hopping bosons on a cubic lattice. In this case the long-range attraction between the stabilizers is mediated by the low-energy collective excitations of the bosons.

physical spins $\boldsymbol{I}_j$ of the surface code are embedded in the bulk of the FM. The interaction Hamiltonian $H_{\text{int}} = A \sum_{\boldsymbol{p}} W_{\boldsymbol{p}} S_{\boldsymbol{p}}^x$ involves five-body interaction terms that are purely local. We define the anyon number $n_{\boldsymbol{p}}$ such that $W_{\boldsymbol{p}} = 1 - 2n_{\boldsymbol{p}}$. Although Hamiltonian (14.16) is three-dimensional, we point out for the sake of clarity, that the actual quantum memory is the two-dimensional surface code. As we show below, the presence of the 3D system is necessary to mediate long-range interactions between the stabilizers. However, the place where the logical qubits are stored is the two-dimensional surface code.

For $A \ll J$, we make use of a perturbative Schrieffer-Wolff transformation [75, 134] to derive the effective plaquette-plaquette interaction

(see 7.A) given by

$$H_{\text{eff}} = \frac{1}{2} \sum_{\boldsymbol{p},\boldsymbol{p}'} J_{\boldsymbol{p},\boldsymbol{p}'} W_{\boldsymbol{p}} W_{\boldsymbol{p}'} , \qquad (7.2)$$

where the coupling is $J_{\boldsymbol{p},\boldsymbol{p}'} = -A^2 \chi_{xx}(\boldsymbol{p} - \boldsymbol{p}')$ and $\chi_{\alpha\beta}(\boldsymbol{r})$ is the static spin susceptibility of the FM. Note that the energy in H_{eff} can be minimized by either all stabilizers $W_{\boldsymbol{p}}$ having a $+1$ or a -1 eigenvalue. Adding the usual toric code Hamiltonian $H_{\text{toric}} = -\Delta \sum_{\boldsymbol{p}} W_{\boldsymbol{p}}$ to (14.16) would explicitly break this symmetry between anyons $n_{\boldsymbol{p}}$ and anyon-holes $\bar{n}_{\boldsymbol{p}} = 1 - n_{\boldsymbol{p}}$. However, H_{toric} is not needed and its effect is vanishing in the limit of large L, as we discuss in the 7.B, so we neglect it for simplicity. The real space static susceptibility $\chi_{\alpha\beta}(\boldsymbol{r})$ is defined as the Fourier transform of

$$\chi_{\alpha\beta}(\boldsymbol{q},\omega) = i \lim_{\eta \to 0^+} \int_0^\infty \mathrm{d}t \, e^{(i\omega - \eta)t} \left\langle \left[S_{\boldsymbol{q}}^\alpha(t), S_{-\boldsymbol{q}}^\beta \right] \right\rangle , \qquad (7.3)$$

for $\omega = 0$, where $\langle \ldots \rangle$ denotes thermal equilibrium expectation values of the $\boldsymbol{S}$-spins at temperature T. The Fourier components are defined as $S_{\boldsymbol{q}}^\alpha = \frac{1}{\sqrt{N_s}} \sum_i e^{-i\boldsymbol{q} \cdot \boldsymbol{R}_i} S_i^\alpha$, where N_s is the number of spins in the FM, and $\boldsymbol{R}_i$ is a 3D vector pointing to the site of spin $\boldsymbol{S}_i$ of the FM.

It is not necessary to explicitly calculate the spin susceptibility in the ferromagnetically ordered state to understand its general behavior at large distances (or small $\boldsymbol{q}$). [135] Indeed, for $h_z = 0$, the spontaneous $SO(3)$ symmetry breaking of the state with finite magnetization pointing along, say, the z-axis, implies the presence of low-frequency Goldstone modes (called magnons in this context) and long-range correlations, i.e., the xx- (and yy-) susceptibility has to diverge for $\boldsymbol{q} \to \boldsymbol{0}$ and takes the following generic form in the hydrodynamic regime (low-energy and long wavelength regime) [135]

$$\chi_{xx}(\boldsymbol{q},\omega = 0) = \frac{M^2}{R|\boldsymbol{q}|^2} \text{ for } \boldsymbol{q} \to \boldsymbol{0} , \qquad (7.4)$$

where $R > 0$ is the stiffness constant of the FM and $M = \langle s^z \rangle$ is the magnetization density with $s^z = \frac{1}{N_s} \sum_i S_i^z$. Equation (7.4) is the expression for the spin susceptibility in the continuum approximation (lattice constant a going formally to zero). To be valid this approximation does not require that the number of spins goes to infinity, but rather that the distance between neighboring spins is much smaller than the distances we are interested in. Since we are concerned with the long-distance physics of our model on the scale of L, this approximation is justified and simply

requires $a/L \ll 1$. In this limit, both the lattice constants of the ferromagnet and of the toric code are taken to zero such that a single plaquette remains coupled to a single FM spin. The divergence at $\boldsymbol{q} \to \boldsymbol{0}$ in Eq. (7.4) is trivially connected with the broken symmetry of the ground state: starting from a ferromagnetic state aligned along the z-direction, the slightest x-magnetic field is able to rotate and align all spins in x-direction and thus the response to an external magnetic field indeed diverges at $\boldsymbol{q} \to \boldsymbol{0}$. Below we give an explicit expression for R in the one-magnon approximation. The presence of the symmetry-breaking magnetic field h_z introduces a gap in the magnon spectrum and thus a mass term in the susceptibility, i.e., $\chi_{xx}(\boldsymbol{q}, \omega = 0) = \frac{M^2}{R|\boldsymbol{q}|^2 + Sh_z}$ for $\boldsymbol{q} \to \boldsymbol{0}$. The real space static susceptibility now follows by Fourier transformation which leads to $\chi_{xx}(\boldsymbol{r}) = \frac{M^2}{R} \frac{1}{4\pi|\boldsymbol{r}|} e^{-|\boldsymbol{r}|/L_h}$, with magnetic length $L_h = \sqrt{R/Sh_z}$. Consequently, Eq. (7.2) describes a stabilizer Hamiltonian with plaquette-plaquette interactions given by a Yukawa-like potential,

$$J_{\boldsymbol{p},\boldsymbol{p}'} = -\frac{A^2 M^2}{4\pi R} \frac{e^{-|\boldsymbol{p}-\boldsymbol{p}'|/L_h}}{|\boldsymbol{p}-\boldsymbol{p}'|} . \tag{7.5}$$

Since $R > 0$ (see also below), the interaction between stabilizer operators $W_{\boldsymbol{p}}$ is *a*ttractive.

For the sake of illustration we calculate R in the one-magnon (harmonic) approximation by making use of the Holstein-Primakoff transformation

$$S_i^z = -S + \hat{n}_i \,, \quad S_i^- = a_i^\dagger \sqrt{2S - \hat{n}_i} \,, \quad S_i^+ = (S_i^-)^\dagger, \tag{7.6}$$

in the formal limit $\hat{n}_i \ll 2S$, where $\hat{n}_i = a_i^\dagger a_i$. [47] Here, a_i and $a_i^\dagger$ satisfy bosonic commutation relations and the associated quasi-particles are called magnons. In Fourier space, we get $H_F \approx \sum_{\boldsymbol{q}}(\omega_{\boldsymbol{q}} + h_z)a_{\boldsymbol{q}}^\dagger a_{\boldsymbol{q}}$, up to some irrelevant constant, with magnon dispersion $\omega_{\boldsymbol{q}} = 4JS[3 - (\cos(q_x) + \cos(q_y) + \cos(q_z))]$, where $a_{\boldsymbol{q}} = \frac{1}{\sqrt{N_s}} \sum_i e^{-i\boldsymbol{q}\cdot\boldsymbol{R}_i} a_i$. Inserting Eq. (7.6) into Eq. (7.4) and using a small $\boldsymbol{q}$ expansion leads to $\chi_{xx}^{(0)}(\boldsymbol{q}, \omega = 0) = \frac{S}{2JS|\boldsymbol{q}|^2 + h_z}$, which allows us to identify $R^{(0)} = 2JS^2$ since here $M^{(0)} = -S$. We thus obtain $\chi_{xx}^{(0)}(\boldsymbol{r}) = \frac{1}{8\pi J|\boldsymbol{r}|} e^{-|\boldsymbol{r}|/L_h}$ and from this the approximate plaquette coupling

$$J_{\boldsymbol{p},\boldsymbol{p}'}^{(0)} = -\frac{A^2}{8\pi J} \frac{e^{-|\boldsymbol{p}-\boldsymbol{p}'|/L_h}}{|\boldsymbol{p}-\boldsymbol{p}'|}, \tag{7.7}$$

which is explicitly attractive since $J > 0$. We emphasize that Eq. (7.7) is the one-magnon approximation of Eq. (7.5). The sole effect of both temperature and damping due to magnon-magnon interactions is to renormalize the coefficients of the interaction (7.7), i.e. $(M^{(0)})^2/R^{(0)} \to M^2/R$

[135], while the form of the potential is not affected. Note that the creation or annihilation of magnons will not generate anyons in the toric code since the coupling terms in Hamiltonian (14.16) commute with the toric code stabilizers. The presence of thermal magnons in the FM will only translate into small fluctuations of the chemical potential for the anyons. Note also that the dimensionality of the 3D FM is critical since Heisenberg FMs in lower dimensions do not order at $T > 0$. [136]

7.3 Coupling to a reservoir of hopping bosons

We present here a second model for a stable quantum memory in three dimensions. It is closely related to Hamiltonian (14.16) but has the additional advantage to be exactly solvable. The Hamiltonian again involves only local couplings of bounded strength A' in three dimensions:

$$H' = H_{\text{Boson}} + A' \sum_{\boldsymbol{p}} W_{\boldsymbol{p}}(a_{\boldsymbol{p}} + a_{\boldsymbol{p}}^\dagger) \,, \tag{7.8}$$

where $H_{\text{Boson}} = \epsilon_{\boldsymbol{0}} \sum_i a_i^\dagger a_i - t \sum_{\langle i,j \rangle} a_i^\dagger a_j$ describes bosons hopping on a cubic lattice with hopping amplitude t and on-site chemical potential $\epsilon_{\boldsymbol{0}}$. Here, $a_i^\dagger$ creates a boson at site i, while a_i destroys a boson at site i of the cubic lattice. In Fourier space the Hamiltonian (7.8) becomes

$$H' = \sum_{\boldsymbol{q}} \epsilon_{\boldsymbol{q}} a_{\boldsymbol{q}}^\dagger a_{\boldsymbol{q}} + \sum_{\boldsymbol{p},\boldsymbol{q}} W_{\boldsymbol{p}}(M_{\boldsymbol{q},\boldsymbol{p}} a_{\boldsymbol{q}} + \text{h.c.}) \,, \tag{7.9}$$

where $\epsilon_{\boldsymbol{q}} = \epsilon_{\boldsymbol{0}} - t_{\boldsymbol{q}}$ with $t_{\boldsymbol{q}} = \frac{1}{N} \sum_{\langle ij \rangle} t e^{i\boldsymbol{q} \cdot (\boldsymbol{r}_i - \boldsymbol{r}_j)}$ and $M_{\boldsymbol{p},\boldsymbol{q}} = A' e^{i\boldsymbol{q} \cdot \boldsymbol{R}_{\boldsymbol{p}}}/\sqrt{N}$. Choosing the on-site potential such that $\epsilon_{\boldsymbol{0}} = t_{\boldsymbol{0}}$, we obtain the dispersion $\epsilon_{\boldsymbol{q}} = 2t \left(3 - (\cos(q_x) + \cos(q_y) + \cos(q_z))\right)$. This Hamiltonian is similar to the independent boson model [137] and thus exactly solvable via the unitary polaron transformation,

$$e^{\mathcal{S}} H' e^{-\mathcal{S}} = \sum_{\boldsymbol{q}} \epsilon_{\boldsymbol{q}} a_{\boldsymbol{q}}^\dagger a_{\boldsymbol{q}} - \sum_{\boldsymbol{p},\boldsymbol{p}',\boldsymbol{q}} W_{\boldsymbol{p}} W_{\boldsymbol{p}'} \frac{M_{-\boldsymbol{q},\boldsymbol{p}} M_{\boldsymbol{q},\boldsymbol{p}'}}{\epsilon_{\boldsymbol{q}}} \,, \tag{7.10}$$

where $\mathcal{S} = \sum_{\boldsymbol{p},\boldsymbol{q}} W_{\boldsymbol{p}} M_{-\boldsymbol{q},\boldsymbol{p}} a_{\boldsymbol{q}}^\dagger/\epsilon_{\boldsymbol{q}} - \text{h.c.}$ Going to the continuum and small-q limit, $\epsilon_{\boldsymbol{q}} \approx t\, q^2$, we have

$$J_{\boldsymbol{p},\boldsymbol{p}'} = \sum_{\boldsymbol{q}} \frac{M_{-\boldsymbol{q},\boldsymbol{p}} M_{\boldsymbol{q},\boldsymbol{p}'}}{\epsilon_{\boldsymbol{q}}} = \frac{A'^2}{(2\pi)^3} \int d\boldsymbol{q} \frac{e^{i\boldsymbol{q} \cdot (\boldsymbol{R}_{\boldsymbol{p}'} - \boldsymbol{R}_{\boldsymbol{p}})}}{t\, q^2} = \frac{A'^2}{4\pi t} \frac{1}{|\boldsymbol{R}_{\boldsymbol{p}'} - \boldsymbol{R}_{\boldsymbol{p}}|} \,. \tag{7.11}$$

Using again $W_{\boldsymbol{p}} = 1 - 2n_{\boldsymbol{p}}$, we recover Eq. (7.2) with $J_{\boldsymbol{p},\boldsymbol{p}'}$ given by Eq. (7.7) in the limit $h_z \to 0$, $t = 2JS$, and $A' = A\sqrt{S/2}$. In fact, for this choice of parameters, the Hamiltonian (7.8) becomes identical to the Hamiltonian (14.16) *in* the harmonic approximation. Thus, we see that within the one-magnon approximation the plaquette interaction (7.2) is *exact* to all orders in A.

7.4 Thermally stable quantum memory

Ferromagnet

Next we show that the attraction (7.5) between the $W_{\boldsymbol{p}}$'s can be made truly long-ranged by choosing h_z appropriately. Equation (7.2) can be rewritten in terms of anyons

$$H_{\text{eff}} = -2\sum_{\boldsymbol{p},\boldsymbol{p}'} J_{\boldsymbol{p},\boldsymbol{p}'} n_{\boldsymbol{p}} + 2\sum_{\boldsymbol{p},\boldsymbol{p}'} J_{\boldsymbol{p},\boldsymbol{p}'} n_{\boldsymbol{p}} n_{\boldsymbol{p}'}. \tag{7.12}$$

In the derivation of Eq. (7.12) we have neglected the constant $\boldsymbol{p} = \boldsymbol{p}'$ terms arising in Eq. (7.2) since $W_{\boldsymbol{p}}^2 = 1$. This is why the $\boldsymbol{p} = \boldsymbol{p}'$ terms cancel in Eq. (7.12), and we can restrict the sums to $\boldsymbol{p} \neq \boldsymbol{p}'$. A similar Hamiltonian has been derived in Ref. [111] by coupling Kitaev's honeycomb model to cavity modes. While the non-locality of cavity modes allowed one to obtain constant plaquette-plaquette interactions, here we start from a purely local Hamiltonian and obtain the Yukawa-like interaction (7.5). As we discuss now, in the regime $L_h \gg L$ this is sufficient to stabilize the memory against thermal fluctuations.

Inserting Eq. (7.5) into Eq. (7.12) and using the fact that in the continuum approximation $\sum_{\boldsymbol{p}\neq 0} \frac{1}{|\boldsymbol{p}|} e^{-|\boldsymbol{p}|/L_h} \approx \int_{D_{L/2}} d\boldsymbol{p} \frac{1}{|\boldsymbol{p}|} e^{-|\boldsymbol{p}|/L_h} = 2\pi L_h (1 - e^{-L/2L_h})$ (where we have approximated the $L \times L$ square surface of the toric code with a disk $D_{L/2}$ of radius $L/2$), we obtain

$$H_{\text{eff}} = \mu(L) \sum_{\boldsymbol{p}} n_{\boldsymbol{p}} + 2\sum_{\boldsymbol{p}\neq\boldsymbol{p}'} J_{\boldsymbol{p},\boldsymbol{p}'} n_{\boldsymbol{p}} n_{\boldsymbol{p}'}, \tag{7.13}$$

where the chemical potential of the anyons is

$$\mu(L) = \frac{A^2 M^2}{R} L_h (1 - e^{-L/2L_h}). \tag{7.14}$$

The continuum approximation used to derive Eq. (7.14) is a calculational tool to estimate the corresponding sum. As we pointed out above, the

continuum approximation is justified when one is concerned with the long-distance physics. Furthermore, in this limit we also let the lattice constant of the surface code go to zero such that a single stabilizer remains coupled to a single FM spin. This approximation is not necessary to obtain the desired behavior since a direct numerical evaluation of the sum shows that it indeed grows linearly with L for $L \ll L_h$, see Figure. 7.4 in 7.E. At this point we note that the external magnetic field h_z stabilizes the magnetization of the FM, keeping it along the z-direction. Indeed, the only condition which needs to be satisfied is that the Zeeman energy $E_z = h_z S \Lambda^3$ due to the h_z field remains much larger than the Zeeman energy $E_x = ASL^2$ due to the surface code. As a specific example, one can make the following scaling choice satisfying all constraints: $h_z \propto 1/L^4$ and $\Lambda \propto L^3$, which satisfy $L_h \propto L^2 \gg L$ and $E_z/E_x \propto L^3 \gg 1$. Under these conditions, it is clear that the total magnetization will not be affected by the presence of the memory and the FM spins will not rotate into the x-direction *on* average. This is in agreement with a Metropolis simulation of the classical Heisenberg FM, see Fig. 7.2. However, we show below that backaction effects become eventually important for the FM spins *c*lose to the memory.

We have now all the arguments needed in order to derive the main result of our work, namely that the chemical potential of the anyons increases linearly with L. Indeed, since $L_h \gg L$, the anyon's chemical potential reads

$$\mu(L) = \frac{A^2 M^2}{2R}(L + O(L/L_h)^2) . \tag{7.15}$$

This implies a quantum information storage time that grows exponentially with L and β, where $\beta = 1/k_B T$ is the inverse temperature of a bath weakly coupled to the memory, as originally demonstrated in Ref. [100] assuming that the interaction with the thermal bath can be described by the Davies equation. In 7.B we present alternative arguments leading to the same conclusion. The second term in Eq. (7.13) describes a gravitation-like attraction between anyons. Since this term helps to keep newly created anyon pairs attached to each other (for temperatures below the interaction strength $\propto A^2 M^2/R$), it will have a further beneficial effect on the memory lifetime. On the other hand this second term effectively reduces the anyon chemical potential. However, this reduction is negligible since the anyon density is exponentially suppressed by the first term, see 7.B.

Hopping Bosons

The interaction between stabilizer operators that is mediated by a reservoir of hopping bosons is truly long-range (there is no cut-off) as demonstrated in Eq. (7.11). The anyon chemical potential in the continuum approximation is then simply given by (we again approximate the surface of the toric code by a disk)

$$\mu(L) = \frac{A^2}{4\pi\,t}\sum_{\boldsymbol{p}}\frac{1}{|\boldsymbol{p}|} \approx \frac{A^2}{4\pi\,t}\int_{D_{L/2}}d\boldsymbol{p}\,\frac{1}{|\boldsymbol{p}|} = \frac{A^2}{4\pi\,t}\,L\,, \qquad (7.16)$$

that leads again to a lifetime increasing exponentially with L. [100]

7.5 Validity of the effective theory

Here we analyze in detail the conditions of validity of our effective theory when we allow for anyon creation, annihilation, and diffusion due to a thermal environment.

Coupling to bosons

The simplest case is the toric code locally coupled to a system of bosons hopping on a lattice. As mentioned above, this model can be treated exactly via the polaron transformation. Since this is a unitary transformation, the spectra of H' and $e^{\mathcal{S}}H'e^{-\mathcal{S}}$ are identical, and so our effective theory is exact.

An upper bound on the creation energy can be found by comparing the energy expectation values for two states $|\Psi\rangle$ and $X_i|\Psi\rangle$. These are defined such that the toric code state is vacuum in the former and has a pair of anyons in the latter created by the Pauli operator X_i on a site i. The state of the hopping bosons is the same in both cases and is chosen such that the difference between expectation values is maximized. The bound is then $\Delta E_A \leq \langle\Psi|X_i H' X_i^\dagger|\Psi\rangle - \langle\Psi|H'|\Psi\rangle = 4A'\langle\Psi|(a_i + a_i^\dagger)|\Psi\rangle$. The unbounded nature of the bosonic operators means that the quantity $\langle\Psi|(a_i+a_i^\dagger)|\Psi\rangle$ is also unbounded. This upper bound is therefore perfectly consistent with the chemical potential $\mu(L) \to +\infty$ for $L \to +\infty$.

Coupling to Ferromagnet

When the toric code is coupled to the FM, the problem cannot be solved exactly and the effective theory does not describe the entire spectrum.

Indeed, the bound ΔE_A for the creation of an anyon pair derived from H is now finite: $\langle\Psi|X_i H X_i^\dagger|\Psi\rangle - \langle\Psi|H|\Psi\rangle \leq 4AS$. This seems to be in contradiction with the chemical potential $\mu(L)$ from H_{eff} (7.13) that diverges in the thermodynamic limit [1]. However, this contradiction is only apparent: the effective Hamiltonian (7.13) describes the system correctly in the *long-wavelength* and *low-energy limit* only. We first note that the Schrieffer-Wolff transformation followed by tracing out the degrees of freedom of the ferromagnet is not a unitary operation. Hence, the spectra of H and H_{eff} are, in general, not identical. They match only in the low-energy sector where H_{eff} leads to bounded results. Indeed, when the quantum memory is in contact with a thermal heat bath, [16] the effective Hamiltonian allows us to calculate the energy of the anyon system

$$\langle H_{\text{eff}}\rangle \approx \mu(L)\sum_{\boldsymbol{p}}\langle n_{\boldsymbol{p}}\rangle \approx \frac{A^2 M^2}{2R}L^3 e^{-\frac{\beta A^2 M^2 L}{2R}} \to 0 \qquad \text{for} \quad L\to\infty\,, \quad (7.17)$$

where we used [16] $\langle n_{\boldsymbol{p}}\rangle = 1/(e^{\beta\mu(L)}+1) \approx e^{-\beta\mu(L)}$. The thermal distribution function $\langle n_{\boldsymbol{p}}\rangle$ of an anyon at plaquette $\boldsymbol{p}$ is self-consistently suppressed by the effective chemical potential and thus the total energy $\langle H_{\text{eff}}\rangle$ remains finite and small even for large L, since we can always reach the regime $\beta\mu(L)\gg 1$ for sufficiently large L at given temperature. This thermal expectation value (7.17) is clearly consistent with the upper bound on the total energy for the code, which is $2AL^2S$ given that the bound is $4AS$ for a single pair and assuming that $n_{\boldsymbol{p}}=1$ for each plaquette. The diverging nature of $\mu(L)$ therefore does not contradict the bound when its full effects are taken into account. The effective description breaks down in the high-temperature limit, $\beta\mu(L)\ll 1$, which corresponds to populating high energy states with finite probability, $\langle n_{\boldsymbol{p}}\rangle \approx 1$. Indeed, in this limit, we get $\langle H_{\text{eff}}\rangle \approx \mu(L)L^2$, which clearly violates the bound $2LA^2S$ for large L (but still $\beta\mu(L)\ll 1$). This breakdown of the low-energy theory is of course not surprising, since in this regime also the magnon expansion for the FM becomes invalid (the magnon occupation number also becomes order one). Thus, our long-wave length and low-energy approximations are self-consistent for L sufficiently large [2].

The effective Hamiltonian (7.13) is not suited to describe the high-energy part of the spectrum ($n_{\boldsymbol{p}}=1$). High-energy excitations are produced when anyons are created non-adiabatically forcing the FM to leave

---

[1]This argument is due to D. Poulin, private communication.

[2]This is similar to e.g. the harmonic approximation of crystal vibrations described by phonons. The Hamiltonian $H_{\text{phonon}} = \sum_{\boldsymbol{q}} D|\boldsymbol{q}|n_{\boldsymbol{q}}$ is only valid in the low-energy regime, and high-energy (large $\boldsymbol{q}$) excitations are self-consistently suppressed by the Bose-Einstein factor $\langle n_{\boldsymbol{q}}\rangle = 1/(e^{\beta D|\boldsymbol{q}|}-1)$.

its local equilibrium. In such a scenario the FM has no time to react and does not penalize the creation of anyons. In fact, the energy cost to create an anyon 'instantaneously'[3] is bounded by $2AS$ as argued above. The fast creation of an anyon produces a bunch of high-energy and short-wavelength excitations in the FM and this kind of processes are not described by our effective theory. In fact, the memory is not protected when the thermal bath is able to create errors on a sufficiently small timescale. We estimate now this timescale. In the derivation of Hamiltonian (7.13) we explicitly assumed that the FM is locally aligned along z and this has to remain valid when thermal anyons are produced. So besides the requirement that the coupling B to the external bath is small, i.e. $B \ll A$, we work in the *a*diabatic regime where the external bath creates errors in the code on a timescale much longer than $1/A$ (we put $\hbar = 1$), or in other words, when the error rate is much smaller than A. For instance, modeling the coupling between code and bath by a generic spin-boson model, [138, 16] the error rate $\gamma(\omega)$ describing the transition probability between two states with energy difference ω takes the following form [16]

$$\gamma(\omega) = \kappa_n \left| \frac{\omega^n}{1 - e^{-\beta\omega}} \right| e^{-\omega/\omega_c}, \tag{7.18}$$

where ω_c is an arbitrary cut-off and κ_n contains the coupling B to the external bath (in Born approximation, $\kappa_n \propto B^2$). For $n = 1$ the bath is called Ohmic, while it is called super-Ohmic for $n \geq 2$. The adiabaticity condition then simply reads $\gamma(-A) \ll A$. In this case, the FM has enough time to adapt to the perturbation generated by an error and stays locally aligned along z. In such a scenario the FM suppresses the creation of anyons as if the energy penalty was effectively $\mu(L)$.

7.6 Backaction effects onto the ferromagnet

As noted above, the external field h_z stabilizes the FM against the effective x-magnetic field induced by the surface code and forbids energetically the turning of the total magnetization. However, backaction effects are substantial for the FM spins close to the code. Here, we study those backaction effects both analytically (via polaron transformation in the harmonic approximation) and numerically with a Metropolis algorithm. Let us consider the situation where the coupling of the surface

---

[3]Strictly speaking, physical processes cannot be instantaneous but take place over a finite interaction time τ. Thus, we just require $\hbar/E \ll \tau \ll \hbar/A$, where E is a typical energy scale of the toric code plus FM. If τ is too small, the system gets destroyed.

code to the FM is turned on at $t = 0$ and let us calculate the dynamics
of the x-component of a FM spin assuming that $W_j = +1 \forall j$. Here we
present the main results and defer details to 7.D. At time $t > 0$ we have,
$\langle S_i^x(t) \rangle = \mathrm{Tr}\rho_F S_i^x(t)$, where $\rho_F = e^{-\beta H_F}/\mathrm{Tr}e^{-\beta H_F}$ and $S_i^x(t) = e^{iHt}S_i^x e^{-iHt}$,
with H the total Hamiltonian Eq. (14.16) after coupling ($\hbar = 1$). Here,
i labels a site of the FM that lies in the plane of the surface code where
the effect of the effective x-magnetic field is strongest, while the backac-
tion effect becomes negligible away from the code. After a lengthy but
straightforward calculation, we obtain (neglecting boundary effects)

$$\langle S_i^x(t) \rangle = \frac{SAL}{4D} \left(\mathrm{FC}\left[\frac{1}{\sqrt{\tau}}\right] + \mathrm{FS}\left[\frac{1}{\sqrt{\tau}}\right] - 1 - \frac{\sqrt{\tau}}{\pi}\left(1 - \cos\left[\frac{\pi}{2\tau}\right] + \sin\left[\frac{\pi}{2\tau}\right]\right) \right),$$
(7.19)

where $\tau = 8\pi Dt/L^2$ is a dimensionless diffusion time, with diffusion
constant $D = 2JS$, and FC/FS are the Fresnel functions. In the limit
$\tau \ll 1$, Eq. (7.19) becomes $\langle S_i^x(t) \rangle \approx -S\sqrt{\frac{A^2 t}{2\pi D}}$. Similarly, in the small τ
limit $\langle S_i^y(t) \rangle \approx -\langle S_i^x(t) \rangle$ and

$$\langle S_i^z(t) \rangle \approx -S(1 - A^2 t/2\pi D) + \frac{1}{N_s}\sum_q \langle \hat{n}_q \rangle,$$
(7.20)

see 7.D. For self-consistency reasons $|\langle S_i^x(t) \rangle|$ should not exceed the max-
imum spin value S. Thus, we trust the polaron approximation up to
times t with $0 \leq t \leq t_r$, where

$$t_r = \frac{2\pi D}{A^2}.$$
(7.21)

Here, t_r is defined by $\langle S_i^x(t_r) \rangle = -S$ so that $-S \leq \langle S_i^x(t) \rangle \leq 0$ for
$0 \leq t \leq t_r$. This is consistent with the behavior of the z component
which satisfies $\langle S_i^z(t_r) \rangle = 0$ (we assume small temperatures and neglect
$\frac{1}{N_s}\sum_q \langle \hat{n}_q \rangle$) and $-S \leq \langle S_i^z(t) \rangle \leq 0$ for $t \leq t_r$. We refer to t_r as the refresh-
ing time: at this time, the backaction of the surface code on the FM has be-
come substantial with the FM spins close to the code pointing now along
the x-axis. To restore the full effect of the FM, we refresh the ferromag-
netic state with, e.g., a magnetic pulse, so that all spins point again along
the z-axis. This procedure has to be repeated periodically on a time scale
t_r, which, importantly, is independent of the code size L. This refreshing
can be considered as part of a cooling cycle to get the heat generated by
the surface code out of the system (note that no measurements of stabiliz-
ers or entangling operations are involved). This refreshing prevents the
total system, FM plus surface code, to reach a new common equilibrium
state, and instead ensures that the FM stays in its own equilibrium state.
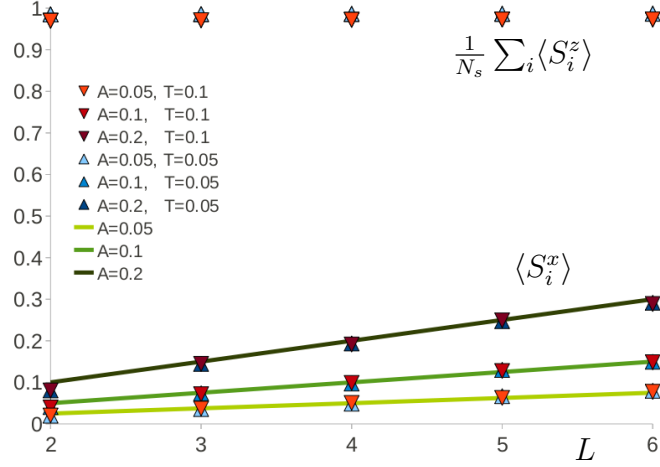
Figure 7.2: A graph of $\langle S_i^x \rangle$ (in the middle of the code) against L for the classical Heisenberg FM with $J = 1$. The data was obtained numerically by using the Metropolis algorithm. The magnetic length is $L_h = L^2$ and the FM size is $\Lambda = 2L_h$. The data shows agreement to the relation $S_i^x(t \to \infty) \propto LA/J$, obtained from Eq. (7.19). On the same graph we plot the total z-magnetization $\frac{1}{N_s} \sum_i \langle S_i^z \rangle$ against L demonstrating that the backaction is only a localized effect. The scaling chosen here is different than the one in the main text. This different choice is only motivated by the difficulty to simulate the classical Heisenberg ferromagnet with a large number of spins. This does not alter the analysis since the chosen scaling satisfies the necessary requirements $E_z \gg E_x$ and $L_h \gg L$.

For L sufficiently small, such that $LA/4D \leq 1$, Eq. (7.19) is applicable for all t and $\langle S_i^x(t \to \infty) \rangle = -SLA/4D$. We compare this result with a Metropolis simulation of the classical Heisenberg FM and obtain good agreement, see Fig. 7.2.

We note that the refreshing process represents a suffcient condition to build a stable memory, however, it does not appear to be necessary. Indeed, let us consider the extreme case where all the spins of the FM tilt into x-direction (possible if we allow E_x to exceed E_z by assuming e.g. $h_z = 0$). In this worst case scenario, the interaction between plaquettes is not given by the transverse susceptibility anymore but by the longitudinal one. The latter has been studied in detail both with a spin wave analysis [139] and with a decoupling method. [140, 141] The small q result reads $\chi_{||}(\boldsymbol{q}, \omega = 0) = k_B T / 8D^2 |\boldsymbol{q}|$ [4]. This is valid when $h \ll Dq^2 \ll k_B T$,

---

[4]We note that, contrary to the transverse susceptibility, $\chi_{||}(\boldsymbol{q}, \omega = 0)$ vanishes at

which is the regime of interest here since we focus on distances smaller than L_h. Here h points in longitudinal direction and is composed of an external magnetic field (which, as above, we assume scales proportional to $1/L^4$) and the magnetic field produced by the surface code. Since the latter scales as $L^2/\Lambda^3 \propto 1/L^7$, see 7.A, the longitudinal field produced by the memory can safely be ignored. The magnetic length thus scales again as $L_h \propto L^2$. In real space we have $\chi_\parallel(\boldsymbol{r}) \propto T/r^2$. Since $\int_{D_{L/2}} \mathrm{d}^2 r \, 1/r^2 \propto \ln(L/2)$, we finally obtain

$$\mu(L) = ck_B T \ln(L/2) \, , \tag{7.22}$$

with $c = 2\pi^2 A^2/D^2$. This implies a lifetime that grows as $L^c/\gamma(0)$ for $c \leq 2$ and as $L^{2c-2}/\gamma(0)$ for $c \geq 2$, as we show in 7.C. The hopping rate of the anyons $\gamma(0)$, and hence the lifetime of the memory, will in general depend on the bath temperature ($\gamma(0) \propto T$ for the bath models considered in Refs. [16, 112, 113]), even though there is no explicit temperature dependence.

7.7 Hindering of anyon's hopping.

The lifetime of the memory that we discussed above does not apply if the initial state of the system has anyons already present. Suppose that errors occur during preparation of the initial state, creating a finite density of anyons. If these errors are sufficiently sparse, it will be possible for error correction to recover the initial state. It is the job of the Hamiltonian to preserve this error correctability until the desired time of readout. The coupling of the quantum memory to the FM or to the hopping bosons will energetically favour the annihilation of anyons on neighboring plaquettes, undoing some of the errors. However, we can expect that a finite density of pairs will have been non-neighbouring, and so will remain. These only need to diffuse a constant distance to make correction ambiguous, which leads to a constant lifetime for the memory. To prevent this we can split the plaquettes into two types. 'Strongly coupled' plaquettes are coupled to the FM or to the hopping bosons with a strength A_s. 'Weakly coupled' plaquettes have a strength $A_w < A_s$. These are chosen such that any sequence of single- or local two-spin errors that move an anyon from one weakly coupled plaquette to another must move it via a strongly coupled plaquette. Example patterns are given in the next section. The chemical potential for the plaquettes will change from the form

---

$T = 0$, since it corresponds to particle-hole excitations.

in Eq. (10) of the main text, giving different values $\mu_s(L)$ and $\mu_w(L)$ for the two types of plaquette. Performing the summation (as described in the next section) shows that the factor A^2 becomes $A_s\bar{A}$ for $\mu_s(L)$ and $A_w\bar{A}$ for $\mu_w(L)$ ($\bar{A}$ being a weighted average). The energy barrier required for anyon movement is therefore of order $(1 - A_w/A_s)\mu_s(L)$, which increases linearly with system size. The resulting suppression of diffusion leads to a lifetime that increases exponentially with system size, even when the initial state has a finite density of anyons.
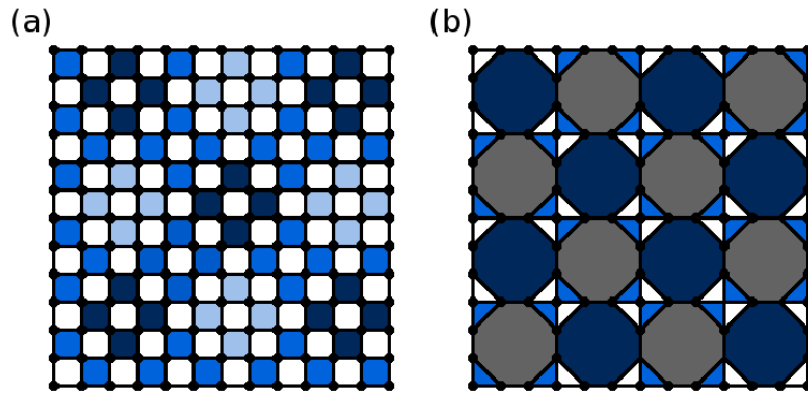
Figure 7.3: Two tilings of plaquettes are shown on which the code may be defined. Spins are located on vertices. (a) The square tiling, as used in the main text. s-plaquettes are shown in dark blue, blue, or light blue, p-plaquettes are shown in white. (b) An alternative tiling, with alternating triangular and octagonal plaquettes. s-plaquettes are shown in dark blue and blue, p-plaquettes are shown in white and grey.

It may come as a surprise that associating some stabilizers with a lower energy penalty has a beneficial effect on the memory. However, note that the weakly coupled plaquettes allow energy to be dissipated from the anyons to the bath by hopping of an anyon from a strongly to a weakly coupled plaquette. On the other hand, if the chemical potential is independent of the anyon position, as in Eq. (10) of the main text, this is only possible through annihilation of anyons.

An example pattern for strongly and weakly coupled plaquettes.

In the toric code model there are two types of anyon, e and m, which reside on two kinds of plaquette, s and p, respectively. Note that, when the

code is defined with spins on the edges of the lattices, these correspond to the stars and plaquettes, respectively.

Consider a spin in the square tiling of Fig. 7.3 (a), shared by two s-plaquettes to the top-left and bottom-right and two p-plaquettes to the top-right and bottom-left. The application of a Pauli I^z to such a spin will affect the e anyon occupations of the two s-plaquettes. If both were initially empty, an anyon pair will be created. If both initially held an anyon, this pair will be annihilated. If only one held an anyon, it will be moved to the other plaquette. The application of a Pauli I^y has the same effect for the m anyons of the p-plaquettes. For spins where the positions of s- and p-plaquettes are exchanged, the roles of I^z and I^y are also exchanged. No operation exists that can move an anyon from an s-plaquette to a p-plaquette, or vice-versa.

Creation, movement and annilation of anyons are therefore achieved by Pauli operations. Using single spin operations, creation of a pair will always lead to the anyons occupying neighboring plaquettes (where neighoring means that they share exactly one spin). Similarly, single spin operations can only move anyons from one plaquette to a neigboring one, or annihilate anyons on neighboring plaquettes. Since we assume that the system-bath coupling supports only single spin errors, it is exactly these processes that we consider during thermalization. However, it should be remembered that two-spin perturbations may also be present in the Hamiltonian. Local two-spin errors should therefore also be considered, which can create, annihilate and transport anyons on next-to-neighboring plaquettes.

With this in mind, we wish to split both s- and p-plaquettes into two groups, one of which will be strongly coupled to the FM or to the hopping bosons with a coupling A_s and the other of which will be weakly coupled with a strength $A_w < A_s$. This will give the plaquettes of the former a higher chemical potential than those of the latter, with an energy difference that increases linearly with system size.

The pattern of strongly and weakly coupled plaquettes should be chosen such that anyons become trapped within the latter, which will occur if two conditions are satisfied. Firstly, any anyons initially on strongly coupled plaquettes should quickly move into a nearby weakly coupled plaquette. Secondly, it should not be possible for anyons to be moved from one weakly coupled plaquette (or a small cluster of weakly coupled plaquettes) to another by a sequence of either single- or two-spin operations without passing through a strongly coupled plaquette.

The first condition can be met if anyons on strongly coupled plaquettes cannot be moved over large distances by a sequence of either single

or two spin operations without either moving through a weakly coupled plaquette, or through a strongly coupled plaquette that neigbors a weakly coupled one. The latter is relevant because it will ensure that the distance an anyon can move before decaying into a weakly coupled plaquette is exponentially suppressed.

Both conditions are satisfied by the pattern shown in Fig. 7.3 (a). Here, weakly coupled s-plaquettes are shown in dark blue. Strongly coupled s-plaquettes that neighbor weakly coupled s-plaquettes are shown in blue, and those that do not are shown in light blue. Regions of strongly coupled plaquettes that do not neighbor weakly coupled plaquettes are separated from each other by a width of three spins. Sequences of one- and two-spin operations therefore cannot move anyons in one such region to another without going via strongly coupled plaquettes that do neighbor weakly coupled plaquettes, which will almost certainly result in the anyon decaying into the neighboring weakly coupled plaquettes. Similarly, regions of weakly coupled plaquettes are separated by the same width, preventing movement between them without going via strongly coupled plaquettes.

The initial movement of anyons on strongly coupled plaquettes to nearby weakly coupled plaquettes may cause ambiguity for error correction if the error rate during initialization is too high. Even so, for sufficiently low error rates this movement will have no effect on correctability. Once the movement is complete, the exponential suppression of diffusion will then ensure that the correctability of the errors is preserved for a time exponential with the system size, since such an exponentially long timescale will be required for the anyons to climb out of the weakly coupled plaquettes.

We will now demonstrate that the difference in chemical potentials between strongly and weakly coupled plaquettes leads to the energy barrier required to suppress diffusion. To determine the chemical potential of an arbitrary plaquette $\boldsymbol{p}$ (which is either s- or p-type), the following sum over all plaquettes must be performed

$$\mu_{\boldsymbol{p}}(L) = \frac{M^2}{2\pi R} A_{\boldsymbol{p}} \sum_{\boldsymbol{p}'}' A_{\boldsymbol{p}'} \frac{1}{|\boldsymbol{p} - \boldsymbol{p}'|} \,, \tag{7.23}$$

where the prime in $\sum'$ means that $\boldsymbol{p}' \neq \boldsymbol{p}$. Here $A_{\boldsymbol{p}'}$ denotes the coupling of plaquette $\boldsymbol{p}'$ which will be A_s or A_w depending on whether this plaquette is weakly or strongly coupled, respectively. By numerically performing the summation we find that, in the $L \to \infty$ limit, it takes the

form

$$\sideset{}{'}\sum_{\boldsymbol{p}'} A_{\boldsymbol{p}'} \frac{1}{|\boldsymbol{p} - \boldsymbol{p}'|} = \frac{3A_s + A_w}{4} c \cdot L \,, \tag{7.24}$$

where c is an $O(1)$ constant. Its value does not depend on whether the sum is centered on a strongly or weakly coupled plaquette, or at least does not do so to a non-negligible degree. To three decimal places its value is found numerically to be $c = 3.524$. The linear combination of A_s and A_w is a weighted average $\bar{A} = (3A_s + A_w)/4$, which arises from the fact that there are three times as many strongly coupled plaquettes as weakly coupled plaquettes. The chemical potentials for weakly and strongly coupled plaquettes are then

$$\mu_s(L) = \frac{cA_s\bar{A}M^2}{2\pi R} \cdot L \,, \quad \mu_w(L) = \frac{cA_w\bar{A}M^2}{2\pi R} \cdot L \,. \tag{7.25}$$

Clearly, $\mu_s(L) - \mu_w(L) = O(L)$, giving the required energy barrier.

Alternative tiling with four-body coupling.

A pattern of strongly and weakly coupled plaquettes, stable against single-spin errors, is shown for an alternative tiling in Fig. 7.3 (b). Strongly (weakly) coupled s-plaquettes are shown in blue (dark blue) and strongly (weakly) coupled p-plaquettes are shown in white (grey). For this tiling it is still true that e anyons can only be created and moved between neighboring s-plaquettes, and m anyons between neighboring p-plaquettes. Note that all strongly coupled plaquettes in this tiling are triangular. The $W_{\boldsymbol{p}}$ for these will therefore be three-body operators, making the code-FM or code-hopping boson coupling only a four-body term. On the other hand, weakly coupled plaquettes are octagons with eight-body $W_{\boldsymbol{p}}$ and nine-body terms required for the code-FM or code-hopping boson coupling. Since these many-body terms will most likely be generated by perturbative methods, with a higher number of spins in a term generated by higher orders of perturbation theory, the difference in coupling strengths will arise naturally.

Due to the practical difficultly in generating many-body terms, we can consider not coupling the octagonal plaquettes to the FM or to the hopping bosons. Only the four-body terms required to couple the triangles are then needed, which should be easier to implement than the five-body terms required for the square tiling. Despite the fact that only a fraction of the plaquettes are coupled to the FM or to the hopping bosons, the memory is still stable against thermal errors. This is because any single spin error must still create at least one anyon on, or move anyons

through, energetically penalized triangular plaquettes. The energy barrier that increases linearly with system size is therefore still intact, and ensures that anyon creation and diffusion are exponentially suppressed.

Unfortunately, stability against local Hamiltonian perturbations does not remain strong without the coupling of octagons. Without an energy penalty, two-body perturbations are free to create and move anyons between next-to-neighboring octagonal plaquettes. This avoids the energy barrier and so leads to uncorrectable errors in a constant time. However, it is possible to avoid this by carefully considering what types of perturbation are present, and then designing the $W_{\boldsymbol{p}}$ such that they are unable to perform such hopping processes. For example, let us use $W_{\boldsymbol{p}} = I^x_{\boldsymbol{p},1} I^y_{\boldsymbol{p},2} I^z_{\boldsymbol{p},3}$ for triangular s-plaquettes. Here spin 1 is that shared with the neighboring triangular s-plaquette and the numbering proceeds clockwise. Let us also use $W_{\boldsymbol{p}} = I^z_{\boldsymbol{p},1} I^y_{\boldsymbol{p},2} I^x_{\boldsymbol{p},3}$ for triangular p-plaquettes with corresponding numbering. No nearest neighbor isotropic perturbation of the form $I^\alpha_i I^\alpha_j$, for $\alpha \in \{x, y, z\}$, commutes with all of these operators. This means such perturbations will be suppressed by the energy barrier and will not be able to move anyons between octagonal plaquettes. If only perturbations of this form are present in the system, the memory will remain stable.

7.8 Conclusions

In this paper we have introduced two 3D-models presenting self-correcting properties with purely local, bounded-strength interactions in three dimensions. The first model consists of a toric code whose stabilizer operators are locally coupled to the transverse component of the spins in a bulk ferromagnet aligned along z direction. The low-energy magnons of the ferromagnet (Goldstone modes) mediate long-range attractive interactions between the stabilizers and thus lead to an energy penalty for the creation of anyons that increases lineraly with the linear size L of the code. We thus obtain a lifetime of the memory increasing exponentially with L. The second model is exactly solvable and consists of a toric code locally coupled to a system of hopping bosons on a cubic lattice. The long-range attractive interaction is mediated by the low-energy collective excitations of the bosonic system (similar to the magnons). This leads again to a memory lifetime increasing exponentially with L. Both models are closely related and in fact coincide in the harmonic approximation. As the ferromagnet model is treated within the framework of standard perturbation theory, our analysis does not represent a full proof

of self-correction but provides evidence towards thermal stability. This is in contrast with the second model (hopping bosons) that is exactly solvable and for which we have exactly demonstrated that the energy barriers grows linearly with L.

We have studied the backaction effects of the toric code onto the ferromagnet and determined that the spins close to the memory tilt along x direction after a so-called refreshing time t_r independent of L. At time $t > t_r$ two scenarios are conceivable. In the first one a magnetic pulse is applied to the ferromagnet in order to realign it along z and to maintain an $O(L)$ energy penalty. In the second case the spins of the ferromagnet reach a new equilibrium position and the energy penalty scales with $\log(L)$ only.

These results obtained from our local model provide strong evidence that the surface code can be made thermally stable in less than 4 dimensions by coupling it to a system with Goldstone modes. Here we have explicitly considered the coupling to a ferromagnet or to a reservoir of hopping bosons. The question of how to engineer such five-body interactions remains open.

7.9 Acknowledgements

7.A Interactions mediated by a translationally invariant system.

For the sake of completeness, we show here a detailed derivation of Eq. (2) of the main text with the use of a perturbative Schrieffer-Wolff transformation similar to Ref. [134]. We start our discussion by introducing the general formalism. Consider a general Hamiltonian

$$H = H_0 + V \,, \tag{7.26}$$

where we identify H_0 as the main part and V as a small perturbation. We decompose the spectrum $\sigma(H_0)$ of H_0 into a high-energy set of eigenvalues M_Q and a low-energy set of eigenvalues M_P such that $\sigma(H_0) = M_P \cup M_Q$, $M_P \cap M_Q = \emptyset$, and there is a gap separating the eigenvalues

in M_P and M_Q. We define the operators P and $Q = 1 - P$ respectively as the projectors onto the low energy subspace $\mathcal{M}_P$ and onto the high-energy subspace $\mathcal{M}_Q$ corresponding to set of eigenvalues M_P and M_Q. The perturbation V can then be decomposed into a diagonal part V_d and an off-diagonal part V_od

$$
\begin{aligned}
V_\mathrm{d} &= PVP + QVQ, & (7.27)\\
V_\mathrm{od} &= PVQ + QVP. & (7.28)
\end{aligned}
$$

The effective Hamiltonian is given by a Schrieffer-Wolff transformation such that the transformed Hamiltonian $H_\mathrm{eff} = e^S H e^{-S}$ is block-diagonal, i.e. $P H_\mathrm{eff} Q = Q H_\mathrm{eff} P = 0$. Up to second order in V the effective Hamiltonian reads [75]

$$
H_\mathrm{eff}^{(2)} = H_0 + V_\mathrm{d} + U = H_0' + U, \qquad (7.29)
$$

where we define $H_0' = H_0 + V_\mathrm{d}$ and

$$
U = -\frac{i}{2} \lim_{\eta \to 0^+} \int_0^\infty \mathrm{d}t\, e^{-\eta t} \left[V_\mathrm{od}(t), V_\mathrm{od} \right], \qquad (7.30)
$$

where $V_\mathrm{od}(t) = e^{iH_0' t} V_\mathrm{od} e^{-iH_0' t}$ is given in the Heisenberg representation ($\hbar = 1$).

Coupling to the transverse component of the FM spins.

We assume here that the FM is in broken-symmetry state with magnetization along z-direction and we couple the surface code to the transverse x component of the FM spins:

$$
H = H_0 + V = H_0 + \sum_{\boldsymbol{q}} S_{\boldsymbol{q}}^x A_{-\boldsymbol{q}}, \qquad (7.31)
$$

where H_0 is a general $\boldsymbol{S}$-spin Hamiltonian and A_i arbitrary operators which commute with H_0 and with each other. The Fourier components are defined through $S_{\boldsymbol{q}} = \frac{1}{\sqrt{N_s}} \sum_i e^{-i\boldsymbol{q}\cdot\boldsymbol{R}_i} \boldsymbol{S}_i$ and $A_{\boldsymbol{q}} = \frac{1}{\sqrt{N_s}} \sum_i e^{-\boldsymbol{q}\cdot\boldsymbol{R}_i} A_i$, where N_s denotes the number of spins $\boldsymbol{S}_i$ and $\boldsymbol{R}_i$ their site. Here we identify the projector P as the operator projecting onto the subspace with a fixed number of magnons $n_{\boldsymbol{q}}$. Since S^x does not conserve the number of magnons, it is clear that $V_\mathrm{d} = 0$ and $V_\mathrm{od} = V$. Note that we have absorbed

the symmetry-breaking term $h_z \sum_i S_i^z$ into H_0. From Eq. (7.30) we obtain

$$
\begin{aligned}
U &= -\frac{i}{2} \lim_{\eta \to 0^+} \sum_{\boldsymbol{q},\boldsymbol{q}'} \int_0^\infty \mathrm{d}t\, e^{-\eta t} \left[S_{\boldsymbol{q}}^x(t) A_{-\boldsymbol{q}}, S_{\boldsymbol{q}'}^x A_{-\boldsymbol{q}'} \right] \\
&= -\frac{i}{2} \lim_{\eta \to 0^+} \sum_{\boldsymbol{q},\boldsymbol{q}'} \int_0^\infty \mathrm{d}t\, e^{-\eta t} ([S_{\boldsymbol{q}}^x(t), S_{\boldsymbol{q}'}^x] A_{-\boldsymbol{q}'} A_{-\boldsymbol{q}} + S_{\boldsymbol{q}}^x(t) S_{\boldsymbol{q}'}^x \underbrace{[A_{-\boldsymbol{q}}, A_{-\boldsymbol{q}'}]}_{=0}) \,.
\end{aligned}
$$
(7.32)

We assume that the $\boldsymbol{S}$-spins are in thermal equilibrium, described by the canonical density matrix $\rho = e^{-\beta H_F}/\mathrm{Tr}\, e^{-\beta H_F}$, where H_F is the $\boldsymbol{S}$-spin Hamiltonian without the coupling to the plaquettes and corresponds to the main part of the Hamiltonian in Eq. (7.31), i.e., $H_F = H_0$. In doing so, we neglect the backaction of the surface code on the ferromagnet. This backaction will be addressed further below where we show that it leads to a localized effect on the ferromagnet which needs to be included (see also main text). Here, we rely on a formal perturbation expansion in powers of A/J. Convergence of this formal expansion is an interesting question by itself and can be approached along the lines discussed in Ref. [75]. However, such rigorous treatment is beyond the present scope and will be addressed elsewhere. Still, as shown in the main text, in the one-magnon (or harmonic) approximation, the effective Hamiltonian Eq. (2) in the main text is exact in all orders of A, thus showing that all higher order contributions of the Schrieffer-Wolff expansion vanish exactly in the one-magnon sector.

The equilibrium expectation values are denoted by $\langle \ldots \rangle$. Since H_0 is translationally invariant, such that $\langle S_{\boldsymbol{r}_i}^\alpha S_{\boldsymbol{r}_j}^\beta \rangle = \langle S_{\boldsymbol{0}}^\alpha S_{\boldsymbol{r}_j - \boldsymbol{r}_i}^\alpha \rangle$, we have $\langle S_{\boldsymbol{q}}^\alpha S_{\boldsymbol{q}'}^\alpha \rangle = \langle S_{\boldsymbol{q}}^\alpha S_{-\boldsymbol{q}}^\alpha \rangle \delta_{\boldsymbol{q}+\boldsymbol{q}',\boldsymbol{0}}$, and thus

$$
U = -\frac{i}{2} \lim_{\eta \to 0^+} \sum_{\boldsymbol{q}} \int_0^\infty \mathrm{d}t\, e^{-\eta t} \left\langle [S_{\boldsymbol{q}}^x(t), S_{-\boldsymbol{q}}^x] \right\rangle A_{\boldsymbol{q}} A_{-\boldsymbol{q}} = -\frac{1}{2} \sum_{\boldsymbol{q}} A_{-\boldsymbol{q}} \chi_{xx}(\boldsymbol{q}) A_{\boldsymbol{q}} \,,
$$
(7.33)

where $\chi_{xx}(\boldsymbol{q})$ is the static spin susceptibility.

Coupling to the longitudinal component of the FM spins.

We are now interested in the case where the surface code is coupled to the longitudinal component of the FM spins:

$$
H = H_0 + V = H_0 + A \sum_i W_i S_i^z \,,
$$
(7.34)

where the sum runs over the L^2 lattice sites lying in the plane of the surface code. The main part H_0 is the Hamiltonian of the FM, i.e. $H_0 = H_F$, which contains the symmetry-braking term $h_z \sum_i S_i^z$. As above, we identify P as the operator projecting onto the subspace with a fixed number of magnons n_q. In order to distinguish between the diagonal and off-diagonal parts of the perturbation, it is useful to apply the Holstein-Primakoff transformation in the harmonic approximation (see Eq. (6) in the main text). Doing so we obtain

$$V = -SA \sum_i W_i + A \sum_i W_i a_i^\dagger a_i \,. \tag{7.35}$$

In Fourier space Eq. (7.35) reads

$$V = -SA \sum_i W_i + \frac{A}{N} \sum_i W_i \sum_{q,q'} e^{i\boldsymbol{R}_i \cdot (\boldsymbol{q}-\boldsymbol{q}')} a_{\boldsymbol{q}}^\dagger a_{\boldsymbol{q}'}. \tag{7.36}$$

It is now straightforward to distinguish between the diagonal and the off-diagonal part of the perturbation, namely

$$V_{\mathrm{d}} = -SA \sum_i W_i + \frac{A}{N} \sum_i W_i \sum_{\boldsymbol{q}} a_{\boldsymbol{q}}^\dagger a_{\boldsymbol{q}} \,, \tag{7.37}$$

$$V_{\mathrm{od}} = \frac{A}{N} \sum_i W_i \sum_{\boldsymbol{q}\neq\boldsymbol{q}'} e^{i\boldsymbol{R}_i \cdot (\boldsymbol{q}-\boldsymbol{q}')} a_{\boldsymbol{q}}^\dagger a_{\boldsymbol{q}'} \,. \tag{7.38}$$

Absorbing V_{d} into the main part of the Hamiltonian, we rewrite

$$H = H_0' + V_{\mathrm{od}} \,, \tag{7.39}$$

with (in the harmonic approximation)

$$H_0' = -SA \sum_i W_i + \sum_{\boldsymbol{q}} \epsilon_{\boldsymbol{q}} n_{\boldsymbol{q}} + \frac{A}{\Lambda^3} L^2 \sum_{\boldsymbol{q}} n_{\boldsymbol{q}}, \tag{7.40}$$

where, as in the main text $\epsilon_{\boldsymbol{q}} = \omega_{\boldsymbol{q}} + h_z$, we assumed that the surface code is free of anyons, i.e. $W_i = +1$, and we used $N_s = \Lambda^3$. We see from Eq. (7.40) that the backaction effect of the surface code increases the gap of the magnons from h_z to $h_z' = h_z + AL^2/\Lambda^3$. However this additional term has no weight in the thermodynamic limit since it scales with Λ^{-3}. Using the specific choice of scaling from the main text, we have $h_z \propto 1/L^4$ while $L^2/\Lambda^3 \propto 1/L^7$. In the thermodynamic limit the magnetic length is thus just given by the external magnetic field h_z

$$L_{h_z'} \to L_{h_z} \propto L^2 \quad \text{for} \quad L \to \infty \,. \tag{7.41}$$

This allows us to safely conclude that the backaction of the surface code is negligible in this case.

From Eq. (7.30) we have

$$
\begin{aligned}
U &= \frac{A^2}{2N^2} \sum_{i,j} W_i W_j \sum_{\boldsymbol{q} \neq \boldsymbol{q}', \boldsymbol{k} \neq \boldsymbol{k}'} \frac{e^{i\boldsymbol{R}_i \cdot (\boldsymbol{q}-\boldsymbol{q}') + \boldsymbol{R}_j \cdot (\boldsymbol{k}-\boldsymbol{k}')}}{\epsilon_{\boldsymbol{q}} - \epsilon_{\boldsymbol{q}'}} \left[a_{\boldsymbol{q}}^\dagger a_{\boldsymbol{q}'}, a_{\boldsymbol{k}}^\dagger a_{\boldsymbol{k}'} \right] \\
&= \frac{A^2}{2N^2} \sum_{i,j} W_i W_j \sum_{\boldsymbol{q} \neq \boldsymbol{q}'} \frac{n_{\boldsymbol{q}} - n_{\boldsymbol{q}'}}{\epsilon_{\boldsymbol{q}} - \epsilon_{\boldsymbol{q}'}} e^{i(\boldsymbol{q}-\boldsymbol{q}') \cdot (\boldsymbol{R}_i - \boldsymbol{R}_j)} \\
&= \frac{A^2}{2N^2} \sum_{i,j} W_i W_j \sum_{\boldsymbol{q}', \boldsymbol{k}} \frac{n_{\boldsymbol{k}+\boldsymbol{q}'} - n_{\boldsymbol{q}'}}{\epsilon_{\boldsymbol{k}+\boldsymbol{q}'} - \epsilon_{\boldsymbol{q}'}} e^{i\boldsymbol{k} \cdot (\boldsymbol{R}_i - \boldsymbol{R}_j)} \\
&= -\frac{A^2}{2N^2} \sum_{i,j} W_i W_j \sum_{\boldsymbol{q}, \boldsymbol{k}} \frac{e^{\beta(\epsilon_{\boldsymbol{k}+\boldsymbol{q}} - \epsilon_{\boldsymbol{k}})}}{\epsilon_{\boldsymbol{k}+\boldsymbol{q}} - \epsilon_{\boldsymbol{k}}} n_{\boldsymbol{k}+\boldsymbol{q}} (n_{\boldsymbol{k}} + 1) e^{i\boldsymbol{q} \cdot (\boldsymbol{R}_i - \boldsymbol{R}_j)} \\
&= -\frac{A^2}{2N} \sum_{i,j} W_i W_j \sum_{\boldsymbol{k}} \chi_{zz}(\boldsymbol{q}, \omega = 0) e^{i\boldsymbol{q}(\boldsymbol{R}_i - \boldsymbol{R}_j)} \qquad (7.42)
\end{aligned}
$$

where the last equality comes from the definition of the susceptibility (3) in the main text evaluated in the one-magnon approximation. Following the approach of Ref. [139] assuming that $\beta\epsilon_{\boldsymbol{q}+\boldsymbol{k}}, \beta\epsilon_{\boldsymbol{q}}, \beta(\epsilon_{\boldsymbol{k}+\boldsymbol{q}} - \epsilon_{\boldsymbol{k}}) \ll 1$, we have that

$$
\chi_{zz}(\boldsymbol{q}, \omega = 0) = \frac{k_B T}{8 D^2} \frac{1}{|\boldsymbol{q}|} \quad \text{for } |\boldsymbol{q}| \to 0, \qquad (7.43)
$$

where $D = 2JS$. From Eqs. (7.42) and (7.43), we finally find a chemical potential for the anyons $\mu \propto k_B T \ln(L/2)$ as shown in the main text. We note that the term $-SA \sum_i W_i$ in H_0' leads to an increase of the chemical potential by $2SA$. However, this term does not scale with L and can be neglected for large L.

7.B Decoherence process with $1/r$-stabilizer interaction.

We have shown in the main part that if the stabilizer interaction is given by the transverse susceptibility, we obtain an $O(L)$ anyon chemical potential and an $1/r$ attractive potential between anyons. For this case, let us try to understand in more detail the decoherence process of the memory in contact with a simple model of a bath. We assume that the bath supports single-spin processes in which an energy ω is transfered from the anyon system to the bath with rate $\gamma(\omega)$ and that $\gamma(0) \neq 0$ [5]. Let $\delta(N)$ denote the average cost to create an anyon pair if there are already

---

[5]If we had $\gamma(0) = 0$, as is the case for super-Ohmic baths, this would of course have a greatly beneficial influence on the memory lifetime as it forbids direct hopping processes of anyons. See [16] for more details about the decoherence of quantum memories under the influence of super-Ohmic baths.

N pairs present. The gravitational interaction will lead to $\delta(N \geq 1) < \delta(0) = 2\mu(L) - A^2 M^2/(\pi R)$. However, below we show that this reduction will not lead to a finite self-consistent number of anyon pairs and that in fact we will have $\delta(N \geq 1) \approx \delta(0)$ in the relevant regime.

Since the presence of only two anyons diffusing across the memory leads to an uncorrectable logical error in times of order $L^2/\gamma(0)$ [16], we need to show that the time for the creation of two nearby anyons that are not directly annihilated increases exponentially with system size. Whenever a new pair of anyons is created, their total hopping rate is given by $6\gamma(0)$ [6] such that the probability that one of the two anyons ever moves before the pair gets annihilated is $6\gamma(0)/[\gamma(\delta(0)) + 6\gamma(0)]$. Since $\gamma(\delta(0)) = \exp(\beta\delta(0))\gamma(-\delta(0))$ (which follows from the detailed balance condition) and the code consists of L^2 physical spins, we conclude that the total rate for creation of anyon pairs that do not directly get annihilated is given by

$$L^2 \gamma(-\delta(0)) \frac{6\gamma(0)}{\gamma(\delta(0)) + 6\gamma(0)} \leq 6L^2 e^{-\beta\delta(0)} \gamma(0) . \tag{7.44}$$

The time needed to create such a pair is thus of order $\exp(\beta\delta(0))/L^2\gamma(0)$. In conclusion, we found a lower bound for the quantum memory storage time that increases exponentially with system size.

Assume that there are already N anyon *pairs* present. We want to determine the average (averaged over all possible positions of the existing anyons) energy cost $\delta(N)$ to create a new pair. From the point of view of one of the two newly created anyons, we assume that the existing $2N$ anyons are uniformly distributed over all $L^2 - 2$ remaining positions. The averaged interaction between one of the newly created anyons and each existing one is thus

$$\frac{1}{L^2 - 2} \left(2 \cdot 2 \sum_{\boldsymbol{p} \neq \boldsymbol{0}} J_{\boldsymbol{p},\boldsymbol{0}} + A^2 M^2/(\pi R) \right) = -\frac{1}{L^2 - 2} \left(2\mu(L) - A^2 M^2/(\pi R) \right) , \tag{7.45}$$

where we have subtract the energy $-A^2 M^2/(\pi R)$ due to attraction with the other anyon of the same pair. Indeed, we are only intersted in the attraction energy due to anyons which are already present before the creation of the pair. The total energy $\delta(N)$ to create the new pair is thus

---

[6]Strictly speaking, the energy cost for hopping is greater than zero since it increases the potential energy in the gravitational potential. However, we approximate this energy cost by zero for simplicity, neglecting the beneficial effect of the anyon attraction and obtaining a lower bound on the actual lifetime.

given by

$$\delta(N) = \delta(0) - \frac{4N}{L^2 - 2}\left(2\mu(L) - A^2 M^2/(\pi R)\right) = \delta(0)\left(1 - \frac{4N}{L^2 - 2}\right),$$
(7.46)

where $\delta(0) = 2\mu(L) - A^2 M^2/(\pi R)$.

The mean-field energy of N anyon pairs is thus

$$E_{mf}(N) = \sum_{i=0}^{N-1} \delta(i) = \delta(0)N\frac{L^2 - 2N}{L^2 - 2}.$$
(7.47)

The symmetry $N \leftrightarrow L^2/2 - N$ is reminiscent of the fact that the energy in Eq. (2) of the main text can be minimized by either all stabilizers having a $+1$ eigenvalue (no anyons present) or a -1 eigenvalue (memory full of anyons). The energetic gap between the sector in which there are almost no anyons and the sector in which the memory is full of anyons is of order $\delta(0)L^2 = O(L^3)$, so transitions between these two sectors happen on time-scales much longer than the time before the stored quantum information is lost. Consequently, each sector may serve as a thermally stable quantum memory, but at each moment in time we can only use one of the two. Without loss of generality, we consider the case where the sector with (almost) no anyons present is used for quantum information storage.

From Eq. (7.46) we have that $\delta(N) = \delta(0)(1 - 2n)$, where n denotes the density of anyons. As there can only be zero or one anyon at each position, we obtain the self-consistent equation for the mean-field anyon density *in equilibrium*

$$n_{mf} = \left[\exp\left(\beta\delta(0)(1 - 2n_{mf})\right) + 1\right]^{-1}.$$
(7.48)

If the left-hand side of this equation is smaller/larger than the right-hand side, the anyon density will tend to increase/decrease. If n_{mf} solves this equation, so does $1 - n_{mf}$. One self-consistent density is $n_{mf} = \frac{1}{2}$. The stability of this density depends on the temperature of the bath. For $\beta\delta(0) < 2$ we have a unique self-consistent density $n_{mf} = \frac{1}{2}$ and this density is also stable. For $\beta\delta(0) > 2$ the density $\frac{1}{2}$ becomes unstable and two new stable self-consistent densities n^* and $1 - n^*$ emerge (let n^* denote the smaller of the two). The system of anyons therefore shows a phase transition and spontaneous breaking of the anyon anyon-hole symmetry at a critical temperature $\delta(0)/2$, which is of order $\frac{A^2}{J}L$. However, this temperature becomes only relevant if it is lower than the critical temperature of the ferromagnet which is of order J, which will not be the case

in the limit of large L. For the purpose of quantum information storage, we are clearly interested in temperatures below both of these critical temperatures.

Adding the toric code Hamiltonian $H_{\text{toric}} = -\Delta \sum_p W_p$ to Eq. (1) in the main text explicitly breaks the symmetry between anyons and anyon holes and will lead to an additional summand $4N\Delta$ in Eq. (7.47). However, the modification of the self-consistent densities n^*, $1 - n^*$, and $\frac{1}{2}$ through this new term becomes vanishing for large L, as Δ does unlike $\delta(0)$ not grow with L.

Let us consider the self-consistent solution n^*. We want to show that n^* is exponentially suppressed with L and consequently that the number of anyons itself goes to zero in the thermodynamic limit. After straight-forward algebra, one can show that $n = 2e^{-\beta\delta(0)} < 1/2$ with $\beta\delta(0)e^{-\beta\delta(0)} < \frac{\log(2)}{4}$ (note that this condition is readily satisfied since $\delta(0)$ grows linearly with L) satisfies

$$[\exp(\beta\delta(0)(1 - 2n)) + 1]^{-1} < n , \qquad (7.49)$$

and therefore $n > n^*$. Since n is by definition exponentially suppressed with L and $n^* < n$ we finally conclude that the self-consistent solution n^* of Eq. (7.48) goes exponentially to zero with L. A direct consequence of this is that the equilibrium number of anyons $n^* L^2$ also vanishes exponentially with L and will generally be much smaller than the minimal positive value 2. Hence the anyon number will fluctuate between 0 and small even integers, such that $\delta(N) \approx \delta(0)$ from Eq. (7.46).

7.C Decoherence process with $1/r^2$-stabilizer interaction.

We have shown in the main part that if the stabilizer interaction is given by the longitudinal susceptibility, we obtain an $O\left(\ln(L)\right)$ anyon chemical potential and an $1/r^2$ attractive potential between anyons. By the same line of reasoning as in 7.B, modifications to the anyon chemical potential due to inter-anyonic interactions are negligible. Let us thus study a simple model in which anyons have a constant energy cost μ independent of the number of anyons which are already present. Ref. [100] predicts in this scenario a lifetime that scales at least with $\exp(2\beta\mu)/L^2$ [7]. Employing

---

[7]The factor 2 in the exponent is due to the fact that anyons can only be created in pairs in a toric code whose boundary conditions are (as its name suggests) periodic. With open boundaries [113], unpaired anyons can be created such that the factor 2 drops out.

the same simple bath model as in the previous paragraph, let us probe the tightness of this bound. As remarked in 7.B, it takes a time of order $t_1 = \exp(2\beta\mu)/(L^2\gamma(0))$ to create an anyon pair that does not immediately annihilate but performs at least one hopping. One such separating pair creates an uncorrectable logical error in times of order $\sim L^2/\gamma(0)$. We ignore here dimensionless $O(1)$ factors which depend on the precise definition of the memory lifetime and on the classical algorithm employed to perform error correction. Thus if we are in the regime $\mu > 2k_BT \ln L$, the quantum information will get destroyed by the first separating pair, which takes a time of order t_1 such that the bound in Ref. [100] is tight.

However, consider now the opposite regime $\mu < 2k_BT \ln L$. In this regime, further anyons will be created before the two anyons of the first separating pair have time to diffuse across a distance of order L. The lifetime of the memory is then given by the time it takes the anyons to diffuse across the average inter-pair distance, which is when error correction will inevitably break down. After a time t, the density of anyons will be of order $t/(t_1L^2) = \gamma(0)t \times \exp(-2\beta\mu)$, taking the possibility for immediate annihilation into account, and existing anyons will have diffused across a distance $\sim \sqrt{\gamma(0)t}$, as the diffusion constant for anyons is essentially given by $\gamma(0)$ [16]. Consequently, after a time $\sim \exp(\beta\mu)/\gamma(0)$ existing anyons will have diffused across the current inter-pair distance, which thus constitutes the lifetime of the memory. Notably, in this case the bound from Ref. [100] is no longer tight, as $\exp(\beta\mu) > \exp(2\beta\mu)/L^2$ in the assumed regime.

To summarize, if anyons can be created at a constant energy cost μ and the quantum memory is in contact with a bath that supports processes which have an energy cost ω with a rate $\gamma(-\omega)$ and fulfills the detailed balance condition, error correction will break down after a time of order

$$\left.\begin{array}{ll} \exp(2\beta\mu)/L^2\gamma(0), & \text{if } \mu \geq 2k_BT \ln L \\ \exp(\beta\mu)/\gamma(0), & \text{if } \mu \leq 2k_BT \ln L \end{array}\right\} = \frac{\max\left\{\exp(2\beta\mu)/L^2, \exp(\beta\mu)\right\}}{\gamma(0)}.$$
(7.50)

Now let us assume that $\mu = \mu(L) = ck_BT \ln L$, which is what we obtain if the stabilizer interaction is given by the longitudinal susceptibility. Then we obtain a lifetime scaling as $\max\left\{L^{2c-2}, L^c\right\}/\gamma(0)$, i.e. polynomially growing for any $c > 0$ with a change in the scaling behavior, depending on whether c is greater or smaller than 2. We note that for bath models as employed in Refs. [16, 112, 113], we have $\gamma(0) \propto T$, so our estimate for the lifetime contains an implicit temperature-dependence, even though the explicit temperature dependence stemming from the Boltz-

mann factor drops out.

7.D   Ferromagnetic spin dynamics under the effective x magnetic field produced by the surface code

Non-equilibrium response for S^x

We calculate now the time-dependent expectation value of the local x magnetization, defined as

$$\langle S_i^x(t) \rangle = \text{Tr} \rho_F S_i^x(t) \tag{7.51}$$

where

$$S_i^x(t) = e^{iHt} S_i^x e^{-iHt}, \quad \rho_F = e^{-H_F/k_B T}/Z_F, \quad Z_F = \text{Tr} e^{-H_F/k_B T}, \tag{7.52}$$

with

$$H = H_F + V, \quad H_F \approx \sum_{\boldsymbol{q}} \epsilon_{\boldsymbol{q}} a_{\boldsymbol{q}}^\dagger a_{\boldsymbol{q}}, \quad V = A \sum_i W_i S_i^x \approx A \sum_i W_i \frac{\sqrt{2S}}{2}(a_i + a_i^\dagger), \tag{7.53}$$

where we used the magnon approximation in lowest order. The canonical density matrix ρ_F contains the unperturbed Hamiltonian H_F, while the time-dependence is given by the full Hamiltonian $H = H_F + V$. The polaron transformation is defined by (see also main text),

$$\tilde{H} = e^{\mathcal{S}} H e^{\mathcal{S}} = \sum_{\boldsymbol{q}} \epsilon_{\boldsymbol{q}} a_{\boldsymbol{q}}^\dagger a_{\boldsymbol{q}} + \mu(L) \sum_i n_i. \tag{7.54}$$

Note that the two terms in $\tilde{H}$ commute. Next, inserting $1 = e^{-\mathcal{S}} e^{\mathcal{S}}$ we rewrite Eq. (7.51) exactly as

$$\langle S_i^x(t) \rangle = \text{Tr} \rho_F e^{-\mathcal{S}} \tilde{S}_i^x(t) e^{\mathcal{S}}, \tag{7.55}$$

where the tilde refers to the transformed quantities, $\tilde{A} = e^{\mathcal{S}} A e^{-\mathcal{S}}$ and ρ_F is untransformed.
The magnon operators transform as

$$e^{\mathcal{S}} a_i e^{-\mathcal{S}} = a_i - d_i = a_i - \frac{A\sqrt{S}}{\sqrt{2}} \sum_j W_j \frac{1}{4\pi D} \frac{1}{|\boldsymbol{R}_i - \boldsymbol{R}_j|} e^{-|\boldsymbol{R}_i - \boldsymbol{R}_j|/L_h}. \tag{7.56}$$

From Eq. (7.56) we directly note that the backaction effect is biggest close to the memory and vanishes as $e^{-|\boldsymbol{r}|/L_h}/|\boldsymbol{r}|$. For what follows we will therefore always consider the worst case and assume that i is a spin lying in the plane of the surface code. Using Eq. (7.56) and assuming that i labels a site lying in the plane of the surface code, we obtain

$$
\begin{aligned}
\tilde{S}_i^x(t) &= e^{i\tilde{H}t}\tilde{S}_i^x e^{-i\tilde{H}t} \approx \frac{\sqrt{2S}}{2} e^{i\tilde{H}t}(\tilde{a}_i + \tilde{a}_i^\dagger)e^{-i\tilde{H}t} = \frac{\sqrt{2S}}{2}(\tilde{a}_i(t) + \tilde{a}_i^\dagger(t)) \\
&= \frac{\sqrt{2S}}{2}(a_i(t) + a_i^\dagger(t) - \sqrt{2S}\frac{A}{2D}(L/2))
\end{aligned}
\tag{7.57}
$$

Now, we find the explicit time-dependence,

$$
a_i(t) = e^{i\tilde{H}t}a_i e^{-i\tilde{H}t} = \frac{1}{\sqrt{N_s}}\sum_{\boldsymbol{q}} a_{\boldsymbol{q}}(t)e^{i\boldsymbol{q}\cdot\boldsymbol{R}_i} = \frac{1}{\sqrt{N_s}}\sum_{\boldsymbol{q}} a_{\boldsymbol{q}}e^{-i\epsilon_{\boldsymbol{q}}t+i\boldsymbol{q}\cdot\boldsymbol{R}_i},
\tag{7.58}
$$

where we used the explicit expression (7.54) for $\tilde{H}$. Now, we insert this back into Eq. (7.55) and get

$$
\begin{aligned}
\langle S_i^x(t)\rangle &= \sqrt{\frac{S}{2N_s}}\mathrm{Tr}\rho_F e^{-S}\sum_{\boldsymbol{q}}(a_{\boldsymbol{q}}e^{-i\epsilon_{\boldsymbol{q}}t+i\boldsymbol{q}\cdot\boldsymbol{R}_i} + h.c.)e^S - e^{-S}\frac{SA}{2D}(L/2)e^S \\
&= \sqrt{\frac{S}{2N_s}}\mathrm{Tr}\rho_F\sum_{\boldsymbol{q}}((a_{\boldsymbol{q}}+d_{\boldsymbol{q}})e^{i\epsilon_{\boldsymbol{q}}t+i\boldsymbol{q}\cdot\boldsymbol{R}_i} + h.c.) - \frac{SA}{2D}(L/2) \\
&= \sqrt{\frac{S}{2N_s}}\underbrace{\mathrm{Tr}\rho_F}_{=1}\sum_{\boldsymbol{q}}d_{\boldsymbol{q}}e^{-i\epsilon_{\boldsymbol{q}}t+i\boldsymbol{q}\cdot\boldsymbol{R}_i} + d_{-\boldsymbol{q}}e^{i\epsilon_{\boldsymbol{q}}t-i\boldsymbol{q}\cdot\boldsymbol{R}_i} - \frac{SA}{2D}(L/2),
\end{aligned}
\tag{7.59}
$$

where we used that $\mathrm{Tr}\rho_F a_{\boldsymbol{q}} = 0$ and defined

$$
d_{\boldsymbol{q}} = \sum_j W_j\frac{M_{-\boldsymbol{q},j}}{\epsilon_{\boldsymbol{q}}} = \sum_j W_j\frac{A\sqrt{2S}}{2\sqrt{N_s}}\frac{e^{-i\boldsymbol{q}\cdot\boldsymbol{R}_j}}{\epsilon_{\boldsymbol{q}}}.
\tag{7.60}
$$

Inserting Eq. (7.60) into Eq. (7.59), we finally obtain

$$
\begin{aligned}
\langle S_i^x(t) \rangle &= \sqrt{\frac{S}{2N_s}} \frac{A\sqrt{2S}}{2\sqrt{N_s}} \sum_j W_j \sum_{\boldsymbol{q}} \frac{1}{\epsilon_{\boldsymbol{q}}} (e^{-i\boldsymbol{q}\cdot\boldsymbol{R}_j} e^{-i\epsilon_q t + i\boldsymbol{q}\cdot\boldsymbol{R}_i} + e^{i\boldsymbol{q}\cdot\boldsymbol{R}_j} e^{i\epsilon_q t - i\boldsymbol{q}\cdot\boldsymbol{R}_i}) \\
&\qquad\qquad\qquad\qquad\qquad\qquad\qquad\qquad\qquad\qquad\qquad -\frac{SA}{2D}(L/2) \\
&= \frac{SA}{2N_s} \sum_j W_j \sum_{\boldsymbol{q}} \frac{1}{\epsilon_{\boldsymbol{q}}} (e^{i\boldsymbol{q}\cdot(\boldsymbol{R}_i-\boldsymbol{R}_j)-i\epsilon_q t} + e^{i\boldsymbol{q}\cdot(\boldsymbol{R}_j-\boldsymbol{R}_i)+i\epsilon_q t}) - \frac{SA}{2D}(L/2) .
\end{aligned}
$$
(7.61)

Going to the continuum approximation ($\sum_{\boldsymbol{q}} \to \frac{N_s}{(2\pi)^3} \int d\boldsymbol{q}$), we now calculate the following integrals (with $V = \Lambda^3 = N_s$),

$$
\begin{aligned}
\int_V d\boldsymbol{q} \frac{1}{Dq^2} e^{i\boldsymbol{q}\cdot\boldsymbol{r} - iDq^2 t} &= 2\pi \int_{-1}^{1} d(\cos(\theta)) \int_0^{\infty} dq q^2 \frac{1}{Dq^2} e^{iqr\cos(\theta)} e^{-iDq^2 t} \\
&= 4\pi \int_0^{+\infty} dq q^2 \frac{1}{Dq^2} \sin(qr) \frac{1}{qr} e^{-iDq^2 t} \\
&= \frac{4\pi}{Dr} \int_0^{\infty} \frac{\sin(qr)}{q} e^{iDq^2 t} dq \\
&= \frac{4\pi}{Dr} \left(\frac{1}{2} + \frac{i}{2}\right) \pi \left(-i\,\mathrm{FC}\left[\frac{r}{\sqrt{2\pi}\sqrt{Dt}}\right] + \mathrm{FS}\left[\frac{r}{\sqrt{2\pi}\sqrt{Dt}}\right]\right) ,
\end{aligned}
$$

$$
\int_V d\boldsymbol{q} \frac{1}{Dq^2} e^{-i\boldsymbol{q}\cdot\boldsymbol{R} + iDq^2 t} = -\frac{4\pi}{Dr} \left(-\frac{1}{2} - \frac{i}{2}\right) \pi \left(\mathrm{FC}\left[\frac{r}{\sqrt{2\pi}\sqrt{Dt}}\right] - i\,\mathrm{FS}\left[\frac{r}{\sqrt{2\pi}\sqrt{Dt}}\right]\right) .
$$
(7.62)

Therefore the sum of both integrals is given by

$$
\frac{4\pi^2}{Dr} \left(\mathrm{FC}\left[\frac{r}{\sqrt{2\pi}\sqrt{Dt}}\right] + \mathrm{FS}\left[\frac{r}{\sqrt{2\pi}\sqrt{Dt}}\right]\right) ,
$$
(7.63)

and thus

$$
\langle S_i^x(t) \rangle = \frac{SA}{2} \frac{4\pi^2}{D(2\pi)^3} \sum_j W_j \frac{1}{r_j} \left(\mathrm{FC}\left[\frac{r_j}{\sqrt{2\pi}\sqrt{Dt}}\right] + \mathrm{FS}\left[\frac{r_j}{\sqrt{2\pi}\sqrt{Dt}}\right]\right) - \frac{SA}{2D}(L/2) .
$$
(7.64)

We remark that here and the following we neglect the finite 'mass term' h_z (i.e. $\epsilon_{\boldsymbol{q}} \approx \omega_{\boldsymbol{q}}$) in the magnon spectrum generated by the magnetic field applied along the z-axis. Since we assume that $h_z \propto 1/L^4$ (in order to

have the magnetic length $L_h \propto \sqrt{1/h_z} \propto L^2$ and thus $L_h \gg L$), this is justified as it would lead to $1/L$ corrections.

Let us now assume $W_j = 1$, i.e. the memory is free of anyons, and assume that the memory is a disk of radius $L/2$:

$$
2\pi \int_0^{L/2} \left(\mathrm{FC} \left[\frac{r}{\sqrt{2\pi}\sqrt{Dt}} \right] + \mathrm{FS} \left[\frac{r}{\sqrt{2\pi}\sqrt{Dt}} \right] \right) dr = 2\pi \left(\frac{L}{2} \mathrm{FC} \left[\frac{L/2}{\sqrt{2\pi}\sqrt{Dt}} \right] + \right.
$$
$$
\left. + \frac{L}{2} \mathrm{FS} \left[\frac{L/2}{\sqrt{2\pi}\sqrt{Dt}} \right] + \sqrt{\frac{2}{\pi}} \sqrt{Dt} \left(-1 + \cos \left[\frac{(L/2)^2}{4Dt} \right] - \sin \left[\frac{(L/2)^2}{4Dt} \right] \right) \right) .
$$

(7.65)

We thus now have the following result for $\langle S_i^x(t) \rangle$,

$$
\begin{aligned}
\langle S_i^x(t) \rangle &= \frac{SA}{2D} \left(\frac{L}{2} \mathrm{FC} \left[\frac{L/2}{\sqrt{2\pi}\sqrt{Dt}} \right] + \frac{L}{2} \mathrm{FS} \left[\frac{L/2}{\sqrt{2\pi}\sqrt{Dt}} \right] \right. \\
&\quad \left. + \sqrt{\frac{2}{\pi}} \sqrt{Dt} \left(-1 + \cos \left[\frac{(L/2)^2}{4Dt} \right] - \sin \left[\frac{(L/2)^2}{4Dt} \right] \right) \right) - \frac{SA}{2D}(L/2) \\
&= F(t) - \frac{SA}{2D}(L/2) .
\end{aligned}
$$

(7.66)

For $t = 0$ we have

$$
2\pi \int_0^{L/2} \left(\mathrm{FC} \left[\frac{r}{\sqrt{2\pi}\sqrt{Dt}} \right] + \mathrm{FS} \left[\frac{r}{\sqrt{2\pi}\sqrt{Dt}} \right] \right) dr = 2\pi(L/2) \qquad (7.67)
$$

and thus

$$
\langle S_i^x(t=0) \rangle = \frac{SA}{2D}(L/2) - \frac{SA}{2D}(L/2) = 0 . \qquad (7.68)
$$

We note that the time-scale of the Fresnel functions is of the diffusive form, $\tau = 2\pi Dt/(L/2)^2$. From Eq. (7.66) it is clear that the time to flip the spins goes like L^2, like in a diffusive process with diffusion constant $D = 2SJ$. Using the representation in form of τ, Eq. (7.66) becomes

$$
\langle S_i^x(t) \rangle = \underbrace{\frac{SA(L/2)}{2D} \left(\mathrm{FC} \left[\frac{1}{\sqrt{\tau}} \right] + \mathrm{FS} \left[\frac{1}{\sqrt{\tau}} \right] + \frac{\sqrt{\tau}}{\pi} \left(-1 + \cos \left[\frac{\pi}{2\tau} \right] - \sin \left[\frac{\pi}{2\tau} \right] \right) \right)}_{\tilde{F}(\tau)}
$$
$$
- \frac{SA}{2D}(L/2) .
$$

(7.69)

We consider now the 'short time limit' in Eq. (7.66), with $\tau = 2\pi Dt/(L/2)^2 \ll 1$ and expand in τ. There are also non-analytic expressions (sin and cos, functions of $1/\tau$) which we just keep as is. For this we perform a series expansion for $\tau \ll 1$ and obtain

$$
\begin{aligned}
\langle S_i^x(t) \rangle &= \frac{SA}{2D}\left(\left(L/2 - \sqrt{J}\sqrt{\frac{2}{\pi}}\sqrt{t} + O[t]^{3/2}\right)\right.\\
&\quad \left. + O[t]^{3/2}\left(\cos\left[\frac{(L/2)^2}{4Dt}\right] + \sin\left[\frac{(L/2)^2}{4Dt}\right]\right)\right) - \frac{SA}{2D}(L/2)\\
&\approx -S\sqrt{\frac{A^2 t}{2\pi D}},
\end{aligned} \tag{7.70}
$$

where we kept only the leading terms in the last line. We emphasize that in the regime $\tau = 2\pi Dt/(L/2)^2 \ll 1$ the x-magnetization $\langle S_i^x(t) \rangle$ becomes independent of L. Thus, the result Eq. (7.70) is formally obtained in the limit $L \to \infty$ (for arbitrary but fixed time t). This limit corresponds to the limit of physical interest: first $L \to \infty$ and then $t \to \infty$. The opposite order, $t \to \infty$ and then $L \to \infty$ (or finite L) leads to unphysical results (for $L \gg 1$ such that the magnetization per spin exceeds the maximum value S), $\langle S_i^x(t \to \infty) \rangle = -SA(L/2)/(2D) \propto L \gg S$. This is an artifact of the harmonic approximation. However, for sufficiently small L the result is physical and can also be used for comparison with the Metropolis simulation, see Fig. (2) in the main text.

Next we note that for self-consistency reasons the magnetization should not exceed the maximum spin value S (this constraint is violated in the harmonic approximation). Thus, we trust our result only up to times t which satisfy

$$
0 \le t \le t_r, \quad t_r = \frac{2\pi D}{A^2}. \tag{7.71}
$$

Here, t_r satisfies $\langle S_i^x(t_r) \rangle = -S$ and $0 \ge \langle S_i^x(t) \rangle \ge -S$ for all positive times $t \le t_r$. We refer to t_r as the refreshing time: at this time the backaction of the memory on the ferromagnet has become substantial with the spins close to the memory pointing now along the x-axis. To maintain the effect of the ferromagnet we refresh the ferromagnetic state with e.g. a magnetic pulse, so that all spins point again along the z-axis. This procedure has to be repeated periodically on a time scale t_r. Note that this time scale is independent of the memory size L. This refreshing can be considered as part of a 'cooling' cycle to get the heat out of the system generated by the memory. This refreshing prevents that the total system,

ferromagnet plus memory, reach a new common equilibrium, and makes sure that the ferromagnet stays in its own equilibrium state.

We further note that the regime $\tau \ll 1$ and $t \leq t_r$ are consistent. Indeed, we can express τ in terms of t_r,

$$\tau = At_r \frac{At}{(L/2)^2} \leq \frac{A^2 t_r^2}{(L/2)^2} \ll 1 \,, \tag{7.72}$$

where we assumed that we consider only times $t \leq t_r$.

Non-equilibrium response for S^y

Here we want to calculate the dynamics of the y-component of ferromagnetic spins which lie in the plane of the surface code:

$$\langle S_i^y(t) \rangle = \mathrm{Tr} \rho_F S_i^y(t) \,, \tag{7.73}$$

where the different quantities are defined as in the previous section. Since

$$
\begin{aligned}
\tilde{S}_i^y(t) &= e^{i\tilde{H}t} \tilde{S}_i^y e^{-i\tilde{H}t} \approx \frac{\sqrt{2S}}{2i} e^{i\tilde{H}t} (\tilde{a}_i - \tilde{a}_i^\dagger) e^{-i\tilde{H}t} = \frac{\sqrt{2S}}{2i} (\tilde{a}_i(t) - \tilde{a}_i^\dagger(t)) \\
&= \frac{\sqrt{2S}}{2i} (a_i(t) - a_i^\dagger(t)) \,,
\end{aligned}
\tag{7.74}
$$

and

$$a_i(t) = e^{i\tilde{H}t} a_i e^{-i\tilde{H}t} = \frac{1}{\sqrt{N}} \sum_{\boldsymbol{q}} a_{\boldsymbol{q}}(t) e^{i\boldsymbol{q}\cdot\boldsymbol{R}_i} = \frac{1}{\sqrt{N}} \sum_{\boldsymbol{q}} a_{\boldsymbol{q}} e^{-i\epsilon_q t + i\boldsymbol{q}\cdot\boldsymbol{R}_i} \,, \tag{7.75}$$

we obtain

$$
\begin{aligned}
\langle S_i^y(t) \rangle &= \sqrt{\frac{S}{2N}} \frac{1}{i} \mathrm{Tr} \rho_F e^{-S} \sum_{\boldsymbol{q}} (a_{\boldsymbol{q}} e^{-i\epsilon_q t + i\boldsymbol{q}\cdot\boldsymbol{R}_i} - h.c.) e^S \\
&= \sqrt{\frac{S}{2N}} \frac{1}{i} \mathrm{Tr} \rho_F \sum_{\boldsymbol{q}} ((a_{\boldsymbol{q}} + d_{\boldsymbol{q}}) e^{-i\epsilon_q t + i\boldsymbol{q}\cdot\boldsymbol{R}_i} - h.c.) \\
&= \sqrt{\frac{S}{2N}} \frac{1}{i} \underbrace{\mathrm{Tr} \rho_F}_{=1} \sum_{\boldsymbol{q}} d_{\boldsymbol{q}} e^{-\epsilon_q t + i\boldsymbol{q}\cdot\boldsymbol{R}_i} - d_{-\boldsymbol{q}} e^{i\epsilon_q t - i\boldsymbol{q}\cdot\boldsymbol{R}_i} \tag{7.76}
\end{aligned}
$$

where we again used that $\mathrm{Tr}\rho_F a_{\boldsymbol{q}} = 0$. Using the explicit definition (7.60) of $M_{\boldsymbol{q}}$, we have

$$
\begin{aligned}
\langle S_i^y(t) \rangle &= \sqrt{\frac{S}{2N}} \frac{A\sqrt{2S}}{2\sqrt{N}} \frac{1}{i} \sum_j W_j \sum_{\boldsymbol{q}} \frac{1}{\epsilon_{\boldsymbol{q}}} (e^{-i\boldsymbol{q}\cdot\boldsymbol{R}_j} e^{-i\epsilon_{\boldsymbol{q}}t + i\boldsymbol{q}\cdot\boldsymbol{R}_i} - e^{i\boldsymbol{q}\cdot\boldsymbol{R}_j} e^{i\epsilon_{\boldsymbol{q}}t - i\boldsymbol{q}\cdot\boldsymbol{R}_i}) \\
&= \frac{SA}{2N} \frac{1}{i} \sum_j W_j \sum_{\boldsymbol{q}} \frac{1}{\epsilon_{\boldsymbol{q}}} (e^{i\boldsymbol{q}\cdot(\boldsymbol{R}_i-\boldsymbol{R}_j)-i\epsilon_{\boldsymbol{q}}t} - e^{i\boldsymbol{q}\cdot(\boldsymbol{R}_j-\boldsymbol{R}_i)+i\epsilon_{\boldsymbol{q}}t}) . \qquad (7.77)
\end{aligned}
$$

Since in the continuum approximation the integrals we need to perform are the same as in the previous section, we obtain that

$$
\langle S_i^y(t) \rangle = \frac{SA}{2} \frac{4\pi^2}{D(2\pi)^3} \sum_j W_j \frac{1}{r_j} \left(\mathrm{FC}\left[\frac{r_j}{\sqrt{2\pi}\sqrt{Dt}} \right] - \mathrm{FS}\left[\frac{r_j}{\sqrt{2\pi}\sqrt{Dt}} \right] \right) .
\tag{7.78}
$$

Assuming again that $W_j = +1$, we finally cocnlude that

$$
\begin{aligned}
\langle S_i^y(t) \rangle &= \frac{SA}{2D} \left(\frac{L}{2} \mathrm{FC}\left[\frac{L/2}{\sqrt{2\pi}\sqrt{Dt}} \right] - \frac{L}{2} \mathrm{FS}\left[\frac{L/2}{\sqrt{2\pi}\sqrt{Dt}} \right] \right. \\
&\quad \left. - \sqrt{\frac{2}{\pi}} \sqrt{Dt} \left(-1 + \cos\left[\frac{(L/2)^2}{4Dt} \right] + \sin\left[\frac{(L/2)^2}{4Dt} \right] \right) \right) .
\end{aligned}
\tag{7.79}
$$

We note that at $t = 0$ and at very long times $\langle S_i^y(t) \rangle$ vanishes. For small τ, we find the following expansion

$$
\langle S_i^y(t \to 0) \rangle = S\sqrt{\frac{A^2 t}{2\pi D}} = -\langle S_i^x(t \to 0) \rangle .
\tag{7.80}
$$

Note that $\langle S_i^y(t) \rangle$ is linear in A (like $\langle S_i^x(t) \rangle$). Thus, the off-diagonal susceptibility $\chi_{yx}(\boldsymbol{R}_i, \omega)$ is non-zero, but only for finite ω. For $\omega \to 0$, $\chi_{yx}(\boldsymbol{R}_i, \omega = 0) = 0$ since $\langle S_i^y(t \to \infty) \rangle = 0$. This agrees with the spin wave evaluation of the susceptibility where all off-diagonal terms vanish in the stationary limit.

Non-equilibrium response for S^z

We calculate now the time-dependent expectation value of the local z-magnetization, defined as

$$
\langle S_i^z(t) \rangle = \mathrm{Tr}\rho_F S_i^z(t) ,
\tag{7.81}
$$

where we use the same definitions as in the two previous sections and i again labels a site which lies in the plane of the surface code. We now have

$$\widetilde{S}_i^z(t) = -S + e^{i\widetilde{H}t}\tilde{a}_i^\dagger \tilde{a}_i e^{-i\widetilde{H}t} = -S + \tilde{a}_i^\dagger(t)\tilde{a}_i(t) = -S + (a_i^\dagger(t) - d_i)(a_i(t) - d_i) \,,$$
(7.82)

where $d_i = \sqrt{S/8}A(L/2)/D$ is defined through Eq. (7.56). As in the two previous sections, we approximate $\epsilon_{\boldsymbol{q}} \approx \omega_{\boldsymbol{q}} \approx Dq^2$ and find

$$
\begin{aligned}
\widetilde{S}_i^z(t) \;=\; & -S + d_i^2 + \frac{1}{N}\sum_{\boldsymbol{q},\boldsymbol{q}'} a_{\boldsymbol{q}}^\dagger a_{\boldsymbol{q}'} e^{i(\boldsymbol{q}'-\boldsymbol{q})\boldsymbol{R}_i} e^{it(\omega_{\boldsymbol{q}}-\omega_{\boldsymbol{q}'})} \\
& -\frac{1}{N}\sum_{\boldsymbol{q},\boldsymbol{q}'} a_{\boldsymbol{q}}^\dagger d_{\boldsymbol{q}'} e^{i\omega_{\boldsymbol{q}}t} e^{i\cdot\boldsymbol{R}_i(\boldsymbol{q}'-\boldsymbol{q})} - \frac{1}{N}\sum_{\boldsymbol{q},\boldsymbol{q}'} a_{\boldsymbol{q}} d_{\boldsymbol{q}'} e^{-i\omega_{\boldsymbol{q}}t} e^{i\boldsymbol{R}_i\cdot(\boldsymbol{q}'+\boldsymbol{q})} \,.
\end{aligned}
$$
(7.83)

Applying the inverse polaron transformation we get

$$
\begin{aligned}
e^{\mathcal{S}}\widetilde{S}_i^z(t)e^{-\mathcal{S}} \;=\; & -S + d_i^2 + \frac{1}{N}\sum_{\boldsymbol{q},\boldsymbol{q}'}(a_{\boldsymbol{q}}^\dagger + d_{\boldsymbol{q}}^*)(a_{\boldsymbol{q}'} + d_{\boldsymbol{q}'}) e^{i(\boldsymbol{q}'-\boldsymbol{q})\boldsymbol{R}_i} e^{it(\omega_{\boldsymbol{q}}-\omega_{\boldsymbol{q}'})} \\
& -\frac{1}{N}\sum_{\boldsymbol{q},\boldsymbol{q}'}(a_{\boldsymbol{q}}^\dagger + d_{\boldsymbol{q}}^*)d_{\boldsymbol{q}'} e^{i\omega_{\boldsymbol{q}}t} e^{i\cdot\boldsymbol{R}_i(\boldsymbol{q}'-\boldsymbol{q})} \\
& -\frac{1}{N}\sum_{\boldsymbol{q},\boldsymbol{q}'}(a_{\boldsymbol{q}} + d_{\boldsymbol{q}})d_{\boldsymbol{q}'} e^{-i\omega_{\boldsymbol{q}}t} e^{i\boldsymbol{R}_i\cdot(\boldsymbol{q}'+\boldsymbol{q})} \,,
\end{aligned}
$$
(7.84)

and thus finally obtain

$$
\begin{aligned}
\langle S_i^z(t)\rangle \;=\; & -S + d_i^2 + \frac{1}{N}\sum_{\boldsymbol{q}}\langle a_{\boldsymbol{q}}^\dagger a_{\boldsymbol{q}}\rangle + \frac{1}{N}\sum_{\boldsymbol{q},\boldsymbol{q}'} d_{\boldsymbol{q}}^* d_{\boldsymbol{q}'}\, e^{i(\boldsymbol{q}'-\boldsymbol{q})\boldsymbol{R}_i}\, e^{it(\omega_{\boldsymbol{q}}-\omega_{\boldsymbol{q}'})} \\[4pt]
& -\frac{1}{N}\sum_{\boldsymbol{q},\boldsymbol{q}'} d_{\boldsymbol{q}}^* d_{\boldsymbol{q}'}\, e^{i\omega_{\boldsymbol{q}} t}\, e^{i\cdot\boldsymbol{R}_i(\boldsymbol{q}'-\boldsymbol{q})} - \frac{1}{N}\sum_{\boldsymbol{q},\boldsymbol{q}'} d_{\boldsymbol{q}} d_{\boldsymbol{q}'}\, e^{-i\omega_{\boldsymbol{q}} t}\, e^{i\boldsymbol{R}_i\cdot(\boldsymbol{q}'+\boldsymbol{q})} \\[6pt]
=\; & -S + d_i^2 + \frac{1}{N}\sum_{\boldsymbol{q}}\langle a_{\boldsymbol{q}}^\dagger a_{\boldsymbol{q}}\rangle \\[4pt]
& + \underbrace{\frac{1}{N}\left(\sum_{kl} W_k W_l \frac{A^2 S}{2N}\right)\sum_{\boldsymbol{q},\boldsymbol{q}'} e^{i(\boldsymbol{q}'-\boldsymbol{q})\boldsymbol{R}_i}\, e^{i\boldsymbol{q}\boldsymbol{R}_k - i\boldsymbol{q}'\boldsymbol{R}_l}\, \frac{e^{it(\omega_{\boldsymbol{q}}-\omega_{\boldsymbol{q}'})}}{\omega_{\boldsymbol{q}}\omega_{\boldsymbol{q}'}}}_{=I} \\[4pt]
& - \underbrace{\frac{1}{N}\left(\sum_{kl} W_k W_l \frac{A^2 S}{2N}\right)\sum_{\boldsymbol{q},\boldsymbol{q}'} e^{i\boldsymbol{q}\boldsymbol{R}_k - i\boldsymbol{q}'\boldsymbol{R}_l}\, e^{i\boldsymbol{R}_i(\boldsymbol{q}'-\boldsymbol{q})}\, \frac{e^{i\omega_{\boldsymbol{q}} t}}{\omega_{\boldsymbol{q}}\omega_{\boldsymbol{q}'}}}_{=II} \\[4pt]
& - \underbrace{\frac{1}{N}\left(\sum_{kl} W_k W_l \frac{A^2 S}{2N}\right)\sum_{\boldsymbol{q},\boldsymbol{q}'} e^{-i\boldsymbol{q}\boldsymbol{R}_k + i\boldsymbol{q}'\boldsymbol{R}_l}\, e^{i\boldsymbol{R}_i(-\boldsymbol{q}'+\boldsymbol{q})}\, \frac{e^{-i\omega_{\boldsymbol{q}} t}}{\omega_{\boldsymbol{q}}\omega_{\boldsymbol{q}'}}}_{=III}\;.
\end{aligned}
\tag{7.85}
$$

Collecting the various results, we have

$$
\langle S_i^z(t)\rangle = -S + \frac{1}{N}\sum_{\boldsymbol{k}}\langle \hat{n}_{\boldsymbol{k}}\rangle + d_i^2 + I - II - III.
\tag{7.86}
$$

The next step is now to calculate integrals I, II, and III in the con-

tinuum approximation:

$$
\begin{aligned}
I &= \left(\sum_{kl} W_k W_l \frac{A^2 S}{2} \right) \frac{1}{(2\pi)^6} \int d\boldsymbol{q} \int d\boldsymbol{q}' e^{i\boldsymbol{q}'(\boldsymbol{R}_i - \boldsymbol{R}_l)} e^{i\boldsymbol{q}(\boldsymbol{R}_k - \boldsymbol{R}_i)} \frac{e^{it(\omega_{\boldsymbol{q}} - \omega_{\boldsymbol{q}'})}}{\omega_{\boldsymbol{q}} \omega_{\boldsymbol{q}'}} \\
&= \left(\sum_{kl} W_k W_l \frac{A^2 S}{2} \right) \frac{4\pi^2}{(2\pi)^6} \frac{4}{|(\boldsymbol{R}_i - \boldsymbol{R}_l)||(\boldsymbol{R}_k - \boldsymbol{R}_i)|} \int dq\, q \sin(q|\boldsymbol{R}_k - \boldsymbol{R}_i|) \frac{e^{i\omega_{\boldsymbol{q}} t}}{\omega_{\boldsymbol{q}}} \times \\
&\qquad\qquad\qquad\qquad\qquad\qquad \times \int dq'\, q' \sin(q'|\boldsymbol{R}_i - \boldsymbol{R}_l|) \frac{e^{-i\omega_{\boldsymbol{q}'} t}}{\omega_{\boldsymbol{q}'}} \\
&= \left(\sum_{kl} W_k W_l \frac{A^2 S}{2} \right) \frac{4\pi^2}{(2\pi)^6} \frac{4}{D|\boldsymbol{R}_{il}||\boldsymbol{R}_{ki}|} \left(\frac{1}{2} + \frac{i}{2} \right) \pi \times \\
&\qquad \left(\mathrm{FC} \left[\frac{|\boldsymbol{R}_{ki}|}{\sqrt{2\pi}\sqrt{Dt}} \right] - i\mathrm{FS} \left[\frac{|\boldsymbol{R}_{ki}|}{\sqrt{2\pi}\sqrt{Dt}} \right] \right) \frac{1}{D} \left(\frac{1}{2} + \frac{i}{2} \right) \pi \times \\
&\qquad \left(-i\mathrm{FC} \left[\frac{|\boldsymbol{R}_{il}|}{\sqrt{2\pi}\sqrt{Dt}} \right] + \mathrm{FS} \left[\frac{|\boldsymbol{R}_{il}|}{\sqrt{2\pi}\sqrt{Dt}} \right] \right) \\
&= \left(\sum_{kl} W_k W_l \frac{A^2 S}{2} \right) \frac{1}{8\pi^2 D^2 |\boldsymbol{R}_{il}||\boldsymbol{R}_{ki}|} \left(\mathrm{FC} \left[\frac{|\boldsymbol{R}_{ki}|}{\sqrt{2\pi}\sqrt{Dt}} \right] \mathrm{FC} \left[\frac{|\boldsymbol{R}_{il}|}{\sqrt{2\pi}\sqrt{Dt}} \right] + \\
&\qquad\qquad + \mathrm{FS} \left[\frac{|\boldsymbol{R}_{ki}|}{\sqrt{2\pi}\sqrt{Dt}} \right] \mathrm{FS} \left[\frac{|\boldsymbol{R}_{il}|}{\sqrt{2\pi}\sqrt{Dt}} \right] \right) , \quad (7.87)
\end{aligned}
$$

where $\boldsymbol{R}_{ki} = \boldsymbol{R}_k - \boldsymbol{R}_i$. Since we are in the continuum approximation we can replace $\sum_r \to \int r\, dr$ and obtain

$$
\begin{aligned}
I &= \left(\frac{A^2 S}{2} \right) \frac{4\pi^2}{8\pi^2 D^2} \int_0^{L/2} dr \int_0^{L/2} dr' \left(\mathrm{FC} \left[\frac{r}{\sqrt{2\pi}\sqrt{Dt}} \right] \mathrm{FC} \left[\frac{r'}{\sqrt{2\pi}\sqrt{Dt}} \right] \right. \\
&\qquad\qquad\qquad\qquad \left. + \mathrm{FS} \left[\frac{r}{\sqrt{2\pi}\sqrt{Dt}} \right] \mathrm{FS} \left[\frac{r'}{\sqrt{2\pi}\sqrt{Dt}} \right] \right) \\
&= \left(\frac{A^2 S}{2} \right) \frac{4\pi^2}{8\pi^3 D^2} \left[(L/2)^2 \pi \left(\mathrm{FC} \left[\frac{L/2}{\sqrt{2\pi}\sqrt{Dt}} \right]^2 + \mathrm{FS} \left[\frac{L/2}{\sqrt{2\pi}\sqrt{Dt}} \right]^2 \right) \right. \\
&\qquad + 8Dt \sin \left[\frac{(L/2)^2}{8Dt} \right]^2 - -4(L/2)\sqrt{2\pi}\sqrt{Dt}\,\mathrm{FS} \left[\frac{L/2}{\sqrt{2\pi}\sqrt{Dt}} \right] \sin \left[\frac{(L/2)^2}{8Dt} \right]^2 \\
&\qquad \left. -2(L/2)\sqrt{2\pi}\sqrt{Dt}\,\mathrm{FC} \left[\frac{L/2}{\sqrt{2\pi}\sqrt{Dt}} \right] \sin \left[\frac{(L/2)^2}{4Dt} \right] \right] . \quad (7.88)
\end{aligned}
$$

The small t expansion of the term I (valid for $\tau \ll 1$) gives

$$
\begin{aligned}
I(t \to 0) \;=\; & \frac{A^2 S}{2} \frac{4\pi^2}{8\pi^3 D^2} \left(\cos\left[\frac{L^2}{2Dt}\right] O[t]^2 \right. \\
& + \left(\frac{L^2 \pi}{2} - \sqrt{D} L \sqrt{2\pi} \sqrt{t} + 2Dt + O[t]^{3/2} \right) \\
& \left. + O[t]^{3/2} \left(\cos\left[\frac{L^2}{4Dt}\right] + \sin\left[\frac{L^2}{4Dt}\right] \right) + O[t]^{5/2} \sin\left[\frac{L^2}{2Dt}\right] \right)
\end{aligned}
\tag{7.89}
$$

Similarly, for integral II we obtain

$$
\begin{aligned}
II \;=\; & \left(\sum_{kl} W_k W_l \frac{A^2 S}{2} \right) \frac{1}{(2\pi)^6} \int d\boldsymbol{q} \int d\boldsymbol{q}' e^{i\boldsymbol{q}'(\boldsymbol{R}_i - \boldsymbol{R}_l)} e^{i\boldsymbol{q}(\boldsymbol{R}_k - \boldsymbol{R}_i)} \frac{e^{it\omega_q}}{\omega_q \omega_{q'}} \\
=\; & \left(\sum_{kl} W_k W_l \frac{A^2 S}{2} \right) \frac{1}{(2\pi)^6} 16\pi^2 \frac{1}{R_{il} R_{ki}} \underbrace{\int dq' \frac{\sin(q' R_{il})}{\omega_{q'}} q'}_{\frac{\pi}{2D}} \int dq \sin(q R_{ki}) \frac{e^{it\omega_q}}{\omega_q} q \\
=\; & \left(\sum_{kl} W_k W_l \frac{A^2 S}{2} \right) \frac{1}{(2\pi)^6} 16\pi^2 \frac{1}{R_{il} R_{ki}} \frac{\pi}{2D} \frac{1}{D} \left(\frac{1}{2} + \frac{i}{2} \right) \pi \left(\mathrm{FC}\left[\frac{R_{ki}}{\sqrt{2\pi}\sqrt{Dt}} \right] \right. \\
& \hspace{8cm} \left. - i\mathrm{FS}\left[\frac{R_{ki}}{\sqrt{2\pi}\sqrt{Dt}} \right] \right) \\
=\; & \left(\sum_{kl} W_k W_l \frac{A^2 S}{2} \right) \frac{1}{8\pi^2 D^2} \frac{1}{R_{il} R_{ik}} \left(\frac{1}{2} + \frac{i}{2} \right) \left(\mathrm{FC}\left[\frac{R_{ki}}{\sqrt{2\pi}\sqrt{Dt}} \right] - i\mathrm{FS}\left[\frac{R_{ki}}{\sqrt{2\pi}\sqrt{Dt}} \right] \right),
\end{aligned}
\tag{7.90}
$$

and since II and III are complex conjugates of each other, we have

$$
II + III = \left(\sum_{kl} W_k W_l \frac{A^2 S}{2} \right) \frac{1}{8\pi^2 D^2} \frac{1}{R_{il} R_{ik}} \left(\mathrm{FC}\left[\frac{R_{ki}}{\sqrt{2\pi}\sqrt{Dt}} \right] + \mathrm{FS}\left[\frac{R_{ki}}{\sqrt{2\pi}\sqrt{Dt}} \right] \right).
\tag{7.91}
$$

As before in the continuum approximation we have $\sum_r \to \int r\,dr$ and thus

$$
\begin{aligned}
II + III \;=\; & \frac{4\pi^2 A^2 S}{16\pi^2 D^2} \int_0^{L/2} dr \int_0^{L/2} dr' \left(\mathrm{FC}\left[\frac{r}{\sqrt{2\pi}\sqrt{Dt}} \right] + \mathrm{FS}\left[\frac{r}{\sqrt{2\pi}\sqrt{Dt}} \right] \right) \\
=\; & \frac{4\pi^2 A^2 S}{16\pi^2 D^2} \frac{L}{2} \left(\frac{L}{2}\mathrm{FC}\left[\frac{L/2}{\sqrt{2\pi}\sqrt{Dt}} \right] + \frac{L}{2}\mathrm{FS}\left[\frac{L/2}{\sqrt{2\pi}\sqrt{Dt}} \right] \right. \\
& \left. + \sqrt{\frac{2}{\pi}} \sqrt{Dt} \left(-1 + \cos\left[\frac{(L/2)^2}{4Dt} \right] - \sin\left[\frac{(L/2)^2}{4Dt} \right] \right) \right).
\end{aligned}
\tag{7.92}
$$

Next, we perform a small t expansion of $II + III$ (valid for $\tau \ll 1$),

$$(II + III)(t \to 0) = \frac{4\pi^2 A^2 S}{16\pi^2 D^2} \frac{L}{2} \left(\left(L/2 - \sqrt{D}\sqrt{\frac{2}{\pi}}\sqrt{t} + O[t]^{3/2} \right) \right)$$

(7.93)

Let us now put all the terms together and obtain the small t behavior of the z magnetization (valid for $\tau \ll 1$):

$$
\begin{aligned}
\langle S_i^z(t \to 0) \rangle &= -S + \frac{1}{N_s} \sum_{\boldsymbol{k}} \langle \hat{n}_{\boldsymbol{k}} \rangle + d_i^2 \\
&\quad + \frac{A^2 S}{2} \frac{4\pi^2}{8\pi^3 D^2} \left(\cos\left[\frac{(L/2)^2}{2Dt}\right] O[t]^2 \right. \\
&\qquad + \left(\frac{(L/2)^2 \pi}{2} - \sqrt{D}(L/2)\sqrt{2\pi}\sqrt{t} + 2Dt + O[t]^{3/2} \right) \\
&\qquad + O[t]^{3/2} \left(\cos\left[\frac{(L/2)^2}{4Dt}\right] + \sin\left[\frac{(L/2)^2}{4Dt}\right] \right) + O[t]^{5/2} \left. \sin\left[\frac{(L/2)^2}{2Dt}\right] \right) \\
&\quad - \frac{4\pi^2 A^2 S}{16\pi^2 D^2} (L/2) \left(\left(\frac{L}{2} - \sqrt{D}\sqrt{\frac{2}{\pi}}\sqrt{t} + O[t]^{3/2} \right) \right. \\
&\qquad + O[t]^{3/2} \left. \left(\cos\left[\frac{(L/2)^2}{4Dt}\right] + \sin\left[\frac{(L/2)^2}{4Dt}\right] \right) \right).
\end{aligned}
$$

(7.94)

Recalling that

$$d_i^2 = \frac{A^2 S}{8D^2} (L/2)^2,$$

(7.95)

we now see that both the terms proportional to L^2 and to L cancel, indeed

$$
\begin{aligned}
\langle S_i^z(t \to 0) \rangle &= -S + \frac{1}{N_s} \sum_{\boldsymbol{k}} \langle \hat{n}_{\boldsymbol{k}} \rangle + \frac{A^2 S}{2} \frac{4\pi^2}{8\pi^3 D^2} \left(\cos\left[\frac{(L/2)^2}{2Dt}\right] O[t]^2 \right. \\
&\quad + \left(2Dt + O[t]^{3/2} \right) + O[t]^{3/2} \left(\cos\left[\frac{(L/2)^2}{4Dt}\right] + \sin\left[\frac{(L/2)^2}{4Dt}\right] \right) \\
&\quad + O[t]^{5/2} \left. \sin\left[\frac{(L/2)^2}{2Dt}\right] \right) \\
&\quad - \frac{4\pi^2 A^2 S}{16\pi^2 D^2} (L/2) \left(\left(O[t]^{3/2} \right) + O[t]^{3/2} \left(\cos\left[\frac{(L/2)^2}{4Dt}\right] + \sin\left[\frac{(L/2)^2}{4Dt}\right] \right) \right) \\
&\approx -S + \frac{1}{N_s} \sum_{\boldsymbol{k}} \langle \hat{n}_{\boldsymbol{k}} \rangle + \frac{S A^2 t}{2\pi D} = -S\left(1 - \frac{A^2 t}{2\pi D}\right) + \frac{1}{N_s} \sum_{\boldsymbol{k}} \langle \hat{n}_{\boldsymbol{k}} \rangle,
\end{aligned}
$$

(7.96)

where we kept only the leading terms in $\tau \ll 1$ (we also neglected $1/L$ corrections). Note that again all L-dependence has disappeared in this regime. The last terms $\frac{1}{N_s} \sum_{\boldsymbol{k}} \langle \hat{n}_{\boldsymbol{k}} \rangle$ describes the finite-temperature effects which reduce the full z-magnetization per spin $-S$ down to zero until it vanishes at the Curie temperature $T_c \approx J$. Let us assume now that we are in the low temperature regime $T \ll T_c$ and for simplicity neglect $\frac{1}{N_s} \sum_{\boldsymbol{k}} \langle \hat{n}_{\boldsymbol{k}} \rangle$. Then, we see again that for self-consistency reasons we can trust the polaron results only up to the refreshing time $t_r = \frac{2\pi D}{A^2}$ defined in Eq. (7.71). Beyond this time, the magnetization along z becomes positive and eventually with even larger amplitude than S which is unphysical.

7.E Continuum approximation

Here we numerically evaluate the sum $\sum_{\boldsymbol{p} \neq \boldsymbol{0}} \frac{1}{|\boldsymbol{p}|} e^{-|\boldsymbol{p}|/L_h}$ and show that the continuum approximation is just a convenient mathematical tool that allows to analytically evaluate the behavior of the sum as function of L.

In Fig. (7.4) we plot the sum $\sum_{\boldsymbol{p} \neq \boldsymbol{0}} \frac{1}{|\boldsymbol{p}|} e^{-|\boldsymbol{p}|/L_h}$ as function of L. Here we choose for the lattice constant $a = 1$ and for the magnetic length $L_h = 1000$. The linear behavior for $L \ll L_h$ is in agreement with the continuum approximation calculation. The other sums appearing in this work can similarly be evaluated numerically and the results agree with the continuum approximation. As mentioned in the main text, we point out again that in the continuum approximation we let the lattice constant a of the surface code go formally to zero such that a single stabilizer remains coupled to a single FM spin.
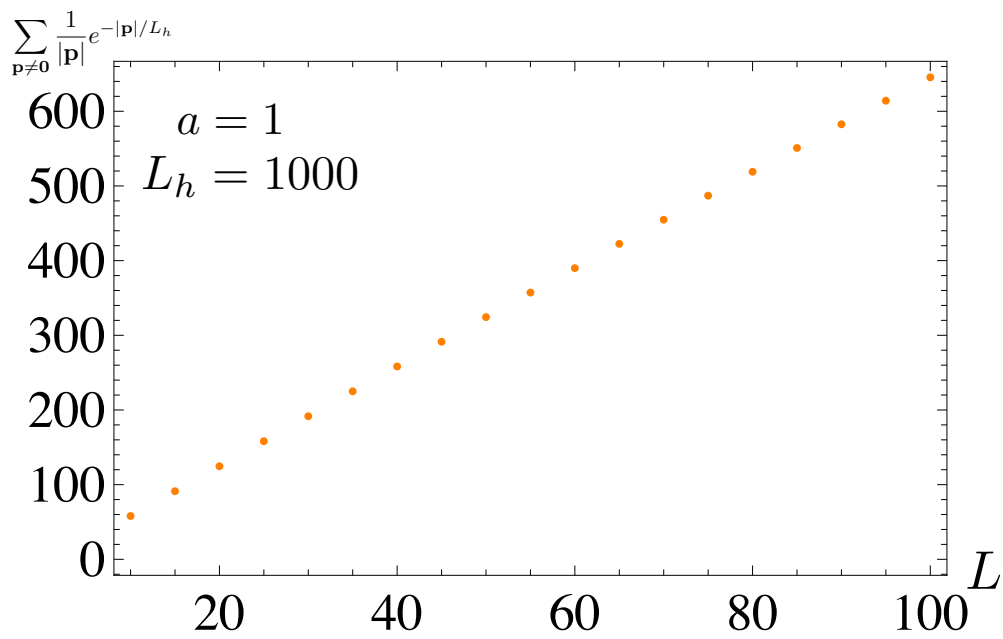
Figure 7.4: Numerical evaluation of the sum $\sum_{p \neq 0} \frac{1}{|p|} e^{-|p|/L_h}$ as function of L for a lattice constant $a = 1$ and magnetic length $L_h = 1000$. For $L \ll L_h$ the sum increases linearly with L, in agreement with the continuum approximation calculation.

Part III

Honeycomb Model, Spin Ladders, Vortex Loops, and Majorana Fermions

CHAPTER 8

Introduction

The Kitaev honeycomb model, with several variations, has attracted a lot of attention over the last years. [14, 16, 27, 30, 31, 32, 111, 114, 142, 143, 144, 145, 146, 147, 148, 149, 150, 151, 152, 153, 154, 155, 156, 157, 158] Many different interesting aspects of it have been studied in detail in the original work of Kitaev. [27] There, an exact method of solution of the model based on the mapping to Majorana fermion operators is discussed. Although alternative mappings and approximation techniques exist, [114, 156, 157] Kitaev's method is widely applied, being ideally suited to this class of spin models. Further, the presence of an abelian and a non-abelian phase (in the presence of an external magnetic perturbation) was demonstrated. [27] The Kitaev honeycomb model has a wide spectrum of physical applications, ranging from the description of strongly correlated materials [31] to the analytical study of critical quantum spin liquids. [147] It is also of central importance in the context of quantum information theory since its gapped phase provides a perturbative realization of the toric code. [14] Extensions of the honeycomb model have been lately proposed as promising candidates for the realization of a topological quantum memory. [16, 111] Although very challenging, its physical realization has become closer to reality thanks to recent proposals. [30, 32]

In the following we study several aspects of the Kitaev honeycomb model and make extensive use of a spin to Majoranas transformation which maps the spin Hamiltonian H to a family of quadratic (easily solvable) Majorana interactions $\{\widetilde{H}_u\}$ in an extended Hilbert space. In Chapter 9, we thus first investigate the exact solution of the Kitaev honeycomb model in detail and derive an explicit formula for the projector onto the

physical subspace. The physical states are shown to be characterized by the parity of the total occupation of the fermionic eigenmodes. We consider physically relevant quantities, as in particular the vortex energies, and show that their true value and associated states can be substantially different from the one calculated in the unprojected space.

In Chapter 10, we propose an inhomogeneous open spin ladder, related to the Kitaev honeycomb model, which can be tuned between topological and non-topological phases. We study the robustness of Majorana end states (MES) which emerge at the boundary between sections in different topological phases and show, among other results, that while the MES in the homogeneous ladder are destroyed by single-body perturbations, in the presence of inhomogeneity at least two-body perturbations are required for destabilizing MES. Furthermore, we present a trijunction setup where MES can be braided. This is of interest since MES in spin ladders potentially follow non-abelian braiding statistics as this is the case in proximity-induced superconducting wires for example.

In Chapter 11, we establish reflection positivity for Gibbs trace states defined by a certain class of Hamiltonians that describe the interaction of Majoranas on a lattice. These Hamiltonians may include many-body interactions, as long as the signs of the associated coupling constants satisfy certain restrictions. We show that reflection positivity holds on an even subalgebra of Majoranas. The class of interactions we consider is relevant to our study of the honeycomb quantum spin model and of its quasi one-dimensional ladder version.

In Chapter 12, we use the results derived in Chapter 11 to investigate the role that vortex loops play in characterizing eigenstates of certain systems of half-integer spins with nearest-neighbor interaction on a trivalent lattice. In particular we focus on ground states (and other low-lying states). We test our ideas on a spin ladder. In certain cases we show how the vortex configuration of the ground state is determined by the relative signs of the coupling constants. Two methods yield exact results: i.) We utilize the equivalence of spin Hamiltonians with quartic interactions of Majorana fermions, and analyze that fermionic Hamiltonian. ii) We use reflection positivity for Majorana fermions to characterize vortices in ground states for reflection-symmetric couplings. Two additional methods suggest potential wider applicability of these results: iii.) Numerical evidence suggests similar behavior for certain systems without reflection symmetry. iv.) A perturbative analysis also suggests similar behavior without the assumption of reflection symmetry. In all the cases we study, we conclude that the ground states of the spin ladders are vortex-free when the sign of the spin couplings are all positive or negative.

Physical Solutions of the Kitaev Honeycomb Model

We investigate the exact solution of the Kitaev honeycomb model and derive an explicit formula for the projector onto the physical subspace. The physical states are simply characterized by the parity of the total occupation of the fermionic eigenmodes. We consider a general lattice on a torus and show that the physical fermion parity depends in a nontrivial way on the vortex configuration and the choice of boundary conditions. In the vortex-free case with a constant gauge field we are able to obtain an analytical expression of the parity. For a general configuration of the gauge field the parity can be easily evaluated numerically, which allows the exact diagonalization of spin models with much larger sizes than the ones accessible to current numerical approaches. We consider physically relevant quantities, as in particular the vortex energies, and show that their true value and associated states can be substantially different from the one calculated in the unprojected space, even in the thermodynamic limit.

9.1 Introduction

In this paper we examine the projection to the physical subspace of the
exact mapping to Majorana fermions proposed by Kitaev. [27] As briefly
discussed in [152, 153, 154], unprojected and projected models have dif-
ferent physical properties, especially the parity of fermions. We derive
here for the first time an explicit and immediately applicable represen-
tation of the projector in terms of the parity of physical fermions. As it
turns out, the physical fermion parity depends in a nontrivial way on the
configuration of vortices and on the lattice topology. Applying the pro-
jection to specific cases, we find large differences between projected and
unprojected physical quantities (e.g. ground state and vortex energies,
or spin-spin correlation functions). Such discrepancies exist both in the
gapped and gapless phase and can also survive the thermodynamic limit.
Our analysis is consequently essential for the exact numerical study via
Kitaev's exact mapping of large spin systems, especially if one wants to
go beyond the small system sizes of about $20 - 100$ spins currently ac-
cessible to various numerical approaches such as direct diagonalization
[143, 145, 146] or density matrix renormalization group (DMRG). [150]

The paper is organized as follows: in Section 9.2 we briefly review
the honeycomb model and the exact mapping to Majorana fermions in-
troduced by Kitaev. [27] In Section 9.3 we compute the parity of physical
fermions with periodic boundary conditions and a generic vortex con-
figuration, which represents our main result. Section 9.4 contains some
applications to specific cases and Section 9.5 our final remarks.

9.2 Model and exact mapping

The Kitaev honeycomb model is a quantum compass model [29] defined
on an hexagonal lattice Λ as follows

$$H = \sum_{\langle i,j \rangle} J_{\alpha_{ij}} \sigma_i^{\alpha_{ij}} \sigma_j^{\alpha_{ij}}, \tag{9.1}$$

where $\boldsymbol{\sigma}_i$ are the Pauli spin operators at site $i \in \Lambda$ ($i = 1, \ldots, 2N$). In
Eq. (14.16), the sum runs over all the pairs of nearest-neighbor sites and
the directions of the Ising interactions are determined by the orientations
of the corresponding links ($\alpha_{ij} = x, y, z$ for x-, y-, z-links respectively, see
Fig. 9.1).

To solve this spin model in an extended Hilbert space $\widetilde{\mathcal{L}}$, one can as-
sociate at each site i four Majorana modes c_i, b_i^x, b_i^y, b_i^z. [27] By defining
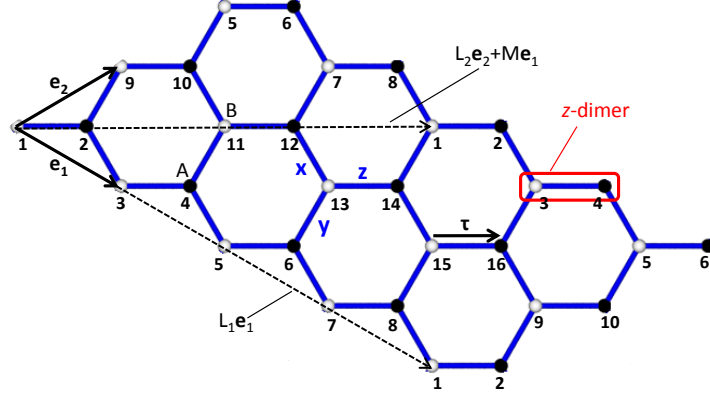
Figure 9.1: Honeycomb lattice, with basis vectors $e_{1,2}$. The directions of x, y, z-links are indicated, as well as the vector τ joining B and A sublattices (white and black dots, respectively). The most general torus on the lattice can be specified by $L_1 e_1$ and $L_2 e_2 + M e_1$ (here $L_1 = 4$, $L_2 = M = 2$). The numbers $1, 2, \ldots 16$ label the sites as described in the main text, see Eq. (9.8).

$\widetilde{\sigma}_i^\alpha = i b_i^\alpha c_i$, the original Hamiltonian in Eq. (14.16) is mapped to

$$\widetilde{H} = i \sum_{\langle i,j \rangle} \widehat{A}_{ij} c_i c_j, \tag{9.2}$$

where for nearest-neighbor sites $\widehat{A}_{ij} = J_{\alpha_{ij}} \widehat{u}_{ij}$ and

$$\widehat{u}_{ij} = i b_i^{\alpha_{ij}} b_j^{\alpha_{ij}} = -\widehat{u}_{ji}. \tag{9.3}$$

These operators satisfy $\widehat{u}_{ij}^2 = 1$. Furthermore, they all commute with each other and also with $\widetilde{H}$. Therefore, the extended Hilbert space splits into $\widetilde{\mathcal{L}} = \oplus_u \widetilde{\mathcal{L}}_u$, where u represents a configuration of $u_{ij} = \pm 1$. Notice that $u_{ij} = -u_{ji}$. So, whenever we specify the values of u_{ij}, we assume conventionally that i is in the A sublattice (see Fig. 9.1). In each subspace $\widetilde{\mathcal{L}}_u$, the operator matrix $\widehat{A}_{ij}$ are replaced by numbers $A_{i,j}^u$ and Eq. (12.4) thus describes non-interacting Majorana fermions.

The eigenmodes can be easily obtained with a canonical transformation Q^u to new Majorana operators

$$(b_1', b_1'', ..., b_N', b_N'') = (c_1, ..., c_{2N}) Q^u, \tag{9.4}$$

which for the specific configuration u brings $\widetilde{H}$ to the form $\widetilde{H}_u = \frac{i}{2} \sum_m \epsilon_m b_m' b_m''$, where ϵ_m are the positive eigenvalues of $2iA^u$. By introducing the fermion

operators $a_m = 1/2(b'_m + ib''_m)$ and $n_m = a^\dagger_m a_m$ we obtain

$$\widetilde{H}_u = \sum_m \epsilon_m \left(n_m - 1/2 \right), \tag{9.5}$$

with ground state energy $E_0 = -1/2 \sum_m \epsilon_m$. The orthoghonal matrix Q^u will have a crucial role in the following to obtain the projection operator.

9.3 Physical fermion parity

The key advantage of Kitaev's solution is to reduce the problem of finding the eigenvalues of a $2^{2N} \times 2^{2N}$ matrix to the diagonalization of the $2N \times 2N$ matrices A^u. However, the final spectrum and eigenstates are in the extended Hilbert space $\widetilde{\mathcal{L}}$, and a projection $\mathcal{P}$ to the physical subspace is necessary. [27] The physical states satisfy $D_i|\Psi\rangle = |\Psi\rangle$ for all the gauge operators $D_i = b^x_i b^y_i b^z_i c_i$ and the explicit form of $\mathcal{P}$ is [27]

$$\mathcal{P} = \prod_{i=1}^{2N} \left(\frac{1 + D_i}{2} \right) = \frac{1}{2^{2N}} \sum_{\{i\}} \prod_{i \in \{i\}} D_i, \tag{9.6}$$

where the summation runs over all possible subsets of indices $\{i\} \subset \Lambda$. Within the physical subspace the $\widetilde{\sigma}^{x,y,z}$ operators satisfy the usual algebra of Pauli matrices and therefore H and $\widetilde{H}$ are equivalent.

To establish a more explicit formula for $\mathcal{P}$ one can note that, in the summation appearing in Eq. (9.6), the two terms corresponding to a subset $\{i\}$ and its complementary set $\Lambda \backslash \{i\}$ simply differ by a factor $\prod_{i=1}^{2N} D_i$. Therefore, $\mathcal{P}$ factorizes as follows [153, 154]

$$\mathcal{P} = \left(\frac{1}{2^{2N-1}} \sum_{\{i\}}' \prod_{i \in \{i\}} D_i \right) \cdot \left(\frac{1 + \prod_{i=1}^{2N} D_i}{2} \right) = \mathcal{S} \cdot \mathcal{P}_0, \tag{9.7}$$

where the prime indicates that the summation in $\mathcal{S}$ (in the first parenthesis) is restricted to half of all possible subset of indices: if $\{i\}$ is included, then $\Lambda \backslash \{i\}$ is not.

We then consider $\prod_{i=1}^{2N} D_i$ in the projector $\mathcal{P}_0$ [the second parenthesis of Eq. (9.7)]. From the definition of D_i, it clearly consists of a product of all the c_i and $b^{x,y,z}_i$ operators. By applying the anticommutation rules we can pair corresponding $b^{x,y,z}_i$ operators, and express them in terms of the conserved quantities u_{ij}. To do this, it is necessary to know the topology of the lattice, from which the correct pairing is determined. We consider

here a model defined on a torus with basis vectors $L_1 e_1$ and $L_2 e_2 + M e_1$, as illustrated in Fig. 9.1 for a special case ($L_1 = 4$, $L_2 = M = 2$). This represents the most general choice of periodic boundary conditions and $N = L_1 L_2$. It is also necessary to fix the correspondence between $i = 1, ..., 2N$ and lattice sites. We fix the labeling as in Fig. 9.1. By taking the origin on site $i = 1$ (on the B sublattice) the position r_i of the sites with odd values of i is given by:

$$r_i = \left(\frac{i-1}{2} \mod L_1 \right) e_1 + \left(\frac{i-1}{2} \backslash L_1 \right) e_2, \qquad (9.8)$$

where $(a \backslash b)$ indicates the integer division and $(a \mod b)$ the reminder. For even i, the position is $r_i = r_{i-1} + \tau$ (see Fig. 9.1). After pairing the $b_i^{x,y,z}$ operators into the u_{ij}, the result is proportional to the parity operator $\hat{\pi}_c = (-i)^N \prod_i c_i$. We then express this quantity in terms of the eigenmodes:

$$\hat{\pi}_c = \det(Q^u) \hat{\pi}, \qquad (9.9)$$

where $\hat{\pi} = \prod_{m=1}^{N}(1 - 2n_m)$ is the parity of the eigenmodes a_m. A proof of Eq. (9.9) is provided in Appendix 9.A. Finally, we find for $\mathcal{P}_0$,

$$2\mathcal{P}_0 = 1 + (-1)^\theta \det(Q^u) \hat{\pi} \prod_{\langle i,j \rangle} u_{ij}, \qquad (9.10)$$

where $\theta = L_1 + L_2 + M(L_1 - M)$ and $\hat{\pi}$ has eigenvalues $+1(-1)$ if the total number of *physical* fermions is even (odd). A complete derivation of Eq. (9.10) is given in Appendix 9.B. It is important to notice that, in applying Eq. (9.10), the labeling of the lattice described above should be used. For example, $\det(Q^u)$ depends on the choice of the labeling.

We would like to point out now the differences between Eq. (9.10) and other discussions in the literature. [152, 153, 154, 155] Firstly, the parity of physical fermions (the only relevant ones) $\hat{\pi}$ is the parity of the eigenmodes a_m and not simply $\hat{\pi}_c$ which is of no calculational use. Eq. (9.9) shows now the precise relation between $\hat{\pi}$ and $\hat{\pi}_c$: for a certain configuration u, the two parities are different if $\det(Q^u) = -1$. We note also that $\hat{\pi}_c$ is not a gauge invariant quantity, while the physical parity $\hat{\pi}$ obviously is, i.e., $[\hat{\pi}, D_i] = 0$. Therefore Eq. (9.9) allows one to form the gauge invariant quantity $\det(Q^u) \prod_{\langle i,j \rangle} u_{ij}$. A second feature revealed by our analysis is that $\hat{\pi}$ (and $\hat{\pi}_c$ as well) depends in a nontrivial way on the boundary conditions through the factor $(-1)^\theta$, which does not appear in Refs. [154, 155].

Being directly applicable to the eigenstates $|\Psi\rangle_u \in \tilde{\mathcal{L}}_u$, identified by their occupation numbers $(2n_m - 1) = \pm 1$, Eq. (9.10) is extremely convenient: it immediately shows whether $\mathcal{P}_0$ gives 0 or 1 on the eigenstate

$|\Psi\rangle_u$. In the former case, the state is clearly unphysical. In the second case, $\mathcal{P}|\Psi\rangle_u = \mathcal{S}|\Psi\rangle_u \neq 0$ since, as seen in Eq. (9.7), the 2^{2N-1} terms of $\mathcal{S}$ all correspond to different configurations of u_{ij}. In conclusion, Eq. (9.10) is sufficient to determine if $|\Psi\rangle_u$ has some overlap with the physical subspace or lies completely outside of it, and makes clear that the crucial quantity is the parity of *physical* fermions $\hat{\pi}$: physical states have either even or odd occupation of the eigenmodes a_m depending on *both* the configuration u and the choice of boundary condition.

9.4 Examples of projected states and energies

We discuss in this Section a few examples illustrating the difference between physical and unphysical results. These examples should make clear that it is not sufficient to calculate the properties of the system in the extended space, but the projection must be carefully applied to take advantage of all the power of Kitaev's exact mapping. While we focus here on the ground state and vortex excitation energy, we expect that similar discrepancies exist for other physical quantities.

By applying Eq. (9.10), the only factor which is not immediately found is $\det(Q^u)$ and we show in the following how it can be explicitly evaluated when $u_{ij} = 1$. The final result, Eq. (9.18), nicely complements Eq. (9.10) for this vortex-free sector.

For an arbitrary configuration of the u_{ij}, the Fourier transformation cannot be used to calculate analytic results. However, $\det(Q^u)$ can be determined numerically with negligible computational effort. This allows us to obtain the exact numerical solution of the spin Hamiltonian at very large values N, otherwise intractable, [143, 146, 150] and to explore the effect of the projection when approaching the thermodynamic limit.

Vortex-free sector

In the vortex-free sector with $u_{ij} = 1$ we can proceed as in Ref. [27] by making use of the Fourier transform on the lattice

$$a_{\boldsymbol{q}B} = \frac{1}{\sqrt{2N}} \sum_{i \text{ odd}} e^{-i\boldsymbol{q}\cdot\boldsymbol{r}_i} c_i,$$

$$a_{\boldsymbol{q}A} = \frac{1}{\sqrt{2N}} \sum_{i \text{ odd}} e^{-i\boldsymbol{q}\cdot\boldsymbol{r}_i} c_{i+1}, \tag{9.11}$$

where the positions $\boldsymbol{r}_i$ of the B lattice sites are given in Eq. (9.8). We now consider a partition of the N possible values of $\boldsymbol{q}$ (fixed by the periodic-
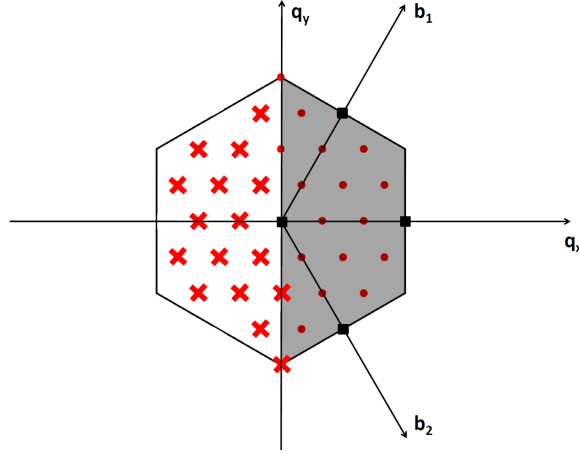
Figure 9.2: An illustration of the partitioning into $\Omega, \Omega_\pm$ described in the main text. The vectors $\boldsymbol{b}_{1,2}$ define the reciprocal lattice and the hexagon is the first Brillouin zone. The four square points are wavevectors in Ω while the dots and crosses are in Ω_+ and Ω_-, respectively. In this example $L_1 = L_2 = 6$ and $M = 0$.

ity of the lattice) in three sets: Ω and $\Omega_\pm$. We say that $\boldsymbol{q} \in \Omega$ if $\pm \boldsymbol{q}$ are the same (up to reciprocal lattice vectors). Ω contains at most 4 wavevectors, depending on $L_{1,2}$ and M, and always contains $\boldsymbol{0}$. The remaining wavevectors can be partitoned in a way that $\pm \boldsymbol{q}$ always belong to two distinct sets $\Omega_\pm$. An example of such partitioning is illustrated in Fig. 9.2 for the special case $L_1 = L_2 = 6$ and $M = 0$. We define new Majorana modes as $\gamma_{\boldsymbol{q}}^\lambda = \sqrt{2} a_{\boldsymbol{q}\lambda}$ for $\boldsymbol{q} \in \Omega$ and

$$\gamma_{\boldsymbol{q},1}^\lambda = a_{\boldsymbol{q}\lambda} + a_{-\boldsymbol{q}\lambda}, \quad \gamma_{\boldsymbol{q},2}^\lambda = i(a_{\boldsymbol{q}\lambda} - a_{-\boldsymbol{q}\lambda}), \tag{9.12}$$

for $\boldsymbol{q} \in \Omega_+$, where $\lambda = A, B$ refers to the sublattice (see Fig. 9.1). This canonical transformation of the c_i can be constructed in two steps. First we rearrange the $(c_1, c_2, \ldots, c_{2N})$ into

$$(c_2, c_4, \ldots, c_{2N}, c_1, c_3, \ldots, c_{2N-1}), \tag{9.13}$$

a transformation which has determinant $(-1)^{N(N+1)/2}$. Notice that, in Eq. (9.13), the modes are partitioned between A (first half) and B (second half). Furthermore, for each sublattice the same order of z-dimers appears, since c_i and c_{i+1} (with odd i) belong to the same z-dimer. Because of this structure, the second transformation [from Eq. (9.13) to the $\gamma_{\boldsymbol{q}}^\lambda, \gamma_{\boldsymbol{q},\alpha}^\lambda$ modes] has two identical blocks labeled by $\lambda = A, B$ and the determinant is simply 1.

The Hamiltonian, rewritten in terms of the new Majorana modes, is diagonal in $\boldsymbol{q}$ and its coefficients are given by $f(\boldsymbol{q}) = 2(J_x e^{i\boldsymbol{q}\cdot\boldsymbol{e}_1} + J_y e^{i\boldsymbol{q}\cdot\boldsymbol{e}_2} + J_z)$ and its complex conjugate. A further diagonalization with respect to the index α of $\gamma_{\boldsymbol{q},\alpha}^\lambda$ is achieved with the rotation of the B operators:

$$\begin{pmatrix} \widetilde{\gamma}_{\boldsymbol{q},1}^B \\ \widetilde{\gamma}_{\boldsymbol{q},2}^B \end{pmatrix} = \begin{pmatrix} \cos(\phi_{\boldsymbol{q}}) & \sin(\phi_{\boldsymbol{q}}) \\ -\sin(\phi_{\boldsymbol{q}}) & \cos(\phi_{\boldsymbol{q}}) \end{pmatrix} \begin{pmatrix} \gamma_{\boldsymbol{q},1}^B \\ \gamma_{\boldsymbol{q},2}^B \end{pmatrix} \tag{9.14}$$

where $\phi_{\boldsymbol{q}}$ is the phase of $f(\boldsymbol{q})$, i.e., $f(\boldsymbol{q}) = |f(\boldsymbol{q})|e^{i\phi_q}$. This transformation has again determinant 1 and brings $\widetilde{H}_u$ to

$$\widetilde{H}_u = \frac{i}{2} \left(\sum_{\boldsymbol{q}\in\Omega_+} |f(\boldsymbol{q})| \sum_{\alpha=1,2} \gamma_{\boldsymbol{q},\alpha}^A \widetilde{\gamma}_{\boldsymbol{q},\alpha}^B + \sum_{\boldsymbol{q}\in\Omega} f(\boldsymbol{q})\gamma_{\boldsymbol{q}}^A \gamma_{\boldsymbol{q}}^B \right). \tag{9.15}$$

Finally, as discussed below Eq. (9.4), Q^u brings the Hamiltonian to the form $\widetilde{H}_u = \frac{i}{2}\sum_{\boldsymbol{q}} \epsilon(\boldsymbol{q})b_{\boldsymbol{q}}' b_{\boldsymbol{q}}''$ with $\epsilon(\boldsymbol{q}) \geq 0$. This can be achieved in Eq. (9.15) by relabeling the Majorana operators. If $\boldsymbol{q} \in \Omega_+$:

$$b_{\boldsymbol{q}}' = \gamma_{\boldsymbol{q},1}^A \quad , \quad b_{\boldsymbol{q}}'' = \widetilde{\gamma}_{\boldsymbol{q},1}^B, \tag{9.16}$$

$$b_{-\boldsymbol{q}}' = \gamma_{\boldsymbol{q},2}^A \quad , \quad b_{-\boldsymbol{q}}'' = \widetilde{\gamma}_{\boldsymbol{q},2}^B. \tag{9.17}$$

If $\boldsymbol{q} \in \Omega$ and $f(\boldsymbol{q}) \geq 0 (< 0)$: $b_{\boldsymbol{q}}' = \gamma_{\boldsymbol{q}}^{A(B)}$, $b_{\boldsymbol{q}}'' = \gamma_{\boldsymbol{q}}^{B(A)}$. The determinant of this last transformation is $(-1)^{\chi+N(N-1)/2}$, where χ is the number of reciprocal lattice vectors $\boldsymbol{q} \in \Omega$ such that $f(\boldsymbol{q}) < 0$. By combining this factor with the one from Eq. (9.13) we obtain:

$$\det(Q^u) = (-1)^{\chi+N^2} \quad \text{for } u_{ij} = 1. \tag{9.18}$$

Notice that χ depends in a non-trivial way on the boundary conditions $L_{1,2}$, M, and the couplings $J_{x,y,z}$. Nevertheless, for a given choice of the model, it can be easily computed.

Following Ref. [27] we examine now the finite size correction $\delta E(N) = E_0(N) - \varepsilon_0 N$ to the ground-state energy $E_0(N)$ with $u_{ij} = 1$, where

$$\varepsilon_0 = \lim_{N\to\infty} E_0(N)/N \tag{9.19}$$

is the energy per unit cell in the thermodynamic limit. We consider in Fig. 9.3 a square lattice ($L_1 = L_2 = L$) with $u_{ij} = 1$ and two different choices of boundary conditions and couplings, and plot $\delta E(N)$ as a function of L ($N = L^2$ in this case). The original result calculated in Ref. [27] is reproduced in the main panel of Fig. 9.3 (dashed lines) and
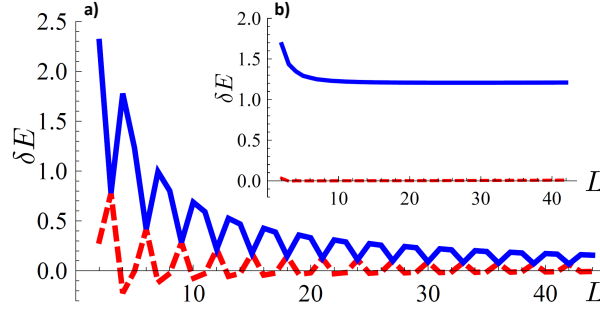
Figure 9.3: Physical (solid line) and unphysical (dashed line) finite size corrections to the thermodynamic energy of a vortex-free configuration $u_{ij} = 1$ for $L_1 = L_2 = L$. The main plot $a)$ refers to the gapless phase with $M = 0$, $J_x = J_y = J_z = 1$, and $\varepsilon_0 \simeq -1.5746$ [27]. The inset $b)$ corresponds to the gapped phase with $M = 1$, $J_x = J_y = 0.2$, $J_z = 1$, and $\varepsilon_0 \simeq -1.0202$.

evidently refers to the unphysical energy, which always underestimates the correct result. The physical and unphysical energies are always distinct, unless $\epsilon_m = 0$ for some fermion mode. Being in the gapless phase, the difference approaches zero at large system size as $1/L$. The inset represents an example in the gapped phase: remarkably, since there is always one fermion in the physical ground state, the difference between projected (solid line) and unprojected (dashed line) results survive the thermodynamic limit where the true energy correction does not vanish. That the state with zero fermions is never physical for any L is immediate from our analytic result Eq. (9.18) since $\chi = 0$ in the gapped phase [$f(\boldsymbol{q}) > 0$]. On the other hand, projected and unprojected *states* are different (have different parity) in the thermodynamic limit in both the gapless and gapped phases. Therefore our projection protocol is necessary to determine the physical quantities of the model in both the gapless and gapped phase even in the thermodynamic limit.

Energy of two adjacent vortices

We consider next the energy to create vortices in the system. These are present on hexagonal cells for which the product of the six u_{ij} is -1. As an interesting example we study configurations with two adjacent vortices, obtained by setting $u_{ij} = -1$ for a single link. The ground state energy of such two-vortex configuration of the u_{ij} is denoted as $E_2(N)$ while, as before, $E_0(N)$ is the ground energy with all $u_{ij} = 1$. We define the
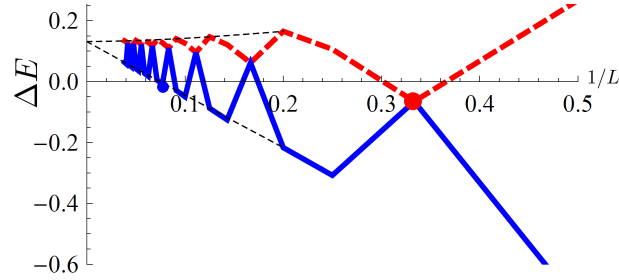
Figure 9.4: Physical (thick solid line) and unphysical (thick dashed line) excitation energy of two adjacent vortices. This plot refers to the gapless phase with $J_x = J_y = J_z = 1$, $L_1 = 2L$, $L_2 = M = L$, and a single $u_{ij} = -1$ with ij being a z-link. Thin dashed lines extrapolate to the thermodynamic limit. The dots at $L = 3$ (unphysical) and $L = 13$ (physical) represent the largest system sizes with negative excitation energy.

excitation energy of a vortex as

$$\Delta E(N) = \frac{1}{2}[E_2(N) - E_0(N)], \tag{9.20}$$

which is plotted in Figs. 9.4 and 9.5 as function of L for different choices of the parameters (given in the captions). In particular, Fig. 9.4 refers to the gapless phase and Fig. 9.5 to the gapped phase. Notice also that it is important in general to specify if $u_{ij} = -1$ refers to an x-, y-, or z-link.

Since the vortex state is not translationally invariant, we obtain the energy spectrum and $\det(Q_u)$ numerically. This can be done efficiently, since it only involves $2N \times 2N$ matrices. In Figs. 9.4 and 9.5 we show physical excitation energies up to $L = 26$ and $L = 35$, respectively (corresponding to $4L^2 = 2704$ and $2L^2 = 2450$ physical spins), obtained with a standard tabletop computer and high level language routines (MATLAB). We have checked that for the lowest possible system size the spectrum obtained with this method is in agreement with direct diagonalization of the physical model. However, direct diagonalization is limited to systems with only a few tens of spins, by making use of very intensive parallel computing numerical routines. [143, 146] Other numerical approaches such as DMRG [150] allow to address larger spin systems ($2N \lesssim 100$) but still much smaller than the ones accessible with the projection protocol presented here.

Similarly to Fig. 9.3, physical and unphysical results are generally different. In Fig. 9.4 (in the gapless phase) they become equal only if there is a zero energy mode or in the thermodynamic limit. On the other hand,
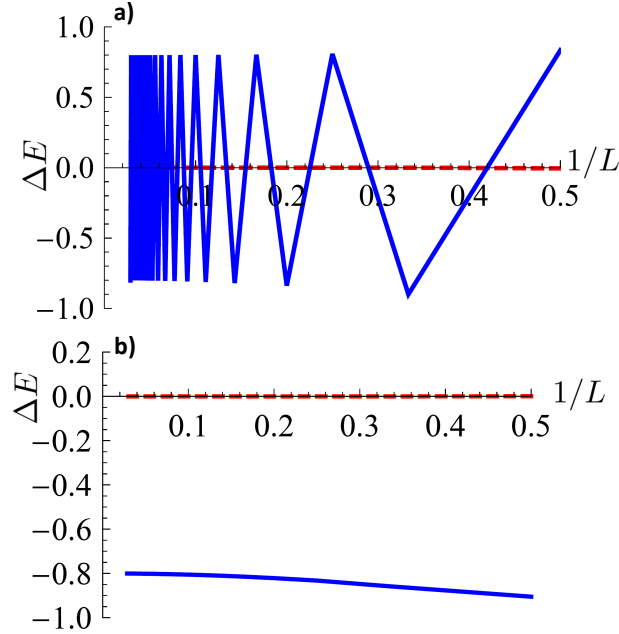
Figure 9.5: Physical (solid line) and unphysical (dashed line) excitation energy of two adjacent vortices in the gapped phase with $J_x = J_y = 0.1$, $J_z = 1$, $L_1 = L_2 = L$, and a single $u_{ij} = -1$ with ij being a y-link. Panel a) refers to $M = 0$ while panel b) to $M = 1$.

finite size corrections are very important: $\Delta E(N)$ shows pronounced oscillations with an amplitude which is of the same order of magnitude of $\Delta E(\infty)$, for up to a few thousand spins. Remarkably, such oscillations result in negative excitation energies of the vortex pair up to 676 spins (instead of 36, in the extended space).

In the gapped phase, the difference between projected and unprojected results can survive the thermodynamic limit. In Fig. 9.5a the oscillations in the physical solution (solid line) persist for $L \to \infty$ and their size is equal to half the gap of the fermions ($\sim J_z$), much larger than the excitation energy of the vortex pair in the unphysical space (dashed line). A different choice of boundary conditions can lead to a situation where ΔE is always large and negative ($\sim -J_z$) and has a well defined thermodynamic limit, as illustrated in Fig. 9.5b.

The thermodynamic limit of the unphysical energies (dashed curves) of Fig. 9.5 is well approximated by a high order perturbative expansion, which allows to derive an accurate effective Hamiltonan including vortex energies and interactions. [27, 114, 111, 151] However such low-energy Hamiltonian does not contain explicitly the constraints on the

allowed vortex configurations, and some care is necessary to establish which states are physical. For example, the vortex-free configuration of Fig. 9.5b does not belong to the low-energy subspace and the two-vortex state has always lower energy. It is worth pointing out here that the negative vortex energies encountered in these examples are not in contradiction with Lieb's theorem as originally formulated in Ref. [159] (see also Ref. [160]).

9.5   Conclusion

We have obtained here an explicit form of the projection operator which allows us to extract the physical properties of the honeycomb model for large lattices. The parity of fermions in the physical sector is directly given through our Eq. (9.10) and depends in a nontrivial way on the vortex configuration and the periodic boundary conditions. By applying Eq. (9.10), we have examined the energies of vortex-free and two-vortex configurations and showed that significant deviation from the physical values can exist if the projection operator is not taken into account. Such differences between projected and unprojected quantities can persist up to large values of N and they can survive the thermodynamic limit in the gapped phase.

Applying the projecion only requires to determine the parity of physical fermions. Therefore, it does not introduce any additional complication related to the symmetrization over all gauge transformations (9.6), a procedure which never needs to be implemented in practice. As known, the energies of projected (i.e. symmetrized) and unprojected (i.e. unsymmetrized) states are the same and the spin correlation functions $S_{ij}^{\alpha\beta}(t) = \langle \sigma_i^\alpha(t) \sigma_j^\beta(0) \rangle$ (whose certain exact properties were discussed in Refs. [142, 156]) can be conveniently computed with unprojected eigenstates $|\Psi\rangle_u$. [142] This is possible thanks to the fact that the spin operators $\widetilde{\sigma}_i^\alpha$ are gauge-invariant. However, one should make sure that only states with $\mathcal{P}|\psi\rangle_u \neq 0$ are included in $S_{ij}^{\alpha\beta}(t)$. Therefore deviations from the unprojected results exist for the $S_{ij}^{\alpha\beta}(t)$ as well.

More generally it is obvious from our discussion that all dynamic and thermodynamic quantities derived from H (for example, the partition function), depend on the physical spectrum and eigenstates and thus differ from those of the unprojected model $\widetilde{H}$. Therefore, we think that it would be interesting to apply our method to problems which have been studied without projection [27, 149, 151, 158] and compare the dif-

ferences. Our work is generally relevant to spin models to which Kitaev's solution applies, like the honeycomb model perturbed by a weak magnetic field, [27, 143, 150] interacting with cavity modes [111] or with different link distributions [151], and a three-dimensional extension of the honeycomb model recently proposed in Ref. [148]. The case of open boundary conditions can also be simply obtained by extending Eq. (14.16) to site-dependent couplings $J_{\alpha_{ij}} \to J_{ij}$ (and $J_{ij} = 0$ on the boundary).

9.6 Acknowledgments.

9.A Derivation of Eq. (9.9)

In this appendix we present a detailed derivation of Eq. (9.9) which gives the relation between the parity $\hat{\pi}_c$ and the parity of the physical fermions $\hat{\pi}$. For the sake of simpler notation we relabel $(b'_1, b''_1, ..., b'_N, b''_N)$ as $(b_1, b_2, ..., b_{2N})$. The relation between the c and b Majorana fermion operators is given by Eq. (9.4):

$$c_i = \sum_j Q_{i,j} b_j, \qquad (9.21)$$

where Q is an orthoghonal matrix. Let us consider the set S_{2N} of the permutations of $1, ..., 2N$. Since the c_i anticommute, we can write the product $c_1 c_2 ... c_{2N}$ as a sum over all permutations $\sigma \in S_{2N}$ as follows:

$$\prod_{i=1}^{2N} c_i = \frac{1}{(2N)!} \sum_\sigma \epsilon(\sigma) \prod_{k=1}^{2N} c_{\sigma(k)}, \qquad (9.22)$$

where $\epsilon(\sigma)$ is the sign of permutation σ. By using Eq. (9.21) we can write $\prod_{k=1}^{2N} c_{\sigma(k)}$ as

$$\sum_{i_1,...,i_{2N}} Q_{\sigma(1),i_{\sigma(1)}}...Q_{\sigma(2N),i_{\sigma(2N)}}\, b_{i_{\sigma(1)}}...b_{i_{\sigma(2N)}}$$

$$= \sum_{i_1,...,i_{2N}} Q_{1,i_1}...Q_{2N,i_{2N}}\, b_{i_{\sigma(1)}}...b_{i_{\sigma(2N)}}, \qquad (9.23)$$

where the numerical factor $\prod_k Q_{k,i_k}$ only depends on the values of i_k, and not on the permutation σ. This allows to express Eq. (9.22) in the following form

$$\frac{1}{(2N)!} \sum_{i_1,..,i_{2N}} \prod_{k=1}^{2N} Q_{k,i_k} \left(\sum_{\sigma} \epsilon(\sigma) b_{i_{\sigma(1)}} ... b_{i_{\sigma(2N)}} \right). \qquad (9.24)$$

It is not difficult to check that the sum over σ gives zero if the values of two of the indexes i_k are equal. When the i_k are all distinct, they are a permutation of $1, ..., 2N$: $i_k = \sigma'(k)$ and $i_{\sigma(k)} = \sigma'(\sigma(k))$. Furthermore, we can anticommute the Majorana operators to the canonical order $b_1 b_2 ... b_{2N}$, which introduces the sign $\epsilon(\sigma)\epsilon(\sigma')$. This leads to

$$\frac{1}{(2N)!} \left(\sum_{\sigma'\sigma} \epsilon(\sigma') \prod_{k=1}^{2N} Q_{k,\sigma'(k)} \right) b_1 b_2 ... b_{2N}. \qquad (9.25)$$

where the $(2N)!$ is canceled by the sum over σ. The remaining factor is simply the determinant of Q, and the following relation is obtained:

$$\prod_{i=1}^{2N} c_i = \det(Q) \prod_{i=1}^{2N} b_i, \qquad (9.26)$$

from which Eq. (9.9) directly follows.

9.B   Derivation of Eq. (9.10)

In this Appendix we present details of the derivation of Eq. (9.10). From Eq. (9.7) we know that

$$2\mathcal{P}_0 = 1 + \prod_{i=1}^{2N} D_i, \qquad (9.27)$$

with gauge operators $D_i = b_i^x b_i^y b_i^z c_i$. The product of all gauge operators can then be rewritten in terms of Majorana operators as

$$\prod_{i=1}^{2N} D_i = b_1^x b_1^y b_1^z c_1 \ ... \ b_{2N}^x b_{2N}^y b_{2N}^z c_{2N}. \qquad (9.28)$$

where $N = L_1 L_2$. In order to pair the b operators and form the corresponding u operators, we first move all the c operators to the right of

the b operators. The fermionic anticommutation relations then lead to a phase factor of $(-1)^{\phi_1}$ with $\phi_1 = 3N(2N-1)$:

$$\prod_{i=1}^{2N} D_i = (-1)^{\phi_1} b_1^x b_1^y b_1^z \ldots b_{2N}^x b_{2N}^y b_{2N}^z \prod_{l=1}^{2N} c_l. \tag{9.29}$$

Since b_i^x and b_{i+1}^x are always separated by two fermionic operators, we can move all the b^x to the left without introducing any phase factor. We then group together all the b^y operators to the right of the b^x, at the cost of an additional phase $(-1)^{\phi_2}$ where $\phi_2 = N(2N-1)$ [notice that $(-1)^{\phi_1+\phi_2} = 1$]:

$$\prod_{i=1}^{2N} D_i = \prod_{i=1}^{2N} b_i^x \prod_{j=1}^{2N} b_j^y \prod_{k=1}^{2N} b_k^z \prod_{l=1}^{2N} c_l, \tag{9.30}$$

For the sake of clarity we explicitly write in this Appendix each u operator as u^α where α refers to the link associated to u: $\hat{u}_{ij} = \hat{u}_{ij}^{\alpha_{ij}} = ib_i^{\alpha_{ij}} b_j^{\alpha_{ij}}$. In order to pair the b^α ($\alpha = x, y, z$) operators into u^α, it is necessary to fix the correspondence between $i = 1, ..., 2N$ and the sites of the lattice. We choose here the labeling defined by Eq. (9.8) and illustrated in Fig. 9.1 for a particular case ($L_1 = 4$ and $L_2 = M = 2$). It is then straightforward to see that

$$\prod_{k=1}^{2N} b_k^z = \frac{(-1)^{\phi_3}}{i^N} \prod_{\langle m,n \rangle} u_{mn}^z \tag{9.31}$$

where the factor $1/i^N$ is from the definition of $u_{ij}^\alpha = ib_i^\alpha b_j^\alpha$ and $\phi_3 = N$ arises from the convention of specifying u_{ij} with $i \in A$. Therefore, the u_{mn}^z above have always the form $u_{i+1\,i}^z$.

It is also not difficult to rearrange the b^x operators:

$$\prod_{i=1}^{2N} b_i^x = \frac{(-1)^{\phi_4}}{i^N} \prod_{\langle m,n \rangle} u_{mn}^x \tag{9.32}$$

where $\phi_4 = L_2$. Note that the phase ϕ_4 arises because of the boundary conditions along e_1. To form the $u_{1\,2L_1}^x$ operator (u_{18}^x in Fig. 9.1) one has to move b_1^x after $b_{2L_1}^x$, which introduces a (-1) factor. This procedure has to be repeated L_2 times, for all pairs of the form $b_{2nL_1}^x b_{2L_1(n-1)+1}^x$ with $n = 1, 2, \ldots, L_2$ (in Fig. 9.1, these are $b_8^x b_1^x$ and $b_{16}^x b_9^x$). Hence, the factor $(-1)^{L_2}$ arises.

Finally, in order to identify $\prod_{j=1}^{2N} b_j^y$ as a product of u^y, we first decompose it in L_2 products of $2L_1$ terms:

$$\prod_{j=1}^{2N} b_j^y = \prod_{n=1}^{L_2} \mathcal{T}_n, \tag{9.33}$$

where $\mathcal{T}_n = \prod_{j=1}^{2L_1} b_{2L_1(n-1)+j}^y$ (e.g., $\mathcal{T}_1 = b_1^y b_2^y \ldots b_8^y$ for Fig. 9.1). As a first step, we rewrite each $\mathcal{T}_n$ by moving all the b_i^y with odd i on the left side (and keeping them in increasing order of i) while rearranging the b_i^y with even i (now on the right side of each $\mathcal{T}_n$) in decreasing order. These operations do not introduce any additional phase factor in the final expressions. For example, in the case of Fig. 9.1 we can write $\mathcal{T}_1 = b_1^y b_3^y b_5^y b_7^y b_8^y b_6^y b_4^y b_2^y$. The advantage of this ordering is that most pairs of b^y operators are now straightforward to form. For example, the pairs $b_2^y b_9^y$, $b_4^y b_{11}^y$, ... of Fig. 9.1 are now easily formed from the rearranged string (9.33), of the form $\ldots b_6^y b_4^y b_2^y b_9^y b_{11}^y b_{13}^y \ldots$. The only difficulty is a remaining product of b_i^y

$$(b_1^y b_3^y \ldots b_{2L_1-1}^y)(b_{2N}^y b_{2N-2}^y \ldots b_{2N-2(L_1-1)}^y), \tag{9.34}$$

which requires some care in pairing to account of the toric boundary conditions. The rearrangement of Eq. (9.34) introduces the phase factor $(-1)^{\phi_5}$ in the final expression:

$$\prod_{j=1}^{2N} b_j^y = \frac{(-1)^{\phi_5}}{i^N} \prod_{\langle m,n \rangle} \hat{u}_{mn}^y, \tag{9.35}$$

where $\phi_5 = M(L_1 - M) + L_1$.

Collecting all the terms, we finally obtain

$$\prod_{i=1}^{2N} D_i = \frac{(-1)^{\phi_3+\phi_4+\phi_5}}{i^{3N}} \prod_{\langle i,j \rangle} \hat{u}_{ij} \prod_{l=1}^{2N} c_l. \tag{9.36}$$

With the aid of Eq. (9.9) we then find

$$2\mathcal{P}_0 = 1 + (-1)^{L_1+L_2+M(L_1-M)} \det(Q^u)\hat{\pi} \prod_{\langle i,j \rangle} \hat{u}_{ij}, \tag{9.37}$$

which is Eq. (9.10) of the main text.

Majornana States in Inhomogeneous Spin Ladders

We propose an inhomogeneous open spin ladder, related to the Kitaev honeycomb model, which can be tuned between topological and non-topological phases. In extension of Lieb's theorem, we show numerically that the ground state of the spin ladder is either vortex free or vortex full. We study the robustness of Majorana end states (MES) which emerge at the boundary between sections in different topological phases and show that while the MES in the homogeneous ladder are destroyed by single-body perturbations, in the presence of inhomogeneity at least two-body perturbations are required for destabilizing MES. Furthermore, we prove that x, y, or z inhomogeneous magnetic fields are not able to destroy the topological degeneracy. Finally, we present a trijunction setup where MES can be braided. A network of such spin ladders provides thus a promising platform for realization and manipulation of Majorana end states.

10.1   Introduction.

The study of Majorana fermions in various solid-state systems has recently attracted a lot of attention. [24, 27, 161, 162, 163, 164, 165, 166, 167, 168, 169, 170, 171, 26, 36, 172, 173, 174] In particular, the possibility of realizing them as zero-energy states localized at the end of one-dimensional systems [so-called Majorana end states (MES)] has been the subject of many recent investigations. [167, 168, 169, 26, 171, 170, 36, 173, 172, 174, 165, 166] Besides being of fundamental interest, the study of MES is motivated by their potential use for topological quantum computing.

While electronic systems are a natural choice for the realization of such MES, well known fermionization techniques have stimulated the study of ME appearing in the Fermionic mapping of one-dimensional spin systems. [36, 170, 171] Since many proposals exist for implementing designer spin-spin interactions, [126] and, in particular, for the experimental realization of Kitaev-like spin models, [30, 32, 33] such one-dimensional systems are interesting candidates for the realization and detection of MES.

Proposals of highly engineered spin interactions also suggest the implementations of inhomogenous systems where regions in different topological phases coexist, which is the main feature of the spin ladder studied in this work. The spin ladder is based on nearest-neighbor Ising interactions, in extension of the Kitaev honeycomb model,[27] and consists in sections which alternate between the topological and non-topological phases. The phase of each section is simply determined by the strength of the Ising couplings and at the boundary between different phases (as well as at the open ends of the ladder) single well-localized MES exist. Being interested in the ground-space properties of the model, we perform an extensive numerical analysis of possible vortex configurations. We always find that the ground state is either vortex-free or vortex-full and thereby give strong evidence that that the Lieb theorem, [159] originally formulated for different boundary conditions, also applies to such open spin ladders. While freely moving vortices would introduce additional degeneracies, the presence of a finite gap for the vortex excitations makes it possible to characterize the ground space in terms of spatially localized Majorana states, and to consider braiding of such MES. We discuss a trijunction setup similar to the one proposed in Ref. [26], which could allow the implementation of topologically protected quantum gates.

In contrast to previous studies, [36, 170, 171] we do not analyze our model by making use of the Jordan-Wigner transformation, but consider the alternative mapping proposed by Kitaev. [27] This method has the in-

teresting feature of mapping local spin operators to local Fermionic operators and has some advantage in analyzing the stability of the MES. In particular, it makes immediately clear that MES in the homogeneous ladder are already fragile against single-body perturbations. This conclusion is consistent with general arguments showing that topological protection in one-dimensional systems can only be effective against local perturbations conserving certain symmetries. [175, 176, 177] In p-wave wires for example, MES are protected against local perturbations which conserve parity. Such symmetry assumption is realistic for superconducting wires (although other limitations exist due to quasiparticle poisoning [178]) but an analogous constraint does not appear for general spin systems. For this reason we study in great detail the robustness of MES and characterize the form of local perturbations which can split the corresponding degeneracy. In the Fermionic language adopted here, the fragility of the topological degeneracy results from the only apparent locality of the Kitaev mapping. Non-local strings of Fermionic operators coupling the MES appear through the projector onto the physical subspace. [27, 179] Nevertheless, we show that the inhomogenous ladder has better properties than the homogenous ladder [36] since single-body perturbations are not sufficient to split the degeneracy but at least two-body interactions are necessary. Furthermore, we show that the topological degeneracy of our model is robust against inhomogeneous magnetic fields along x, y, or z.

The paper is organized as follows, in Section 10.2 we introduce the inhomogeneous ladder and the spin-to-fermion mapping we use to study MES properties. In Section 10.3, we derive the topological invariant of the spin ladder for both the vortex-free and vortex-full sectors. We show that well-localized MES appear at the junction between topological and non-topological sections and demonstrate how to move MES along the ladder. In Section 10.4 we investigate numerically the validity of the Lieb theorem [159] and show that it also applies to this type of open spin ladders, since the ground state is either vortex-free (when one of the coupling is negative) or vortex-full (when all couplings are positive). In Section 10.5, we perform an analysis of the robustness of MES under local perturbations. We demonstrate that single-body perturbations split the topological degeneracy of the homogeneous ladder while two-body terms are required in the inhomogeneous case. Furthermore, we prove that x, y, or z inhomogeneous magnetic fields alone are not able to split the topological degeneracy of the ladder. In Section 10.6 we present a trijunction setup which could allow braiding of MES following the scheme of Ref. [26] and Section 10.7 contains our final remarks. We present ad-

ditional details and interesting aspects of the model in Appendices 10.A-10.E.

10.2 Inhomogeneous spin ladder and Kitaev's mapping.
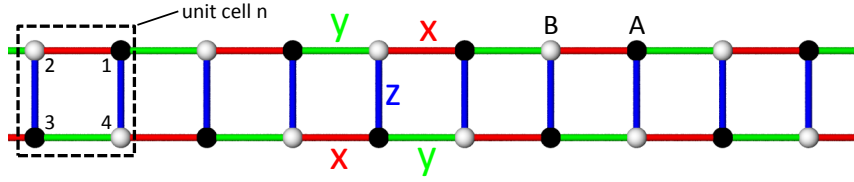
Figure 10.1: Inhomogeneous spin ladder. Each site contains a quantum spin-1/2 which interacts with its nearest neighbor spins via bond-dependent Ising interactions J_x, J_y, J_z. The x, y, and z bonds are indicated by red, green, and blue lines *r*esp., the A (B) sublattice site by black (white) dots, and the n*t*h unit cell composed of four spins by the black dashed square. In contrast to the standard honeycomb model, the z couplings are inhomogeneous, *i.*e., site-dependent $J_z \to J_{z_{ij}}$.

The spin model we propose is an inhomogeneous ladder version of the compass [29] or Kitaev honeycomb [27] model with Hamiltonian

$$H = \sum_{\langle i,j \rangle} J_{\alpha_{ij}} \sigma_i^{\alpha_{ij}} \sigma_j^{\alpha_{ij}}, \tag{10.1}$$

where $\boldsymbol{\sigma}_i = (\sigma_i^x, \sigma_i^y, \sigma_i^z)$ are the Pauli operators for the spin-1/2 located at the site i of the ladder, and where the sum runs over all pairs of nearest-neighbor sites of the open ladder containing N unit cells. We assume that the ladder is of length $2N - 1$ (lattice constant set to one) , *i.*e. consists of an odd number $2N - 1$ of square plaquettes, see Fig. 10.1. The anisotropy direction in spin space of the Ising interaction $J_{\alpha_{ij}}$ depends on the orbital location of the bond which is labeled by the index $\alpha_{ij} = x, y, z$ for x-, y-, and z-bonds, *r*esp., see Fig. 10.1. Furthermore, we allow the z-couplings to depend on position, *i.*e., $J_z \to J_{z_{ij}}$. Without loss of generality we will assume that $J_{z_{ij}} > 0$. Following Ref. [27], this model can be solved exactly in an extended Hilbert space $\widetilde{\mathcal{L}}$ by assigning four Majorana fermion operators $b_i^{x,y,z}$ and c_i (all self-adjoint) to each site of the lattice and mapping each spin operator to a product of two Majoranas

$$\widetilde{\sigma}_i^\alpha = i b_i^\alpha c_i. \tag{10.2}$$

In fermionic representation, the spin Hamiltonian in Eq. (14.16) takes the form $\widetilde{H} = i \sum_{\langle i,j \rangle} \widehat{A}_{ij} c_i c_j$, where $\widehat{A}_{ij} = J_{\alpha_{ij}} \hat{u}_{ij}$ and $\hat{u}_{ij} = i b_i^{\alpha_{ij}} b_j^{\alpha_{ij}}$. The u operators commute with each other and with $\tilde{H}$, and satisfy $\hat{u}_{ij}^2 = 1$. Therefore, the extended Hilbert space splits into subspaces $\widetilde{\mathcal{L}}_u$, i.e., $\widetilde{\mathcal{L}} = \oplus \widetilde{\mathcal{L}}_u$, where u represents a certain configuration of eigenvalues $u_{ij} = \pm 1$. To remove the ambiguity due to $\hat{u}_{ij} = -\hat{u}_{ji}$, we assume that for a chosen value u_{ij} the first index i belongs to sublattice A (see Fig. 10.1). The physical subspace is defibded through the gauge operators $D_i = b_i^x b_i^y b_i^z c_i$ as $\mathcal{L} = \{|\Psi\rangle \; : \; D_i |\Psi\rangle = |\Psi\rangle\}$. Starting from a state $|\Psi\rangle$ in the extended space, the corresponding physical state $|\Psi\rangle_{\text{phys}}$ is given by symmetrization over all gauge operators D_i, i.e., [27]

$$|\Psi\rangle_{\text{phys}} = \prod_{i=1}^{4N} \left(\frac{1 + D_i}{2} \right) |\Psi\rangle. \tag{10.3}$$

In each subspace $\widetilde{\mathcal{L}}^u$, the operators $\widehat{A}_{ij}$ are replaced by numbers A_{ij}^u and thus the quadratic Hamiltonian $\widetilde{H}$ is easily solvable with a canonical transformation Q^u to new Majorana modes [27]

$$(b_1, b_2, ..., b_{4N-1}, b_{4N}) = (c_1, ..., c_{4N}) Q^u. \tag{10.4}$$

Under this transformation, $\widetilde{H}$ takes, for a given configuration u, the form $\widetilde{H}_u = \frac{i}{2} \sum_{m=1}^N \epsilon_m b_{2m-1} b_{2m}$, where $\epsilon_m > 0$ are the positive eigenvalues of $2iA^u$. By defining new complex fermion operators $a_m = (b_{2m-1} + ib_{2m})/2$, we finally obtain $\widetilde{H}_u = \sum_m \epsilon_m (a_m^\dagger a_m - 1/2)$.

The spin ladder Eq. (14.16) possesses as conserved quantities two types of plaquettes that are naturally associated with each unit cell n, i.e., $W_n = -\sigma_{n,1}^y \sigma_{n,2}^y \sigma_{n,3}^x \sigma_{n,4}^x$ and $\overline{W}_n = -\sigma_{n,1}^x \sigma_{n+1,2}^x \sigma_{n+1,3}^y \sigma_{n,4}^y$, where each spin $\sigma_{n,\alpha}$ is labeled by the index n for the unit cell and $\alpha = 1, ..., 4$ for one of the four spins inside the unit cell (see Fig. 10.1). We say that a square plaquette p carries a vortex if $W_n = -1$ for $p = 2n - 1$ and if $\overline{W}_n = -1$ for $p = 2n$. In fermionic representation, the plaquettes are products of u operators around each unit cell. In the following, we study the robustness of MES against local perturbations and show that not all the degeneracies due to MES can be splitted by single-body perturbations. Additionally, we show that the topological degeneracy cannot be fully splitted by inhomogeneous x, y, or z magnetic fields. We note that in the special case with $J_{z_{ij}} = J_z$ our model is equivalent to the usual honeycomb model studied in Refs. [36] and [34]. As we show below, the Majorana degeneracy present in the homogeneous ladder is less protected in the sense

that it is fully splitted by single-body local perturbations. Similar homogeneous Kitaev ladders have been studied in Refs. [34] and [35].

10.3   Topological phases of spin ladders.
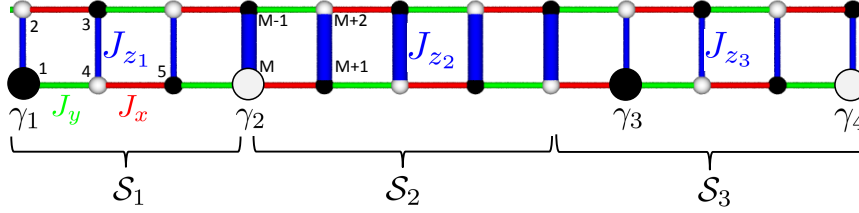
Figure 10.2: Inhomogeneous spin ladder with different topological sections. Shown are two topological sections $\mathcal{S}_1$ and $\mathcal{S}_3$ (thin z-bonds J_{z_1} and J_{z_3}) separated by a non-topological section $\mathcal{S}_2$ (thick z-bonds J_{z_2}). For the corresponding $J_{x,y,z}$-values see main text. The wave functions of the four MES $\gamma_{1,...,4}$ are mainly localized at the phase-boundaries and, for $J_x > J_y$, on the lower sites of the ladder as indicated by the large dots.

We consider now a spin ladder with sections in different topological phases, $\mathcal{S}_1$, $\mathcal{S}_2$, and $\mathcal{S}_3$, which are distinguished by the value of the $J_{z_{ij}}$ couplings (see Fig. 10.2). If we focus on the vortex-free/vortex-full sector, then we choose the $J_{z_{ij}}$ couplings as follows: for the $\mathcal{S}_1$ and $\mathcal{S}_3$ parts, $J_{z_{ij}} = J_{z_1} = J_{z_3}$ and $|J_{z_1}| < |J_x \pm J_y|$, while for the $\mathcal{S}_2$ part we have $J_{z_{ij}} = J_{z_2}$ and $|J_{z_2}| > |J_x \pm J_y|$ (see Fig. 10.2). Below we derive the conditions for the existence of zero-energy MES in the vortex-free (vortex-full) sector with the use of the mapping (10.2) and prove that sections $\mathcal{S}_1$ and $\mathcal{S}_3$ are topological, while section $\mathcal{S}_2$ is non-topological.

The vortex-free sector corresponds to all $u_{ij} = +1$. In contrast, the configuration where all the u's along only one of the axis (say x-axis) takes on the value -1 is vortex-full. From the explicit expression of A^u_{ij} we obtain the bulk spectrum in the vortex-free sector for $J_{z_{ij}} = J_z$,

$$\epsilon_{\substack{1+m \\ 2+m}}(k) = \pm 2\sqrt{J^2 + 2J_x J_y \cos(k) - (1-m)\gamma_k},$$ (10.5)

where $J^2 = J_x^2 + J_y^2 + J_z^2$, $\gamma_k = \sqrt{(2+2\cos(k))(J_x + J_y)^2 J_z^2}$, k is the wavevector, and $m = 0, 2$.

In the vortex-free sector, the MES eigenvectors ϕ with eigenvalues $\epsilon = 0$ can be shown to satisfy the following transfer equations $(\phi_{n+1,\alpha+\xi}, \phi_{n,\alpha+\xi})^T = \mathcal{T}_\alpha(\phi_{n,\alpha+\xi}, \phi_{n-1,\alpha+\xi})^T$ (the two labels of $\phi_{n,\alpha}$ correspond to the unit cell n

and one site α of the unit cell), with $\xi = 0, 2$, and $\mathcal{T}_{1,2} = \begin{pmatrix} \frac{J_z^2}{J_{x,y}^2} - \frac{2J_{y,x}}{J_{x,y}} & -\frac{J_{y,x}^2}{J_{x,y}^2} \\ 1 & 0 \end{pmatrix}$.

MES can only exist when both eigenvalues of $\mathcal{T}_\alpha$ have absolute value larger or smaller than one. Therefore, we define the topological invariants $\nu_\alpha = -\text{sgn}((1 - |\tau_1^\alpha|)(1 - |\tau_2^\alpha|))$, where $\tau_{1,2}^\alpha$ are the two eigenvalues of $\mathcal{T}_\alpha$. The system is in the *non*-topological phase when $\nu = +1$, and in the *t*opological phase with MES when $\nu = -1$. From the above explicit expression for $\mathcal{T}_{1,2}$, we obtain the following result for the topological invariants in agreement with Refs. [36] and [34]

$$\nu_1 = \nu_2 = \text{sgn}(2|J_z| - 2|J_x + J_y|). \tag{10.6}$$

In the vortex-full sector, the topological invariant is given by Eq. (10.6) with $J_x + J_y$ replaced by $J_x - J_y$. From Eq. (10.6) it follows that sections $\mathcal{S}_1$ and $\mathcal{S}_3$ of our model are topological, while section $\mathcal{S}_2$ lies in the non-topological phase. This system thus contains four c Majoranas: $\gamma_{1,4}$ localized at each end of the ladder and $\gamma_{2,3}$ at each junction between topological and non-topological sections of the ladder, see Fig. 10.2. Note that for $J_x > J_y$ ($J_y < J_x$), γ_1 and γ_3 will reside on the A (B) sublattice while γ_2 and γ_4 on the B (A) sublattice. For the rest of this work we will always consider the case where $|J_x| > |J_y|$ and $J_z > 0$, since the case $|J_x| < |J_y|$ can be treated analogously. It is worth pointing out that $\mathcal{T}_1 = \mathcal{T}_2$ when $|J_x| = |J_y|$, and consequently all the $|\phi_{n,\alpha=1,...,4}|$ will decrease (increase) with n if both eigenvalues of $\mathcal{T}_{1,2}$ have their absolute values smaller (larger) than one. This excludes the presence of MES localized at the right (left) end of the ladder. Consequently, Eq. (10.6) is strictly valid only for $|J_x| \neq |J_y|$.

The four MES operators $\gamma_{1,...,4}$ can be easily expressed in terms of Majorana operators c_i through relation (10.4): $\gamma_{1,...,4} = \sum_j Q_{i_{1,...,4},j}^u c_j$, where the coefficients $Q_{i_{1(2)},j}^u$ and $Q_{i_{3(4)},j}$ are the elements of the imaginary (real) part of the $\epsilon = 0$ eigenvectors of matrix iA^u. Figure 10.3 shows a plot of the wavefunctions of four Majoranas $\gamma_{1,...,4}$ for a ladder with $N = 60$ with all $u_{ij} = +1$, and $J_x = 1.0$, $J_y = -0.4$, $J_{z_1} = J_{z_3} = 0.2$ for the $\mathcal{S}_1$ and $\mathcal{S}_3$ sections, and $J_{z_2} = 3$ for the middle section $\mathcal{S}_2$. We can see that the MES γ_1 and γ_4 are respectively localized at the left and right ends of the ladder, while MES γ_2 and γ_3 are localized at the junctions between topological and non-topological sections of the ladder (the precise shape of MES can be understood more intuitively by mapping the spin ladder to two coupled p-wave superconducting wires, see Appendix 10.A). The four zero-energy eigenvalues of iA_{ij}^u (corresponding to $\gamma_{1,...,4}$) reside inside a gap of about 1.7 for this choice of parameters . From Eq. (10.6) one concludes
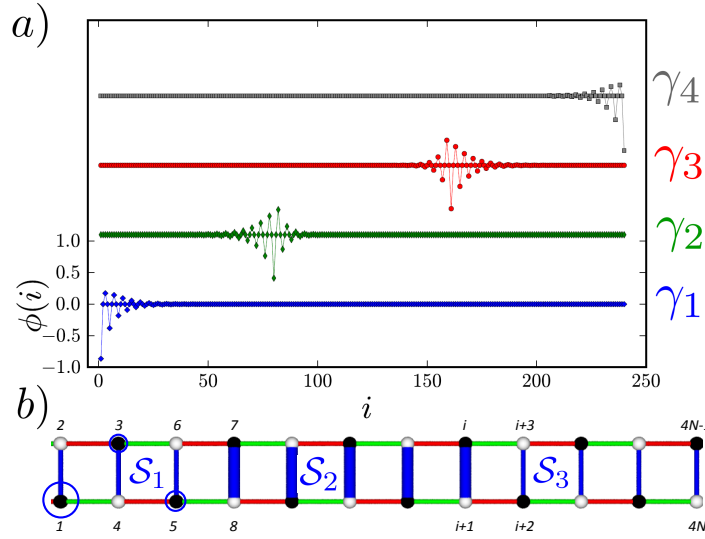
Figure 10.3: Inhomogeneous spin ladder as defined in Fig. (10.2). a) MES wavefunctions $\phi(i)$ (corresponding to $\gamma_{1,...,4}$) as function of site i. The curves for $\gamma_{2,3,4}$ are shifted vertically for clarity. The order used for the site-labeling of the spin ladder is shown in b). The circles represent the wavefunction weight of γ_1 (proportional to the area enclosed by the circle) at the corresponding site. For both plots we have all $u_{ij} = +1$ (vortex-free), $N = 60$, $J_x = 1.0$, $J_y = -0.4$, $J_{z_1} = J_{z_3} = 0.2$ in $\mathcal{S}_{1,3}$ and $J_{z_2} = 3$ in $\mathcal{S}_2$. Section $\mathcal{S}_2$ starts at unit cell $n = 41$ and ends at $n = 79$.

that it is possible to move from the topological to the non-topological phase by changing the relative strengths of $J_{x,y,z}$. Since MES will exist at the junction between sections in different topological phases, MES can be created, destroyed, and transported by locally (and adiabatically) changing the relative strengths of $J_{x,y,z}$ along the spin ladder. Finally, it is well-known that, in principle, exchange interactions can be controlled electrically (for atomistic or nano-structures see e.g. Refs. [180, 181]). Thus, applying gates over portions of the spin-ladder will allow one to move the MES along the ladder. This is similar to what is done in superconducting wires with local tuning of the chemical potential, see Ref. [26].

For the sake of completeness, we study in Appendix 10.E long-range static correlations which exist in the topological phase only. In the standard honeycomb model spin spin correlations vanish rapidly with distance. [142, 156]

10.4 Vortex-free (full) ground state.

In this section we give numerical evidence that the ground state is either vortex-free or vortex-full for a certain range of $J_{x,y,z}$ parameters. It is tempting to invoke Lieb's theorem [159] (see also Ref. [160]). However, this theorem is not directly applicable to our system since it requires periodic boundary conditions in the horizontal direction or $|J_x| = |J_y|$ with open boundaries (when the reflection plane is taken to be horizontal and going through the middle of the ladder). However, different numerical checks lead us to conclude that the ground state of our spin model is vortex-free/vortex-full for $\text{sgn}(J_x) = (-/+)\text{sgn}(J_y)$ and general $J_{z_{ij}} > 0$. Figure 10.4 is a plot of the single-vortex energy for different N and couplings $J_x = 1.0$, $J_y = -0.4$, $J_{z_{ij}} = J_{z_1} = J_{z_3} = 0.2$ in sections $\mathcal{S}_1$ and $\mathcal{S}_3$, while $J_{z_{ij}} = J_{z_2} = 4$ in section $\mathcal{S}_2$. The vortex energy converges quickly with N and is positive. We also see that a vortex lying in the non-topological section $\mathcal{S}_2$ has a larger energy since J_z is stronger there. Figure 10.4 reveals that the energy becomes independent of the vortex position in the bulk of the ladder when N is large. However, the ground-state is vortex-free or vortex-full and such additional degeneracies are not present. All groundstate degeneracies can thus be associated to MES.

We have numerically investigated the energy of multi-vortex configurations and found that, although the vortex-vortex interaction is attractive, the attraction is not strong enough to favor the creation of additional vortices and the ground state remains a vortex-free state, see Appendix 10.B for more details. Additional numerical checks with different $J_{x,y,z}$ configurations are also reported there. For all the numerical checks we performed, the conclusion remains the same: the ground state is vortex-free. Since changing the sign of $J_{x,y}$ is equivalent to $u_{ij}^{x,y} = -1$ for the corresponding bond, the system with $\text{sgn}(J_x) = \text{sgn}(J_y)$ has thus a vortex-full ground state, as expected. Although an analytical proof, to the best of our knowledge, is lacking, we conjecture that Lieb's theorem can be formally extended to the spin ladder considered in this work.

10.5 Robustness of the topological degeneracy

As mentioned in the introduction, topological order does not exist in one-dimensional systems. [175, 176, 177] Especially, if no symmetry constraints are present, it is always possible to find local perturbations which split the Majorana degeneracy.

In line with this general result, we are thus interested in determining
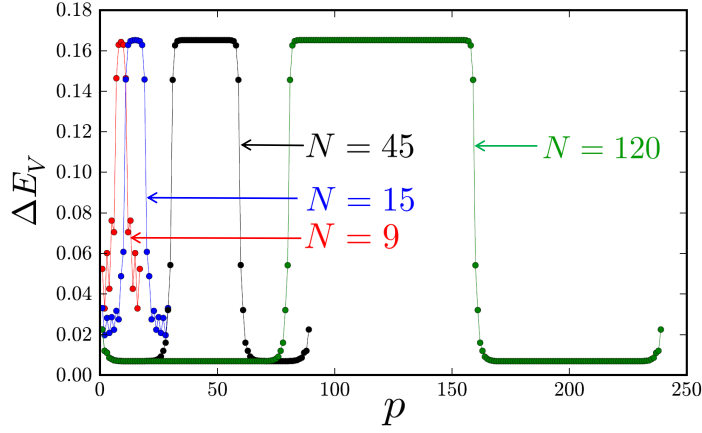
Figure 10.4: Excitation energy ΔE_V of a single vortex as function of its position p (square plaquette) on the ladder for different N. The values of $J_{x,y}$ and $J_{z_{ij}}$ are given in the main text. The junction between sections $\mathcal{S}_1$ and $\mathcal{S}_2$ is at $p = 2N/3$ and between $\mathcal{S}_2$ and $\mathcal{S}_3$ at $p = 4N/3$. Note the slight increase of ΔE_V (as compared to the bulk) for $N = 45$ and 120 when the vortex is located at the end of the ladder.

what type of local spin perturbations can split the topological degeneracy and against which type of perturbations the MES of the inhomogeneous ladder are robust. Indeed, as we shall see, only certain form of local perturbations can split the topological degeneracy. A symmetry-based analysis of perturbations that can split the topological degeneracy in different spin ladders have recently been performed in Ref. [182].

Here we demonstrate that single-body terms cannot fully split the topological degeneracy present in the inhomogeneous ladder and that at least two-body perturbations are required. Furthermore, we also demonstrate that a twofold degeneracy always remain when x, y, or z inhomogeneous magnetic fields are applied. The presence of inhomogeneity in the ladder is important, since much simpler perturbations destroy the topological degeneracy of the homogeneous ladder as we show below.

Homogeneous ladder

Here we first focus on the homogeneous ladder, while we study the inhomogeneous ladder in the next section. In order to study the robustness of MES, we recall that the spin system carries four additional b Majoranas arising from the b operators at the ends of the ladder (b_1^x, b_2^y, b_{4N-1}^y, and b_{4N}^x) which are completely decoupled from the Hamiltonian $\widetilde{H}_u$. These

b Majoranas are always present in the model (in the extended space) independent of the strength of the couplings $J_{x,y,z}$. Such a model carries six Majoranas in the topological phase, namely two spatially separated c Majoranas and two b Majoranas at each end. From Eq. (10.2) it is thus clear that a local single-body perturbation $V = h_1 \sigma_1^x + h_{4N} \sigma_{4N}^x$ will combine two of the three Majoranas at each end of the ladder leaving only one Majorana at the right and one Majorana at the left end of the ladder (and thus one zero-energy fermion state). It has recently been shown [179] that, given a certain vortex configuration and lattice topology, only half of the states in the extended space are physical and these physical states have a definite fermionic parity. If the physical states have even parity, then the remaining zero-energy fermion state is unfilled, while it is filled for physical states with odd parity. In any case this means that one of the states of the remaining zero-energy fermion is unphysical. We thus conclude that the topological degeneracy of the homogeneous ladder has been lifted by x single-body terms only.

Inhomogeneous ladder

Let us now consider the inhomogeneous ladder. The ladder possesses eight MES, namely four spatially separated γ_i (see Fig. 10.2) and two b Majorana operators at each end. An indentical argument as the one presented for the homogeneous ladder is thus applicable here and single-body local perturbations $V = h_1 \sigma_1^x + h_{4N} \sigma_{4N}^x$ will mix one b with one c Majorana at each end of the ladder. Since four Majoranas are left in the extended space, we still have a twofold degeneracy in the physical space. The corresponding states in a given u configuration are denoted by $|\Psi_1^u\rangle$ and $|\Psi_2^u\rangle$. The four Majoranas are well-separated from each other, hence, it seems impossible to remove this remaining degeneracy with local perturbations V, indeed $\langle \Psi_1^u | V | \Psi_2^u \rangle = 0$. However, one has to be careful with the fact that the physical states are given by symmetrization over all gauge operators, see Eq. (10.3). The physical vortex-free degenerate groundstates $|\Psi_{1,2}^{\mathrm{VF}}\rangle$ are thus given by

$$|\Psi_{1,2}^{\mathrm{VF}}\rangle = \underbrace{\prod_i \left(\frac{1 + D_i}{2} \right)}_{\mathcal{P}} |\Psi_{1,2}^u\rangle, \qquad (10.7)$$

where u is the configuration with all $u_{ij} = +1$.

From Eq. (10.7), we realize that the projection onto the physical subspace introduces string of D_i operators and that the spin to fermion mapping (10.2) is only apparently local. Similar to the case encountered with

a Jordan-Wigner transformation [171], the nonlocality of the mapping means that a local spin perturbation is nonlocal in the fermionic language and can thus connect well-separated MES. In order to check whether a local perturbation V splits the Majorana degeneracy, we thus need to calculate the following matrix elements

$$\langle \Psi_{1,2}^{\text{VF}} | V | \Psi_{1,2}^{\text{VF}} \rangle = \langle \Psi_{1,2}^{u} | V \mathcal{P} | \Psi_{1,2}^{u} \rangle. \tag{10.8}$$

Since $\mathcal{P}$ contains string of D_i operators, we need to check whether V introduces transition between $|\Psi_{1,2}^{u}\rangle$ and $\prod_{i \in \Lambda} D_i |\Psi_{1,2}^{u}\rangle$, where Λ is a subset of indices. If this is the case, then the perturbation V can split the remaining degeneracy.

In the following we explicitly construct a local perturbation which splits the remaining degeneracy in agreement with the general result of Ref. [175, 176, 177] stating that topological order is impossible in one-dimensional systems. Furthermore, we show that such a perturbation has to contain at least two-body terms.

A necessary criterion for a local perturbation V to split the degeneracy is that it does not create vortices. This is so because the degenerate groundstates are vortex-free and states with different u configurations are orthogonal. Let us thus first consider all possible single-body terms which do not create any vortex and show that they cannot split the degeneracy. The effect of $V_1 = \epsilon_1 \sigma_1^x$ and $V_{4N} = \epsilon_{4N} \sigma_{4N}^x$ has been considered already. The remaining single-body terms which do not create vortices are:

$$V_2 = \epsilon_2 \sigma_2^y, \quad V_{4N-1} = \epsilon_{4N-1} \sigma_{4N-1}^y. \tag{10.9}$$

For these single-body perturbations, the only string of D_i operators which leaves the u-configuration invariant is the product of all D_i, i.e., $\prod_{i=1}^{4N} D_i$. As an explicit example, let us now consider the effect of V_2:

$$\sigma_2^y \prod_i^{4N} D_i = i b_2^y c_2 \prod_{i=1}^{4N} b_i^x b_i^y b_i^z c_i \tag{10.10}$$

$$\propto i b_2^y c_2 b_1^x b_2^y b_{4N-1}^y b_{4N}^x \prod_{\langle ij \rangle} u_{ij} \prod_{i=1}^{4N} c_i \tag{10.11}$$

$$\propto i b_2^y c_2 \hat{\pi}, \tag{10.12}$$

where $\hat{\pi} = b_1^x b_2^y b_{4N-1}^y b_{4N}^x \prod_{i=1}^{4N} c_i$ is a parity operator and we used the fact that all $u_{ij} = +1$. We thus have

$$\langle \Psi_{1,2}^{u} | i b_2^y c_2 \hat{\pi} | \Psi_{1,2}^{u} \rangle = \pi \langle \Psi_{1,2}^{u} | i b_2^y c_2 | \Psi_{1,2}^{u} \rangle = 0, \tag{10.13}$$

where π is the parity of $|\Psi_{1,2}^u\rangle$ and the last equality comes from the fact that c_2 creates a finite-energy fermion (the contribution of c_2 in the remaining MES is exponentially supressed with system's size). We thus finally conclude that single-body perturbations cannot fully split the topological degeneracy.

In the following we show that two-body interactions are enough to destroy the remaining MES and we construct explicitly a perturbation which splits them:

$$V = \epsilon \sigma_{M-1}^x \sigma_M^y, \tag{10.14}$$

where M is even and belongs to the nontopological section $\mathcal{S}_2$, see Fig. (10.2). An in important point to notice is that such a perturbation will not create any vortices since σ_{M-1}^x changes the values of $u_{M-2,M-1}^x$ while σ_M^y changes the value of $u_{M-3,M}^y$. If this was not the case, then all matrix elements $\langle \Psi_{1,2}^u | V \prod_{i \in \Lambda} D_i | \Psi_{1,2}^u \rangle$ would trivially vanish, since states with different u configuration are orthogonal. The fact that states with different u configurations are orthogonal implies that the matrix elements $\langle \Psi_{1,2}^u | \prod_{i \in \Lambda} D_i \sigma_{M-1}^x \sigma_M^y | \Psi_{1,2}^u \rangle$ can be different than zero only if there exists a string of D_i operators which connect the two different configurations of u. Having in mind that D_i changes the value of u for the the three links connected to site i, it is easy to check that $\prod_{i=1}^{M-2} D_i$ introduces transitions between these two configurations of u. We have

$$\prod_{i=1}^{M-2} D_i \propto b_1^x b_2^y b_{M-3}^y b_{M-2}^x \prod_{i=1}^{M-2} c_i, \tag{10.15}$$

where we used that the other b operators combine into u operators which are all equal to one. From Eq. (10.15) we then obtain

$$\sigma_{M-1}^x \sigma_M^y \prod_{i=1}^{M-2} D_i \propto b_2^y b_1^x \prod_{i=1}^{M} c_i \tag{10.16}$$

The string of c_i operators in Eq. (10.16) is nonlocal and connect MES b_2^y with MES c_M. This allows to conclude that $\sigma_{M-1}^x \sigma_M^y \prod_{i=1}^{M-2} D_i$ can split the remaining topological degeneracy. However, checking that the matrix elements are really different from zero, i.e.,

$$\langle \Psi_{1,2}^u | \prod_{i=1}^{M-2} D_i \sigma_{M-1}^x \sigma_M^y | \Psi_{1,2}^u \rangle \neq 0, \tag{10.17}$$

requires determining whether the string operator $\prod_{i=1}^{M} c_i$ allows to come back to the groundsubspace. This is in principle the case since c_i's are

superpositions of all eigenmodes. In Appendix 10.C we use a different approach and show explicilty that V can indeed induce splitting between the Majorana states (all these considerations remain valid for a perturbation $V = \epsilon \sigma_M^y \sigma_{M+1}^x$ as well). Although single-body terms are not able to fully split the topological degeneracy, we showed that local two-body terms does it. From this result, it appears that MES are quite fragile against external magnetic fields since two-body interactions are easily generated in second order perturbation theory. However, on the positive side, we show below that the topological degeneracy is protected against inhomogeneous x, y, and z magnetic field components.

Protection against magnetic fields aligned along x-, y-, or z-direction.

Let us consider a local perturbation V which represents an inhomogeneous magnetic field in direction $\alpha = x, y, z$:

$$V = \sum_i h_i \sigma_i^\alpha. \tag{10.18}$$

As we demonstrated in the previous section, single-body terms cannot fully split the topological degeneracy. As a consequence, the perturbation V is not able to split the topological degeneracy at first order. We thus ask here the question whether this is possible at higher orders. The answer in principle is yes. For MES well-separated by L sites, the degeneracy can obviously be splitted in L^{th} order. However, L^{th} order terms are exponentially supressed with system's size and the effect of such perturbation is thus negligible for large systems. We are then interested in determining whether this is possible at order n independent of system's size.

As mentioned previously, a necessary condition for a local perturbation to split the degeneracy is that it does not create any vortices. The good candidates V^n generated at order n have thus to be products of terms $\sigma_i^\alpha \sigma_j^\alpha$ and $\sigma_{1,4N}^x$ or $\sigma_{2,4N-1}^y$ where i, j are nearest-neighbor sites along an α-link $\langle i, j \rangle_\alpha$. Note that V^n of this form not only do not create vortices, but also do not change the configuration of u. Thus, the two matrix elements which need to be considered are

$$\langle \Psi_{1,2}^u | V^n | \Psi_{1,2}^u \rangle \quad \text{and} \quad \langle \Psi_{1,2}^u | V^n \prod_{i=1}^{4N} D_i | \Psi_{1,2}^u \rangle, \tag{10.19}$$

since $\prod_{i=1}^{4N} D_i$ leaves the configuration of u invariant. If we recall that (the remaining four) MES are well-separated from each other, it is then

clear that $\langle \Psi_{1,2}^u | V^n | \Psi_{1,2}^u \rangle = 0$ for $n < L$. Furthermore, as mentioned previously, the operator $\prod_{i=1}^{4N} D_i$ is proportional to the parity operator of the eigenmodes [179] and we thus have for $n < L$

$$\langle \Psi_{1,2}^u | V^n \prod_{i=1}^{4N} D_i | \Psi_{1,2}^u \rangle \propto \pi \langle \Psi_{1,2}^u | V^n | \Psi_{1,2}^u \rangle = 0, \qquad (10.20)$$

where π is the eigenmodes parity of $|\Psi_{1,2}^u\rangle$.

From this we conclude that the effect of x, y, or z magnetic field components on the inhomogeneous spin ladder is exponentially supressed with system size. In other words, the topological degeneracy cannot be fully splitted by inhomogeneous magnetic fields purely along x-, y-, or z-direction.

10.6 Braiding MES in a tri-junction setup

The recent demonstration of non-abelian character of MES in p-wave wires [26] makes the possibility to realize topological quantum computing by braiding MES an attractive and promising method. Majorana end states in spin ladders can be moved by locally tuning the value of J_z couplings (similar to the local tuning of chemical potential in p-wave wires) and it is thus in principle also possible to braid them (following the scheme of Ref. [26]) in the tri-junction setup presented in Fig. 10.5. The tri-junction in Fig. 10.5 possesses the interesting property that no spurious Majorana modes are created in the course of braiding. Indeed, when all three parts building the tri-junction are in the topological phase, the $J_{x,y}$ couplings (dashed lines in Fig. 5) between the MES will combine two of them into an ordinary complex fermion. We note that such braiding processes in the simpler $xx-yy$ chain would be difficult to realize because of the many additional zero-energy modes, see Appendix 10.D. This is why we are interested in inhomogeneous spin ladders where such additional degeneracies do not appear all Majorana modes are well-separated from each other.

In order to be of use for topological quantum computing, an important property of MES is that they follow non-abelian exchange statistics (as it is the case in p-wave wires [26]). As mentioned above, the projection operator (onto the physical subspace) $\mathcal{P}$ introduces strings of operators and renders mapping (10.2) only apparently local. In such a case the study of braiding statistics is more complicated and especially mapping the Hamiltonian onto Kitaev's toy model Hamiltonian is not enough to

conclude anything about the statistics of MES. [171] We leave here the question of the MES statistics as an open problem.

To perform a robust topological quantum computation by exchanging MES, the two-body perturbations splitting the topological degeneracy have to be excluded. This requirement is analogous to the parity conservation requirement in p-wave wires and can in principle be achieved by carefully screening magnetic fields. Since Ising interactions can be tuned by means of electric fields only [180, 181], magnetic fields are not required for braiding and there is no intrinsic contradiction between exchanging MES and screening external magnetic fields.
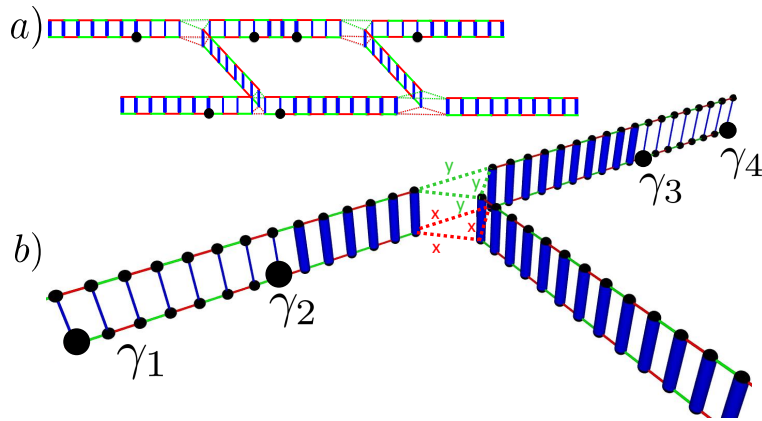
Figure 10.5: Network of spin ladders. a) Majoranas are exchanged through the tri-junctions which are shown in detail in b). The connection between the three spin ladders is given by Ising couplings J_x (red dashed lines) and J_y (green dashed lines). Braiding is performed by varying $J_{x,y}$, see main text. MES $\gamma_{1,\dots,4}$ (large dots) are localized at the left and right ends of the ladder and at the junction between topological (thin z-links) and non-topological (thick z-links) sections.

10.7 Conclusions

We have proposed inhomogeneous spin ladders and shown that they support a topological phase with localized Majorana states. We have studied the robustness of MES under local perturbations and demonstrated that single-body perturbations are not enough to split the topological degeneracy. We have explicitly constructed a two-body perturbation which does this, in agreement with the general fact that topological order is not possible in one-dimensional systems. [175, 176, 177] On the

positive side, we showed that the topological degeneracy cannot be destroyed by inhomogeneous magnetic fields aligned purely along x-, y-, or z-direction. Finally, we have presented a tri-junction setup where MES can be exchanged similar to Ref. [26].

While the spin ladders envisioned here are not yet available, we hope that the present study provides a strong encouragement for their experimental realization since they represent a promising framework for the realization and manipulation of MES.

10.8 Acknowledgement

10.A Mapping to two coupled Kitaev p-wave superconducting wires
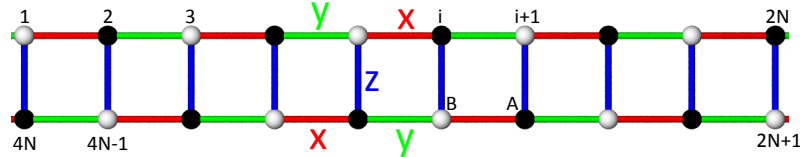
Figure 10.6: Inhomogeneous Kitaev spin ladder. The directions of x, y, and z links are indicated, as well as the A (black dots) and B (white dots) sublattices. In contrast to the standard Kitaev model, the z-coupling are allowed to be inhomogeneous, i.e., site-dependent $J_z \to J_{z_{ij}}$.

As presented in the main text, the model we consider possesses three different sections $\mathcal{S}_1$, $\mathcal{S}_2$, and $\mathcal{S}_3$ which are distinguished by the value of the $J_{z_{ij}}$ couplings [see Fig. 10.6]. We focus on the vortex-free and vortex-full sectors where we choose $J_{x,y,z,z'}$ such that $\mathcal{S}_1$ and $\mathcal{S}_3$ are topological, while section $\mathcal{S}_2$ is non-topological. This system carries four MES: γ_1 and γ_4 at the left and right end of the ladder, respectively, while γ_2 and γ_3 sit at the junction between topological ($\mathcal{S}_2$) and non-topological ($\mathcal{S}_{1,3}$) sections of the ladder.

Let us focus on a topological section, say $\mathcal{S}_1$, in the vortex-free sector (i.e. $u_{ij} = +1$), and study the location of MES $\gamma_{1,2}$ and their behavior under the modification of $J_{x,y,z}$ couplings. We disregard here the presence of the two other sections $\mathcal{S}_{2,3}$. It is useful to consider our spin system as two xx-yy chains coupled via J_z Ising couplings. Let us now introduce the following complex fermion operators

$$d_j = \frac{1}{2}(c_{2j-1} + ic_{2j}) \ \text{ and } \ d_j^\dagger = \frac{1}{2}(c_{2j-1} - ic_{2j}), \qquad (10.21)$$

with $j = 1...2N$ [the site labeling is shown in Fig. 10.3], $\{d_j, d_{j'}\} = 0$, and $\{d_j, d_{j'}^\dagger\} = \delta_{jj'}$. Then the upper ($u$) xx-yy chain is mapped to the Kitaev model for a one-dimensional p-wave superconductor [25, 24, 183]

$$H^u = -\mu^u \sum_{j=1}^{N} d_j^\dagger d_j - \sum_{j=1}^{N-1} \left(t^u d_j^\dagger d_{j+1} + \Delta^u d_j d_{j+1} + \text{h.c.} \right), \qquad (10.22)$$

with $\mu^u = 2J_x$ and $t^u = -\Delta^u = J_y$, while the lower (l) xx-yy spin chain is mapped to

$$H^l = -\mu^l \sum_{j=N+1}^{2N} d_j^\dagger d_j - \sum_{j=N+1}^{2N-1} \left(t^l d_j^\dagger d_{j+1} + \Delta^l d_j d_{j+1} + \text{h.c.} \right), \qquad (10.23)$$

with $\mu^l = 2J_y$ and $t^l = -\Delta^l = J_x$.

The J_z spin couplings between upper and lower xx-yy chain leads to a hopping term H^{ul} between upper and lower wire in the fermionic representation,

$$H^{ul} = -\sum_{j=1}^{N} \left(t^{ul} d_j^\dagger d_{2N-(j-1)} + \text{h.c.} \right), \qquad (10.24)$$

where $t^{ul} = 2J_z$.

Let us first focus on the case $J_z = 0$. Then, the system consists of two decoupled wires Eqs. (10.22) and (10.23), and we can distinguish between the following cases: If $J_x > J_y$, then the upper wire lies in the non-topological and the lower wire in the topological phase, i.e., the two MES are localized in the lower wire, one at the left and one at the right end. And vice versa for $J_y > J_x$.

When the z-couplings are turned on, i.e. $J_z > 0$, then the MES spread over both the upper and lower wires as shown in Fig. 3 of the main text. If J_z increases, then the MES continue to spread until they completely split

when $|J_z| > |J_x + J_y|$ in the vortex-free sector and $|J_z| > |J_x - J_y|$ in the vortex-full sector, see Eq. (6) in the main text. It is also straightforward to understand the exact site localization of the two MES. For $J_x > J_y$, most of the weight of the left γ_1 (right γ_2) MES resides at respectively the first and last site of the lower xx-yy chain and spreads only over A (B) sublattice sites. Indeed, the $J_{x,y,z}$-couplings between spins residing on different sublattices forbids γ_1 (γ_2) to spread over B (A) sites. Similarly, for $J_y > J_x$, most of the weight of the left γ_1 (right γ_2) MES resides at respectively the first a nd last site of the upper xx-yy chain and spreads only over B (A) sublattice sites.

10.B Vortex-free and vortex-full ground states

As discussed in the main text, although Lieb's theorem [159, 160] is not directly applicable to our system, we nevertheless are able to show numerically that the ground state is indeed vortex-free for $\text{sgn}(J_x) = -\text{sgn}(J_y)$ and $J_{z_{ij}} > 0$, while it is vortex-full for $\text{sgn}(J_x) = \text{sgn}(J_y)$. Let us focus on the case $\text{sgn}(J_x) = -\text{sgn}(J_y)$, since the other one can easily be deduced from it as discussed in the main text. Figure 10.7 shows single-vortex energies for different ladder lengths and $J_{x,y,z,z'}$ coupling configurations. All the results are consistent with our assumption that the ground state is vortex-free. We have furthermore investigated the effect of vortex-vortex interactions and plotted in Figs. 10.8 and 10.9 multi-vortex energies for different N, $J_{x,y,z}$ couplings, and distance between the vortices. Again, all the plots indicate a vortex-free ground state since the *attractive* vortex-vortex interaction is not strong enough to favor the creation of additional vortices. Finally, we plot in Fig. 10.10 the energy of the vortex-full sector as function of N for $J_x = 1.0$, $J_y = -0.55$, $J_z = 0.25$ in $\mathcal{S}_{1,3}$, while $J_{z'} = 4$ in $\mathcal{S}_2$. The energy of the vortex-full sector is always positive and increases linearly with the system size N. This result again shows that vortex-vortex interactions do not favour the creation of vortices and the ground state is free of vortices. We have checked that this result is valid for many other choices of parameters $J_{x,y,z}$. A detailed explanation of the plots is given in the figure captions.

As a final remark, we would like to mention that the groundstate of the tri-junction setup presented in the main text (see Fig. 5 of the main text) is also vortex-free/full. Indeed, each ladder forming the tri-junction is separately free/full of vortices and thus by a continuity argument it is clear that switching on (small) couplings between different ladders cannot create vortices.
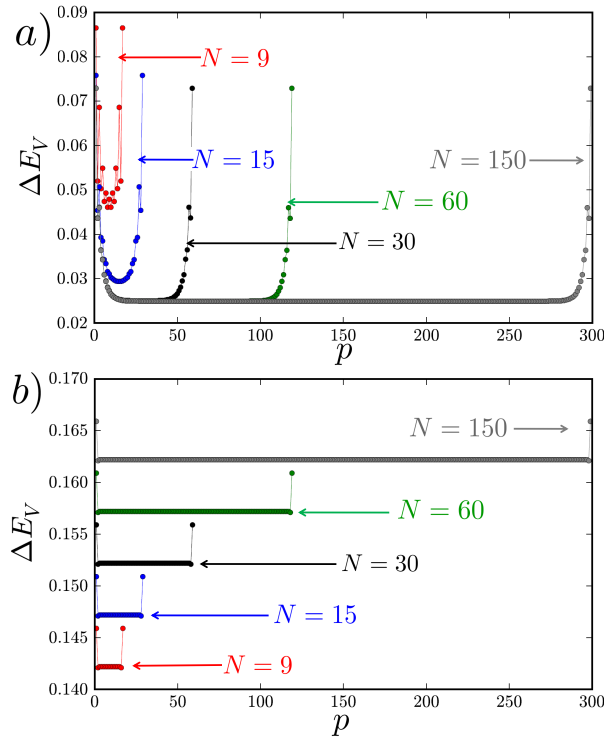
Figure 10.7: Energy ΔE_V of a single vortex as function of its position p on the ladder. We recall that a vortex can be placed at $2N - 1$ different positions on a ladder with N unit cells. The five different curves correspond to $N = 9, 15, 30, 60, 150$. We see a clear difference between the vortex energy in the bulk and near the boundaries: boundary effects increase the energy of a vortex lying near to one end of the ladder. It is also worth pointing out that the vortex energy converges quickly (with N) to its thermodynamic limit value. We see that the vortex energy is positive for each curve irrespective of the vortex's position. This plot thus supports our claim that the ground state is vortex free. The value of the different couplings chosen is: *a)* $J_x = 1.0$, $J_y = -0.5$, $J_z = 0.3$ in $\mathcal{S}_{1,3}$, and $J_{z'} = 0.3$ in $\mathcal{S}_2$. *b)* $J_x = 1.0$, $J_y = -0.65$, $J_z = 4.3$ in $\mathcal{S}_{1,3}$ and $J_{z'} = 4.3$ in $\mathcal{S}_2$. The curves for $N = 15, 30, 60, 150$ are shifted vertically by $0.005, 0.01, 0.015$, and 0.02, respectively, for clarity.

10.C   Different mapping to study the robustness of MES

The aim of this Appendix is to propose another mapping to study the robustness of MES in the homogeneous and inhomogeneous ladder. We
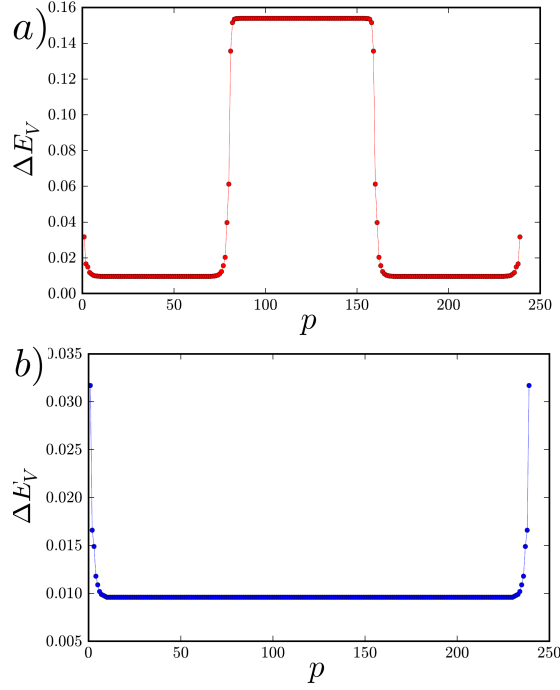
Figure 10.8: a, b) Energy ΔE_V of a single vortex as function of its position p on a ladder with $N = 120$, $J_x = 1.0$, $J_y = -0.37$, $J_z = 0.25$ in $\mathcal{S}_{1,3}$, while $J_{z'} = 4$ in $\mathcal{S}_2$ for a) and $J_x = 1.0$, $J_y = -0.37$, $J_z = 0.25$ in $\mathcal{S}_{1,3}$ and $J_{z'} = 0.25$ in $\mathcal{S}_2$ for b). The junction between sections $\mathcal{S}_1$ and $\mathcal{S}_2$ is at $p = 2N/3$ and between $\mathcal{S}_2$ and $\mathcal{S}_3$ at $p = 4N/3$

use the same labeling as Fig. 10.3 but now make use of the following spin-to-spin mapping: [34, 184]

$$\sigma_i^z \quad \rightarrow \quad \tau_{i-1}^z \tau_i^z, \tag{10.25}$$

$$\sigma_i^x \quad \rightarrow \quad \prod_{i=1}^{4N} \tau_i^x, \tag{10.26}$$

$$\tag{10.27}$$

where $\tau_i^{x,y,z}$ are ususal Pauli matrices. The mapping is thus to an auxiliary system of $4N + 1$ τ_i spins ($i = 0, 1, 2, ..., 4N$). Therefore, the mapping introduces a doubling of the Hilbert space which can be taken into account by imposing the constraint $\tau_0^z = +1$.

The spin ladder Hamiltonian (14.16) takes in this new language the
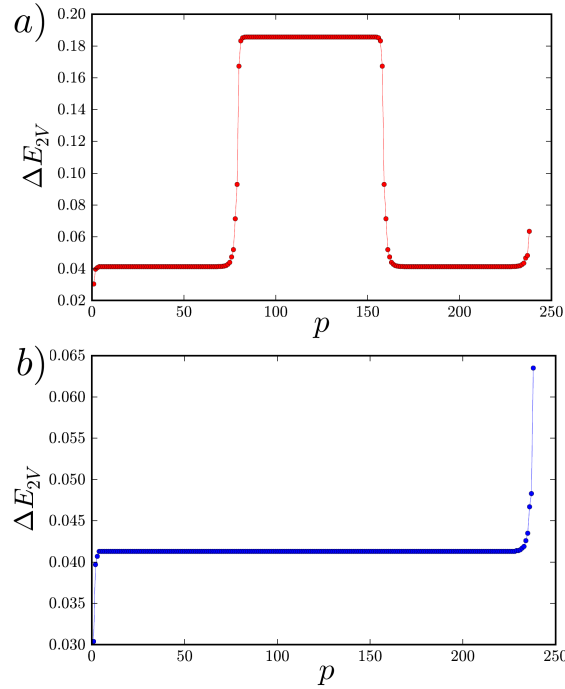
Figure 10.9: a, b) Energy ΔE_{2V} of two vortices as function of the position p of the second vortex. The first vortex lies on the $p = 1$ square plaquette. The $J_{x,y,z,z'}$ parameters are chosen respectively as in Fig. 10.8. The vortex-vortex interaction is attractive and rapidly decaying as function of distance between the two vortices. Indeed, already for $p = 5$ the energy of the two vortices is roughly 0.04 [0.03 (energy of the vortex at the boundary $p = 1$) plus 0.01 (energy of the vortex in the bulk)]. However, as mentioned in the main text, the attraction is never strong enough to favor the creation of vortices and the energy of the two vortices is always positive. The junction between sections $\mathcal{S}_1$ and $\mathcal{S}_2$ is at $p = 2N/3$ and between $\mathcal{S}_2$ and $\mathcal{S}_3$ at $p = 4N/3$

following form:

$$
\begin{aligned}
H = {} & J_x \left(\tau_2^x + \tau_4^x + ... + \tau_{N-2}^x \right) \\
& + J_z \big(\underbrace{\tau_0^z}_{+1} \tau_2^z + \tau_2^z \tau_4^z + \tau_4^z \tau_6^z + ... + \tau_{N-2}^z \tau_N^z \big) \\
& + J_y \big(\tau_0^z \tau_1^y \tau_2^x \tau_3^y \tau_4^z + ... + \tau_{N-4}^z \tau_{N-3}^y \tau_{N-2}^x \tau_{N-1}^y \tau_N^z \big).
\end{aligned}
$$

$$(10.28)$$

This Hamiltonian possesses many conserved quantities since all τ_i^y with odd i commute with H and are straightforwardly connected to the vortex
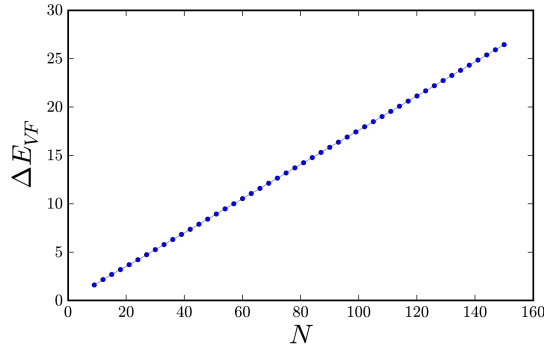
Figure 10.10: Energy E_{VF} of the vortex full sector as function of N with $J_x = 1.0$, $J_y = -0.55$, $J_z = 0.25$ in $\mathcal{S}_{1,3}$, while $J_{z'} = 4$ in $\mathcal{S}_2$. As expected, the energy of the vortex-full sector is always positive and grows linearly with N. The slope of the of the straight line can be interpreted as an average vortex energy. This plot indicates again that the vortex-vortex interaction does not favour the creation of vortices and the ground state is vortex-free. The junction between sections $\mathcal{S}_1$ and $\mathcal{S}_2$ is at $p = 2N/3$ and between $\mathcal{S}_2$ and $\mathcal{S}_3$ at $p = 4N/3$

operators:

$$W_n = \tau_{n,1}^y \tau_{n,3}^y \quad \text{and} \quad \bar{W}_n = \tau_{n,1}^y \tau_{n+1,3}^y. \tag{10.29}$$

Homogeneous ladder

As a first step, let us now study the homogeneous ladder and consider the case where $J_x \gg J_{y,z}$ which, according to Eq. (10.6), is in the topological phase. For $J_{y,z} = 0$, the odd spins are completely decoupled and the corresponding $2^{N/2-1}$ degeneracy is due to the absence of gap to create a vortex. However, there is an additional and interesting degeneracy coming from the fact that the last spin τ_N^x does not appear in the Hamiltonian and the total degeneracy in the topological phase is thus $2^{N/2}$. In the opposite limit, i.e., when $J_z \neq 0$ and $J_{x,y} = 0$ which, according to Eq. (10.6), corresponds to the nontopological phase, then by construction $\tau_0^z = +1$ and no additional degeneracy is present. In this limit the degeneracy is thus $2^{N/2-1}$. We thus identify the additional degeneracy due to the Nth spin as the topological degeneracy. In the strong J_x limit, the two corresponding degenerate groundstates take the following form

$$|\psi_{\uparrow\downarrow}\rangle = |\uparrow_0 +_2 +_4 \ldots +_{N-2} \uparrow\downarrow_N\rangle, \tag{10.30}$$

where $+_i$ is eigenstate of τ_i^x while $\uparrow_j$ and $\downarrow_j$ are eigenstates of τ_j^z.

It is now straightforward to understand that the single-body pertur-
bation $V = \sigma_N^x = \tau_N^x$ will split the topological degeneracy since

$$\langle \psi_1 | V | \psi_2 \rangle = \langle \psi_1 | \tau_N^x | \psi_2 \rangle \neq 0. \tag{10.31}$$

With the Kitave's mapping, we noticed the presence of an additional de-
generacy because of the presence of six MES in the extended space. In
the new language, this additional degeneracy correpsonds to the sign of
τ_1^y (the state with all $\tau_{2i-1}^y = +1$ is degenerate with the state where all
$\tau_{2i-1}^y = -1$). This degeneracy is splitted by $\sigma_1^x = \prod_{i=1}^N \tau_i^x$ since it induces
transition between the states with all $\tau_{2i-1}^y = +1$ and all $\tau_{2i-1}^y = -1$.

Inhomogeneous ladder

Let us now consider the inhomogeneous ladder with two topological sec-
tions $\mathcal{S}_{1,3}$ separated by the nontopological section $\mathcal{S}_2$, see Fig. 10.2. In the
case where $J_x \neq 0$ and $J_{y,z} = 0$ in $S_{1,3}$ while $J_z \neq 0$ and $J_{x,y} = 0$ in S_2 it
is easy to see the origin of the eightfold degeneracy, see Fig. 10.11. One
degeneracy is related to the sign of $\tau_1^y = \pm 1$. This degeneracy is easy to
split with a local perturbation $\epsilon \tau_1^y = \epsilon \sigma_1^y \sigma_2^x$ (as we showed with Kitaev's
mapping (10.2), $\sigma_1^x = \prod_{i=1}^N \tau_i^x$ also splits this degeneracy). The origin of
the remaining fourfold degeneracy can be understood easily in the limit-
ing case we consider. The first twofold degeneracy is due to the Nth spin
which is decoupled from the other spins while the other twofold degen-
eracy comes from the middle Ising section which has the same energy if
all spins are up or down. The former degeneracy is trivially splitted by a
perturbation $\epsilon \tau_N^x = \epsilon \sigma_N^x$ while the later is clearly splitted by the pertuba-
tion in Eq. (10.14)

$$\epsilon \sigma_{M-1}^x \sigma_M^y = \epsilon i \sigma_{M-1}^x \sigma_M^x \sigma_M^z \tag{10.32}$$
$$= \epsilon i \tau_{M-1}^x \tau_{M-1}^z \tau_M^z = \epsilon \tau_{M-1}^y \tau_M^z \tag{10.33}$$

since τ_{M-1}^y is a conserved quantity ($M - 1$ is an odd site here). We have
thus shown here explicitly that two-body perturbations are enough to
split the remaining degeneracies in agreement with the discussion in the
main text.
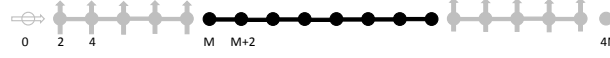
Figure 10.11: Pictorial representation of the groundstates in the limit $J_x \neq 0$ and $J_{y,z} = 0$ in sections $\mathcal{S}_{1,3}$ and $J_z \neq 0$ and $J_{x,y} = 0$ in $\mathcal{S}_2$. Here $\Uparrow$ and $\Downarrow$ are a pictorial representations of τ^x eigenstates.

10.D Proliferation of π-junction zero-modes in XX-YY spin chain

In this section we study some properties of the zero-energy modes present in a xx-yy spin chain of length $2N$, described by the Hamiltonian

$$H_{xx-yy} = J_x \sum_{\substack{i=1 \\ i\,\mathrm{odd}}}^{2N-1} \sigma_i^x \sigma_{i+1}^x + J_y \sum_{\substack{i=1 \\ i\,\mathrm{even}}}^{2N} \sigma_i^y \sigma_{i+1}^y. \qquad (10.34)$$

We show that the xx-yy spin chains contain many additional zero-energy modes besides the two c Majoranas localized at the ends of the chain. In the language of mapping (10.2), this arises because all non-equivalent u configurations are degenerate, i.e. putting a $u_{ij}^\alpha = -1$ does not cost energy. It is instructive to study this model with a Jordan-Wigner transformation

$$\sigma_j^+ = \prod_{k=1}^{j-1} (-1)^{n_k} a_j \quad \text{and} \quad \sigma_j^- = \prod_{k=1}^{j-1} (-1)^{n_k} a_j^\dagger, \qquad (10.35)$$

where a_j annihilates a complex fermion at site j, i.e., $\{a_j^{(\dagger)}, a_{j'}^{(\dagger)}\} = 0$ and $\{a_j, a_{j'}^\dagger\} = \delta_{jj'}$, and $n_j = a_j^\dagger a_j$. With the use of Eq. (10.35), H_{xx-yy} takes the form

$$\begin{aligned}
\widetilde{H}_{xx-yy} &= \sum_{\substack{i\,\mathrm{odd}}} \left(-w_x a_i^\dagger a_{i+1} + \Delta_x a_i a_{i+1} + \mathrm{h.c.} \right) \\
&+ \sum_{\substack{i\,\mathrm{even}}} \left(-w_y a_i^+ a_{i+1} + \Delta_y a_i a_{i+1} + \mathrm{h.c.} \right),
\end{aligned}$$

$$(10.36)$$

where $w_x = \Delta_x = J_x/4$ and $w_y = -\Delta_y = -J_y/4$.

Since there is a difference of π in the pase of Δ_x and Δ_y, we thus conclude that Hamiltonian (10.36) represents an array of π-junctions and thus possesses $2N$ additional zero-energy modes. [26] To find the spectrum ϵ_k of Hamiltonian (10.36), we artificially double the number of de-

grees of freedom and rewrite Eq. (10.36) as

$$\widetilde{H}_{xx-yy} = \frac{1}{2} \boldsymbol{a}\, \mathcal{H}\, \boldsymbol{a}^\dagger, \qquad (10.37)$$

where $\boldsymbol{a} = \begin{pmatrix} a_1 & \ldots & a_{2N} & a_1^\dagger & \ldots & a_{2N}^\dagger \end{pmatrix}$, and $\mathcal{H}$ is a real $4N \times 4N$ symmetric matrix defined through Eq. (10.36). Fig. 10.12 is a plot of the eigenvalues ϵ_k of $\mathcal{H}$ which corresponds to the modes of a xx-yy spin chain with $J_x = 0.4$, $J_y = 1.0$, and length $2N = 20$ for a) and $2N = 100$ for b). As expected, the number of additional zero-energy modes is $2N$. It is thus possible to generate zero-energy modes in the xx-yy spin chain by increasing the system size.
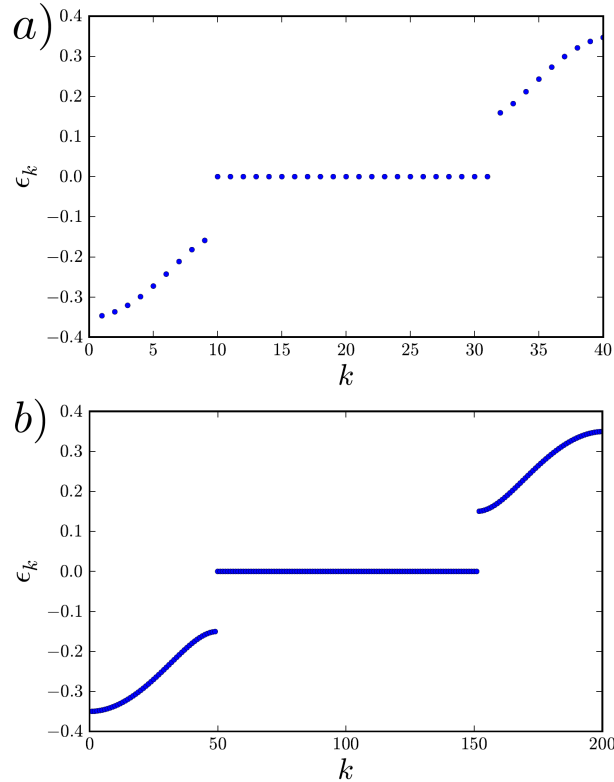
Figure 10.12: Energy eigenvalues ϵ_k of $\mathcal{H}$ in Eq. (10.37) for xx-yy chains with $J_x = 0.4$, $J_y = 1.0$, and $2N = 20$ for a) and $2N = 100$ for b). There are $2N$ zero-energy modes in addition to the two expected MES. The presence of these additional zero modes can be understood by mapping Hamiltonain H_{xx-yy} to an array of π-junctions [see Eq. 10.36].

10.E Long-distance spin-spin correlation function

In this section we study the static long-distance spin-spin correlation function $\langle \sigma_1^x \sigma_{4N}^x \rangle$ (the site labeling is shown in Fig. 3 of the main text). We note that this correlator vanishes in the standard honeycomb model [?, 156] but is non-zero for the ladder in the topological phase due to the presence of MES localized at sites 1 and $4N$ when $J_x > J_y$ (the scenario with $J_x < J_y$ can be treated analogously by considering $\langle \sigma_2^x \sigma_{4N-1}^x \rangle$). Let us first give an explicit expression for $\langle \sigma_1^x \sigma_{4N}^x \rangle$. Since

$$\sigma_i^x \sigma_j^x = -i u_{ij}^x c_i c_j \tag{10.38}$$

and

$$(b_1, b_2, ..., b_{4N-1}, b_{4N})Q^u = (c_1, ..., c_{4N}), \tag{10.39}$$

we have

$$c_i = \sum_k Q_{ki}^u b_k \tag{10.40}$$

$$c_i c_j = \sum_{k,k'} Q_{ki}^u Q_{k'j}^u b_k b_{k'}. \tag{10.41}$$

Using

$$\begin{aligned} a_k^\dagger &= (b_{2k-1} - i b_{2k})/2 \\ a_k &= (b_{2k-1} + i b_{2k})/2, \end{aligned} \tag{10.42}$$

and

$$\begin{aligned} c_i c_j &= \sum_{l,k} Q_{2k-1i}^u Q_{2l-1j}^u b_{2k-1} b_{2l-1} + \sum_{l,k} Q_{2k-1i}^u Q_{2lj}^u b_{2k-1} b_{2l} + \sum_{l,k} Q_{2ki}^u Q_{2l-1j}^u b_{2k} b_{2l-1}' \\ &\quad + \sum_{l,k} Q_{2ki}^u Q_{2lj}^u b_{2k} b_{2l}, \end{aligned} \tag{10.43}$$

we obtain

$$\begin{aligned} c_i c_j &= \sum_{l,k} Q_{2k-1i}^u Q_{2l-1j}^u (a_k + a_k^\dagger)(a_l + a_l^\dagger) + \sum_{l,k} Q_{2k-1i}^u Q_{2lj}^u (a_k + a_k^\dagger)(1/i)(a_l - a_l^\dagger) \\ &\quad + \sum_{l,k} Q_{2ki}^u Q_{2l-1j}^u (1/i)(a_k - a_k^\dagger)(a_l + a_l^\dagger) + \sum_{l,k} Q_{2ki}^u Q_{2lj}^u (1/i^2)(a_k - a_k^\dagger)(a_l - a_l^\dagger), \end{aligned} \tag{10.44}$$

and thus

$$
\begin{aligned}
c_i c_j &= \sum_{k,l} \Big[Q^u_{2k-1i} Q^u_{2l-1j} (a_k a_l + a_k a_l^\dagger + a_k^\dagger a_l + a_k^\dagger a_l^\dagger) \\
&\quad + Q^u_{2k-1i} Q^u_{2lj} (1/i) (a_k a_l - a_k a_l^\dagger + a_k^\dagger a_l - a_k^\dagger a_l^\dagger) \\
&\quad + Q^u_{2ki} Q^u_{2l-1j} (1/i) (a_k a_l + a_k a_l^\dagger - a_k^\dagger a_l - a_k^\dagger a_l^\dagger) \\
&\quad + Q^u_{2ki} Q^u_{2lj} (-a_k a_l + a_k a_l^\dagger + a_k^\dagger a_l - a_k^\dagger a_{2l}^\dagger) \Big] \; .
\end{aligned}
\tag{10.45}
$$

It is now straightforward to calculate $\langle \Psi_{n=0} | \sigma_1^x \sigma_{4N}^x | \Psi_{n=0} \rangle$, where n ($n = 0, 1$) represents the filling of MES while all the high-energy modes are unfilled,

$$
\begin{aligned}
\langle \Psi_{n=0} | \sigma_1^x \sigma_{4N}^x | \Psi_{n=0} \rangle &= -i u_{14N}^x \langle n = 0 | c_1 c_{4N} | n = 0 \rangle \\
&= -i u_{14N}^x \langle n = 0 | \sum_k \Big[Q^u_{2k-1i} Q^u_{2k-1j} (a_{2k-1} a_{2k-1}^\dagger + a_{2k-1}^\dagger a_{2k-1}) \\
&\quad + Q^u_{2ki} Q^u_{2k-1j} (1/i) (a_k a_k^\dagger - a_k^\dagger a_k) \\
&\quad + Q^u_{2k-1i} Q^u_{2kj} (1/i) (-a_k a_k^\dagger + a_k^\dagger a_k) \\
&\quad + Q^u_{2ki} Q^u_{2kj} (a_k a_k^\dagger + a_k^\dagger a_k) \Big] | n = 0 \rangle \; ,
\end{aligned}
\tag{10.46}
$$

where $i = 1$ and $j = 4N$.

With the use of the fermionic anticommutation relation $\{a_k, a_k^\dagger\} = 1$ we obtain

$$
\begin{aligned}
\langle \Psi_{n=0} | \sigma_1^x \sigma_{4N}^x | \Psi_{n=0} \rangle &= -i u_{14N}^x \sum_k \Big[Q^u_{2k-1i} Q^u_{2k-1j} - (1/i) Q^u_{2k-1i} Q^u_{2kj} \\
&\qquad\qquad + (1/i) Q^u_{2ki} Q^u_{2k-1j} + Q^u_{2ki} Q^u_{2kj} \Big] \\
&\quad + \sum_k \Big[(2/i) Q^u_{2k-1i} Q^u_{2kj} - (2/i) Q^u_{2ki} Q^u_{2k-1j} \Big] (n_k = 0) \\
&= -i u_{14N}^x \sum_k \Big[Q^u_{2k-1i} Q^u_{2k-1j} - (1/i) Q^u_{2k-1i} Q^u_{2kj} \\
&\qquad\qquad + (1/i) Q^u_{2ki} Q^u_{2k-1j} + Q^u_{2ki} Q^u_{2kj} \Big] \; .
\end{aligned}
\tag{10.47}
$$

Since the matrix Q^u is orthogonal we finally obtain

$$
\begin{aligned}
\langle \Psi_{n=0} | \sigma_1^x \sigma_{4N}^x | \Psi_{n=0} \rangle &= -i u_{14N}^x \sum_k \Big[-(1/i) Q^u_{2k-1i} Q^u_{2kj} + (1/i) Q^u_{2ki} Q^u_{2k-1j} \Big] \\
&= u_{14N}^x \sum_k \Big[Q^u_{2k-1i} Q^u_{2kj} - Q^u_{2ki} Q^u_{2k-1j} \Big] \; ,
\end{aligned}
\tag{10.48}
$$

where we recall that $u_{14N}^x = \pm 1$ decouples from the Hamiltonian in the absence of external perturbations.

Similarly we can show that

$$\langle \Psi_{n=1} | \sigma_1^x \sigma_{4N}^x | \Psi_{n=1} \rangle = u_{14N}^x \Big(\sum_k \big[Q_{2k-1i}^u Q_{2kj}^u - Q_{2ki}^u Q_{2k-1j}^u \big] + 2 Q_{2\alpha i}^u Q_{2\alpha-1j}^u$$

$$-2 Q_{2\alpha-1i}^u Q_{2\alpha j}^u \Big),$$

(10.49)

where α is the index of the fermonic mode formed by the Majoranas, i.e., $n_\alpha = n = 1$ is the filling of MES. As mentioned above, the long-distance spin-spin correlation $\langle \sigma_1^x \sigma_{4N}^x \rangle$ vanishes in the standard honeycomb model [?, 156] and is non-zero here only in the topological phase due to the presence of MES state with components on both sites 1 and $4N$. We show in Fig. 10.13 a) and b) a plot of $-\langle \Psi_n | \sigma_1^x \sigma_{4N}^x | \Psi_n \rangle$ as function of N with all $u_{ij} = +1$, $J_x = 1.0$, $J_y = -0.4$, and $J_{z_1} = J_{z_2} = J_{z_3} = 0.2$ for the topological phase in a) and $J_{z_1} = J_{z_2} = J_{z_3} = 2$ for the non-topological phase in b). We make use of the projection protocol of Ref. [179] in order to determine if the physical ground state of the vortex-free sector has even ($n = 0$) or odd ($n = 1$) parity. As expected, the long-distance spin-spin correlation takes a finite value in a) while it vanishes in b). In the remainder of this section, we want to investigate the effects of vortices on the long-distance correlation function. Figure 10.14a) shows a plot of $-\langle \Psi_n | \sigma_1^x \sigma_{4N}^x | \Psi_n \rangle$ as function of position of a single vortex, p, for $N = 50$, $J_x = 1.0$, $J_y = -0.4$, $J_{z_1} = J_{z_2} = J_{z_3} = 0.2$. This ladder has one topological section with two MES $\gamma_{1,2}$ localized on the left and right ends. The oscillations between positive and negative values of the correlator show that the vortex changes the value of $\langle \Psi_n | \sigma_1^x \sigma_{4N}^x | \Psi_n \rangle$ and thus the MES parity $i\gamma_1\gamma_2$ as function of its position on the ladder. Indeed, using Eqs. (10.48) and (10.49) we show numerically that $\langle \Psi_{n=0} | \sigma_1^x \sigma_{4N}^x | \Psi_{n=0} \rangle = -\langle \Psi_{n=1} | \sigma_1^x \sigma_{4N}^x | \Psi_{n=1} \rangle$, and thus conclude that a change of sign in the correlator implies a change of the parity $i\gamma_1\gamma_2$ (i.e., $n = 0 \leftrightarrow n = 1$). We make use of the projection protocol of Ref. [179] in order to determine if the physical ground state of the one-vortex sectors have even ($n = 0$) or odd ($n = 1$) parity. In Fig. 10.14 b) we plot $-\langle \Psi_n | \sigma_1^x \sigma_{4N}^x | \Psi_n \rangle$ as function of position of a single vortex, p, for $N = 50$, $J_x = 1.0$, $J_y = -0.4$, $J_{z_1} = J_{z_3} = 0.2$, $J_{z_2} = 2$. This ladder carries four MES: $\gamma_{1,4}$ at respectively the left and right ends of the ladder and $\gamma_{2,3}$ at the junction between topological and non-topological sections. The oscillations in the correlator demonstrates again oscillations in the parity $i\gamma_1\gamma_4$. As mentioned in the main text, the one-vortex state is highly degenerate since it does not cost
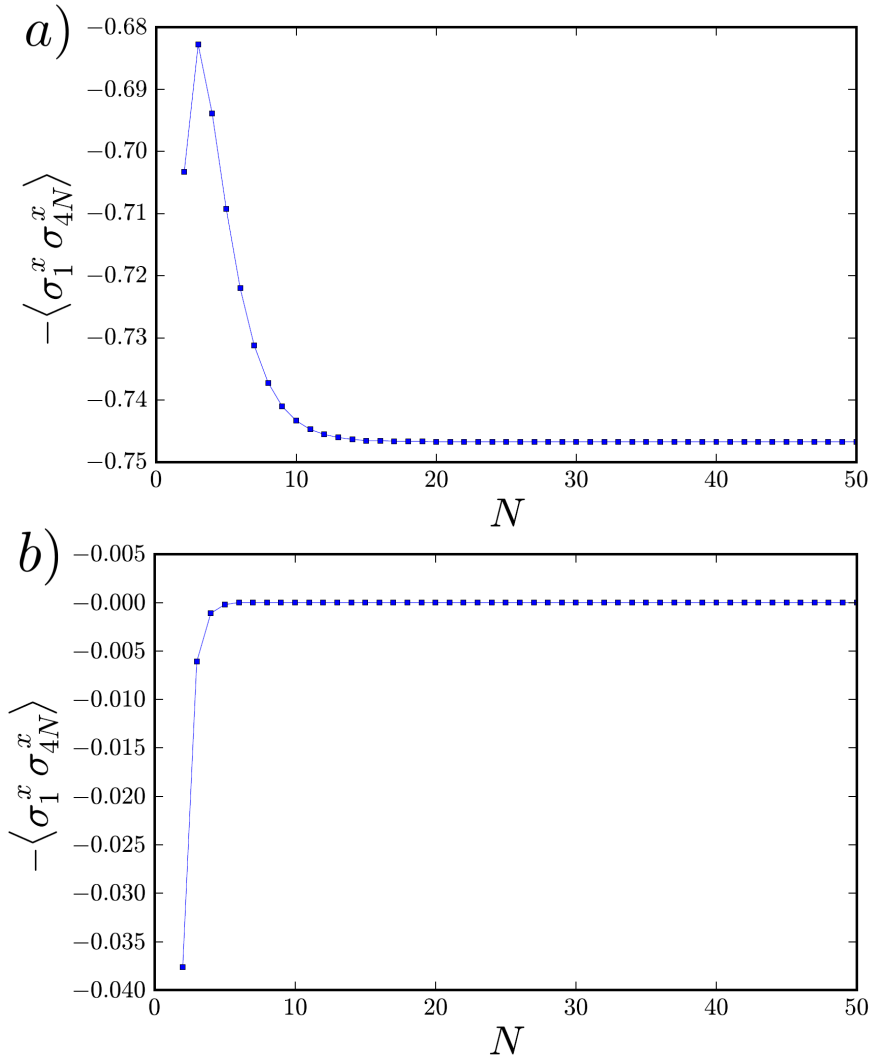
Figure 10.13: $-\langle\Psi_n|\sigma_1^x\sigma_{4N}^x|\Psi_n\rangle$ as function of N, with all $u_{ij} = +1$, $J_x = 1.0$, $J_y = -0.4$, and $J_{z_1} = J_{z_2} = J_{z_3} = 0.2$ for a), and $J_{z_1} = J_{z_2} = J_{z_3} = 2$ for b). We make use of the projection protocol of Ref. [179] in order to determine if the physical ground state of the vortex-free sector has even ($n = 0$) or odd ($n = 1$) parity.

energy to move a vortex to a nearby plaquette, and thus, without any prior measurement, the position of a vortex is generally not known, and so neither is the parity of the MES. In the case where MES are used for topological computing (braiding), it is thus essential that the groundstate is vortex-free or vortex-full.
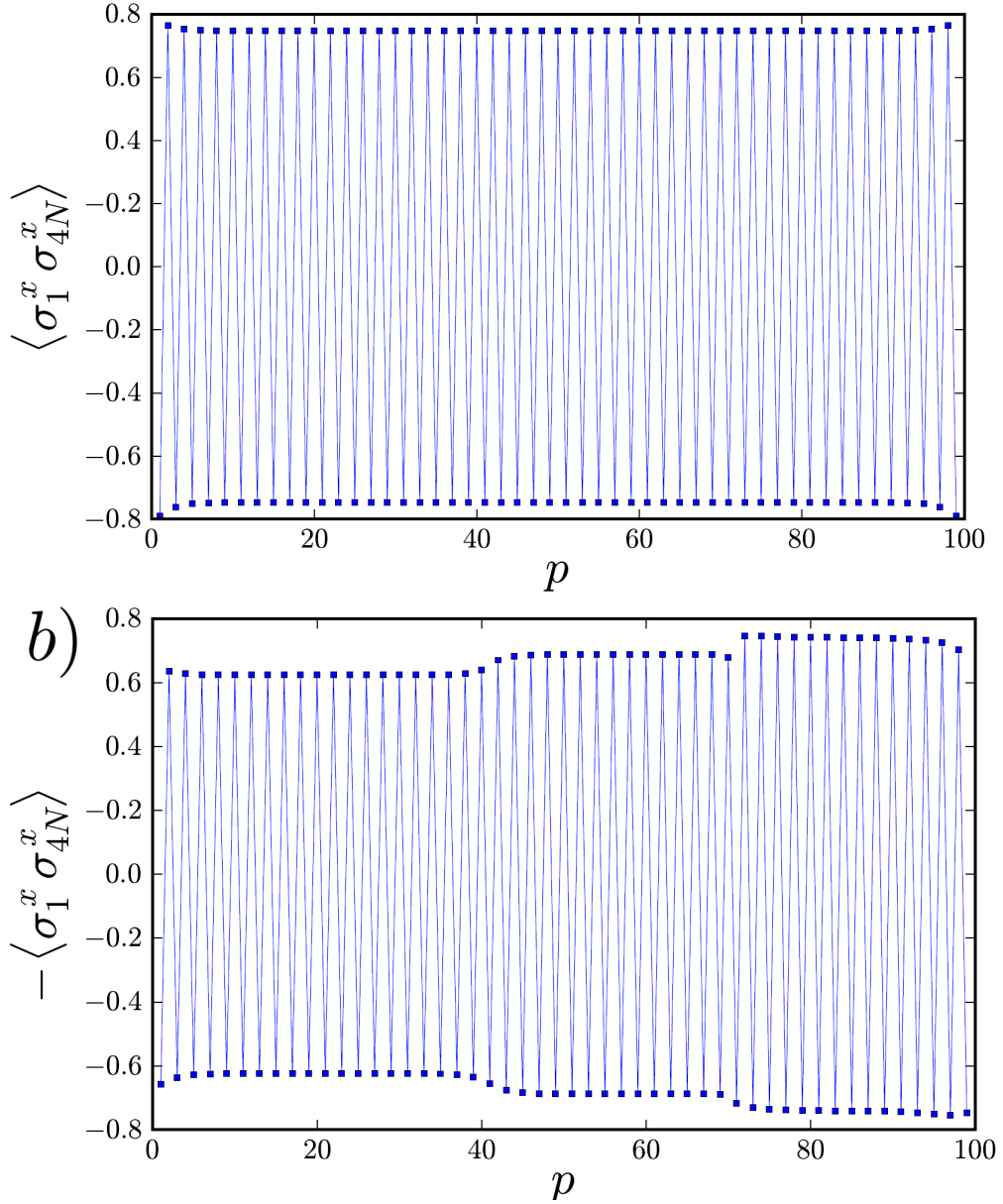
Figure 10.14: Plot of correlator $-\langle \Psi_n | \sigma_1^x \sigma_{4N}^x | \Psi_n \rangle$ as function of position of a single vortex, p, for $N = 50$, $J_x = 1.0$, $J_y = -0.4$, and $J_{z_1} = J_{z_2} = J_{z_3} = 0.2$ in a) and $J_{z_1} = J_{z_3} = 0.2$, $J_{z_2} = 2$ in b). The junctions between sections $\mathcal{S}_{1,3}$ and $\mathcal{S}_2$ are at plaquettes $p = 41, 71$. We used the projection protocol of Ref. [179] to determine if the physical ground state of the corresponding single-vortex sector has even ($n = 0$) or odd ($n = 1$) parity. Note that the physical groundstates we consider have a fixed parity $i\gamma_2\gamma_3 = +1$ and oscillating parity $i\gamma_1\gamma_4$.

Reflection Positivity for Majoranas

We establish reflection positivity for Gibbs trace states defined by a certain class of Hamiltonians that describe the interaction of Majoranas on a lattice. These Hamiltonians may include many-body interactions, as long as the signs of the associated coupling constants satisfy certain restrictions. We show that reflection positivity holds on an even subalgebra of Majoranas.

11.1   Introduction

In this paper we prove reflection positivity for trace functionals defined by a certain class of interactions of (neutral) Majoranas on a lattice. Earlier results on reflection positivity for fermions in the framework of quantum statistical mechanics focus on the case of charged excitations. In §11.3 we isolate conditions that entail reflection positivity on an interaction Hamiltonian H, expressed in terms of Majoranas. Our main result is Theorem 3 of §11.6,

$$0 \leqslant Tr(A\,\vartheta(A)\,e^{-H})\,, \tag{11.1}$$

which is valid for certain functions A of Majoranas, and for a reflection ϑ. Some related bounds are given in §11.8.

Our formulation and proof of Theorem 3 in §11.6 involve familiar methods, but they also require new ideas. As the present paper describes interactions without charge, one does not have the useful charge-conservation symmetry to aid in their analysis. In this case we establish reflection positivity on an even sub-algebra of fermions. The corresponding positivity is not valid on the full fermionic algebra for a half-space on one side of the reflection plane, as we show with an explicit counterexample in (11.9).

Recently the present authors have studied certain quantum spin interactions, which are of interest in quantum information theory, [185] where we apply the reflection positivity results of this present paper. These quantum spin systems have certain features similar to lattice gauge theory. However one must also deal with the additional complication that the basic fermionic variables anti-commute at different sites, rather than commute.

Reflection positivity has played an important role in analysis of quantum fields as well as the analysis of classical and quantum spin systems. Osterwalder and Schrader discovered reflection positivity in their study of classical fields on Euclidean space [186]; it provided the key notion of quantization and allowed one to go from a classical field to a quantum-mechanical Hilbert space and a positive Hamiltonian acting on that Hilbert space.

Multiple reflection bounds, based on reflection positivity for classical fields, played a crucial role in Glimm, Jaffe, and Spencer's mathematical proof [187] of the physicists' assumption that phase transitions and symmetry breaking exist in quantum field theory. This first example of a phase transition in field theory [187] concerned breaking of a discrete $\mathbb{Z}_2$ symmetry. Reflection positivity also turned out be be extremely useful in the analysis of lattice models for boson and fermion interactions by Fröhlich, Simon, Spencer, Dyson, Israel, Lieb, Macris, Nachtergale, and others. [188, 189, 190, 159, 160] This included the analysis of phase transitions and the breaking of certain continuous symmetry groups in lattice spin systems. In addition, reflection positivity was crucial in the study by Osterwalder and Seiler of the Wilson action for lattice gauge theory. [191]

11.2 Definitions and basic properties

Majoranas on a lattice are a self-adjoint representation of a Clifford algebra with $2N$ generators c_i. They satisfy

$$\{c_i, c_j\} = 2\delta_{ij}, \qquad c_i^* = c_i, \qquad \text{for } i, j = 1, \ldots, 2N. \tag{11.1}$$

One can realize $2N$ Majoranas in a standard way on a complex Hilbert space of dimension 2^N, and we use this representation. Start with the real Hilbert space $\mathcal{H}_r = \wedge \mathbb{R}^N$, the real exterior algebra over $\mathbb{R}^N$. Let a_j^* denote the linear transformation on $\mathcal{H}_r$ given the exterior product $e_j \wedge$ with the jth basis element e_j in $\mathbb{R}^N$. These operators and their adjoint a_j are N fermionic creation and annihilation operators. Let $\mathcal{H}$ denote the complexification of $\mathcal{H}_r$ and define the Majorana operators c_{2j-1}, c_{2j} as linear combinations, $c_{2j-1} = a_j + a_j^*$ and $c_{2j} = i\left(a_j - a_j^*\right)$. Thus our odd indexed Majoranas are real and the even Majoranas are purely imaginary.

We consider the index j of the Majoranas to have a geometric significance as an element of a simple cubic lattice $\Lambda = \Lambda_- \cup \Lambda_+$. We assume that Λ is invariant under a reflection ϑ in a plane Π normal to a coordinate direction and intersecting no sites in Λ, so $\vartheta(\Lambda) = \Lambda$. Here $\Lambda_\pm$ denote the sites on the $\pm$ side of Π. We assume that the reflection ϑ maps $\Lambda_\pm$ into $\Lambda_\mp$.

For any subset $\mathcal{B} \subset \Lambda$, let $\mathfrak{A}(\mathcal{B})$ denote the algebra generated by the c_j's with $j \in \mathcal{B}$. Let $\mathfrak{A} = \mathfrak{A}(\Lambda)$ and $\mathfrak{A}_\pm = \mathfrak{A}(\Lambda_\pm)$. Also introduce the even algebras $\mathfrak{A}(\mathcal{B})^{even}$, as the subset of $\mathfrak{A}(\mathcal{B})$ generated by even monomials in the c_j's, with $j \in \mathcal{B}$. Note that $\mathfrak{A}^{even}$ is not abelian, but $\mathfrak{A}^{even}(\mathcal{B})$ commutes with $\mathfrak{A}^{even}(\mathcal{B}')$ when $\mathcal{B} \cap \mathcal{B}' = \varnothing$.

Anti-unitary transformations

An antilinear transformation Θ on the finite-dimensional complex Hilbert space $\mathcal{H}$ has the property $\Theta(f + \lambda g) = \Theta f + \bar{\lambda}\Theta g$ for $f, g \in \mathcal{H}$ and $\lambda \in \mathbb{C}$. Here $\bar{\lambda}$ denotes the complex conjugate of λ. Assuming $\mathcal{H}$ has the hermitian inner product $\langle \cdot, \cdot \rangle$, the adjoint Θ^* of Θ is the anti-linear transformation

$$\langle f, \Theta^* g \rangle = \langle g, \Theta f \rangle. \tag{11.2}$$

Also Θ is said to be anti-unitary if for all $f, g \in \mathcal{H}$,

$$\langle f, g \rangle = \langle \Theta g, \Theta f \rangle = \langle \Theta^* g, \Theta^* f \rangle. \tag{11.3}$$

As a consequence an anti-unitary satisfies $\Theta\Theta^* = \Theta^*\Theta = I$ or $\Theta^* = \Theta^{-1}$.

We are especially interested in an anti-unitary representation of the reflection ϑ on $\mathcal{H}$, which we also denote by ϑ. The anti-unitary ϑ defines an anti-linear map on $\mathfrak{A}$, with $\vartheta : \mathfrak{A}_\pm \to \mathfrak{A}_\mp$ with the property

$$\vartheta(c_j) = \vartheta c_j \vartheta^{-1} = \overline{c_{\vartheta j}} \,. \tag{11.4}$$

By the general properties of the anti-unitary ϑ,

$$\vartheta(AB) = \vartheta(A)\,\vartheta(B)\,, \qquad \text{and} \quad \vartheta(A)^* = \vartheta(A^*)\,. \tag{11.5}$$

In addition

$$\mathrm{Tr}(\vartheta(A)) = \overline{\mathrm{Tr}(A)}\,, \qquad \text{for all } A \in \mathfrak{A}\,. \tag{11.6}$$

Thus the Clifford algebra relations are also satisfied by $\vartheta(c_j)$,

$$\{\vartheta(c_i), \vartheta(c_j)\} = 2\delta_{ij}I\,. \tag{11.7}$$

In our representation of $\mathfrak{A}$ each Majorana c_j is real or imaginary, so

$$\vartheta(c_j) = \alpha_{\vartheta j}\, c_{\vartheta j}\,, \qquad \text{with} \quad \alpha_{\vartheta j} = \pm 1\,. \tag{11.8}$$

It is no complication to allow a set of n Majorana operators at each lattice site i.

11.3   Hamiltonians

We consider self-adjoint Hamiltonians of the form

$$H = H_- + H_0 + H_+\,, \tag{11.1}$$

where $H_- = H_-^* \in \mathfrak{A}_-^{even}$ and $H_+ = H_+^* \in \mathfrak{A}_+^{even}$. The operator $H_0 = H_0^*$ denotes a coupling across the reflection plane Π. Let $\mathfrak{I} = \{i_1, \ldots, i_k\}$ denote a subset of points in Λ_- with cardinality $n(\mathfrak{I}) = |\mathfrak{I}|$. Define

$$\sigma(\mathfrak{I}) = n(\mathfrak{I}) \mod 2\,. \tag{11.2}$$

We assume that H_0 has the form

$$H_0 = \sum_{\mathfrak{I}} J_{\mathfrak{I}\,\vartheta\mathfrak{I}}\, i^{\sigma(\mathfrak{I})}\, C_{\mathfrak{I}}\, \vartheta(C_{\mathfrak{I}})\,, \qquad \text{where} \quad J_{\mathfrak{I}\,\vartheta\mathfrak{I}} \in \mathbb{R}\,, \tag{11.3}$$

and $C_{\mathfrak{I}} = c_{i_1} c_{i_2} \cdots c_{i_k} \in \mathfrak{A}_-$.

Remark: The Hamiltonian H_0 is self-adjoint and reflection-symmetric,

$$H_0 = H_0^* = \vartheta(H_0)\,. \tag{11.4}$$

Each term in the sum (11.3) defining H_0 is self-adjoint. In fact

$$\left(C_\mathfrak{J}\, \vartheta(C_\mathfrak{J})\right)^* = \vartheta(C_\mathfrak{J})^*\, C_\mathfrak{J}^* = (-1)^{|\mathfrak{J}|}\, C_\mathfrak{J}\, \vartheta(C_\mathfrak{J})\,. \tag{11.5}$$

So from $\overline{i^{\sigma(\mathfrak{J})}} = (-1)^{\sigma(\mathfrak{J})}\, i^{\sigma(\mathfrak{J})}$, and $(-1)^{\sigma(\mathfrak{J})} = (-1)^{|\mathfrak{J}|}$, we infer

$$\left(i^{\sigma(\mathfrak{J})}\, C_\mathfrak{J}\, \vartheta(C_\mathfrak{J})\right)^* = i^{\sigma(\mathfrak{J})}\, C_\mathfrak{J}\, \vartheta(C_\mathfrak{J})\,. \tag{11.6}$$

Likewise

$$\vartheta(H_0) = \sum_\mathfrak{J} (-1)^{|\mathfrak{J}|}\, i^{\sigma(\mathfrak{J})}\, \vartheta(C_\mathfrak{J})\, C_\mathfrak{J} = \sum_\mathfrak{J} i^{\sigma(\mathfrak{J})}\, C_\mathfrak{J}\, \vartheta(C_\mathfrak{J})\,. \tag{11.7}$$

Here we use the fact that the $|\mathfrak{J}|$ Majoranas in $C_\mathfrak{J}$ all anti-commute with the ones in $\vartheta(C_\mathfrak{J})$, yielding another factor $(-1)^{|\mathfrak{J}|}$ in the final equality.

Assumptions on the Couplings: We require that the sign of the couplings $J_{\mathfrak{J}\,\vartheta\mathfrak{J}}$ in (11.3) satisfy

$$\begin{array}{ll} \text{all } J_{\mathfrak{J}\,\vartheta\mathfrak{J}} \leqslant 0\,, \text{ or all } J_{\mathfrak{J}\,\vartheta\mathfrak{J}} \geqslant 0\,, & \text{for terms with } \sigma(\mathfrak{J}) = 1\,, \\ \text{all } J_{\mathfrak{J}\,\vartheta\mathfrak{J}} \leqslant 0\,, & \text{for terms with } \sigma(\mathfrak{J}) = 0\,. \end{array} \tag{11.8}$$

We restrict the sign of couplings only for interaction terms (11.3) that cross the plane Π. Nearest-neighbor two-body interactions have $\sigma(\mathfrak{J}) = 1$.

11.4 Monomial basis

The $2N$ operators c_i yield monomials of the form $M_\beta = c_{i_1} c_{i_2} \cdots c_{i_j}$ of degree j, with $i_1 < i_2 < \cdots i_j$. (Other orders of the c's are the same up to a $\pm$ sign.) Denote by $\beta = 0$ the monomial $M_0 = I$. There are $\binom{2N}{j}$ such monomials M_β of degree j, so there are a total of 2^{2N} such monomials. As $2^{2N} = (\dim \mathcal{H})^2$, these monomials are a candidate for a basis of the space of matrices acting on $\mathcal{H}$.

Proposition 1. *If $\beta \neq 0$, the monomials M_β have vanishing trace, $Tr\,(M_\beta) = 0$. Any linear transformation A on $\mathcal{H}$ can be written in terms of the basis M_β as*

$$A = \sum_\beta a_\beta\, M_\beta\,, \quad where \quad a_\beta = 2^{-N} Tr\,(M_\beta^* A)\,. \tag{11.1}$$

The monomials M_β are an irreducible set of matrices.

Proof. If $\deg M_\beta$ is odd, there is at least one of the c's, say c_j, not contained in M_β. Thus

$$\mathrm{Tr}\,(M_\beta) = \mathrm{Tr}\,(c_j c_j M_\beta) = \mathrm{Tr}\,(c_j M_\beta c_j) = (-1)^{\deg M_\beta}\mathrm{Tr}\,(M_\beta) = -\mathrm{Tr}\,(M_\beta) = 0 \ .$$

On the other hand, if $\deg M_\beta = 2k > 0$, and c_j does occur in M_β, then also

$$\mathrm{Tr}\,(M_\beta) = \mathrm{Tr}\,\left(c_j^2 M_\beta\right) = \mathrm{Tr}\,(c_j M_\beta c_j) = (-1)^{\deg M_\beta - 1}\mathrm{Tr}\,(M_\beta) = -\mathrm{Tr}\,(M_\beta) = 0 \ .$$

Thus we have verified the first statement in the proposition. Also $M_\beta^* M_\beta = I$, and $M_{\beta'}^* M_\beta = \pm M_\gamma$ for some $\gamma \neq 0$.

Suppose that there are coefficients $a_\beta \in \mathbb{C}$ such that $\sum_\beta a_\beta M_\beta = 0$. Then for any β', one has $M_{\beta'}^* \sum_\beta a_\beta M_\beta = \sum_\beta a_\beta M_{\beta'}^* M_\beta = 0$. Taking the trace shows that $a_{\beta'} = 0$, so the M_β are actually linear independent. As there are 2^{2N} matrices M_β, they are a basis for all matrices on $\mathcal{H}$.

Expanding an arbitrary matrix A in this basis, we calculate the coefficients in (11.1) using $\mathrm{Tr}\,I = 2^N$. As the set of all matrices on $\mathcal{H}$ is irreducible, the basis M_β is also irreducible. $\qquad\square$

11.5   Reflection positivity

In this section we consider traces on the Hilbert space $\mathcal{H} = \wedge\mathbb{C}^N$.

Proposition 2 (Reflection Positivity I). *Consider an operator $A \in \mathfrak{A}_\pm$, then*

$$Tr(A\,\vartheta(A)) \geqslant 0\,. \tag{11.1}$$

Proof. The operator $A \in \mathfrak{A}_\pm$ can be expanded as a polynomial in the basis M_β of Proposition 15. The monomials that appear in the expansion all belong to $\mathfrak{A}_\pm$. Write

$$A = \sum_\beta a_\beta\, M_\beta\,, \qquad \text{and} \quad \vartheta(A) = \sum_\beta \overline{a_\beta}\,\vartheta(M_\beta)\,. \tag{11.2}$$

We now consider the case $A \in \mathfrak{A}_-$. Let ι_β denote the number of purely-imaginary Majoranas in M_β. For $M_\beta = c_{i_1}\cdots c_{i_k}$, define $M_{\vartheta\beta} = c_{\vartheta i_1}\cdots c_{\vartheta i_k}$. One then has

$$\mathrm{Tr}\,(A\,\vartheta(A)) = \sum_{\beta,\beta'} a_\beta\,\overline{a_{\beta'}}\,\mathrm{Tr}\,(M_\beta\,\vartheta(M_{\beta'})) = \sum_{\beta,\beta'}(-1)^{\iota_{\beta'}}a_\beta\,\overline{a_{\beta'}}\,\mathrm{Tr}\,(M_\beta\,M_{\vartheta\beta'})\,.$$

$$\tag{11.3}$$

Since $M_\beta \in \mathfrak{A}_-$ and $M_{\vartheta\beta'} \in \mathfrak{A}_+$, they are products of different Majoranas. We infer from Proposition 15 that the trace vanishes unless $\beta = \vartheta\beta' = 0$. As $\iota_0 = 0$,

$$\mathrm{Tr}\,(A\,\vartheta(A)) = 2^N\,|a_0|^2 \geqslant 0\,, \tag{11.4}$$

as claimed. $\qquad\qquad\qquad\qquad\qquad\qquad\qquad\qquad\qquad\qquad\qquad\qquad$ $\square$

This reflection positivity allows one to define a pre-inner product on $\mathfrak{A}_\pm$ given by

$$\langle A, B\rangle_{\mathrm{RP}} = \mathrm{T}r(A\,\vartheta(B))\,. \tag{11.5}$$

This pre-inner product satisfies the Schwarz inequality

$$|\langle A, B\rangle_{\mathrm{RP}}|^2 \leqslant \langle A, A\rangle_{\mathrm{RP}}\,\langle B, B\rangle_{\mathrm{RP}}\,. \tag{11.6}$$

In the standard way, one obtains an inner product $\langle \widehat{A}, \widehat{B}\rangle_{\mathrm{RP}}$ and norm $\|\widehat{A}\|_{\mathrm{RP}}$ by defining the inner product on equivalence classes $\widehat{A} = \{A + n\}$ of A's, modulo elements n of the null space of the functional (11.5) on the diagonal. In order to simplify notation, we ignore this distinction.

11.6 The main result

Here we consider reflection-positivity of the functional

$$\mathrm{T}r(A\,\vartheta(B)\,e^{-H})\,, \qquad \text{for} \quad A, B \in \mathfrak{A}_\pm^{even}\,, \tag{11.7}$$

that is linear in A and anti-linear in B.

Theorem 3 (Reflection Positivity II). *Consider* $A \in \mathfrak{A}_\pm^{even}$ *and* H *of the form (14.16), with* $H_+ = \vartheta(H_-)$*. Then the functional (11.7) is positive on the diagonal,*

$$0 \leqslant Tr(A\,\vartheta(A)\,e^{-H})\,. \tag{11.8}$$

Remark: The functional (11.8) does not satisfy reflection positivity on the full fermonic algebra $\mathfrak{A}_\pm$. Even for $N = 1$, with $H_\pm = 0$, $H_0 = -i\,c_1\vartheta(c_1)$, and $A = c_1$, reflection positivity fails. In this case

$$\mathrm{T}r(A\,\vartheta(A)\,e^{-H}) = -2i\sinh 1\,, \tag{11.9}$$

is purely imaginary. A similar argument shows that reflection positivity fails in case the coupling constants do not obey the restrictions (11.8).

If the interaction terms in H_0 all have $\sigma_{\mathfrak{I}} = 0$, then the functional (11.8) vanishes on odd elements of $\mathfrak{A}$, and in this case reflection-positivity extends trivially to the full algebra.

There is a natural second reflection positivity condition connected with the functional

$$\text{Tr}(\vartheta(A)B\,e^{-H}), \qquad \text{for} \quad A, B \in \mathfrak{A}_{\pm}^{even}, \tag{11.10}$$

in place of (11.8). The properties (11.5)–(11.6) ensure that

$$\text{Tr}(\vartheta(A)B\,e^{-H}) = \overline{\text{Tr}(A\vartheta(B)\,e^{-\vartheta(H)})}. \tag{11.11}$$

Since the assumed properties for H hold also for $\vartheta(H)$ with $H_{\mp}$ replaced by $\vartheta(H_{\pm})$, we infer the following corollary.

Corollary 4 (**Reflection Positivity III**). *Consider $A \in \mathfrak{A}_{\pm}^{even}$ and H of the form (14.16), with $H_+ = \vartheta(H_-)$. Then the functional (11.10) is positive on the diagonal,*

$$0 \leqslant \text{Tr}(\vartheta(A)A\,e^{-H}). \tag{11.12}$$

of Theorem 3. Our argument is motivated by [189, 190, 159], but has its own special features. Take $A \in \mathfrak{A}_{-}^{even}$. Use the Lie product formula for matrices α_1, α_2, and α_3 in the form

$$e^{\alpha_1+\alpha_2+\alpha_3} = \lim_{k\to\infty} \left((1+\alpha_1/k)e^{\alpha_2/k}e^{\alpha_3/k}\right)^k. \tag{11.13}$$

This is norm-convergent for matrices.

Take $\alpha_1 = -H_0$, $\alpha_2 = -H_-$, and $\alpha_3 = -H_+ = -\vartheta(H_-)$ in (11.13). Here H_0 is defined in (11.3), and it can be written

$$H_0 = \sum_{\ell=1}^{L-1} J_{\mathfrak{I}_\ell \vartheta \mathfrak{I}_\ell}\, i^{\sigma(\mathfrak{I}_\ell)}\, C_{\mathfrak{I}_\ell}\, \vartheta(C_{\mathfrak{I}_\ell}). \tag{11.14}$$

Here we label the non-empty subsets of Λ_- by $\mathfrak{I}_\ell$, for $\ell = 1, \ldots, L-1$, with $L = 2^{|\Lambda_-|}$. Label the empty subset $\varnothing$ by $\mathfrak{I}_0$. The sum (11.3) defining H_0 ranges over the non-empty subsets. Then using (11.13),

$$A\,\vartheta(A)\,e^{-H} = \lim_{k\to\infty} A\,\vartheta(A)\left(e^{-H}\right)_k, \tag{11.15}$$

where

$$\left(e^{-H}\right)_k = \left((I - \sum_{\ell=1}^{L-1} J_{\mathfrak{I}_\ell \vartheta \mathfrak{I}_\ell}\, i^{\sigma(\mathfrak{I}_\ell)}\, C_{\mathfrak{I}_\ell}\, \vartheta(C_{\mathfrak{I}_\ell})/k)\, e^{-H_-/k}\, e^{-\vartheta(H_-)/k}\right)^k. \tag{11.16}$$

One can include the term I in the sums in (11.16) by defining $-J_{\varnothing\,\vartheta\varnothing} = k$, $C_\varnothing = C_{\vartheta\varnothing} = I$, and $n(\mathfrak{I}_{\ell_0}) = n(\varnothing) = 0$. Then

$$
\left(e^{-H}\right)_k = \frac{1}{k^k}\left(-\sum_{\ell=0}^{L-1} J_{\mathfrak{I}_\ell\,\vartheta\mathfrak{I}_\ell}\, i^{\sigma(\mathfrak{I}_\ell)}\, C_{\mathfrak{I}_\ell}\,\vartheta(C_{\mathfrak{I}_\ell})\, e^{-H_-/k}\, e^{-\vartheta(H_-)/k}\right)^k
$$

$$
= \sum_{\ell_1,\dots,\ell_k=0}^{L-1} i^{\sum_{i=1}^k \sigma(\mathfrak{I}_{\ell_i})}\, \mathfrak{c}_{\ell_1,\dots,\ell_k}\, Y_{\ell_1,\dots,\ell_k}\,. \tag{11.17}
$$

In the second equality we have expanded the expression into a linear combination of L^k terms with coefficients

$$
\mathfrak{c}_{\ell_1,\dots,\ell_k} = \frac{1}{k^k}\prod_{i=1}^k\left(-J_{\mathfrak{I}_{\ell_i}\,\vartheta\mathfrak{I}_{\ell_i}}\right), \tag{11.18}
$$

and with

$$
Y_{\ell_1,\dots,\ell_k} = C_{\mathfrak{I}_{\ell_1}}\vartheta(C_{\mathfrak{I}_{\ell_1}})\, e^{-H_-/k}\, e^{-\vartheta(H_-)/k}\cdots C_{\mathfrak{I}_{\ell_k}}\vartheta(C_{\mathfrak{I}_{\ell_k}})\, e^{-H_-/k}\, e^{-\vartheta(H_-)/k}\,. \tag{11.19}
$$

Using this expansion, (11.15) can be written

$$
A\,\vartheta(A)\left(e^{-H}\right)_k = \sum_{\ell_1,\dots,\ell_k=0}^{L-1} i^{\sum_{i=1}^k \sigma(\mathfrak{I}_{\ell_i})}\, \mathfrak{c}_{\ell_1,\dots,\ell_k}\, A\,\vartheta(A)\, Y_{\ell_1,\dots,\ell_k}\,. \tag{11.20}
$$

Lemma 5. *The trace $\mathrm{Tr}(A\,\vartheta(A)\,Y_{\ell_1,\dots,\ell_k}) = 0$ vanishes unless*

$$
\sum_{i=1}^k n(\mathfrak{I}_{\ell_i}) = 2\mathfrak{N}\,, \tag{11.21}
$$

is an even integer. In this case,

$$
\sum_{i=1}^k \sigma(\mathfrak{I}_{\ell_i}) = 0 \quad \mathrm{mod}\ 2\,, \qquad and \quad 0 \leqslant \mathfrak{c}_{\ell_1,\dots,\ell_k}\,. \tag{11.22}
$$

Proof. In order to establish (11.21), recall that we assume that the factor A in $A\,\vartheta(A)\,Y_{\ell_1,\dots,\ell_k}$ is an element of $\mathfrak{A}_-^{even}$. Therefore we can expand it as a sum of the form (11.1), with all the basis elements $M_\beta \in \mathfrak{A}_-^{even}$. As $H_- \in \mathfrak{A}_-^{even}$, one can also expand each factor $e^{-H_-/k}$ as a sum of even basis elements $M_\beta \in \mathfrak{A}_-^{even}$. Each *interaction term*, defined as a summand $C_{\mathfrak{I}_{\ell_j}}\vartheta(C_{\mathfrak{I}_{\ell_j}})$ in H_0, contains $n(\mathfrak{I}_{\ell_j})$ Majoranas in $\mathfrak{A}_-$ and an equal number in $\mathfrak{A}_+$.

We infer from Proposition 15 that the trace of $A\,\vartheta(A)\,Y_{\ell_1,\ldots,\ell_k}$ vanishes unless each c_i occurs in $A\,\vartheta(A)\,Y_{\ell_1,\ldots,\ell_k}$ an even number of times. Consequently any $A\,\vartheta(A)\,Y_{\ell_1,\ldots,\ell_k}$ with non-zero trace must have an even number of Majoranas in $\mathfrak{A}_-$. In other words, the condition (11.21) must hold. This ensures the number of odd $n(\mathfrak{I}_{\ell_j})$ is even. As $\sigma(\mathfrak{I}_{\ell_j}) = n(\mathfrak{I}_{\ell_j}) \mod 2$, the sum of $\sigma(\mathfrak{I}_{\ell_j})$'s equals $0 \mod 2$.

We next show that $0 \leqslant \mathfrak{c}_{\ell_1,\ldots,\ell_k}$. Suppose the interaction term $C_{\mathfrak{I}_{\ell_j}}\vartheta(C_{\mathfrak{I}_{\ell_j}})$ occurs as a factor in $A\,\vartheta(A)\,Y_{\ell_1,\ldots,\ell_k}$ and has $\sigma(\mathfrak{I}_{\ell_j}) = 0$. Then the restriction on the coupling constants (11.8) means that $0 \leqslant -J_{\mathfrak{I}_{\ell_j}\vartheta\mathfrak{I}_{\ell_j}}$. On the other hand, the condition (11.22) on $\sigma(\mathfrak{I}_{\ell_j})$ means that an even number of interaction terms in $A\,\vartheta(A)\,Y_{\ell_1,\ldots,\ell_k}$ have $\sigma(\mathfrak{I}_{\ell_j}) = 1$. From the restriction (11.8), we infer that these couplings all have the same sign. Hence the product of the negative of these coupling constants is also positive. Finally we use $0 < J_{\varnothing\,\vartheta\varnothing}$ to complete the proof. $\square$

Lemma 6. *Assume relations (11.21)–(11.22). Then the $Y_{\ell_1,\ldots,\ell_k}$ in (11.19) satisfy the identities*

$$Y_{\ell_1,\ldots,\ell_k} = i^{-\sum_{i=1}^{k}\sigma(\mathfrak{I}_{\ell_i})}\; D_{\ell_1,\ldots,\ell_k}\,\vartheta(D_{\ell_1,\ldots,\ell_k})\,, \tag{11.23}$$

where

$$D_{\ell_1,\ldots,\ell_k} = C_{\mathfrak{I}_{\ell_1}}\,e^{-H_-/k}\,C_{\mathfrak{I}_{\ell_2}}\,e^{-H_-/k}\cdots C_{\mathfrak{I}_{\ell_k}}\,e^{-H_-/k} \in \mathfrak{A}_-^{even}\,. \tag{11.24}$$

Proof. As $e^{-H_+/k} = e^{-\vartheta(H_-)/k} = \vartheta(e^{-H_-/k})$, the product $Y_{\ell_1,\ldots,\ell_k}$ in (11.19) differs from the product $D_{\ell_1,\ldots,\ell_k}\,\vartheta(D_{\ell_1,\ldots,\ell_k})$, only in the order of its factors. In order to transform from one product into the other, we need to move all the Majorana operators of $Y_{\ell_1,\ldots,\ell_k}$ that are localized in $\mathfrak{A}_-$ to the left, and all operators of $Y_{\ell_1,\ldots,\ell_k}$ in $\mathfrak{A}_+$ to the right. We move each operator c_j as far as possible to the left, without permuting the order of any operator in $\mathfrak{A}_-$. As $H_+ \in \mathfrak{A}_+^{even}$, it commutes with each $c_j \in \mathfrak{A}_-$. Likewise $H_- \in \mathfrak{A}_-^{even}$, it commutes with each $c_j \in \mathfrak{A}_+$. This procedure neither changes any of the exponentials $e^{-H_\pm/k}$. It gives rise to a minus sign only each time we permute a c_j in an interaction term to the left past an operator $\vartheta(c_{j'})$ in another interaction term.

We count the minus signs that occur from permuting the c's in the interaction terms. In order to simplify notation, let $n_{\ell_i} = n(\mathfrak{I}_{\ell_i})$. The term $C_{\mathfrak{I}_{\ell_1}}\vartheta(C_{\mathfrak{I}_{\ell_1}})$ contributes no minus sign. The term $C_{\mathfrak{I}_{\ell_2}}\vartheta(C_{\mathfrak{I}_{\ell_2}})$ contributes $n_{\ell_2}n_{\ell_1}$ minus signs. The term $C_{\mathfrak{I}_{\ell_3}}\vartheta(C_{\mathfrak{I}_{\ell_3}})$ contributes $n_{\ell_3}(n_{\ell_1}+n_{\ell_2})$ minus signs. The term $C_{\mathfrak{I}_{\ell_4}}\vartheta(C_{\mathfrak{I}_{\ell_4}})$ contributes $n_{\ell_4}(n_{\ell_1}+n_{\ell_2}+n_{\ell_3})$ minus signs, and so on. Finally, the term

$$C_{\mathfrak{I}_{\ell_k}}\vartheta(C_{\mathfrak{I}_{\ell_k}})$$

contributes $n_{\ell_k} \sum_{i=1}^{k-1} n_{\ell_i}$ minus signs. Adding these numbers, one obtains a total number of minus signs equal to

$$\frac{1}{2} \sum_{i,i'=1}^{k} n_{\ell_i} \, n_{\ell_{i'}} - \frac{1}{2} \sum_{i=1}^{k} n_{\ell_i}^2 = \frac{1}{2} \left(\sum_{i=1}^{k} n_{\ell_i} \right)^2 - \frac{1}{2} \sum_{i=1}^{k} n_{\ell_i}^2 = 2\mathfrak{N}^2 - \frac{1}{2} \sum_{i=1}^{k} n_{\ell_i}^2 \,. \tag{11.25}$$

Here $\mathfrak{N}$ is defined in (11.21). We infer that

$$\left(2\mathfrak{N}^2 - \frac{1}{2} \sum_{i=1}^{k} n_{\ell_i}^2 \right) \mod 2 = -\frac{1}{2} \sum_{i=1}^{k} n_{\ell_i}^2 \mod 2 \,. \tag{11.26}$$

The overall sign arising from the permutation of the c's in going from (11.19) to (11.23) is (-1) raised to the power (11.26). This is

$$(-1)^{-\frac{1}{2} \sum_{i=1}^{k} n_{\ell_i}^2} = i^{-\sum_{i=1}^{k} n_{\ell_i}^2} = i^{-\sum_{i=1}^{k} (n_{\ell_i} \mod 2)} = i^{-\sum_{i=1}^{k} \sigma_{\ell_i}} \,. \tag{11.27}$$

In the second equality we use an identity for natural numbers n, namely

$$n^2 \mod 4 = n \mod 2 \,. \tag{11.28}$$

In the final equality we use the definition $\sigma_{\ell_i} = n_{\ell_i} \mod 2$. $\qquad \square$

Completion of the proof of Theorem 3. In case $\mathrm{Tr}(A\,\vartheta(A)\,Y_{\ell_1,\dots,\ell_k}) \neq 0$, we infer from (11.20) along with Lemmas 5 and 6 and the fact that $\vartheta(A)$ commutes with $D_{\ell_1,\dots,\ell_k}$ that

$$\mathrm{Tr}\left(A\,\vartheta(A)\,e^{-H} \right) = \lim_{k \to \infty} \sum_{\ell_1,\dots,\ell_k=0}^{L-1} \mathfrak{c}_{\ell_1,\dots,\ell_k} \, \mathrm{Tr}\left(A D_{\ell_1,\dots,\ell_k} \vartheta\left(A D_{\ell_1,\dots,\ell_k} \right) \right) \,. \tag{11.29}$$

From Lemma 5, we know that $0 \leqslant \mathfrak{c}_{\ell_1,\dots,\ell_k}$. And from Proposition 2, we know that $0 \leqslant \mathrm{Tr}\left(A D_{\ell_1,\dots,\ell_k} \vartheta\left(A D_{\ell_1,\dots,\ell_k} \right) \right)$. Thus (11.29) is a sum of positive terms. This completes the proof in the case that $A \in \mathfrak{A}_{-}^{even}$.

The remaining case is $A \in \mathfrak{A}_{+}^{even}$. Then one has $A = \vartheta(\widetilde{A})$ with $\widetilde{A} \in \mathfrak{A}_{-}^{even}$. As A commutes with $\vartheta(A)$, we infer that $A\,\vartheta(A) = \widetilde{A}\,\vartheta(\widetilde{A})$, and $\mathrm{Tr}\left(A\,\vartheta(A)\,e^{-H} \right) = \mathrm{Tr}\left(\widetilde{A}\,\vartheta(\widetilde{A})\,e^{-H} \right) \geqslant 0$ as a consequence of the case already established. $\qquad \square$

Reflection-positive inner product

Let us introduce the modified pre-inner product on $\mathfrak{A}_{\pm}^{even}$ defined by the functional (11.8). Let

$$\langle A, B \rangle_{\mathrm{RP}} = \mathrm{Tr}(A\,\vartheta(B)\,e^{-H}) \,. \tag{11.30}$$

Denote the corresponding semi-norm by $\|A\|_{\mathrm{RP}}$.

The theorem shows that one has an elementary reflection positivity bound, arising from the Schwarz inequality. Also ϑ acts as anti-unitary transformation on the Hilbert space $\mathfrak{A}_{\pm}^{even}$ with inner product (11.30).

Corollary 7. *For $A, B \in \mathfrak{A}_{\pm}^{even}$, one has*

$$|\langle A, B \rangle_{RP}| \leqslant \|A\|_{RP} \, \|B\|_{RP} \, , \tag{11.31}$$

and

$$\langle A, B \rangle_{RP} = \langle \vartheta(B), \vartheta(A) \rangle_{RP} \, , \qquad so \quad \|\vartheta(A)\|_{RP} = \|A\|_{RP} \, . \tag{11.32}$$

11.7   Relation to spin systems

It is well-known that the ferromagnetic Ising model is reflection-positive, but the quantum Heisenberg model is not reflection-positive [**?**]. We can also infer these facts from the point of view of Majoranas.

One can consider the infinitesimal rotation matrices in the (α, β)-plane, $\Sigma^{\alpha\beta} = \frac{-i}{2}\left[\gamma^\alpha, \gamma^\beta\right]$, with γ^α the Euclidean Dirac matrices on 4-space with coordinate labels $\alpha, \beta \in \{0, x, y, z\}$. In the notation sometimes used in condensed-matter physics, one assigns Dirac matrices γ_j^α as four Majoranas c_j, b_j^x, b_j^y, b_j^z at each lattice site. We use a real representation for b_j^x and b_j^z, and an imaginary representation for b_j^y and c_j. One could also use a real representation for b_j^y and c_j, and an imaginary representation for b_j^x and b_j^z.

Then the three $(0, \alpha)$ planes yield $\Sigma_j^{0\alpha} = \sigma_j^\alpha = i \, b_j^\alpha c_j$. They agree with the Pauli matrices when projected to one chiral copy, namely to the subspace of the Hilbert space $\mathcal{H}$ of the Majoranas, on which each of the mutually commuting operators $\gamma_j^5 = b_j^x b_j^y b_j^z c_j$ has the eigenvalue $+1$. Note that each γ_j commutes with all the $\boldsymbol{\sigma}_{j'}$. With these choices, the $\sigma_j^{x,z}$ are real, while σ_j^y is imaginary.[1]

For a reflection across a nearest-neighbor bond (ij), a ferromagnetic Ising interaction term is

$$-\sigma_i^z \sigma_j^z = b_i^z c_i b_j^z c_j = -b_i^z c_i \, \vartheta \left(b_i^z c_i\right) \, . \tag{11.33}$$

---

[1] These three operators correspond to half of the generators $\Sigma_j^{\alpha\beta}$, and we use this representation. The other three generators $\Sigma_j^{\alpha\beta}$ for $\alpha, \beta \neq 0$ act the same on both chiral copies, and as they are isomorphic on each copy they yield an alternative representation $\sigma_j^x = -i b_j^y \, b_j^z$, etc., which is also sometimes used in the condensed-matter literature.

This satisfies condition (11.8) with $k = 2$ and $\sigma = 0$. Similarly, the quantum "rotator" Hamiltonian has an interaction term,

$$-\sigma_i^x \, \sigma_j^x - \sigma_i^z \, \sigma_j^z = -b_i^x c_i \, \vartheta \left(b_i^x c_i \right) - b_i^z c_i \, \vartheta \left(b_i^z c_i \right) \ . \tag{11.34}$$

This also satisfies condition (11.8), and so is reflection-positive. The corresponding quantum Heisenberg interaction term is

$$-\boldsymbol{\sigma}_i \cdot \boldsymbol{\sigma}_j = -\sigma_i^x \, \sigma_j^x - \sigma_i^y \, \sigma_j^y - \sigma_i^z \, \sigma_j^z = -b_i^x c_i \, \vartheta \left(b_i^x c_i \right) + b_i^y c_i \, \vartheta \left(b_i^y c_i \right) - b_i^z c_i \, \vartheta \left(b_i^z c_i \right) \ . \tag{11.35}$$

This does not satisfy (11.8), since one of the interaction coefficients of the term $b_i^y c_i \, \vartheta \left(b_i^y c_i \right)$ arising from $-\sigma_i^y \, \sigma_j^y$ is positive. (Note these properties are the same in the alternative representation.)

11.8 Reflection bounds

The use of reflection bounds and their iteration has many applications, both in statistical physics and quantum field theory. Here we study some bounds which follow from the results of Section 11.5, that we apply in [185].

Let us introduce two pre-inner products $\langle \, \cdot \, , \cdot \, \rangle_{\mathrm{RP}\pm}$ on the algebras $\mathfrak{A}_{\pm}^{even}$, corresponding to two reflection symmetric Hamiltonians. Let

$$\langle A, B \rangle_{\mathrm{RP}-} = \mathrm{Tr}(A \, \vartheta(B) \, e^{-H}) \, , \quad \text{for} \quad H = H_- + H_0 + \vartheta(H_-) \, . \tag{11.1}$$

Similarly define

$$\langle A, B \rangle_{\mathrm{RP}+} = \mathrm{Tr}(A \, \vartheta(B) \, e^{-H}) \, , \quad \text{for} \quad H = \vartheta(H_+) + H_0 + H_+ \, . \tag{11.2}$$

As previously, one can define inner products on equivalence classes, yielding norms $\| \cdot \|$.

Proposition 8 (RP-Bounds). *Let $H = H_- + H_0 + H_+$ with $H_\pm \in \mathfrak{A}_\pm^{even}$ and H_0 of the form (11.3). Then*

$$\left| Tr(A \, \vartheta(B) \, e^{-H}) \right| \leqslant \|A\|_{RP-} \, \|B\|_{RP+} \, , \quad \text{for} \quad A, B \in \mathfrak{A}_-^{even} \, . \tag{11.3}$$

Also

$$\left| Tr(A \, \vartheta(B) \, e^{-H}) \right| \leqslant \|A\|_{RP+} \, \|B\|_{RP-} \, , \quad \text{for} \quad A, B \in \mathfrak{A}_+^{even} \, . \tag{11.4}$$

In particular for $A = B = I$,

$$Tr(e^{-H}) \leqslant Tr(e^{-(H_- + H_0 + \vartheta(H_-))})^{1/2} \, Tr(e^{-(\vartheta(H_+) + H_0 + H_+)})^{1/2} \, . \tag{11.5}$$

Proof. The proof of (11.3) follows the proof of Theorem 3. Use the expression (11.16) to write $A\,\vartheta(B)\left(e^{-H}\right)_k$, which converges to $A\,\vartheta(B)\,e^{-H}$ as $k \to \infty$, namely

$$
\begin{aligned}
\mathrm{Tr}\left(A\,\vartheta(B)\left(e^{-H}\right)_k\right) &= \sum_{\ell_1,\dots,\ell_k=0}^{L-1} \mathfrak{c}_{\ell_1,\dots,\ell_k}\,\mathrm{Tr}\left(AD^-_{\ell_1,\dots,\ell_k}\,\vartheta\left(BD^+_{\ell_1,\dots,\ell_k}\right)\right) \\
&= \sum_{\ell_1,\dots,\ell_k=0}^{L-1} \mathfrak{c}_{\ell_1,\dots,\ell_k}\langle AD^-_{\ell_1,\dots,\ell_k}, BD^+_{\ell_1,\dots,\ell_k}\rangle_{\mathrm{RP}} \,.
\end{aligned}
$$

(11.6)

The form $\langle\,\cdot\,,\,\cdot\,\rangle_{\mathrm{RP}}$ in (11.6) is defined in (11.5). The difference is that now the terms contain $\vartheta(B)$ in place of $\vartheta(A)$, and $D^\pm_{\ell_1,\dots,\ell_k}$ depends on $H_\pm$. Thus the constants $\mathfrak{c}_{\ell_1,\dots,\ell_k}$ are given by (11.18), the matrices $D^-_{\ell_1,\dots,\ell_k} \in \mathfrak{A}^{even}_-$ are given by (11.24), and

$$
\vartheta(D^+_{\ell_1,\dots,\ell_k}) = \vartheta(C_{\mathfrak{I}_{\ell_1}})e^{-H_+/k}\vartheta(C_{\mathfrak{I}_{\ell_2}})e^{-H_+/k}\cdots\vartheta(C_{\mathfrak{I}_{\ell_k}})e^{-H_+/k} \in \mathfrak{A}^{even}_+ \,.
$$

(11.7)

Lemma 5 depends only on the form of H_0 and the fact that $H_\pm \in \mathfrak{A}^{even}_\pm$. Thus the lemma applies in this case as well. With these substitutions, the proof of Lemma 6 also applies.

To establish (11.3), note that the product of couplings $\mathfrak{c}_{\ell_1,\dots,\ell_k}$ defined in (11.18) are independent of A and B, so as before we infer from Lemma 5 that $\mathfrak{c}_{\ell_1,\dots,\ell_k} \geqslant 0$ whenever $\langle AD^-_{\ell_1,\dots,\ell_k}, BD^+_{\ell_1,\dots,\ell_k}\rangle_{\mathrm{RP}} \neq 0$. Use the Schwarz inequality for $\langle\,\cdot\,,\cdot\,\rangle_{\mathrm{RP}}$ and the positivity of $\mathfrak{c}_{\ell_1,\dots,\ell_k}$ to obtain

$$
\begin{aligned}
\left|\mathrm{Tr}\left(A\,\vartheta(B)\,e^{-H}\right)\right| &= \left|\lim_{k\to\infty}\sum_{\ell_1,\dots,\ell_k=0}^{L-1}\mathfrak{c}_{\ell_1,\dots,\ell_k}\langle AD^-_{\ell_1,\dots,\ell_k}, BD^+_{\ell_1,\dots,\ell_k}\rangle_{\mathrm{RP}}\right| \\
&\leqslant \lim_{k\to\infty}\sum_{\ell_1,\dots,\ell_k=0}^{L-1}\mathfrak{c}^{1/2}_{\ell_1,\dots,\ell_k}\langle AD^-_{\ell_1,\dots,\ell_k}, AD^-_{\ell_1,\dots,\ell_k}\rangle^{1/2}_{\mathrm{RP}} \\
&\qquad\times \mathfrak{c}^{1/2}_{\ell_1,\dots,\ell_k}\langle BD^+_{\ell_1,\dots,\ell_k}, BD^+_{\ell_1,\dots,\ell_k}\rangle^{1/2}_{\mathrm{RP}} \\
&\leqslant \lim_{k\to\infty}\left(\sum_{\ell_1,\dots,\ell_k=0}^{L-1}\mathfrak{c}_{\ell_1,\dots,\ell_k}\langle AD^-_{\ell_1,\dots,\ell_k}, AD^-_{\ell_1,\dots,\ell_k}\rangle_{\mathrm{RP}}\right)^{1/2} \\
&\qquad\times\left(\sum_{\ell_1,\dots,\ell_k=0}^{L-1}\mathfrak{c}_{\ell_1,\dots,\ell_k}\langle BD^+_{\ell_1,\dots,\ell_k}, BD^+_{\ell_1,\dots,\ell_k}\rangle_{\mathrm{RP}}\right)^{1/2} \\
&= \langle A, A\rangle^{1/2}_{\mathrm{RP}-}\langle B, B\rangle^{1/2}_{\mathrm{RP}+} = \|A\|_{\mathrm{RP}-}\|B\|_{\mathrm{RP}+}\,. \qquad (11.8)
\end{aligned}
$$

This completes the proof of relation (11.3).

When $A, B \in \mathfrak{A}_+^{even}$, substitute in the left-hand side of (11.4) $A = \vartheta(\widetilde{A})$ and $B = \vartheta(\widetilde{B})$ with $\widetilde{A}, \widetilde{B} \in \mathfrak{A}_-^{even}$. Since A and B commute with $\vartheta(A)$ and $\vartheta(B)$,

$$\left| \mathrm{Tr}(A\,\vartheta(B)\,e^{-H}) \right| = \left| \mathrm{Tr}(\widetilde{B}\,\vartheta(\widetilde{A})\,e^{-H}) \right| . \tag{11.9}$$

Replacing H_- by $\vartheta(H_+)$ and $\vartheta(H_-)$ by H_+ in the bound (11.3) completes the proof of (11.4). $\qquad\square$

11.9 Acknowledgement

Vortex Loops and Majoranas

We investigate the role that vortex loops play in characterizing eigenstates of interacting Majoranas. As an application of our general result, we investigate the ground states of certain ladder Hamiltonians. We show how the relative signs of the coupling constants determine the vortex configuration of ground states. Two methods yield exact results: i.) We utilize the equivalence of spin Hamiltonians with quartic interactions of Majoranas. ii) We use reflection positivity for Majoranas to characterize vortices. Two additional methods suggest potential wider applicability of these results: iii.) Numerical evidence suggests similar behavior for certain systems without reflection symmetry. iv.) A perturbative analysis also suggests similar behavior without the assumption of reflection symmetry.

12.1   Introduction

In §12.2 we define a family of Hamiltonians with nearest-neighbor Majorana interactions on a cubic lattice in arbitrary dimension. In this section we assume the existence of a reflection plane leaving the lattice invariant

and transforming the Hamiltonians in a simple way. Using reflection-positivity one can characterize vortex loop configurations of the Hamiltonians that minimize the ground state energy within the given family.When all the coupling constants are positive (or negative), the minimal-energy is achieved for a vortex-free ground state. This property of vortex loops is related to results of Lieb, [159] Macris, and Nachtergaele [160] for hopping Hamiltonians.

In §12.3–§12.6 we apply these results to spin ladders and their Majorana fermionic representations. The ladders we study have their origin in the "compass model" introduced by Kugel and Khomskii [29] to study the Jahn-Teller effect in magnetic insulators. Kitaev studied a honeycomb version of this model extensively. [27] This and other similar models arise frequently in the study of quantum information theory, see for instance [34, 143, 156, 170, 35, 36, 182, 193, 194]. While in much of this paper we analyze ladders as an example, most of our results extend in a straightforward way to models defined on a honeycomb lattice with similar trivalent couplings at each site.

In §12.5 we show that the spectrum of an open spin ladder coincides with the spectrum of its Majorana fermionic representation, aside from multiplicity. While the spectrum of a closed spin ladder seems not to have this property, we conjecture that the ground state energies are the same.

In §12.7 we study certain ladders numerically. These ladders do not possess the symmetry required to use reflection-positivity arguments. Numerical evidence suggests that the ground state energy of a closed spin ladder coincides with the ground state energy of its fermionic representation. Furthermore, the numerical calculations suggest that the ground states remain vortex-free (or vortex-full) as for the spin ladders for which reflection-positivity applies.

In §12.8 we use third-order perturbation theory (the lowest non-trivial order) to complement the picture. These results also show that for certain regions of the coupling constants for non-symmetric, open and closed ladders, the ground states are vortex-free (or vortex-full).

12.2 Nearest-neighbor Majorana interactions on a cubic lattice

The cubic lattice

We consider a finite subset Λ of the cubic lattice $\mathbb{Z}^d$ in Euclidean d-space, with an even number $|\Lambda|$ of sites i. We assume Λ to be a rectangular box, with sites $i \in \mathbb{Z}^d$ and bonds (ij) connecting nearest-neighbor sites. The side length of the box along each coordinate axis may be different. We call this an *open* box. We sometimes *close* the box in one or more coordinate directions. One closes the box in the kth direction by defining sites with minimum and maximum value of the kth coordinate, but the same value of each of the other coordinates, to be nearest-neighbors.

The Majoranas and the Hilbert space

A set of Majoranas is a self-adjoint representation of an even-dimensional Clifford algebra,

$$\{c_i, c_j\} = 2\delta_{ij}\,, \qquad \text{where} \quad c_j = c_j^* = c_j^{-1}\,. \tag{12.1}$$

We assign a Majorana c_j to each site j. Majoranas can be represented on a Fock-Hilbert space $\widetilde{\mathcal{H}}_c$ of dimension $2^{|\Lambda|/2}$ and we use this representation. We consider the family of Hamiltonians

$$\widetilde{H}_u = \sum_{(ij)} J_{(ij)}\, u_{ij}\, i\, c_i c_j\,, \tag{12.2}$$

with $J_{(ij)} = J_{(ji)} \geqslant 0$ and $u_{ij} = -u_{ji} = \pm 1$. In case the subscripts are difficult to distinguish, we write $J_{(i,j)}$ in place of $J_{(ij)}$.

Vortex loops

Define a loop $\mathfrak{C}$ of length $|\mathfrak{C}| = \ell$ as an ordered sequence of nearest-neighbor sites $\{i_1, i_2, \ldots, i_\ell, i_1\}$ in Λ, starting and ending at the same site. In addition we assume $i_1, \ldots, i_\ell$ are distinct so the loop is not self-intersecting. We identify the loop with a closed, directed path connecting nearest-neighbor sites i_k and i_{k+1} by bonds $(i_k i_{k+1})$. Denote $-\mathfrak{C}$ as the reverse loop which contains the same sites as $\mathfrak{C}$ but the opposite orientation, $\{i_1, i_\ell, i_{\ell-1}, \ldots, i_2, i_1\}$. Let $\prod_{(ij)\in\mathfrak{C}} K_{ij}$ denote the ordered product around the loop,

$$\prod_{(ij)\in\mathfrak{C}} K_{ij} = K_{i_1 i_2}\, K_{i_2 i_3} \cdots K_{i_{\ell-1} i_\ell}\, K_{i_\ell i_1}\,. \tag{12.3}$$

In the case where K_{ij} are matrices, the starting point of the loop is important, though the trace $\mathrm{T}r\left(\prod_{(ij)\in\mathfrak{C}} K_{ij}\right)$ is independent of the cyclic permutation of sites in the loop. The smallest loop contains four sites, which are the corner of a square or plaquette p bounded by the loop $\mathfrak{C} = \partial p$. Define a loop to be *non-degenerate* if the coupling constants on the loop do not vanish:

$$\mathfrak{C} \text{ is non-degenerate } \Leftrightarrow \prod_{(ij)\in\mathfrak{C}} J_{(ij)} \neq 0 \, . \tag{12.4}$$

Define the vortex loop $\widetilde{\mathfrak{B}}(\mathfrak{C})$ as

$$\widetilde{\mathfrak{B}}(\mathfrak{C}) = -\prod_{(ij)\in\mathfrak{C}} u_{ij} \, . \tag{12.5}$$

In case $\widetilde{\mathfrak{B}}(\mathfrak{C}) = 1$ we say that the loop $\mathfrak{C}$ is *vortex-free*. In case $\widetilde{\mathfrak{B}}(\mathfrak{C}) = -1$ we say that $\mathfrak{C}$ is *vortex-full*. We say that a state is vortex-free or vortex-full, in case all loops $\mathfrak{C}$ are vortex-free or vortex-full. In case $\mathfrak{C}$ bounds a surface, one can interpret the vortex configuration $\widetilde{\mathfrak{B}}(\mathfrak{C})$ in terms of flux through the surface.

Fermionic Fock representation

We represent the Hilbert space $\widetilde{\mathcal{H}}_c$ as a fermionic Fock space generated by $|\Lambda|/2$ real creation operators a_μ^* and their adjoints a_μ are the corresponding annihilation operators. Here $\mu = 1,\ldots,|\Lambda|/2$. Each creation-annihilation pair gives rise to two Majoranas

$$m_{\mu 1} = a_\mu + a_\mu^*, \qquad \text{and} \quad m_{\mu 2} = i\left(a_\mu - a_\mu^*\right) \, . \tag{12.6}$$

The reality condition on a_μ means that complex conjugation on $\widetilde{\mathcal{H}}_c$ maps the first Majorana to itself and changes the sign of the second one. In other words the Majoranas occur in pairs that are purely real or purely imaginary

$$\overline{m_{\mu 1}} = m_{\mu 1} \, , \qquad \text{and} \qquad \overline{m_{\mu 2}} = -m_{\mu 2} \, , \tag{12.7}$$

where $\overline{}$ denotes complex conjugation, which also acts in a natural way on $\widetilde{\mathcal{H}}_c$. Note that there are $|\Lambda|$ Majoranas $m_{\mu\beta}$ and the same number of c_j's. We can and do identify the $m_{\mu\beta}$'s with the c_j's.

The $\mathbb{Z}_2$ gauge group on $\widetilde{\mathcal{H}}_c$

It is convenient to introduce the gauge group $\mathfrak{G}^c$ that acts on $\widetilde{\mathcal{H}}_c$. The generators of this group are the operators

$$U_j^c = c_j \, \mathcal{U}^c, \qquad \text{where} \quad \mathcal{U}^c = \prod_{j=1}^{4N} c_j \, . \tag{12.8}$$

We later choose an order for the product $\mathcal{U}^c$, but conjugation by $\mathcal{U}^c$ does not depend on the choice. The group $\mathfrak{G}^c$ has dimension $2^{|\Lambda|+1}$, since $\left(U_j^c\right)^2 = -I$.

A general gauge transformation $W \in \mathfrak{G}^c$ on $\widetilde{\mathcal{H}}_c$ depends upon $|\Lambda| + 1$ two-valued parameters $\mathfrak{n} = \{n_0, n_1, \ldots, n_{|\Lambda|}\}$. It has the form

$$W(\mathfrak{n}) = (-1)^{n_0} \left(U_1^c\right)^{n_1} \left(U_2^c\right)^{n_2} \cdots \left(U_{|\Lambda|}^c\right)^{n_{|\Lambda|}} , \tag{12.9}$$

where $n_k = 0, 1$. Conjugation by the unitary $W(\mathfrak{n})$ acts on the c_k's as an automorphism that we also denote by $W(\mathfrak{n})$. We write,

$$W(\mathfrak{n})(c_k) = W(\mathfrak{n}) \, c_k \, W(\mathfrak{n})^* = (-1)^{n_k} c_k \, . \tag{12.10}$$

Reflection-symmetry

In certain sections we consider lattices that are symmetric under a reflection ϑ in a hyperplane Π, that intersects no lattice sites. The reflection defines two disjoint subsets of the lattice $\Lambda_\pm$ of $\Lambda = \Lambda_- \cup \Lambda_+$ that map into each other,

$$\vartheta \, \Lambda_\pm = \Lambda_\mp, \qquad \vartheta^2 = \mathrm{Id}, \qquad \text{with} \quad \vartheta : i \mapsto \vartheta i \, . \tag{12.11}$$

The reflection ϑ acts on loops as

$$\vartheta(\mathfrak{C}) = \vartheta(\{i_1, i_2, \ldots, i_\ell, i_1\}) = \{\vartheta i_1, \vartheta i_2, \ldots, \vartheta i_\ell, \vartheta i_1\} \, . \tag{12.12}$$

We say that a loop $\mathfrak{C}$ is reflection-symmetric under the action of ϑ, if $\vartheta(\mathfrak{C}) = -\mathfrak{C}$.

We represent ϑ on $\widetilde{\mathcal{H}}_c$ as an *anti-unitary* transformation. Introduce the constants $\alpha_j = \pm 1$ for which

$$\vartheta(c_j) = \vartheta \, c_j \, \vartheta^{-1} = \overline{c_{\vartheta j}} = \alpha_{\vartheta j} \, c_{\vartheta j} \, . \tag{12.13}$$

The transformation ϑ defines an anti-linear automorphism of the algebra generated by the c_j's, which we also denote by ϑ.

Definition 9. *The Hamiltonian $\widetilde{H}_u$ is reflection-symmetric if $\vartheta(\widetilde{H}_u) = \widetilde{H}_u$.*

The fermionic algebra on $\widetilde{\mathcal{H}}_c$

Define the fermionic algebra $\mathfrak{A}_c$ as the algebra generated by the c_j's for $j \in \Lambda$. Let $\mathfrak{A}_c^{\mathrm{even}}$ denote the even subalgebra of $\mathfrak{A}_c$, generated by even monomials in the fermionic operators. Similarly let $\mathfrak{A}_{c,\pm} \subset \mathfrak{A}_c$ denote the subalgebras generated by the c_j's with $j \in \Lambda_\pm$. Also let $\mathfrak{A}_{c,\pm}^{\mathrm{even}}$ denote the even subalgebras of $\mathfrak{A}_{c,\pm}$.

Reflection positivity

Reflection positivity (RP) for Majoranas is a condition on a Hilbert space, an algebra of operators on the Hilbert space, a reflection ϑ through a plane Π, and a Hamiltonian. Here we study the Hilbert space $\widetilde{\mathcal{H}}_c$, the algebras $\mathfrak{A}_{c,\pm}^{even}$, an implementation of the reflection ϑ on $\widetilde{\mathcal{H}}_c$, and a reflection-symmetric Hamiltonian $\widetilde{H}$. The RP condition states that

$$\mathrm{Tr}_{\widetilde{\mathcal{H}}_c}\left(B\,\vartheta(B)\,e^{-\widetilde{H}} \right) \geqslant 0\,, \qquad \text{for all } B \in \mathfrak{A}_{c,\pm}^{even}\,. \tag{12.14}$$

Time-reflection positivity was originally discovered in quantum field theory by Osterwalder and Schrader in the context of relating classical fields with quantum fields. [186] In particular they introduced the method of "multiple reflection bounds," involving iterated applications of a reflection-positivity bound. Such bounds have been key for the first mathematical proof of the existence of phase transitions (ground-state degeneracy) in quantum field theory, [187] and in proving that certain field theories have infinite volume limits. [192]

RP has also had many applications in the study of phase transitions for classical and quantum spin systems on a lattice; see Fröhlich, Israel, Lieb, and Simon [190] for more details. In the context of nearest-neighbor hopping interactions, the vortex configuration of the ground state has been analyzed by Lieb [159] and Macris and Nachtergaele. [160] Recently one has shown that RP is also valid for a class of many-body Majorana interactions; [195] this family of interactions includes the two-body $\widetilde{H}_u$ in (12.2) with certain restrictions on the coupling constants J_{ij}.

Vortex loops and reflection positivity

We study vortex loops $\widetilde{\mathfrak{B}}(\mathfrak{C})$ for ground states of the family of Hamiltonians $\{\widetilde{H}_u\}$ with ground state energies $\{\widetilde{E}_0(u)\}$.

Theorem 10. *Let $\widetilde{H}_u$ denote a Hamiltonian of the form (12.2). Let $\mathfrak{C}$ denote a non-degenerate, reflection-symmetric loop with respect to a reflection ϑ in the plane Π. Assume that the magnitudes of the couplings are reflection-symmetric, $\left|J_{(ij)}\right| = \left|J_{(\vartheta i\,\vartheta j)}\right|$. Then $\min_u \widetilde{E}_0(u)$ is achieved for a "vortex-free" configuration of the u_{ij}'s, namely*

$$\widetilde{\mathfrak{B}}(\mathfrak{C}) = 1\,. \tag{12.15}$$

Proof. Consider a loop $\mathfrak{C}$ of length $2L$ symmetrically crossed by the hyperplane Π. This means that $\Lambda_\pm \cap \mathfrak{C}$ each contain L sites. Relabel the sites of $\mathfrak{C}$ as $1, \ldots, 2L$ so that the bonds in order on $\mathfrak{C} \cap \Lambda_-$ are $(i\,i+1)$ with $i = 1, \ldots, L-1$. Similarly on $\mathfrak{C} \cap \Lambda_+$ the bonds are $(i\,i+1)$ with $i = L+1, \ldots, 2L-1$. Choose the starting point of $\mathfrak{C}$ so that the bonds cutting Π are $(2L,\,1)$ and $(L,\,L+1)$.

Define $\Lambda_{\Pi\pm} \subset \Lambda_\pm$ as those sites in $\Lambda_\pm$ that border Π. Decompose $\widetilde{H}_u = \widetilde{H}_{u,-} + \widetilde{H}_{u,0} + \widetilde{H}_{u,+}$ where $\widetilde{H}_{u,\pm} \in \mathfrak{A}_\pm$ and

$$\widetilde{H}_{u,0} = \sum_i J_{(i\,\vartheta i)}\, u_{i\,\vartheta i}\, \alpha_{\vartheta i}\, ic_i\vartheta(c_i)\,, \qquad \text{with } i \in \Lambda_{\Pi-}\,. \tag{12.16}$$

Perform a gauge transformation $W(\mathfrak{n}) \in \mathfrak{G}^c$ of the form (12.9), with $n_i = 0$ except for $i \in \Lambda_{\Pi-}$. Choose n_i to ensure that the interactions in $\widetilde{\widetilde{H}}_{u,0} = W(\mathfrak{n})\,\widetilde{H}_{u,0}\,W(\mathfrak{n})^*$ across Π are positive, namely

$$J_{(i\,\vartheta i)}\, u_{i\,\vartheta i}\, (-1)^{n_i}\, \alpha_{\vartheta i} > 0\,, \qquad \text{for } i \in \Lambda_{\Pi-}\,. \tag{12.17}$$

Also define the Hamiltonians $\widetilde{\widetilde{H}}_{u,1}$ and $\widetilde{\widetilde{H}}_{u,2}$ as

$$\widetilde{\widetilde{H}}_{u,1} = \widetilde{\widetilde{H}}_{u,-} + \widetilde{\widetilde{H}}_{u,0} + \vartheta(\widetilde{\widetilde{H}}_{u,-})\,, \quad \text{and} \quad \widetilde{\widetilde{H}}_{u,2} = \vartheta(\widetilde{\widetilde{H}}_{u,+}) + \widetilde{\widetilde{H}}_{u,0} + \widetilde{\widetilde{H}}_{u,+}\,, \tag{12.18}$$

where

$$\widetilde{\widetilde{H}}_{u,-} = W(\mathfrak{n})\,\widetilde{H}_{u,-}\,W(\mathfrak{n})^*\,, \qquad \text{and} \qquad \widetilde{\widetilde{H}}_{u,+} = W(\mathfrak{n})\,\widetilde{H}_{u,+}\,W(\mathfrak{n})^*\,. \tag{12.19}$$

Since $\vartheta(\widetilde{\widetilde{H}}_{u,0}) = \widetilde{\widetilde{H}}_{u,0}$, the Hamiltonians $\widetilde{\widetilde{H}}_{u,1}$ and $\widetilde{\widetilde{H}}_{u,2}$ are reflection-symmetric,

$$\vartheta(\widetilde{\widetilde{H}}_{u,1}) = \widetilde{\widetilde{H}}_{u,1}\,, \qquad \text{and} \qquad \vartheta(\widetilde{\widetilde{H}}_{u,2}) = \widetilde{\widetilde{H}}_{u,2}\,. \tag{12.20}$$

Furthermore the coupling constants in $\widetilde{\widetilde{H}}_{u,0}$ that cross the reflection plane Π are positive.

The Hamiltonians $\widetilde{\widetilde{H}}_{u,1}$ and $\widetilde{\widetilde{H}}_{u,2}$ satisfy the hypothesis of Theorem 3 in [195]. In that paper one studies reflection-positivity for a class of interacting Majorana systems including the present one satisfying (12.17) and (12.20). From this result one concludes the reflection-positivity conditions. For $B \in \mathfrak{A}_{\pm}^{\text{even}}$,

$$\mathrm{Tr}_{\widetilde{\mathcal{H}}_c} \left(B\, \vartheta(B)\, e^{-\widetilde{\widetilde{H}}_{u,1}} \right) \geqslant 0\,, \quad \text{and} \quad \mathrm{Tr}_{\widetilde{\mathcal{H}}_c} \left(B\, \vartheta(B)\, e^{-\widetilde{\widetilde{H}}_{u,2}} \right) \geqslant 0\,. \quad (12.21)$$

A direct consequence of the reflection-positivity conditions (12.21) is the reflection-positivity bound for any $\beta \geqslant 0$,

$$\mathrm{Tr}_{\widetilde{\mathcal{H}}_c}\, e^{-\beta \widetilde{\widetilde{H}}_u} \leqslant \left(\mathrm{Tr}_{\widetilde{\mathcal{H}}_c}\, e^{-\beta \widetilde{\widetilde{H}}_{u,1}} \right)^{1/2} \left(\mathrm{Tr}_{\widetilde{\mathcal{H}}_c}\, e^{-\beta \widetilde{\widetilde{H}}_{u,2}} \right)^{1/2}\,. \quad (12.22)$$

This bound is a special case of the reflection-positivity inequality for interacting Majorana systems proved in Proposition 8 of [195]. The reflection-positivity bound (12.22) allows one to establish an inequality on the ground state energy $\widetilde{\widetilde{E}}_0(u)$ of the Hamiltonian $\widetilde{\widetilde{H}}_u$ in terms of the ground-state energies $\widetilde{\widetilde{E}}_0(u,1)$ and $\widetilde{\widetilde{E}}_0(u,2)$ of the Hamiltonians $\widetilde{\widetilde{H}}_{u,1}$ and $\widetilde{\widetilde{H}}_{u,2}$, namely

$$0 \geqslant \widetilde{\widetilde{E}}_0(u) \geqslant \frac{\widetilde{\widetilde{E}}_0(u,1) + \widetilde{\widetilde{E}}_0(u,2)}{2}\,. \quad (12.23)$$

Taking β large in (12.22) proves (12.23).

Conjugation by the gauge transformation $W(\mathfrak{n})$ does not change the ground state energy $\widetilde{E}_0(u)$ of $\widetilde{H}_u$, so $\widetilde{\widetilde{E}}_0(u) = \widetilde{E}_0(u)$. Nor does conjugation by the gauge transformation $W(\mathfrak{n})$ change the value of any vortex loop $\widetilde{B}(\mathfrak{C})$. Thus $\min_u \widetilde{E}_0(u)$ is obtained from some configuration $u = u_0$ that is both reflection-symmetric and has positive interactions across Π. Call this Hamiltonian $\widetilde{H}_{u_0}$.

Let $\widetilde{H}_{u_0}(\mathfrak{C})$ denote the Hamiltonian that is the restriction of $\widetilde{H}_{u_0}$ to bonds $(ij) \in \mathfrak{C}$. Decompose $\widetilde{H}_{u_0}(\mathfrak{C})$ as

$$\widetilde{H}_{u_0}(\mathfrak{C}) = \widetilde{H}_{u_0,-}(\mathfrak{C}) + \widetilde{H}_{u_0,0}(\mathfrak{C}) + \widetilde{H}_{u_0,+}(\mathfrak{C})\,, \quad (12.24)$$

where positivity of the $J_{(ij)}$'s ensures

$$\widetilde{H}_{u_0,-}(\mathfrak{C}) = \sum_{i=1}^{L-1} J_{(i,i+1)}\, u_{i\,i+1}\, i\, c_i c_{i+1}\,,$$

$$\widetilde{H}_{u_0,+}(\mathfrak{C}) = \sum_{i=L+1}^{2L-1} J_{(i,i+1)}\, u_{i\,i+1}\, i\, c_i c_{i+1}\,, \quad (12.25)$$

$$\widetilde{H}_{u_0,0}(\mathfrak{C}) = J_{(1,2L)}\, u_{1\,2L}\, \alpha_{\vartheta 1}\, i\, c_1\, \vartheta(c_1) + J_{(L,L+1)}\, u_{L\,L+1}\, \alpha_{\vartheta L}\, i\, c_L\, \vartheta(c_L)\,.$$

With our chosen representation

$$J_{(1,\,2L)}\,u_{1\,2L}\,\alpha_{\vartheta 1} > 0\,, \qquad \text{and} \qquad J_{(L,\,L+1)}\,u_{L\,L+1}\,\alpha_{\vartheta L} > 0\,, \qquad (12.26)$$

and also reflection-symmetry $\vartheta(\widetilde{H}_{u_0,-}(\mathfrak{C})) = \widetilde{H}_{u_0,+}(\mathfrak{C})$ yields for $i = 1, \ldots, L-1$,

$$\begin{aligned} J_{(i,\,i+1)}\,u_{i\,i+1}\,\alpha_{2L-i}\,\alpha_{2L-i+1}\,i\,c_{2L-i}\,c_{2L-i+1} \\ = \quad J_{(2L-i,\,2L-i+1)}\,u_{2L-i\,2L-i+1}\,i\,c_{2L-i}\,c_{2L-i+1}\,. \end{aligned} \qquad (12.27)$$

Consequently, since the loop $\mathfrak{C}$ is non-degenerate, for $i = 1, \ldots, L-1$ one has

$$J_{(i,\,i+1)}J_{(2L-i,\,2L-i+1)}\,u_{i\,i+1}\,u_{2L-i\,2L-i+1}\,\alpha_{2L-i}\,\alpha_{2L-i+1} > 0\,. \qquad (12.28)$$

Multiply together conditions (12.26) with all the conditions (12.28), and identify site $2L + 1$ with site 1. One obtains

$$\mathfrak{B}(\mathfrak{C}) = -\prod_{(ij)\in\mathfrak{C}} u_{ij} = -\prod_{i=1}^{2L} u_{i\,i+1} = \operatorname{sgn}\left(\prod_{i=1}^{2L} J_{(i,\,i+1)}\right) = 1\,. \qquad (12.29)$$

The first two equalities and the last equality in (12.29) are definitions, so one only needs to verify the third equality. This means one needs to show that the factors α_j cancel, and this occurs because each α_j appears twice in the product. There is one additional minus sign, which comes from $u_{1\,2L} = -u_{2L\,1}$, with the former appearing in (12.26) and the later in the product $\prod_{i=1}^{2L} u_{i\,i+1}$. This minus sign cancels the explicit minus sign in (12.29). □

12.3 Quantum spin ladders

One way to realize the family of Hamiltonians $\widetilde{H}_u$ defined in (12.2) is to study nearest-neighbor spin interactions on a trivalent lattice. We consider the simplest example, the quantum spin ladder, corresponding to the case $d = 2$ in §12.2.

Even spin ladders

An open, even spin ladder is a $2 \times 2N$ square lattice array. The sites of the lattice are connected by bonds linking nearest-neighbor sites. We call one given plaquette the *unit cell* of the ladder. One obtains the lattice of

the ladder as a union of N translates of the unit cell by integer multiples of twice the side-length of the unit cell, along one of its coordinate axes (which we choose horizontal). One completes the ladder with bonds (ij) that link site i with a nearest-neighbor site j.
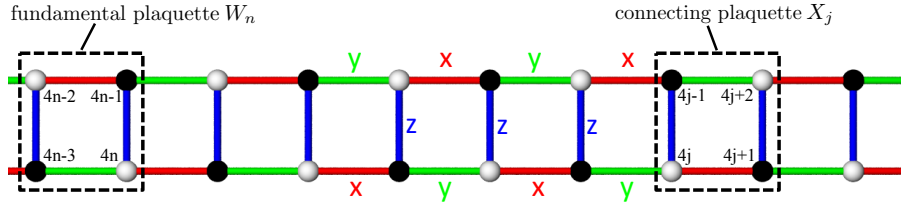
Figure 12.1: Ladder

We illustrate such a ladder in Fig. 12.1, where we label the plaquettes, vertices, and bonds. Divide the $2N-1$ plaquettes of the ladder into two sets: the first set comprises N *fundamental plaquettes* $p_1, p_3, \ldots, p_{2k-1}, \ldots, p_{2N-1}$ that are the translates of the unit cell that generates the ladder. The other set contains $(N-1)$ *connecting plaquettes* $p_2, p_4, \ldots, p_{2k}, \ldots, p_{2N-2}$, each of which links two fundamental plaquettes, by sharing two of its bonds with two different fundamental plaquettes.

In order to discuss both "open" and "closed" ladders in a unified way, we introduce one additional connecting plaquette p_{2N} linking p_{2N-1} with p_1, and two additional bonds to the open ladder, connecting the site $4N$ to the site 1, and connecting the site $4N-1$ to the site 2. The closed ladder corresponds to periodic boundary conditions. Another way to characterize a closed ladder, is the property that one must remove at least four bonds to divide it into two disconnected pieces.

Label the sites in the fundamental plaquette p_{2n-1} clockwise, starting in the lower-left corner, by $4n-3, 4n-2, 4n-1, 4n$. As a consequence, the sites in the connecting plaquette p_{2j} are labeled clockwise by $4j, 4j-1, 4j+2, 4j+1$. The open ladders we consider have $(6N-2)$ bonds, which we divide into three types. There are $(2N-1)$ type-x bonds, $(2N-1)$ type-y bonds, and $2N$ type-z bonds. All the vertical bonds will be type-z bonds. The horizontal bonds on top of each fundamental plaquette, and on the bottom of each connecting plaquette are type-x bonds. The remaining bonds are type-y bonds.

The Hamiltonian

The spins at each site $\boldsymbol{\sigma}_i = (\sigma_i^x, \sigma_i^y, \sigma_i^z)$ are Pauli matrices. Here i denotes the lattice site (using the labels above), and x, y, z denotes the three Pauli

matrices. The Hamiltonian we study is a nearest-neighbor quadratic interaction of the form

$$H = -\sum_{(ij)} J_{(ij)}\, \sigma_i^{(ij)}\sigma_j^{(ij)}\ , \qquad J_{(ij)} = J_{(ji)} \text{ real.} \qquad (12.1)$$

Here the sum over (ij) denotes a sum over unoriented bonds (ij) between nearest neighbor lattice sites in the ladder. Also $\sigma_i^{(ij)}$ equals σ_i^x, σ_i^y, or σ_i^z, according to whether the bond (ij) is type-x, type-y, or type-z, respectively, as defined above; thus the couplings labeled by a bond depends only on products of the same components of $\boldsymbol{\sigma}$ at different sites.

A simple case of this Hamiltonian which we call *homogeneous couplings* is the case for which every type-x bond has coupling J_x, every type-y bond has coupling J_y, and every type-z bond has coupling J_z. The open ladder Hamiltonian corresponds to taking the two coupling constants closing the ladder equal to zero, namely $J_{(4N\,1)} = J_{(4N-1\,2)} = 0$.

Vortex loops

For each loop $\mathfrak{C}$, we assign a *vortex-loop operator* (or simply a *vortex*) $\mathfrak{B}(\mathfrak{C})$. This is proportional to the *ordered* product along the loop of terms in the interaction. Recall that $\sigma_i^{(ij)}\sigma_j^{(ij)}$ is the term in the Hamiltonian (14.16) on the bond (ij). Define

$$\mathfrak{B}(\mathfrak{C}) \;=\; i^{|\mathfrak{C}|+2} \prod_{(ij)\in\mathfrak{C}} \left(\sigma_i^{(ij)}\sigma_j^{(ij)}\right)\ , \qquad (12.2)$$

similar to (5-6) in Kitaev. [27] As $\sigma_i^{(ij)}$ is self-adjoint with square I, we infer that $\mathfrak{B}(\mathfrak{C})$ is unitary. We devote the rest of this paper to the study of properties of the operators $\mathfrak{B}(\mathfrak{C})$.

12.4 Fermionic ladders

Mapping of spins to fermions

We use a representation of the Pauli matrices as quadratic expressions in Majoranas. Choose four Majoranas at each lattice site j and denoted them b_j^x, b_j^y, b_j^z, and c_j. Define the algebra $\mathfrak{A}$ as the algebra generated by the $b_j^{x,y,z}$ and c_j for $j \in \Lambda$. Let $\mathfrak{A}^{\text{even}}$ denote the even subalgebra of $\mathfrak{A}$, generated by even monomials in the fermionic operators. One defines for the single site j,

$$\widetilde{\sigma}_j^\alpha = ib_j^\alpha\, c_j\ , \qquad (12.1)$$

as in the usual construction of boost operators for the Dirac equation. For a single chiral component of the spin-1/2 Dirac wave function, the boost generator is isomorphic to the spin.

Denote the vector space of the four Majoranas as $\widetilde{\mathcal{H}}_j$. In order to project onto a single chiral component, one restricts to the eigenspace $+1$ of the self-adjoint matrix $\gamma_j^5 = b_j^x \, b_j^y \, b_j^z \, c_j$ with square one. On the full Hilbert space $\widetilde{H}$ these γ_j^5's mutually commute and commute with each $\widetilde{\sigma}_j^{x,y,z}$. The corresponding orthogonal projection onto this eigenspace is $P = \prod_j P_j = \prod_j \frac{1}{2}\left(I + \gamma_j^5\right)$, and it yields $\mathcal{H} = P\widetilde{\mathcal{H}}$ of dimension 2^{4N}. The $\sigma_j^\alpha = P_j \, \widetilde{\sigma}_j^\alpha \, P_j$'s satisfy the correct multiplication laws for spin matrices on $\mathcal{H}$.

Representation of the Hamiltonian

Introduce the three skew $4N \times 4N$ matrices u, A, and C with entries that are hermitian operators,

$$u_{ij} = -u_{ji} = u_{ij}^*, \qquad A_{ij} = -A_{ji} = A_{ij}^*, \qquad \text{and} \quad C_{ij} = -C_{ji} = C_{ij}^*. \tag{12.2}$$

We define these matrix elements to vanish unless i, j are nearest-neighbors. In this case

$$u_{ij} = ib_i^{(ij)} \, b_j^{(ij)}, \qquad C_{ij} = ic_i c_j, \qquad \text{and} \quad A_{ij} = J_{(ij)} \, u_{ij}, \tag{12.3}$$

with $J_{(ij)} = J_{(ji)}$ real. A representation of the spin-ladder Hamiltonian on the fermionic Hilbert space is

$$\widetilde{H} = \sum_{(ij)} A_{ij} \, C_{ij} = \sum_{(ij)} J_{(ij)} \, u_{ij} \, i \, c_i \, c_j = \widetilde{H}^* . \tag{12.4}$$

The u_{ij} operators mutually commute, and they also commute with the Hamiltonian $\widetilde{H}$. They satisfy $u_{ij}^2 = +1$, so the eigenvalues of u_{ij} are ± 1. Also all the γ_j^5 commute with $\widetilde{H}$. Furthermore the Hamiltonian $\widetilde{H}$ commutes with P, so it maps the subspace $\mathcal{H}$ into itself and on this subspace the Hamiltonian has the representation as a sum of self-adjoint operators,

$$H = P\widetilde{H}P = \sum_{(ij)} P \, A_{ij} \, C_{ij} \, P . \tag{12.5}$$

The properties of $\widetilde{H}$ on $\widetilde{\mathcal{H}}$ are different from those of H on $\mathcal{H}$, and in particular the eigenvalues might different (aside from multiplicity). One should be careful not to jump to conclusions, as we give numerical evidence for the existence of both types of behavior in §12.7.

Representation of the vortices

A fermionic representation of $\widetilde{\mathfrak{B}}(\mathfrak{C})$ of $\mathfrak{B}(\mathfrak{C})$ commutes with the projection P. Its projection $P\,\widetilde{\mathfrak{B}}(\mathfrak{C})\,P$, agrees with the original definition (12.2) of the vortex $\mathfrak{B}(\mathfrak{C})$. We give such a fermionic representation $\widetilde{\mathfrak{B}}(\mathfrak{C})$, similar to [27] and observe that the spin vortices $\mathfrak{B}(\mathfrak{C})$ are mutually commuting, conserved quantities.

Proposition 11. *A fermionic representation of the vortex loop-operator is given in terms of the mutually-commuting operators u_{ij} as*

$$\widetilde{\mathfrak{B}}(\mathfrak{C}) = -\prod_{(ij)\in\mathfrak{C}} u_{ij}\,. \tag{12.6}$$

Each γ_k^5 commutes with $\widetilde{\mathfrak{B}}(\mathfrak{C})$, namely

$$\left[\widetilde{\mathfrak{B}}(\mathfrak{C}), \gamma_k^5\right] = 0\,. \tag{12.7}$$

Proof. The contribution to the vortex loop-operator $\mathfrak{B}(\mathfrak{C})$ from the spins at site i_j, for $j \neq 1$, is $\sigma_{i_j}^{(i_{j-1}\,i_j)}\sigma_{i_j}^{(i_j\,i_{j+1})}$. (In case $j = \ell$, set $\ell + 1 = 1$.) This product has the fermionic representation $-b_{i_j}^{(i_{j-1}\,i_j)} c_j\, b_{i_j}^{(i_j\,i_{j+1})} c_j = b_{i_j}^{(i_{j-1}\,i_j)} b_{i_j}^{(i_j\,i_{j+1})}$. Taking the product of these representations and adding the contribution from the spins at site i_1, one has a fermionic representation for $\mathfrak{B}(\mathfrak{C})$ defined in (12.2) equal to

$$
\begin{aligned}
\widetilde{\mathfrak{B}}(\mathfrak{C}) \;=\;& -i^{|\mathfrak{C}|+2}\, b_{i_1}^{(i_1\,i_2)}\, c_{i_1}\, b_{i_2}^{(i_1\,i_2)}\, b_{i_2}^{(i_2\,i_3)}\, b_{i_3}^{(i_2\,i_3)}\, b_{i_3}^{(i_3\,i_4)} \cdots \\
& \quad b_{i_{\ell-1}}^{(i_{\ell-2}\,i_{\ell-1})}\, b_{i_{\ell-1}}^{(i_{\ell-1}\,i_\ell)}\, b_{i_\ell}^{(i_{\ell-1}\,i_\ell)}\, b_{i_\ell}^{(i_\ell\,i_1)}\, b_{i_1}^{(i_\ell\,i_1)}\, c_{i_1} \\
\;=\;& i^{|\mathfrak{C}|+2}\, c_{i_1}\, b_{i_1}^{(i_1\,i_2)}\, b_{i_2}^{(i_1\,i_2)}\, b_{i_2}^{(i_2\,i_3)}\, b_{i_3}^{(i_2\,i_3)}\, b_{i_3}^{(i_3\,i_4)} \cdots \\
& \quad b_{i_{\ell-1}}^{(i_{\ell-2}\,i_{\ell-1})}\, b_{i_{\ell-1}}^{(i_{\ell-1}\,i_\ell)}\, b_{i_\ell}^{(i_{\ell-1}\,i_\ell)}\, b_{i_\ell}^{(i_\ell\,i_1)}\, b_{i_1}^{(i_\ell\,i_1)}\, c_{i_1} \\
\;=\;& -c_{i_1}\, u_{i_1 i_2}\, u_{i_2 i_3} \cdots u_{i_{\ell-1} i_\ell}\, u_{i_\ell i_1}\, c_{i_1} \\
\;=\;& -u_{i_1 i_2}\, u_{i_2 i_3} \cdots u_{i_{\ell-1} i_\ell}\, u_{i_\ell i_1}\,. \tag{12.8}
\end{aligned}
$$

In the last equality we use the fact that c_{i_1} commutes with all the u_{ij}'s. This establishes the fermionic representation (12.6). As each u_{ij} is hermitian and the u_{ij} mutually commute, we infer that $\widetilde{\mathfrak{B}}(\mathfrak{C})$ is hermitian. Since $\widetilde{\mathfrak{B}}(\mathfrak{C})$ is a product of b Majoranas, with an even number of b's at each site $i_j \in \mathfrak{C}$, we infer that $\widetilde{\mathfrak{B}}(\mathfrak{C})$ commutes with each γ_j^5. Therefore $\widetilde{\mathfrak{B}}(\mathfrak{C})$ commutes with P. $\qquad\square$

From the representation (12.6) for $\widetilde{\mathfrak{B}}(\mathfrak{C})$ and the representation (12.4) for $\widetilde{H}$ in terms of the mutually-commuting, self-adjoint operators u_{ij} with square one, one infers the following two corollaries:

Corollary 12. *The fermionic vortex representatives $\widetilde{\mathfrak{B}}(\mathfrak{C})$ are all self-adjoint and have eigenvalues ± 1. Different $\widetilde{\mathfrak{B}}(\mathfrak{C})$ mutually commute,*

$$\left[\widetilde{\mathfrak{B}}(\mathfrak{C}), \widetilde{\mathfrak{B}}(\mathfrak{C}')\right] = 0 \,. \tag{12.9}$$

All the $\widetilde{\mathfrak{B}}(\mathfrak{C})$ are conserved by $\widetilde{H}$, namely

$$\left[\widetilde{\mathfrak{B}}(\mathfrak{C}), \widetilde{H}\right] = 0 \,. \tag{12.10}$$

Corollary 13. *The vortex loop operators $\mathfrak{B}(\mathfrak{C})$ are self-adjoint on $\mathcal{H}$, and have eigenvalues ± 1. Different $\mathfrak{B}(\mathfrak{C})$ mutually commute,*

$$[\mathfrak{B}(\mathfrak{C}), \mathfrak{B}(\mathfrak{C}')] = 0 \,. \tag{12.11}$$

The vortex loop-operators are all conserved, namely

$$[\mathfrak{B}(\mathfrak{C}), H] = 0 \,. \tag{12.12}$$

The reduced fermionic Hamiltonians

Define $\widetilde{H}_u$ as the Hamiltonian $\widetilde{H}$ restricted to an eigenspace of the u_{ij}'s. Therefore it is useful to represent the Hilbert space $\widetilde{\mathcal{H}}$ in the form of a tensor product

$$\widetilde{\mathcal{H}} = \widetilde{\mathcal{H}}_u \otimes \widetilde{\mathcal{H}}_c \,. \tag{12.13}$$

Here we consider the $6N$ mutually commuting variables u_{ij} corresponding to the products of $ib_i^{(ij)} b_j^{(ij)}$ on the $6N$ bonds of a closed ladder. In the case of an open ladder the couplings on the two extra bonds $(1, 4N)$ and $(2, 4N - 1)$ are zero. Each u_{ij} is self-adjoint and has square equal to one, so it can be represented on a two-dimensional Hilbert space. Therefore the Hilbert space $\widetilde{H}_u$ has dimension 2^{6N}, which is exactly $2^{\#_b/2}$, where $\#_b$ equals the total number of $b^{x,y,z}$ Majoranas. These Majoranas can be represented on a Hilbert space of the same dimension 2^{6N}.

Define the fermionic algebra $\mathfrak{A}_c$ as the subalgebra of $\mathfrak{A}$ generated by the c_j-Majoranas. Since this algebra commutes with all the u_{ij}'s, it acts as $I \otimes \mathfrak{A}_c$ on $\widetilde{\mathcal{H}} = \widetilde{\mathcal{H}}_u \otimes \widetilde{\mathcal{H}}_c$.

12.5 Eigenvalues of $\widetilde{H}$ and of H

Let $\widetilde{E}_0$ denote the ground-state energy of $\widetilde{H}$ given in (12.4), and let E_0 denote the ground-state energy of H. We are interested to know when these two ground state energies coincide. By the variational principle, there is a normalized vector $\widetilde{\Omega} \in \widetilde{\mathcal{H}}$, such that

$$\widetilde{E}_0 = \langle \widetilde{\Omega}, \widetilde{H}\widetilde{\Omega} \rangle = \inf_{\|\widetilde{\chi}\|=1} \langle \widetilde{\chi}, \widetilde{H}\widetilde{\chi} \rangle \leq E_0 \ .$$

One obtains E_0 by restricting $\widetilde{\chi}$ to the range of P. So if $P\widetilde{\Omega} = \widetilde{\Omega}$, then $\widetilde{E}_0 = E_0$. More generally, we investigate the eigenvalues of $\widetilde{H}$, and determine in certain cases that they are the same as the eigenvalues of H. In other cases there is evidence that they are different.

For an open ladder, we prove in Proposition 14 that $\widetilde{H}$ and H have the same eigenvalues. We analyze the ground state of H using the fermionic representation and demonstrate that the ground state is vortex-free. In reflection symmetric cases we do this in §12.6 using reflection positivity. In §12.8 we analyze some non-reflection symmetric cases using perturbation theory.

In Proposition 15 we explain why the proof of Proposition 14 for the open ladder does not apply to the closed ladder. More to the point, numerical calculation shows that the spectra are really different, see the discussion in §12.7 and in particular in §12.7.

Proposition 14. *Consider an open ladder. The eigenvalues of H defined in (14.16) are the same as those of $\widetilde{H}$ defined in (12.4), aside from multiplicity.*

Proof. The operators γ_i^5 mutually commute and commute with $\widetilde{H}$, so we can simultaneously diagonalize them. We find an operator Q_j with square ± 1, which anti-commutes with γ_j^5 and commutes with $\widetilde{H}$ and γ_i^5, for $i \neq j$. Let $\widetilde{\Omega}$ be a simultaneous eigenstate of the γ_i^5 and $\widetilde{H}$ with eigenvalues $(\mu_i, \widetilde{E})$, where $\mu_i = \pm 1$ are the eigenvalues of the γ_i^5. Then the vector $Q_j\widetilde{\Omega}$ is an eigenstate with the same eigenvalues except for the one μ_i with $i = j$, that has the opposite sign. (Note $Q_j\widetilde{\Omega} \neq 0$, as $Q_j^2 = \pm 1$.) By applying Q_j for each negative μ_j, we obtain a simultaneous eigenstate with energy $\widetilde{E}$, and with all the $\mu_i = +1$. Calling this vector $\widetilde{\Omega}'$, the projected state $P\widetilde{\Omega}' = \Omega'$ is an eigenstate of H with eigenvalue $\widetilde{E}$. This also shows that to each eigenvalue E of H is associated 2^{4N} eigenvalues of $\widetilde{H}$, of which all but one of the corresponding eigenvectors project to zero.

Define the operator Q_j by considering a non-self-intersecting path Γ through the ladder from site j to site $4N$. The operator Q_j equals the product of the $u_{i'j'}$ operators along the bonds $(i'j')$ on this path, followed by b^x_{4N}. This Q_j is a product of b operators, so its square is ± 1. The operator b^x_{4N} does not enter the expression (12.4) for $\widetilde{H}$, and each term in $\widetilde{H}$ is a product of an even number of other fermion operators. Therefore Q_j commutes with $\widetilde{H}$.

To complete the proof, we need to check the commutativity of Q_j with the operators γ^5_i. Consider four cases: first suppose the path Γ does not pass through i. Then γ^5_i commutes with each b belonging to Q_j, so it commutes with Q_j.

Second suppose that i is a site on the path Γ, but $i \neq j$ and $i \neq 4N$. In this case the site i contributes a product of two different b_i operators to Q_j; this is the case, because in the ladders we consider, the three bonds ending at site i are of three different types, and the path Γ contains two of these bonds. Each of these two b_i's anti-commutes with γ^5_i, so their product commutes. Also γ^5_i commutes with b_k's at other sites, so it commutes with Q_j.

The third case is $i = 4N$. As before, γ^5_{4N} commutes with the b's at sites different from $4N$. Only one bond in Γ ends at site $4N$, so only one b_{4N} at site $4N$ arises from the path; for our ladders, this must be either b^y_{4N} or b^z_{4N}. But Q_j also includes the extra b^x_{4N}. So γ^5_{4N} anti-commutes with this extra b^x_{4N} and therefore commutes with the product of the two distinct b_{4N}'s that occur in Q_j.

The fourth case is $i = j$. In this case only one bond in Γ enters site i, so only one b_i occurs in Q_j. Hence γ^5_j anti-commutes with the b_j's in Q_j. As γ^5_j commutes with the b's at other sites, γ^5_j anti-commutes with Q_j. These cases cover all possibilities, so we have established all the desired properties of the operators Q_j. $\square$

We remark that an alternate proof could be based on the explicit form of the projection $P : \widetilde{\mathcal{H}} \to \mathcal{H}$ as a function of the variables u_{ij} derived in Appendix A of [179]. We now show that the proof of Proposition 14 does not extend in a straightforward way to the closed ladder. This is in line with the numerical calculations we perform in §12.7 suggesting that the spectrum of H is different from the spectrum of $\widetilde{H}$ for the closed ladder.

Proposition 15. *Consider a closed ladder Hamiltonian $\widetilde{H}$ of the form (12.4) with all couplings $J_{(ij)}$ different from 0. There is no non-zero monomial Q_j in the b's and c's that anti-commutes with γ^5_j and commutes with $\widetilde{H}$ and γ^5_k for $k \neq j$.*

Proof. Each site k in the ladder gives rise to a 4-dimensional Hilbert space $\widetilde{\mathcal{H}}_k$. There are 16 linearly-independent operators on $\widetilde{\mathcal{H}}_k$, and this space is spanned by monomials M_k^α in the $b_k^{x,y,z}$ or c_k of degree 4 or less. Of these, four monomials that we denote $m_k^{1,\dots,4}$ are the Majoranas themselves and have degree 1, and four others $m_k^{1,\dots,4}\gamma_k^5$ have degree 3. We write these eight odd degree monomials as $M_k^{-,\alpha}$. Each $M_j^{-,\alpha}$ anti-commutes with γ_j^5 and commutes with γ_k^5 for $k \neq j$.

There are eight monomials $M_k^{+,\alpha}$ of degree 0, 2, or 4, and these commute with all the γ_j^5. All 16 of the $M_k^{\pm,\alpha}$ commute with $\gamma_{k'}^5$ for $k' \neq k$. The monomials in the b's and c's are linearly independent and span the operators on $\widetilde{\mathcal{H}}$, as shown in Proposition 1 of [195]. From these properties, we infer that

$$Q_j = \pm\, M_j^{-,\alpha} \prod_{k \neq j} M_k^{+,\alpha_k} \;. \tag{12.1}$$

We now consider further restrictions on Q_j, imposed by the fact that one wants $\left[Q_j, \widetilde{H}\right] = 0$. We show this is impossible for Q_j of form (12.1). These restrictions use the assumption that all $J_{(ij)} \neq 0$, so they do not apply in the case of an open ladder.

Let us denote the interaction on bond (ji) by $\langle ji \rangle$, so the Hamiltonian (12.4) can be written

$$\widetilde{H} = \sum_{(ji)} \langle ji \rangle \;, \qquad \text{where} \quad \langle ji \rangle = J_{(ji)}\, u_{ji}\, i c_j c_i = -J_{(ji)}\, b_j^{(ji)}\, b_i^{(ji)}\, c_j c_i \;. \tag{12.2}$$

We claim that

    I. $M_j^{-,\alpha}$ anti-commutes with either one or three terms in the sum (12.2).

    II. $\prod_{k\neq j}^3 M_k^{+,\alpha_k}$ anti-commutes with an even number of terms in (12.2).

These two properties show that Q_j of the form (12.1) cannot commute with $\widetilde{H}$.

In order to establish property (I), notice that a single Majorana c_j anti-commutes with three terms $\langle ji \rangle$ in the sum (12.2), where i are the three nearest neighbors to j. Also the Majorana $b_j^{x,y,z}$ anti-commutes with one such term. As γ_j^5 commutes with $\langle ji \rangle$, the same anti-commutativity properties hold for $m_j^{1,\dots,4}\gamma_j^5$ as for $m_j^{1,\dots,4}$.

Property (II) also follows by considering the anti-commutation properties of the eight possible M_k^{+,α_k}. The identity and monomial of degree 4 commute with each $\langle ji \rangle$. The monomials M_k^{+,α_k} of degree 2 all anti-commmute with two of the $\langle ji \rangle$'s. The statement then follows. $\qquad\square$

12.6   Ladder Hamiltonians and reflections

In the following we consider ladder Hamiltonians $\widetilde{H}$ of the form (12.4) with reflection-symmetric absolute value of the couplings $J_{(ij)}$, namely

$$\left|J_{(\vartheta i\, \vartheta j)}\right| = \left|J_{(ij)}\right| . \qquad (12.3)$$

We determine the value of reflection-symmetric vortex loops in the ground states of $\widetilde{H}$ and H for such couplings.

   The open or closed ladder in Fig. 12.1 satisfies (12.3) in three cases:

Case I. Reflection through a horizontal plane. We illustrate this case in Fig. 12.2. We make no restriction on the couplings $J_{(i\, i+1)}$ on vertical bonds.
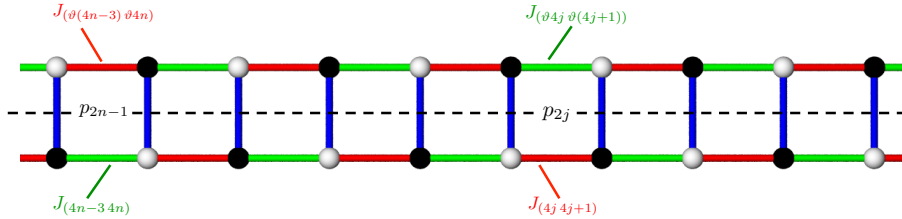
Figure 12.2: Case I: Horizontal reflection plane for an open or closed ladder.

Case II. Vertical reflection plane bisecting an open ladder, see Fig. 12.3.
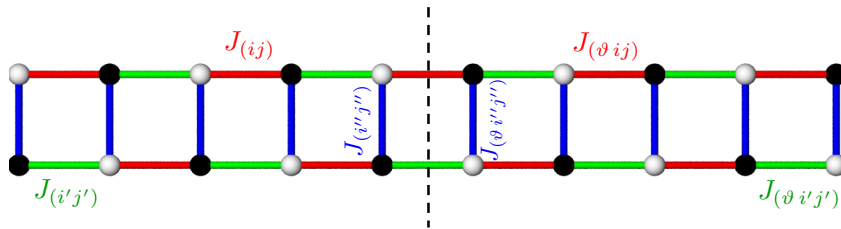
Figure 12.3: Case II: Vertical reflection plane. Recall that $J_{(ij)} = J_{(ji)}$.

Case III. Reflection through any vertical plane bisecting a closed ladder, see Fig. 12.4. The dotted reflection plane intersects the ladder twice.

Vortex loops and reflection-symmetric ladders

In this section we apply Theorem 10 to characterize the vortex configurations of the ground-state of $\widetilde{H}$, for ladders satisfying conditions (12.3).
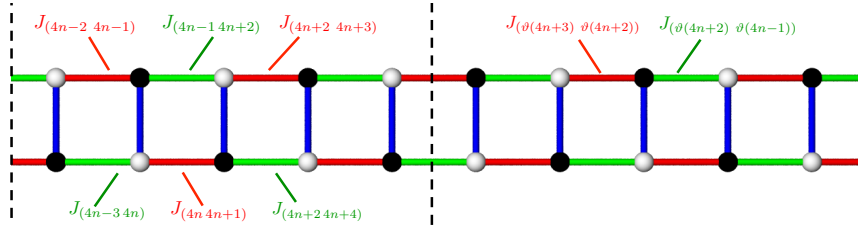
Figure 12.4: Case III: Vertical reflection of a closed ladder.

Theorem 16. *Let $\widetilde{H}$ denote a fermionic ladder Hamiltonian of the form (12.4) satisfying condition (12.3) with respect to a reflection ϑ and a reflection plane Π. Let $\mathfrak{C}$ denote a non-degenerate, reflection-symmetric loop. Then the vortex configuration of $\mathfrak{C}$ in the ground state of $\widetilde{H}$ is*

$$\widetilde{\mathfrak{B}}(\mathfrak{C}) = sgn\left(\prod_{(ij)\in\mathfrak{C}} J_{(ij)} \right). \tag{12.4}$$

In case the couplings have all the same sign, then $\widetilde{\mathfrak{B}}(\mathfrak{C}) = +1$ and the loop $\mathfrak{C}$ is vortex-free.

Corollary 17 (Vortex-free ladders). *For closed ladders with homogeneous couplings which all have the same sign, every loop $\mathfrak{C}$ is vortex-free in the ground state of $\widetilde{H}$.*

Proof. Each Hamiltonian $\widetilde{H}$ acting on $\widetilde{\mathcal{H}}$ corresponds to 2^{6N} Hamiltonians $\widetilde{H}_u$ acting on $\widetilde{\mathcal{H}}_c$, some of which could be the same. Each $\widetilde{H}_u$ arises from a particular choice of $u_{ij} = \pm 1$. The eigenvalues of $\widetilde{H}$ are the union of the eigenvalues of these 2^{6N} Hamiltonians $\widetilde{H}_u$. A gauge transformation of the variables $b_j^{x,y,z}$ transforms one $\widetilde{H}_u$ into another $\widetilde{H}_{u'}$. This justifies our present study of the individual Hamiltonians $\widetilde{H}_u$.

Each Hamiltonian $\widetilde{H}_u$ is of the form (12.2), although the couplings $J_{(ij)}$ may not be positive. In case all the $J_{(ij)} > 0$, we infer from Theorem 10 that the minimum energy of $\widetilde{H}$ is achieved for a $\widetilde{H}_u$ with a configuration of the u_{ij}'s such that

$$\widetilde{\mathfrak{B}}(\mathfrak{C}) = -\prod_{(ij)\in\mathfrak{C}} u_{ij} = 1, \tag{12.5}$$

for any loop $\mathfrak{C}$ that is reflection-symmetric. Changing the sign of $J_{(ij)}$ with $(ij) \in \mathfrak{C}$ is equivalent to changing the sign of the corresponding u_{ij},

so one infers from (12.5) that

$$\widetilde{\mathfrak{B}}(\mathfrak{C}) = - \prod_{(ij)\in\mathfrak{C}} u_{ij} = \text{sgn}\left(\prod_{(ij)\in\mathfrak{C}} J_{(ij)}\right). \tag{12.6}$$

This completes the proof of the proposition. The corollary follows as every plaquette in the ladder is reflection-symmetric and hence vortex free, and the same then follows for the loop $\mathfrak{C}$. $\qquad\square$

Implications for reflection-symmetric spin ladders

For open ladders, we know that the ground-state energies of $\widetilde{H}$ and H agree, as shown in Proposition 14. We also know that the projection P commutes with all the vortex operators, see Proposition 11. On the other hand, in the case of a closed ladder we do not know whether the spectra coincide, and in particular whether the ground-state energies are the same. We have shown the following:

Theorem 18. *The ground-state of the Hamiltonian H for an open spin ladder satisfying condition (12.3) with respect to a reflection plane Π has the vortex configuration*

$$\mathfrak{B}(\mathfrak{C}) = sgn\left(\prod_{(ij)\in\mathfrak{C}} J_{(ij)}\right), \tag{12.7}$$

in each non-degenerate, reflection-symmetric loop $\mathfrak{C}$ that crosses Π. In case the couplings have all the same sign, the ground-state is vortex-free in those loops.

12.7   Numerical evidence

In this section we give some numerical evidence for the spectral properties of H and $\widetilde{H}$, both in the case of open and of closed ladders. We have shown in Proposition 14 that the spectra of H and $\widetilde{H}$ are identical for an open ladder. However this is not true for a closed ladder. Even a simple closed ladder with $N = 2$ (four plaquettes) shows by explicit numerical diagonalization that $\widetilde{H}$ has eigenvalues not present in the spectrum of H, see §12.7. For this Hamiltonian, we plot the energies and show the vortex configurations for a number of eigenvalues.

We inspect the low-lying spectrum of the Hamiltonians H and $\widetilde{H}$ for a number of ladders of length N, in case that N is as large as 100, so with

up to 400 spins and $1,600$ Majoranas. We use Mathematica 8.0.4.0 and Matlab 7.10.0.499 (R2010a). In order to find which eigenvalues of $\widetilde{H}$ are eigenvalues of H, we use the method introduced in [179].

Our numerical analysis suggests that the ground state of $\widetilde{H}$ and also the ground state of H is vortex free, whether or not they have the symmetry (12.3), leading to the conjecture at the end of the section.

Open ladders

We first analyze an open ladder with $N = 2$ (three plaquettes). In Fig. 12.5 we plot the low-lying eigenvalues of both H and $\widetilde{H}$. We have chosen the
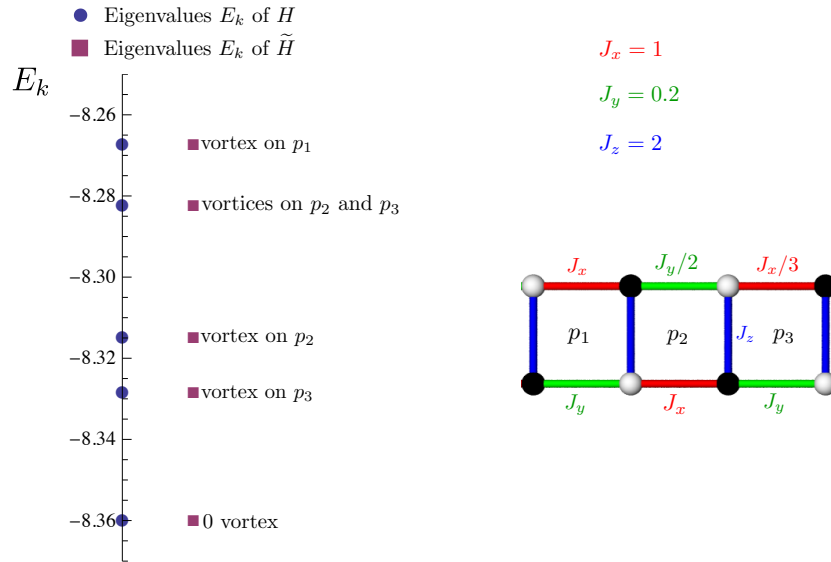
Figure 12.5: Low-lying eigenvalues of H and $\widetilde{H}$ for an open ladder with the illustrated couplings. We plot eigenvalues of H with circles and those of $\widetilde{H}$ with squares, and we ignore multiplicities. Other couplings yield qualitatively similar plots.

couplings $J_z = 2$, and the x and y couplings to decrease from left to right on the top of the ladder, but not on the bottom. These couplings are neither reflection-symmetric nor homogeneous. The plaquettes are labeled p_n with $n = 1, 2, 3$ from left to right as illustrated in Fig. 12.5. The numerical eigenvalues of H and $\widetilde{H}$ agree, as we already have shown in Proposition 14. It is interesting that the one-vortex configurations yield the first excited states (aside from multiplicity) and the placement on the ladder
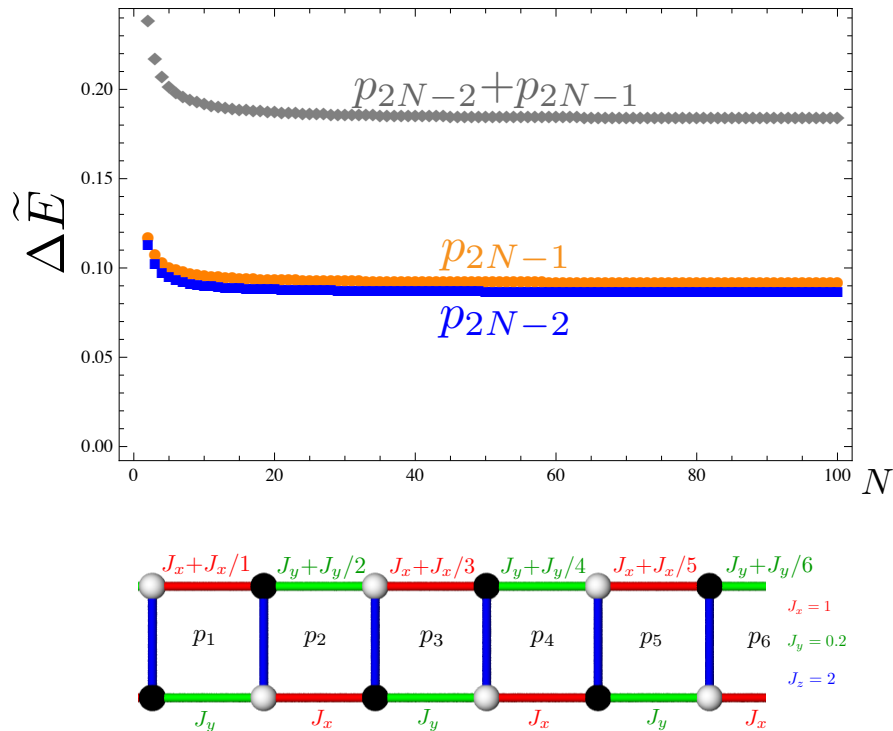
Figure 12.6: We plot the lowest energies of excitation for an open ladder of length N, with a vortex on plaquette p_{2N-2}, on plaquette p_{2N-1}, or on both. The choice of the couplings is shown in the figure, and the vortex configurations are explained in the text.

of the vortex that creates the minimal-energy excitation corresponds to the configuration of coupling constants that one intuitively expects.

Hamiltonians for open ladders of Length N

Next we consider a sequence of Hamiltonians $\widetilde{H}$ for open ladders with variable length N. We choose non-homogeneous couplings that decay on the upper rungs of the ladder from $2J_x$ and $3J_y/2$ on the left, to $J_x + J_x/(2N-1)$ and $J_y + J_y/(2N-2)$ on the right. On the bottom rungs we take homogeneous couplings. We plot the case $J_x = 1$, $J_y = 0.2$, and $J_z = 2$, as illustrated in Fig. 12.6. We find that the ground state energy corresponds to a vortex-free configuration. We then consider the minimal energy excitation above the ground state (neglecting multiplicity).

Among the configuration we have tested, the minimal energy excitation above the vortex-free configuration appears to occur with a single

vortex on a plaquette p_{2N-j} for small j. The effect of the boundary of the ladder at plaquette p_{2N-1} seems to raise slightly the energy of the single vortex in that plaquette, as illustrated in two curves labeled by p_{2N-2} and p_{2N-1}. We have computed other single-vortex excitations that confirm this picture.

We also plot the excitation energy of a configuration with two vortices on plaquettes p_{2N-2} and p_{2N-1}. This is approximately twice the energy of a single vortex.

Closed ladders

We present numerical evidence for several closed ladders, and contrast the results with the case of the open ladders. In spite of the fact that we observe numerically that $\widetilde{H}$ and H have different spectra, the ground-state energy of $\widetilde{H}$ coincides with the ground-state energy of H and the ground-state vortex-loop configuration is vortex-free.
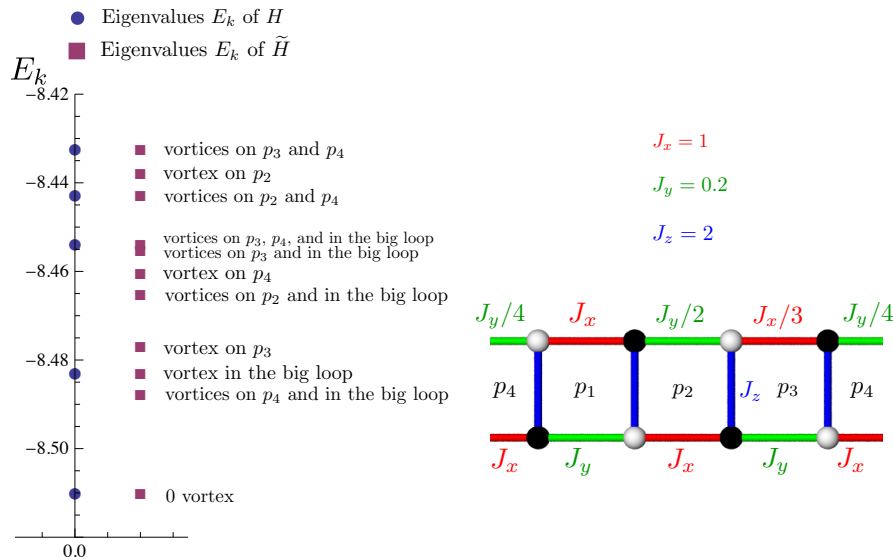
Figure 12.7: Low-lying eigenvalues of H and $\widetilde{H}$ for an $N = 2$ closed ladder without symmetry. Here $\widetilde{H}$ has eigenvalues that do not occur in H. We refer to the "big loop" as a loop with four horizontal bonds (around either the top or the bottom of the ladder). As in Fig. 12.5 we ignore multiplicities.

Hamiltonians $\widetilde{H}$ and H for closed ladders of length $N = 2$

We first analyze the $N = 2$ ladder with couplings of the same sort as in Fig. 12.5, but with non-zero couplings on the bonds closing the ladder, as illustrated in Fig. 12.7. We plot the low-lying eigenvalues of H and $\widetilde{H}$, aside from multiplicity. We label the eigenvalues we plot by their vortex loop configuration.

Hamiltonians $\widetilde{H}$ and H for closed ladders of length N

Here we consider the two smallest excitations above the ground state of the Hamiltonians $\widetilde{H}$ and H for ladders of variable length $2 \leqslant N \leqslant 100$. We choose non-homogeneous couplings that decay on the upper rungs of the ladder from $2J_x$ and $3J_y/2$ on the left, to $J_x + J_x/(2N - 1)$ and $J_y + J_y/(2N)$ on the right. On the bottom rungs we take homogeneous couplings. We plot the case $J_x = 1$, $J_y = 0.2$, and $J_z = 2$. See Fig. 12.8.

We find that the lowest energy of the configurations we tested is a zero-vortex state. We redefine this energy to be zero. However, we also find that the energy for the state with lowest energy and having a vortex in the big loop, decays rapidly with N. We plot the energy $\Delta \widetilde{E}$ (relative to the vortex-free state) for one vortex in the big loop (BL), two vortices in the big loop and on plaquette p_{2N} (BL+p_{2N}), and finally three vortices in the big loop, on p_{2N-1} and p_{2N} (BL+p_{2N-1}+p_{2N}). The configurations BL and BL+p_{2N} appear to be the lowest-energy excitations of $\widetilde{H}$. By computing the eigenvalues of H, we find that the minimal-energy configuration is vortex-free, and the eigenvalue equals the ground state energy of $\widetilde{H}$. However the lowest-energy excitations of H appear to arise from the vortex-loop configurations BL and BL+p_{2N-1}+p_{2N}.

Conjecture based on numerical evidence

We have performed numerical calculations for different ladder lengths and coupling configurations that we do not show here, but they all result in similar behavior. Even though these configurations of the couplings approximate homogeneous configuration for large N, this motivates:

Conjecture 19. *For a closed ladder, the ground state energies of H in (14.16) and $\widetilde{H}$ in (12.4) coincide. For a closed or open ladder with the coupling constants $J_{(ij)}$ all positive or all negative, the ground states of H and $\widetilde{H}$ are vortex-free.*
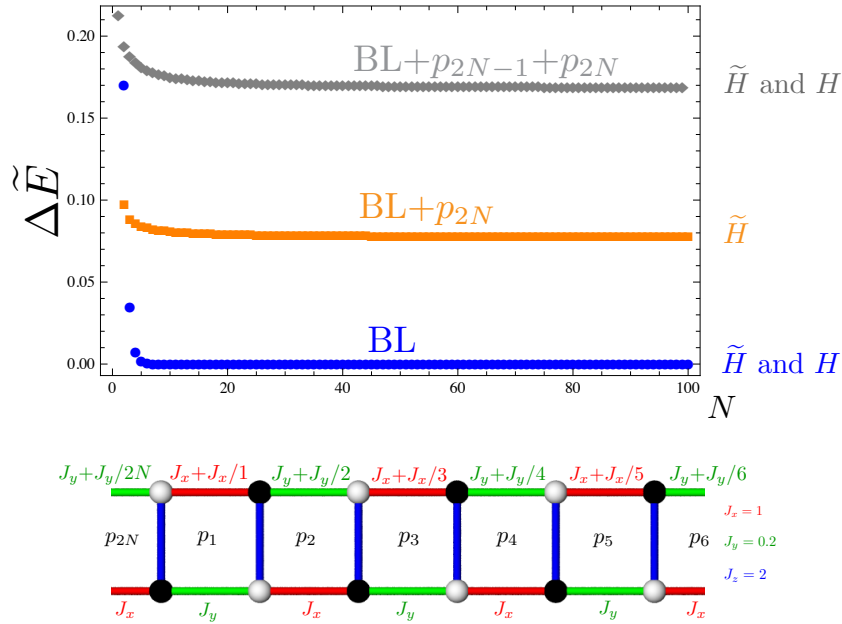
Figure 12.8: Excitation energies for closed ladders of length N compared with the vortex-free configuration. The choice of the couplings is shown in the figure, and the vortex configurations are explained in the text.

12.8 Perturbative results without reflection symmetry

In the previous sections we found that ladders satisfying (12.3) and all positive couplings (or all negative couplings) have ground states with no vortex in any reflection-symmetric loop $\mathfrak{C}$. It is of interest to understand whether the vortex-free property extends to open and closed ladders that do not satisfy (12.3). Here we investigate this question by perturbation theory, and find evidence that certain ladders have vortex-free ground-state configurations.

We study ladders for which the x-couplings are all equal to J_x, but for which

$$J_x \gg J_{(i,\,i+3)},\ J_{(i,\,i+1)} \geqslant 0\,. \tag{12.1}$$

For homogeneous couplings with $J_z \gg |J_x|\,, |J_y|$, the ground-state of the open ladder in lowest-order perturbation theory (depending upon N) has been shown to be vortex-free when $J_x\,J_y > 0$ or vortex-full when $J_x\,J_y < 0$. [36] Qualitatively this situation is different from the one we

study here, as our perturbation satisfying (12.1) gives a vortex contribution to the energy only in third order perturbation theory, rather than in second order. On the other hand the perturbation theory evidence in [36] that the ground state is vortex-free or vortex-full agrees with Conjecture 19 in §12.7.

Write the Hamiltonian as

$$H = H_0 + V \,, \tag{12.2}$$

where

$$H_0 = -J_x \sum_{(ij)_x} \sigma_i^x \sigma_j^x \,, \quad \text{and} \quad V = -\sum_{(ij)_y} J_{(ij)} \, \sigma_i^y \sigma_j^y - \sum_{(ij)_z} J_{(ij)} \, \sigma_i^z \sigma_j^z \,, \tag{12.3}$$

where $(ij)_{x,y,z}$ denotes type-x, y, z bonds. We consider perturbations of H_0 by V. In the case of the open ladder, $\boldsymbol{\sigma}_1$ and $\boldsymbol{\sigma}_{4N}$ do not occur in H_0.

Proposition 20 (Open Ladder**).** *Assume that $0 < J_{(ij)}$ for all bonds (ij). Also assume that there are constants $0 < M_1$, $0 < M_2$ such that $J_{(ij)} < M_1$ for y and z bonds (ij) and $M_2 < J_x$. Then for M_1/M_2 sufficiently small, the ground state of Hamiltonian (14.16) is vortex-free.*

Remark. We believe that in Proposition 20 one can choose M_1/M_2 sufficiently small, uniformly in N. Establishing such a result about the boundedness of the magnitude of differences of eigenvalues of H requires detailed analysis of the local nature of the perturbation. One needs to estimate non-perturbatively the error in the low-energy perturbation analysis, within a small region of couplings bounded by M_1/M_2, uniformly in N. Cluster expansions have been used to do this, both in field theory [196] and in lattice systems. For the latter a framework is given in [197, 198] and several related papers. Working out the details to bound the energy differences for the ladder Hamiltonian H remains an interesting project.

Proof. First we establish the notation we use. The ground-state eigenspace $\mathcal{P}_0$ of the Hamiltonian H_0 has 2^{2N+1} ground states, which we label by the eigenvalues of σ_j^x, for $j = 1, \ldots, 4N$, with the constraint $\sigma_i^x \sigma_j^x = +1$ for all bonds $(ij)_x$. We use m to denote the set of eigenvalues of σ_j^x for $j = 1, \ldots, 4N$ that satisfy the constraint. Let $\mathcal{P}_0^\perp = 1 - \mathcal{P}_0$. Note that $\mathfrak{B}(\partial p_n)$ commutes with H_0 and thus with $\mathcal{P}_0$. Decompose the perturbation V in two parts, $V = V_z + V_y$ with

$$V_z = \sum_{j=1}^{2N} V_z^j = -\sum_{j=1}^{2N} J_{(2j-1, 2j)} \, \sigma_{2j-1}^z \sigma_{2j}^z \,, \tag{12.4}$$

and

$$V_y = \sum_{j=1}^{2N-1} V_y^j = -\sum_{j=1}^{2N-1} J_{(2j-1,\,2j+2)} \sigma_{2j-1}^y \sigma_{2j+2}^y \ . \tag{12.5}$$

The First-Order Effective Hamiltonian. The first-order effective Hamiltonian is

$$\mathcal{P}_0 \, H_{\text{eff}}^{(1)} \, \mathcal{P}_0 = \mathcal{P}_0 \, V \, \mathcal{P}_0 = 0 \ . \tag{12.6}$$

The Second-Order Effective Hamiltonian. The second-order effective Hamiltonian has matrix elements

$$(\mathcal{P}_0 \, H_{\text{eff}}^{(2)} \, \mathcal{P}_0)_{m,m'} = \frac{1}{2} \sum_l V_{m,l} V_{l,m'} \left[\frac{1}{E_m - E_l} + \frac{1}{E_{m'} - E_l} \right] , \tag{12.7}$$

where l labels eigenstates in $\mathcal{P}_0^\perp$. Here $V_{m,l}$, and E_l are the corresponding matrix elements of V and H_0. As $\mathcal{P}_0 \, V_j^z V_{j'}^z \, \mathcal{P}_0 = 0$, $\mathcal{P}_0 \, V_j^y V_{j'}^y \, \mathcal{P}_0 = 0$ for $j \neq j'$, and $\mathcal{P}_0 \, V_j^z V_{j'}^y \, \mathcal{P}_0 = 0$ for all j and j', so one obtains

$$\begin{aligned}
&\mathcal{P}_0 \, H_{\text{eff}}^{(2)} \, \mathcal{P}_0 \\
&= \ -\frac{1}{4J_x} \left(\sum_{j=1}^{2N-1} J_{(2j-1,\,2j+2)}^2 + \sum_{j=1}^{2N} J_{(2j-1,\,2j)}^2 \right. \\
&\qquad \left. + J_{(1,\,4)}^2 + J_{(4N-3,\,4N)}^2 + J_{(1,\,2)}^2 + J_{(4N-1,\,4N)}^2 \right) \mathcal{P}_0 \ .
\end{aligned}$$

This Hamiltonian does not involve the σ's, so it does not introduce any splitting of the different vortex configurations.

The Third-Order Effective Hamiltonian. The third-order effective Hamiltonian has matrix elements

$$\begin{aligned}
&(\mathcal{P}_0 \, H_{\text{eff}}^{(3)} \, \mathcal{P}_0)_{m,m'} \\
&= -\frac{1}{2} \sum_{l,m''} \left[\frac{V_{m,l} V_{l,m''} V_{m'',m'}}{(E_{m'} - E_l)(E_{m''} - E_l)} + \frac{V_{m,m''} V_{m'',l} V_{l,m'}}{(E_m - E_l)(E_{m''} - E_l)} \right] \tag{12.8} \\
&+ \frac{1}{2} \sum_{l,l'} V_{m,l} V_{l,l'} V_{l',m'} \left[\frac{1}{(E_m - E_l)(E_m - E_{l'})} + \frac{1}{(E_{m'} - E_l)(E_{m'} - E_{l'})} \right] \ .
\end{aligned}$$

We claim this simplifies to

$$
\mathcal{P}_0\, H_{\text{eff}}^{(3)}\, \mathcal{P}_0 = -\sum_{k=2}^{2N-2} \frac{J_{(2k-1,\,2k)}\, J_{(2k-1,\,2k+2)}\, J_{(2k+1,\,2k+2)}}{8 J_x^2} \mathfrak{B}(\partial p_k)\, \mathcal{P}_0
$$
$$
-\frac{J_{(1,\,2)}\, J_{(1,\,4)}\, J_{(3,\,4)}}{2 J_x^2} \mathfrak{B}(\partial p_1)\, \mathcal{P}_0
$$
$$
-\frac{J_{(4N-3,\,4N-2)}\, J_{(4N-3,\,4N)}\, J_{(4N-1,\,4N)}}{2 J_x^2} \mathfrak{B}(\partial p_{2N-1})\, \mathcal{P}_0 .
$$

$$(12.9)$$

The minimal energy configuration for the Hamiltonian (12.9) therefore occurs in the case that all $\mathfrak{B}(\partial p_k) = +1$. The single sum over k reflects the extensive nature of the eigenvalues in perturbation theory, see for example [75]. The splitting of the degenerate ground states occurs in case a single vortex $\mathfrak{B}(\partial p_k) = -1$. This raises the energy of such a state by the quantity

$$
\delta E = \begin{cases} \frac{J_{(2k-1,\,2k)}\, J_{(2k-1,\,2k+2)}\, J_{(2k+1,\,2k+2)}}{4 J_x^2}, & \text{for } k = 2, \ldots, 2N-2 \\ \frac{J_{(1,\,2)}\, J_{(1,\,4)}\, J_{(3,\,4)}}{J_x^2}, & \text{for } k = 1 \\ \frac{J_{(4N-3,\,4N-2)}\, J_{(4N-3,\,4N)}\, J_{(4N-1,\,4N)}}{J_x^2}, & \text{for } k = 2N-1 \end{cases} \quad . \quad (12.10)
$$

Which plaquette p_k gives rise to the minimal energy shift depends upon the choice of the coupling constants $J_{(ij)}$. In every case, the energy shift is positive as long as $J_{(ij)} > 0$. For given M_1 and M_2, the energy shifts δE due to a single vortex on one plaquette—as given by third-order perturbation theory—are bounded away from zero, and also from above, uniformly in N.

We justify the expression (12.9) as follows. The first sum in (12.8) vanishes because $\mathcal{P}_0 V \mathcal{P}_0 = 0$. The perturbation V_z^j contains the product $\sigma_{2j-1}^z \sigma_{2j}^z$ and V_y^j contains the product $\sigma_{2j-1}^y \sigma_{2j+2}^y$, so the only possible third-order terms have the form $V_z V_y V_z$, $V_z V_z V_y$, or $V_y V_z V_z$, where

$$
V_z V_y V_z = -\sum_{j,k,l} J_{(2j-1,\,2j)}\, J_{(2k-1,\,2k+2)}\, J_{(2l-1,\,2l)}\, \sigma_{2j-1}^z \sigma_{2j}^z\, \sigma_{2k-1}^y \sigma_{2k+2}^y\, \sigma_{2l-1}^z \sigma_{2l}^z ,
$$

etc. There are only two possible choices of indices such that $\mathcal{P}_0 V_z V_y V_z \mathcal{P}_0$ does not vanish, namely $j = k$, $l = k + 1$, and $l = k$ and $j = k + 1$. One

thus obtains

$$
\begin{aligned}
&\mathcal{P}_0 \, V_z V_y V_z \, \mathcal{P}_0 \\
&= \; -2 \sum_k J_{(2k-1,\,2k)} J_{(2k-1,\,2k+2)} J_{(2k+1,\,2k+2)} \mathcal{P}_0 \, \sigma^x_{2k-1} \, \sigma^z_{2k} \sigma^z_{2k+1} \sigma^x_{2k+2} \, \mathcal{P}_0 \\
&= \; 2 \sum_k J_{(2k-1,\,2k)} J_{(2k-1,\,2k+2)} J_{(2k+1,\,2k+2)} \, \mathfrak{B}(\partial p_k) \, \mathcal{P}_0 \,. \qquad (12.11)
\end{aligned}
$$

Here we use $\mathcal{P}_0 \, \sigma^z_{2k}\sigma^z_{2k+1} \, \mathcal{P}_0 = -\mathcal{P}_0 \, \sigma^y_{2k}\sigma^y_{2k+1} \, \mathcal{P}_0$ and the definition of $\mathfrak{B}(\partial p_k)$ in (12.2). Similarly

$$
\begin{aligned}
&\mathcal{P}_0 \, V_z V_z V_y \, \mathcal{P}_0 \\
&= \; 2 \sum_k J_{(2k-1,\,2k)} J_{(2k-1,\,2k+2)} J_{(2k+1,\,2k+2)} \, \mathcal{P}_0 \sigma^x_{2k-1} \sigma^z_{2k} \sigma^z_{2k+1} \sigma^x_{2k+2} \mathcal{P}_0 \\
&= \; -2 \sum_k J_{(2k-1,\,2k)} J_{(2k-1,\,2k+2)} J_{(2k+1,\,2k+2)} \, \mathfrak{B}(\partial p_k) \, \mathcal{P}_0 \,. \qquad (12.12)
\end{aligned}
$$

The terms in (12.11)–(12.12) that do not contain the boundary plaquettes $\mathfrak{B}(\partial p_1)$ and $\mathfrak{B}(\partial p_{2N-1})$ cancel identically; they have the same energy denominators and opposite signs. Finally

$$
\begin{aligned}
&\mathcal{P}_0 V_y V_z V_z \, \mathcal{P}_0 \\
&= \; 2 \sum_k J_{(2k-1,\,2k)} J_{(2k-1,\,2k+2)} J_{(2k+1,\,2k+2)} \, \mathcal{P}_0 \sigma^x_{2k-1} \sigma^z_{2k} \sigma^z_{2k+1} \sigma^x_{2k+2} \, \mathcal{P}_0 \\
&= \; -2 \sum_k J_{(2k-1,\,2k)} J_{(2k-1,\,2k+2)} J_{(2k+1,\,2k+2)} \, \mathfrak{B}(\partial p_k) \, \mathcal{P}_0 \,. \qquad (12.13)
\end{aligned}
$$

Therefore the contribution to $\mathcal{P}_0 H^{(3)}_{\text{eff}} \mathcal{P}_0$ that does not involve the boundary plaquettes p_1 and p_{2N-1} is

$$
-\sum_{k=2}^{2N-2} \frac{J_{(2k-1,\,2k)} J_{(2k-1,\,2k+2)} J_{(2k+1,\,2k+2)}}{8 J_x^2} \, \mathfrak{B}(\partial p_k) \, \mathcal{P}_0 \,.
$$

The situation is different for terms entering in the perturbations $V_z V_y V_z$, $V_z V_z V_y$, and $V_y V_z V_z$ and involving plaquettes p_1 and p_{2N-1}. The reason is that $\boldsymbol{\sigma}_1$ and $\boldsymbol{\sigma}_{4N}$ do not enter into H_0. Taking this into account, the coefficients of the boundary terms differ. However, they are still negative and the third-order effective Hamiltonian is (12.9).

The fact that the perturbation theory result applies in a region of couplings for small M_1/M_2 is a consequence of the analyticity of the eigenvalues, see [199] and §II.1.3–II.1.4 of [200] . $\qquad \square \qquad\qquad \square$

Proposition 21 (**Closed Ladder with** $N > 2$). *Under the hypothesis of Proposition 20, the ground state of the Hamiltonian H in (14.16) with closed boundaries is vortex-free on each plaquette $p_1, \ldots, p_{2N}$. The effective Hamiltonian to third order is*

$$
\mathcal{P}_0 H_{\text{eff}}^{\leqslant 3} \mathcal{P}_0 \;=\; H_0 \mathcal{P}_0 - \frac{1}{4J_x} \left(\sum_{j=1}^{2N-1} J_{(2j-1,\,2j+2)}^2 + \sum_{j=1}^{2N} J_{(2j-1,\,2j)}^2 + J_{(2,\,4N-1)}^2 \right) \mathcal{P}_0
$$

$$
- \sum_{k=1}^{2N-1} \frac{J_{(2k-1,\,2k)}\, J_{(2k-1,\,2k+2)}\, J_{(2k+1,\,2k+2)}}{8J_x^2} \, \mathfrak{B}(\partial p_k) \, \mathcal{P}_0 \,. \qquad (12.14)
$$

Remark. The perturbative expansion up to third order will not give a splitting in energy due to a vortex on the big loop (the shortest loop around the top or bottom of the closed ladder). This will occur only in perturbation theory of order $O(N)$; but a single vortex in this loop gives an energy shift that is exponentially small in N.

Proof. The Hamiltonian H in (14.16) possesses two additional bonds $(2,\,4N-1)$ and $(1,\,4N)$ that do not occur in the open ladder. They yield interaction terms

$$
H_x^{\text{closed}} = -J_x\, \sigma_1^x\, \sigma_{4N}^x \qquad \text{and} \qquad V_y^{\text{closed}} = -J_{(2,\,4N-1)}\, \sigma_2^y \sigma_{4N-1}^y \,. \quad (12.15)
$$

We incorporate H_x^{closed} in the unperturbed Hamiltonian H_0 and V_y^{closed} in the perturbation V_y. Define $V_y^{2N} = V_y^{\text{closed}}$, we have $V_y = \sum_{j=1}^{2N} V_y^j$. We now derive the first order, second order, and third order effective Hamiltonians.

The First-Order Effective Hamiltonian. As in the proof of Proposition 20, the first-order effective Hamiltonian vanishes.

The Second-Order Effective Hamiltonian. Also as in the proof of Proposition 20, the second-order is given in (12.7). For ladders with $N > 2$ the only second order terms that do not vanish are $\mathcal{P}_0 \left(V_z^j \right)^2 \mathcal{P}_0$ and $\mathcal{P}_0 \left(V_y^j \right)^2 \mathcal{P}_0$. The ladder being closed, all the energy denominators in (12.7) are the same. One thus obtains the second-order term.

The Third-Order Effective Hamiltonian. As for the open ladder, the third-order effective Hamiltonian is given in (12.8). For the same reason as in the case of the open ladder, the first sum in (12.8) vanishes. Again the relevant perturbations are $\mathcal{P}_0 V_z V_y V_z \mathcal{P}_0$, $\mathcal{P}_0 V_z V_z V_y \mathcal{P}_0$, $\mathcal{P}_0 V_y V_z V_z \mathcal{P}_0$. The cancelation of the terms (12.11) and (12.12) of the first two perturbations for the open ladder also takes place for the closed ladder. Furthermore, since the ladder is closed, the energy denominators appearing in

$\mathcal{P}_0 V_z V_y V_z \mathcal{P}_0$, $\mathcal{P}_0 V_z V_z V_y \mathcal{P}_0$, $\mathcal{P}_0 V_y V_z V_z \mathcal{P}_0$ are all the same and no "boundary" terms appear in the third-order effective Hamiltonian. $\qquad\square$

12.9 Acknowledgements

Part IV

Absence of Spontaneous Magnetic Order of Lattice Spins Coupled to Itinerant Interacting Electrons in One and Two Dimensions

CHAPTER 13

Introduction

Since the seminal work on phase transitions by Hohenberg [201] and Mermin and Wagner [136] it has become common knowledge that spontaneous order in low-dimensional systems is generically not possible at any finite temperature. In these studies, the use of the Bogoliubov inequality [202] was essential: Hohenberg used it to rule out superfuidity [201] and Mermin and Wagner to rule out magnetic order in Heisenberg spin systems [136] in dimensions $d < 3$. This approach is very powerful and was then applied to many different systems, [203, 204, 205, 206, 207, 208, 209] including the Anderson and Kondo lattice models. [210, 211]

For systems in the continuum, the weak coupling approximation is often applied leading to an effective exchange coupling between the localized spins which is of the RKKY-type. [212] RKKY interactions occur in many physical systems, prominent examples of present interest are heavy-fermion systems, [213] diluted magnetic semiconductors, [214, 215, 216, 217] and nuclear spins in low-dimensional conducting nanostructures. [218, 219, 220] The latter system plays an important role as noise source for spin qubits in GaAs or InAs quantum dots, [5, 221, 222] and much effort goes into understanding and controling the nuclear spin bath, with one possibility being to freeze out the nuclear noise by magnetic order. [223, 224]

In contrast to the Heisenberg exchange, however, the RKKY interaction is long-ranged and thus is not covered by the original Mermin-Wagner theorem which requires the spin interactions to decay sufficiently fast with distance r (faster than $1/r^{2+d}$). [136] Addressing precisely this issue, Bruno [209] was able to rule out in RKKY systems magnetic order in one dimension. A similar conclusion, however, for the two-dimensional

counterpart appears still to be missing. Here we will fill this gap by rigorously proving the absence of order for a rather general class of systems which consist of lattice spins embedded in a continuum of itinerant electrons with which they interact by an isotropic on-site spin interaction. The allowed electron Hamiltonian H_e is very general and may include electron-electron interactions as well as any single-particle potential (such as lattice or disorder potential) that does not depend on spin. For this class of models we prove then that in the thermodynamic limit ferro- and antiferromagnetic, as well as helical, long-range order of the lattice spins is excluded at any finite temperature in dimensions one and two. We show that this conclusion remains valid when short-range Heisenberg interaction between lattice spins is included. Our result also applies to the RKKY case, since this regime is obtained from the full one by lowest order perturbation expansion in the on-site spin interaction [212] including the full H_e. [224]

Moreover, we consider the effect of Rashba [225] and Dresselhaus [226] spin-orbit interactions (SOI) which explicitly break the spin symmetry. Our argument becomes then inconclusive and magnetic order cannot be excluded. While this finding is not unexpected it is remarkable that it is closely linked to the existence of equilibrium spin currents studied recently in spintronics. [227, 228, 229] Even more remarkably, we find that in the special case when Rashba (α) and Dresselhaus (β) SOIs become equal, magnetic order is excluded again. Since α can be electrically tuned to β, [230, 231, 232] this opens up a new way to tune magnetism by electrical gates.

Finally, we note that the absence of spontaneous order proven here is valid only in the thermodynamic limit; thus, effective ordering in nanostructures of finite size at sufficiently low (but finite) temperatures is not in conflict with our findings.

Extended Mermin-Wagner Theorem

We extend the Mermin-Wagner theorem to a system of lattice spins which are spin-coupled to itinerant and interacting charge carriers. We use the Bogoliubov inequality to rigorously prove that neither (anti-) ferromagnetic nor helical long-range order is possible in one and two dimensions at any finite temperature. Our proof applies to a wide class of models including any form of electron-electron and single-electron interactions that are independent of spin. In the presence of Rashba or Dresselhaus spin-orbit interactions (SOI) magnetic order is not excluded and intimately connected to equilibrium spin currents. However, in the special case when Rashba and Dresselhaus SOIs are tuned to be equal, magnetic order is excluded again. This opens up a new possibility to control magnetism electrically.

14.1 Model

We consider a lattice $\{\boldsymbol{R}_j\}_{j=1}^{N_I}$ filled with N_I spins $\hat{\boldsymbol{I}}_j = (\hat{I}_j^x, \hat{I}_j^y, \hat{I}_j^z)$ located at the sites $\boldsymbol{R}_j$. The lattice is embedded into a volume Ω containing N_e itinerant electrons which couple to the lattice spins via on-site spin-spin interactions. The Hamiltonian for the entire system reads,

$$H = H_e + J \sum_{j=1}^{N_I} \hat{\boldsymbol{S}}_j \cdot \hat{\boldsymbol{I}}_j + h \sum_{j=1}^{N_I} (e^{-i\boldsymbol{Q}\cdot\boldsymbol{R}_j} \hat{I}_j^z + \text{h.c.}), \qquad (14.1)$$

where $H_e = H_0 + V + U = \sum_{i=1}^{N_e} \hat{\boldsymbol{p}}_i^2/2m + \sum_{i<j}^{N_e} V_{ij} + \sum_{i=1}^{N_e} U(\hat{\boldsymbol{r}}_i)$ is the Hamiltonian describing the electron system. Here, m is the mass and $\hat{\boldsymbol{p}}_i$ the momentum operator of the ith electron, $V_{ij} = V(\hat{\boldsymbol{r}}_i - \hat{\boldsymbol{r}}_j)$ the electron-electron interaction of electrons at positions $\hat{\boldsymbol{r}}_i$ and $\hat{\boldsymbol{r}}_j$, and $U(\hat{\boldsymbol{r}}_i)$ an arbitrary spin-independent single-electron potential. Typical examples for $U(\hat{\boldsymbol{r}}_i)$ are periodic lattice potentials, disorder potentials, electron-phonon interactions [1], etc. We remark that in contrast to previous work on lattice models, [210, 211] we do not restrict the motion of the electrons to the sites of a lattice (tight binding limit) but allow them to move in the real space continuum. Further, J denotes the coupling strength of the isotropic spin interaction at lattice site $\boldsymbol{R}_j$, $H_J = J \sum_{j=1}^{N_I} \hat{\boldsymbol{S}}_j \cdot \hat{\boldsymbol{I}}_j$, where $\hat{\boldsymbol{S}}_j \equiv \hat{\boldsymbol{S}}(\boldsymbol{R}_j)$ is the electron spin density operator $\hat{\boldsymbol{S}}(\boldsymbol{r}) = \sum_{i=1}^{N_e} \hat{\boldsymbol{s}}_i \delta(\boldsymbol{r} - \hat{\boldsymbol{r}}_i)$, with $\hat{\boldsymbol{s}}_i = (\hat{s}_i^x, \hat{s}_i^y, \hat{s}_i^z)$ being the spin-$1/2$ of the ith electron. The vector components of each spin, $\hat{s}_i^k$ and $\hat{I}_j^l$, satisfy standard spin commutation relations. Finally, to probe the order for the lattice spins $\hat{\boldsymbol{I}}_j$ we break the symmetry by an external (fictitious) field h pointing in, say, z direction, which we let then go to zero at the end. This leads to an additional Zeeman term $H_Z(\boldsymbol{Q}) = h \sum_{j=1}^{N_I} e^{-i\boldsymbol{Q}\cdot\boldsymbol{R}_j} \hat{I}_j^z + \text{h.c.}$ To rule out ferromagnetic order we will choose $\boldsymbol{Q} = 0$, whereas to exclude antiferromagnetic order we will choose $\boldsymbol{Q}$ such that $e^{-i\boldsymbol{Q}\cdot\boldsymbol{R}} = +1$, if $\boldsymbol{R}$ connects sites from the same sublattice, and $e^{-i\boldsymbol{Q}\cdot\boldsymbol{R}} = -1$, if $\boldsymbol{R}$ connects sites from different sublattices.

To prove the absence of spontaneous order for the lattice spins $\hat{\boldsymbol{I}}_j$ we follow Ref. [136] and make use of the Bogoliubov inequality, [202] which is an exact relation between two operators A, C, and a Hamiltonian H,

$$\frac{1}{2}\langle\{A, A^\dagger\}\rangle\langle[[C, H], C^\dagger]\rangle \geq k_B T |\langle[C, A]\rangle|^2. \qquad (14.2)$$

Here, $\langle A \rangle = Tr e^{-H/k_B T} A / Tr e^{-H/k_B T}$ denotes the expectation value in a canonical ensemble, T the temperature, k_B the Boltzmann constant, and

---

[1] H also contains then a free-phonon part, which, however, is of no consequence since Eq. (14.6) remains valid.

$\{A, B\} = AB + BA$ the anticommutator and $[A, B] = AB - BA$ the commutator. It is assumed that all expectation values are well-defined and exist in the thermodynamic limit defined by $N_e, N_I, \Omega \to \infty$ with electron density $n_e = N_e/\Omega$ and density of lattice spins $n_I = N_I/\Omega$ finite.

14.2 Proof

The strategy of the proof consists of using the Bogoliubov inequality to derive an upper bound for the order parameter corresponding to the phase transition we want to discuss. If this bound turns out to be in contradiction with the presence of long-range magnetic order, then the absence of the corresponding phase transition is rigorously demonstrated. The success of the procedure depends crucially on the choice of the operators A and C in (14.18). As we shall see, the appropriate choice for our case is given by

$$C_{\boldsymbol{q}} = \hat{S}_{-\boldsymbol{q}}^- + \hat{I}_{-\boldsymbol{q}}^- + \hat{S}_{-\boldsymbol{q}}^+ + \hat{I}_{-\boldsymbol{q}}^+ \,, \ A_{\boldsymbol{q}} = \hat{I}_{\boldsymbol{q}+Q}^+ + \hat{I}_{\boldsymbol{q}-Q}^+, \qquad (14.3)$$

where the Fourier transforms are given by $\hat{\boldsymbol{S}}_{\boldsymbol{q}} = \sum_{i=1}^{N_e} e^{-i\boldsymbol{q}\cdot\hat{\boldsymbol{r}}_i} \hat{\boldsymbol{s}}_i$ and $\hat{\boldsymbol{I}}_{\boldsymbol{q}} = \sum_{j=1}^{N_I} e^{-i\boldsymbol{q}\cdot\boldsymbol{R}_j} \hat{\boldsymbol{I}}_j$ [2], and where $B^\pm \equiv B^x \pm iB^y$. Note that $C_{\boldsymbol{q}}$ and $A_{\boldsymbol{q}}$ are not hermitian in general. Since the Bogoliubov inequality (14.18) is valid for any wave vector $\boldsymbol{q}$, it can be generalized to

$$\frac{1}{2} \sum_{\boldsymbol{q}} \langle \{A_{\boldsymbol{q}}, A_{\boldsymbol{q}}^\dagger\} \rangle \geq k_B T \sum_{\boldsymbol{q}} \frac{|\langle [C_{\boldsymbol{q}}, A_{\boldsymbol{q}}] \rangle|^2}{\langle [[C_{\boldsymbol{q}}, H], C_{\boldsymbol{q}}^\dagger] \rangle}, \qquad (14.4)$$

where the sum runs over all $\boldsymbol{q}$'s in the first Brillouin zone of the reciprocal lattice. We note that the above choice for $C_{\boldsymbol{q}}$ and $A_{\boldsymbol{q}}$ is essential also for the following reason. Besides the fact that $\sum_{\boldsymbol{q}} \langle [C_{\boldsymbol{q}}, A_{\boldsymbol{q}}] \rangle$ can be expressed in terms of the lattice spin magnetization, the generally complicated interaction terms V and U in H_e simply drop out of the calculation since they commute with $C_{\boldsymbol{q}}$,

$$[C_{\boldsymbol{q}}, H_e] = [\hat{S}_{-\boldsymbol{q}}^- + \hat{S}_{-\boldsymbol{q}}^+, H_0]. \qquad (14.5)$$

This simplification is a crucial advantage of first over second quantization formalism since spin and position operators of the electrons trivially commute. [Note, however, that the expectation values still contain the

_____

[2]Here, $\boldsymbol{q}$ is restricted to the first Brillouin zone, and thus $\hat{\boldsymbol{S}}_{\boldsymbol{q}}$ is defined on the reciprocal lattice only, while $\hat{\boldsymbol{S}}(\boldsymbol{r})$ is a function in the real space continuum.

full Hamiltonian including U and V.] Hence, our proof goes through for any form of the potentials V and U as long as they are spin independent.

We now focus on the various terms in Eq. (14.4) and find bounds for them. Here, we outline only the main steps of the calculations and defer details to the Appendix. As a first step, let us evaluate the double commutator on the right-hand-side of inequality (14.4). By virtue of the commutation relation $[\hat{S}^{\pm}_{-\boldsymbol{q}}, H_0] = -\frac{\boldsymbol{q}}{2m}\sum_i \hat{s}^{\pm}_i \{\hat{\boldsymbol{p}}_i, e^{i\boldsymbol{q}\cdot\hat{\boldsymbol{r}}_i}\}$, we obtain that $[[C_{\boldsymbol{q}}, H_e], C^{\dagger}_{\boldsymbol{q}}] = \frac{1}{m}N_e q^2$. The part of the double commutator with H_J vanishes since $[C_{\boldsymbol{q}}, H_J] = 0$. Indeed, $[\hat{S}^{\pm}_{-\boldsymbol{q}}, H_J] = i\sum_{i,j} e^{i\boldsymbol{q}\cdot\hat{\boldsymbol{r}}_i}\delta(\hat{\boldsymbol{r}}_i - \boldsymbol{R}_j)(\hat{\boldsymbol{I}}_j \times \hat{\boldsymbol{s}}_i)^{\pm}$, and thus $[\hat{S}^{\pm}_{-\boldsymbol{q}}, H_J] = -[\hat{\boldsymbol{I}}^{\pm}_{-\boldsymbol{q}}, H_J]$. After some calculations (see Appendix) we find that $[[C_{\boldsymbol{q}}, H_z(\boldsymbol{Q})], C^{\dagger}_{\boldsymbol{q}}] = -4h(\sum_j e^{-i\boldsymbol{Q}\cdot\boldsymbol{R}_j}\hat{I}^z_j + h.c.)$. Hence,

$$\langle[[C_{\boldsymbol{q}}, H], C^{\dagger}_{\boldsymbol{q}}]\rangle = N_e \left(\frac{1}{m}q^2 - 4h\frac{N_I}{N_e}m^z_I(\boldsymbol{Q})\right), \qquad (14.6)$$

where the lattice spin magnetization appearing in Eq. (14.6), which we identify as the order parameter, is defined by $m^z_I(\boldsymbol{Q}) = \frac{1}{N_I}\langle\sum_j e^{-i\boldsymbol{Q}\cdot\boldsymbol{R}_j}\hat{I}^z_j + e^{i\boldsymbol{Q}\cdot\boldsymbol{R}_j}\hat{I}^z_j\rangle$. The commutator on the right-hand side of inequality (14.4) can also be expressed in terms of $m^z_I(\boldsymbol{Q})$,

$$\langle[C_{\boldsymbol{q}}, A_{\boldsymbol{q}}]\rangle = -2N_I m^z_I(\boldsymbol{Q}). \qquad (14.7)$$

Finally, the sum on the left-hand side of Eq. (14.4) can be bounded as follows,

$$\sum_{\boldsymbol{q}}\langle\{A_{\boldsymbol{q}}, A^{\dagger}_{\boldsymbol{q}}\}\rangle = 2N_I\sum_j\langle\{\hat{I}^+_j, \hat{I}^-_j\}(1 + \cos(\boldsymbol{Q}\cdot\boldsymbol{R}_j))\rangle$$
$$\leq 4N^2_I(2I)^2, \qquad (14.8)$$

where we have used that $\sum_{\boldsymbol{q}} e^{i\boldsymbol{q}\cdot(\boldsymbol{R}_i-\boldsymbol{R}_j)} = N_I\boldsymbol{\delta}_{\boldsymbol{R}_i,\boldsymbol{R}_j}$, and $\langle\{\hat{I}^+_j, \hat{I}^-_j\}\rangle \leq (2I)^2$. Using Eqs. (14.6), (14.7), and (14.8), we obtain from the Bogoliubov inequality (14.4)

$$4N^2_I(2I)^2/2 \geq k_B T\sum_{\boldsymbol{q}}\frac{4N^2_I m^z_I(\boldsymbol{Q})^2}{\langle[[C_{\boldsymbol{q}}, H], C^{\dagger}_{\boldsymbol{q}}]\rangle}. \qquad (14.9)$$

Our goal is to rule out spontaneous magnetization in the lattice spin system, therefore we are interested in the behavior of the order parameter $m^z_I(\boldsymbol{Q})$ in the limit of vanishing external field, i.e., $h \to 0$, after we have taken the thermodynamic limit. We need to distinguish two cases: $i)$ $m^z_I(\boldsymbol{Q}) = 0, \forall h$ around $h = 0$; $ii)$ $m^z_I(\boldsymbol{Q}) \neq 0, \forall h$ around $h = 0$. If $i)$ is

satisfied, there is no order and the proof is completed. If $ii)$ is satisfied, we need to show that $\lim_{h\to 0} m_I^z(\boldsymbol{Q}) = 0$ follows from inequality (14.9) in the thermodynamic limit. In this limit, the sum can be replaced by an integral,

$$(2I)^2 \;\geq\; \frac{k_B T N_I v}{N_e (2\pi)^d} \int\limits_{|\boldsymbol{q}|\leq|\boldsymbol{q}_c|} d^d q \; \frac{m_I^z(\boldsymbol{Q})^2}{\frac{q^2}{2m} + |\nu h m_I^z(\boldsymbol{Q})|}, \qquad (14.10)$$

where $\nu = 2N_I/N_e$, $\boldsymbol{q}_c$ is an arbitrary cut-off vector lying in the first Brillouin zone, $v = \Omega/N_I$, and we have used that $\langle [[C_{\boldsymbol{q}}, H], C_{\boldsymbol{q}}^\dagger] \rangle \leq N_e(q^2/m + |2\nu h m_I^z(\boldsymbol{Q})|)$. In the one-dimensional case ($d = 1$), Eq. (14.10) gives

$$\frac{\lambda_1 \sqrt{|h|}}{T} \left[\arctan\left(\frac{|\boldsymbol{q}_c|}{\sqrt{2m|\nu h m_I^z(\boldsymbol{Q})|}} \right) \right]^{-1} \geq \frac{m_I^z(\boldsymbol{Q})^2}{\sqrt{|m_I^z(\boldsymbol{Q})|}}, \qquad (14.11)$$

where $\lambda_1 = \pi(2I)^2 n_e \sqrt{\nu}/(k_B \sqrt{2m})$. In the limit $h \to 0$, the left hand-side of inequality (14.11) vanishes and this implies that $\lim_{h\to 0} m_I^z(\boldsymbol{Q}) = 0$. The two-dimensional case can be treated in a similar way. For $d = 2$, inequality (14.10) leads to the following relation

$$\frac{\lambda_2}{T} \left[\log\left(1 + \frac{|\boldsymbol{q}_c|^2}{2m|\nu h m_I^z(\boldsymbol{Q})|} \right) \right]^{-1} \geq m_I^z(\boldsymbol{Q})^2, \qquad (14.12)$$

where $\lambda_2 = 2\sqrt{2}\lambda_1/\sqrt{\nu m}$. It follows from inequality (14.12) that $\lim_{h\to 0} m_I^z(\boldsymbol{Q}) = 0$ here, too. Since our arguments were independent of the choice of $\boldsymbol{Q}$, we have proven that neither ferromagnetic nor antiferromagnetic long-range order of the lattice spins is possible at any finite temperature $T > 0$ in one and two dimensions.

The absence of order can be traced back to the increased fluctuations in the lattice spin system in lower dimensions. These fluctuations, in turn, have their origin in the kinetic energy of the electrons, as one can explicitly see from Eq. (14.10) where the term $q^2/2m$ is responsible for the divergency in above q-integrals for $d = 1$ and 2.

Next, we show that helical long-range order of the lattice spins is also excluded. The strategy of the proof remains the same and we shall be brief (for details see Appendix). To study this type of order, we consider the symmetry breaking Zeeman term $\tilde{H}_Z(\boldsymbol{Q}) = \sqrt{2/3} h \sum_j e^{-i\boldsymbol{Q}\cdot\boldsymbol{R}_j} \hat{I}_j^+ + h.c.$ and the magnetic order parameter $m_I^\perp(\boldsymbol{Q}) = \sqrt{2/3}\frac{1}{N_I}\langle \sum_j e^{-i\boldsymbol{Q}\cdot\boldsymbol{R}_j} \hat{I}_j^+ + h.c. \rangle$ which corresponds to a spin helix in the xy-plane. Note that the spin part of Hamiltonian (14.16) is isotropic and consequently all choices for

the helix are equivalent. The operators $\widetilde{C}_{\boldsymbol{q}}$ and $\widetilde{A}_{\boldsymbol{q}}$ for the Bogoliubov inequality (14.4) are now chosen to be

$$\widetilde{C}_{\boldsymbol{q}} = \hat{S}^z_{-\boldsymbol{q}} + \hat{I}^z_{-\boldsymbol{q}} \quad \text{and} \quad \widetilde{A}_{\boldsymbol{q}} = \frac{1}{\sqrt{3}} \left(\hat{I}^+_{\boldsymbol{q}+\boldsymbol{Q}} - \hat{I}^-_{\boldsymbol{q}-\boldsymbol{Q}} \right). \tag{14.13}$$

The double commutator on the right-hand side of Eq. (14.4) becomes then $\langle [[\widetilde{C}_{\boldsymbol{q}}, H], \widetilde{C}^\dagger_{\boldsymbol{q}}] \rangle = N_e \, (q^2/4m - \nu h m_I(\boldsymbol{Q})/2)$. Since $\langle [\widetilde{C}_{\boldsymbol{q}}, \widetilde{A}_{\boldsymbol{q}}] \rangle = (N_I/\sqrt{2}) m^\perp_I(\boldsymbol{Q})$ and $\sum_{\boldsymbol{q}} \langle \{ \widetilde{A}_{\boldsymbol{q}}, \widetilde{A}^\dagger_{\boldsymbol{q}} \} \rangle \leq 2 N_I^2 (2I)^2$, Eq. (14.4) takes in the thermodynamic limit exactly the same form as Eq. (14.10), where $m^z_I(\boldsymbol{Q})$ must be replaced by $m^\perp_I(\boldsymbol{Q})$. We thus conclude that $\lim_{h\to 0} m^\perp_I(\boldsymbol{Q}) = 0$ for any $\boldsymbol{Q}$ and hence long-range helical order is also excluded in one and two dimensions at any $T > 0$ [3].

As a further generalization, short-range impurity-spin Heisenberg interaction $H_{\mathcal{I}} = \sum_{i,j} \mathcal{I}_{ij} \hat{\boldsymbol{I}}_i \cdot \hat{\boldsymbol{I}}_j$ is added to Hamiltonian (14.16). When the couplings $\mathcal{I}_{ij}$ satisfy $1/N_I \sum_{ij} |\mathcal{I}_{ij}| (\boldsymbol{R}_i - \boldsymbol{R}_j)^2 < \infty$, then both proofs to exclude (anti-) ferromagnetic and helical ordering remain valid and lead to Eq. (14.10) with renormalized mass $m^* = m/(1 + 8mI^2 \frac{n_I}{n_e} \frac{1}{N_I} \sum_{ij} |\mathcal{I}_{ij}| (\boldsymbol{R}_i - \boldsymbol{R}_j)^2)$, see Appendix.

14.3   Presence of spin orbit interaction

Next we investigate the question of magnetic order in a low-dimensional electron gas in the presence of Rashba [225] and/or Dresselhaus [226] spin orbit interaction which break the rotational spin symmetry of the Hamiltonian (14.16) explicitly. The spin-orbit Hamiltonian is given by $H_{\mathrm{SO}} = H_{\mathrm{R}} + H_{\mathrm{D}}$, with $H_{\mathrm{R}} = \alpha \sum_{i=1}^{N_e} (\hat{p}^y_i \hat{s}^x_i - \hat{p}^x_i \hat{s}^y_i)$, $H_{\mathrm{D}} = \beta \sum_{i=1}^{N_e} (\hat{p}^x_i \hat{s}^x_i - \hat{p}^y_i \hat{s}^y_i)$, where α (β) is the Rashba (Dresselhaus) coefficient. Using Eq. (14.3) for $C_{\boldsymbol{q}}$, we obtain $[[C_{\boldsymbol{q}}, H_{\mathrm{SO}}], C^\dagger_{\boldsymbol{q}}] = 4m\alpha \hat{j}^y_{\boldsymbol{q}=0,x} + 4m\beta \hat{j}^y_{\boldsymbol{q}=0,y}$, where we have defined the spin-current density operator as $\hat{\boldsymbol{j}}^\alpha(\boldsymbol{r}) = \frac{1}{2m} \sum_{i=1}^{N_e} \hat{s}^\alpha_i \{ \hat{\boldsymbol{p}}_i, \delta(\hat{\boldsymbol{r}}_i - \boldsymbol{r}) \}$ and its corresponding Fourier component $\hat{j}^\alpha_{\boldsymbol{q}} = \frac{1}{2m} \sum_i \hat{s}^\alpha_i \{ \hat{\boldsymbol{p}}_i, e^{-i\boldsymbol{q}\cdot\hat{\boldsymbol{r}}_i} \}$. These spin currents may lead to an intrinsic cut-off for the fluctuations in q, and thus help to establish order. To see this, we evaluate now the spin currents perturbatively around the free electron limit, i.e. $U, V, J = 0$, and

---

[3]If $\boldsymbol{Q}$ corresponds to the (anti-) ferromagnetic case, then $m^z_I(\boldsymbol{Q})$ and $m^\perp_I(\boldsymbol{Q})$ are equivalent for isotropic systems.

at $T = 0$ [4],

$$\langle \hat{j}^y_{\boldsymbol{q}=0,x} \rangle_0 \;=\; \Omega \frac{mE_F}{4\pi} \alpha \tag{14.14}$$

$$\langle \hat{j}^y_{\boldsymbol{q}=0,y} \rangle_0 \;=\; -\Omega \frac{mE_F}{4\pi} \beta \,, \tag{14.15}$$

where E_F is the Fermi energy and the results are valid in the regime $m\alpha^2, m\beta^2 \ll \hbar^2 E_F$ [5]. Performing now a perturbative expansion in the parameters V, U, J, T around above free case, we conclude that $\langle \hat{j}^y_y \rangle \neq 0$ and $\langle \hat{j}^y_x \rangle \neq 0$ [6]. (In passing we note that in the stationary and homogeneous limit, the spin-currents satisfy the relations $\langle \hat{j}^x_x \rangle = -\langle \hat{j}^y_y \rangle$ and $\langle \hat{j}^y_x \rangle = -\langle \hat{j}^x_y \rangle$ due to a generalized continuity equation, see Appendix.) As a consequence, the commutator $\langle [[C_{\boldsymbol{q}}, H_{\mathrm{SO}}], C^\dagger_{\boldsymbol{q}}] \rangle$ appearing in Eq. (14.9) does not vanish anymore and thus provides an intrinsic cut-off to the q-integral (cf. Eq. (14.10)). Hence, the bound for the order parameter we extract from inequality (14.10) is a constant which does not vanish in the limit $h \to 0$. Thus, our argument becomes inconclusive and we cannot rule out (anti-) ferromagnetic order in this case.

Similarly, for helical order our argument remains inconclusive, since $[[\widetilde{C}_{\boldsymbol{q}}, H_{SO}], \widetilde{C}^\dagger_{\boldsymbol{q}}] = m\alpha(\hat{j}^y_{\boldsymbol{q}=0,x} - \hat{j}^x_{\boldsymbol{q}=0,y}) + m\beta(\hat{j}^y_{\boldsymbol{q}=0,y} - \hat{j}^x_{\boldsymbol{q}=0,x})$, which, will not vanish in general.

Next, let us consider the special case $\alpha = \beta$ where new symmetries emerge. [233] Then, the leading terms, Eqs. (14.14), (14.15), cancel, indicating that the physics changes dramatically. Indeed, by making use of the 'gauge transformation' $U = e^{i\sum_k \hat{\boldsymbol{A}}_k \cdot \hat{\boldsymbol{r}}_k}$, where $\hat{\boldsymbol{A}}_k = -\alpha m(\hat{s}^x_k - \hat{s}^y_k)(1,1,0)$, to remove the SOI from the Hamiltonian, we can prove as before (see Appendix) that (anti-) ferromagnetic order in z-direction can now be excluded rigorously for any $T > 0$ and $d = 1, 2$. Similarly, we can rule out helical ordering described by the order parameter $m^{\perp'}_I = \frac{1}{N_I}\langle \sum_j e^{-i\boldsymbol{Q}\cdot\boldsymbol{R}_j} \hat{I}^{+'}_j + h.c.\rangle$ with $\boldsymbol{Q} = \sqrt{2}\alpha m(1,1,0)$ (for rotated coordinates $(x,y,z) \to (x',y',z') = (z, (x+y)/\sqrt{2}, (x-y)/\sqrt{2})$, see Appendix).

Thus, quite remarkably, this spin orbit effect suggests the control of magnetism by electrical gates, namely by tuning the Rashba SOI (α) [230, 231, 232] from the regime $\alpha \neq \beta$ (ordering not excluded) to $\alpha = \beta$ (ordering excluded).

---

[4]The leading contribution to the spin-currents are linear in α, β, in contrast to Refs. [227, 229]. This is due to the different definitions of spin-currents, see Appendix.

[5]Eqs. (14.14,14.15) are valid for $h \neq 0$ since the Zeeman term simply drops out when $J = 0$.

[6]Presumably, the spin currents can remain non-zero even beyond the perturbative regime.

14.4   Conclusions

We proved an extension of the Mermin-Wagner theorem for lattice spins interacting with itinerant electrons, and showed that spontaneous order of the lattice spins is ruled out in one and two dimensions at finite temperature. In the presence of Rashba (α) and Dresselhaus (β) spin-orbit interactions, however, spontaneous order could not be excluded, unless for $\alpha = \beta$.

14.5   Acknowledgments

14.A   Model Hamiltonian

To make the Appendix largely self-contained we restate the problem defined in the main text briefly. We consider a lattice $\{\boldsymbol{R}_j\}_{j=1}^{N_I}$ filled with N_I spins $\hat{\boldsymbol{I}}_j = (\hat{I}_j^x, \hat{I}_j^y, \hat{I}_j^z)$ located at the sites $\boldsymbol{R}_j$. The lattice is embedded into a volume Ω containing N_e itinerant electrons which couple to the lattice spins via on-site spin-spin interactions. The Hamiltonian for the entire system reads,

$$H = H_e + H_{\mathcal{I}} + J \sum_{j=1}^{N_I} \hat{\boldsymbol{S}}_j \cdot \hat{\boldsymbol{I}}_j + H_Z(\boldsymbol{Q}), \qquad (14.16)$$

where $H_e = H_0 + V + U = \sum_{i=1}^{N_e} \hat{\boldsymbol{p}}_i^2/2m + \sum_{i<j} V_{ij} + \sum_i U(\hat{\boldsymbol{r}}_i)$ is the interacting electron gas Hamiltonian, $V_{ij} = V(\hat{\boldsymbol{r}}_i - \hat{\boldsymbol{r}}_j)$ the potential describing the interaction between two electrons at position $\hat{\boldsymbol{r}}_i$ and $\hat{\boldsymbol{r}}_j$, respectively, and $U(\hat{\boldsymbol{r}}_i)$ is an arbitrary potential for an electron at position $\hat{\boldsymbol{r}}_i$. Further, J denotes the coupling strength of the isotropic spin interaction at lattice site $\boldsymbol{R}_j$, $H_J = J \sum_{j=1}^{N_I} \hat{\boldsymbol{S}}_j \cdot \hat{\boldsymbol{I}}_j$, where $\hat{\boldsymbol{S}}_j \equiv \hat{\boldsymbol{S}}(\boldsymbol{R}_j)$ is the electron spin density operator $\hat{\boldsymbol{S}}(\boldsymbol{r}) = \sum_{i=1}^{N_e} \hat{\boldsymbol{s}}_i \delta(\boldsymbol{r} - \hat{\boldsymbol{r}}_i)$ with $\hat{\boldsymbol{s}}_i = (\hat{s}_i^x, \hat{s}_i^y, \hat{s}_i^z)$ being the spin-1/2 of the ith electron. The lattice spin Hamiltonian $H_{\mathcal{I}} = \sum_{ij} \mathcal{I}_{ij} \hat{\boldsymbol{I}}_i \cdot \hat{\boldsymbol{I}}_j$ describes an isotropic interaction between lattice spins with coupling constants $\mathcal{I}_{ij}$ satisfying $1/N_I \sum_{ij} |\mathcal{I}_{ij}| (\boldsymbol{R}_i - \boldsymbol{R}_j)^2 < \infty$. Finally, the Zeeman term $H_Z(\boldsymbol{Q})$, accounts for the presence of an external (fictitious) magnetic field which breaks the symmetry of the lattice spins. To rule out (anti-)ferromagnetic

order we choose $H_Z(\boldsymbol{Q}) = h \sum_{j=1}^{N_I} e^{-i\boldsymbol{Q}\cdot\boldsymbol{R}_j} \hat{I}_j^z + \text{h.c.}$ and to exlcude helical order we choose $\widetilde{H}_Z(\boldsymbol{Q}) = h \sum_{j=1}^{N_I} e^{-i\boldsymbol{Q}\cdot\boldsymbol{R}_j} \hat{I}_j^+ + \text{h.c.}$

14.B Bogoliubov inequality

For the proof to rule out order we follow Ref. [136] and make use of the Bogoliubov inequality, [202] which is an exact relation between two operators A, C, and a Hamiltonian H,

$$\frac{1}{2}\langle\{A, A^\dagger\}\rangle\langle[[C, H], C^\dagger]\rangle \geq k_B T |\langle[C, A]\rangle|^2, \tag{14.17}$$

where, $\langle A \rangle = Tr e^{-H/k_B T} A / Tr e^{-H/k_B T}$ denotes the expectation value in a canonical ensemble, T the temperature, k_B the Boltzmann constant, and $\{A, B\} = AB + BA$ the anticommutator and $[A, B] = AB - BA$ the commutator. It is assumed that all expectation values are well-defined and exist in the thermodynamic limit defined by $N_e, N_I, \Omega \to \infty$ with electron density $n_e = N_e/\Omega$ and density of lattice spins $n_I = N_I/\Omega$ finite.

If the operators A and B depend on the reciprocal vector $\boldsymbol{q}$, then the Bogoliubov inequality can be generalized to

$$\frac{1}{2}\sum_{\boldsymbol{q}}\langle\{A_{\boldsymbol{q}}, A_{\boldsymbol{q}}^\dagger\}\rangle \geq k_B T \sum_{\boldsymbol{q}} \frac{|\langle[C_{\boldsymbol{q}}, A_{\boldsymbol{q}}]\rangle|^2}{\langle[[C_{\boldsymbol{q}}, H], C_{\boldsymbol{q}}^\dagger]\rangle}, \tag{14.18}$$

where the sum runs over all $\boldsymbol{q}$'s in the first Brillouin zone of the reciprocal lattice.

14.C (Anti-)Ferromagnetic ordering

In this case, the Zeeman term is given by $H_Z(\boldsymbol{Q}) = h \sum_j e^{-i\boldsymbol{Q}\cdot\boldsymbol{R}_j} \hat{I}_j^z + \text{h.c.}$ and the magnetization is defined by

$$m_I^z(\boldsymbol{Q}) = \frac{1}{N_I}\left\langle \sum_j \left(e^{-i\boldsymbol{Q}\cdot\boldsymbol{R}_j} \hat{I}_j^z + e^{i\boldsymbol{Q}\cdot\boldsymbol{R}_j} \hat{I}_j^z \right) \right\rangle. \tag{14.19}$$

We choose $C_{\boldsymbol{q}}$ and $A_{\boldsymbol{q}}$ in the Bogoliubov inequality (14.18) such that

$$C_{\boldsymbol{q}} = \underbrace{\hat{S}_{-\boldsymbol{q}}^- + \hat{I}_{-\boldsymbol{q}}^-}_{C_{\boldsymbol{q}}^-} + \underbrace{\hat{S}_{-\boldsymbol{q}}^+ + \hat{I}_{-\boldsymbol{q}}^+}_{C_{\boldsymbol{q}}^+} \quad \text{and} \quad A_{\boldsymbol{q}} = \hat{I}_{\boldsymbol{q}+\boldsymbol{Q}}^+ + I_{\boldsymbol{q}-\boldsymbol{Q}}^+. \tag{14.20}$$

The strategy of the proof consists in evaluating every term which enters the Bogoliubov inequality (14.18) to derive an upper bound for the order parameter corresponding to the phase transition we want to discuss. If this bound turns out to be in contradiction with the presence of long-range magnetic ordering, then the absence of the corresponding magnetic phase transition is rigorously demonstrated.

Evaluation of $[[C_{\boldsymbol{q}}, H], (C_{\boldsymbol{q}})^{\dagger}]$

We decompose the double commutator $[[C_{\boldsymbol{q}}, H], (C_{\boldsymbol{q}})^{\dagger}]$ into the following four parts which we calculate below,

$$i)[[C_{\boldsymbol{q}}^{-} + C_{\boldsymbol{q}}^{+}, H_e], (C_{\boldsymbol{q}}^{-} + C_{\boldsymbol{q}}^{+})^{\dagger}], \quad ii)[[C_{\boldsymbol{q}}^{-} + C_{\boldsymbol{q}}^{+}, H_A], (C_{\boldsymbol{q}}^{-} + C_{\boldsymbol{q}}^{+})^{\dagger}], \quad (14.21)$$

$$iii)[[C_{\boldsymbol{q}}^{-} + C_{\boldsymbol{q}}^{+}, H_Z(\boldsymbol{Q})], (C_{\boldsymbol{q}}^{-} + C_{\boldsymbol{q}}^{+})^{\dagger}] \quad \text{and} \quad iv)[[C_{\boldsymbol{q}}^{-} + C_{\boldsymbol{q}}^{+}, H_{\mathcal{I}}]. \quad (14.22)$$

Evaluation of $i)$

Let us first determine $[C_{\boldsymbol{q}}^{-}, H_e]$,

$$
\begin{aligned}
[C_{\boldsymbol{q}}^{-}, H_e] &= [\hat{S}_{-\boldsymbol{q}}^{-} + \hat{I}_{-\boldsymbol{q}}^{-}, H_0 + V + U] = [\sum_i e^{i\boldsymbol{q}\cdot\hat{\boldsymbol{r}}_i}\hat{s}_i^{-} + \sum_j e^{i\boldsymbol{q}\cdot\boldsymbol{R}_j}\hat{I}_j^{-}, H_0 + V + U] \\
&= [\sum_i e^{i\boldsymbol{q}\cdot\hat{\boldsymbol{r}}_i}\hat{s}_i^{-}, \sum_k \hat{\boldsymbol{p}}_k^2/2m] = \sum_i \frac{s_i^{-}}{2m}[e^{i\boldsymbol{q}\cdot\hat{\boldsymbol{r}}_i}, \hat{\boldsymbol{p}}_i^2] \\
&= \sum_i \frac{s_i^{-}}{2m}\hat{\boldsymbol{p}}_i \cdot [e^{i\boldsymbol{q}\cdot\hat{\boldsymbol{r}}_i}, \hat{\boldsymbol{p}}_i] + \sum_i \frac{s_i^{-}}{2m}[e^{i\boldsymbol{q}\cdot\hat{\boldsymbol{r}}_i}, \hat{\boldsymbol{p}}_i] \cdot \hat{\boldsymbol{p}}_i. \quad (14.23)
\end{aligned}
$$

Since

$$[e^{i\boldsymbol{q}\cdot\hat{\boldsymbol{r}}_i}, \hat{\boldsymbol{p}}_i]\psi = (e^{i\boldsymbol{q}\cdot\hat{\boldsymbol{r}}_i}\hat{\boldsymbol{p}}_i - \hat{\boldsymbol{p}}_i e^{i q\hat{\boldsymbol{r}}_i})\psi = -ie^{i\boldsymbol{q}\cdot\hat{\boldsymbol{r}}_i}\psi^{'} - \boldsymbol{q}e^{i\boldsymbol{q}\cdot\hat{\boldsymbol{r}}_i}\psi + ie^{i\boldsymbol{q}\cdot\hat{\boldsymbol{r}}_i}\psi^{'} = -\boldsymbol{q}e^{i\boldsymbol{q}\cdot\hat{\boldsymbol{r}}_i}\psi, \quad (14.24)$$

we can conclude that

$$[C_{\boldsymbol{q}}^{-}, H_e] = -\boldsymbol{q}\sum_i \frac{s_i^{-}}{2m}\{\hat{\boldsymbol{p}}_i, e^{i\boldsymbol{q}\cdot\hat{\boldsymbol{r}}_i}\}, \quad (14.25)$$

and thus that

$$
\begin{aligned}
[[C_{\boldsymbol{q}}^-, H_e], (C_{\boldsymbol{q}}^-)^\dagger] &= -\frac{1}{2m}\sum_i [\hat{s}_i^- \boldsymbol{q} \cdot \{\hat{\boldsymbol{p}}_i, e^{i\boldsymbol{q}\cdot\hat{\boldsymbol{r}}_i}\}, (C_{\boldsymbol{q}}^-)^\dagger] \\
&= -\frac{1}{2m}[\sum_i s_i^- \boldsymbol{q}\cdot\{\hat{\boldsymbol{p}}_i, e^{i\boldsymbol{q}\cdot\hat{\boldsymbol{r}}_i}\}, \sum_k \hat{s}_k^+ e^{-i\boldsymbol{q}\cdot\hat{\boldsymbol{r}}_k}] \\
&= -\frac{1}{2m}\sum_i \left(\underbrace{\hat{s}_i^- \hat{s}_i^+ [\boldsymbol{q}\cdot\{\hat{\boldsymbol{p}}_i, e^{i\boldsymbol{q}\cdot\hat{\boldsymbol{r}}_i}\}, e^{-i\boldsymbol{q}\cdot\hat{\boldsymbol{r}}_i}]}_{A} \right. \\
&\qquad\qquad\qquad \left. + \underbrace{[\hat{s}_i^-, \hat{s}_i^+]e^{-i\boldsymbol{q}\cdot\hat{\boldsymbol{r}}_i}\boldsymbol{q}\cdot\{\hat{\boldsymbol{p}}_i, e^{i\boldsymbol{q}\cdot\hat{\boldsymbol{r}}_i}\}}_{B} \right).
\end{aligned}
\tag{14.26}
$$

We can now evaluate expressions A and B,

$$
\begin{aligned}
A &= (1/2 - \hat{s}_i^z)\boldsymbol{q}\cdot\left([\hat{\boldsymbol{p}}_i e^{i\boldsymbol{q}\cdot\hat{\boldsymbol{r}}_i}, e^{-i\boldsymbol{q}\cdot\hat{\boldsymbol{r}}_i}] + [e^{i\boldsymbol{q}\cdot\hat{\boldsymbol{r}}_i}\hat{\boldsymbol{p}}_i, e^{-i\boldsymbol{q}\cdot\hat{\boldsymbol{r}}_i}]\right) \\
&= (1/2 - \hat{s}_i^z)\boldsymbol{q}\cdot\left(e^{i\boldsymbol{q}\cdot\hat{\boldsymbol{r}}_i}\hat{\boldsymbol{p}}_i e^{-i\boldsymbol{q}\cdot\hat{\boldsymbol{r}}_i} - e^{-i\boldsymbol{q}\cdot\hat{\boldsymbol{r}}_i}\hat{\boldsymbol{p}}_i e^{i\boldsymbol{q}\cdot\hat{\boldsymbol{r}}_i}\right) \\
&= (1/2 - \hat{s}_i^z)\boldsymbol{q}\cdot(\hat{\boldsymbol{p}}_i - \boldsymbol{q} - \hat{\boldsymbol{p}}_i - \boldsymbol{q}) = -2(1/2 - \hat{s}_i^z)q^2, \quad (14.27)
\end{aligned}
$$

$$
B = -2\hat{s}_i^z \boldsymbol{q}\cdot\left(\underbrace{e^{-i\boldsymbol{q}\cdot\hat{\boldsymbol{r}}_i}\hat{\boldsymbol{p}}_i e^{i\boldsymbol{q}\cdot\hat{\boldsymbol{r}}_i}}_{\hat{\boldsymbol{p}}_i + \boldsymbol{q}} + \hat{\boldsymbol{p}}_i\right) = -2\hat{s}_i^z(2\boldsymbol{q}\cdot\hat{\boldsymbol{p}}_i + q^2). \tag{14.28}
$$

With the help of the above results, we can finally conclude that

$$
\begin{aligned}
[[C_{\boldsymbol{q}}^-, H_e], (C_{\boldsymbol{q}}^-)^\dagger] &= -\frac{1}{2m}\sum_i (1/2 - s_i^z)(-2q^2) - \frac{1}{2m}\sum_i (-2\hat{s}_i^z)(2\boldsymbol{q}\cdot\hat{\boldsymbol{p}}_i + q^2) \\
&= \frac{4\boldsymbol{q}}{2m}\sum_i \hat{s}_i^z\hat{\boldsymbol{p}}_i + \frac{1}{2m}N_e q^2.
\end{aligned}
\tag{14.29}
$$

Let us now calculate $[[C_{\boldsymbol{q}}^+, H_e], (C_{\boldsymbol{q}}^+)^\dagger]$. Since

$$
[C_{\boldsymbol{q}}^+, H_e] = \sum_i \left(\frac{\hat{s}_i^+}{2m}\hat{\boldsymbol{p}}_i \cdot [e^{i\boldsymbol{q}\cdot\hat{\boldsymbol{r}}_i}, \hat{\boldsymbol{p}}_i] + \frac{\hat{s}_i^+}{2m}[e^{i\boldsymbol{q}\cdot\hat{\boldsymbol{r}}_i}, \hat{\boldsymbol{p}}_i]\cdot\hat{\boldsymbol{p}}_i\right) = -\boldsymbol{q}\cdot\sum_i \frac{\hat{s}_i^+}{2m}\{\hat{\boldsymbol{p}}_i, e^{i\boldsymbol{q}\cdot\hat{\boldsymbol{r}}_i}\},
\tag{14.30}
$$

we thus have that

$$
\begin{aligned}
[[C_{\boldsymbol{q}}^{+}, H_e],(C_{\boldsymbol{q}}^{+})^{\dagger}] \;=\; & -\frac{1}{2m}\sum_i \hat{s}_i^{+}\hat{s}_i^{-}[\boldsymbol{q}\cdot\{\hat{\boldsymbol{p}}_i, e^{i\boldsymbol{q}\cdot\hat{\boldsymbol{r}}_i}\}, e^{-i\boldsymbol{q}\cdot\hat{\boldsymbol{r}}_i}] \\
& -\frac{1}{2m}\sum_i [\hat{s}_i^{+},\hat{s}_i^{-}]e^{-i\boldsymbol{q}\cdot\hat{\boldsymbol{r}}_i}\boldsymbol{q}\cdot\{\hat{\boldsymbol{p}}_i, e^{i\boldsymbol{q}\cdot\hat{\boldsymbol{r}}_i}\} \\
=\; & -\frac{1}{2m}\sum_i (1/2+\hat{s}_i^z)(-2q^2) - \frac{1}{2m}\sum_i 2\hat{s}_i^z(2\boldsymbol{q}\cdot\hat{\boldsymbol{p}}_i+q^2) \\
=\; & \frac{1}{2m}N_e q^2 - \frac{4\boldsymbol{q}}{2m}\sum_i \hat{s}_i^z\hat{\boldsymbol{p}}_i .
\end{aligned}
\tag{14.31}
$$

Let us now calculate the mixed term $[[C_{\boldsymbol{q}}^{+}, H_e],(C_{\boldsymbol{q}}^{-})^{\dagger}]$. From

$$
[C_{\boldsymbol{q}}^{+}, H_e] \;=\; -\boldsymbol{q}\cdot\sum_i \frac{\hat{s}_i^{+}}{2m}\{\hat{\boldsymbol{p}}_i, e^{i\boldsymbol{q}\cdot\hat{\boldsymbol{r}}_i}\},
\tag{14.32}
$$

we have that

$$
\begin{aligned}
[[C_{\boldsymbol{q}}^{+}, H_e],(C_{\boldsymbol{q}}^{-})^{\dagger}] \;=\; & -\frac{1}{2m}\sum_i [\hat{s}_i^{+}\boldsymbol{q}\cdot\{\hat{\boldsymbol{p}}_i, e^{i\boldsymbol{q}\cdot\hat{\boldsymbol{r}}_i}\}, \hat{s}_i^{+}e^{-i\boldsymbol{q}\cdot\hat{\boldsymbol{r}}_i}] \\
=\; & -\frac{1}{2m}\sum_i \hat{s}_i^{+}\hat{s}_i^{+}[\boldsymbol{q}\cdot\{\hat{\boldsymbol{p}}_i, e^{i\boldsymbol{q}\cdot\hat{\boldsymbol{r}}_i}\}, e^{-i\boldsymbol{q}\cdot\hat{\boldsymbol{r}}_i}] \\
& -\frac{1}{2m}\sum_i [\hat{s}_i^{+},\hat{s}_i^{+}]e^{-i\boldsymbol{q}\cdot\hat{\boldsymbol{r}}_i}\boldsymbol{q}\cdot\{\hat{\boldsymbol{p}}_i, e^{i\boldsymbol{q}\cdot\hat{\boldsymbol{r}}_i}\} = 0
\end{aligned}
\tag{14.33}
$$

An exactly analogous calculation shows that $[[C_{\boldsymbol{q}}^{-}, H_e],(C_{\boldsymbol{q}}^{+})^{\dagger}] = 0$. This finally allows us to conclude that

$$
[[C_{\boldsymbol{q}}, H], C_{\boldsymbol{q}}^{\dagger}] = \frac{1}{m}N_e q^2 .
\tag{14.34}
$$

Evaluation of $ii)$

Let us calculate $[[C_{\boldsymbol{q}}^{-} + C_{\boldsymbol{q}}^{+}, H_J],(C_{\boldsymbol{q}}^{-} + C_{\boldsymbol{q}}^{+})^{\dagger}]$. As a first step we evaluate

$$
[C_{\boldsymbol{q}}^{-} + C_{\boldsymbol{q}}^{+}, H_J] \;=\; J[C_{\boldsymbol{q}}^{-} + C_{\boldsymbol{q}}^{+}, \sum_j \hat{\boldsymbol{S}}_j\cdot\hat{\boldsymbol{I}}_j].
\tag{14.35}
$$

From

$$
\begin{aligned}
[\hat{S}_{-\boldsymbol{q}}^-, \sum_j \hat{\boldsymbol{S}}_j \cdot \hat{\boldsymbol{I}}_j] &= [\sum_i e^{i\boldsymbol{q}\cdot\hat{\boldsymbol{r}}_i} \hat{s}_i^-, \sum_{j,k} \hat{\boldsymbol{s}}_k \delta(\hat{\boldsymbol{r}}_k - \boldsymbol{R}_j)\hat{\boldsymbol{I}}_j] = \sum_{i,j}[e^{i\boldsymbol{q}\hat{\boldsymbol{r}}_i}\hat{s}_i^-, \delta(\hat{\boldsymbol{r}}_i - \boldsymbol{R}_j)\hat{\boldsymbol{s}}_i \cdot \hat{\boldsymbol{I}}_j] \\
&= \sum_{\alpha=x,y,z} \sum_{i,j} e^{i\boldsymbol{q}\cdot\hat{\boldsymbol{r}}_i} \delta(\hat{\boldsymbol{r}}_i - \boldsymbol{R}_j)\hat{I}_j^\alpha [\hat{s}_i^-, \hat{s}_i^\alpha] \\
&= \sum_{\alpha=x,y,z} \sum_{i,j} e^{i\boldsymbol{q}\cdot\hat{\boldsymbol{r}}_i} \delta(\hat{\boldsymbol{r}}_i - \boldsymbol{R}_j)\hat{I}_j^\alpha i\hat{s}_i^\beta (\epsilon_{x\alpha\beta} - i\epsilon_{y\alpha\beta}) \\
&= \sum_{i,j} e^{i\boldsymbol{q}\cdot\hat{\boldsymbol{r}}_i} \delta(\hat{\boldsymbol{r}}_i - \boldsymbol{R}_j)i(\hat{\boldsymbol{I}}_j \times \hat{\boldsymbol{s}}_i)^-,
\end{aligned} \tag{14.36}
$$

and

$$
\begin{aligned}
[\hat{I}_{-\boldsymbol{q}}^-, \sum_j \hat{\boldsymbol{S}}_j \cdot \hat{\boldsymbol{I}}_j] &= [\sum_l e^{i\boldsymbol{q}\cdot\boldsymbol{R}_l} \hat{I}_l^-, \sum_{j,i} \hat{\boldsymbol{s}}_i \delta(\hat{\boldsymbol{r}}_i - \boldsymbol{R}_j)\hat{\boldsymbol{I}}_j] \\
&= \sum_{\alpha=x,y,z} \sum_{i,j} e^{i\boldsymbol{q}\cdot\boldsymbol{R}_j} \hat{s}_i^\alpha \delta(\hat{\boldsymbol{r}}_i - \boldsymbol{R}_j)[I_j^-, I_j^\alpha] \\
&= \sum_{\alpha=x,y,z} \sum_{i,j} e^{i\boldsymbol{q}\cdot\boldsymbol{R}_j} \delta(\hat{\boldsymbol{r}}_i - \boldsymbol{R}_j)i\hat{s}_i^\alpha \hat{I}_j^\beta (\epsilon_{x\alpha\beta} - i\epsilon_{y\alpha\beta}) \\
&= \sum_{i,j} e^{i\boldsymbol{q}\cdot\boldsymbol{R}_j} \delta(\hat{\boldsymbol{r}}_i - \boldsymbol{R}_j)i(\hat{\boldsymbol{s}}_i \times \hat{\boldsymbol{I}}_j)^-,
\end{aligned} \tag{14.37}
$$

we have that $[\hat{S}_{-\boldsymbol{q}}^-, \sum_j \hat{\boldsymbol{S}}_j \cdot \hat{\boldsymbol{I}}_j] = -[\hat{I}_{-\boldsymbol{q}}^-, \sum_j \hat{\boldsymbol{S}}_j \cdot \hat{\boldsymbol{I}}_j]$ and consequently $[C_{\boldsymbol{q}}^-, H_J] = 0$. A similar calculation for $[C_{\boldsymbol{q}}^+, H_J]$ shows that

$$
\begin{aligned}
[C_{\boldsymbol{q}}^+, H_J] &= J\sum_{i,j} e^{i\boldsymbol{q}\cdot\hat{\boldsymbol{r}}_i} \delta(\hat{\boldsymbol{r}}_i - \boldsymbol{R}_j)i(\hat{\boldsymbol{I}}_j \times \hat{\boldsymbol{s}}_i)^+ \\
&\quad + J\sum_{i,j} e^{i\boldsymbol{q}\cdot\boldsymbol{R}_j} \delta(\hat{\boldsymbol{r}}_i - \boldsymbol{R}_j)i(\hat{\boldsymbol{s}}_i \times \hat{\boldsymbol{I}}_j)^+ = 0.
\end{aligned} \tag{14.38}
$$

From this it follows that $[[C_{\boldsymbol{q}}^- + C_{\boldsymbol{q}}^+, H_J], (C_{\boldsymbol{q}}^- + C_{\boldsymbol{q}}^+)^\dagger] = 0$.

Evaluation of $iii)$

Let us calculate $[[C_{\boldsymbol{q}}, H_Z(\boldsymbol{Q})], C_{\boldsymbol{q}}^\dagger]$. From

$$
\begin{aligned}
[C_{\boldsymbol{q}}, H_Z(\boldsymbol{Q})] &= [\hat{I}_{-\boldsymbol{q}}^- + \hat{I}_{-\boldsymbol{q}}^+, H_Z(\boldsymbol{Q})] \\
&= h \sum_j \left(e^{i\boldsymbol{R}_j\cdot(\boldsymbol{q}-\boldsymbol{Q})}[\hat{I}_j^-, \hat{I}_j^z] + e^{i\boldsymbol{R}_j\cdot(\boldsymbol{q}+\boldsymbol{Q})}[\hat{I}_j^-, \hat{I}_j^z] \right. \\
&\qquad \left. + e^{i\boldsymbol{R}_j\cdot(\boldsymbol{q}-\boldsymbol{Q})}[\hat{I}_j^+, \hat{I}_j^z] + e^{i\boldsymbol{R}_j\cdot(\boldsymbol{q}+\boldsymbol{Q})}[\hat{I}_j^+, \hat{I}_j^z] \right) \\
&= h \sum_j \left(e^{i\boldsymbol{R}_j\cdot(\boldsymbol{q}-\boldsymbol{Q})}(\hat{I}_j^- - \hat{I}_j^+) + e^{i\boldsymbol{R}_j\cdot(\boldsymbol{q}+\boldsymbol{Q})}(\hat{I}_j^- - \hat{I}_j^+) \right),
\end{aligned}
$$
$$(14.39)$$

we obtain

$$
\begin{aligned}
[[C_{\boldsymbol{q}}, H_Z(\boldsymbol{Q})], C_{\boldsymbol{q}}^\dagger] &= h[\sum_j \left(e^{i\boldsymbol{R}_j\cdot(\boldsymbol{q}-\boldsymbol{Q})}(\hat{I}_j^- - \hat{I}_j^+) + e^{i\boldsymbol{R}_j\cdot(\boldsymbol{q}+\boldsymbol{Q})}(\hat{I}_j^- - \hat{I}_j^+) \right), \\
&\qquad\qquad\qquad \sum_l \left(e^{-i\boldsymbol{q}\cdot\boldsymbol{R}_l}\hat{I}_l^+ + e^{-i\boldsymbol{q}\cdot\boldsymbol{R}_l}\hat{I}_l^- \right)] \\
&= \sum_j e^{-i\boldsymbol{Q}\cdot\boldsymbol{R}_j}[\hat{I}_j^-, \hat{I}_j^+] - \sum_j e^{-i\boldsymbol{Q}\cdot\boldsymbol{R}_j}[\hat{I}_j^+, \hat{I}_j^-] + \sum_j e^{i\boldsymbol{Q}\cdot\boldsymbol{R}_j}[\hat{I}_j^-, \hat{I}_j^+] \\
&\qquad - \sum_j e^{i\boldsymbol{Q}\cdot\boldsymbol{R}_j}[\hat{I}_j^+, \hat{I}_j^-] \\
&= 2h \sum_j e^{-i\boldsymbol{Q}\cdot\boldsymbol{R}_j}[\hat{I}_j^-, \hat{I}_j^+] + 2h \sum_j e^{i\boldsymbol{Q}\cdot\boldsymbol{R}_j}[\hat{I}_j^-, \hat{I}_j^+] \\
&= -4h \sum_j \left(e^{-i\boldsymbol{Q}\cdot\boldsymbol{R}_j}\hat{I}_j^z + e^{i\boldsymbol{Q}\cdot\boldsymbol{R}_j}\hat{I}_j^z \right).
\end{aligned}
$$
$$(14.40)$$

Evaluation of $iv)$

Let us calculate $[[C_{\boldsymbol{q}}^- + C_{\boldsymbol{q}}^+, H_\mathcal{I}], (C_{\boldsymbol{q}}^- + C_{\boldsymbol{q}}^+)^\dagger]$. Since

$$
\begin{aligned}
[C_{\boldsymbol{q}}^- + C_{\boldsymbol{q}}^+, H_\mathcal{I}] &= [\hat{I}_{-\boldsymbol{q}}^+ + \hat{I}_{-\boldsymbol{q}}^-, \sum_{\alpha,j,l}\mathcal{I}_{jl}\hat{I}_j^\alpha \hat{I}_l^\alpha] = [2\sum_k e^{i\boldsymbol{q}\cdot\boldsymbol{R}_k}\hat{I}_k^x, \sum_{\alpha,j,l}\mathcal{I}_{jl}\hat{I}_j^\alpha \hat{I}_l^\alpha] \\
&= 2 \sum_{\alpha,k,j,l} \mathcal{I}_{jl}e^{i\boldsymbol{q}\cdot\boldsymbol{R}_k}[\hat{I}_k^x, \hat{I}_j^\alpha \hat{I}_l^\alpha] = 2 \sum_{\alpha,k,j,l} \mathcal{I}_{jl}e^{i\boldsymbol{q}\cdot\boldsymbol{R}_k}\left([\hat{I}_k^x, \hat{I}_j^\alpha]\hat{I}_l^\alpha + \hat{I}_j^\alpha[\hat{I}_k^x, \hat{I}_l^\alpha] \right) \\
&= 2 \sum_{\alpha,j,l} \mathcal{I}_{jl}e^{i\boldsymbol{q}\cdot\boldsymbol{R}_j} i\epsilon_{x\alpha\beta}\hat{I}_j^\beta \hat{I}_l^\alpha + 2 \sum_{\alpha,j,l} \mathcal{I}_{jl}e^{i\boldsymbol{q}\cdot\boldsymbol{R}_l}\hat{I}_j^\alpha i\epsilon_{x\alpha\beta}\hat{I}_l^\beta \\
&= 2 \sum_{\alpha,j,l} i\mathcal{I}_{jl}(e^{i\boldsymbol{q}\cdot\boldsymbol{R}_j} - e^{i\boldsymbol{q}\cdot\boldsymbol{R}_l})(\hat{\boldsymbol{I}}_l \times \hat{\boldsymbol{I}}_j)_x,
\end{aligned}
$$
$$(14.41)$$

we obtain

$$
\begin{aligned}
[[C_{\boldsymbol{q}}, H_{\mathcal{I}}], C_{\boldsymbol{q}}^{\dagger}] &= [2\sum_{\alpha,j,l} i\mathcal{I}_{jl}(e^{i\boldsymbol{q}\cdot\boldsymbol{R}_j} - e^{i\boldsymbol{q}\cdot\boldsymbol{R}_l})(\hat{\boldsymbol{I}}_l \times \hat{\boldsymbol{I}}_j)_x, 2\sum_{k} e^{-i\boldsymbol{q}\cdot\boldsymbol{R}_k}\hat{I}_k^x] \\
&= -4i\sum_{k,j,l} \mathcal{I}_{jl}e^{-i\boldsymbol{q}\cdot\boldsymbol{R}_k}(e^{i\boldsymbol{q}\cdot\boldsymbol{R}_j} - e^{i\boldsymbol{q}\cdot\boldsymbol{R}_l})[\hat{I}_k^x, (\hat{\boldsymbol{I}}_l \times \hat{\boldsymbol{I}}_j)_x] \\
&= -4i\sum_{k,j,l} \mathcal{I}_{jl}e^{-i\boldsymbol{q}\cdot\boldsymbol{R}_k}(e^{i\boldsymbol{q}\cdot\boldsymbol{R}_j} - e^{i\boldsymbol{q}\cdot\boldsymbol{R}_l})\left(\sum_{\alpha} \epsilon_{x\alpha\beta}\{[\hat{I}_k^x, \hat{I}_l^\alpha]\hat{I}_j^\beta + \hat{I}_l^\alpha[\hat{I}_k^x, \hat{I}_j^\beta]\}\right) \\
&= -4i\sum_{j,l} \mathcal{I}_{jl}e^{-i\boldsymbol{q}\cdot\boldsymbol{R}_l}(e^{i\boldsymbol{q}\cdot\boldsymbol{R}_j} - e^{i\boldsymbol{q}\cdot\boldsymbol{R}_l})i\sum_{\alpha} \epsilon_{x\alpha\beta}\epsilon_{x\alpha\gamma}\hat{I}_l^\gamma \hat{I}_j^\beta \\
&\quad -4i\sum_{j,l} \mathcal{I}_{jl}e^{-i\boldsymbol{q}\cdot\boldsymbol{R}_j}(e^{i\boldsymbol{q}\cdot\boldsymbol{R}_j} - e^{i\boldsymbol{q}\cdot\boldsymbol{R}_l})i\sum_{\alpha} \epsilon_{x\alpha\beta}\epsilon_{x\beta\gamma}\hat{I}_l^\alpha \hat{I}_j^\gamma \\
&= -4i\sum_{j,l} \mathcal{I}_{jl}e^{-i\boldsymbol{q}\cdot\boldsymbol{R}_l}(e^{i\boldsymbol{q}\cdot\boldsymbol{R}_j} - e^{i\boldsymbol{q}\cdot\boldsymbol{R}_l})i(\hat{I}_l^z\hat{I}_j^z + \hat{I}_l^y\hat{I}_j^y) \\
&\quad +4i\sum_{j,l} \mathcal{I}_{jl}e^{-i\boldsymbol{q}\cdot\boldsymbol{R}_j}(e^{i\boldsymbol{q}\cdot\boldsymbol{R}_j} - e^{i\boldsymbol{q}\cdot\boldsymbol{R}_l})i(\hat{I}_l^z\hat{I}_j^z + \hat{I}_l^y\hat{I}_j^y) \\
\\
&= 4\sum_{j,l} \mathcal{I}_{jl}(e^{i\boldsymbol{q}\cdot(\boldsymbol{R}_j-\boldsymbol{R}_l)} - 1)(\hat{I}_l^z\hat{I}_j^z + \hat{I}_l^y\hat{I}_j^y) - 4\sum_{j,l} \mathcal{I}_{jl}(1 - e^{i\boldsymbol{q}\cdot(\boldsymbol{R}_l-\boldsymbol{R}_j)})(\hat{I}_l^z\hat{I}_j^z + \hat{I}_l^y\hat{I}_j^y) \\
&= -8\sum_{j,l} \mathcal{I}_{jl}(\hat{I}_l^z\hat{I}_j^z + \hat{I}_l^y\hat{I}_j^y) + 4\sum_{j,l} \mathcal{I}_{jl}(e^{i\boldsymbol{q}\cdot(\boldsymbol{R}_j-\boldsymbol{R}_l)} + e^{i\boldsymbol{q}\cdot(\boldsymbol{R}_l-\boldsymbol{R}_j)})(\hat{I}_l^z\hat{I}_j^z + \hat{I}_l^y\hat{I}_j^y) \\
&= -8\sum_{j,l} \mathcal{I}_{jl}[1 - \cos(\boldsymbol{q}\cdot(\boldsymbol{R}_j - \boldsymbol{R}_l))](\hat{I}_l^z\hat{I}_j^z + \hat{I}_l^y\hat{I}_j^y). \qquad (14.42)
\end{aligned}
$$

The expectation value is then given by

$$
\begin{aligned}
\langle[[C_{\boldsymbol{q}}, H_{\mathcal{I}}], C_{\boldsymbol{q}}^{\dagger}]\rangle &= -8\sum_{j,l} \mathcal{I}_{jl}(1 - \cos(\boldsymbol{q}\cdot(\boldsymbol{R}_j - \boldsymbol{R}_l)))\langle\hat{I}_l^z\hat{I}_j^z + \hat{I}_l^y\hat{I}_j^y\rangle \\
&\leq 8\sum_{j,l} |\mathcal{I}_{jl}|\frac{q^2(\boldsymbol{R}_j - \boldsymbol{R}_l)^2}{2}2I^2 \\
&= 8I^2q^2\sum_{j,l} |\mathcal{I}_{jl}|(\boldsymbol{R}_j - \boldsymbol{R}_l)^2 \\
&= 8I^2q^2 N_I \underbrace{\frac{1}{N_I}\sum_{j,l} |\mathcal{I}_{jl}|(\boldsymbol{R}_j - \boldsymbol{R}_l)^2}_{<\infty}. \qquad (14.43)
\end{aligned}
$$

Evaluation of $[C_q, A_q]$

Let us calculate $[C_q, A_q]$:

$$
\begin{aligned}
[C_q, A_q] &= [\hat{I}^-_{-q} + \hat{I}^+_{-q}, \hat{I}^+_{q+Q} + \hat{I}^+_{q-Q}] = [\hat{I}^-_{-q}, \hat{I}^+_{q+Q} + \hat{I}^+_{q-Q}] \\
&= \sum_j \left(e^{-iQ\cdot R_j}[\hat{I}^-_j, \hat{I}^+_j] + e^{iQ\cdot R_j}[\hat{I}^-_j, \hat{I}^+_j] \right) \\
&= -2\sum_j \left(e^{-iQ\cdot R_j}\hat{I}^z_j + e^{iQ\cdot R_j}\hat{I}^z_j \right). \qquad (14.44)
\end{aligned}
$$

Evaluation of $\sum_q \{A_q, A^\dagger_q\}$

As a first step let us calculate $\{A_q, A^\dagger_q\}$,

$$
\begin{aligned}
\{A_q, A^\dagger_q\} &= \left\{ \sum_l \left(e^{-i(q+Q)\cdot R_l}\hat{I}^+_l + e^{-i(q-Q)\cdot R_l}\hat{I}^+_l \right), \sum_j \left(e^{i(q+Q)\cdot R_j}\hat{I}^-_j + e^{i(q-Q)\cdot R_j}\hat{I}^-_j \right) \right\} \\
&= \sum_{l,j} \left(e^{i(q+Q)\cdot(R_j-R_l)}\{\hat{I}^+_l, \hat{I}^-_j\} + e^{iq\cdot(R_j-R_l)}e^{-iQ\cdot(R_l+R_j)}\{\hat{I}^+_l, \hat{I}^-_j\} \right) \\
&\quad + \sum_{l,j} \left(e^{iq\cdot(R_j-R_l)}e^{iQ\cdot(R_l+R_j)}\{\hat{I}^+_l, \hat{I}^-_j\} + e^{i(q-Q)(R_j-R_l)}\{\hat{I}^+_l, \hat{I}^-_j\} \right). \qquad (14.45)
\end{aligned}
$$

With the use of $\sum_q e^{iq\cdot(R_j-R_l)} = N_I \delta_{R_l, R_j}$, we obtain

$$
\begin{aligned}
\sum_q \{A_q, A^\dagger_q\} &= N_I \left(2\sum_j \{\hat{I}^+_j, \hat{I}^-_j\} + \sum_j (e^{-i2Q\cdot R_j} + e^{i2Q\cdot R_j})\{\hat{I}^+_j, \hat{I}^-_j\} \right) \\
&= N_I \sum_j \{\hat{I}^+_j, \hat{I}^-_j\}(2 + 2\cos(Q\cdot R_j)),
\end{aligned}
$$

$$\qquad (14.46)$$

and consequently

$$
\left\langle \sum_q \{A_q, A^\dagger_q\} \right\rangle \leq 4N_I \sum_j \langle \{\hat{I}^+_j, \hat{I}^-_j\} \rangle \leq 4N_I^2(2I)^2, \qquad (14.47)
$$

where we have used $\langle \{\hat{I}^+_i, \hat{I}^-_i\} \rangle \leq (2I)^2$. Indeed, $\{\hat{I}^-_i, \hat{I}^+_i\} = 2(\hat{I}^x_i)^2 + 2(\hat{I}^y_i)^2 \leq 4I^2$.

Putting everything together

The Bogoliubov inequality (14.18) takes now the following form,

$$4N_I^2(2I)^2/2 \geq k_B T \sum_q \frac{4N_I^2 m_I^z(Q)^2}{(\frac{N_e}{m} + 8I^2 N_I \frac{1}{N_I} \sum_{jl} |\mathcal{I}_{jl}|(R_j - R_l)^2)q^2 - 4hN_I m_I^z(Q)} .$$

(14.48)

In the thermodynamic limit we can replace the sum by an integral and obtain

$$4N_I^2(2I)^2/2 \geq \frac{k_B T N_I v}{(2\pi)^d} \int_{|q| \leq |q_c|} d^d q \frac{4N_I^2 m_I^z(Q)^2}{\frac{N_e}{m^*} q^2 - 4hN_I m_I^z(Q)}, \qquad (14.49)$$

where $v = \Omega/N_I$, d is the dimensionality of the system, $m^* = m/(1 + 8I^2 N_I/N_e m \frac{1}{N_I} \sum_{ij} |\mathcal{I}_{ij}|(R_i - R_j)^2)$, and q_c is an arbitrary cut-off vector lying in the first Brillouin zone. Since $\langle [[C_q, H], C_q^\dagger] \rangle \leq N_e(q^2/m^* + |2\nu h m_I^z(Q)|)$, inequality (14.49) can be simplified to

$$(2I)^2 \geq \frac{k_B T N_I v}{N_e(2\pi)^d} \int_{|q| \leq |q_c|} d^d q \frac{m_I^z(Q)^2}{\frac{q^2}{2m^*} + |\nu h m_I^z(Q)|}, \qquad (14.50)$$

where $\nu = 2N_I/N_e$.

14.D   Helical ordering

In this case the symmetry-breaking Zeeman term is given by $\widetilde{H}_Z(Q) = h\sqrt{2/3} \sum_j \left(e^{-iQ\cdot R_j} \hat{I}_j^+ + e^{iQ\cdot R_j} \hat{I}_j^- \right)$ and the order parameter is a helix in the xy-plane: $m_I^\perp(Q) = \sqrt{2/3} \frac{1}{N_I} \left\langle \sum_j \left(e^{-iQ\cdot R_j} \hat{I}_j^+ + e^{iQ\cdot R_j} \hat{I}_j^- \right) \right\rangle$. The choice of operators $\widetilde{A}_q$ and $\widetilde{C}_q$ in the Bogoliubov inequality (14.18) is as follows,

$$\widetilde{C}_q = \hat{S}_{-q}^z + \hat{I}_{-q}^z \quad \text{and} \quad \widetilde{A}_q = \frac{1}{\sqrt{3}} \left(\hat{I}_{q+Q}^+ - \hat{I}_{q-Q}^- \right). \qquad (14.51)$$

The numerical prefactor $1/\sqrt{3}$ is chosen for later convenience.

Evaluation of $[[\widetilde{C}_q, H_e], \widetilde{C}_q^\dagger]$

Let us first calculate

$$
\begin{aligned}
[\widetilde{C}_q, H_e] &= [\sum_i e^{iq\cdot\hat{r}_i} \hat{s}_i^z, \sum_k \hat{p}_k^2/2m] \\
&= \sum_i \frac{\hat{s}_i^z}{2m} \left([e^{iq\cdot\hat{r}_i}, \hat{p}_i] \cdot \hat{p}_i + \hat{p}_i \cdot [e^{iq\cdot\hat{r}_i}, \hat{p}_i] \right) .
\end{aligned}
$$

(14.52)

Since $[e^{i\boldsymbol{q}\cdot\hat{\boldsymbol{r}}_i}, \hat{\boldsymbol{p}}_i] = -\boldsymbol{q}e^{i\boldsymbol{q}\cdot\hat{\boldsymbol{r}}_i}$, it follows that

$$[\widetilde{C}_{\boldsymbol{q}}, H_e] = -\boldsymbol{q}\sum_i \frac{\hat{s}_i^z}{2m}\{\hat{\boldsymbol{p}}_i, e^{i\boldsymbol{q}\cdot\hat{\boldsymbol{r}}_i}\}, \tag{14.53}$$

and consequently that

$$\begin{aligned}
[[\widetilde{C}_{\boldsymbol{q}}, H_e], \widetilde{C}_{\boldsymbol{q}}^\dagger] &= -\frac{1}{2m}[\sum_i \hat{s}_i^z \boldsymbol{q}\cdot\{\hat{\boldsymbol{p}}_i, e^{i\boldsymbol{q}\cdot\hat{\boldsymbol{r}}_i}\}, \sum_i e^{-i\boldsymbol{q}\hat{\boldsymbol{r}}_i}\hat{s}_i^z] \\
&= -\frac{1}{2m}\sum_i \hat{s}_i^z s_i^z[\boldsymbol{q}\cdot\{\hat{\boldsymbol{p}}_i, e^{i\boldsymbol{q}\cdot\hat{\boldsymbol{r}}_i}\}, e^{-i\boldsymbol{q}\hat{\boldsymbol{r}}_i}] \\
&\quad -\frac{1}{2m}\sum_i \underbrace{[\hat{s}_i^z, \hat{s}_i^z]}_{=0} e^{-i\boldsymbol{q}\cdot\hat{\boldsymbol{r}}_i}\boldsymbol{q}\cdot\{\hat{\boldsymbol{p}}_i, e^{i\boldsymbol{q}\cdot\hat{\boldsymbol{r}}_i}\} \\
&= -\frac{1}{2m}\sum_i \frac{1}{4}(-2q^2) = \frac{1}{4m}N_e q^2. \tag{14.54}
\end{aligned}$$

Evaluation of $[[\widetilde{C}_{\boldsymbol{q}}, \widetilde{H}_Z(\boldsymbol{Q})], \widetilde{C}_{\boldsymbol{q}}^\dagger]$

From

$$\begin{aligned}
[\widetilde{C}_{\boldsymbol{q}}, \widetilde{H}_Z(\boldsymbol{Q})] &= [\sum_j e^{i\boldsymbol{q}\cdot\boldsymbol{R}_j}\hat{I}_j^z, \sqrt{2/3}h\sum_j e^{-i\boldsymbol{Q}\cdot\boldsymbol{R}_j}\hat{I}_j^+ + \sqrt{2/3}h\sum_j e^{i\boldsymbol{Q}\cdot\boldsymbol{R}_j}\hat{I}_j^-] \\
&= \sqrt{2/3}h\sum_j e^{i(\boldsymbol{q}-\boldsymbol{Q})\cdot\boldsymbol{R}_j}\hat{I}_j^+ - \sqrt{2/3}h\sum_j e^{i(\boldsymbol{q}+\boldsymbol{Q})\cdot\boldsymbol{R}_j}\hat{I}_j^-, \tag{14.55}
\end{aligned}$$

we obtain

$$\begin{aligned}
[[\widetilde{C}_{\boldsymbol{q}}, \widetilde{H}_z(\boldsymbol{Q})], \widetilde{C}_{\boldsymbol{q}}^\dagger] &= [\sqrt{2/3}h\sum_l e^{i(\boldsymbol{q}-\boldsymbol{Q})\cdot\boldsymbol{R}_l}\hat{I}_l^+ - \sqrt{2/3}h\sum_l e^{i(\boldsymbol{q}+\boldsymbol{Q})\cdot\boldsymbol{R}_l}\hat{I}_l^-, \sum_j e^{-i\boldsymbol{q}\cdot\boldsymbol{R}_j}\hat{I}_j^z] \\
&= -\sqrt{2/3}h\sum_j e^{-i\boldsymbol{Q}\cdot\boldsymbol{R}_j}\hat{I}_j^+ - \sqrt{2/3}h\sum_j e^{i\boldsymbol{Q}\cdot\boldsymbol{R}_j}\hat{I}_j^-. \tag{14.56}
\end{aligned}$$

Evaluation of $[[\widetilde{C}_{\boldsymbol{q}}, H_J], \widetilde{C}_{\boldsymbol{q}}^\dagger]$

As a first step let us calculate

$$[\widetilde{C}_{\boldsymbol{q}}, H_J] = [\hat{S}_{-\boldsymbol{q}}^z + \hat{I}_{-\boldsymbol{q}}^z, J\sum_j \hat{\boldsymbol{S}}_j \cdot \hat{\boldsymbol{I}}_j]. \tag{14.57}$$

Since

$$
\begin{aligned}
[\hat{S}_{-\boldsymbol{q}}^z, \sum_j \hat{\boldsymbol{S}}_j \cdot \hat{\boldsymbol{I}}_j] &= [\sum_i e^{i\boldsymbol{q}\cdot\hat{\boldsymbol{r}}_i}\hat{s}_i^z, \sum_{j,k} \hat{\boldsymbol{s}}_k \delta(\hat{\boldsymbol{r}}_k - \hat{\boldsymbol{R}}_j)\hat{\boldsymbol{I}}_j] \\
&= \sum_{\alpha=x,y,z}\sum_{i,j} e^{i\boldsymbol{q}\cdot\hat{\boldsymbol{r}}_i}\delta(\hat{\boldsymbol{r}}_i - \boldsymbol{R}_j)\hat{I}_j^\alpha[\hat{s}_i^z, \hat{s}_i^\alpha] \\
&= \sum_{\alpha=x,y,z}\sum_{i,j} e^{i\boldsymbol{q}\cdot\hat{\boldsymbol{r}}_i}\delta(\hat{\boldsymbol{r}}_i - \boldsymbol{R}_j)i\hat{I}_j^\alpha \hat{s}_i^\beta \epsilon_{z\alpha\beta} \\
&= \sum_{i,j} e^{i\boldsymbol{q}\cdot\hat{\boldsymbol{r}}_i}\delta(\hat{\boldsymbol{r}}_i - \boldsymbol{R}_j)i(\hat{\boldsymbol{I}}_j \times \hat{\boldsymbol{s}}_i)_z, \qquad (14.58)
\end{aligned}
$$

and

$$
\begin{aligned}
[\hat{I}_{-\boldsymbol{q}}^z, \sum_j \hat{\boldsymbol{S}}_j \cdot \hat{\boldsymbol{I}}_j] &= [\sum_l e^{i\boldsymbol{q}\cdot\boldsymbol{R}_l}\hat{I}_l^z, \sum_{i,j} \hat{\boldsymbol{s}}_i \delta(\hat{\boldsymbol{r}}_i - \boldsymbol{R}_j)\hat{\boldsymbol{I}}_j] \\
&= \sum_{\alpha=x,y,z}\sum_{i,j} e^{i\boldsymbol{q}\cdot\boldsymbol{R}_i}\delta(\hat{\boldsymbol{r}}_i - \boldsymbol{R}_j)i\hat{s}_i^\alpha \hat{I}_j^\beta \epsilon_{z\alpha\beta} \\
&= \sum_{i,j} e^{i\boldsymbol{q}\cdot\boldsymbol{R}_i}\delta(\hat{\boldsymbol{r}}_i - \boldsymbol{R}_j)i(\hat{\boldsymbol{s}}_i \times \hat{\boldsymbol{I}}_j)_z, \qquad (14.59)
\end{aligned}
$$

we have $[\hat{S}_{-\boldsymbol{q}}^z, \sum_j \hat{\boldsymbol{S}}_j \cdot \hat{\boldsymbol{I}}_j] + [\hat{I}_{-\boldsymbol{q}}^z, \sum_j \hat{\boldsymbol{S}}_j \cdot \hat{\boldsymbol{I}}_j] = 0$ and consequently $[\widetilde{C}_{\boldsymbol{q}}, H_J] = 0$.

Evaluation of $[[\widetilde{C}_{\boldsymbol{q}}, H_{\mathcal{I}}], \widetilde{C}_{\boldsymbol{q}}^\dagger]$

From

$$
\begin{aligned}
[\widetilde{C}_{\boldsymbol{q}}, H_{\mathcal{I}}] &= \sum_{\alpha,k,j,l} e^{i\boldsymbol{q}\cdot\boldsymbol{R}_k}\mathcal{I}_{jl}[\hat{I}_k^z, \hat{I}_j^\alpha \hat{I}_l^\alpha] = \sum_{\alpha,k,j,l} \mathcal{I}_{jl}e^{i\boldsymbol{q}\cdot\boldsymbol{R}_k}\left([\hat{I}_k^z, \hat{I}_j^\alpha]\hat{I}_l^\alpha + \hat{I}_j^\alpha[\hat{I}_k^z, \hat{I}_l^\alpha]\right) \\
&= \sum_{\alpha,j,l} \mathcal{I}_{jl}e^{i\boldsymbol{q}\cdot\boldsymbol{R}_j}i\epsilon_{z\alpha\beta}\hat{I}_j^\beta \hat{I}_l^\alpha + \sum_{\alpha,j,l} \mathcal{I}_{jl}e^{i\boldsymbol{q}\cdot\boldsymbol{R}_l}\hat{I}_j^\alpha i\epsilon_{z\alpha\beta}\hat{I}_l^\beta \\
&= i\sum_{j,l} \mathcal{I}_{jl}(e^{i\boldsymbol{q}\cdot\boldsymbol{R}_j} - e^{i\boldsymbol{q}\cdot\boldsymbol{R}_l})(\hat{\boldsymbol{I}}_l \times \hat{\boldsymbol{I}}_j)_z, \qquad (14.60)
\end{aligned}
$$

we obtain

$$
\begin{aligned}
[[\widetilde{C}_{\boldsymbol{q}}, H_{\mathcal{I}}], \widetilde{C}_{\boldsymbol{q}}^{\dagger}] &= -i \sum_{k,j,l} \mathcal{I}_{jl} e^{-i\boldsymbol{q}\cdot\boldsymbol{R}_k} (e^{i\boldsymbol{q}\cdot\boldsymbol{R}_j} - e^{i\boldsymbol{q}\cdot\boldsymbol{R}_l}) [\hat{I}_k^z, (\hat{\boldsymbol{I}}_l \times \hat{\boldsymbol{I}}_j)_z] \\
&= -i \sum_{jl} \mathcal{I}_{jl} e^{-i\boldsymbol{q}\cdot\boldsymbol{R}_l} (e^{i\boldsymbol{q}\cdot\boldsymbol{R}_j} - e^{i\boldsymbol{q}\cdot\boldsymbol{R}_l}) \sum_{\alpha} i\epsilon_{z\alpha\beta}\epsilon_{z\alpha\gamma} \hat{I}_l^\gamma \hat{I}_j^\beta \\
&\quad -i \sum_{jl} \mathcal{I}_{jl} e^{-i\boldsymbol{q}\cdot\boldsymbol{R}_j} (e^{i\boldsymbol{q}\cdot\boldsymbol{R}_j} - e^{i\boldsymbol{q}\cdot\boldsymbol{R}_l}) \sum_{\alpha} i\epsilon_{z\alpha\beta}\epsilon_{z\beta\gamma} \hat{I}_l^\alpha \hat{I}_j^\gamma \\
&= -2 \sum_{jl} \mathcal{I}_{jl}(1 - \cos(\boldsymbol{q}\cdot(\boldsymbol{R}_j - \boldsymbol{R}_l)))(\hat{I}_j^x \hat{I}_l^x + \hat{I}_j^y \hat{I}_l^y).
\end{aligned}
$$

$$(14.61)$$

The expectation value is then given by

$$
\begin{aligned}
\langle[[\widetilde{C}_{\boldsymbol{q}}, H_{\mathcal{I}}], \widetilde{C}_{\boldsymbol{q}}^{\dagger}]\rangle &= -2 \sum_{jl} \mathcal{I}_{jl}(1 - \cos(\boldsymbol{q}\cdot(\boldsymbol{R}_j - \boldsymbol{R}_l))) \left\langle (\hat{I}_j^x \hat{I}_l^x + \hat{I}_j^y \hat{I}_l^y) \right\rangle \\
&\leq 2 \sum_{jl} |\mathcal{I}_{jl}| \frac{q^2(\boldsymbol{R}_j - \boldsymbol{R}_l)^2}{2} 2I^2 \\
&= 2q^2 I^2 \sum_{jl} |\mathcal{I}_{jl}|(\boldsymbol{R}_j - \boldsymbol{R}_l)^2 \\
&= 2q^2 N_I I^2 \frac{1}{N_I} \sum_{j,l} |\mathcal{I}_{jl}|(\boldsymbol{R}_j - \boldsymbol{R}_l)^2.
\end{aligned}
$$

$$(14.62)$$

Evaluation of $[\widetilde{C}_{\boldsymbol{q}}, \widetilde{A}_{\boldsymbol{q}}]$

Let us now calculate $[\widetilde{C}_{\boldsymbol{q}}, \widetilde{A}_{\boldsymbol{q}}]$,

$$
\begin{aligned}
[\widetilde{C}_{\boldsymbol{q}}, \widetilde{A}_{\boldsymbol{q}}] &= [\sum_{l} e^{i\boldsymbol{q}\cdot\boldsymbol{R}_l} \hat{I}_l^z, \frac{1}{\sqrt{3}} \sum_{j} e^{-i(\boldsymbol{q}+\boldsymbol{Q})\cdot\boldsymbol{R}_j} \hat{I}_j^+ - \frac{1}{\sqrt{3}} \sum_{j} e^{-i(\boldsymbol{q}-\boldsymbol{Q})\cdot\boldsymbol{R}_j} \hat{I}_j^-] \\
&= \frac{1}{\sqrt{3}} \sum_{j} e^{-i\boldsymbol{Q}\cdot\boldsymbol{R}_j} \hat{I}_j^+ + \frac{1}{\sqrt{3}} \sum_{j} e^{i\boldsymbol{Q}\cdot\boldsymbol{R}_j} \hat{I}_j^-.
\end{aligned}
$$

$$(14.63)$$

Evaluation of $\sum_q \{\widetilde{A}_q, \widetilde{A}_q^\dagger\}$

Let us first calculate $\{\widetilde{A}_q, \widetilde{A}_q^\dagger\}$,

$$
\begin{aligned}
\left\{\widetilde{A}_q, \widetilde{A}_q^\dagger\right\} &= \left\{\frac{1}{\sqrt{3}}\left(\hat{I}_{q+Q}^+ - \hat{I}_{q-Q}^-\right), \frac{1}{\sqrt{3}}\left(\hat{I}_{-q-Q}^- - \hat{I}_{-q+Q}^+\right)\right\} \\
&= \left\{\frac{1}{\sqrt{3}}\left(\sum_l e^{-i(q+Q)\cdot R_l}\hat{I}_l^+ - \sum_l e^{-i(q-Q)\cdot R_l}\hat{I}_l^-\right),\right. \\
&\qquad\qquad \left.\frac{1}{\sqrt{3}}\left(\sum_j e^{i(q+Q)\cdot R_j}\hat{I}_j^- - \sum_j e^{i(q-Q)\cdot R_j}\hat{I}_j^+\right)\right\} \\
&= \frac{1}{3}\sum_{l,j} e^{i(q+Q)\cdot(R_j-R_l)}\{\hat{I}_l^+, \hat{I}_j^-\} - \frac{1}{3}\sum_{l,j} e^{iq(R_j-R_l)}e^{-iQ\cdot(R_j+R_l)}\{\hat{I}_l^+, \hat{I}_j^+\} \\
&\quad -\frac{1}{3}\sum_{l,j} e^{iq\cdot(R_j-R_l)}e^{iQ\cdot(R_l+R_j)}\{\hat{I}_l^-, \hat{I}_j^-\} + \frac{1}{3}\sum_{l,j} e^{i(q-Q)\cdot(R_j-R_l)}\{\hat{I}_l^-, \hat{I}_j^+\}.
\end{aligned}
\tag{14.64}
$$

By using $\sum_q e^{iq\cdot(R_j-R_l)} = N_I \delta_{R_l, R_j}$, we obtain

$$
\begin{aligned}
\sum_q \left\{\widetilde{A}_q, \widetilde{A}_q^\dagger\right\} &= \frac{1}{3}N_I\left(\sum_j \{\hat{I}_j^+, \hat{I}_j^-\} - \sum_j e^{-i2Q\cdot R_j}\{\hat{I}_j^+, \hat{I}_j^+\}\right. \\
&\qquad\qquad\qquad \left. -\sum_j e^{i2Q\cdot R_j}\{\hat{I}_j^-, \hat{I}_j^-\} + \sum_j \{\hat{I}_j^-, \hat{I}_j^+\}\right) \\
&= \frac{1}{3}N_I\left(2\sum_j \{\hat{I}_j^+, \hat{I}_j^-\} - \sum_j e^{-i2Q\cdot R_j}\{\hat{I}_j^+, \hat{I}_j^+\} - \sum_j e^{i2Q\cdot R_j}\{\hat{I}_j^-, \hat{I}_j^-\}\right) \\
&= \frac{1}{3}N_I\left(2\sum_j \{\hat{I}_j^+, \hat{I}_j^-\} + 2\sum_j ((\hat{I}_j^y)^2 - (\hat{I}_j^x)^2)2\cos(2Q\cdot R_j)\right. \\
&\qquad\qquad\qquad\qquad\qquad \left. -2\sum_j \{\hat{I}_j^x, \hat{I}_j^y\}2\sin(2Q\cdot R_j)\right) \\
&\leq \frac{1}{3}N_I\left(2\sum_j \{\hat{I}_j^+, \hat{I}_j^-\} + 4\sum_j ((\hat{I}_j^y)^2 - (\hat{I}_j^x)^2) + 4\sum_j \{\hat{I}_j^x, \hat{I}_j^y\}\right) \\
&\leq 2N_I^2(2I)^2,
\end{aligned}
\tag{14.65}
$$

where we have used that

$$\{I_j^\pm, I_j^\pm\} = 2((I_j^x)^2 - (I_j^y)^2 \pm i\{I_j^x, I_j^y\}), \tag{14.66}$$

$$\langle (I_j^y)^2 - (I_j^x)^2 \rangle \leq 2I^2, \tag{14.67}$$

$$\langle \{I_j^x, I_j^y\} \rangle \leq 2I^2, \tag{14.68}$$

$$\langle \{I_j^+, I_j^-\} \rangle \leq (2I)^2. \tag{14.69}$$

Putting everything together

With the use of the above results the Bogoliubov inequality (14.18) reads as follows,

$$2N_I^2(2I)^2/2 \geq k_B T \sum_{\boldsymbol{q}} \frac{N_I^2 m_I^\perp(\boldsymbol{Q})^2/2}{\frac{N_e}{4m^*}q^2 - hN_I m_I^\perp(\boldsymbol{Q})}, \tag{14.70}$$

where m^* is defined as above. In the thermodynamic limit we thus obtain

$$(2I)^2 \geq \frac{k_B T N_I v}{N_e(2\pi)^d} \int_{|\boldsymbol{q}| \leq |\boldsymbol{q}_c|} d^d q \frac{m_I^\perp(\boldsymbol{Q})^2}{\frac{q^2}{2m^*} + |\nu h m_I^\perp(\boldsymbol{Q})|}, \tag{14.71}$$

where v and ν are defined as above.

14.E Presence of spin-orbit interaction

In this section we want to investigate the effect of the presence of Rashba and Dresselhaus spin-orbit terms which break the rotational spin symmetry of Hamiltonian (14.16). The spin-orbit Hamiltonian under consideration is thus given by

$$H_{\text{SO}} = H_R + H_D = \alpha \sum_i (\hat{p}_i^y \hat{s}_i^x - \hat{p}_i^x \hat{s}_i^y) + \beta \sum_i (\hat{p}_i^x \hat{s}_i^x - \hat{p}_i^y \hat{s}_i^y), \tag{14.72}$$

where H_R and H_D are the Rashba and the Dresselhaus spin-orbit Hamiltonian, respectively. [225, 226]

(Anti-)ferromagnetic ordering

In this case, the operator $C_{\boldsymbol{q}}$ entering the Bogoliubov inequality (14.18) is given by $C_{\boldsymbol{q}} = \hat{S}_{-\boldsymbol{q}}^- + \hat{I}_{-\boldsymbol{q}}^- + \hat{S}_{-\boldsymbol{q}}^+ + \hat{I}_{-\boldsymbol{q}}^+$.

Let us first calculate $[[C_{\boldsymbol{q}}, H_R], (C_{\boldsymbol{q}})^\dagger]$. From

$$
\begin{aligned}
[C_{\boldsymbol{q}}, H_R] &= [\hat{S}^-_{-\boldsymbol{q}} + \hat{S}^+_{-\boldsymbol{q}}, H_R] = [\sum_i e^{i\boldsymbol{q}\cdot\hat{\boldsymbol{r}}_i}(\hat{s}^+_i + \hat{s}^-_i), \alpha \sum_i (\hat{p}^y_i \hat{s}^x_i - \hat{p}^x_i \hat{s}^y_i)] \\
&= \alpha \sum_i \left((\hat{s}^+_i + \hat{s}^-_i)\hat{s}^x_i[e^{i\boldsymbol{q}\cdot\hat{\boldsymbol{r}}_i}, \hat{p}^y_i] + \underbrace{[\hat{s}^+_i + \hat{s}^-_i, \hat{s}^x_i]}_{=0}\hat{p}^y_i e^{i\boldsymbol{q}\hat{\boldsymbol{r}}_i} \right. \\
&\qquad\qquad \left. -(\hat{s}^+_i + \hat{s}^-_i)\hat{s}^y_i[e^{i\boldsymbol{q}\cdot\hat{\boldsymbol{r}}_i}, \hat{p}^x_i] - [\hat{s}^+_i + \hat{s}^-_i, \hat{s}^y_i]\hat{p}^x_i e^{i\boldsymbol{q}\cdot\hat{\boldsymbol{r}}_i} \right),
\end{aligned}
\tag{14.73}
$$

and with the aid of

$$
\begin{aligned}
(\hat{s}^+_i + \hat{s}^-_i)\hat{s}^x_i &= 2\hat{s}^x_i \hat{s}^x_i = \frac{1}{2}, & (14.74) \\
(\hat{s}^+_i + \hat{s}^-_i)\hat{s}^y_i &= 2\hat{s}^x_i \hat{s}^y_i = i\hat{s}^z_i, & (14.75) \\
[\hat{s}^+_i + \hat{s}^-_i, \hat{s}^y_i] &= [2\hat{s}^x_i, \hat{s}^y_i] = 2i\hat{s}^z_i, & (14.76)
\end{aligned}
$$

we have that

$$
\begin{aligned}
[C_{\boldsymbol{q}}, H_R] &= \alpha \sum_i \left(\frac{1}{2}[e^{i\boldsymbol{q}\hat{\boldsymbol{r}}_i}, \hat{p}^y_i] - i\hat{s}^z_i[e^{i\boldsymbol{q}\cdot\hat{\boldsymbol{r}}_i}, \hat{p}^x_i] - 2i\hat{s}^z_i \hat{p}^x_i e^{i\boldsymbol{q}\cdot\hat{\boldsymbol{r}}_i} \right) \\
&= \alpha \sum_i \left(\frac{1}{2}[e^{i\boldsymbol{q}\cdot\hat{\boldsymbol{r}}_i}, \hat{p}^y_i] - i\hat{s}^z_i\{\hat{p}^x_i, e^{i\boldsymbol{q}\cdot\hat{\boldsymbol{r}}_i}\} \right).
\end{aligned}
\tag{14.77}
$$

Therefore,

$$
\begin{aligned}
[[C_{\boldsymbol{q}}, H_R], C^\dagger_{\boldsymbol{q}}] &= [\alpha \sum_i \left(\frac{1}{2}[e^{i\boldsymbol{q}\cdot\hat{\boldsymbol{r}}_i}, \hat{p}^y_i] - i\hat{s}^z_i\{\hat{p}^x_i, e^{i\boldsymbol{q}\cdot\hat{\boldsymbol{r}}_i}\} \right), \sum_i e^{-i\boldsymbol{q}\cdot\hat{\boldsymbol{r}}_i}(\hat{s}^+_i + \hat{s}^-_i)] \\
&= \alpha \sum_i (\hat{s}^+_i + \hat{s}^-_i) \underbrace{[\frac{1}{2}[e^{i\boldsymbol{q}\cdot\hat{\boldsymbol{r}}_i}, \hat{p}^y_i], e^{-i\boldsymbol{q}\cdot\hat{\boldsymbol{r}}_i}]}_{=0} \\
&\quad -\alpha \sum_i i\underbrace{\hat{s}^z_i(\hat{s}^+_i + \hat{s}^-_i)}_{-\hat{s}^y_i}\underbrace{[\{\hat{p}^x_i, e^{i\boldsymbol{q}\cdot\hat{\boldsymbol{r}}_i}\}, e^{-i\boldsymbol{q}\cdot\hat{\boldsymbol{r}}_i}]}_{-2q_x} \\
&\quad -\alpha \sum_i i\underbrace{[\hat{s}^z_i, \hat{s}^+_i + \hat{s}^-_i]}_{-2\hat{s}^y_i}\underbrace{e^{-i\boldsymbol{q}\cdot\hat{\boldsymbol{r}}_i}\{\hat{p}^x_i, e^{i\boldsymbol{q}\cdot\hat{\boldsymbol{r}}_i}\}}_{2\hat{p}^x_i + q_x} \\
&= \alpha \sum_i 4\hat{p}^x_i \hat{s}^y_i.
\end{aligned}
\tag{14.78}
$$

Let us now calculate $[[C_{\boldsymbol{q}}, H_D], (C_{\boldsymbol{q}})^\dagger]$. Analogously to the above case we have that

$$
\begin{aligned}
[C_{\boldsymbol{q}}, H_D] &= [\hat{S}^-_{-\boldsymbol{q}} + \hat{S}^+_{-\boldsymbol{q}}, H_D] = [\sum_i e^{i\boldsymbol{q}\cdot\hat{\boldsymbol{r}}_i}(\hat{s}^+_i + \hat{s}^-_i), \beta \sum_i (\hat{p}^x_i \hat{s}^x_i - \hat{p}^y_i \hat{s}^y_i)] \\
&= \beta \sum_i \left((\hat{s}^+_i + \hat{s}^-_i)\hat{s}^x_i [e^{i\boldsymbol{q}\cdot\hat{\boldsymbol{r}}_i}, \hat{p}^x_i] + \underbrace{[\hat{s}^+_i + \hat{s}^-_i, \hat{s}^x_i]}_{=0} \hat{p}^x_i e^{i\boldsymbol{q}\cdot\hat{\boldsymbol{r}}_i} \right. \\
&\qquad\qquad \left. -(\hat{s}^+_i + \hat{s}^-_i)\hat{s}^y_i [e^{i\boldsymbol{q}\cdot\hat{\boldsymbol{r}}_i}, \hat{p}^y_i] - [\hat{s}^+_i + \hat{s}^-_i, \hat{s}^y_i]\hat{p}^y_i e^{i\boldsymbol{q}\hat{\boldsymbol{r}}_i} \right) \\
&= \beta \sum_i \left(\frac{1}{2}[e^{i\boldsymbol{q}\cdot\hat{\boldsymbol{r}}_i}, \hat{p}^x_i] - i\hat{s}^z_i [e^{i\boldsymbol{q}\cdot\hat{\boldsymbol{r}}_i}, \hat{p}^y_i] - 2i\hat{s}^z_i \hat{p}^y_i e^{i\boldsymbol{q}\cdot\hat{\boldsymbol{r}}_i} \right) \\
&= \beta \sum_i \left(\frac{1}{2}[e^{i\boldsymbol{q}\cdot\hat{\boldsymbol{r}}_i}, \hat{p}^x_i] - i\hat{s}^z_i \{\hat{p}^y_i, e^{i\boldsymbol{q}\cdot\hat{\boldsymbol{r}}_i}\} \right),
\end{aligned} \tag{14.79}
$$

and consequently we obtain

$$
\begin{aligned}
[[C_{\boldsymbol{q}}, H_D], C^\dagger_{\boldsymbol{q}}] &= [\beta \sum_i \left(\frac{1}{2}[e^{i\boldsymbol{q}\hat{\boldsymbol{r}}_i}, \hat{p}^x_i] - i\hat{s}^z_i \{\hat{p}^y_i, e^{i\boldsymbol{q}\cdot\hat{\boldsymbol{r}}_i}\} \right), \sum_i e^{-i\boldsymbol{q}\cdot\hat{\boldsymbol{r}}_i}(\hat{s}^+_i + \hat{s}^-_i)] \\
&= \beta \sum_i (\hat{s}^+_i + \hat{s}^-_i) \underbrace{[\frac{1}{2}[e^{i\boldsymbol{q}\cdot\hat{\boldsymbol{r}}_i}, \hat{p}^x_i], e^{-i\boldsymbol{q}\hat{\boldsymbol{r}}_i}]}_{=0} \\
&\quad -\beta \sum_i i\underbrace{\hat{s}^z_i(\hat{s}^+_i + \hat{s}^-_i)}_{-\hat{s}^y_i} \underbrace{[\{\hat{p}^y_i, e^{i\boldsymbol{q}\cdot\hat{\boldsymbol{r}}_i}\}, e^{-i\boldsymbol{q}\cdot\hat{\boldsymbol{r}}_i}]}_{-2q_y} \\
&\quad -\beta \sum_i i\underbrace{[\hat{s}^z_i, \hat{s}^+_i + \hat{s}^-_i]}_{-2\hat{s}^y_i} \underbrace{e^{-i\boldsymbol{q}\cdot\hat{\boldsymbol{r}}_i}\{\hat{p}^y_i, e^{i\boldsymbol{q}\cdot\hat{\boldsymbol{r}}_i}\}}_{2\hat{p}^y_i+q_y} \\
&= \beta \sum_i 4\hat{p}^y_i \hat{s}^y_i.
\end{aligned} \tag{14.80}
$$

We thus finally conclude that

$$
[[C_{\boldsymbol{q}}, H_{\text{SO}}], C^\dagger_{\boldsymbol{q}}] = 4\sum_i (\alpha\hat{p}^x_i + \beta\hat{p}^y_i)\hat{s}^y_i. \tag{14.81}
$$

Helical ordering

In this case, $\widetilde{C}_{\boldsymbol{q}}$ is chosen to be $\widetilde{C}_{\boldsymbol{q}} = \hat{S}^z_{-\boldsymbol{q}} + \hat{I}^z_{-\boldsymbol{q}}$. From

$$
\begin{aligned}
[\widetilde{C}_{\boldsymbol{q}}, H_R] &= [\sum_i e^{i\boldsymbol{q}\cdot\hat{\boldsymbol{r}}_i}\hat{s}^z_i, \alpha\sum_i(\hat{p}^y_i\hat{s}^x_i - \hat{p}^x_i\hat{s}^y_i)] = \alpha\sum_i\left([e^{i\boldsymbol{q}\cdot\hat{\boldsymbol{r}}_i}\hat{s}^z_i, \hat{p}^y_i\hat{s}^x_i] - [e^{i\boldsymbol{q}\cdot\hat{\boldsymbol{r}}_i}\hat{s}^z_i, \hat{p}^x_i\hat{s}^y_i]\right) \\
&= \alpha\sum_i\left(\underbrace{\hat{s}^z_i\hat{s}^x_i}_{\frac{i}{2}\hat{s}^y_i}[e^{i\boldsymbol{q}\cdot\hat{\boldsymbol{r}}_i}, \hat{p}^y_i] + \underbrace{[\hat{s}^z_i, \hat{s}^x_i]}_{i\hat{s}^y_i}\hat{p}^y_i e^{i\boldsymbol{q}\cdot\hat{\boldsymbol{r}}_i} - \underbrace{\hat{s}^z_i\hat{s}^y_i}_{-\frac{i}{2}\hat{s}^x_i}[e^{i\boldsymbol{q}\cdot\hat{\boldsymbol{r}}_i}, \hat{p}^x_i] - \underbrace{[\hat{s}^z_i, \hat{s}^y_i]}_{-i\hat{s}^x_i}\hat{p}^x_i e^{i\boldsymbol{q}\hat{\boldsymbol{r}}_i}\right) \\
&= \alpha\sum_i\left(\frac{1}{2}i\hat{s}^y_i\{\hat{p}^y_i, e^{i\boldsymbol{q}\hat{\boldsymbol{r}}_i}\} + \frac{1}{2}i\hat{s}^x_i\{\hat{p}^x_i, e^{i\boldsymbol{q}\cdot\hat{\boldsymbol{r}}_i}\}\right),
\end{aligned}
\tag{14.82}
$$

we obtain

$$
\begin{aligned}
[[\widetilde{C}_{\boldsymbol{q}}, H_R], \widetilde{C}^\dagger_{\boldsymbol{q}}] &= [\alpha\sum_i\left(\frac{1}{2}i\hat{s}^y_i\{\hat{p}^y_i, e^{i\boldsymbol{q}\cdot\hat{\boldsymbol{r}}_i}\} + \frac{1}{2}i\hat{s}^x_i\{\hat{p}^x_i, e^{i\boldsymbol{q}\cdot\hat{\boldsymbol{r}}_i}\}\right), \sum_i e^{-i\boldsymbol{q}\cdot\hat{\boldsymbol{r}}_i}\hat{s}^z_i] \\
&= \alpha\sum_i\left(\frac{1}{2}i[\hat{s}^y_i\{\hat{p}^y_i, e^{i\boldsymbol{q}\cdot\hat{\boldsymbol{r}}_i}\}, e^{-i\boldsymbol{q}\cdot\hat{\boldsymbol{r}}_i}\hat{s}^z_i] + \frac{1}{2}i[\hat{s}^x_i\{\hat{p}^x_i, e^{i\boldsymbol{q}\cdot\hat{\boldsymbol{r}}_i}\}, e^{-i\boldsymbol{q}\cdot\hat{\boldsymbol{r}}_i}\hat{s}^z_i]\right) \\
&= \alpha\sum_i\frac{1}{2}i\left(\underbrace{\hat{s}^y_i\hat{s}^z_i}_{\frac{i}{2}\hat{s}^x_i}\underbrace{[\{\hat{p}^y_i, e^{i\boldsymbol{q}\cdot\hat{\boldsymbol{r}}_i}\}, e^{-i\boldsymbol{q}\cdot\hat{\boldsymbol{r}}_i}]}_{-2q_y} + \underbrace{[\hat{s}^y_i, \hat{s}^z_i]}_{i\hat{s}^x_i}\underbrace{e^{-i\boldsymbol{q}\cdot\hat{\boldsymbol{r}}_i}\{\hat{p}^y_i, e^{i\boldsymbol{q}\cdot\hat{\boldsymbol{r}}_i}\}}_{2\hat{p}^y_i+q_y}\right) \\
&\quad +\alpha\sum_i\frac{1}{2}i\left(\underbrace{\hat{s}^x_i\hat{s}^z_i}_{-\frac{i}{2}\hat{s}^y_i}\underbrace{[\{\hat{p}^x_i, e^{i\boldsymbol{q}\cdot\hat{\boldsymbol{r}}_i}\}, e^{-i\boldsymbol{q}\cdot\hat{\boldsymbol{r}}_i}]}_{-2q_x} + \underbrace{[\hat{s}^x_i, \hat{s}^z_i]}_{-i\hat{s}^y_i}\underbrace{e^{-i\boldsymbol{q}\cdot\hat{\boldsymbol{r}}_i}\{\hat{p}^x_i, e^{i\boldsymbol{q}\cdot\hat{\boldsymbol{r}}_i}\}}_{2\hat{p}^x_i+q_x}\right) \\
&= \alpha\sum_i(\hat{p}^x_i\hat{s}^y_i - \hat{p}^y_i\hat{s}^x_i) = -H_R.
\end{aligned}
\tag{14.83}
$$

Similarly, from

$$
\begin{aligned}
[\widetilde{C}_{\boldsymbol{q}}, H_D] &= [\sum_i e^{i\boldsymbol{q}\hat{\boldsymbol{r}}_i}\hat{s}^z_i, \beta\sum_i(\hat{p}^x_i\hat{s}^x_i - \hat{p}^y_i\hat{s}^y_i)] = \beta\sum_i\left([e^{i\boldsymbol{q}\hat{\boldsymbol{r}}_i}\hat{s}^z_i, \hat{p}^x_i\hat{s}^x_i] - [e^{i\boldsymbol{q}\cdot\hat{\boldsymbol{r}}_i}\hat{s}^z_i, \hat{p}^y_i\hat{s}^y_i]\right) \\
&= \beta\sum_i\left(\underbrace{\hat{s}^z_i\hat{s}^x_i}_{\frac{i}{2}\hat{s}^y_i}[e^{i\boldsymbol{q}\cdot\hat{\boldsymbol{r}}_i}, \hat{p}^x_i] + \underbrace{[\hat{s}^z_i, \hat{s}^x_i]}_{i\hat{s}^y_i}\hat{p}^x_i e^{i\boldsymbol{q}\cdot\hat{\boldsymbol{r}}_i} - \underbrace{\hat{s}^z_i\hat{s}^y_i}_{-\frac{i}{2}\hat{s}^x_i}[e^{i\boldsymbol{q}\cdot\hat{\boldsymbol{r}}_i}, \hat{p}^y_i] - \underbrace{[\hat{s}^z_i, \hat{s}^y_i]}_{-i\hat{s}^x_i}\hat{p}^y_i e^{i\boldsymbol{q}\cdot\hat{\boldsymbol{r}}_i}\right) \\
&= \beta\sum_i\left(\frac{i}{2}\hat{s}^y_i\{\hat{p}^x_i, e^{i\boldsymbol{q}\cdot\hat{\boldsymbol{r}}_i}\} + \frac{i}{2}\hat{s}^x_i\{\hat{p}^y_i, e^{i\boldsymbol{q}\cdot\hat{\boldsymbol{r}}_i}\}\right),
\end{aligned}
\tag{14.84}
$$

we obtain

$$
\begin{aligned}
[[\widetilde{C}_{\boldsymbol{q}}, H_D], \widetilde{C}_{\boldsymbol{q}}^\dagger] &= [\beta \sum_i \left(\frac{i}{2} \hat{s}_i^y \{\hat{p}_i^x, e^{i\boldsymbol{q}\cdot\hat{\boldsymbol{r}}_i}\} + \frac{i}{2} \hat{s}_i^x \{\hat{p}_i^y, e^{i\boldsymbol{q}\cdot\hat{\boldsymbol{r}}_i}\} \right), \sum_i e^{-i\boldsymbol{q}\cdot\hat{\boldsymbol{r}}_i} \hat{s}_i^z] \\
&= \beta \sum_i \left(\frac{i}{2} [\hat{s}_i^y \{\hat{p}_i^x, e^{i\boldsymbol{q}\cdot\hat{\boldsymbol{r}}_i}\}, e^{-i\boldsymbol{q}\cdot\hat{\boldsymbol{r}}_i} \hat{s}_i^z] + \frac{i}{2} [\hat{s}_i^x \{\hat{p}_i^y, e^{i\boldsymbol{q}\cdot\hat{\boldsymbol{r}}_i}\}, e^{-i\boldsymbol{q}\cdot\hat{\boldsymbol{r}}_i} \hat{s}_i^z] \right) \\
&= \beta \sum_i \left(\frac{i}{2} \underbrace{\hat{s}_i^y \hat{s}_i^z}_{\frac{i}{2}\hat{s}_i^x} \underbrace{[\{\hat{p}_i^x, e^{i\boldsymbol{q}\cdot\hat{\boldsymbol{r}}_i}\}, e^{-i\boldsymbol{q}\cdot\hat{\boldsymbol{r}}_i}]}_{-2q_x} + \frac{i}{2} \underbrace{[\hat{s}_i^y, \hat{s}_i^z]}_{i\hat{s}_i^x} \underbrace{e^{-i\boldsymbol{q}\cdot\hat{\boldsymbol{r}}_i} \{\hat{p}_i^x, e^{i\boldsymbol{q}\cdot\hat{\boldsymbol{r}}_i}\}}_{2\hat{p}_i^x + q_x} \right) \\
&\quad + \beta \sum_i \left(\frac{i}{2} \underbrace{\hat{s}_i^x \hat{s}_i^z}_{-\frac{i}{2}\hat{s}_i^y} \underbrace{[\{\hat{p}_i^y, e^{i\boldsymbol{q}\cdot\hat{\boldsymbol{r}}_i}\}, e^{-i\boldsymbol{q}\cdot\hat{\boldsymbol{r}}_i}]}_{-2q_y} + \frac{i}{2} \underbrace{[\hat{s}_i^x, \hat{s}_i^z]}_{-i\hat{s}_i^y} \underbrace{e^{-i\boldsymbol{q}\cdot\hat{\boldsymbol{r}}_i} \{\hat{p}_i^y, e^{i\boldsymbol{q}\cdot\hat{\boldsymbol{r}}_i}\}}_{2\hat{p}_i^y + q_y} \right) \\
&= \beta \sum_i (\hat{p}_i^y \hat{s}_i^y - \hat{p}_i^x \hat{s}_i^x) = -H_D. \tag{14.85}
\end{aligned}
$$

We can thus finally conclude that

$$
[[\widetilde{C}_{\boldsymbol{q}}, H_{\text{SO}}], \widetilde{C}_{\boldsymbol{q}}^\dagger] = -H_{\text{SO}}. \tag{14.86}
$$

14.F   Continuity equation for spin-currents

Similar to Refs. [228, 229], we can derive a continuity equation for the total spin density operator $\hat{\Sigma}(\boldsymbol{r}) = \hat{\boldsymbol{S}}(\boldsymbol{r}) + \hat{\boldsymbol{I}}(\boldsymbol{r})$, where the lattice spin density is defined as $\hat{\boldsymbol{I}}(\boldsymbol{r}) = \sum_{j=1}^{N_I} \hat{\boldsymbol{I}}_j \delta(\boldsymbol{r} - \boldsymbol{R}_j)$. Let us first recall that $\hat{S}^\alpha(\boldsymbol{r})$ satisfies the Born-von Karman periodic boundary conditions and can thus be expanded as a Fourier series,

$$
\hat{S}^\alpha(\boldsymbol{r}) = \frac{1}{\Omega} \sum_{\boldsymbol{q}} e^{i\boldsymbol{q}\cdot\boldsymbol{r}} \hat{S}_{\boldsymbol{q}}^\alpha, \tag{14.87}
$$

where $\hat{S}_{\boldsymbol{q}}^\alpha = \sum_i e^{-i\boldsymbol{q}\cdot\hat{\boldsymbol{r}}_i} \hat{s}_i^\alpha$.

The Heisenberg equation of motion for the component $\alpha = x, y, z$ of the electron spin density is given by

$$
\dot{\hat{S}}^\alpha(\boldsymbol{r}) = i[H, \hat{S}^\alpha(\boldsymbol{r})]. \tag{14.88}
$$

Since $i[V, \hat{S}^\alpha(\boldsymbol{r})] = 0$, $i[U, \hat{S}^\alpha(\boldsymbol{r})] = 0$, and $i[H_Z(\boldsymbol{Q}), \hat{S}^\alpha(\boldsymbol{r})] = 0$, we only need to consider $i[H_0, \hat{S}^\alpha(\boldsymbol{r})]$, $i[H_J, \hat{S}^\alpha(\boldsymbol{r})]$, and $i[H_{\text{SO}}, \hat{S}^\alpha(\boldsymbol{r})]$. Let us first

calculate $i[H_0, \hat{S}^\alpha(\boldsymbol{r})]$. By using the Fourier decomposition from Eq. (14.87) we obtain

$$i[H_0, \hat{S}^\alpha(\boldsymbol{r})] = i\frac{1}{\Omega}\sum_{\boldsymbol{q}} e^{i\boldsymbol{q}\cdot\boldsymbol{r}}\sum_i \frac{\hat{s}_i^\alpha}{2m}[\hat{\boldsymbol{p}}_i^2, e^{-i\boldsymbol{q}\cdot\hat{\boldsymbol{r}}_i}]. \tag{14.89}$$

From

$$[\hat{\boldsymbol{p}}_i, e^{-i\boldsymbol{q}\cdot\hat{\boldsymbol{r}}_i}] = -\boldsymbol{q}e^{-i\boldsymbol{q}\cdot\hat{\boldsymbol{r}}_i}, \tag{14.90}$$

we have

$$
\begin{aligned}
i[H_0, \hat{S}^\alpha(\boldsymbol{r})] &= i\frac{1}{\Omega}\sum_{\boldsymbol{q}} e^{i\boldsymbol{q}\cdot\boldsymbol{r}}\sum_i \frac{\hat{s}_i^\alpha}{2m}(-\boldsymbol{q})\cdot\{\hat{\boldsymbol{p}}_i, e^{-i\boldsymbol{q}\cdot\hat{\boldsymbol{r}}_i}\} \\
&= -i\frac{1}{\Omega}\sum_{\boldsymbol{q}} e^{i\boldsymbol{q}\cdot\boldsymbol{r}}\boldsymbol{q}\cdot\boldsymbol{j}_{\boldsymbol{q}}^\alpha = -\nabla\cdot\boldsymbol{j}^\alpha(\boldsymbol{r}),
\end{aligned} \tag{14.91}
$$

where the spin current density operator is defined as

$$\boldsymbol{j}^\alpha(\boldsymbol{r}) = \sum_{i=1}^{N_e} \frac{1}{2m}\hat{s}_i^\alpha\{\hat{\boldsymbol{p}}_i, \delta(\hat{\boldsymbol{r}}_i - \boldsymbol{r})\}$$

and its Fourier decomposition reads $\boldsymbol{j}^\lambda(\boldsymbol{r}) = \frac{1}{\Omega}\sum_{\boldsymbol{q}} e^{i\boldsymbol{q}\cdot\boldsymbol{r}}\boldsymbol{j}_{\boldsymbol{q}}^\lambda$, with $\boldsymbol{j}_{\boldsymbol{q}}^\lambda = \frac{1}{2m}\sum_i \hat{s}_i^\lambda\{\hat{\boldsymbol{p}}_i, e^{-i\boldsymbol{q}\cdot\hat{\boldsymbol{r}}_i}\}$ ($\lambda = x, y, z$). We note that above definition of spin currents emerges naturally in the present context, and must be carefully distinguished from the one commonly used in the literature, [227, 228, 229] $\tilde{\boldsymbol{j}}^\alpha(\boldsymbol{r}) = \sum_{j=1}^{N_e} \frac{1}{2}\{\hat{\boldsymbol{v}}_j, \hat{s}_j^\alpha\delta(\hat{\boldsymbol{r}}_j - \boldsymbol{r})\}$, where the velocity operator, defined by $\hat{\boldsymbol{v}}_j = i[H, \hat{\boldsymbol{r}}_j]/\hbar$, picks up an additional anomalous spin-dependent term due to the presence of the SOI term H_{SO}. This anomalous term is absent in $\boldsymbol{j}^\alpha(\boldsymbol{r})$.

Let us now calculate $i[H_J, \hat{S}^\alpha(\boldsymbol{r})]$,

$$
\begin{aligned}
i[H_J, \hat{S}^\alpha(\boldsymbol{r})] &= i[J\sum_{j,k} \hat{\boldsymbol{s}}_k\delta(\hat{\boldsymbol{r}}_k - \boldsymbol{R}_j)\hat{\boldsymbol{I}}_j, \sum_i \hat{s}_i^\alpha\delta(\hat{\boldsymbol{r}}_i - \boldsymbol{r})] \\
&= J\sum_{\beta=x,y,z}\sum_{i,j} i\delta(\hat{\boldsymbol{r}}_i - \boldsymbol{R}_j)\delta(\hat{\boldsymbol{r}}_i - \boldsymbol{r})i\hat{I}_j^\beta\hat{s}_i^\gamma\epsilon_{\beta\alpha\gamma} \\
&= -J\sum_{\beta=x,y,z}\sum_j \delta(\boldsymbol{R}_j - \boldsymbol{r})\hat{I}_j^\beta\hat{s}_j^\gamma\epsilon_{\beta\alpha\gamma} = J\sum_j \delta(\boldsymbol{R}_j - \boldsymbol{r})(\hat{\boldsymbol{I}}_j \wedge \hat{\boldsymbol{s}}_j)_\alpha .
\end{aligned}
$$
$$\tag{14.92}$$

Finally we consider $i[H_{\mathrm{SO}}, \hat{S}^\alpha(\boldsymbol{r})]$. Since

$$i[H_R, \hat{S}^\alpha(\boldsymbol{r})] = i\frac{1}{\Omega}\sum_{\boldsymbol{q}} e^{i\boldsymbol{q}\cdot\boldsymbol{r}}[H_R, \hat{S}_{\boldsymbol{q}}^\alpha], \tag{14.93}$$

and

$$[H_R, \hat{S}_{\boldsymbol{q}}^\alpha] = \alpha \sum_i \underbrace{[\hat{p}_i^y \hat{s}_i^x, \sum_k e^{-i\boldsymbol{q}\cdot\hat{\boldsymbol{r}}_k} \hat{s}_k^\alpha]}_{=A} - \alpha \sum_i \underbrace{[\hat{p}_i^x \hat{s}_i^y, \sum_k e^{-i\boldsymbol{q}\cdot\hat{\boldsymbol{r}}_k} \hat{s}_k^\alpha]}_{=B},$$

(14.94)

with

$$A = \hat{s}_i^x \hat{s}_i^\alpha [\hat{p}_i^y, e^{-i\boldsymbol{q}\cdot\hat{\boldsymbol{r}}_i}] + [\hat{s}_i^x, \hat{s}_i^\alpha] e^{-i\boldsymbol{q}\cdot\hat{\boldsymbol{r}}_i} \hat{p}_i^y = \frac{i}{2}\epsilon_{x\alpha\gamma} \hat{s}_i^\gamma \{\hat{p}_i^y, e^{-i\boldsymbol{q}\cdot\hat{\boldsymbol{r}}_i}\}$$

(14.95)

$$\Rightarrow \alpha \frac{i}{2}\epsilon_{x\alpha\gamma} \sum_i \hat{s}_i^\gamma \{\hat{p}_i^y, e^{-i\boldsymbol{q}\cdot\hat{\boldsymbol{r}}_i}\} = \frac{i}{2}\alpha\epsilon_{x\alpha\gamma} 2m j_{\boldsymbol{q},y}^\gamma,$$

(14.96)

$$B = \hat{s}_i^y \hat{s}_i^\alpha [\hat{p}_i^x, e^{-i\boldsymbol{q}\cdot\hat{\boldsymbol{r}}_i}] + [\hat{s}_i^y, \hat{s}_i^\alpha] e^{-i\boldsymbol{q}\cdot\hat{\boldsymbol{r}}_i} \hat{p}_i^x = \frac{i}{2}\epsilon_{y\alpha\gamma} \hat{s}_i^\gamma \{\hat{p}_i^x, e^{-i\boldsymbol{q}\cdot\hat{\boldsymbol{r}}_i}\}$$

(14.97)

$$\Rightarrow \frac{i}{2}\alpha\epsilon_{y\alpha\gamma} \sum_i \hat{s}_i^\gamma \{\hat{p}_i^x, e^{-i\boldsymbol{q}\cdot\hat{\boldsymbol{r}}_i}\} = \frac{i}{2}\alpha\epsilon_{y\alpha\gamma} 2m j_{\boldsymbol{q},x}^\gamma,$$

(14.98)

we have that

$$i[H_R, \hat{S}^\alpha(\boldsymbol{r})] = -\frac{1}{2}\alpha\epsilon_{x\alpha\gamma} 2m j_y^\gamma + \frac{1}{2}\alpha\epsilon_{y\alpha\gamma} 2m j_x^\gamma,$$

(14.99)

where we have used $j_\gamma^\lambda(\boldsymbol{r}) = \frac{1}{\Omega} \sum_{\boldsymbol{q}} e^{i\boldsymbol{q}\cdot\boldsymbol{r}} j_{\boldsymbol{q},\gamma}^\lambda$ ($\gamma = x, y, z$).

For the Dresselhaus term the calculation is similar. Since $i[H_D, \hat{S}^\alpha(\boldsymbol{r})] = i\frac{1}{\Omega} \sum_{\boldsymbol{q}} e^{i\boldsymbol{q}\cdot\boldsymbol{r}} [H_D, \hat{S}_{\boldsymbol{q}}^\alpha]$ and

$$[H_D, \hat{S}_{\boldsymbol{q}}^\alpha] = \beta \sum_i \underbrace{[\hat{p}_i^x \hat{s}_i^x, e^{-i\boldsymbol{q}\cdot\hat{\boldsymbol{r}}_i} \hat{s}_i^\alpha]}_{=A} - \beta \sum_i \underbrace{[\hat{p}_i^y \hat{s}_i^y, e^{-i\boldsymbol{q}\cdot\hat{\boldsymbol{r}}_i} \hat{s}_i^\alpha]}_{=B}, \quad (14.100)$$

with

$$A = \hat{s}_i^x \hat{s}_i^\alpha [\hat{p}_i^x, e^{-i\boldsymbol{q}\cdot\hat{\boldsymbol{r}}_i}] + [\hat{s}_i^x, \hat{s}_i^\alpha] e^{-i\boldsymbol{q}\cdot\hat{\boldsymbol{r}}_i} \hat{p}_i^x = \frac{i}{2}\epsilon_{x\alpha\gamma} \hat{s}_i^\gamma \{\hat{p}_i^x, e^{-i\boldsymbol{q}\cdot\hat{\boldsymbol{r}}_i}\}$$

(14.101)

$$\Rightarrow \frac{i}{2}\beta\epsilon_{x\alpha\gamma} \sum_i \hat{s}_i^\gamma \{\hat{p}_i^x, e^{-i\boldsymbol{q}\cdot\hat{\boldsymbol{r}}_i}\} = \frac{i}{2}\beta\epsilon_{x\alpha\gamma} 2m j_{\boldsymbol{q},x}^\gamma,$$

(14.102)

$$B = \hat{s}_i^y \hat{s}_i^\alpha [\hat{p}_i^y, e^{-i\boldsymbol{q}\cdot\hat{\boldsymbol{r}}_i}] + [\hat{s}_i^y, \hat{s}_i^\alpha] e^{-i\boldsymbol{q}\cdot\hat{\boldsymbol{r}}_i} \hat{p}_i^y = \frac{i}{2}\epsilon_{y\alpha\gamma} \hat{s}_i^\gamma \{\hat{p}_i^y, e^{-i\boldsymbol{q}\cdot\hat{\boldsymbol{r}}_i}\}$$

(14.103)

$$\Rightarrow \frac{i}{2}\beta\epsilon_{y\alpha\gamma} \sum_i \hat{s}_i^\gamma \{\hat{p}_i^y, e^{-i\boldsymbol{q}\cdot\hat{\boldsymbol{r}}_i}\} = \frac{i}{2}\beta\epsilon_{y\alpha\gamma} 2m j_{\boldsymbol{q},y}^\gamma,$$

(14.104)

we can conclude that

$$i[H_D, \hat{S}^\alpha(\boldsymbol{r})] = -\frac{1}{2}\beta\epsilon_{x\alpha\gamma}2mj_x^\gamma + \frac{1}{2}\beta\epsilon_{y\alpha\gamma}2mj_y^\gamma, \quad (14.105)$$

where we used $j_\gamma^\lambda(\boldsymbol{r}) = \frac{1}{\Omega}\sum_{\boldsymbol{q}} e^{i\boldsymbol{q}\cdot\boldsymbol{r}} j_{\boldsymbol{q},\gamma}^\lambda$ as above.

Let us now derive the Heisenberg equation of motion for the lattice spin density. Since $i[H_e, \hat{I}^\alpha(\boldsymbol{r})] = 0$, we only need to consider $i[H_J, \hat{I}^\alpha(\boldsymbol{r})]$ and $i[H_Z(\boldsymbol{Q}), \hat{I}^\alpha(\boldsymbol{r})]$. Let us first calculate $i[H_J, \hat{I}^\alpha(\boldsymbol{r})]$:

$$\begin{aligned}
i[H_J, \hat{I}^\alpha(\boldsymbol{r})] &= i[J\sum_{i,j} \hat{\boldsymbol{s}}_i\delta(\hat{\boldsymbol{r}}_i - \boldsymbol{R}_j)\hat{\boldsymbol{I}}_j, \sum_l \hat{I}_l^\alpha\delta(\boldsymbol{R}_l - \boldsymbol{r})] \\
&= iJ\sum_{\beta=x,y,z}\sum_{i,j} \delta(\hat{\boldsymbol{r}}_i - \boldsymbol{R}_j)\delta(\boldsymbol{R}_j - \boldsymbol{r})i\hat{s}_i^\beta\hat{I}_j^\gamma\epsilon_{\beta\alpha\gamma} \\
&= -J\sum_{\beta=x,y,z}\sum_j \delta(\boldsymbol{R}_j - \boldsymbol{r})\hat{s}_j^\beta\hat{I}_j^\gamma\epsilon_{\alpha\gamma\beta} \\
&= -J\sum_j \delta(\boldsymbol{R}_j - \boldsymbol{r})(\hat{\boldsymbol{I}}_j \times \hat{\boldsymbol{s}}_j)_\alpha = -i[H_J, \hat{S}^\alpha(\boldsymbol{r})].
\end{aligned}$$

$$(14.106)$$

For the (anti-)ferromagnetic case the Zeeman term is

$$H_Z(\boldsymbol{Q}) = h\sum_j \left(e^{-\boldsymbol{Q}\cdot\hat{\boldsymbol{R}}_j}\hat{I}_j^z + e^{i\boldsymbol{Q}\cdot\hat{\boldsymbol{R}}_j}\hat{I}_j^z\right)$$

, and

$$\begin{aligned}
i[H_Z(\boldsymbol{Q}), \hat{I}^\alpha(\boldsymbol{r})] &= i[h\sum_l \left(e^{-\boldsymbol{Q}\cdot\hat{\boldsymbol{R}}_l}\hat{I}_l^z + e^{i\boldsymbol{Q}\cdot\hat{\boldsymbol{R}}_l}\hat{I}_l^z\right), \sum_j \hat{I}_j^\alpha\delta(\boldsymbol{R}_j - \boldsymbol{r})] \\
&= ih\sum_{j,l}(e^{-i\boldsymbol{Q}\cdot\boldsymbol{R}_l} + e^{i\boldsymbol{Q}\cdot\boldsymbol{R}_l})\delta(\boldsymbol{R}_j - \boldsymbol{r})[\hat{I}_l^z, \hat{I}_j^\alpha] \\
&= ih\sum_j(e^{-i\boldsymbol{Q}\cdot\boldsymbol{R}_j} + e^{i\boldsymbol{Q}\cdot\boldsymbol{R}_j})\delta(\boldsymbol{R}_j - \boldsymbol{r})i\epsilon_{z\alpha\gamma}\hat{I}_j^\gamma. \quad (14.107)
\end{aligned}$$

The continuity equation for the z-component of the total spin density takes the following form,

$$\dot{\Sigma}^z(\boldsymbol{r}) = -\nabla\cdot\boldsymbol{j}^z(\boldsymbol{r}) - \alpha\epsilon_{xzy}mj_y^y + \alpha\epsilon_{yzx}mj_x^x - \beta\epsilon_{xzy}mj_x^y + \beta\epsilon_{yzx}mj_y^x,$$

$$(14.108)$$

$$\Rightarrow \dot{\Sigma}^z(\boldsymbol{r}) + \nabla\cdot\boldsymbol{j}^z(\boldsymbol{r}) = m\alpha(j_y^y + j_x^x) + m\beta(j_x^y + j_y^x). \quad (14.109)$$

In the homogeneous and stationary limit, the left-hand side of Eq. (14.108) vanishes and this leads to

$$\langle j_x^x \rangle = -\langle j_y^y \rangle \quad \text{and} \quad \langle j_x^y \rangle = -\langle j_y^x \rangle. \tag{14.110}$$

For the helical case, the Zeeman term is

$$\widetilde{H}_Z(\boldsymbol{Q}) = \sqrt{2/3}h \sum_j \left(e^{-i\boldsymbol{Q}\cdot\boldsymbol{R}_j} \hat{I}_j^+ + e^{i\boldsymbol{Q}\cdot\boldsymbol{R}_j} \hat{I}_j^- \right)$$

and

$$
\begin{aligned}
i[\widetilde{H}_Z(\boldsymbol{Q}), \hat{I}^\alpha(\boldsymbol{r})] &= i[\sqrt{2/3}h \sum_l \left(e^{-i\boldsymbol{Q}\cdot\boldsymbol{R}_l} \hat{I}_l^+ + e^{i\boldsymbol{Q}\cdot\boldsymbol{R}_l} \hat{I}_l^- \right), \sum_j \hat{I}_j^\alpha \delta(\boldsymbol{R}_j - \boldsymbol{r})] \\
&= i\sqrt{2/3}h \sum_j \left(e^{-i\boldsymbol{Q}\cdot\boldsymbol{R}_j} \delta(\boldsymbol{R}_j - \boldsymbol{r})[\hat{I}_j^+, \hat{I}_j^\alpha] + e^{i\boldsymbol{Q}\cdot\boldsymbol{R}_j} \delta(\boldsymbol{R}_j - \boldsymbol{r})[\hat{I}_j^-, \hat{I}_j^\alpha] \right) \\
&= i\sqrt{2/3}h \sum_j e^{-i\boldsymbol{Q}\cdot\boldsymbol{R}_j} \delta(\boldsymbol{R}_j - \boldsymbol{r})(i\epsilon_{x\alpha\gamma}\hat{I}_j^\gamma - \epsilon_{y\alpha\gamma}\hat{I}_j^\gamma) \\
&\quad + i\sqrt{2/3}h \sum_j e^{i\boldsymbol{Q}\cdot\boldsymbol{R}_j} \delta(\boldsymbol{R}_j - \boldsymbol{r})(i\epsilon_{x\alpha\gamma}\hat{I}_j^\gamma + \epsilon_{y\alpha\gamma}\hat{I}_j^\gamma).
\end{aligned}
\tag{14.111}
$$

For $\alpha = z$ we thus have

$$i[\widetilde{H}_Z(\boldsymbol{Q}), \hat{I}^\alpha(\boldsymbol{r})] = i\sqrt{2/3}h \sum_j \left(e^{-i\boldsymbol{Q}\cdot\boldsymbol{R}_j} \delta(\boldsymbol{R}_j - \boldsymbol{r})(-\hat{I}_j^+) + e^{i\boldsymbol{Q}\cdot\boldsymbol{R}_j} \delta(\boldsymbol{R}_j - \boldsymbol{r})\hat{I}_j^- \right). \tag{14.112}$$

In this case the continuity equation for the z-component of the total spin density reads

$$
\begin{aligned}
\dot{\Sigma}^z(\boldsymbol{r}) + \nabla \cdot \boldsymbol{j}^z(\boldsymbol{r}) &= m\alpha(j_y^y + j_x^x) + m\beta(j_x^y + j_y^x) \\
&\quad + i\sqrt{2/3}h \sum_j \left(e^{-i\boldsymbol{Q}\cdot\boldsymbol{R}_j} \delta(\boldsymbol{R}_j - \boldsymbol{r})(-\hat{I}_j^+) + e^{i\boldsymbol{Q}\cdot\boldsymbol{R}_j} \delta(\boldsymbol{R}_j - \boldsymbol{r})\hat{I}_j^- \right).
\end{aligned}
\tag{14.113}
$$

In the presence of the lattice spin-spin interaction term $H_\mathcal{I}$, the right-hand

side of Eqs. (14.108) and (14.113) acquires an additional term

$$
\begin{aligned}
i[H_{\mathcal{I}}, \hat{I}^\alpha(\boldsymbol{r})] &= i[\sum_{j,l} \sum_{\beta=x,y,z} \mathcal{I}_{jl} \hat{I}_j^\beta \hat{I}_l^\beta, \sum_k \hat{I}_k^\alpha \delta(\boldsymbol{R}_k - \boldsymbol{r})] \\
&= i \sum_{j,l,k,\beta} \mathcal{I}_{jl} \delta(\boldsymbol{R}_k - \boldsymbol{r}) \left(\hat{I}_j^\beta [\hat{I}_l^\beta, \hat{I}_k^\alpha] + [\hat{I}_j^\beta, \hat{I}_k^\alpha] \hat{I}_l^\beta \right) \\
&= i \sum_{j,l,\beta} \mathcal{I}_{jl} \left(\delta(\boldsymbol{R}_l - \boldsymbol{r}) \hat{I}_j^\beta i\epsilon_{\beta\alpha\gamma} \hat{I}_l^\gamma + \delta(\boldsymbol{R}_j - \boldsymbol{r}) i\epsilon_{\beta\alpha\gamma} \hat{I}_j^\gamma \hat{I}_l^\beta \right) \\
&= \sum_{j,l,\beta} \mathcal{I}_{jl} \delta(\boldsymbol{R}_l - \boldsymbol{r}) \epsilon_{\alpha\beta\gamma} \hat{I}_j^\beta \hat{I}_l^\gamma + \sum_{j,l,\beta} \mathcal{I}_{jl} \delta(\boldsymbol{R}_j - \boldsymbol{r}) \epsilon_{\alpha\beta\gamma} \hat{I}_l^\beta \hat{I}_j^\gamma \\
&= 2 \sum_{jl} \mathcal{I}_{jl} \delta(\boldsymbol{R}_l - \boldsymbol{r}) (\hat{I}_j \times \hat{I}_l)_\alpha.
\end{aligned}
\tag{14.114}
$$

14.G Equilibrium spin-currents for $U, V, J, T = 0$

The aim of this section is to calculate uniform equilibrium spin currents for a system described by Hamiltonian (14.16) in the special case $V, U, J, T = 0$. The calculation follows the ones given in Refs. [227, 229]; however, due to the spin currents occcurring here without anomalous velocity term (see text after Eq. (14.91)), the leading term will turn out to be first order in the SOIs (instead of 3rd order [227, 229]). The single-particle Hamiltonian we consider takes the following form,

$$
H = \frac{\hat{\boldsymbol{p}}^2}{2m} + \frac{\alpha}{\hbar}(\sigma_x \hat{p}_y - \sigma_y \hat{p}_x) + \frac{\beta}{\hbar}(\sigma_y \hat{p}_y + \sigma_x \hat{p}_x),
\tag{14.115}
$$

where $\hat{\boldsymbol{p}}$ is the electron momentum operator and $\sigma_{x,y,z}$ are the usual Pauli matrices. The eigenstates of the system are

$$
\psi_{\boldsymbol{k},s}(\boldsymbol{r}) = \frac{e^{i\boldsymbol{k}\cdot\boldsymbol{r}}}{\sqrt{A}} \boldsymbol{u}_s(\boldsymbol{k}),
\tag{14.116}
$$

where A is the area of the system and $\boldsymbol{u}_s(\boldsymbol{k}) = \begin{pmatrix} 1 \\ s\frac{\Gamma^+}{|\Gamma^+|} \end{pmatrix}$, with

$$
\Gamma = \frac{1}{\sqrt{2}} \begin{pmatrix} -\beta k_x + \alpha k_y \\ \beta k_y - \alpha k_x \\ 0 \end{pmatrix}
$$

. The spectrum is given by

$$E_s(k_x, k_y) = \frac{\hbar^2 k^2}{2m} + s\sqrt{(\alpha^2 + \beta^2)k^2 - 4k_x k_y \alpha \beta}, \qquad (14.117)$$

and it takes the following form in polar coordinates $(k_x, k_y) = (k\cos(\theta), k\sin(\theta))$:

$$E_s(k, \theta) = \frac{\hbar^2 k^2}{2m} + sk \underbrace{\sqrt{(\alpha^2 + \beta^2) - 4\cos(\theta)\sin(\theta)\alpha\beta}}_{=:\alpha(\theta)}. \qquad (14.118)$$

The Fermi wavevectors $k_\pm(\theta)$ of the two branches are defined by $E_F = E_{s=\mp1}(k_\pm(\theta)) = \frac{\hbar^2 k_\pm(\theta)^2}{2m} + sk_\pm(\theta)\alpha(\theta)$ and the explicit expressions read

$$k_\pm(\theta) = \pm\frac{\alpha(\theta)m}{\hbar^2} + \sqrt{\left(\frac{m}{\hbar^2}\alpha(\theta)\right)^2 + \frac{2m}{\hbar^2}E_F}. \qquad (14.119)$$

In the perturbative limit where $m\alpha(\theta)^2 \ll \hbar^2 E_F$, we expand $k_\pm(\theta)$ up to second order in $\alpha(\theta)$ and obtain

$$k_\pm(\theta) = \sqrt{\frac{2m}{\hbar^2}E_F}\frac{m}{4\hbar^2 E_F}\alpha(\theta)^2 \pm \frac{m}{\hbar^2}\alpha(\theta) + \sqrt{\frac{2m}{\hbar^2}E_F}. \qquad (14.120)$$

The spin-current tensor $\mathcal{T}_{lm}$ is given by

$$\mathcal{T}_{lm} = \frac{1}{\Omega}\langle j_{q=0,l}^m \rangle_0 = \frac{1}{2}\sum_s \int \frac{d^2k}{(2\pi)^2}\langle \sigma_m v_l + v_l \sigma_m \rangle_{k,s}, \qquad (14.121)$$

where $\langle ... \rangle_{k,s}$ denotes the expectation value in the eigenstates $\psi_{k,s}$ and the integration must be performed over $k \leq k_\pm(\theta)$.

Let us first calculate $\mathcal{T}_{xy}$. Since $v_x = \hbar k_x/m$, we have that $\{\sigma_y, v_x\} = 2\hbar k_x \sigma_y/m$, and

$$\frac{2\hbar}{m}\langle \sigma_y k_x \rangle_{k,s} = \frac{2\hbar}{m}s\frac{k_x \Gamma_y}{|\Gamma^+|} = \frac{2\hbar}{m}s\frac{k_x(\beta k_y - \alpha k_x)}{\sqrt{k^2(\alpha^2 + \beta^2) - 4k_x k_y \alpha \beta}}. \qquad (14.122)$$

With the use of polar coordinates we obtain

$$\frac{2\hbar}{m}\langle \sigma_y k_x \rangle_{k,s} = \frac{2\hbar}{m}s\frac{\beta k^2 \cos(\theta)\sin(\theta) - \alpha k^2 \cos^2(\theta)}{k\underbrace{\sqrt{(\alpha^2 + \beta^2) - 4\cos(\theta)\sin(\theta)\alpha\beta}}_{=\alpha(\theta)}}. \qquad (14.123)$$

From Eqs. (14.121,14.123) we obtain

$$
\begin{aligned}
\mathcal{T}_{xy} &= \frac{1}{2}\frac{2\hbar}{m}\frac{1}{(2\pi)^2}\int_{k_+(\theta)}^{k_-(\theta)}\int_0^{2\pi} dk d\theta k \frac{\beta k \cos(\theta)\sin(\theta) - \alpha k \cos^2(\theta)}{\alpha(\theta)} \\
&= \frac{\hbar}{m}\frac{1}{(2\pi)^2}\int_0^{2\pi} d\theta \frac{k_-(\theta)^3 - k_+(\theta)^3}{3}\frac{\beta\cos(\theta)\sin(\theta) - \alpha\cos^2(\theta)}{\alpha(\theta)} \\
&= -\frac{\hbar}{m}\frac{1}{(2\pi)^2}\frac{1}{3}\int_0^{2\pi} d\theta[\frac{8m^3}{\hbar^6}\alpha(\theta)^3 + \frac{12m^2}{\hbar^4}E_F\alpha(\theta)]\frac{\beta\cos(\theta)\sin(\theta) - \alpha\cos^2(\theta)}{\alpha(\theta)}.
\end{aligned}
$$

$$(14.124)$$

Let us now split the above integral in two parts:

$$
\begin{aligned}
I_1 &= -\frac{\hbar}{m}\frac{1}{(2\pi)^2}\frac{1}{3}\frac{8m^3}{\hbar^6}\int_0^{2\pi} d\theta\alpha(\theta)^2(\beta\cos(\theta)\sin(\theta) - \alpha\cos^2(\theta)) \\
&= -\frac{2m^2}{3\pi^2\hbar^5}\int_0^{2\pi} d\theta(\alpha^2 + \beta^2 - 4\cos(\theta)\sin(\theta)\alpha\beta)(\beta\cos(\theta)\sin(\theta) - \alpha\cos^2(\theta)) \\
&= \frac{2m^2}{3\pi\hbar^5}\alpha(\alpha^2 + 2\beta^2),
\end{aligned}
$$

$$(14.125)$$

$$
\begin{aligned}
I_2 &= -\frac{\hbar}{m}\frac{1}{(2\pi)^2}\frac{1}{3}\frac{12m^2}{\hbar^4}E_F\int_0^{2\pi} d\theta(\beta\cos(\theta)\sin(\theta) - \alpha\cos^2(\theta)) \\
&= \frac{mE_F}{\pi\hbar^3}\alpha.
\end{aligned}
$$

$$(14.126)$$

The spin-current $\mathcal{T}_{xy}$ is thus given by

$$
\mathcal{T}_{xy} \approx \frac{2m^2}{3\pi\hbar^5}\alpha(\alpha^2 + 2\beta^2) + \frac{mE_F}{\pi\hbar^3}\alpha.
$$

$$(14.127)$$

Note that the term cubic in SOI agrees with earlier results, [227, 229] while the linear term survives here due to the absence of an anomalous velocity term. However, since $m\alpha(\theta)^2 \ll \hbar^2 E_F$ the cubic term is negligible and we obtain

$$
\mathcal{T}_{xy} \approx \frac{mE_F}{\pi\hbar^3}\alpha.
$$

$$(14.128)$$

A similar calculation shows that

$$
\mathcal{T}_{yy} \approx -\frac{mE_F}{\pi\hbar^3}\beta.
$$

$$(14.129)$$

Note that differently from the main text, both Hamiltonian (14.115) and the spin current density are expressed in terms of Pauli matrices and not

in terms of spin operators. Therefore, we need to multiply our results by a factor $(\hbar/2)^2$. Another multiplication with a factor $\hbar$ arises from the fact that the spin-orbit part is multiplied by $1/\hbar$ in (14.115) as compared to our definition in the main text,

$$\mathcal{T}_{xy} \approx \frac{mE_F}{4\pi}\alpha, \tag{14.130}$$

$$\mathcal{T}_{yy} \approx -\frac{mE_F}{4\pi}\beta. \tag{14.131}$$

14.H   Spin-orbit interaction with $\alpha = \beta$

Let us consider the special case when Rashba and Dresselhaus coefficients are equal, i.e., $\alpha = \beta$. In such a case, the spin-orbit Hamiltonian takes the following form

$$H_{\text{SO}} = \alpha \sum_i (\hat{p}_i^x + \hat{p}_i^y)(\hat{s}_i^x - \hat{s}_i^y), \tag{14.132}$$

and we define a gauge transformation $U = e^{i\sum_k \hat{\boldsymbol{A}}_k \cdot \hat{\boldsymbol{r}}_k}$ with gauge vector field $\boldsymbol{A}_k = (-\alpha m(\hat{s}_k^x - \hat{s}_k^y), -\alpha m(\hat{s}_k^x - \hat{s}_k^y), 0)$. Since

$$U\hat{p}_i^{x,y}U^{-1} = e^{i\sum_k \hat{\boldsymbol{A}}_k \cdot \hat{\boldsymbol{r}}_k}\hat{p}_i^{x,y}e^{-i\sum_k \hat{\boldsymbol{A}}_k \cdot \hat{\boldsymbol{r}}_k} = \hat{p}_i^{x,y} + \alpha m(\hat{s}_i^x - \hat{s}_i^y), \tag{14.133}$$

we have that

$$
\begin{aligned}
U\sum_i \frac{\hat{\boldsymbol{p}}_i^2}{2m}U^{-1} &= \sum_i \frac{(\hat{p}_i^x + \alpha m(\hat{s}_i^x - \hat{s}_i^y))^2 + (\hat{p}_i^y + \alpha m(\hat{s}_i^x - \hat{s}_i^y))^2}{2m} \\
&= \sum_i \frac{\hat{\boldsymbol{p}}_i^2}{2m} + H_{\text{SO}} + \frac{\alpha^2 m}{2},
\end{aligned}
\tag{14.134}
$$

where the constant $\alpha^2 m/2$ can be neglected without loss of generality. Under gauge transformation the spin isotropic term $H_J = J\sum_{j=1}^{N_I} \hat{\boldsymbol{S}}_j \cdot \hat{\boldsymbol{I}}_j$

transforms as follows,

$$
\begin{aligned}
U H_J U^{-1} &= U J \sum_{j=1}^{N_I} \hat{\boldsymbol{S}}_j \cdot \hat{\boldsymbol{I}}_j U^{-1} = J \sum_{j=1}^{N_I} U \hat{\boldsymbol{S}}_j U^{-1} \cdot \hat{\boldsymbol{I}}_j \\
&= J \sum_{j=1}^{N_I} e^{i \sum_k \hat{\boldsymbol{A}}_k \cdot \hat{\boldsymbol{r}}_k} \sum_{i=1}^{N_e} \hat{\boldsymbol{s}}_i \delta(\hat{\boldsymbol{r}}_i - \boldsymbol{R}_j) e^{-i \sum_k \hat{\boldsymbol{A}}_k \cdot \hat{\boldsymbol{r}}_k} \hat{\boldsymbol{I}}_j \\
&= J \sum_{j=1}^{N_I} \sum_{i=1}^{N_e} \underbrace{e^{i \sum_k \hat{\boldsymbol{A}}_k \cdot \hat{\boldsymbol{r}}_k} \hat{\boldsymbol{s}}_i e^{-i \sum_k \hat{\boldsymbol{A}}_k \cdot \hat{\boldsymbol{r}}_k}}_{=\mathcal{R}(\hat{\boldsymbol{r}}_i) \hat{\boldsymbol{s}}_i} \delta(\hat{\boldsymbol{r}}_i - \boldsymbol{R}_j) \hat{\boldsymbol{I}}_j \\
&= J \sum_{j=1}^{N_I} \sum_{i=1}^{N_e} \delta(\hat{\boldsymbol{r}}_i - \boldsymbol{R}_j) \mathcal{R}(\boldsymbol{R}_j) \hat{\boldsymbol{s}}_i \cdot \hat{\boldsymbol{I}}_j \\
&= J \sum_{j=1}^{N_I} \sum_{i=1}^{N_e} \delta(\hat{\boldsymbol{r}}_i - \boldsymbol{R}_j) \hat{\boldsymbol{s}}_i \cdot \underbrace{\mathcal{R}(\boldsymbol{R}_j)^T \hat{\boldsymbol{I}}_j}_{=:\hat{\boldsymbol{I}}_j^{\mathcal{R}^T}} = J \sum_{j=1}^{N_I} \sum_{i=1}^{N_e} \delta(\hat{\boldsymbol{r}}_i - \boldsymbol{R}_j) \hat{\boldsymbol{s}}_i \cdot \hat{\boldsymbol{I}}_j^{\mathcal{R}^T},
\end{aligned}
$$

$$(14.135)$$

where $\mathcal{R} \in SO(3)$ is a 3×3 special orthogonal matrix. The lattice spin Hamiltonian $H_{\mathcal{I}}$ remains unchanged under gauge transformation. From this, we can conclude that Hamiltonian $H = H_e + H_{\mathcal{I}} + H_J + H_{\text{SO}}$ and Hamiltonian

$$
H^{\mathcal{R}^T} = \underbrace{\sum_i \frac{\hat{\boldsymbol{p}}_i^2}{2m} + \sum_{i<j} V(\hat{\boldsymbol{r}}_i - \hat{\boldsymbol{r}}_j) + \sum_i U(\hat{\boldsymbol{r}}_i)}_{=H_e} + \underbrace{\sum_{j,l} \mathcal{I}_{jl} \hat{\boldsymbol{I}}_j \cdot \hat{\boldsymbol{I}}_l}_{=H_{\mathcal{I}}} + J \sum_{j=1}^{N_I} \hat{\boldsymbol{S}}_j \cdot \hat{\boldsymbol{I}}_j^{\mathcal{R}^T},
$$

$$(14.136)$$

are equivalent, i.e., $U^{-1} H^{\mathcal{R}^T} U = H$. Let us now introduce an impurity spin rotation $\widetilde{U}$ such that $\widetilde{U}^{-1} \hat{\boldsymbol{I}}_j \widetilde{U} = \hat{\boldsymbol{I}}_j^{\mathcal{R}^T}$:

$$
\widetilde{U}^{-1} H_0 \widetilde{U} = H^{\mathcal{R}^T}, \tag{14.137}
$$

where $H_0 = H_e + H_{\mathcal{I}} + \sum_{j=1}^{N_I} \hat{\boldsymbol{S}}_j \cdot \hat{\boldsymbol{I}}_j$. We conclude that

$$
U^{-1} \widetilde{U}^{-1} H_0 \widetilde{U} U = H. \tag{14.138}
$$

The canonical ensemble average of an operator $\mathcal{O}$ is given by $\langle \mathcal{O} \rangle_H = \text{Tr}(e^{-\beta H} \mathcal{O})/\text{Tr}(e^{-\beta H})$. Therefore, if we use the fact that $U^{-1} \widetilde{U}^{-1} H_0 \widetilde{U} U =$

H, we obtain

$$
\begin{aligned}
\langle \mathcal{O} \rangle_H &= \mathrm{Tr}\left(e^{-\beta \widetilde{U} U H U^{-1} \widetilde{U}^{-1}} \left[\widetilde{U} U \mathcal{O} U^{-1} \widetilde{U}^{-1} \right] \right) / \mathrm{Tr}\left(e^{-\beta \widetilde{U} U H U^{-1} \widetilde{U}^{-1}} \right) \\
&= \mathrm{Tr}\left(e^{-\beta H_0} \left[\widetilde{U} U \mathcal{O} U^{-1} \widetilde{U}^{-1} \right] \right) / \mathrm{Tr}\left(e^{-\beta H_0} \right) \\
&= \langle \widetilde{U} U \mathcal{O} U^{-1} \widetilde{U}^{-1} \rangle_{H_0}.
\end{aligned}
\tag{14.139}
$$

For the impurity spin magnetization $\hat{m}_I$ Eq. (14.139) implies that

$$
\langle \hat{m}_I \rangle_H = \mathrm{Tr}\left(e^{-\beta H_0} \hat{m}_I^{\mathcal{R}} \right) / \mathrm{Tr}\left(e^{-\beta H_0} \right) = \langle \hat{m}_I^{\mathcal{R}} \rangle_{H_0},
\tag{14.140}
$$

where $\hat{m}_I^{\mathcal{R}} = \widetilde{U} U \hat{m}_I U^{-1} \widetilde{U}^{-1} = \widetilde{U} \hat{m}_I \widetilde{U}^{-1}$ is defined analogously as $\hat{m}_I$ but with rotated spins $\hat{\boldsymbol{I}}_j^{\mathcal{R}} = \mathcal{R}(\boldsymbol{R}_j) \hat{\boldsymbol{I}}_j$. The explicit form of the matrix $\mathcal{R}(\boldsymbol{R}_j)$ is given by

$$
\mathcal{R}(\boldsymbol{R}_j) = \begin{pmatrix} 1/2 + 1/2 \cos(\theta_j) & -1/2 + 1/2 \cos(\theta_j) & -1/\sqrt{2} \sin(\theta_j) \\ -1/2 + 1/2 \cos(\theta_j) & 1/2 + 1/2 \cos(\theta_j) & -1/\sqrt{2} \sin(\theta_j) \\ 1/\sqrt{2} \sin(\theta_j) & 1/\sqrt{2} \sin(\theta_j) & \cos(\theta_j) \end{pmatrix},
\tag{14.141}
$$

and it corresponds to a rotation around the axis $\boldsymbol{n} = (1/\sqrt{2}, -1/\sqrt{2}, 0)$ by an angle of $\theta_j = -\sqrt{2}\alpha m (R_j^x + R_j^y)$. Note that the lattice vectors $\boldsymbol{R}_j = (R_j^x, R_j^y, R_j^z)$ should not be confused with the rotation matrix $\mathcal{R}$.

(Anti-) ferromagnetic ordering

The aim of this section is to rule out ferromagnetic ordering in a system defined by Hamiltonian $H = H_e + H_{\mathcal{I}} + H_J + H_{\mathrm{SO}} + H_Z(\boldsymbol{Q})$, where H_{SO} is defined as in Eq. (14.132) and the Zeeman term is chosen to be $H_Z(\boldsymbol{Q}) = h \sum_{j=1}^{N_I} (e^{-i\boldsymbol{Q}\cdot\boldsymbol{R}_j} \hat{I}_j^z + e^{i\boldsymbol{Q}\cdot\boldsymbol{R}_j} \hat{I}_j^z)$. The magnetization is given by $m_I^z(\boldsymbol{Q}) = \langle \hat{m}_I^z(\boldsymbol{Q}) \rangle_H = \frac{1}{N_I} \langle \sum_{j=1}^{N_I} (e^{-i\boldsymbol{Q}\cdot\boldsymbol{R}_j} \hat{I}_j^z + e^{i\boldsymbol{Q}\cdot\boldsymbol{R}_j} \hat{I}_j^z) \rangle_H$. We know that

$$
H_Z^{\mathcal{R}}(\boldsymbol{Q}) = \widetilde{U} U H_Z(\boldsymbol{Q}) U^{-1} \widetilde{U}^{-1} = h \sum_{j=1}^{N_I} (e^{-i\boldsymbol{Q}\cdot\boldsymbol{R}_j} (\hat{I}_j^{\mathcal{R}})^z + e^{i\boldsymbol{Q}\cdot\boldsymbol{R}_j} (\hat{I}_j^{\mathcal{R}})^z)
$$

and from Eq. (14.140) that

$$
\langle \hat{m}_I^z(\boldsymbol{Q}) \rangle_H = \langle (\hat{m}_I^{\mathcal{R}})^z(\boldsymbol{Q}) \rangle_{H_0} = \frac{1}{N_I} \langle \sum_{j=1}^{N_I} (e^{-i\boldsymbol{Q}\cdot\boldsymbol{R}_j} (\hat{I}_j^{\mathcal{R}})^z + e^{i\boldsymbol{Q}\cdot\boldsymbol{R}_j} (\hat{I}_j^{\mathcal{R}})^z) \rangle_{H_0}
$$

, with $H_0 = H_e + H_{\mathcal{I}} + H_J + H_Z^{\mathcal{R}}(\boldsymbol{Q})$. Since the rotation matrix $\mathcal{R}$ corresponds to a rotation around axis $\boldsymbol{n} = (1/\sqrt{2}, -1/\sqrt{2}, 0)$ (see Eq. (14.141)),

we define a new coordinate system, namely: $\boldsymbol{z} \to \boldsymbol{z}' = (1/\sqrt{2}, -1/\sqrt{2}, 0)$, $\boldsymbol{y} \to \boldsymbol{y}' = (1/\sqrt{2}, 1/\sqrt{2}, 0)$, and $\boldsymbol{x} \to \boldsymbol{x}' = \boldsymbol{z} = (0, 0, 1)$. In this new coordinate system we obtain

$$
H_Z^{\mathcal{R}}(\boldsymbol{Q}) = \frac{h}{2} \sum_{j=1}^{N_I} \left(e^{-i(\boldsymbol{Q}'+\boldsymbol{Q})\cdot\boldsymbol{R}_j} \hat{I}_j^{+'} + e^{i(\boldsymbol{Q}'-\boldsymbol{Q})\cdot\boldsymbol{R}_j} \hat{I}_j^{-'} + e^{i(\boldsymbol{Q}-\boldsymbol{Q}')\cdot\boldsymbol{R}_j} \hat{I}_j^{+'} \right.
$$
$$
\left. + e^{i(\boldsymbol{Q}'+\boldsymbol{Q})\cdot\boldsymbol{R}_j} \hat{I}_j^{-'} \right),
$$

$$(14.142)$$

$$
\langle (m_I^{\mathcal{R}})^z(\boldsymbol{Q}) \rangle_{H_0} = \frac{1}{2N_I} \left\langle \sum_{j=1}^{N_I} \left(e^{-i(\boldsymbol{Q}'+\boldsymbol{Q})\cdot\boldsymbol{R}_j} \hat{I}_j^{+'} + e^{i(\boldsymbol{Q}'-\boldsymbol{Q})\cdot\boldsymbol{R}_j} \hat{I}_j^{-'} + e^{i(\boldsymbol{Q}-\boldsymbol{Q}')\cdot\boldsymbol{R}_j} \hat{I}_j^{+'} \right.\right.
$$
$$
\left.\left. + e^{i(\boldsymbol{Q}'+\boldsymbol{Q})\cdot\boldsymbol{R}_j} \hat{I}_j^{-'} \right) \right\rangle_{H_0},
$$

$$(14.143)$$

where $\hat{I}_j^{\pm'} = \hat{I}_j^{x'} \pm i\hat{I}_j^{y'}$ and $\boldsymbol{Q}' = (-\sqrt{2}\alpha m, -\sqrt{2}\alpha m, 0)$. Note that in the new coordinate system $x'y'z'$, $H_{\mathcal{I}}$ and H_J does not change their form.

The proof in section 14.D can be generalized in a straightforward way to a slightly different choice of operator $\widetilde{A}_{\boldsymbol{q}} = \hat{I}_{\boldsymbol{q}+\boldsymbol{K}}^+ - \hat{I}_{\boldsymbol{q}-\boldsymbol{K}}^- + \hat{I}_{\boldsymbol{q}+\boldsymbol{K}'}^+ - \hat{I}_{\boldsymbol{q}-\boldsymbol{K}'}^-$ and symmetry-breaking Zemman term $H_Z(\boldsymbol{K}, \boldsymbol{K}') = h \sum_{j=1}^{N_I} (e^{-i\boldsymbol{K}\cdot\boldsymbol{R}_j} \hat{I}_j^{+'} + e^{i\boldsymbol{K}\cdot\boldsymbol{R}_j} \hat{I}_j^{-'} + e^{-i\boldsymbol{K}'\cdot\boldsymbol{R}_j} \hat{I}_j^{+'} + e^{i\boldsymbol{K}'\cdot\boldsymbol{R}_j} \hat{I}_j^{-'})$, with $\boldsymbol{K} = \boldsymbol{Q} + \boldsymbol{Q}'$ and $\boldsymbol{K}' = \boldsymbol{Q}' - \boldsymbol{Q}$. We thus conclude that in the limit of vanishing external magnetic field ($h \to 0$) $\langle (\hat{m}_I^{\mathcal{R}})^z \rangle_{H_0} = 0$ and consequently that $\langle \hat{m}_I^z \rangle_H = 0$. Since the proof is valid for any possible $\boldsymbol{Q}$, we have ruled out (anti-) ferromagnetic ordering along the z-direction in this case, too.

Helical Ordering

Here we rigorously rule out helical ordering in the direction of $\boldsymbol{n} = (1/\sqrt{2}, -1/\sqrt{2}, 0)$ for a system described by the Hamiltonian $H = H_e + H_{\mathcal{I}} + H_J + H_{SO} + H_Z^{\mathcal{R}^T}$, where H_{SO} is defined as in Eq. (14.132) and the Zeeman term is $H_Z^{\mathcal{R}^T} = h \sum_{j=1}^{N_I} (\hat{I}_j^{\mathcal{R}^T})^z$. The magnetization is given by $(m_I^{\mathcal{R}^T})^z = \langle (\hat{m}_I^{\mathcal{R}^T})^z \rangle_H = \frac{1}{N_I} \langle \sum_{j=1}^{N_I} (\hat{I}_j^{\mathcal{R}^T})^z \rangle_H$. From $\widetilde{U} U H_Z^{\mathcal{R}^T} U^{-1} \widetilde{U}^{-1} = H_Z = h \sum_{j=1}^{N_I} \hat{I}_j^z$ and Eq. (14.140), we have

$$
\langle (\hat{m}_I^{\mathcal{R}^T})^z \rangle_H = \langle \hat{m}_I^z \rangle_{H_0},
$$

$$(14.144)$$

where $H_0 = H_e + H_{\mathcal{I}} + H_J + H_Z$. From the proof in section 14.C, we know that in in the limit of vanishing external magnetic field ($h \to 0$) $\langle \hat{m}_I^z \rangle_{H_0} = 0$. From Eq. (14.144) we can thus conclude that $\langle (\hat{m}_I^{\mathcal{R}^T})^z \rangle_H = 0$ for $h \to 0$.

In order to have a better idea of the type of helical order excluded here, we can rewrite the magnetization $(m_I^{\mathcal{R}^T})^z$ in the transformed coordinate system $x'y'z'$ defined in the paragraph above,

$$(m_I^{\mathcal{R}^T})^z = \frac{1}{2N_I} \left\langle \sum_{j=1}^{N_I} \left(e^{-i\boldsymbol{Q}\cdot\boldsymbol{R}_j} \hat{I}_j^{+'} + e^{i\boldsymbol{Q}\cdot\boldsymbol{R}_j} \hat{I}_j^{-'} \right) \right\rangle_H , \qquad (14.145)$$

where $\boldsymbol{Q} = (\sqrt{2}\alpha m, \sqrt{2}\alpha m, 0)$. This corresponds to a helix in the $x'y'$-plane.

Bibliography

[1]   P. W. Shor, "Algortihms for quantum computation: discrete log and factoring",in *Proceedings of the 35th Anual Symposium on the Foundations of Computer Science*, (Los Alamos), p. 124, IEEE Computer Society Press, 1994.

[2]   D. Loss and D. P. DiVincenzo, Phys. Rev. A **57**, 120 (1998).

[3]   D. P. DiVincenzo, Report No. cond-mat/9612126; in *Mesoscopic Electron Transport*, Vol. 345 of NATO *Advanced Study Institute, Series E: Applied Sciences*, edited by L. Sohn, L. Kouwenhoven, and F. Schoen (Kluwer, Dordrecht, 1997).

[4]   L. P. Kouwenhoven, D. G. Austing, and S. Tarucha, Rep. Prog. Phys. **64**, 701 (2001).

[5]   R. Hanson, L. P. Kouwenhoven, J. R. Petta, S. Tarucha, L. M. K. Vandersypen, Rev. Mod. Phys. **79**, 1217 (2007).

[6]   C. Kloeffel and D. Loss, Ann. Rev. Condens. Matter Phys. **4**, 51 (2013).

[7]   J. J. Pla, K. Y. Tan, J. P. Dehollain, W. H. Lim, J. J. L. Morton, D. N. Jamieson, A. S. Dzurak, and A. Morello, Nature **489**, 541 (2012).

[8]   J. J. Pla, K. Y. Tan, J. P. Dehollain, W. H. Lim, J. J. L Morton, F. A. Zwanenburg, D. N. Jamieson, A. S. Dzurak, and A. Morello, ArXiv: 1302.0047 (2013).

[9]   V. Dobrovitski, G. Fuchs, A. Falk, C. Santori, and D. Awschalom, Ann. Rev. Condens. Matter Phys. **4**, 23 (2013).

[10]   J. Preskill, Proc. R. Soc. London, Ser. A **454**, 385 (1998).

[11]   M. A. Nielsen and I. L. Chuang, *Quantum Computation and Quantum Information* (Cambridge University Press, New York, 2000).

[12]   S. Bravyi, M. B. Hastings, and S. Michalakis, J. Math. Phys. **51**, 093512 (2010).

[13]   A. Y. Kitaev, *Proceedings of the 3rd International Conference of Quantum Communication and Measurement*, Ed. O. Hirota, A. S. Holevo, and C. M. Caves (New York, Plenum, 1997).

[14]   A. Kitaev, Ann. Phys. **303**, 2-30 (2003).

[15]   E. Dennis, A. Kitaev, A. Landahl, and J. Preskill, J. Math. Phys. **43**, 4452 (2002).

[16]   S. Chesi, B. Röthlisberger, and D. Loss, Phys. Rev. A **82**, 022305 (2010).

[17]   F. Wilczek, Quantum Mechanics of Fractional-Spin Particles, Phys. Rev. Lett. **49**, 957–959 (1982).

[18]   R. F. Streater and I. F. Wilde, Nuclear Physics B **24**, 561 (1970).

[19]   J. M. Leinaas and J. Myrheim, Nuovo Cimento B **37**, 1 (1977).

[20]   J. Preskill, Lecture Notes for Physics 219: Quantum computation, http://www.theory.caltech.edu/ preskill/ph219/topological.pdf.

[21]   Jiannis K. Pachos, *Introduction to Topological Quantum Computation*, Cambridge University Press (2012).

[22]   G. Moore and N. Read, Nucl. Phys. B **360**, 362 (1991).

[23]   D. A. Ivanov, Phys. Rev. Lett. **86**, 268 (2001).

[24]   A. Y. Kitaev, Phys. Usp. **44**, 131 (2001).

[25]   E. Lieb, T. Schultz, and D. Mattis, Ann. of Phys. **16**, 407 (1961).

[26]   J. Alicea, Y. Oreg, G. Refael, F. von Oppen, and M. P. A. Fisher, Nat. Phys. **7**, 412 (2011).

[27]   A. Kitaev, Ann. Phys. **321**, 2-111 (2006).

[28]   S. Bravyi and A. Kitaev, Phys. Rev. A **71**, 022316 (2005).

[29]   K. I. Kugel' and D. I. Khomskii, Sov. Phys.-Usp. **25**, 231 (1982).

[30]   L.-M. Duan, E. Demler, and M. D. Lukin, Phys. Rev. Lett. **91**, 090402 (2003).

[31]   G. Jackeli and G. Khaliullin, Phys. Rev. Lett. **102**, 017205 (2009).

[32]   J. Q. You, X.-F. Shi, X. Hu, and F. Nori, Phys. Rev. B **81**, 014505 (2010).

[33]   R. Schmied, J. H. Wesenberg, and D. Leibfried, New. J. Phys. **13**, 115011 (2011).

[34]   X.-Y. Feng, G.-M. Zhang, and T. Xiang, Phys. Rev. Lett. **98**, 087204 (2007)

[35]   H.-H. Lai and O. I. Motrunich, Phys. Rev. B **84**, 235148 (2011).

[36]   W. DeGottardi, D. Sen, and S. Vishveshwara, New. J. Phys. **13**, 065028 (2011).

[37]   F. Jelezko, T. Gaebel, I. Popa, A. Gruber, and J. Wrachtrup, Phys. Rev. Lett. **92**, 076401 (2004).

[38]   F. Jelezko, T. Gaebel, I. Popa, M. Domhan, A. Gruber, and J. Wrachtrup, Phys. rev. Lett. **93**, 130501 (2004).

[39]   L. Childress, M. V. Gurudev Dutt, J. M. Taylor, A. S. Zibrov, F. Jelezko, J. Wrachtrup, P. R. Hemmer, and M. D. Lukin, Science **314**, 281 (2006).

[40]   M. V. G. Dutt, L. Childress, L. Jiang, E. Togan, J. Maze, F. Jelezko, A. S. Zibrov, P. R. Hemmer, and M. D. Lukin, Science **316**, 1312 (2007).

[41]   R. Hanson, V. V. Dobrovitski, A. E. Feiguin, O. Gywat, and D. D. Awschalom, Science **320**, 352 (2008).

[42]　　　　P. Neumann, N. Mizuochi, F. Rempp, P. Hemmer, H. Watanabe, S. Yamasaki, V. Jacques, T. Gaebel, F. Jelezko, and J. Wrachtrup, Science **320**, 1326 (2008).

[43]　　　　L. Jiang, J. S. Hodges, J. R. Maze, P. Maurer, J. M. Taylor, D. G. Cory, P. R. Hemmer, R. L. Walsworth, A. Yacoby, A. S. Zibrov, and M. D. Lukin, Science **326**, 1520 (2009).

[44]　　　　G. D. Fuchs, V. V. Dobrovitski, D. M. Toyli, F. J. Heremans, and D. D. Awschalom, Science **326**, 1520 (2009).

[45]　　　　P. Neumann, J. Beck, M. Steiner, F. Rempp, H. Fedder, P. R. Hemmer, J. Wrachtrup, and F. Jelezko, Science **329**, 542 (2010).

[46]　　　　B. B. Buckley, G. D. Fuchs, L. C. Bassett, and D. D. Awschalom, Science **330**, 1212 (2010).

[47]　　　　W. Nolting and A. Ramakanth, *Quantum Theory of Magnetism* (Springer, Berlin, 2009).

[48]　　　　E. Togan, Y. Chu, A. Trifonov, L. Jiang, J. Maze, L. Childress, M. Dutt, A. Sorensen, P. Hemmer, A. Zibrov, and M. Lukin, Nature **466**, 730 (2010).

[49]　　　　L. Robledo, L. Childress, H. Bernien, B. Hensen, P. F. Alkemade, and R. Hanson, Nature **477**, 574 (2011).

[50]　　　　G. Balasubramanian, P. Neumann, D. Twitchen, M. Markham, R. Kolesov, N. Mizuochi, J. Isoya, J. Achard, J. Beck, J. Tissler, V. Jacques, P. R. Hemmer, F. Jelezko, and J. Wrachtrup, Nat. Mater. **8**, 383 (2009).

[51]　　　　S. Amashm K. MacLean, I. P. Radu, D. M. Zumbühl, M. A. Kastner, M. O. Hanson, and A. C. Gossard, Phys. Rev. Lett. **100**, 046803 (2008).

[52]　　　　H. Bluhm, S. Foletti, I. Neder, M. Rudner, S. Mahalu, V. Umansky, and A. Yacoby, Nat. Phys. **7**, 109 (2011).

[53]　　　　J. R. Petta, A. C. Johnson, J. M. Taylor, E. A. Laird, A. Yacoby, M. D. Lukin, C. M. Marcus, M. P. Hanson, and A. C. Gossard, Science **309**, 2180 (2005).

[54]   F. H. L. Koppens, K. C. Nowack, and L. M. K. Vandersypen, Phys. Rev. Lett. **100**, 236802 (2008).

[55]   R. Brunner, Y.-S. Shin, T. Obata, M. Pioro-Ladrière, T. Kubo, K. Yoshida, T. Taniyama, Y. Tokura, and S. Tarucha, Phys. Rev. Lett. **107**, 146801 (2011).

[56]   M.-S. Choi, C. Bruder, and D. Loss, Phys. Rev. B **62**, 13569 (2000).

[57]   A. Wallraff, D. I. Schuster, A. Blaids, L. Frunzio, R.-S. Huang, J. Majer, D. Kumar, S. M. Girvin, and R. J. Schoelkopf, Nature **431**, 162 (2004).

[58]   L. Childress, A. S. Sorensen, and M. D. Lukin, Phys. Rev. A **69**, 042302 (2004).

[59]   Y. Rikitake and H. Imamura, Phys. Rev. B **72**, 033308 (2005).

[60]   G. Burkard and A. Imamoglu, Phys. Rev. B. **74**, 041307 (2006).

[61]   C. Flindt, A. S. Sørensen, and K. Flensberg, Phys. Rev. B **75**, 085307 (2006).

[62]   M. Trif, V. N. Golovach, and D. Loss, Phys. Rev. B **75**, 085307 (2007).

[63]   M. Trif, V. N. Golovach, and D. Loss, Phys. Rev. B **77**, 045434 (2008).

[64]   K. Flensberg and C. M. Marcus, Phys. Rev. B **81**, 195418 (2010).

[65]   L. Trifunovic, O. Dial, M. Trif, J. R. Wootton, R. Abebe, A. Yacoby, and D. Loss, Phys. Rev. X **2**, 011006 (2012).

[66]   M. D. Shulman, O. E. Dial, S. P. Harvey, H. Bluhm, V. Umansky, and A. Yacoby, Science **336**, 202 (2012).

[67]   M. Leijnse and K. Flensberg, arXiv: 1303.3507 (2013).

[68]   A. Imamoglu, D. D. Awschalom, G. Burkard, D. P. DiVincenzo, D. Loss, M. Sherwin, and A. Small, Phys. Rev. Lett. **83**, 4204 (1999).

[69]   T. Tanamoto, K. Maruyama, Y. X. Liu, X. Hu, and F. Nori, Phys. Rev. A **78**, 062313 (2008).

[70]   D. S. Wang, A. G. Fowler, and L. C. L. Hollenberg, Phys. Rev. A **83**, 020302 (2011).

[71]   Y. Makhlin and A. Shnirman, Phys. Rev. Lett. **92**, 178301 (2004).

[72]   A. A. Abrikosov, L. P. Gorkov, and I. E. Dzyaloshinski, *Methods of Quantum Field Theory in Statistical Physics* (Dover, 1975).

[73]   Y. Makhlin, G. Schön, and A. Shnirman, Chem. Phys. **296**, 315 (2004).

[74]   D. P. DiVincenzo and D. Loss, Phys. Rev. B **71**, 035318 (2005).

[75]   S. Bravyi, D.P. DiVincenzo, and D. Loss, Ann. Phys. **326**, 2793 (2011).

[76]   J. Hauptmann, J. Paaske, and P. Lindelof, Nat. Phys. **4**, 373 (2008).

[77]   L. Hofstetter, A. Geresdi, M. Aagesen, J. Nygard, C. Schönenberger, and S. Csonka, Phys. Rev. Lett. **104**, 246804 (2010).

[78]   R. Raussendorf and J. Harrington, Phys. Rev. Lett. **98**, 190504 (2007).

[79]   K. Khodjasteh and L. Viola, Phys. Rev. Lett. **102**, 080501 (2009).

[80]   X. Xu, W. Yao, B. Sun, D. G. Steel, A. S. Bracker, D. Gammon, and L. J. Sham, Nature **459**, 1105 (2009).

[81]   I. T. Vink, K. C. Nowack, F. H. L. Koppens, J. Danon, Y. V. Nazarov, and L. M. K. Vandersypen, Nat. Phys. **5**, 764 (2009).

[82]   H. Ohno, D. Chiba, F. Matsukura, T. Omiya, E. Abe, T. Dietl, Y. Ohno, and K. Ohtani, Nature **408**, 944 (2000).

[83]   L. Trifunovic, F. L. Pedrocchi, and D. Loss, ArXiv: 1302. 4017 (2013).

[84]   J. Levy, Phys. Rev. Lett. **89**, 147902 (2002).

[85]   J. Klinovaja, D. Stepanenko, B. I. Halperin, and D. Loss, Phys. Rev. B **86**, 085423 (2012).

[86]   D. Stepanenko, M. Rudner, B. I. Halperin, and D. Loss, Phys. Rev. B **85**, 075416 (2012).

[87]   Y. Tserkovnyak, A. Brataas, G. E. W. Bauer, and B. I. Halperin, Rev. Mod. Phys. **77**, 1375 (2005).

[88]   D. P. DiVincenzo, Fortschr. Phys. **48**, 771 (2000).

[89]   D. Gottesman, Ph.D. thesis, California Institute of Technology (1997), see also Phys. Rev. A **57**, 127 (1998).

[90]   S. Bravyi and M. B. Hastings, Commun. Math. Phys. **307**, 609 (2011).

[91]   F. Wegner, J. Math. Phys. **12**, 2259 (1971).

[92]   J. B. Kogut, Rev. Mod. Phys. **51**, 659 (1979).

[93]   C. Castelnovo and C. Chamon, Phys. Rev. B **76**, 184442 (2007).

[94]   Z. Nussinov and G. Ortiz, Phys. Rev. B **77**, 064302 (2008).

[95]   R. Alicki, M. Fannes, and M. Horodecki, J. Phys. A **42**, 065303 (2009).

[96]   S. Iblisdir, D. Pérez-García, M. Aguado, and J. Pachos, Phys. Rev. B **79**, 134303 (2009).

[97]   A. Hamma, C. Castelnovo, and C. Chamon, Phys. Rev. B **79**, 245122 (2009).

[98]   S. Bravyi and B. Terhal, New. J. Phys. **11**, 043029 (2009).

[99]   A. Kay and R. Colbeck, arxiv:0810.3557.

[100]   S. Chesi, D. Loss, S. Bravyi, and B. M. Terhal, New J. Phys. **12**, 025013 (2010).

[101]   F. Pastawski, A. Kay, N. Schuch, and I. Cirac, Phys. Rev. Lett. **103**, 080501 (2009).

[102]   F. Pastawski, A. Kay, N. Schuch, and I. Cirac, Quantum Inf. Comput. **10**, 580 (2010).

[103]   R. Alicki, M. Fannes, and M. Horodecki, J. Phys. A: Math. Theor. **40**, 6451 (2007).

[104]   J. Haah and J. Preskill, Phys. Rev. A. **86**, 032308 (2012).

[105]   B. Yoshida, Ann. Phys. **326**, 2566 (2011).

[106]   R. Alicki, M. Horodecki, P. Horodecki, and R. Horodecki, Open Syst. Inf. Dyn. **17**, 1 (2010).

[107]   D. Bacon, Phys. Rev. A **73**, 012340 (2006).

[108]   J. Haah, Phys. Rev. A **83**, 042330 (2011).

[109]   S. Bravyi and J. Haah, Phys. Rev. Lett. **107**, 150504 (2011).

[110]   K. Michnicki, arXiv:1208.3496 (2012).

[111]   F. L. Pedrocchi, S. Chesi, and D. Loss, Phys. Rev. B **83**, 115415 (2011).

[112]   B. Röthlisberger, J. R. Wootton, R. M. Heath, J. K. Pachos, and D. Loss, Phys. Rev. A **85**, 022313 (2012).

[113]   A. Hutter, J. R. Wootton, B. Röthlisberger, and D. Loss, Phys. Rev. A **86**, 052340 (2012).

[114]   J. Vidal, K. P. Schmidt, and S. Dusuel, Phys. Rev. B **78**, 245121 (2008).

[115]   J. R. Wootton and J. K. Pachos, Phys. Rev. Lett. **107**, 030503 (2011).

[116]   C. Stark, L. Pollet, A. Imamoglu, and R. Renner, Phys. Rev. Lett. **107**, 030504 (2011).

[117]   M. Trif, F. Troiani, D. Stepanenko, and D. Loss, Phys. Rev. Lett. **101**, 217201 (2008).

[118]   M. Trif, F. Troiani, D. Stepanenko, and D. Loss, Phys. Rev. B **82**, 045429 (2010).

[119]   M. F. Islam, J. F. Nossa, C. M. Canali, and M. Pederson, Phys. Rev. B **82**, 155446 (2010).

[120]   A. Blais, R.-S. Huang, A. Wallraff, S. M. Girvin, and R. J. Schoelkopf, Phys. Rev. A **69**, 062320 (2004).

[121]   A. Wallraff, D. I. Schuster, A. Blais, L. Frunzio, J. Majer, M. H. Devoret, S. M. Girvin, and R. J. Schoelkopf, Phys. Rev. Lett. **95**, 060501 (2005).

[122]   J. R. Schrieffer and P. A. Wolff, Phys. Rev. **149**, 491 (1966).

[123]   M. Trif, V. N. Golovach, and D. Loss, Phys. Rev. B **75**, 085307 (2007).

[124]   Yu. A. Pashkin, T. Yamamoto, O. Astafiev, Y. Nakamura, D. V. Averin, and J. S. Tsai, Nature (London) **421**, 823 (2003).

[125]   D. V. Averin and C. Bruder, Phys. Rev. Lett. **91**, 057003 (2003).

[126]   H. Weimer, M. Müller, I. Lesanovsky, P. Zoller, and H. P. Büchler, Nat. Phys. **6**, 382 (2010).

[127]   A. Kay and D. G. Angelakis, Eur. Phys. Lett. **84**, 20001 (2008).

[128]   J. Chaloupka, G. Jackeli, and G. Khaliullin, Phys. Rev. Lett. **105**, 027204 (2010).

[129]   L. Chirolli, G. Burkard, S. Kumar, and D. P. DiVincenzo, Phys. Rev. Lett. **104**, 230502 (2010).

[130]   C. Knetter and G. S. Uhrig, Eur. Phys. J. B. **13**, 209 (2000).

[131]   F. Wegner, Ann. Physik **3**, 77 (2004).

[132]   M. Trif, V. N. Golovach, and D. Loss, Phys. Rev. B **77**, 045434 (2008).

[133]   G. Duclos-Cianci and D. Poulin, Phys. Rev. Lett. **104**, 050504 (2010).

[134]   P. Simon, B. Braunecker, and D. Loss, Phys. Rev. B **77**, 045108 (2008).

[135]   D. Forster, *Hydrodynamic Fluctuations, Broken Symmetry, and Correlation Functions* (Benjamin, MA 1975).

[136]   N.D. Mermin and H. Wagner, Phys. Rev. Lett. **17**, 1133 (1966).

[137]   G. D. Mahan, *Many-Particle Physics* (Plenum 1990).

[138]   D. P. DiVincenzo and D. Loss, Phys. Rev. B **71**, 035318 (2005).

[139]   H. Mori and K. Kawasaki, Prog. Theor. Phys. **27**, 529 (1962).

[140]   H. B. Callen, Phys. Rev. **130**, 890 (1963).

[141]   R. A. Tahir-Kheli and H. B. Callen, Phys. Rev. **135**, A679 (1964).

[142]   G. Baskaran, S. Mandal, and R. Shankar, Phys. Rev. Lett **98**, 247201 (2007).

[143]   V. Lahtinen, G. Kells, A. Carollo, T. Stitt, J. Vala, and J. K. Pachos, Ann. Phys. **323**, 2286 (2008).

[144]   G. Kells, A. T. Bolukbasi, V. Lahtinen, J. K. Slingerland, J. K. Pachos, and J. Vala, Phys. Rev. Lett. **101**, 240404 (2008).

[145]   G. Kells, N. Moran, and J. Vala, J. Stat. Mech. (2009) P03006.

[146]   J. Chaloupka, G. Jackeli, and G. Khaliullin, Phys. Rev. Lett. **105**, 027204 (2010).

[147]   K. S. Tikhonov, M. V. Feigel'man, and A. Yu. Kitaev, Phys. Rev. Lett. **106**, 067203 (2011).

[148]   S. Mandal and N. Surendran, Phys. Rev. B **79**, 024426 (2009).

[149]   H. Xu and J. M. Taylor, arXiv:1104.0024 (2011).

[150]   H.-C. Jiang, Z.-C. Gu, X.-L. Qi, and S. Trebst, arxiv:1101.1145 (2011).

[151]   M. Kamfor, S. Dusuel, J. Vidal, and K. P. Schmidt, J. Stat. Mech. (2010) P08010.

[152]   H. Yao and S. A. Kivelson, Phys. Rev. Lett. **99**, 247203 (2007).

[153]   H. Yao, S.-C. Zhang, and S. A. Kivelson, Phys. Rev. Lett. **102**, 217202 (2009).

[154]   H. Yao and X.-L. Qi, Phys. Rev. Lett. **105**, 080501 (2010).

[155]   A. J. Willans, J. T. Chalker, and R. Moessner, arxiv:1106.0732

[156]   H.-D. Chen and Z. Nussinov, J. Phys. A: Math. Theor. **41**, 0705001 (2008).

[157]   G. Kells, J. K. Slingerland, and J. Vala, Phys. Rev. B **80**, 125415 (2009).

[158]   V. Lahtinen, New J. Phys. **13**, 075009 (2011).

[159]   E. H. Lieb, Phys. Rev. Lett. **73**, 2158 (1994).

[160]   N. Macris and B. Nachtergaele, J. Stat. Phys. **85**, 745 (1996).

[161]   S. Bravyi, Phys. Rev. A **73**, 042313 (2006).

[162]   L. Fu and C. L. Kane, Phys. Rev. Lett. **100**, 096407 (2008).

[163]   C. Nayak, S. H. Simon, A. Stern, M. Freedman, and S. Das Sarma, Rev. Mod. Phys. **80**, 1083 (2008).

[164]   B. M. Terhal, F. Hassler, and D. P. DiVincenzo, arxiv:1201.3757 (2012).

[165]   M. Sato, Y. Takahashi, and S. Fujimoto, Phys. Rev. Lett. **103**, 020401 (2009).

[166]   M. Sato, Y. Takahashi, and S. Fujimoto, Phys. Rev. B. **82**, 134521 (2010).

[167]   J. Alicea, Phys. Rev. B **81**, 125318 (2010).

[168]   R. M. Lutchyn, J. D. Sau, and S. Das Sarma, Phys. Rev. Lett. **105**, 077001 (2010).

[169]   Y. Oreg, G. Refael, and F. von Oppen, Phys. Rev. Lett. **105**, 177002 (2010).

[170]   A. Saket, S. R. Hassan, and R. Shankar, Phys. Rev. B **82**, 174409 (2010).

[171]   Y. Tserkovnyak and D. Loss, Phys. Rev. A **84**, 032333 (2011).

[172]   S. Gangadharaiah, B. Braunecker, P. Simon, and D. Loss, Phys. Rev. Lett. **107**, 036801 (2011).

[173]   J. Klinovaja, S. Gangadharaiah, and D. Loss, Phys. Rev. Lett. **108**, 196804 (2012).

[174]   M. Trif and Y. Tserkovnyak, PRL **109**, 257002 (2012).

[175]   F. Verstraete, J. I. Cirac, J. I. Latorre, E. Rico, and M. M. Wolf, Phys. Rev. Lett. **94**, 140601 (2005).

[176]   X. Chen, Z.-C. Gu, and X.-G. Wen, Phys. Rev. B **83**, 035107 (2011).

[177]   N. Schuch, D. Pérez-García, and I. Cirac, Phys. Rev. B **84**, 165139 (2011).

[178]   D. Rainis and D. Loss, Phys. Rev. B **85**, 174533 (2012).

[179]   F. L. Pedrocchi, S. Chesi, and D. Loss, Phys. Rev. B **84**, 165414 (2011).

[180]   R. Wiesendanger, Rev. Mod. Phys. **81**, 1495 (2009).

[181]   R. Hanson, L. P. Kouwenhoven, J. R. Petta, S. Tarucha, L. M. K. Vandersypen, Rev. Mod. Phys., **79** 1217 (2007).

[182]   Z.-X. Liu, Z.-B. Yang, Y.-J. Han, W. Yi, and X.-G. Wen, Arxiv:1204.5162 (2012).

[183]   O. Motrunich, K. Damle, and D. A. Huse, Phys. Rev. B **63**, 224204 (2001).

[184]   E. Fradkin and L. Susskind, Phys. Rev. D **17**, 2637 (1978).

[185]   S. Chesi, A. Jaffe, D. Loss, and F. L. Pedrocchi, ArXiv:1305.6270 (2013).

[186]   K. Osterwalder and R. Schrader, Commun. Math. Phys. **31**, 83–112 (1973), and Commun. Math. Phys. **42**, 281–305 (1975).

[187]   J. Glimm, A. Jaffe, and T. Spencer, Commun. Math. Phys. **45**, 203–216 (1975).

[188]   J. Fröhlich, Commun. Math. Phys. **50**, 79–85 (1976).

[189]   F. J. Dyson, E. H. Lieb, and B. Simon, J. Stat. Phys. **18**, 335–383 (1978).

[190]   J. Fröhlich, R. Israel, E. H. , and B. Simon, Commun. Math. Phys. **62**, 1–34 (1978), and J. Stat. Phys. **22**, 297–347 (1980).

[191]   K. Osterwalder and E. Seiler, Gauge Field Theories on a Lattice, *Ann. Phys.* **110**, 440–471 (1978).

[192]   J. Glimm and A. Jaffe, *Quantum Physics*, 2nd Edition, Springer Verlag, 1987.

[193]   Fabio L. Pedrocchi, Stefano Chesi, Suhas Gangadharaiah, and Daniel Loss, Phys. Rev. B **86**, 205412 (2012).

[194]   Y.-C. He and Y. Chen, ArXiv: 1210.5139 (2012).

[195]   A. Jaffe and F. L. Pedrocchi, ArXiv: 1305.1792 (2013).

[196]   J. Glimm, A. Jaffe, and T. Spencer, Ann. Math. **100**, 585–632 (1974).

[197]   N. Datta, R. Fernández, and J. Fröhlich, J. Stat. Phys. **84**, 455–534 (1996).

[198]   N. Datta, R. Fernàndez, J. Fröhlich, L. Rey-Bellet, Helv. Phys. Acta **69**, 752–820 (1996).

[199]   T. Kato, Prog. Theor. Phys. **IV**, 514–523 (1949).

[200]   T. Kato, *Perturbation Theory for Linear Operators*, Springer-Verlag, New York (1966).

[201]   P. C. Hohenberg, Phys. Rev. **158**, 158 (1967).

[202]   N. N. Bogoliubov, Phys. Abh. Sowjetunion **6**, 1, 113, 229 (1962).

[203]   A. Gelfert and W. Nolting, J. Phys.: Condens. Matter **13**, R505-R524 (2001).

[204]   F. Wegner, Phys. Lett. A **24**, 131 (1967).

[205]   M. B. Walker and Th. W. Ruijgrok, Phys. Rev. **171**, 513 (1968).

[206]   D. K. Ghosh, Phys. Rev. Lett. **27**, 1584 (1971).

[207]   E. Rastelli and A. Tassi, Phys. Rev. B **40**, 5282 (1989).

[208]   G. S. Uhrig, Phys. Rev. B **45**, 4738 (1992).

[209]   P. Bruno, Phys. Rev. Lett. **87**, 137203 (2001).

[210] C. Proetto and A. Lopez, J. Physique Lett. **44**, L635 (1983).

[211] C. Noce and M. Cuoco, Phys. Rev. B **59**, 7409 (1999).

[212] M. A. Ruderman and C. Kittel, Phys. Rev. **96**, 99 (1954); T. Kasuya, Prog. Theor. Phys. **16**, 45 (1956); K. Yosida, Phys. Rev. **106**, 893 (1957).

[213] H. Tsunetsugu, M. Sigrist, and K. Ueda, Rev. Mod. Phys. **69**, 809 (1997).

[214] T. Dietl, A. Haury, and Y. M. d'Aubigné, Phys. Rev. B **55**, 3347(R) (1997).

[215] H. Ohno, D. Chiba, F. Matsukura, T. Omiya, E. Abe, T. Dietl, Y. Ohno, and K. Ohtani, Nature **408**, 944 (2000).

[216] D. Chiba, M. Sawicki, Y. Nishitani, Y. Nakatani, F. Matsukura, and H. Ohno, Nature **455**, 515 (2008).

[217] A. Richardella, P. Roushan, S. Mack, B. Zhou, D. A. Huse, D. D. Awschalom, A. Yazdani, Science **327**, 665 (2010).

[218] J. R. Petta, A. C. Johnson, J. M.Taylor, E. A. Laird, A. Yacoby, M. D. Lukin, C. M. Marcus, M. P. Hanson, A. C. Gossard, Science **309**, 2180 (2005).

[219] H. Bluhm, S. Foletti, I. Neder, M. Rudner, D. Mahalu, V. Umansky, and A. Yacoby, Nat. Phys. **7**, 109 (2011).

[220] S. Nadj-Perge, S. M. Frolov, E. P. A. M. Bakkers, and L. P. Kouwenhoven, Nature **468**, 1084 (2010).

[221] A. V. Khaetskii, D. Loss, and L. Glazman, Phys. Rev. Lett. **88**, 186802 (2002).

[222] W. A. Coish and D. Loss, Phys. Rev. B **70**, 195340 (2004).

[223] P. Simon and D. Loss, Phys. Rev. Lett. **98**, 156401 (2007).

[224] P. Simon, B. Braunecker, and D. Loss, Phys. Rev. B **77**, 045108 (2008); B. Braunecker, P. Simon, and D. Loss, Phys. Rev. B **80**, 165119 (2009).

[225] Y. A. Bychkov and E. I. Rashba, J. Phys. C **17**, 6039 (1984).

[226]   G. Dresselhaus, Phys. Rev. **100**, 580 (1955).

[227]   E. I. Rashba, Phys. Rev. B **68**, 241315(R) (2003).

[228]   A. A. Burkov, A. S. Núñez, and A. H. MacDonald, Phys. Rev. B **70**, 155308 (2004).

[229]   S. I. Erlingsson, J. Schliemann, and D. Loss, Phys. Rev. B **71**, 035319 (2005).

[230]   J. Nitta, T. Akazaki, and H. Takayanagi, Phys. Rev. Lett. **78**, 1335 (1997).

[231]   J. D. Koralek, C. P. Weber, J. Orenstein, B. A. Bernevig, S.-C. Zhang, S. Mack, and D. D. Awschalom, Nature **458**, 610 (2009).

[232]   M. Studer, G. Salis, K. Ensslin, D. C. Driscoll, and A. C. Gossard, Phys. Rev. Lett. **103**, 027201 (2009).

[233]   J. Schliemann, J. C. Egues, and D. Loss, Phys. Rev. Lett. **90**, 146801 (2003).

Fabio Luigi Pedrocchi
Curriculum Vitae

Personal Data

Citizen of Switzerland.

20.10.1985   **Born in Delémont**, *2800 Delémont*, Switzerland.

Education

2009-2013   **PhD in Physics**, *Physics Department*, University of Basel, Switzerland.
Spin systems and long-range interactions for quantum memories and quantum computing''
Advisor: Prof. Dr. Daniel Loss,   *Summa Cum Laude*.

2007-2009   **Master of Science in Physics (with distinction)**, *ETH Zürich*, Zürich, Switzerland.
Supervisor: Prof. Dr. Renato Renner.

2004-2007   **Bachelor of Science in Physics**, *ETH Zürich*, Zürich, Switzerland.

2001-2004   **Maturité Cantonale**, *Lycée Cantonal de Porrentruy*, Porrentruy, Switzerland.

List of Publications

2013   Stefano Chesi, Arthur Jaffe, Daniel Loss, and Fabio L. Pedrocchi
ArXiv: 1305.6270
Vortex Loops and Majoranas

2013   Luka Trifunovic, Fabio L. Pedrocchi, and Daniel Loss
ArXiv:1305.2451
Long-Range Interaction of Singlet-Triplet Qubits via Ferromagnets

2013   Arthur Jaffe and Fabio L. Pedrocchi
ArXiv: 1305.1792
Reflection Positivity for Majoranas

2013   Luka Trifunovic, Fabio L. Pedrocchi, and Daniel Loss
ArXiv: 1302.4017
Long-Range Interaction of Spin-Qubits via Ferromagnets

2013   Daniel Becker, Tetsufumi Tanamoto, Adrian Hutter, Fabio L. Pedrocchi, and Daniel Loss
Phys. Rev. A **87**, 042340 and arXiv:1302.3998
Dynamic Generation of Topologically Protected Self-Correcting Quantum Memory

2013   Fabio L. Pedrocchi, Adrian Hutter, James R. Wootton, and Daniel Loss
ArXiv:1309.062, ArXiv: 1209.5289
Enhanced thermal stability of the toric code through coupling to a bosonic bath

2012   Fabio L. Pedrocchi, Stefano Chesi, Suhas Gangadharaiah, and Daniel Loss
Phys. Rev. B **86**, 205412 and arXiv:1204.3044
Majorana states in inhomogeneous spin ladders

2011   Daniel Loss, Fabio L. Pedrocchi, and Anthony J. Leggett
Phys. Rev. Lett. **107**, 107201 and arXiv:1107.1223
Absence of spontaneous magnetic order of lattice spins coupled to itinerant interacting electrons in one and two dimensions

2011   Fabio L. Pedrocchi, Stefano Chesi, and Daniel Loss
Phys. Rev. B **84**, 165414 and arXiv:1105.4573
Physical solutions of the Kitaev honeycomb model

2011   Fabio L. Pedrocchi, Stefano Chesi, and Daniel Loss
Phys. Rev. B **83**, 115414 and arXiv:1011.3762
Quantum memory coupled to cavity modes